UNIVERSITAT DE BARCELONA

TP53INP2 at the crossroad of transcription, autophagy and liver metabolism

Jia Liang Sun Wang

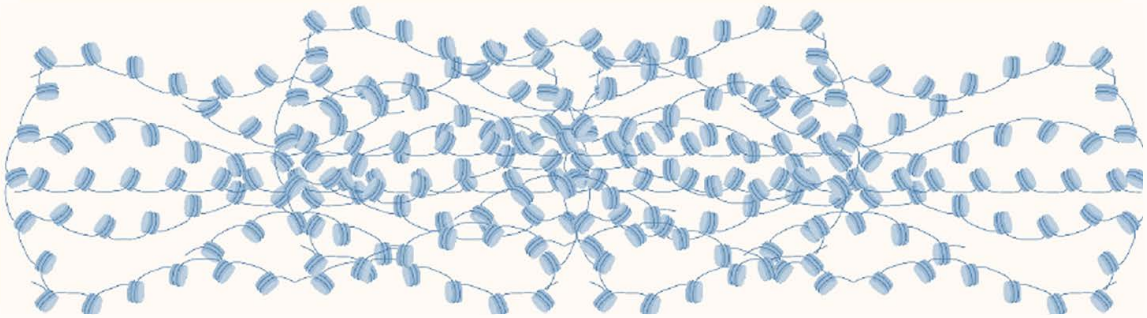

NRCA1 at the crossroad of transcription, autophagy and liver metabolism

Doctoral Thesis

Jia Liang Sun Wang

Universitat de Barcelona

Barcelona, 2024

DISCLAIMER

The research project carried out in this thesis is currently unfinished. Moreover, part of the results from this thesis are being considered for patenting. Therefore, to protect this thesis, we have changed the name of our target protein for a fictional one. Based on the findings of this thesis, we have named our target protein NRCA1 (Nuclear Receptor CoActivator-1). We have also encrypted all the references, part of the introduction, as well as material and methods information about our target protein.

FACULTAT DE BIOLOGIA

DEPARTAMENT DE BIOQUÍMICA I BIOMEDICINA MOLECULAR

INSTITUTE FOR RESEARCH IN BIOMEDICINE (IRB BARCELONA)

PROGRAMA DE DOCTORAT EN BIOMEDICINA

NRCA1 at the crossroad of transcription, autophagy and liver metabolism

Memòria presentada per Jia Liang Sun Wang per optar al grau de doctor per la Universitat de Barcelona

Jia Liang Sun Wang	Antonio Zorzano Olarte	Saška Ivanova
Doctorand	Co-director i tutor	Co-directora

Barcelona, 2024

FACULTAT DE BIOLOGIA

DEPARTAMENT DE BIOQUÍMICA I BIOMEDICINA MOLECULAR

INSTITUTE FOR RESEARCH IN BIOMEDICINE (IRB BARCELONA)

PROGRAMA DE DOCTORAT EN BIOMEDICINA

NRCA1 at the crossroad of transcription, autophagy, and liver metabolism

Jia Liang Sun Wang

Doctoral Thesis

Barcelona, 2024

“Innovation is the key to the future, but basic research is the key to future innovation”

Jerome I. Friedman, PhD, Nobel Prize in Physics (1990)

“Dream on, dream until your dreams come true”

Steven Tyler

ACKNOWLEDGEMENTS

Después de un arduo y largo camino, el doctorado por fin llega a su fin. Han sido 4 años y medio de autoaprendizaje, crecimiento y superación personal. Y, sobre todo, de disfrutar la ciencia. Si hoy estoy aquí, es gracias al apoyo incondicional de mi familia y de la persona más importante de mi vida: mi esposa. Gracias cariño, por siempre creer en mí, por haberme dado un lugar al que llamar hogar y por animarme en los momentos de máxima frustración. Sin ti, no habría llegado hasta aquí. Sin ti, no sería la persona que soy a día de hoy. También gracias a ti Melanie, por haberme acompañado durante esta aventura. Los viajes a Londres, aunque no tan frecuentes últimamente, me han ayudado a desconectar y descansar de la rutina en el laboratorio. Ahora que vuelves a Barcelona, ya no te echaré tanto de menos y te podré ver más a menudo.

Este, es un momento muy importante, y me hubiera gustado que fueran testigos de este instante familiares que ya no se encuentran aquí presentes, sobretodo mi papá Liu. Espero que me estés viendo desde ahí arriba. Esta tesis va fuertemente dedicada a ti.

感谢爸爸妈妈对我付出的一切. 我要深表感谢你们对我学习的支持以及对我一直以来的的信任. 感谢你们教会我的价值观以及生活的各个方面. 是因为有你们才会有今天的我. 我也想对我岳父岳母深表感谢.谢谢你们一直相信我, 一直对待我像对待你们自己的儿子一样. 留爸爸，这本博士论文是我特殊想献给你的， 希望你能见证到.

Doy gracias también a aquellas personas que forman parte de mi más íntimo círculo de amistades. En especial, quiero agradecerte a ti Alejo, por haberme acompañado, no solo en la etapa del doctorado, sino en toda mi etapa de crecimiento académico y personal, desde que nos conocimos en el instituto. Gracias por todos aquellos momentos de desconexión, tanto presenciales como online, a través de la PS4 y de la Switch. Nuestras “cacerías” en MH, Elden Ring y COD han sido un gran apoyo emocional. A ti tampoco te queda nada para terminar la tesis, ¡esos bros ahí! Muchos ánimos y espero ver ese Nature pronto, se te echa de menos hermano. Gracias a vosotros también Guille, Guillem y Roger, por nuestras cenas y quedadas rememorando nuestros momentos en la universidad (éramos sumamente felices en aquella época) y por nuestras profundas conversaciones sobre el actual sistema académico (no entraré en más detalle).

También quisiera agradecer a todas aquellas personas que me han acompañado activamente durante el doctorado y que han hecho que esta aventura sea más llevadera. En este sentido, he tenido la suerte de contar con unos fantásticos compañeros de laboratorio (past and present) y compañeros de la comunidad IRB. Me gustaría dar gracias en especial a: David A., Dragana, Ekaitz, Inés, Isa, Ivan, Josep, Judith, Katerina, Laura, Marina, Paula N., Paula S., Petra, Sergio y Valentina. Muchas gracias de todo corazón.

Acho Marina, ¿Qué haría yo sin tu esencia murciana en el laboratorio? Gracias por ser la alegría de la huerta (nunca mejor dicho) y por darme vidilla dentro del laboratorio. Aún recuerdo los primeros meses después de tu llegada al laboratorio, ni siquiera habíamos hablado. Sin embargo, creo que fue después de la cena de Navidad del 2022, que de repente nuestra amistad se disparó exponencialmente. Gracias por todos esos coffee breaks, muy necesarios para no caer absorbido en el trabajo, y por todas las risas. Y también por todas las noches de fiesta, aunque desde que se pasó el verano ya no hemos vuelto a salir. Ah, y también gracias por los limones que siempre me traes de Murcia, están tan ricos que ya ni me apetece comprar limones de los supermercados. ¡Viva la región de Murcia!

Hey you! Judith, quan em vaig assabentar que tornaves al laboratori de Palacín a fer la tesi, em vaig alegrar molt. És molt curiós, tots dos vam començar a fer el TFG en els laboratoris on hem fet ara la tesi. Però després del TFG, vam prendre rumbs diferents. Tot i que després del TFG no havíem mantingut el contacte, quan et vaig tornar a veure al laboratori, tenia la sensació que m'havia retrobat amb una vella amiga que no veia des de fa molt temps. He tingut molta sort de tenir-te com a partner-in-crime al laboratori i també de tenir-te com a companya de running. Aquestes sessions, no només m'han ajudat a cuidar-me físicament, sinó també mentalment (el doctorat desgasta molt, com bé saps). T'admiro molt a nivell professional, ets una gran científica i ets el clar exemple de "multitasking" ben fet, tot i que ara et veig una mica més relaxada, eh doctora! També he trobat una mica a faltar la teva presència a les cool-offs del IRB. Tant de bo no visquessis a Igualada per poder fer més plans junts!

¡Inés! ¡Cabesa! Tengo la suerte de haberte conocido durante el máster y de haber coincidido contigo durante el PhD. Para mí, no eres solo una gran amiga, sino también una gran científica por la que siento mucha admiración. Y esa admiración, me ha motivado a ser mejor científico. Gracias por todos esos momentos que hemos compartido juntos tanto en el IRB como fuera, por esos fines de semana de juegos de mesa y por las sesiones de body pump, que siempre me dejaban destrozado. Te echo mucho de menos, ¡defendiste demasiado pronto! Y para colmo, te fuiste a la otra punta del mundo. ¡Espero verte pronto!

Joseeeeep! Yo, what up m**********r. Ha sigut tot un plaer coincidir amb tu al laboratori. Amb tu he pogut donar "rienda suelta" al meu humor negre. Crec que ets la persona del laboratori amb qui més he rigut, principalment per tonteries que no tenen ni caps ni peus. També ha sigut un honor per mi compartir amb tu música de veritat i depositar la tesi el mateix dia que tu. No deixis de ser com ets, no deixis d'emborratxar-te a la mínima, no deixis d'anar a pica piques del IRB, no deixis d'anar a defenses de tesis sense ser convidat, i sobretot, no deixis de treballar dur com fas sempre. Perquè ja saps, "quien no sacrifica, no *******". Espero tenir també una bona dedicatòria als agraïments de la teva tesi. Per acabar, et dedico les següents paraules: "don't believe everything you read".

Katerina, do you still remember when we first started the PhD together? It's been such a long way since then. You know, I've always appreciated working in an international environment, and you were the person who brought that to the lab when I started the PhD. I'm so glad that we embarked on this journey together because of all the fun we've had, which made the PhD adventure significantly more bearable. I am also grateful to you for being the person who re-ignited my interest and passion for innovation. I am also overly happy that the delivery date of my PhD Thesis is so close to your birthing date, because then when I think about my thesis submission, I will also think about Eva. Soon it will be your turn to submit your thesis, and I can't wait for that to happen! ¡Muchos ánimos!

¡Qué pasa bro! Iván, tu y yo también empezamos juntos el PhD, y creo que conectamos muy rápido, gracias a que compartimos una gran pasión: el manga y el anime. Y que también somos unos viciados del Pokémon, del MH, y un largo etcétera. Gracias por ser un friki como yo, porque si no, no tendría con quien hablar de One Piece, que, por cierto, está muy interesante, desde luego más que esta tesis, seguro. Admiro mucho tu arte para dibujar personajes de manga, y te tengo que dar las gracias por las maravillosas ilustraciones de Monkey D. Luffy que me has regalado, shishishi. Gracias por estos años de amistad y de buenos momentos que hemos pasado juntos, especialmente en las cool-offs, y ¡ánimos con la tesis! Que tienes los días contados. Ah, por cierto, que sepas que nunca pararé de mandarte reels.

¡Paula! Encara recordo el dia que ens vam trobar a la cambra del WB, em va fer molta gràcia i il·lusió que em saludessis, tot i que jo no et vaig reconèixer. Per mi ha sigut un gran plaer compartir passadís amb tu durant tots aquests anys. Jo que em pensava que era el rei dels WBs, vas arribar tu i em vas treure el títol! A tu encara et queda una mica per acabar la tesi, però no t'esveris, ja arribarà el teu moment, gaudeix del moment. Segur que descobriràs quelcom molt interessant amb els teus ratolins. Et dic el mateix que li he dit a la Judith, també t'he trobat a faltar a les cool-offs del IRB, i mira que tu vius aquí a prop, no tens excuses eh!

Hey there, Dragana! Despite not talking to you during your master's, I wanted to say a few words to you as well, because now I do care! In fact, when word was spread that you were re-joining the lab to do your PhD, I was actually very excited to see you again. You also bring a sense of internationality to the lab that not only do I appreciate, but also Josep. And that is fantastic, because I have so much fun when Josep starts joking around with you about Eastern Europe and whatnot. I'm also glad that I could help you with your proteomic studies, even if it's just scrapping plates, I'm beyond excited to see what you discover, keep up the hard work!

¡Qué pasa jefe! Sergio, ha sido un gran placer coincidir contigo en el laboratorio. Tus seminarios de grupo han sido de lo mejorcito del grupo. Como también lo han sido tus tubulinas y tus actinas. Me alegra mucho saber que educarás las futuras generaciones de científicos valencianos, eres todo un referente. Muchas gracias por todas las risas que nos hemos echado.

Vanessa, muchas gracias a ti también por toda la ayuda con los experimentos *in vivo*, sin ti, ¡no hubieran sido posible!

Jordi, moltes gràcies a tu també per la fantàstica feina que fas com lab manager. Trobaré a faltar el teus concerts (a mi no m'han molestat gaire, a diferència d'altra gent).

Estoy eternamente agradecido a mis supervisores, Antonio y Saška. Gracias por todos estos años de aprendizaje, mentoría y supervisión. Gracias por las magníficas discusiones científicas que hemos tenido a lo largo de todos estos años y por contagiarme vuestra pasión y curiosidad por la ciencia. De no ser por vosotros, no habría podido crecer tanto a nivel académico y profesional. Para mi sois grandes modelos científicos a seguir, mis dos pilares de la ciencia. Antonio, sempre m'encordaré de la següent frase que em vas ensenyar: "si no pots convèncer, confon". Saška, I'm very grateful to you for all the good moments and the fun we've had in the lab. Thanks to both of you for this amazing project and experience!

También me gustaría dar las gracias a mis mentores del Máster. Muchas gracias Luis, Ekaitz, Pau y Manuel. Gracias a vosotros, maduré mucho a nivel científico y aprendí que las colaboraciones interdisciplinarias son esenciales para resolver los grandes misterios de la ciencia. Siempre llevaré

También quisiera agradecer a todos los programas de innovación en los que he participado por abrirme nuevos horizontes, por hacerme ver que más allá de la ciencia básica, que es esencial para la innovación, se pueden transformar grandes descubrimientos científicos en soluciones tangibles para el beneficio de nuestra sociedad. Muchas gracias a EIT Health, ESADE, al programa "De la ciencia al mercat" y a los Tech Transfer Officers del IRB Barcelona, en especial, gràcies a tu, Alba.

I would also like to thank very special and talented people that through their continuous work, have made my PhD journey less arduous and have brought joy to it in moments of darkness. A big thanks to all mangakas, especially to Toriyama-sensei, Oda-sensei and Kishimoto-sensei, because I essentially grew up following your works. You taught me what dreams are, that you have to work hard to chase your dreams and never give up. You also taught me that you can achieve greatness through discipline. You also taught me how to appreciate friendship, to smile in difficult situations, and that no matter how dark the tunnel is, there is always a ray of light in it. Thank you. R.I.P Toriyama-sensei.

I also have to thank music artists around the world, because without their music, I would have never been able to finish my PhD journey. Thank you Linkin Park, Aerosmith, Bon Jovi, Guns N' Roses, Avenged Sevenfold, Tupac, Dr.Dre, Snoop Dogg and Biggie.

Last but not least, I want to thank me for believing in me. I want to thank me for doing all this hard work. I want to thank me for having no days off. And I want to thank me for never quitting.

ABSTRACT

Metabolic-associated steatotic liver disease (MASLD) is the leading global liver chronic disease and it is estimated to affect 30% of the world population. MASLD is a progressive multi-stage disease characterized by an abnormal accumulation of fat in liver, also known as steatosis. Major risk factors for developing MASLD include obesity and metabolic syndrome. Patients with MASLD are at risk of developing co-morbidities such as cardiovascular disease, diabetes and chronic kidney disease. Unfortunately, there is no approved pharmacological treatment for MASLD.

PPARα is a nuclear receptor that is activated upon fasting to coordinate the hepatic response against this cue. It promotes the expression of genes that are essential for fatty acid oxidation (FAO) and ketone body (KB) synthesis. It emerged as a promising therapeutic target for MASLD due to its strong protective role against the development of MASLD in mouse models. In addition, treatment of MASLD mouse models with PPARα agonists improves steatosis.

In this thesis, we have identified NRCA1 as a novel regulator of PPARα. NRCA1 is a multifaceted protein that regulates many aspects of metabolic homeostasis through its action in different tissues. It also modulates many cellular processes, including autophagy and apoptosis. Essentially, liver-specific NRCA1 ablation impaired the activation of PPARα upon fasting, which caused a blunted upregulation of FAO and KB synthesis genes. This resulted in increased hepatic fat accumulation. These effects were more pronounced in aged mice. By using PPARα agonists, we uncovered that NRCA1 is required to fully activate PPARα.

Interestingly, NRCA1 ablation also impaired the transcriptional activation of autophagy during fasting. This may be a direct effect of impaired PPARα activation, as PPARα was shown to be a master regulator of hepatic autophagy in response to fasting. Autophagy has also been established to be a protective against MASLD.

We used a methionine- and choline-deficient (MCD) diet to promote MASLD in control and NRCA1-deficient mice and treated them with the PPARα agonist GW7647 to assess the potential role of NRCA1 in the development and treatment of MASLD. Interestingly, female NRCA1-deficient mice subjected to a one-week regime of MCD diet showed impaired activation of PPARα by the agonist GW7647. In addition, male NRCA1-deficient mice fed with MCD diet during 3 weeks and treated chronically with GW7647 during the diet showed lower response to GW7647.

To elucidate how NRCA1 regulates PPARα activation we used the BioID technology to map the binding partners of NRCA1. Most of the identified interactors are involved in the regulation of chromatin dynamics and epigenetics, with coregulator activity and nuclear receptor binding functions. In keeping with this, we have also shown that NRCA1 is a chromatin-binding protein that interacts with RING1A, a ubiquitin ligase (E3) that acts as the catalytic component of the Polycomb repressive complex 1 (PRC1). The PRC1 is an epigenetic modulator that ubiquitinates histone H2A to suppress gene expression. In addition, NRCA1 interacts with UBR5, another E3 that is involved in the turnover of nuclear receptors. These results indicate that NRCA1 may regulate PPARα-dependent gene expression through

its interaction with players of the epigenetic machinery. ChIP-Seq experiments will be key to confirm this hypothesis.

In conclusion, NRCA1 is required for the full activation of PPARα in response to fasting and to agonists. When NRCA1 is ablated in the liver, upregulation of FAO, KB synthesis and autophagy genes in response to fasting is blunted. This renders NRCA1-deficient hepatocytes incapable of ridding of the fat overload coming from adipose tissue lipolysis, leading to increased hepatic fat accumulation.

TABLE OF CONTENTS

TABLE OF FIGURES

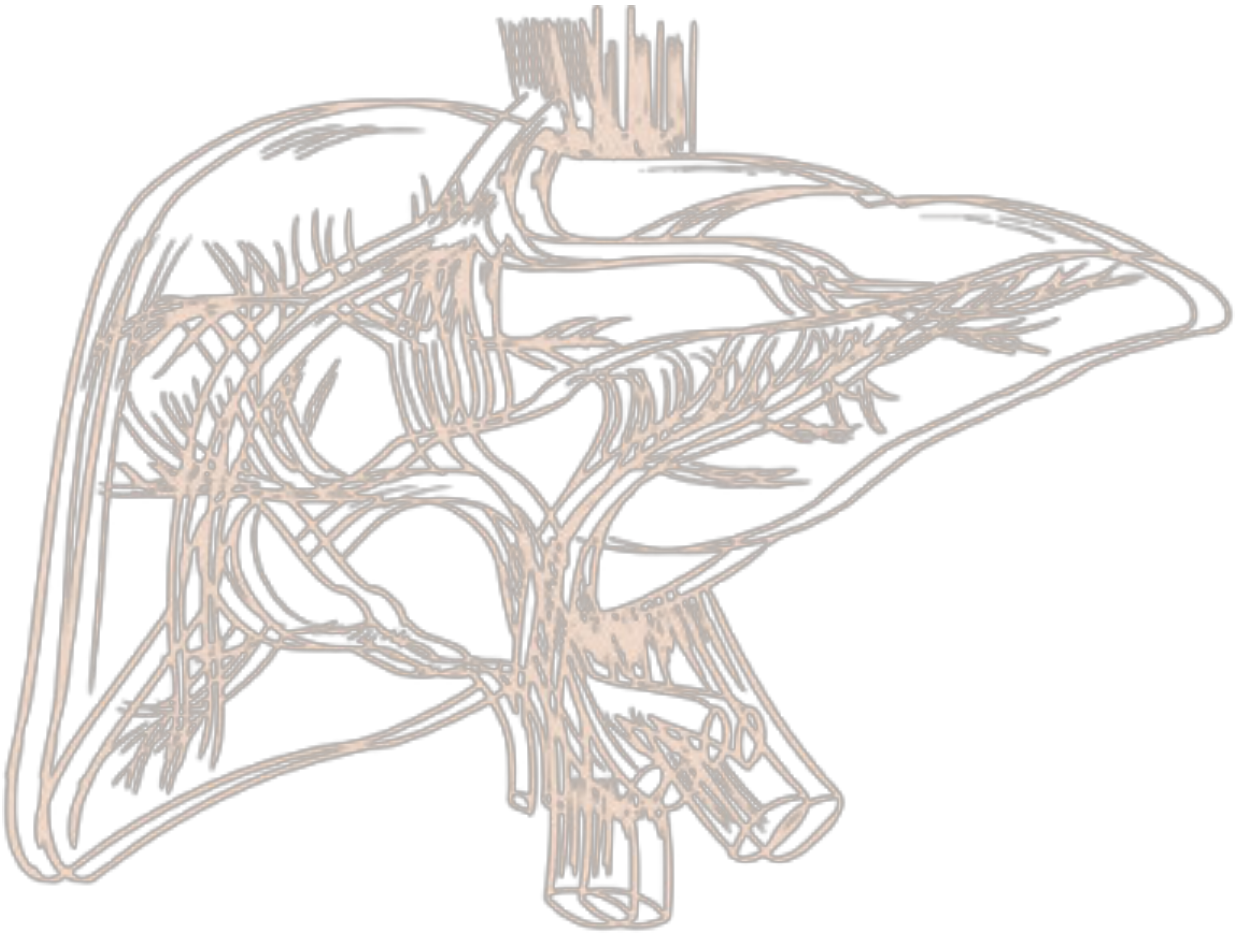

ABBREVIATIONS

1. ABBREVIATIONS

A

ABCA1	ATP-binding cassette transporter subfamily A member 1
ABCG1/5/8	ATP-binding cassette transporter subfamily G member 1/5/8
AKT	AKT serine/threonine kinase 1
ALT	Alanine transaminase
AMPK	Adenosine monophosphate-activated protein kinase
AST	Aspartate transaminase
AT	Adipose tissue
ATG	Autophagy related

B

BFDR	Bayesian false discovery rate

C

cAMP	Cyclic adenosine monophosphate
ChEA	ChIP enrichment analysis
ChIP	Chromatin immunoprecipitation
CMA	Chaperone-mediated autophagy
CREB	cAMP responsive element binding protein
CRTC	CREB regulated transcription coactivator
CST	Cell Signaling Technologies
Cyp4a10/14	Cytochrome p450 family 4 subfamily A member 10/14
Cyp7a1	Cytochrome p450 family 7 subfamily A member 1

D

Dgat2	Diglyceride acyltransferase 2
DNL	De novo lipogenesis
[redacted]	[redacted]

E

E3	Ubiquitin ligase
ER	Endoplasmic reticulum
ERK5	Extracellular-signal-regulated kinase 5

F

FAO	Fatty acid oxidation
FFA	Free fatty acid
FIP200	FAK family kinase-interacting protein of 200 kDa
F-TP	Flag-NRCA1
FXR	Farnesoid X receptor

G

GABARAP	GABA type A receptor-associated protein
GO	Gene ontology
GRα	Glucocorticoid receptor α
GSEA	Gene set enrichment analysis

H

HCC	Hepatocellular carcinoma
HDL	High-density lipoprotein
HOMA-IR	Homeostasis model index of insulin resistance

K

KB	Ketone body

L

LC3A/B	Microtubule associated protein 1 light chain 3 alpha/beta
LD	Lipid droplet
LDL	Low-density lipoprotein
LIR	LC3-interacting region
Lpin1	Lipin-1
LRH-1	Liver receptor homolog-1
LXR	Liver X receptor

M

MASLD	Metabolic dysfunction-associated steatotic liver disease
MASL	Metabolic dysfunction-associated steatotic liver
MASH	Metabolic dysfunction-associated steatohepatitis
MCD	Methionine- and choline-deficient

MRI	Magnetic resonance imaging
mTORC1	Mammalian target of rapamycin complex 1

N

NAFLD	Non-alcoholic fatty liver disease
NES	Nuclear export signal
NLS	Nuclear localization signal
NR	Nuclear receptor

P

PE	Phosphatidylethanolamine
PI3K	Phosphoinositide 3-kinase
PI3P	Phosphoinositide 3-phosphate
PKA	Protein kinase A
PPAR	Peroxisome proliferator-activated receptor

R

RCT	Reverse cholesterol transport
RXR	Retinoid X receptor

S

Scd1	Stearoyl-Coenzyme A desaturase-1
SHP	Small heterodimer partner

T

TG	Triglyceride
TID	TurboID
TIM	TRAF6-interacting motif
TFEB	Transcription factor EB
NRCA1	[redacted]
NRCA1-TID	NRCA1-TurboID
TRAF6	Tumor necrosis factor receptor-associated factor 6
TRα	Thyroid hormone receptor α

U

UBA	Ubiquitin-associated

UBL	Ubiquitin-like
UIM	Ubiquitin-interacting motif
ULK1	Unc-51 like autophagy activating kinase 1

V

VDR	Vitamin D receptor
VLDL	Very low-density lipoprotein
VPS34	Vacuolar protein sorting 34

W

WAT	White adipose tissue
WIPI	WD repeat domain phosphoinositide-interacting protein

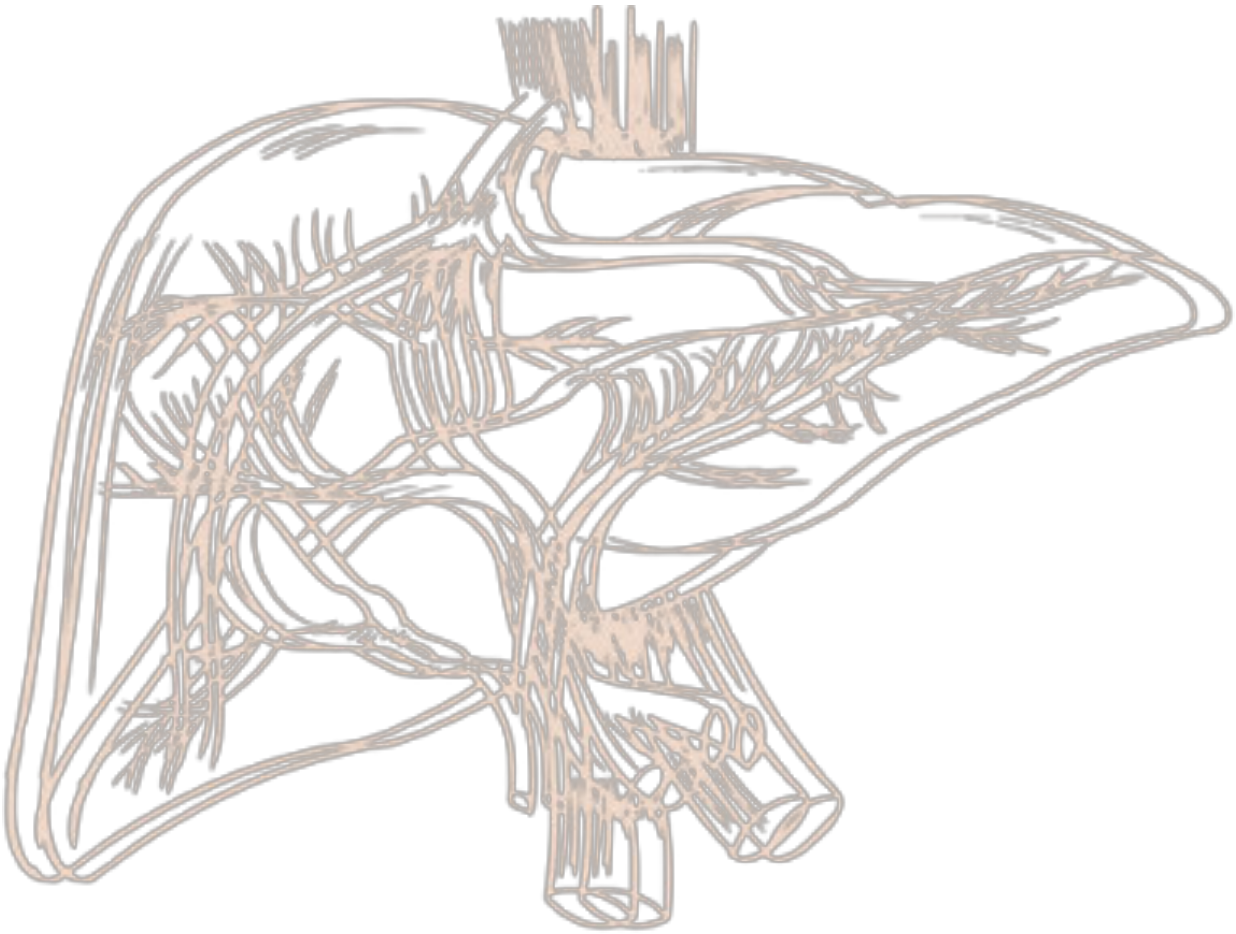

INTRODUCTION

2. INTRODUCTION

2.1. The liver: a key organ in metabolic homeostasis

The liver is a key organ in metabolic homeostasis. As a central organ of metabolic control, it plays crucial functions for maintaining homeostasis, including nutrient sensing and regulation, detoxification and protein synthesis.

The liver plays a pivotal role in nutrient sensing and regulation. In glucose metabolism, it regulates the production of glucose by gluconeogenesis, as well as the metabolism of glucose (glycolysis) and the pentose phosphate pathway. Simultaneously, it also serves as the main reservoir for glycogen storage, releasing glucose as needed to meet energy demands through glycogenolysis. These processes are finely tuned to maintain blood glucose levels within a physiological range[1].

In lipid metabolism, the liver modulates the synthesis and breakdown of fatty acids, triglycerides and cholesterol. Additionally, the liver regulates lipoprotein production, thus influencing the transport of lipids in the bloodstream and to distal organs. Through these intricate processes, the liver ensures a delicate balance between energy storage and utilization, responding to the body's metabolic demand[2].

Detoxification is another critical facet of the liver's functions. It acts as a primary site for the clearance of toxins and metabolic byproducts, such as urea, and converts them into less harmful substances that can be eliminated through excretion. This detoxification capacity protects the organism from potentially toxic chemical insults[3].

The liver synthesizes numerous proteins, including clotting factors, albumin and enzymes involved in various metabolic pathways. Many of the proteins produced by the liver are secreted to the bloodstream and are essential for the regulation of blood composition[4]. The liver also secretes hormone-like proteins termed hepatokines, such as FGF-21 and insulin-like growth factors (IGFs), including IGF-I and IGF-II[5]. Hepatokines regulate systemic metabolic homeostasis by modulating energy expenditure, glucose and lipid metabolism[5].

Dysregulation of any of the above-mentioned hepatic functions can lead to liver disease. This thesis will focus on a particular disease: metabolic dysfunction-associated steatotic liver disease (MASLD).

2.1.1. Metabolic dysfunction-associated liver disease (MASLD)

2.1.1.1. MASLD, a silent epidemic

Metabolic dysfunction-associated steatotic liver disease (MASLD), also known as non-alcoholic fatty liver disease (NAFLD)[6], is the leading chronic liver disease worldwide. It is estimated to affect approximately 25 to 30% of the world population, with varying prevalence across geographic regions[7]. The new nomenclature was introduced as an overarching term to include the metabolic aspects of the disease, as it is associated with metabolic dysfunction. Moreover, the use of the term steatotic liver disease (SLD) was adopted to incorporate a less stigmatizing language compared to the term fatty liver disease (FLD)[6].

MASLD is a progressive multi-stage disease characterized by an abnormal accumulation of fat in liver, also known as steatosis, and elevated serum levels of hepatic enzymes, including alanine aminotransferase (ALT) and aspartate aminotransferase (AST). MASLD is diagnosed when at least 5% of hepatocytes show signs of steatosis in individuals without secondary causes, with little to no alcohol consumption and without any indirect causes, such as drug consumption or other metabolic liver diseases (e.g., lipodystrophy, etc.).

The stages of MASLD include metabolic dysfunction-associated steatotic liver (MASL), metabolic dysfunction-associated steatohepatitis (MASH), liver fibrosis and cirrhosis, which can progress to hepatocellular carcinoma (HCC) (Figure 1). MASLD is histologically classified into MASL and MASH. MASL is characterized by ≥ 5% hepatic steatosis without evidence of hepatocellular injury. MASH manifests with ≥ 5% hepatic steatosis, and inflammation with hepatocyte injury (e.g., ballooning) with or without fibrosis[8]. It is estimated that 20% of individuals with MASLD have MASH, and 20% of these individuals may progress to cirrhosis[9]. Individuals with cirrhosis are at an increased risk of developing HCC[10].

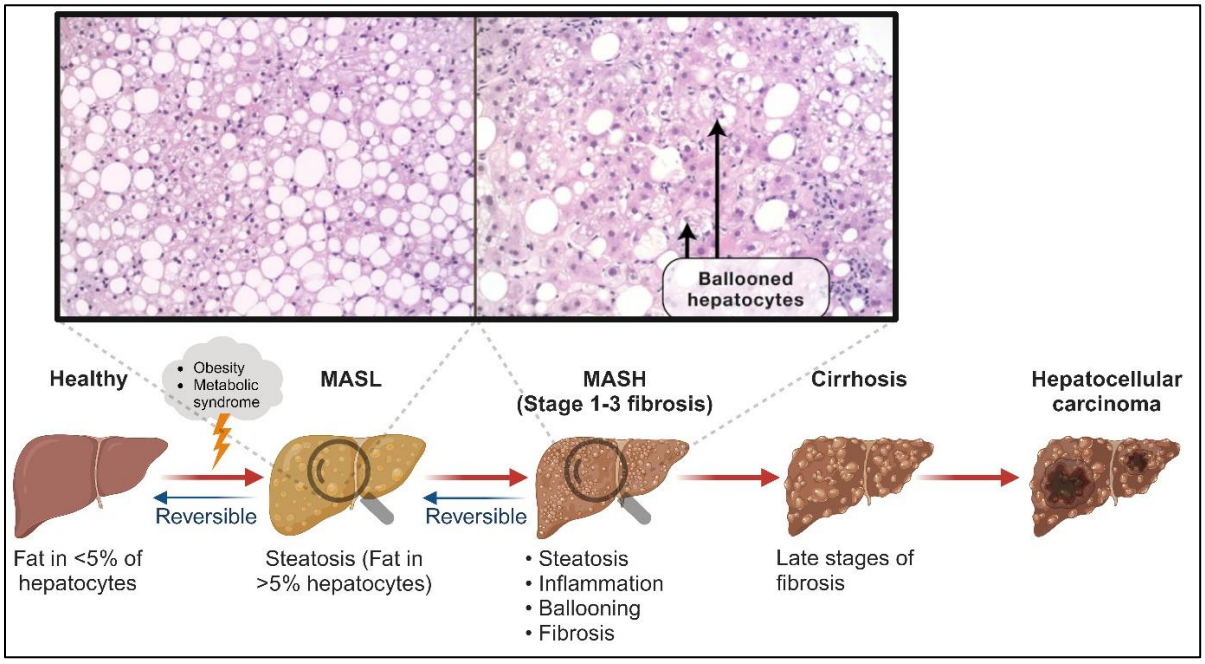

Figure 1: MASLD spectrum. Adapted from[7]. Created with BioRender.

MASLD can be considered a silent epidemic[11], as it usually manifests with no symptoms in most individuals until it has progressed to cirrhosis, making it difficult to detect the pathology in early stages. The most common symptom is right upper quadrant pain and fatigue, which is then confirmed by ultrasonic evidence or MRI and serum biochemistry tests showing increased levels of hepatic enzymes (e.g. ALT, AST, etc.) and lower albumin levels[8].

2.1.1.2. Metabolic syndrome and genetic factors in the development of MASLD

The metabolic mechanisms leading to MASLD are complex and involve other tissues such as skeletal muscle and white adipose tissue (WAT). The main cause of MASLD is a chronic imbalance of energy metabolism in the liver, in the form of excess energy (mostly carbohydrates and fat) due to excess food intake. This surplus of energy supplies is far superior to the capability of the liver to oxidize it or transport it as very low density lipoproteins (VLDLs), resulting in a net accumulation of energy in the liver as triglycerides (TGs). Mono- and disaccharides, especially fructose, sucrose and high-fructose corn syrup, which is ubiquitously present in processed foods, can activate hepatic *de novo* lipogenesis (DNL). Additionally, fructose is exclusively metabolized in the liver and is mostly converted into triglycerides by DNL. Skeletal muscle insulin resistance, an early sign of metabolic syndrome (Box 1) and prediabetes, also contributes to the development of MASLD by diverting glucose away from skeletal muscle into the liver for DNL. Furthermore, white adipose tissue dysfunction in the context of obesity also redirects lipid storage to the liver, exacerbating MASLD[7]. Hepatic insulin resistance impairs glycogen synthesis and thus repurposes glucose for lipogenic pathways, further promoting MASLD[12].

Genetic predisposition can also influence the development of MASLD. GWAS studies have provided valuable information on gene loci associated with MASLD susceptibility[13]. A major genetic variant concerns the gene encoding for PNPLA3 (rs738409 C>G), which results in the substitution of isoleucine to methionine at position 148. PNPLA3 is a lipase involved in the breakdown of TGs, and the I148M mutation induces a loss-of-function in its enzymatic activity[14], which may be responsible for increased hepatic fat accumulation. This mutant variant has also been reported to evade proteasomal degradation and accumulate in lipid droplets (LDs)[15], where it may affect the activity of other lipases such as ATGL.

Epigenetic factors are also involved in the pathogenesis of MASLD[13]. It has been reported that maternal fat intake contributes to the development of MASLD in adult offspring[16]. In this study, female mice were fed either a chow diet (CD) or a high-fat-diet (HFD) during gestation and lactation. The offspring were fed either a CD or a HFD after weaning, resulting in four offspring groups: CD/CD (offspring fed with a CD born from a mother that was fed a CD), CD/HFD, HFD/CD and HFD/HFD. Offspring mice were fed with CD or HFD for 15 weeks or 30 weeks. Interestingly, at 15 weeks of age, CD/HFD and HFD/CD offspring developed MASL, whereas HFD/HFD offspring developed MASH. At 30 weeks, HFD/HFD offspring had a more severe form of MASH compared to CD/HFD and HFD/CD offspring[16].

MASLD also has a heritable component. It has been reported that first degree relatives of patients with MASLD are at considerably increased risk of manifesting the disease[13]. In a family study, MASLD was significantly more common in siblings (59%) and parents (78%) of children with MASLD, independently of adiposity[17]. Moreover, studies conducted with twins

showed that circulating liver enzymes such as ALT have between 35-61% heritability, and phenotype concordance was higher in monozygotic that in dizygotic twins[14].

Currently, there is no approved pharmacological treatment for MASLD and therapeutic options may vary depending on the stage of the disease. Several drugs are in clinical trials, which target a plethora of liver proteins including nuclear receptors, among others[18]. Lifestyle intervention has also proved to ameliorate MASLD. In a 12-month weight-loss intervention study, it was shown that weight reduction improved histological parameters including steatosis, hepatocyte ballooning, inflammation and fibrosis[19]. Moreover, this improvement was dependent on the percentage of weight loss (with a positive correlation), for example 35% of patients who lost less than 5% of their weight (1.78 ± 0.16) had improved steatosis, whereas 100% of patients who lost more than 10% of their weight (13.04 ± 6.6) had improved steatosis. Exercise also improves liver steatosis and liver stiffness independently of changes in diet[20,21]. In a study with a cohort of 233,676 subjects, moderate to vigorous exercise was shown to be beneficial in decreasing risk of fatty liver incidence as well as improving existing fatty liver during a 5-year follow-up[22]. In addition, a dose-response relationship between exercise volume and steatosis reduction has been established, independent of weight reduction[23]. Individuals performing moderate to vigorous physical activity over 400 minutes (409.7 ± 10.7) per week experienced higher responses compared to individuals exercising over 200 minutes (216 ± 15.4) per week, which in turn showed higher responses compared to individuals exercising over 100 minutes (101.6 ± 15.8) per week[23].

In conclusion, MASLD emerges as a complex liver disorder driven by an energy imbalance within the liver, with insulin resistance in key tissues and the compounding effects of metabolic syndrome and obesity collectively contributing to its progression and severity. Therefore, MASLD can be considered the hepatic manifestation of the metabolic syndrome. Due to its systemic nature, MASLD constitutes a risk factor for many other diseases, including cardiovascular diseases, diabetes and chronic kidney disease, among others[24]. Overall, among people with MASLD, cardiovascular disease are the leading cause of death, followed by cancer. Pharmacological treatment of MASLD is currently under evaluation with several drugs in clinical trials. However, lifestyle interventions, including dietary weight loss and exercise, look promising in the management and treatment of MASLD.

Box 1 | **Metabolic syndrome**

Metabolic syndrome is a cluster of interconnected risk factors that significantly increase the likelihood of developing cardiovascular diseases, type 2 diabetes, and other health complications such as MASLD. At the core of metabolic syndrome is insulin resistance, a condition where the cells become less responsive to the effects of insulin. Insulin resistance results in impaired glucose uptake in insulin-sensitive tissues such as white adipose tissue and skeletal muscle, leading to elevated blood sugar levels and contributing to the development of metabolic syndrome. Increased glucose levels in circulation are diverted to other tissues such as liver, where it becomes a main substrate for DNL.

WAT plays a critical role in metabolic health. Obesity, or excessive accumulation of visceral fat, particularly around the abdominal area, is associated with insulin resistance and inflammation, resulting in metabolic syndrome. AT is not merely a passive energy storage site; it secretes hormones and cytokines, also known as adipokines, which can disrupt insulin signaling and promote inflammation. This inflammatory state exacerbates insulin resistance at autocrine and endocrine level, reaching other tissues like skeletal muscle, thus creating a detrimental cycle that fuels the progression of metabolic syndrome.

Skeletal muscle, a major site for glucose utilization, also plays a key role in metabolic syndrome. Impaired insulin signaling in skeletal muscle, influenced by adipokines, hampers glucose uptake, contributing to elevated blood sugar levels. Additionally, reduced physical activity and muscle mass, common in sedentary lifestyles, further exacerbate metabolic syndrome.

The intricate relationship between metabolic syndrome and liver health is evident in the context of MASLD. Insulin resistance contributes to the accumulation of fat in the liver through various mechanisms, including DNL, leading to hepatic steatosis. Therefore, MASLD is often considered the hepatic manifestation of metabolic syndrome.

At the molecular level, metabolic syndrome is associated with autophagy dysfunction. Numerous studies indicate that suppression of autophagy in WAT and liver impairs metabolic homeostasis in mouse models (discussed later in the thesis). Dysregulated or aberrant activation of nuclear receptors can also contribute to metabolic syndrome (discussed later in the thesis).

In conclusion, metabolic syndrome is a complex condition characterized by the interplay of insulin resistance, dysfunctional white adipose tissue, and impaired skeletal muscle function. These components collectively contribute to the cascade of events leading to metabolic syndrome and its associated health risks including cardiovascular diseases, type 2 diabetes, and MASLD. Understanding these key components is crucial for effective prevention and management strategies.

2.1.2. The role of nuclear receptors in liver metabolism and homeostasis

2.1.2.1. General aspects of nuclear receptors

Nuclear receptors (NRs) are a class of proteins that play a crucial role in the regulation of various physiological processes, including metabolism, development, immunity, and reproduction. These receptors act as transcription factors and their key feature is their ability to bind to specific ligands, which can be hormones, vitamins, or other signaling molecules. Upon ligand binding, NRs undergo conformational changes that enable them to interact with DNA and modulate the transcription of target genes. Mammals express a diverse array of NRs, and the total number can vary among species. In humans, there are approximately 48 NRs identified to date and they are classified according to their association with ligands (Figure 2). The diversity of NRs allows for a finely tuned and dynamic regulation of gene expression in response to a variety of signals, such as hormones, metabolites, and environmental cues in a tissue-specific manner[25]. This thesis will focus on NRs that regulate the transcriptional control of energy metabolism, with special emphasis on liver metabolism.

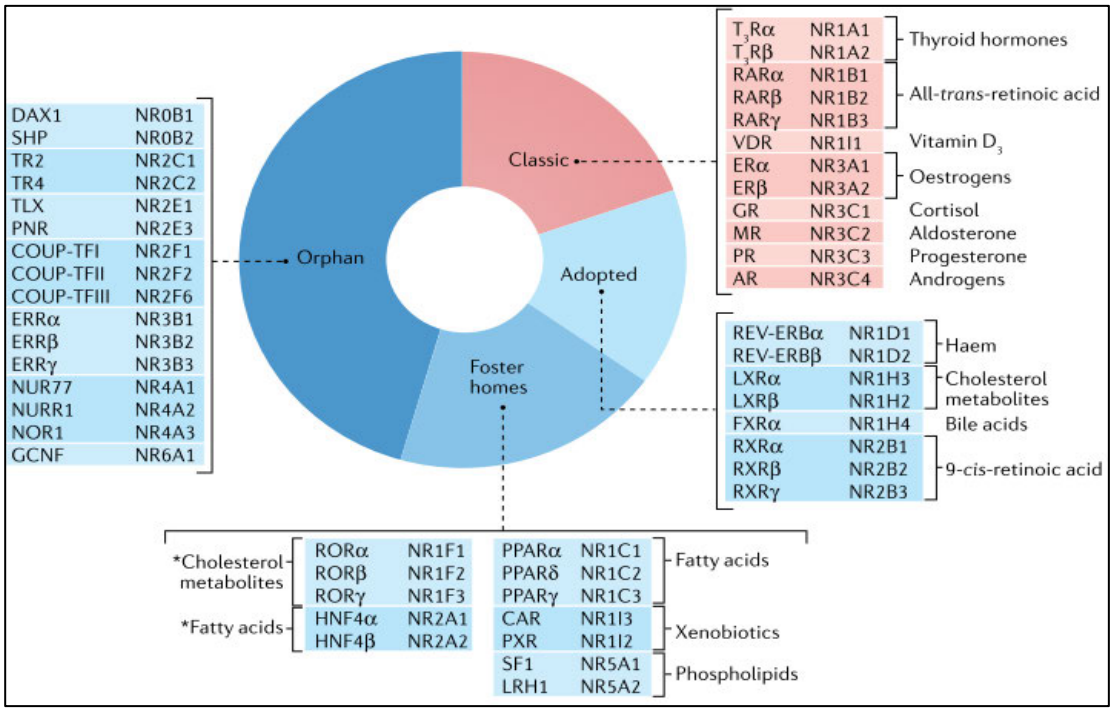

Figure 2: NR classification. The NR superfamily comprises 48 members in humans and they are classified according to their association with ligands. Classic NRs (red) belong to the group of receptors for which natural ligands were known before the receptor was identified by molecular cloning (e.g. thyroid hormones receptors and all-trans-retinoic acid receptors). Orphan NRs (distinct shades of blue) were identified without prior knowledge of their ligand association, and they remain in this class even after the identification of their ligands. Orphan NRs can be further classified into adopted and foster homes NRs. Adopted NRs are those for which association with one or more well-defined high-affinity ligands has been firmly established. Foster homes NRs are those functionally linked to broad, ill-defined class of ligands. The remaining 16 orphan NRs have yet to be associated with a natural ligand. Adapted from[25].

The general mechanism of action of NRs can be briefly summarized in the following steps (Figure 3):

1. Ligand binding: NRs are activated by binding to specific ligands, which can be hormones, vitamins, or other signaling molecules. Ligand binding induces conformational changes in the receptor, leading to an active state.
2. Dimerization: Some NRs function as homodimers or heterodimers. Dimerization is essential for the receptor's ability to bind to specific DNA sequences.
3. DNA binding: Activated NR dimers translocate to the cell nucleus, where they bind to specific DNA sequences called 'response elements'. These response elements are typically located in the promoter regions or enhancers of target genes.
4. Transcriptional regulation: Upon DNA binding, NRs interact with co-regulator proteins (coactivators or corepressors). Through the recruitment of epigenetic regulators[26] (Box 2), coactivators enhance gene transcription, while corepressors inhibit it. Typically, NR activation by ligand recruits co-activators. When NRs are inactive, they are bound to corepressors.
5. Transcription initiation: The presence of coactivators leads to the recruitment of the transcriptional machinery, including RNA polymerase. This results in the initiation of transcription and the synthesis of mRNA from the target gene, which is eventually processed and translated into a protein with a biological effect.

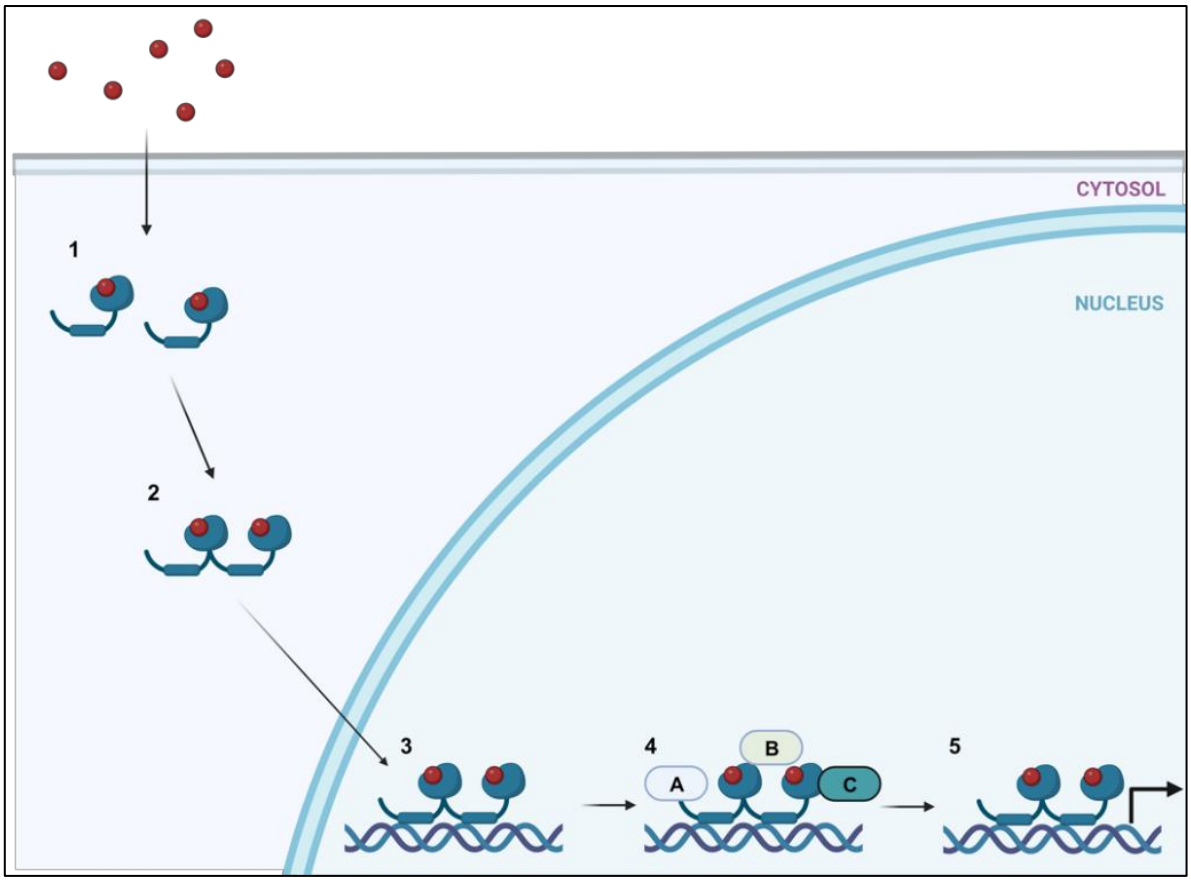

Figure 3: Mechanism of action of NRs. 1) Ligand binding, 2) Dimerization, 3) DNA binding, 4) Recruitment of coactivators, 5) Transcription of target genes. Created with BioRender.

Box 2 | **Epigenetic regulators**

Epigenetics refers to changes in gene function (or expression) that do not entail a change in DNA sequence and it constitutes a key regulatory mechanism for gene expression. Epigenetics permits spatiotemporal control of gene expression in response to endogenous and environmental stimuli. Epigenetic regulation is achieved through reversible modifications in the DNA or histones:

- DNA modifications: DNA methylation is the main DNA modification and results in repression of gene expression.
- Histone modifications: DNA is wrapped around histones, forming a structure called chromatin. The fundamental subunit of chromatin is the nucleosome, which consists of a little less than two turns of DNA wrapped around 8 histones (histone octamer). Common histone modifications are acetylation, methylation and ubiquitination. These modifications affect the structure of chromatin, influencing gene accessibility and expression. When chromatin is accessible for gene expression, it is called euchromatin. When chromatin is not accessible, it is called heterochromatin.

Epigenetic regulators are proteins that modulate epigenetic modifications, also known as epigenetic marks, and their subsequent outcomes. These proteins can be classified according to their action:

- Epigenetic writers: epigenetic writers are enzymes responsible for adding epigenetic marks. For example, DNA methyltransferases add methyl groups to DNA, and histone acetyltransferases add acetyl groups to histone.
- Epigenetic erasers: epigenetic erasers are enzymes responsible for removing epigenetic marks. Examples include DNA demethylases that remove methyl groups from DNA and histone deacetylases that remove acetyl groups from histones.
- Epigenetic readers: epigenetic readers are proteins that recognize and bind to specific epigenetic marks. They interpret the epigenetic code and recruit downstream effectors to mediate an effect in gene expression. Examples include proteins with chromodomains or bromodomains that recognize methylated or acetylated histones, respectively.
- Chromatin remodelers: chromatin remodelers are enzymes that alter the structure of chromatin by moving, ejecting, or repositioning nucleosomes. They are primarily involved in the dynamic restructuring of chromatin, allowing or restricting the binding of transcriptional machinery to gene regulatory regions.

Epigenetic modifications collectively contribute to the regulation of gene activity, cellular differentiation, development, and response to environmental stimuli.

2.1.2.2. Hepatic nuclear receptors and metabolic homeostasis

The liver expresses a subset of NRs that play a crucial role in regulating key aspects of liver metabolism, such as glucose and lipid metabolism. Some of the key hepatic NRs that are involved in liver health and disease are: farnesoid X receptor (FXR), hepatocyte nuclear factor 4α (HNF4α), peroxisome proliferator-activated receptors (PPARs), retinoid X receptor (RXR), liver X receptors (LXRs) and liver receptor homolog-1 (LRH-1)[27].

- **FXR**: FXR is activated by bile acids and heterodimerizes with RXR. Upon activation, it regulates bile acid synthesis and transport, maintaining bile acid homeostasis. FXR also influences glucose and lipid metabolism by regulating genes involved in lipogenesis, gluconeogenesis and TG synthesis[28].
- **PPARs**: PPARs are activated by long-chain fatty acids and are key regulators of lipid metabolism. They heterodimerize with RXR. There are three PPARs: PPARα (encoded by PPARA), PPARβ/δ (encoded by PPARD) and PPARγ (encoded by PPARG) and they have different tissue distribution. PPARα is highly expressed and active in the liver, PPARβ/δ is predominantly active in skeletal muscle and PPARγ highest expression is in adipose tissues[29]. This thesis will focus on PPARα, as it is the PPAR with the highest expression in the liver[30].
- **RXR**: RXR forms heterodimers with several NRs, including PPARs, LXRs and FXR. These heterodimers play a key role in coordinating the regulation of liver metabolism and energy balance.
- **LXR**: LXRs, including LXRα and LXRβ, are activated by cholesterol metabolites such as oxysterols and act as heterodimers with RXR. LXRs play an important role in cholesterol homeostasis by regulating the expression of genes involved in cholesterol uptake, efflux and conversion to bile acids. LXRs are also involved in the regulation of lipogenesis[31].
- **LRH-1**: LRH-1 is activated by phospholipids and it is involved in the regulation of bile acid homeostasis, together with FXR. It is also involved in the regulation of glucose, TG and phospholipid metabolism[32].

Liver metabolism is finely regulated by nutrient status, and NRs play a central role in orchestrating the metabolic adaptations in response to variations in nutrient availability. The liver serves as a metabolic hub, integrating signals from the fed and fasting states to ensure proper utilization and storage of nutrients through the action of NRs.

Fed state

In the fed state, elevated nutrient levels trigger the activation of the following NRs:

FXR

The release of bile acids to the intestine under fed conditions activates FXR. Activation of FXR inhibits bile acid synthesis through a feedback mechanism that involves SHP (small heterodimer partner). SHP is also a NR, but unlike others, it lacks the well-conserved DNA-binding domain, and thus functions as a coregulator (mostly as a corepressor). FXR activation promotes transcription of SHP, which in turn binds and represses the transcriptional activity of LRH-1 and LXR. LRH-1 and LXR promote the expression of Cyp7a1, the first and rate-

limiting enzyme in the bile acid synthesis pathway. Therefore, SHP-mediated repression of LRH-1 and LXR blunts bile acid synthesis. FXR activation also increases the expression of bile acid exporters to promote its excretion to the bile duct. Overall, FXR prevents the accumulation of bile acids in the liver, protecting it from its toxic effects[33].

Activation of FXR has implications other than modulating bile acid homeostasis. It was recently shown that FXR activation reduces the expression of key lipogenic enzymes, including Scd1, Lpin1 and Dgat2[34]. FXR also represses the transcription of genes involved in the regulation of autophagy, thus limiting autophagy activation during the fed state[35,36]. Autophagy is cellular catabolic process of utmost importance in the liver and other tissues, which will also be discussed in detail in this thesis. Moreover, FXR activation ameliorates MASLD in mouse models through two mechanisms of action: 1) by lowering lipid intestinal absorption as a consequence of lowering bile acid production and 2) by repressing hepatic lipogenesis[34]. In fact, there are several FXR agonist drugs on clinical trials for MASLD[18].

LXR

LXR activation in the liver by oxysterols, which are oxidized cholesterol derivatives, promotes the transcription of genes involved in cholesterol excretion and catabolism, while also decreases the uptake of cholesterol in the form of low density lipoprotein (LDL)[31]. LXR controls the expression of ATP-binding cassette transporters ABCG5 and ABCG8, which act as heterodimers to promote hepatic cholesterol excretion into the bile duct, which is then eliminated through bile. It also induces the expression of the rate-limiting enzyme in the bile acid synthesis pathway Cyp7a1, thus promoting cholesterol conversion into bile acids.

LXR activation also promotes DNL and TG synthesis through the expression of key enzymes involved in these pathways. In concert with this, LXR drives the production and secretion of VLDLs, providing an additional mechanism to rid the liver of cholesterol[31].

LXR also plays an important role in cholesterol homeostasis in peripheral tissues, through a process known as reverse cholesterol transport (RCT). In extra-hepatic tissues, LXR activation induces the expression of ABCA1 and ABCG1, which transfer cholesterol to high density lipoprotein (HDL). HDL particles deliver cholesterol to the liver for its eventual catabolism.

Coordinated response of FXR and LXR

Early in the fed state upon nutrient intake, bile acids are released into the gut to emulsify and promote the absorption of dietary lipids. In response to increased levels of bile acids, FXR is activated. Activation of FXR limits the synthesis of bile acids and lipogenesis. Lipids are then absorbed by the intestine and reach the liver in the form of chylomicrons, which contains TGs and cholesterol. LXR senses cholesterol derivatives and is activated, which promotes DNL, TGs synthesis, VLDL production, bile acid synthesis and cholesterol efflux. The LXR-mediated bile acid synthesis may also activate FXR, which promotes bile acid efflux and exerts a negative feedback loop on LXR. In conclusion, the coordinated activation of FXR and LXR in the fed state finely tunes the management and handling of dietary lipids.

Fasting state

The major NR that modulates the fasting response in the liver is PPARα[37]. Ligands of PPARα include different types of fatty acids with a clear preference for long-chain poly-unsaturated fatty acids, as well as fatty-acid derivatives, such as eicosanoids. During fasting, adipose tissue lipolysis is activated through the action of several hormones, including catecholamines, cortisol, and glucagon, among others. This event leads to increased levels of glycerol and free fatty acids (FFAs) in circulation and elevated flux of fatty acids into many tissues including the liver. These FFAs serve as the source of endogenous ligands that activate PPARα in the fasting state[38].

Activation of PPARα triggers a shift in fuel utilization in the liver towards fatty acids, given the high abundance of FFAs provided by WAT and low glucose availability during fasting, which is mostly diverted to the brain. Hence, PPARα activation upregulates the expression of genes involved in fatty acid oxidation (FAO) and ketone body (KB) formation, also known as ketogenesis. Brain cannot rely on fatty acids as fuel because of the blood-brain barrier, as they cannot pass through it, but it can use KBs, which is why fasting activates ketogenesis in the liver.

PPARα also activates the transcription of genes involved in the regulation of autophagy, also known as ATG (autophagy-related) genes[36]. Autophagy is a cellular recycling process that permits the degradation of a broad variety of substrates ranging from proteins to whole organelles including LDs and mitochondria, among others. Activation of hepatic autophagy during fasting permits the degradation of LDs, further increasing the pool of fatty acids for their subsequent oxidation.

PPARα is regarded as a therapeutic target for MASLD as it was shown to be protective against MASLD in mouse models[39], with several PPARα agonist drugs that have dual agonism (activates simultaneously PPARα and another PPAR, such as PPARγ or PPARδ) in clinical trials[18]. Ablation of PPARα in liver aggravates MASLD in mice in response to a methionine- and choline-deficient diet (MCD), a diet used for pre-clinical MALFD studies. Moreover, liver-specific knockout mice develop spontaneous hepatic steatosis during ageing. Along these lines, it was reported that PPARα expression and activity is downregulated during aging[40], and growing evidence suggests that aging is a relevant risk factor in the development of MASLD[41].

2.2. Autophagy

Autophagy targets cytosolic components, including proteins and organelles, to the lysosome for degradation. Three types of autophagy occur in mammals: macroautophagy[42], microautophagy[43], and chaperone-mediated autophagy (CMA)[44]. Macroautophagy (autophagy hereafter) is the most characterized type of autophagy and it requires the formation of autophagosomes, namely double-membrane vesicles that deliver the cargo to lysosomes. Once autophagosomes are formed, they fuse with lysosomes into autolysosomes, where the cargo and autophagosomes are degraded into building blocks that are recycled by the cell. Autophagy is a tightly regulated process that requires a complex signaling cascade and ATG proteins. mTORC1 and AMPK, two key metabolic sensors, control the initial events in autophagosome biogenesis[45].

Autophagy can take place in a non-selective manner (non-selective autophagy), which involves the random uptake of cytosolic material for degradation (e.g., upon nutrient deprivation). On the other hand, during selective autophagy, autophagosomes recruit specific cellular components[46]. Selective degradation through autophagy receives a distinct nomenclature depending on the cargo recruited: aggrephagy (protein aggregates), mitophagy (mitochondria), lipophagy (lipid droplets) etc. The degradation of cellular material by autophagy serves as a quality control mechanism to maintain homeostasis.

2.2.1. Mechanistic regulation of autophagy

Autophagy relies on the formation of autophagosomes. The initial structure that precedes the autophagosome is called phagophore. The upstream signaling complex in autophagosome biogenesis is the ULK1 complex, formed by the heterotetramer ULK1, ATG13, ATG101 and FIP200 (Figure 4). This complex plays a central role in autophagy signaling as it is regulated by the mammalian target of rapamycin complex 1 (mTORC1) and the AMP-activated protein kinase (AMPK), both key metabolic sensors[47]. The ULK1 complex anchors at autophagosome assembly sites, where it recruits, phosphorylates and activates the class III phosphoinositide 3-kinase (PI3K) complex I (also known as VPS34 complex)[48]— composed of Vps34 (also known as the catalytic subunit), Vps15 (also known as the regulatory subunit), Beclin-1 and ATG14. This complex generates phosphatidylinositol 3-phosphates (PI3Ps) at phagophores[49] for the anchoring of the ATG2-WIPI complex, a PI3P effector that allows the recruitment of downstream machinery[42] (Figure 4).

Downstream of ATG2-WIPI are the ubiquitin-like (UBL) conjugation systems. As their name indicates, these systems resemble ubiquitin conjugation systems and they consist of a UBL protein, an E1-like enzyme, an E2-like enzyme and an E3-like enzyme[50]. The autophagic machinery contains two UBL-conjugation systems with shared factors: ATG12 and ATG8 are UBL proteins, ATG7 acts as an E1-like enzyme, ATG10 and ATG3 as E2-like enzymes and the conjugated ATG12-ATG5-ATG16L complex as an E3-like enzyme. In the first conjugation system, ATG12 is conjugated to ATG5 through ATG7 and ATG10 and subsequently binds to ATG16L to form an E3-like enzyme complex. In the second conjugation system, ATG8 is processed by the cysteine protease ATG4[51] and conjugated to phosphatidylethanolamine (PE) moieties present in nascent autophagosomes through ATG7, ATG3 and the ATG12-

ATG5-ATG16L complex[50,52] (Figure 4). Conjugated ATG8 to PE is referred to as ATG8-II and serves many functions: (i) further recruitment of upstream factors, generating a positive feedback loop, (ii) elongation and closure of nascent autophagosomes, (iii) cargo recruitment and (iv) fusion of autophagosomes with lysosomes[53]. Mammalian cells express 6 distinct ATG8 homolog proteins, of which the most widely studied is LC3B[54]. In this regard, LC3B-II serves as a bonafide autophagosome marker[55].

Autophagosomes recruit cargo through a variety of adaptor proteins, also known as autophagic adaptors or receptors, such as p62[46]. These adaptors recognize both the cargo, through ubiquitin-associated (UBA) domains and ATG8 proteins in the autophagosome membrane via LC3-interacting region (LIR) motives[54] (Figure 4). Once the cargo has been engulfed, autophagosomes fuse with lysosomes, forming autolysosomes, where the cargo and autophagosomes themselves are degraded into recyclable building blocks (Figure 4).

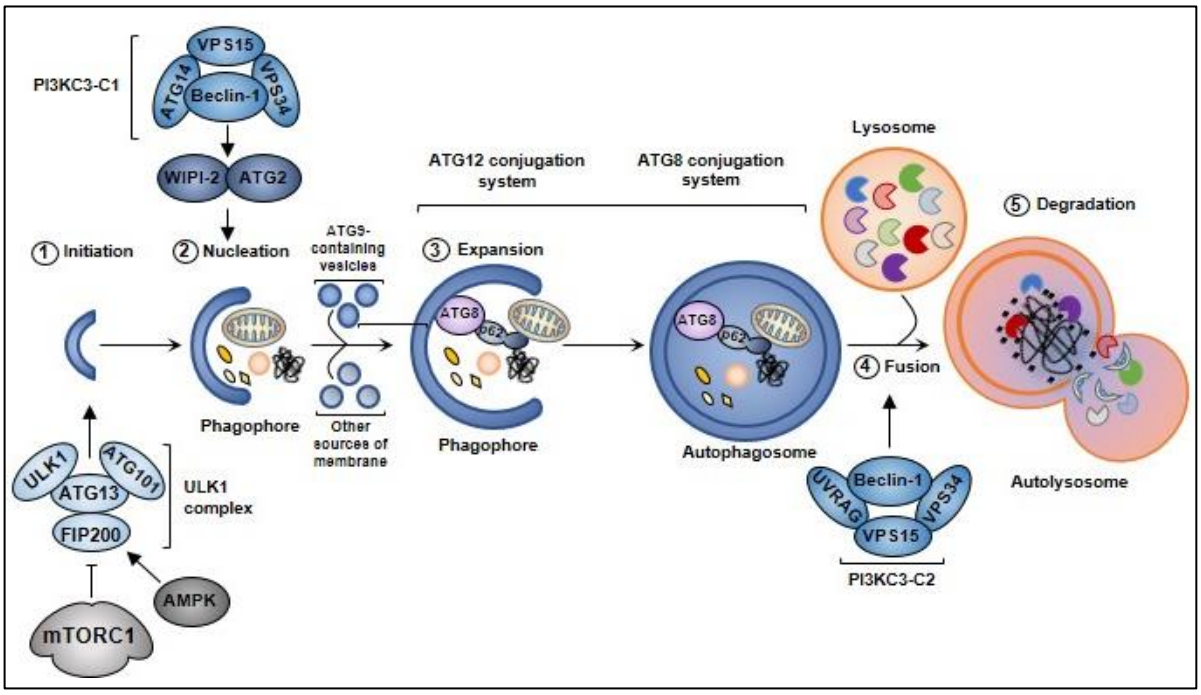

Figure 4: Mechanisms of autophagy. Autophagy is initiated by the ULK1 complex, which can be activated via mTORC1 inhibition or AMPK activation (1). The nucleation step results in the formation of the phagophore and requires the class III phosphatidylinositol 3-kinase complex I (PI3KC3-C1) and the WIPI2-ATG2 complex (2). Phagophore expansion and maturation into autophagosome requires delivery of membranes by ATG9-containing vesicles and other sources of membrane like the endoplasmic reticulum, and the conjugation of ATG8 homolog proteins to the phagophore membrane (3). Autophagic adaptors such as p62 mediate cargo recruitment. ATG8 proteins are also required for cargo recruitment and are conjugated to autophagosome membranes through the action of the ATG12 and ATG8 conjugation systems. Autophagic cargo can be ubiquitinated, which may be essential for recognition by adaptor proteins[46], which recognize both the cargo and conjugated ATG8 on the autophagosome membrane. For instance, p62 binds ubiquitinated protein aggregates and ubiquitinated mitochondria through a UBA (ubiquitin-associated) domain and interacts with LC3B (an ATG8 protein) anchored at the autophagosome membrane through an LC3-interacting region (LIR). The fusion between autophagosomes and lysosomes is mediated by the class III phosphatidylinositol 3-kinase complex II (PI3KC3-C2) (4). The fusion event results in the formation autolysosomes, where cargo and autophagic adaptors are degraded (5). Adapted from[56].

2.2.2. Autophagy and liver physiology

Autophagy is a fundamental cellular process in the adaptation to starvation/fasting. Hepatic autophagy activity fluctuates periodically depending on the fasting-feeding cycle and is under regulation by nutrients and hormones, including insulin and glucagon[57]. Activation of hepatic autophagy in the fasting state permits the breakdown of glycogen, lipid droplets (LDs) and proteins, in this order[57] during severe nutrient deprivation to supply glucose, fatty acids and amino acids. However, during steady state conditions, basal selective autophagy also occur, which serves as a quality and quantity control of organelles, including mitochondria. This in turn regulates features of hepatic metabolism such as β-oxidation.

2.2.2.1. Regulation of autophagy in the fed state

Autophagy in the liver is tightly regulated by nutrient status, which is primarily sensed via mTORC1, a sensor of amino acids. Under nutrient rich conditions, mTORC1 is directly activated by increased levels of amino acids and phosphorylates many target proteins to inhibit autophagy at the machinery level and at the transcriptional level. For example, mTORC1 phosphorylates and inhibits ULK1, therefore blunting the autophagosome formation signaling cascade. mTORC1 also phosphorylates transcription factor EB (TFEB), the master transcription factor of lysosomal and autophagy genes[58], to keep it inactive in the cytoplasm. Insulin also inhibits autophagy in the liver, although to a lesser extent compared to amino acids[59], through the phosphatidylinositol 3-kinase (PI3K)/AKT pathway[60].

The activation of FXR in the fed state also contributes to the inhibition of autophagy[35,36], through two possible mechanisms. FXR activation upon feeding disrupts and transrepresses the CREB-CRTC complex, which is a key transcriptional effector complex of glucagon in the fasting state (discussed later). FXR also binds directly promoters autophagy genes upon its activation, which promotes the recruitment of corepressors and reduces the recruitment of RNA polymerase II, thus repressing the expression of autophagy genes[36].

2.2.2.2. Regulation of autophagy in the fasting state

In the fasting state, low amino acid levels and insulin lead to inactive mTORC1, therefore it can no longer phosphorylate its substrates. Thus, all the mTORC1-mediated inhibitory inputs are alleviated, which permits the activation of the autophagy machinery and the transcription of autophagy and lysosomal genes via TFEB[58].

Glucagon, a key hormone secreted by pancreatic α cells in response to fasting, plays an important role in the activation of autophagy in liver. Glucagon stimulates production of the second messenger cAMP by adenylyl cyclase, which in turn activates the protein kinase A (PKA). PKA phosphorylates many substrates, including regulators of glucose metabolism to promote glycogenolysis and gluconeogenesis. An important effector of PKA is the transcription factor cAMP response-element binding protein (CREB). PKA phosphorylates CREB to induce its nuclear translocation, and it also activates the nuclear translocation of CREB-regulated transcription coactivator (CRTC). As a consequence, CREB forms a complex with CRTC that binds cAMP response elements, thus upregulating the expression of genes related to gluconeogenesis (e.g. pyruvate carboxylase, phosphoenol pyruvate cabroxykinase

and glucose-6-phosphatase) and autophagy[35]. In addition, CREB-CRTC also induces the expression of TFEB[35].

PPARα activation during fasting also upregulates the expression of autophagy genes directly[36]. It has been reported that PPARα binds to enhancer regions in LC3a and LC3b, key autophagy genes, upon fasting or treatment with PPARα agonist GW7646, which increased RNA polymerase II recruitment to the genes[36]. In fact, PPARα and FXR compete for the same elements in autophagy genes with opposite transcriptional outputs[36].

2.2.2.3. Metabolic implications of hepatic autophagy

In the liver, suppression of hepatic autophagy in Atg7-deficient mice results in increased total TG content in the liver, which can be observed in the fed state, but it becomes much more pronounced upon overnight fasting. This increased accumulation of TGs in autophagy-deficient livers is due to impaired autophagy-mediated LD breakdown, also known as lipophagy[61] (Box 3). During lipophagy, LDs associate with autophagosomes through lipophagy receptors and are delivered to lysosomes for their subsequent breakdown to release free fatty acids for β-oxidation. Not surprisingly, rates of β-oxidation are decreased in autophagy deficient cells[61].

In the context of obesity, genetically obese mice and high fat diet-induced obese mice show impaired autophagy activity, also known as autophagy flux, in liver[62]. In agreement with this observation, livers of mice challenged with a high-fat diet during 16 weeks show a remarkable reduction in LD-containing autophagosomes. These results suggest that fat overload (obesity) can impair hepatic autophagy, resulting in decreased lipophagy. Decreased lipophagy leads to increased accumulation of fat in the liver (steatosis), thus promoting a detrimental feed-forward loop.

Autophagy ablation also impairs glucose metabolism. Adenoviral repression of Atg7 induces ER stress and insulin resistance in the liver, and systemic insulin resistance resulting in increased blood glucose levels[62], suggesting that suppression of autophagy may lead to metabolic syndrome. Additionally, restoration of autophagy in obese mice via reconstitution of Atg7 attenuates hepatic ER stress, improves insulin action and alleviates hepatic steatosis[62]. Moreover, it has been reported that autophagy is necessary for circadian-dependent regulation of gluconeogenesis in mice[63].

In conclusion, autophagy is a finely tuned cellular recycling system that is important in the regulation of lipid and glucose homeostasis through various mechanisms of action. Therefore, autophagy is necessary for metabolic health[56]. Alterations in hepatic autophagy, such as in the context of obesity, may lead to metabolic syndrome. Sustained insulin resistance and the inability to breakdown LDs may eventually cause hepatic steatosis and MASLD. Interestingly, activation of lipophagy with a synthetic lipophagy adapter protein using adeno-associated virus ameliorated steatohepatitis in mouse MASLD models[64]. Additionally, numerous studies suggest that autophagy declines upon aging[65], which is an important risk factor for developing MASLD. Furthermore, autophagy is impaired in the livers of patients with MASLD[66]. Thus, autophagy emerges as a potential therapeutic target to treat metabolic syndrome and MASLD.

2.3. NRCA1 – a multifaceted protein

[redacted] (NRCA1) is a 9kb-long gene in humans located in chromosome [redacted]. It harbors 5 exons and encodes for a [redacted] amino acid-long protein with a predicted molecular weight of [redacted] kDa[67]. The human NRCA1 protein sequence shares 84% amino acid identity with murine NRCA1 protein, which contains [redacted] amino acids[redacted]. NRCA1 has a paralog protein, [redacted] ([redacted]1), which originated from gene duplication[redacted]. The two paralogs share a 36% amino acid identity[redacted]. [redacted].

NRCA1 was first identified in [redacted] in a substractive hybridization assay. [redacted], PhD thesis, [redacted].

The murine NRCA1 protein sequence bears several functional regions and motives. There are two well conserved regions, [redacted] (Figure 5). [redacted].

The second conserved region contains an [redacted].

Figure 5: Murine NRCA1 protein amino acid sequence. [redacted].

2.3.1. NRCA1 regulates transcription

Initial sequence analysis of NRCA1 using subcellular localization prediction tools suggested that NRCA1 was predominantly a nuclear protein. Subsequent immunocytochemistry studies confirmed the nuclear localization of NRCA1 in proliferative cells, such as HeLa cells, C2C12 myoblast cells and 1C9 myoblast cells [redacted]. NRCA1 localization also varies from tissue to tissue. [redacted].

Sequence analysis also revealed that NRCA1 has a LXXLL box, also known as NR box[redacted], [redacted]. The NR box is present in coregulators and allows them to bind NRs to repress or activate gene expression. Transcription reporter assays were performed to assess whether NRCA1 had the capacity to act as a coregulator of NRs. Overexpression of NRCA1 was able to [redacted] Additionally, there is a functional interaction between the coactivator effect of NRCA1 on NRs and known NR coactivators [redacted].

The role of NRCA1 as a NR coactivator was also confirmed in endogenous conditions. [redacted].

The molecular mechanisms underlying the NR coactivator function of NRCA1 has yet to be elucidated. The NR box suggests that NRCA1 may interact physically with NRs to regulate their transcriptional output. [redacted] It could also be that NRCA1 enhances the activity of NRs through interaction with other coactivators.

Apart from regulating transcription of NR target genes, NRCA1 also induces the transcription [redacted]. These data suggest that NRCA1 regulates transcription and protein synthesis.

2.3.2. NRCA1 is an autophagy activator

Early indications that NRCA1 had a potential role in the regulation of autophagy stem from a yeast two-hybrid screening of interacting partners. [redacted] [54].

Two independent studies, [redacted] showed that NRCA1 is a positive regulator of autophagy in mammalian cells, and this function is conserved in *Drosophila* cells [redacted].

Using live imaging techniques, we found that NRCA1 is constantly shuttling from the nucleus to the cytoplasm [redacted].

NRCA1 interacts [redacted]. However, why this interaction induces autophagy? In fact, [redacted]. This observation suggests that

while the whole protein promotes autophagy, small fragments of NRCA1 could inhibit it.

The role of NRCA1 as an autophagy activator has also been confirmed *in vivo* studies in mice. On one hand, depletion of NRCA1

2.3.3. NRCA1 promotes death receptor-mediated apoptosis

Many proteins involved in the regulation of autophagy participate in the crosstalk between autophagy and apoptosis[89], including NRCA1 [redacted].

NRCA1-deficient cells were less sensitive to [redacted].

NRCA1-mediated induction of [redacted]

In a recent report, it was shown that kinase [redacted]

2.3.4. NRCA1 is a master regulator of metabolic homeostasis

2.3.4.1. Skeletal muscle

Early indications that NRCA1 could be involved in the regulation of metabolic homeostasis stem from the initial hybridization assay [redacted] Reduced expression of NRCA1 was also [redacted].

2.3.4.2. White adipose tissue

In white adipose tissue, NRCA1 is a negative regulator of adipogenesis [redacted]

Total NRCA1 ablation also promoted adipogenesis in mice. These mice showed white adipose hyperplasia and thus accumulated more subcutaneous and visceral adipose tissues. In addition, adipocytes from 4-month old NRCA1-deficient mice showed higher expression of [redacted].

Transcriptomic analysis in NRCA1-deficient preadipocytes indicated impaired [redacted]

[redacted], thus repressesing adipogenesis.

2.3.4.3. Brown adipose tissue

In brown adipose tissue (BAT), NRCA1 plays the opposite role, it promotes adipogenesis [redacted].

NRCA1 ablation *in vivo* substantially increased [redacted]. In keeping with all these data, [redacted].

Transcriptomic analysis revealed that NRCA1-deficient BAT have impaired [redacted].

2.3.4.4. Liver

In liver, NRCA1 ablation did not cause any changes in body weight, body composition nor liver weight in young mice (16-week old) [redacted].

Under fasting conditions, NRCA1-KO mice showed [redacted]. On the other hand, fasting induced enhanced [redacted].

Transcriptomic and gene set enrichment analysis (GSEA) in fed conditions revealed a downregulation in PPAR signaling and fatty acid metabolism pathways [redacted]. ChIP enrichment analysis (ChEA) was performed to assess the putative transcription factors regulating the expression of downregulated genes. LXR, RXR and PPARα were the top enriched transcription factors, which regulate many aspects of lipid metabolism (2.1.2.2).

In order to evaluate the effects of NRCA1 depletion upon nutrient overload, LoxP and NRCA1-KO mice at the age of 8 weeks were subjected to HFD (60% kcal of fat) for 8 weeks or 16 weeks. Upon 8 weeks and 16 weeks of HFD, there were no differences in body weight gain between genotypes. Food intake and fecal excretion were comparable between genotypes. However, liver weight was increased in NRCA1-KO mice after 16 weeks of HFD pathways [redacted].

Glucose metabolism was impaired in NRCA1-KO mice upon HFD. In this regard, these mice showed higher fasting glucose levels, together with a tendency towards higher fasting insulin levels. The homeostasis model index of insulin resistance (HOMA-IR) is a calculation widely used as an estimate of insulin resistance[56] and it takes into consideration fasting glucose and insulin levels. NRCA1-KO mice showed higher HOMA-IR values. Concomitantly, these mice also showed impaired glucose handling as evidenced by glucose tolerance test [redacted].

Histological analysis showed increased hepatic fat accumulation of NRCA1-depleted mice. HFD caused a slight infiltration of F4/80-positive immune cells in NRCA1-KO animals, but not in LoxP littermates. Moreover, plasma analysis showed a tendency towards increased ALT and AST values in HFD-fed NRCA1-KO mice. Plasma KB levels were reduced in HFD-fed NRCA1-KO mice, similarly to fed conditions. In addition, plasma cholesterol and TG levels were also reduced in HFD-fed NRCA1-depleted animals. These mice also showed increased hepatic accumulation of TGs upon 8 weeks and 16 weeks of HFD, and also increased hepatic cholesterol upon 8 weeks of HFD. However, 16 weeks of HFD did not further increase liver cholesterol levels in NRCA1-KO mice, and were actually reduced compared to LoxP animals [redacted]

Since the increase in hepatic cholesterol upon 8 weeks of HFD was abrogated upon 16 week of HFD, cholesterol metabolism was investigated in more detail in mice fed a HFD for 8 weeks. ApoA1, which is mainly synthesized in the liver and the small intestine, serves as an important component of high-density lipoproteins (HDLs) and accounts for up to 70% of the total protein content of HDLs. ApoA1 is upregulated at the mRNA and protein levels in HFD-fed NRCA1-KO mice. ApoA1 is essential for HDL structure, stability and function. In this regard, NRCA1-KO animals showed decreased number of HDL particles, but these particles had increased size [redacted]. Mechanistically, primary hepatocytes isolated from livers of NRCA1-KO mice showed increased accumulation of free cholesterol in the presence of LDL, which may explain why cholesterol is more accumulated in NRCA1-KO livers upon an 8-week HFD. However, alterations observed in HDLs were not observed in LDLs.

To further analyze the implications of NRCA1 ablation in cholesterol metabolism, mice were subjected to a 16-week long western diet (WD) at the age of 8 weeks. WD contains 40% of kcal of fat, 35% of sucrose (w/w) and 0.2% cholesterol (w/w). Under these conditions, there were no differences in body weight, liver weight, hepatic cholesterol nor hepatic TGs between genotypes. WD led to a dramatic increase in plasma cholesterol levels, but there were no differences between genotypes. Histological analysis showed no differences in number of lipid droplets, fibrosis nor glycogen content between genotypes. WD induced infiltration of F4/80-positive immune cells in NRCA1-KO animals, but not in LoxP animals. In addition, plasma ALT levels tended to be higher in WD-fed NRCA1-KO mice. Strikingly, plasma bile acids and fecal bile acids were dramatically reduced in WD-fed NRCA1-KO animals. Interestingly, expression of FXRα was slightly upregulated in these mice. However, FXRα target genes were not upregulated in NRCA1-deficient mice.

Despite all these alterations in glucose, TG and cholesterol metabolism upon HFD and WD, transcriptomic analysis did not show major changes in gene expression between genotypes under these conditions. Although hepatic NRCA1 ablation seems to be protective in response to HFD, the implications of NRCA1 deficiency in liver needs further investigation.

2.3.5. NRCA1 and other processes

Numerous reports suggest that NRCA1 has antitumor effects and suggest that it may negatively correlate with tumor progression and malignancy[redacted]. Bioinformatics analysis of

publicly available transcriptomics data from cancer patients show that NRCA1 expression is downregulated in several cancers, including breast cancer, colorectal cancer, skin cutaneous melanoma and papillary thyroid carcinoma, among others. In a similar study, the expression of NRCA1 negatively correlated with estrogen receptor-negative breast cancer risk. These observations indicate that NRCA1 may have a tumor suppressive role, which would be consistent with the role of NRCA1 in apoptosis.

It has also been reported that NRCA1 promotes the differentiation of . NRCA1 expression increases during differentiation. To monitor differentiation, activity can be measured, as differentiated exhibit higher activity. Silencing of NRCA1 resulted in reduced activity, which indicates impaired differentiation, whereas NRCA1 overexpression increased activity.

Another study revealed that NRCA1 mRNA is the most abundant mRNA in and it is essential for and target innervation *in vivo*. .

In all, NRCA1 is a gene/protein that exerts tissue-specific functions. It seems that NRCA1 has a prominent role in cellular differentiation, as observed in brown and white adipocytes, and myoblasts. Interestingly, expression levels of NRCA1 are remarkably affected by the differentiation process in all these cells. In this regard, NRCA1 expression is upregulated during differentiation (unpublished data), suggesting that NRCA1 may also be important for differentiation. Another important role of NRCA1 is that of regulation of metabolism, as specific deletion of NRCA1 in metabolically relevant tissues, such as BAT, WAT and skeletal muscle, results in metabolic dysregulation. Therefore, this thesis is focused on the study of NRCA1 depletion in the liver, a major organ in metabolic homeostasis.

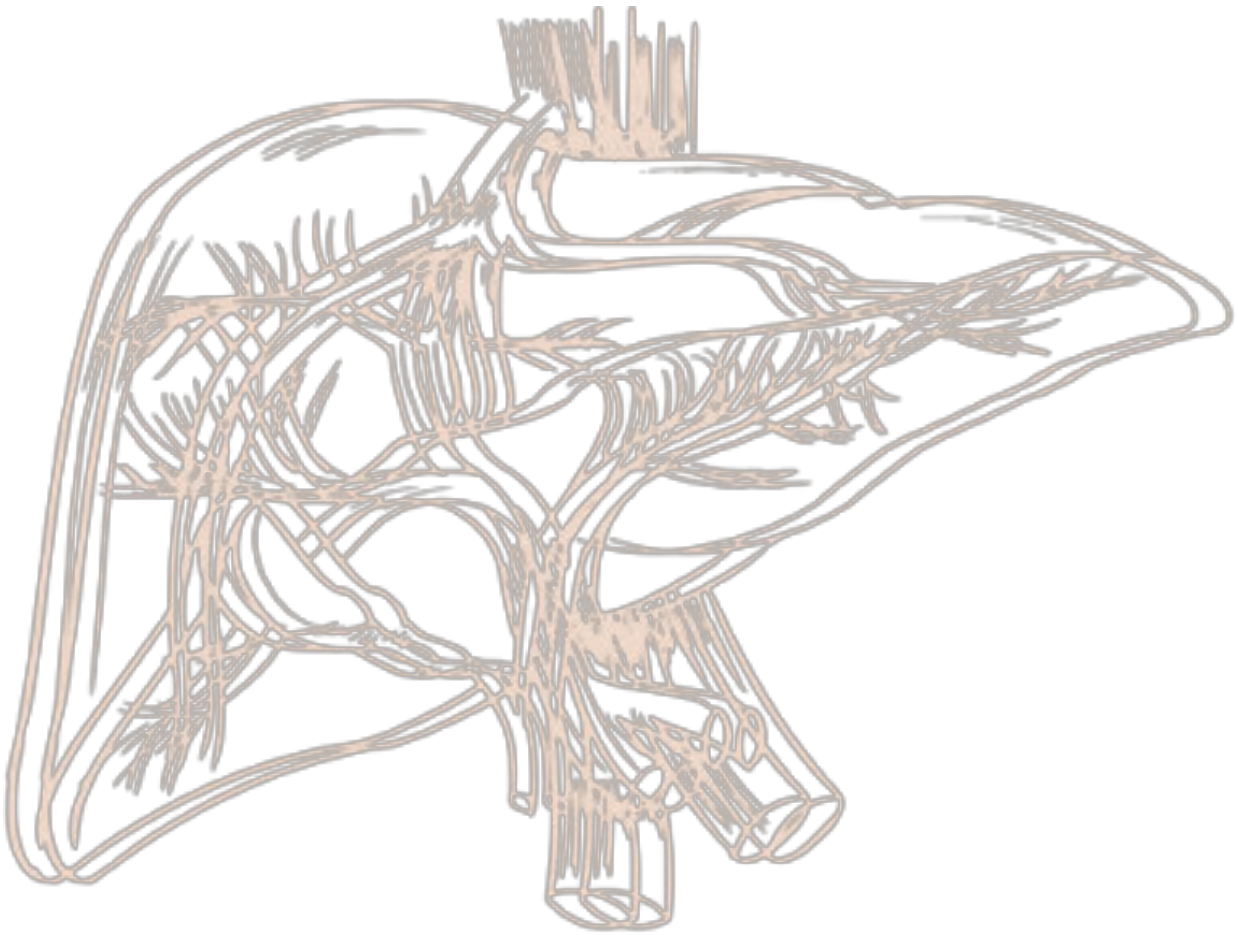

OBJECTIVES

3. OBJECTIVES

NRCA1 is a multifaceted protein that regulates numerous physiological and cellular processes. The implications of NRCA1 ablation in liver has been studied, but requires further investigation. Considering the available data from [redacted], we hypothesize that NRCA1 ablation impairs PPARα activation in response to fasting and synthetic agonists, and that this has implications in the development and treatment of MASLD. To test this hypothesis, we have set the following objectives for this thesis:

- To further characterize the loss-of-function effects of NRCA1 in liver metabolism. This aim will be divided in the following sub-objectives:
    - To characterize the implications of NRCA1 ablation in liver metabolism during aging.
    - To characterize the implications of NRCA1 in the development of MASLD.
- To elucidate the molecular mechanisms responsible for the effects of NRCA1 ablation in the liver. To achieve this aim, we will identify the molecular partners of NRCA1 and perform functional studies with validated interactors.

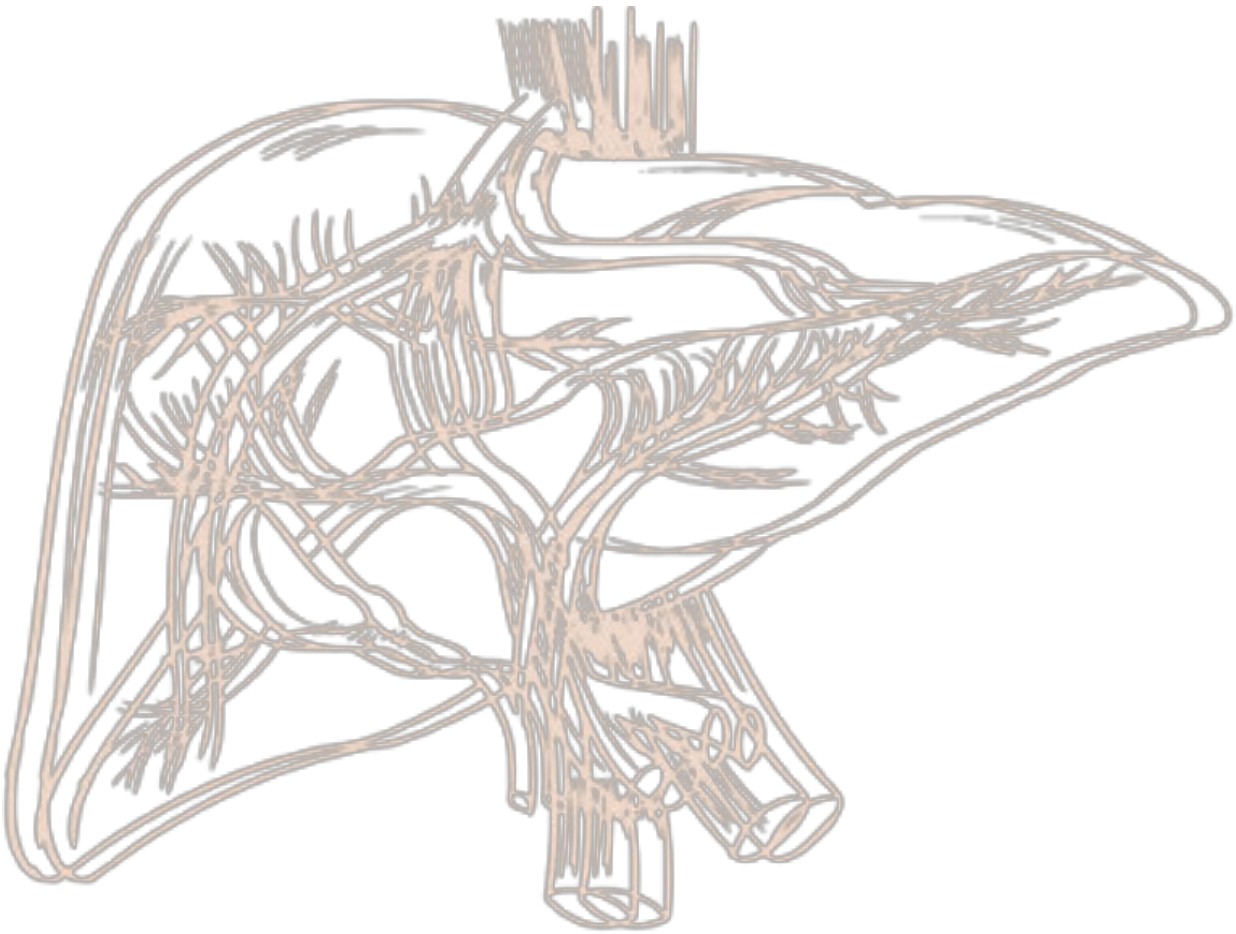

RESULTS

4. RESULTS

4.1. NRCA1 regulates PPARα and liver lipid metabolism

4.1.1. NRCA1 ablation impairs PPARα-dependent response to fasting in male mice

Initial transcriptomic analysis indicated that NRCA1 ablation led to downregulation of PPARα target genes [redacted] (Figure 6).

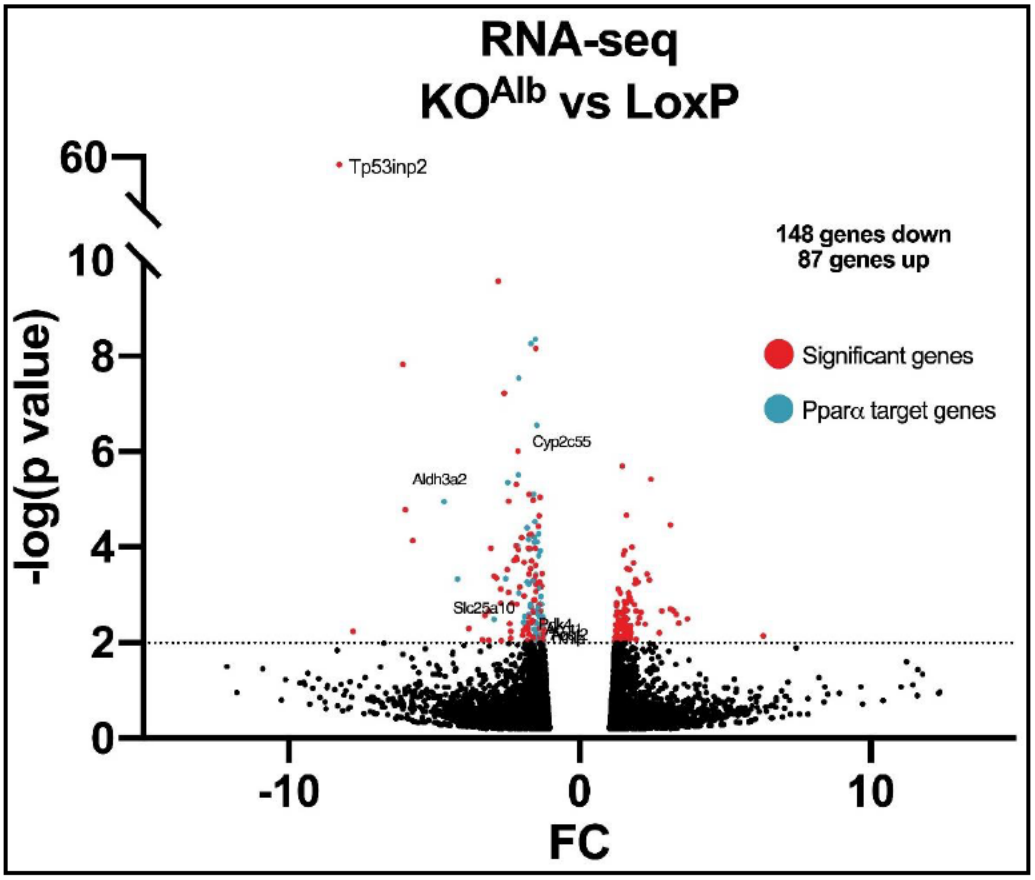

Figure 6: NRCA1 liver-specific ablation leads to downregulation of PPARα target genes. Livers were collected from LoxP and NRCA1-liver specific KO mice under fed conditions and subjected to transcriptomic analysis.

As described in 2.1.2, PPARα is a NR that is activated under fasting conditions. However, initial transcriptomics analysis was performed under fed conditions. Therefore, we subjected LoxP and NRCA1-KO^{Alb} to overnight fasting and performed RNA-seq. We performed ChiP enrichment analysis (ChEA) to assess the putative transcription factors regulating the expression of downregulated genes in fasted NRCA1-KO^{Alb} mice (Figure 7A). In agreement with previous data, we observed a significant enrichment of genes under the regulation of PPARα. Next, we analyzed the relative expression of PPARα target genes in our RNA-seq dataset and found that many of them were downregulated in NRCA1-KO^{Alb} fasted mice (Figure 7B).

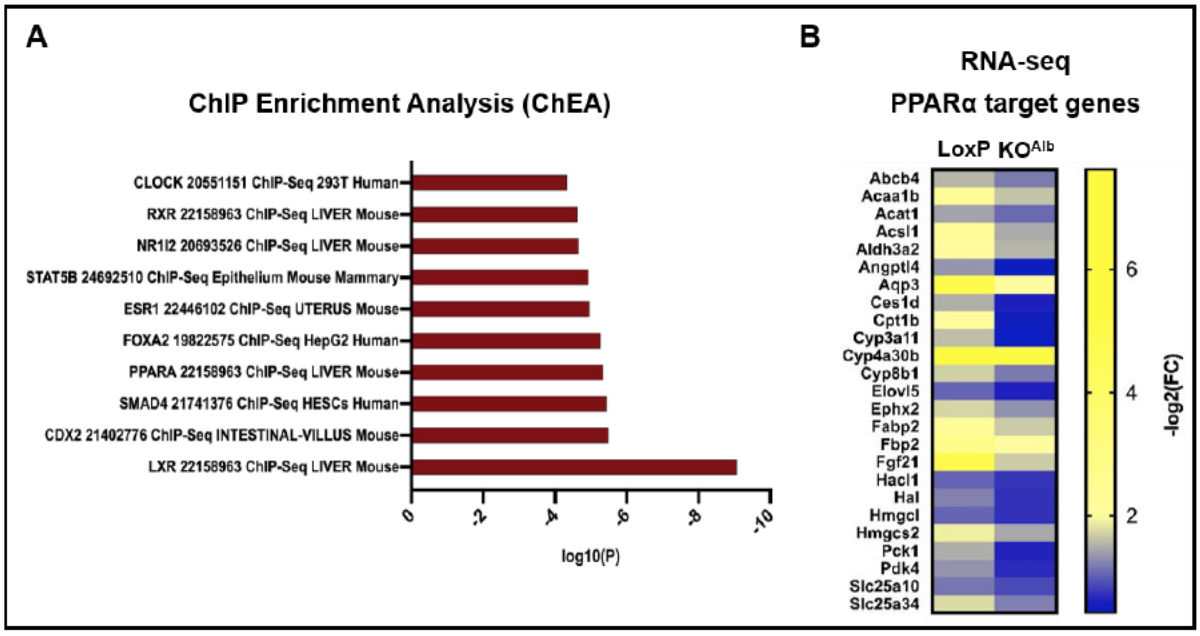

Figure 7: PPARα target genes are downregulated in NRCA1-KO^{Alb} mice upon fasting. A) ChIP enrichment analysis (ChEA) of downregulated genes in fasted NRCA1-KO^{Alb} mice. **B**) Heatmap of relative expression of PPARα target genes in LoxP and NRCA1-KO^{Alb} mice. Values are shown as –log2 of fasted/fed FC ratio.

To validate our transcriptomics data, we analyzed the relative expression of PPARα target genes through real-time quantitative PCR (RT-qPCR) assays in livers of 16-week old male LoxP and NRCA1-KO^{Alb} mice under fasting conditions (16 h). We observed that fasting triggers a remarkable upregulation of PPARα target genes in LoxP mice (Figure 8). However, this upregulation of PPARα target genes is blunted in NRCA1-KO^{Alb} mice (Figure 8). No differences were found in the expression of PPARα target genes in fed conditions between genotypes.

Cyp4a genes encode for enzymes involved in microsomal fatty acid oxidation[102]. Hepatic expression of these genes have been established to be almost completely dependent on PPARα, including Cyp4a10, Cyp4a12 and Cyp4a14[102], and therefore they serve as robust PPARα target genes. By analyzing the expression of Cyp4a10, we could observe that NRCA1 is necessary for the full activation of PPARα, as upregulation of Cyp4a10 expression upon fasting in NRCA1-KO^{Alb} mice is much lower compared to LoxP animals (Figure 8).

PPARα activation upregulates genes involved in FAO and KB synthesis (2.1.2.2). In keeping with downregulated activation of PPARα target genes in NRCA1-KO^{Alb} mice, these mice also exhibit higher liver triglyceride content and lower plasma levels of the KB β-hydroxybutyrate under fasting conditions (Figure 9) [redacted]

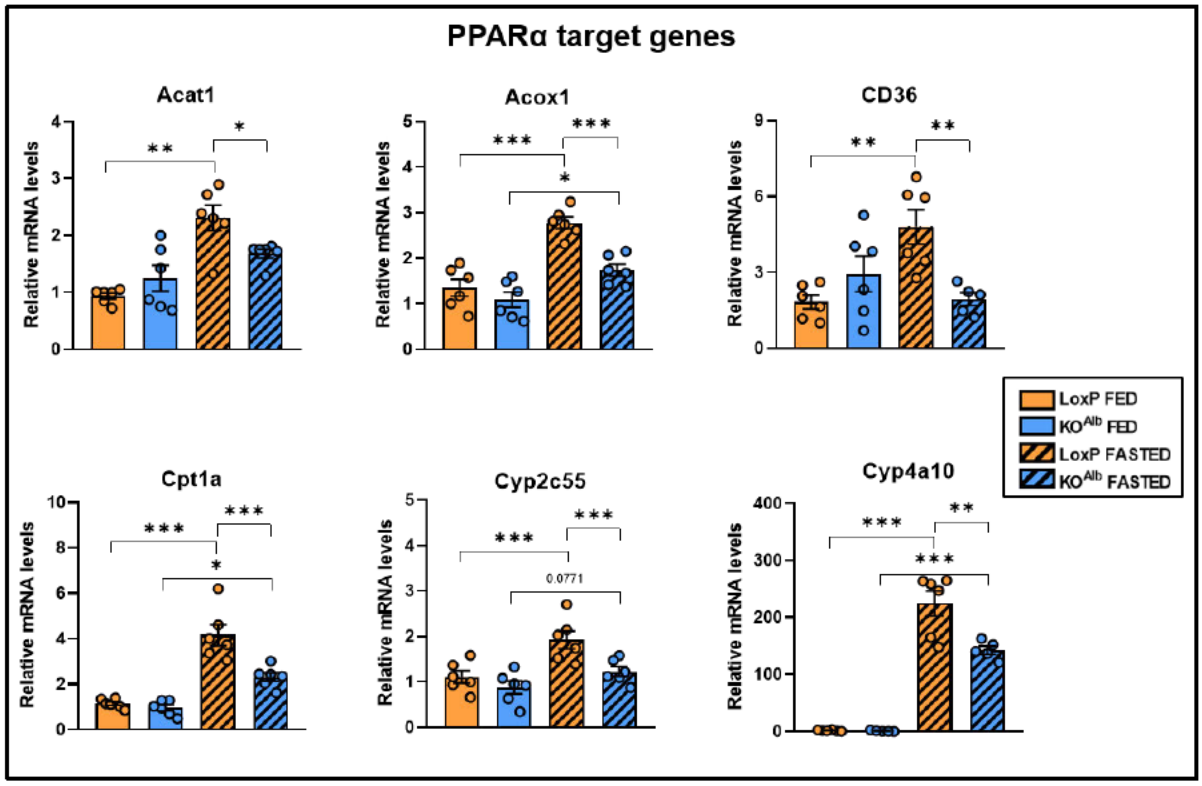

Figure 8: NRCA1 ablation impairs induction of PPARα target genes upon fasting. Livers were collected from 16-week old fed LoxP (orange) and NRCA1-KO^{Alb} mice (blue), and fasted LoxP (orange, dashed) and NRCA1-KO^{Alb} mice (blue, dashed). RT-qPCR was performed to analyze the expression of PPARα target genes. One-way Anova test coupled with multiple-comparisons was performed. * $P < 0.05$, ** $P < 0.01$, *** $P < 0.001$.

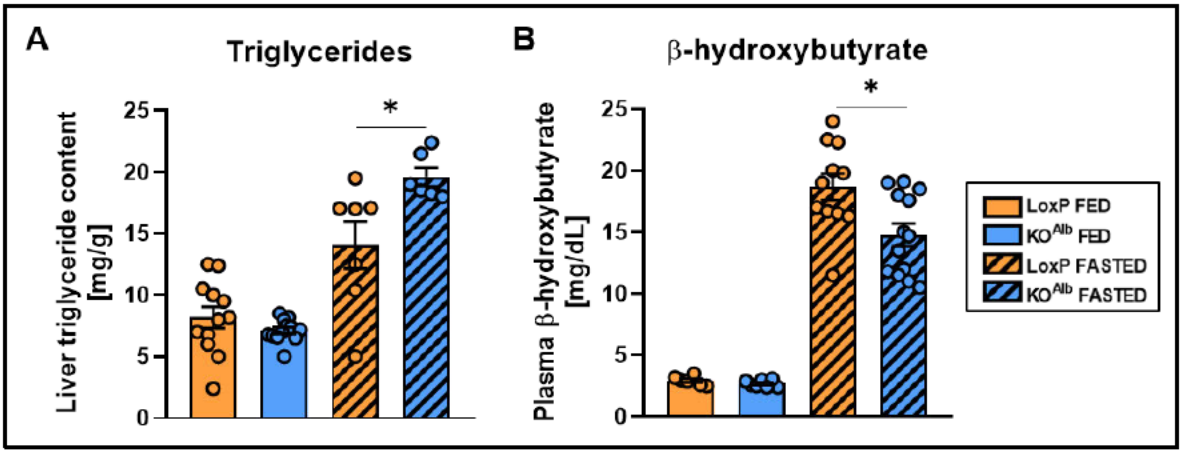

Figure 9: NRCA1 ablation leads to increased hepatic triglyceride content and decreased plasma levels of β-hydroxybutyrate during fasting. Livers and plasma were collected from 16-week old fed LoxP (orange) and NRCA1-KO^{Alb} mice (blue), and fasted LoxP (orange, dashed) and NRCA1-KO^{Alb} mice (blue, dashed). **A**) Hepatic triglyceride content. **B**) Plasma β-hydroxybutyrate levels. Data represented as mean ± SEM. Student t-test was performed. * $P < 0.05$.

We also analyzed the expression of PPARα coregulators, but there were no major differences between genotypes (Figure 10). However, auto-induction of PPARα[103] upon fasting was higher in LoxP animals compared to NRCA1-KO^{Alb} mice (Figure 10).

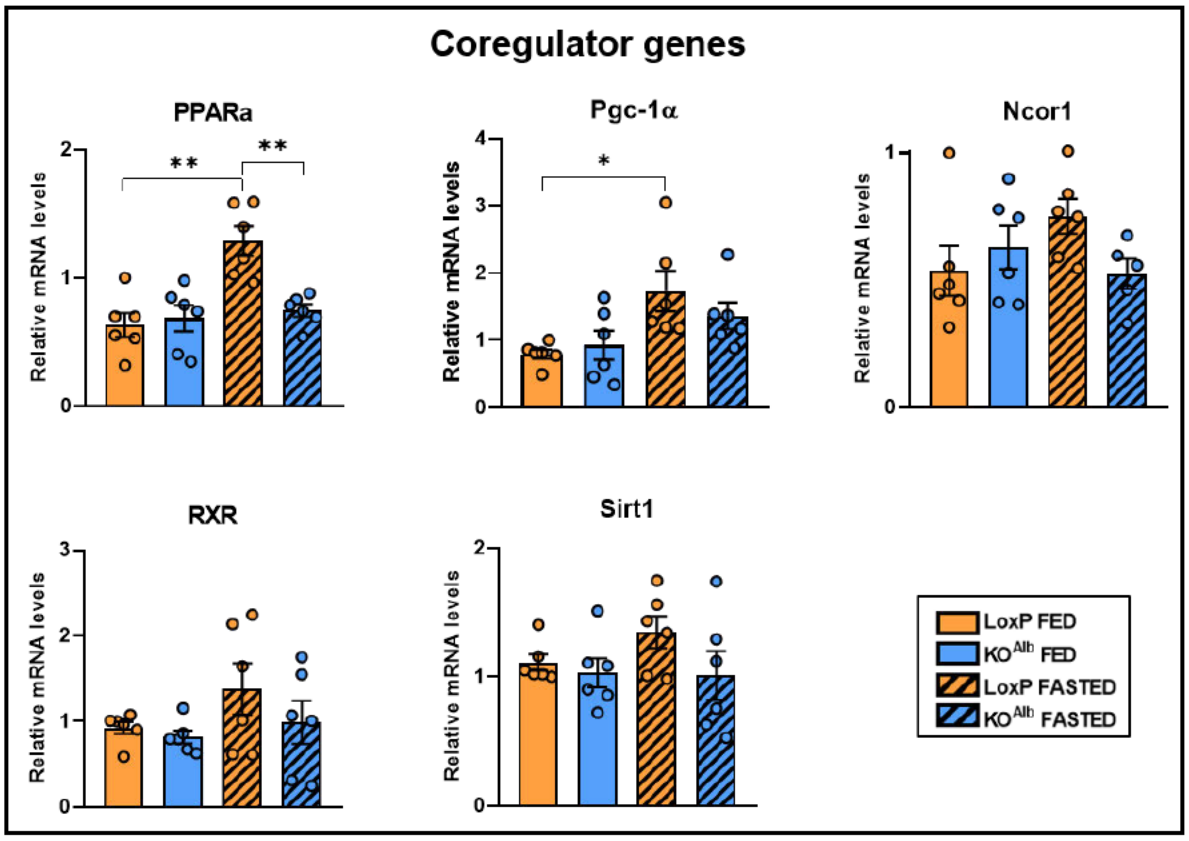

Figure 10: NRCA1 ablation does not affect expression of PPARα coregulators. Livers were collected from 16-week old fed LoxP (orange) and NRCA1-KO^{Alb} mice (blue), and fasted LoxP (orange, dashed) and NRCA1-KO^{Alb} mice (blue, dashed). RT-qPCR was performed to analyze the expression of PPARα target genes. Data represented as mean ± SEM. One-way Anova test coupled with multiple-comparisons was performed. * $P < 0.05$, ** $P < 0.01$, *** $P < 0.001$.

To further validate our results, we measured the expression of PPARα target genes under fasting conditions in a tamoxifen-inducible NRCA1 total KO mouse model[88] (NRCA1-KO^{Ubc}). 8-week male mice were subjected to a tamoxifen-containing chow diet for 4 weeks to induce NRCA1 ablation, and then were sacrificed at 12 weeks of age. Livers of NRCA1-KO^{Ubc} also show impaired PPARα-dependent response to fasting (Figure 11).

Interestingly, we observed that NRCA1 expression is upregulated upon fasting in LoxP animals, suggesting that NRCA1 may be a PPARα target gene and that NRCA1 upregulation upon fasting may be needed for PPARα activation, acting as a feed-forward mechanism (Figure 12).

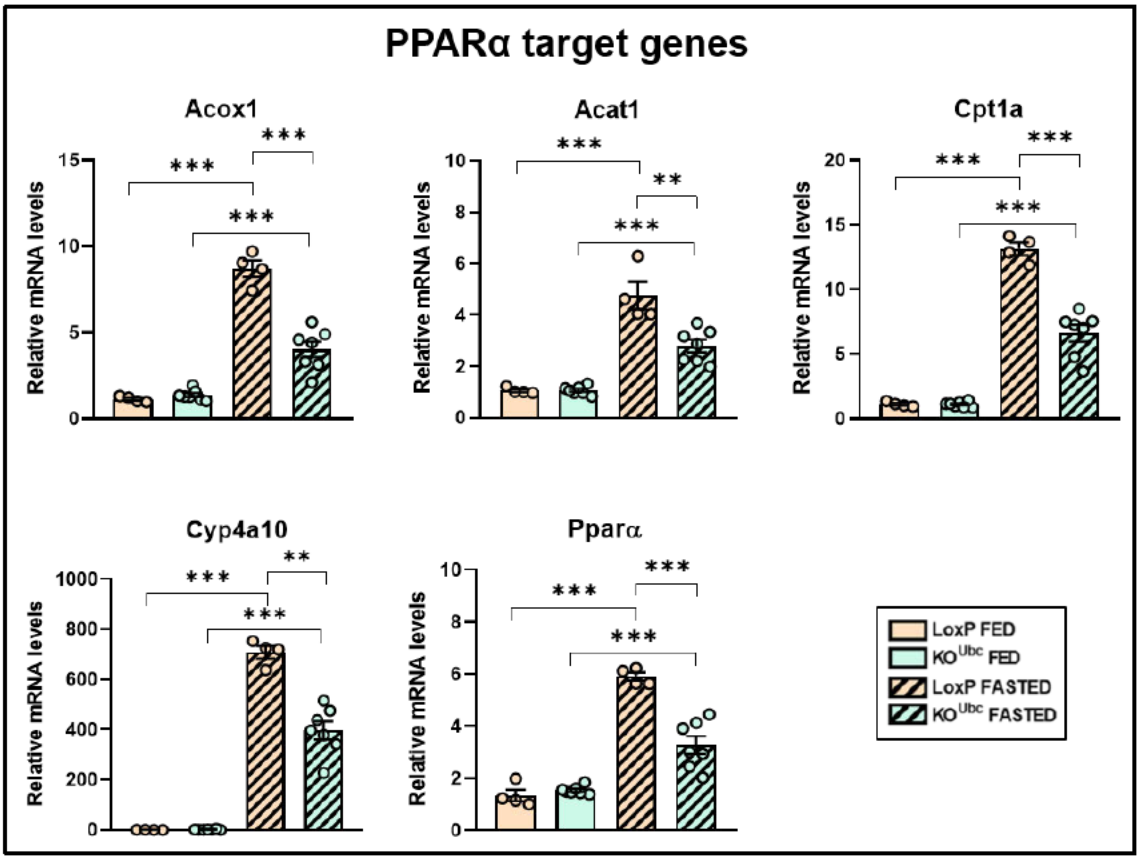

Figure 11: NRCA1 ablation impairs induction of PPARα target genes upon fasting in a tamoxifen-inducible total KO model. Livers were collected from 12-week old fed LoxP (light orange) and NRCA1-KO^{Ubc} mice (greenish blue), and fasted LoxP (light orange, dashed) and NRCA1-KO^{Ubc} mice (greenish blue, dashed). RT-qPCR was performed to analyze the expression of PPARα target genes. Data represented as mean ± SEM. One-way Anova test coupled with multiple-comparisons was performed. * $P < 0.05$, ** $P < 0.01$, *** $P < 0.001$.

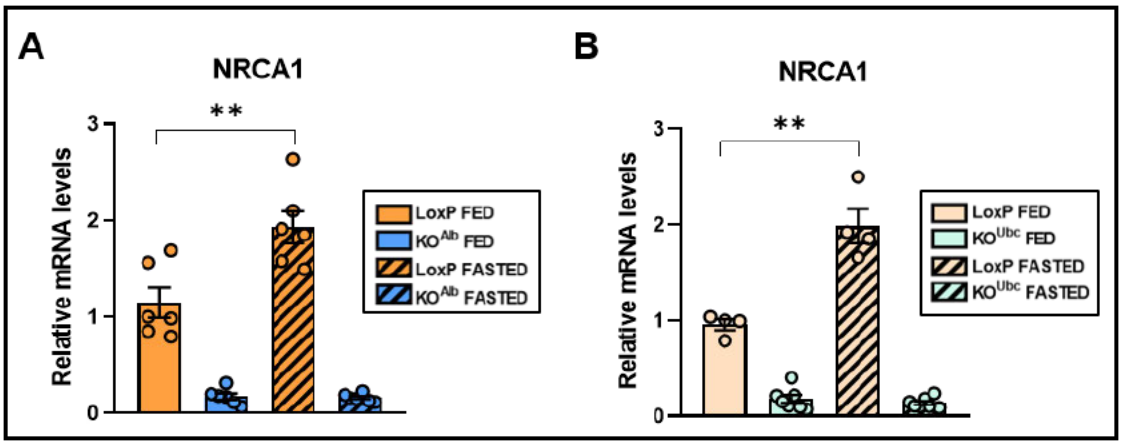

Figure 12: NRCA1 expression is upregulated upon fasting. **A**) NRCA1 expression in livers of the liver-specific KO cohort mice. **B**) NRCA1 expression in livers of the total KO cohort mice. Data represented as mean ± SEM. One-way Anova test coupled with multiple-comparisons was performed. * $P < 0.05$, ** $P < 0.01$, *** $P < 0.001$.

NRCA1 has been established as an activator of autophagy through interaction with the ATG8 family of proteins (2.3.2). However, considering our proteomics data, we wondered whether NRCA1 could also be regulating autophagy at the transcriptional level. Moreover, PPARα was identified as a master transcriptional regulator of autophagy genes during fasting[36]. Therefore, we subjected both NRCA1-deficient mouse models to overnight fasting. Autophagy genes are upregulated upon fasting in LoxP mice, but to a lesser extent in both KO mouse models (Figure 13). These results are consistent with the observation that autophagy flux is impaired in mouse primary hepatocytes derived from livers of NRCA1-KO^{Alb} mice[redacted]. Therefore, NRCA1 not only regulates autophagy via protein interactions but also at the transcriptional level. It is likely that NRCA1 regulates the expression of autophagy genes through PPARα.

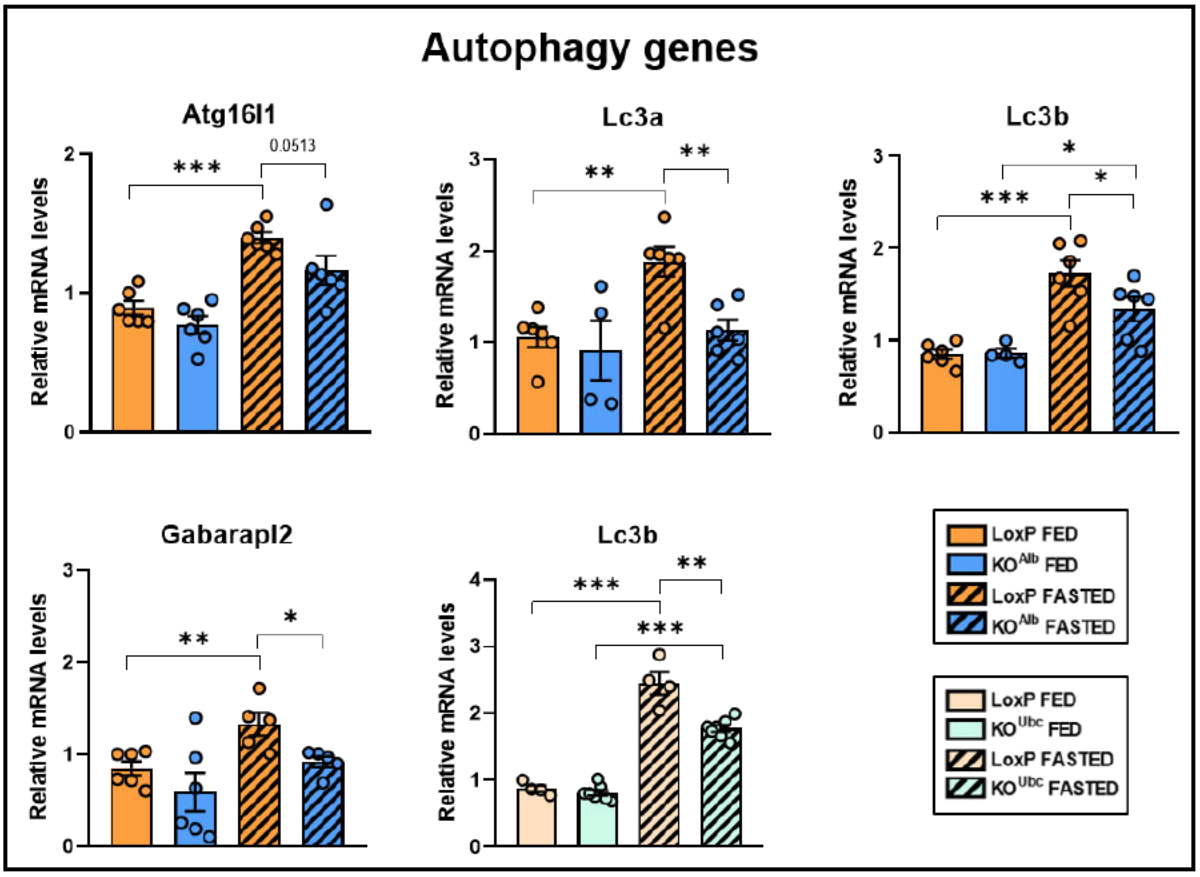

Figure 13: NRCA1 ablation impairs fasting-induced transcriptional activation of autophagy. Relative expression of autophagy genes in livers of the liver-specific KO cohort mice and livers of the total KO cohort mice. Data represented as mean ± SEM. One-way Anova test coupled with multiple-comparisons was performed. * $P < 0.05$, ** $P < 0.01$, *** $P < 0.001$.

4.1.2. Effects of [redacted] ablation on PPARα-dependent response also occur in female mice

To further validate the effects of NRCA1 ablation on the fasting response, we subjected 16-week old female mice to fasting and examined the hepatic expression of PPARα target gens. We observed that NRCA1 is also upregulated upon fasting in female mice (Figure 14). However, despite no differences in the auto-induction of PPARα between genotypes, the induction of PPARα target genes and the autophagy gene Lc3b are impaired in female NRCA1-KO^{Alb} mice (Figure 14). These observation suggests that impaired induction of PPARα target genes during fasting in NRCA1-deficient mice may be due to impaired PPARα activity and not due to decreased auto-induction of PPARα. Interestingly, the induction of Cyp4a10, one of the most sensitive and exclusively PPARα-dependent genes[102], is ten-fold higher in male mice compared to female counterparts (Figure 15), suggesting sex differences in the activation of PPARα.

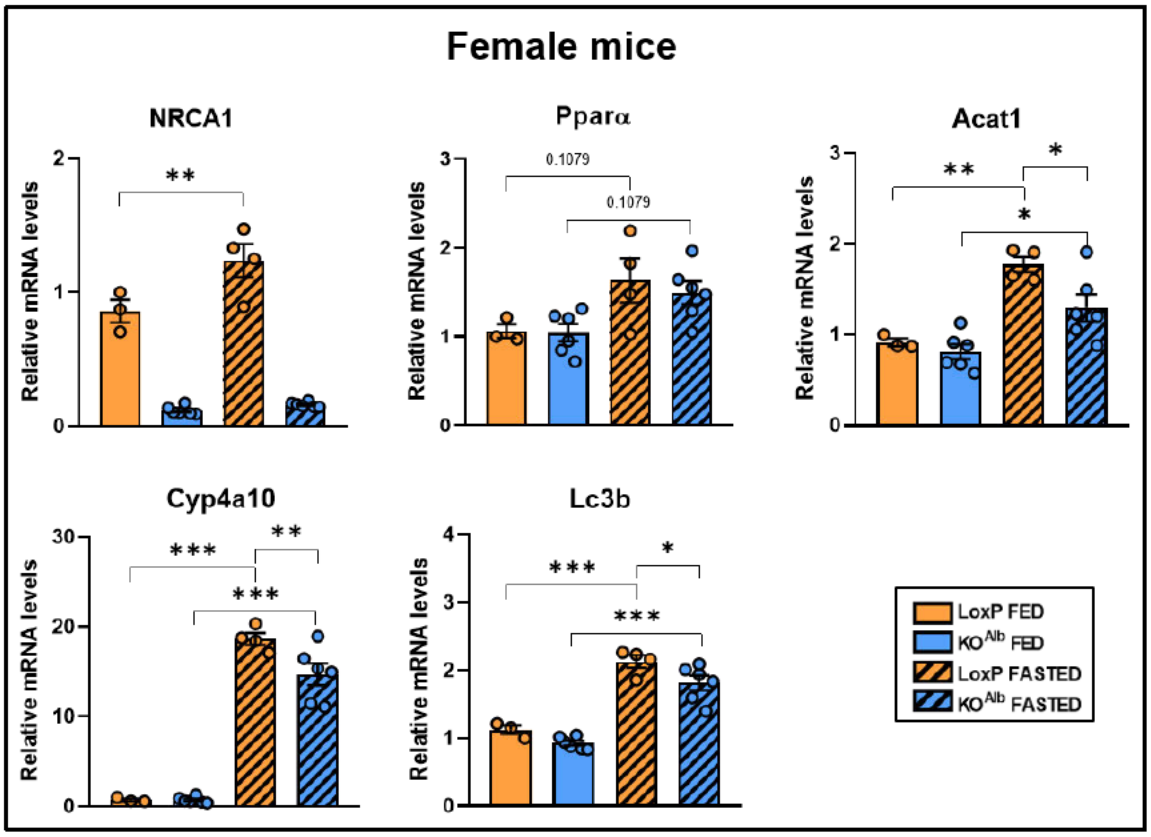

Figure 14: Fasting-induced PPARα response and transcriptional activation of autophagy are also impaired in female mice. Livers were collected from female 16-week old fed LoxP (orange) and NRCA1-KO^{Alb} mice (blue), and fasted LoxP (orange, dashed) and NRCA1-KO^{Alb} mice (blue, dashed). RT-qPCR was performed to analyze the expression of PPARα target genes. Data represented as mean ± SEM. One-way Anova test coupled with multiple-comparisons was performed. * $P < 0.05$, ** $P < 0.01$, *** $P < 0.001$.

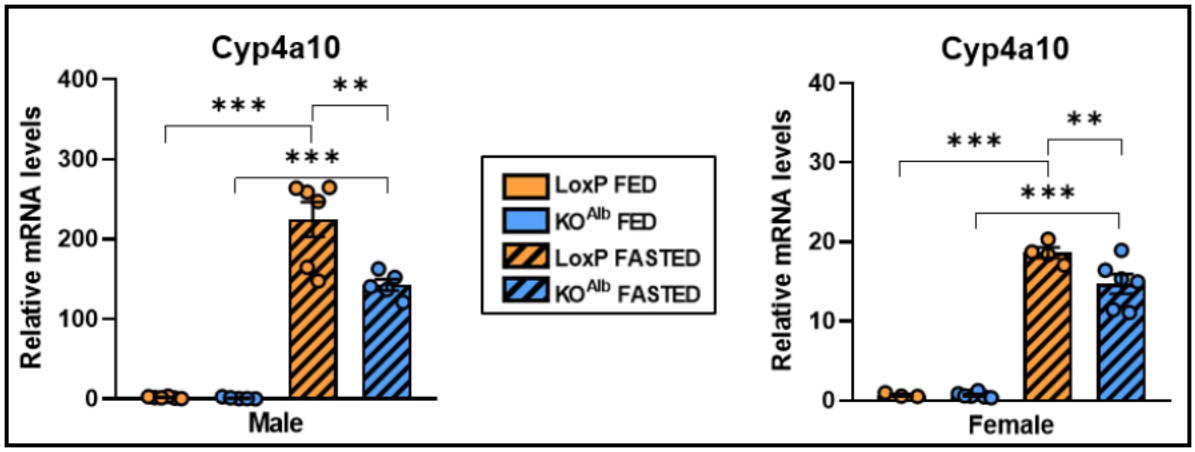

Figure 15: Sex differences in the induction of Cyp4a10 upon fasting. Relative expression of Cyp4a10 in male (left) and female (right) mice. . Data represented as mean ± SEM. One-way Anova test coupled with multiple-comparisons was performed. * $P < 0.05$, ** $P < 0.01$, *** $P < 0.001$.

4.1.3. The effects of NRCA1 ablation on PPARα-dependent response to fasting are aggravated during aging in male mice

Growing evidence suggests that aging is a major risk factor for developing MASLD[41] and that PPARα expression and activity declines with age in mice[40]. Considering our data, we examined the PPARα-dependent fasting response in one-year and two-year old male mice. Livers of one-year old male NRCA1-KO^{Alb} mice also show impaired induction of PPARα target genes upon fasting, including PPARα itself (Figure 16). Consistently, protein levels of Cyp4a family members are downregulated in fasted NRCA1-KO^{Alb} mice (Figure 17).

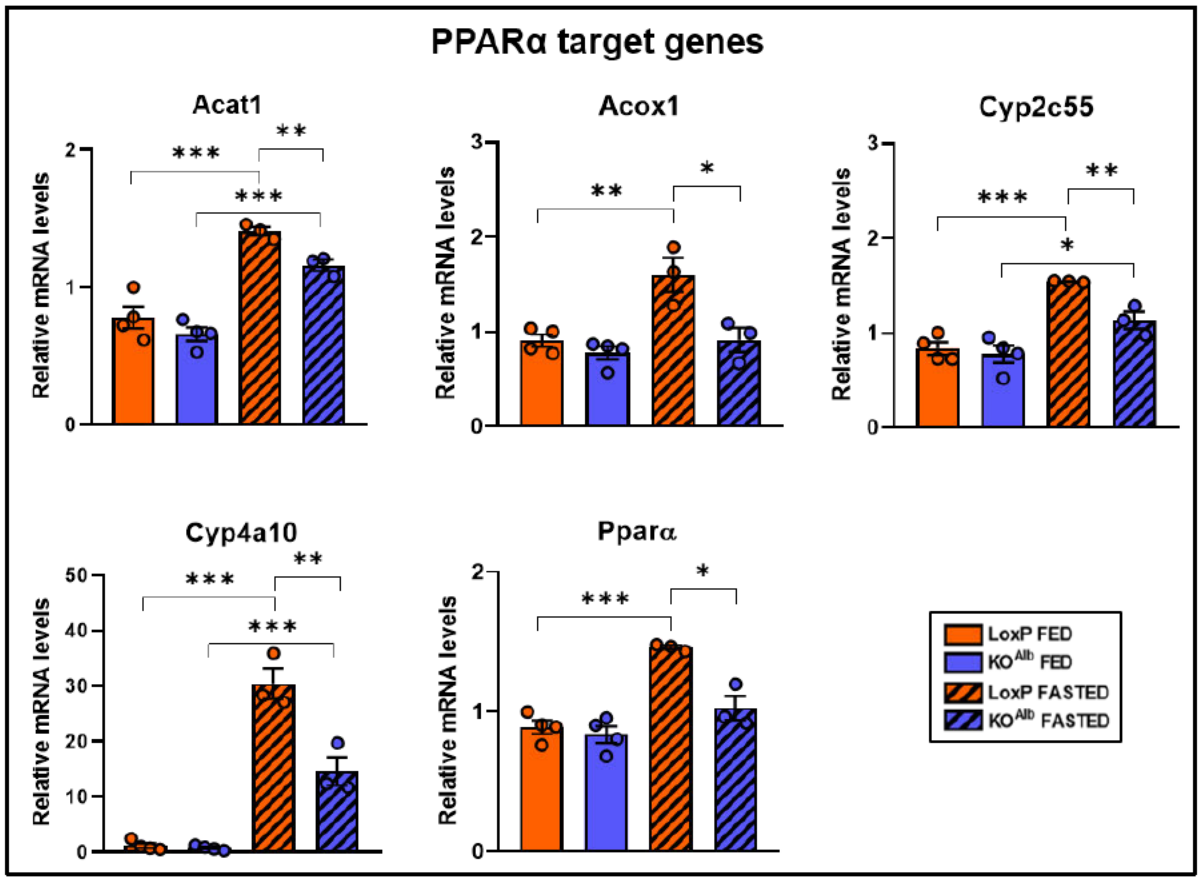

Figure 16: NRCA1 ablation impairs induction of PPARα target genes upon fasting in one-year old mice. Livers were collected from one-year old fed LoxP (dark orange) and NRCA1-KO^{Alb} mice (navy blue), and fasted LoxP (dark orange, dashed) and NRCA1-KO^{Alb} mice (navy blue, dashed). RT-qPCR was performed to analyze the expression of PPARα target genes. Data represented as mean ± SEM. One-way Anova test coupled with multiple-comparisons was performed. * $P < 0.05$, ** $P < 0.01$, *** $P < 0.001$.

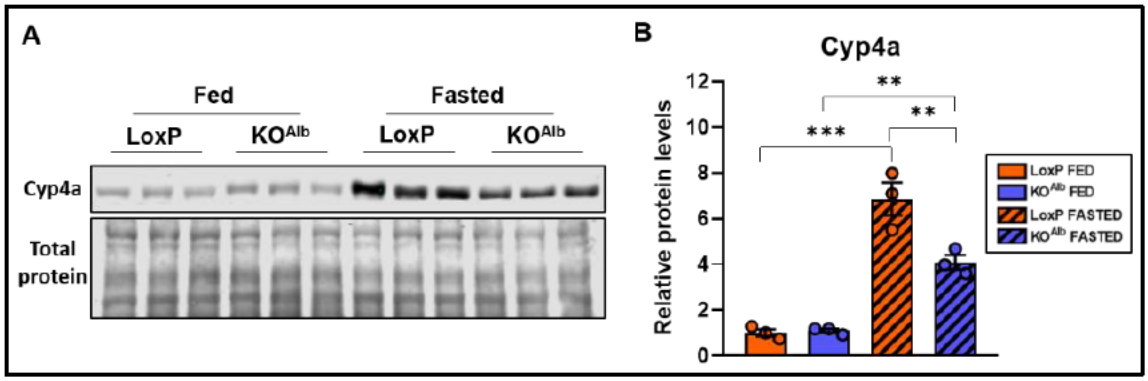

Figure 17: Cyp4a protein levels are downregulated in fasted NRCA1-KO^{Alb} mice. **A**) Western blot analysis of livers from one-year old fed LoxP (dark orange) and NRCA1-KO^{Alb} mice (navy blue), and fasted LoxP (dark orange, dashed) and NRCA1-KO^{Alb} mice (navy blue, dashed). **B**) Quantification. Data represented as mean ± SEM. One-way Anova test coupled with multiple-comparisons was performed. $P < 0.05$, ** $P < 0.01$, *** $P < 0.001$.

Growing evidence also suggests that autophagy declines with age[65]. While we do see an upregulation of NRCA1 in LoxP mice, the induction of autophagy genes upon fasting is also impaired in one-year old NRCA1-KO^{Alb} mice (Figure 18). These results are consistent with the fact that autophagy genes are PPARα target genes[36].

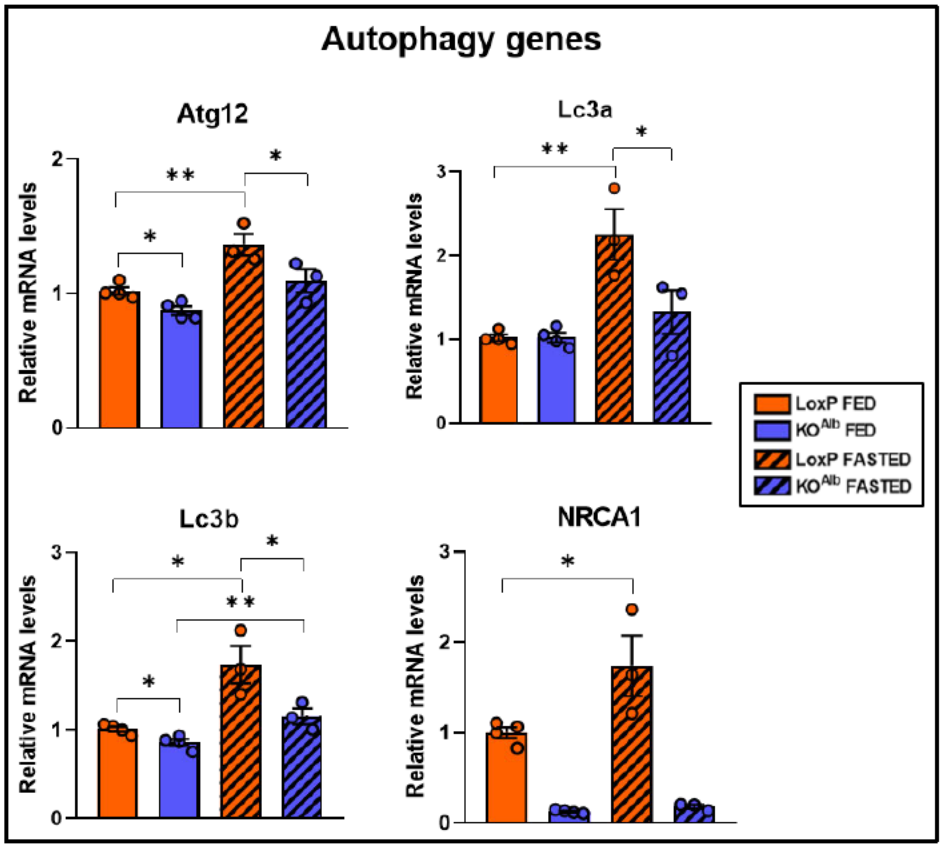

Figure 18: Fasting-induced transcriptional activation of autophagy is impaired in one-year old NRCA1-KO^{Alb} mice. One-year old fed LoxP (dark orange) and NRCA1-KO^{Alb} mice (navy blue), and fasted LoxP (dark orange, dashed) and NRCA1-KO^{Alb} mice (navy blue, dashed). Relative expression of autophagy genes. One-way Anova test coupled with multiple-comparisons was performed. * $P < 0.05$, ** $P < 0.01$, *** $P < 0.001$.

Livers of two-year old NRCA1-KO^{Alb} mice also show impaired induction of PPARα target genes upon fasting, as well as the autophagy gene LC3B (Figure 19). However, upregulation of NRCA1 upon fasting is maintained in two-year old mice and the expression of PPARα is equally induced in both LoxP and NRCA1-KO^{Alb} animals, suggesting that impaired induction of PPARα target genes during fasting in NRCA1-deficient mice is due to impaired PPARα activity and not due to decreased auto-induction of PPARα.

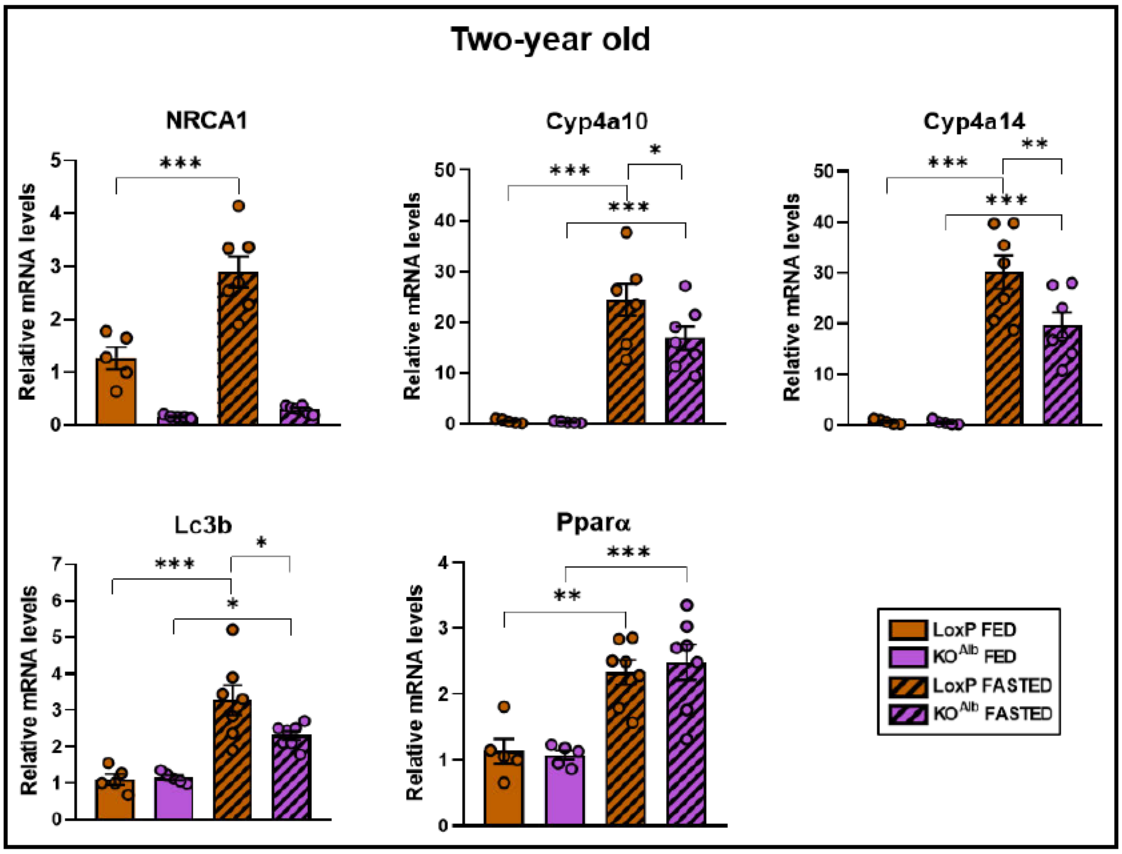

Figure 19: Two-year old mice show impaired fasting-induced expression of PPARα target genes and autophagy genes. Livers were collected from one-year old fed LoxP (brown) and NRCA1-KO^{Alb} mice (violet) and fasted LoxP (brown, dashed) and NRCA1-KO^{Alb} mice (violet, dashed). RT-qPCR was performed to analyze the expression of NRCA1 and PPARα target genes. Data represented as mean ± SEM. One-way Anova test coupled with multiple-comparisons was performed. * $P < 0.05$, ** $P < 0.01$, *** $P < 0.001$.

Next, we assessed fasting-induced upregulation of PPARα target genes across different ages (i.e. 16-week, one-year and two-year old male mice). To do this, we checked the expression of Cyp4a10 and Cyp4a14, which are the most sensitive and exclusively PPARα-dependent genes[102]. We observed an age-dependent decline in the activity of PPARα, as the fasting-induced expression of Cyp4a10 and Cyp4a14 was markedly impaired in one-year old male mice, and further exacerbated in two-year old male mice (Figure 20A). This age-dependent impairment of Cyp4a10 and Cyp4a14 expression is even more remarkable in NRCA1-deficient animals. Moreover, there is a slight tendency suggesting that NRCA1 expression is downregulated upon aging (Figure 20B) and fasting-induced expression of NRCA1 is compromised (Figure 20B).

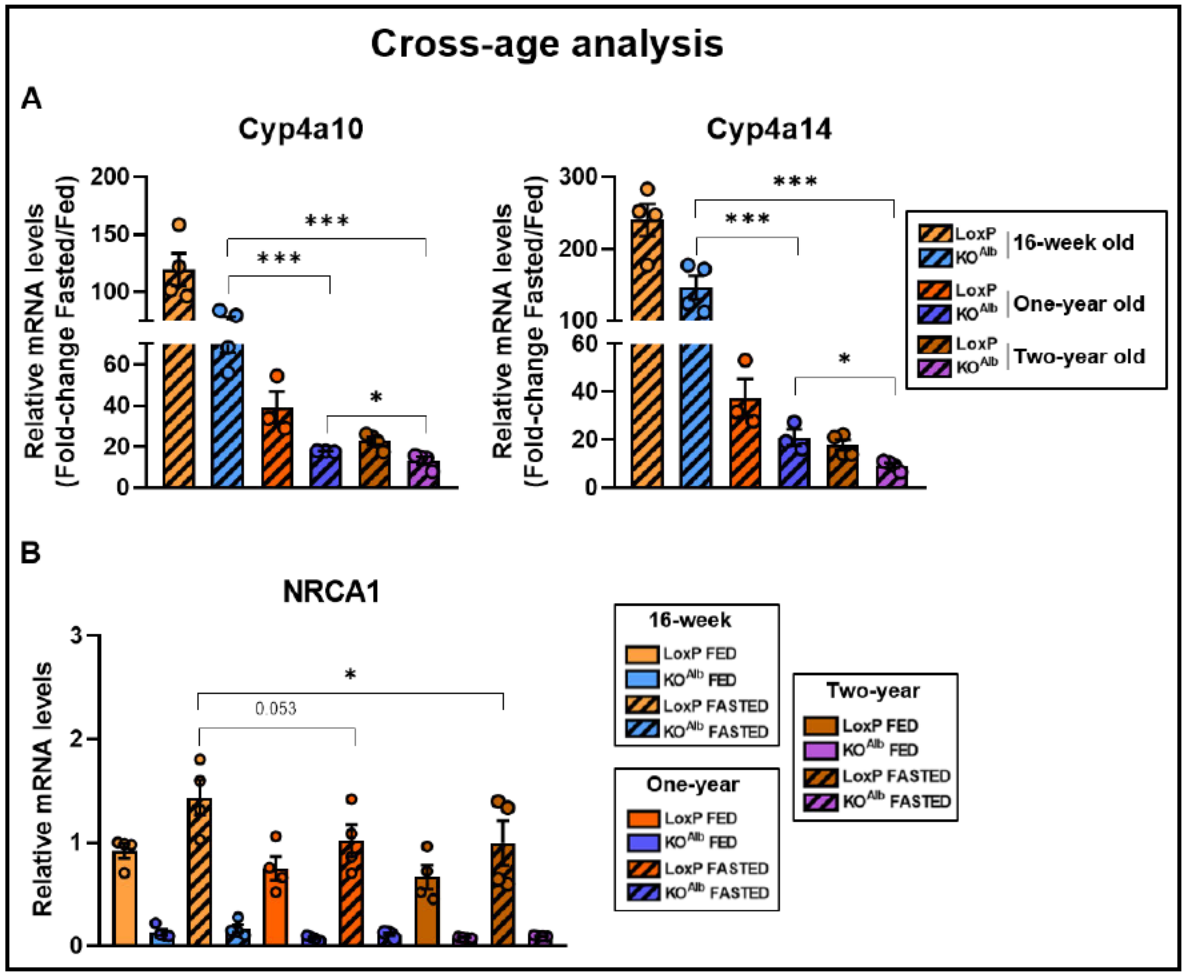

Figure 20: NRCA1 ablation aggravates aging-induced decline of PPARα activity. **A**) Relative expression of Cyp4a10 and Cyp4a14 in livers of 16-week, one-year and two-year old mice. Data represented as fold-change of fasted and fed values. **B**) Relative expression of NRCA1 in livers of fed and fasted 16-week, one-year and two-year old mice. Data represented as mean ± SEM. One-way Anova test coupled with multiple-comparisons was performed. $P < 0.05$, ** $P < 0.01$, *** $P < 0.001$.

4.1.4. NRCA1 ablation impairs western diet-induced PPARα response and transcriptional activation of autophagy

We have shown that NRCA1 ablation compromises fasting-induced PPARα response, which occurs across different ages. PPARα can also be activated by stimuli other than fasting, such as in response to high fat diet[104]. To study whether PPARα activation by other stimuli, we subjected male LoxP and NRCA1-KO^{Alb} to a high-fat diet (HFD), containing 60% kcal of fat, at 8 weeks of age for 16 weeks, as described in [redacted]. Upon HFD, we observed an upregulation of PPARα target genes in LoxP animals, as reported in the literature (Figure 21). HFD also induced the expression of NRCA1 (Figure 21). However, the impaired induction of PPARα target genes in HFD-fed NRCA1-KO^{Alb} mice is not as clear as in fasting conditions. When we analyzed the expression of autophagy genes, HFD has a clear effect in inducing autophagy genes, probably as a coping mechanism to get rid of fat overload. However, similarly to PPARα target genes, there are no major differences in the upregulation of autophagy genes between genotypes (Figure 22).

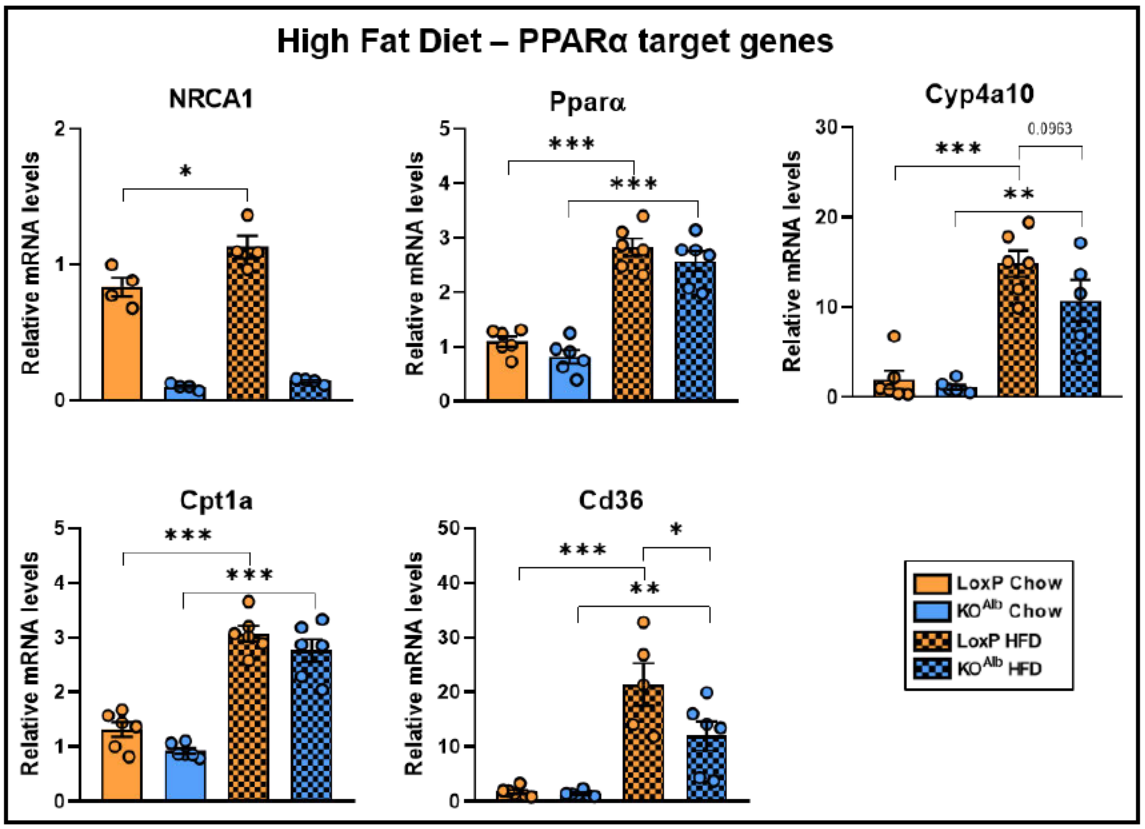

Figure 21: NRCA1 ablation has little effect on PPARα-dependent response to HFD. Mice at 8 weeks of age were subjected to HFD for 16 weeks and then sacrificed. Livers were collected from chow diet-fed LoxP (orange) and NRCA1-KO^{Alb} mice (blue) and HFD-fed LoxP (orange, squared) and NRCA1-KO^{Alb} mice (blue, squared). RT-qPCR was performed to analyze the expression of NRCA1 and PPARα target genes. Data represented as mean ± SEM. One-way Anova test coupled with multiple-comparisons was performed. * $P < 0.05$, ** $P < 0.01$, *** $P < 0.001$.

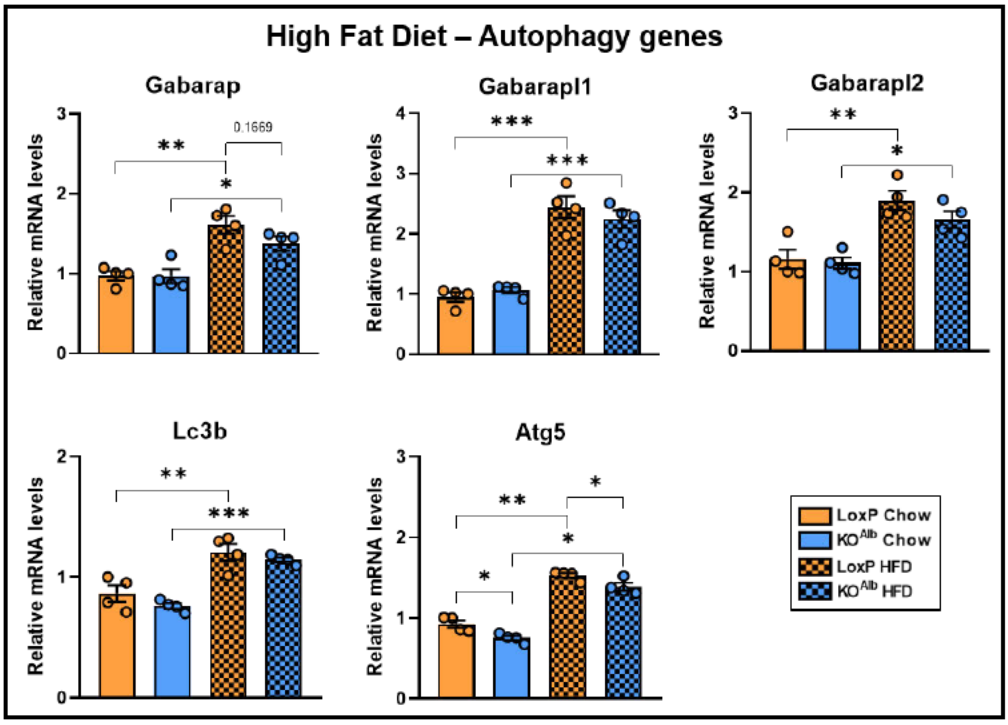

Figure 22: NRCA1 ablation has little effect on the induction of autophagy genes in response to HFD. Mice at 8 weeks of age were subjected to HFD for 16 weeks and then sacrificed. Livers were collected from chow diet-fed LoxP (orange) and NRCA1-KO^{Alb} mice (blue) and HFD-fed LoxP (orange, squared) and NRCA1-KO^{Alb} mice (blue, squared). RT-qPCR was performed to analyze the expression of autophagy genes. Data represented as mean ± SEM. One-way Anova test coupled with multiple-comparisons was performed. * $P < 0.05$, ** $P < 0.01$, *** $P < 0.001$.

Despite little effects of NRCA1 ablation in the induction of PPARα target genes and autophagy genes, we observed a substantial increase in the accumulation of hepatic triglycerides and decreased KB plasma levels in HFD-fed NRCA1-KO^{Alb} mice compared to LoxP littermates. [redacted] (Figure 23). These observations are similar to those of fasting conditions, albeit induction PPARα target genes and autophagy genes was impaired in NRCA1-KO^{Alb} animals upon fasting (Figure 8, Figure 13).

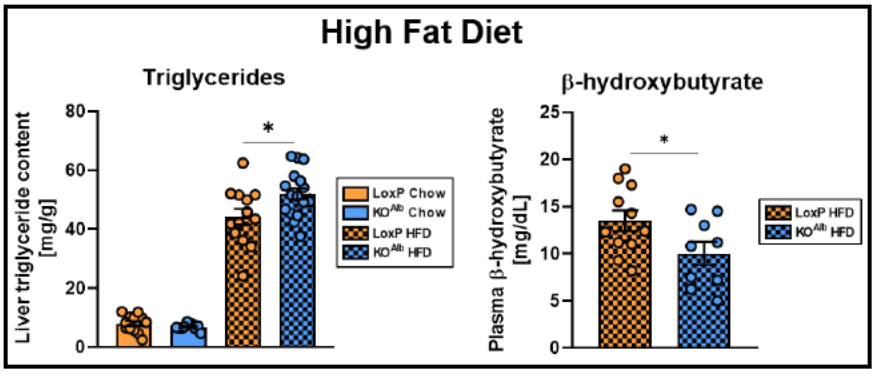

Figure 23: NRCA1 ablation leads to increased hepatic triglyceride content and decreased plasma levels of β-hydroxybutyrate in response to HFD. **A**) Hepatic triglyceride content. Livers were collected from chow diet-fed LoxP (orange) and NRCA1-KO^{Alb} mice (blue) and HFD-fed LoxP (orange, squared) and NRCA1-KO^{Alb} mice (blue, squared). **B**) Plasma β-hydroxybutyrate levels. Plasmas were collected from fasted HFD-fed LoxP (orange, squared) and NRCA1-KO^{Alb} mice (blue, squared). Data represented as mean ± SEM. Student t-test was performed. * $P < 0.05$. Adapted from Petra Frager, PhD Thesis, 2022.

PPARα and autophagy have a protective role against the development of MASLD, as described in 2.1.2.2 and 2.2.2.3, respectively. Fatty liver in mice can be modeled with different types of diets, such as western diet (WD) and methionine- and choline-deficient (MCD) diet. Given the role of NRCA1 in the activation of PPARα during fasting, we sought to test whether NRCA1 ablation had any effect in the development of fatty liver. To do this, we subjected LoxP and NRCA1-KO^{Alb} mice at 8 weeks of age to a WD. The WD is a HFD (40% kcal of fat) with a high content of sucrose (35% w/w) and supplemented with cholesterol (0.2% w/w). The expression of NRCA1 is also induced by western diet (Figure 24). As the WD is a HFD, we also observe an induction of PPARα target genes in response to WD. However, this induction is impaired in NRCA1-KO^{Alb} mice (Figure 24), similarly to what we observed in fasted NRCA1-KO^{Alb} animals (Figure 8).

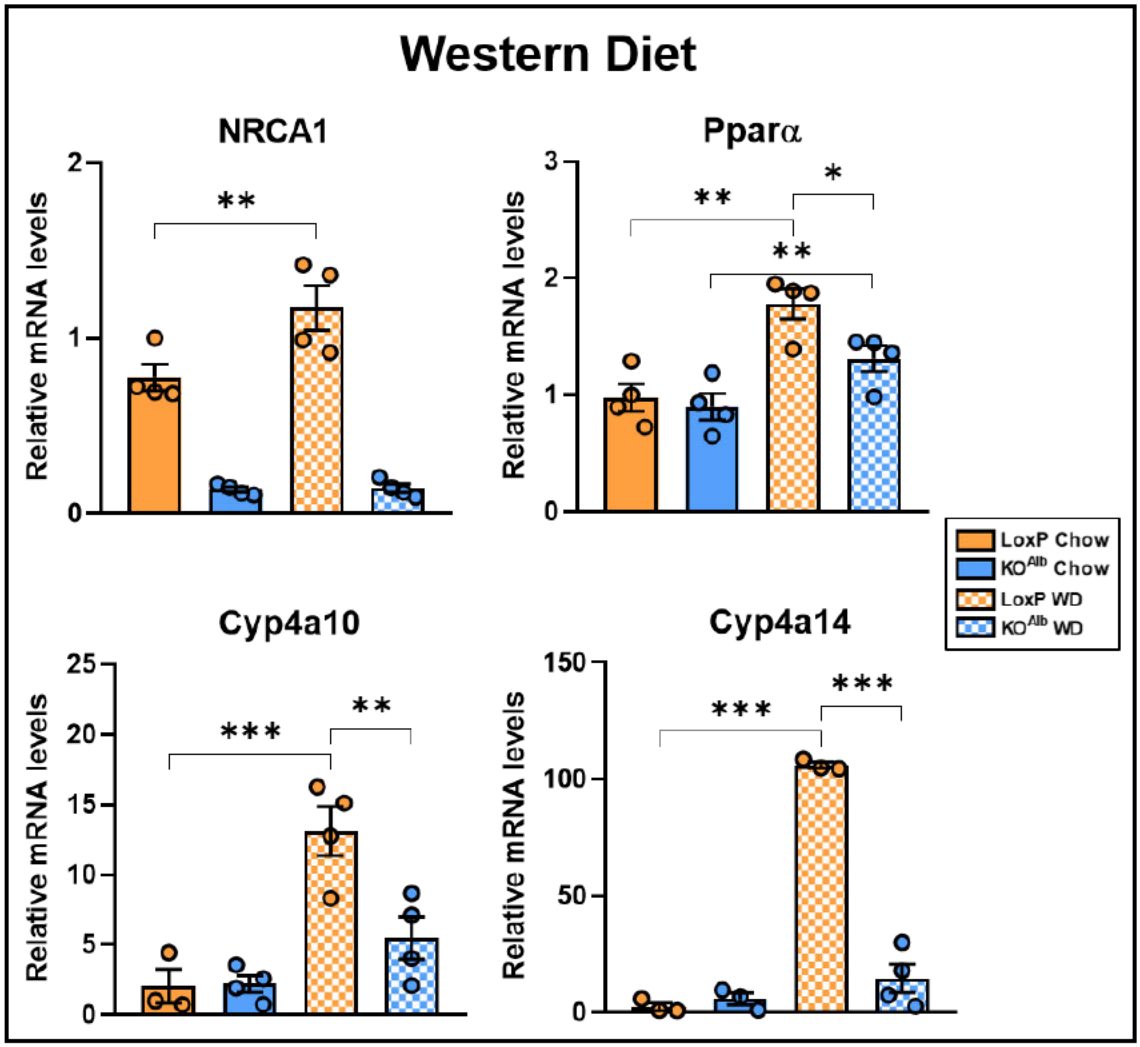

Figure 24: NRCA1 ablation impairs induction of PPARα target genes in response to WD. Mice at 8 weeks of age were subjected to WD for 16 weeks and then sacrificed. Livers were collected from chow diet-fed LoxP (orange) and NRCA1-KO^{Alb} mice (blue) and WD-fed LoxP (orange, white squares) and NRCA1-KO^{Alb} mice (blue, white squares). RT-qPCR was performed to analyze the expression of NRCA1 and PPARα target genes. Data represented as mean ± SEM. One-way Anova test coupled with multiple-comparisons was performed. * $P < 0.05$, ** $P < 0.01$, *** $P < 0.001$.

Similarly to HFD, WD also activates the expression of autophagy genes. However, unlike HFD, NRCA1-KO^{Alb} mice are not able upregulate the expression of autophagy genes in response to WD (Figure 25). Although NRCA1 ablation impaired WD-induced expression of PPARα target genes and autophagy genes, an increased accumulation of hepatic TGs in WD-fed KO^{Alb} animals was not observed [redacted].

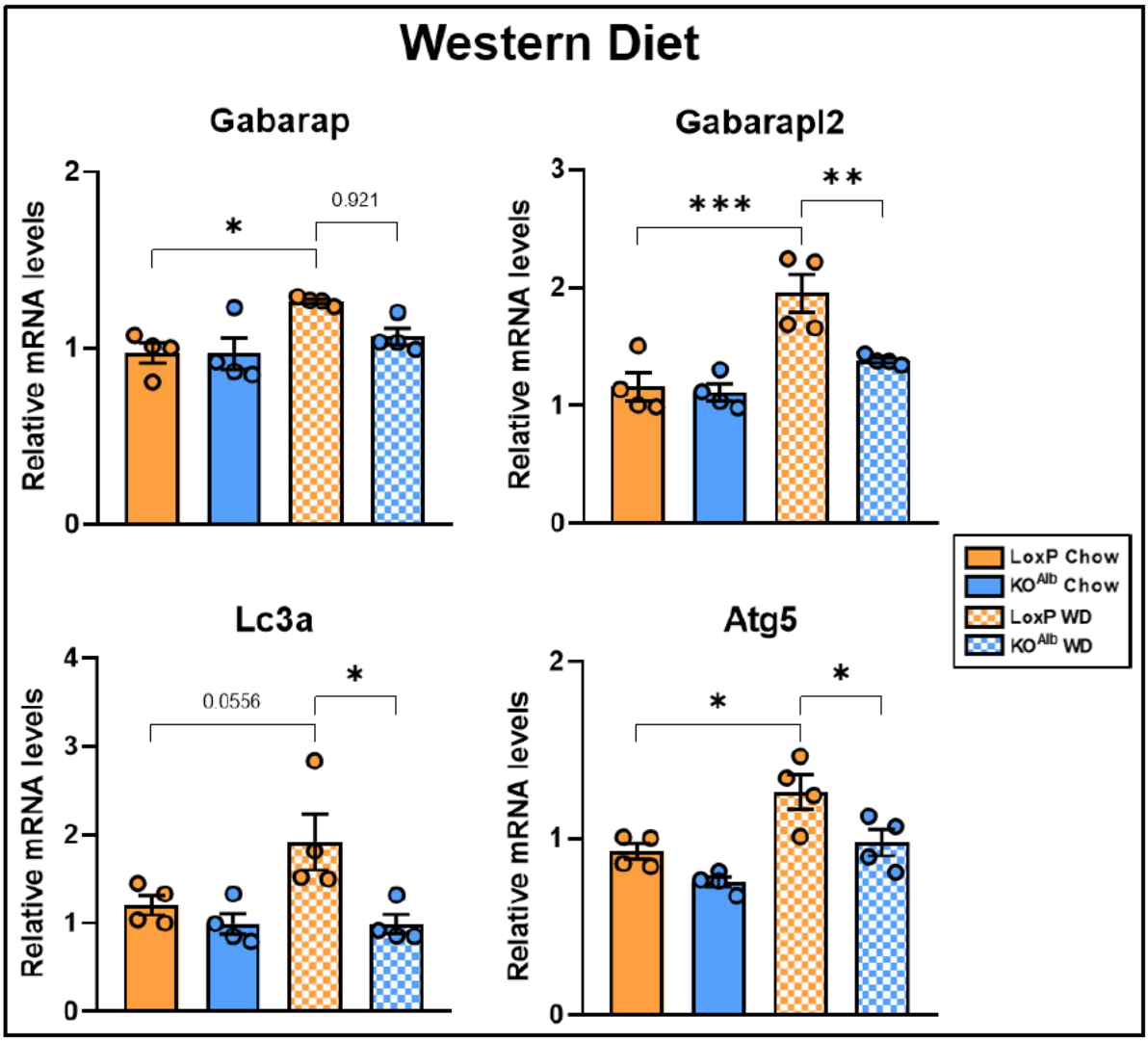

Figure 25: NRCA1 ablation impairs induction of autophagy genes in response to WD. Mice at 8 weeks of age were subjected to WD for 16 weeks and then sacrificed. Livers were collected from chow diet-fed LoxP (orange) and NRCA1-KO^{Alb} mice (blue) and WD-fed LoxP (orange, white squares) and NRCA1-KO^{Alb} mice (blue, white squares). RT-qPCR was performed to analyze the expression of autophagy genes. Data represented as mean ± SEM. One-way Anova test coupled with multiple-comparisons was performed. * $P < 0.05$, ** $P < 0.01$, *** $P < 0.001$.

4.1.5. NRCA1 is required to fully activate PPARα

We have shown so far that NRCA1 ablation impairs activation of PPARα in response to fasting and to WD. To dissect whether NRCA1 is indeed an activator of PPARα, we treated 16-week old female LoxP and NRCA1-KO^{Alb} mice with the PPARα agonist GW7647. We observed that upon GW7647 treatment, NRCA1 levels were not upregulated (Figure 26). PPARα auto-induction was higher in LoxP animals compared to NRCA1-KO^{Alb} mice and the expression of PPARα target genes were induced to a greater extent in LoxP animals, suggesting that NRCA1 is required for the full activation of PPARα.

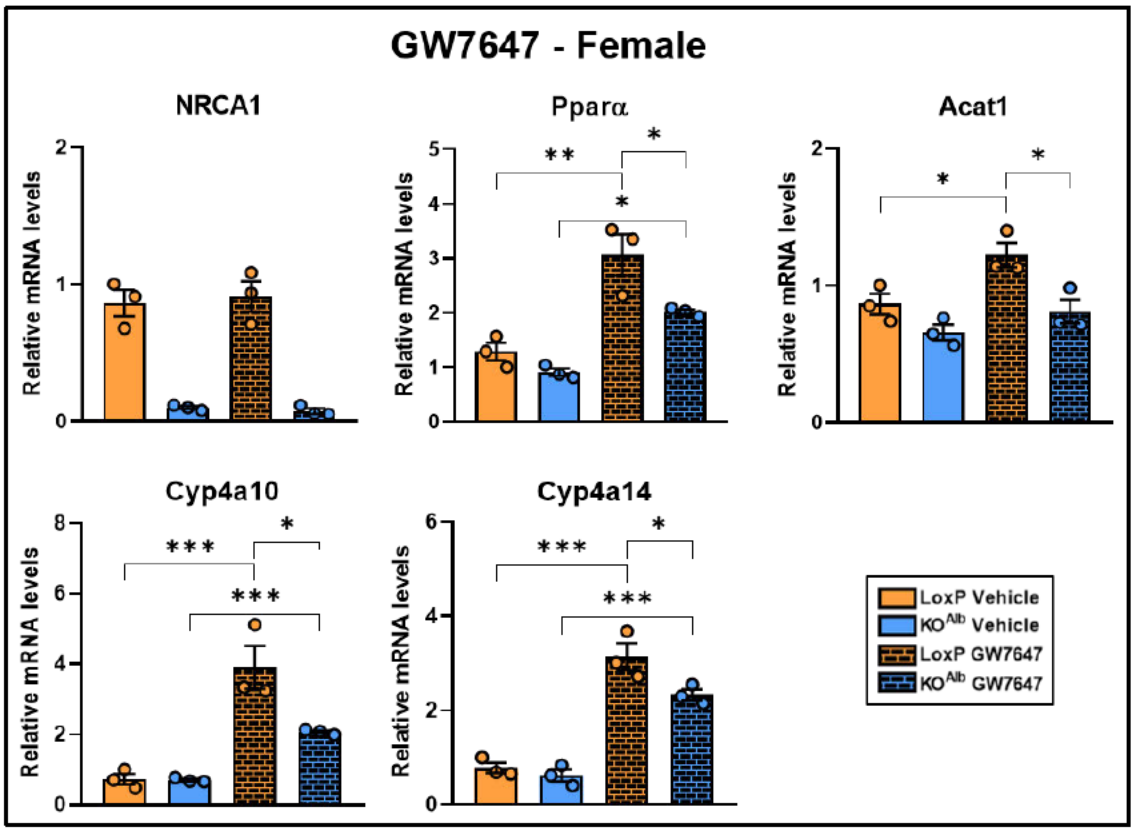

Figure 26: NRCA1 is required to fully activate PPARα by GW7647. Female animals were subjected to a 4-hour treatment through oral gavage with vehicle or GW7647. LoxP vehicle (orange), NRCA1-KO^{Alb} mice vehicle (blue), LoxP GW7647 (orange, black tiled) and NRCA1-KO^{Alb} mice GW7647 (blue, black tiled). RT-qPCR was performed to analyze the expression of NRCA1 and PPARα target genes. Data represented as mean ± SEM. One-way Anova test coupled with multiple-comparisons was performed. * $P < 0.05$, ** $P < 0.01$, *** $P < 0.001$.

To further validate these results, we treated female mice with Wy14643, another PPARα agonist. Wy14643, unlike GW7647, induced the expression of NRCA1 (Figure 27). PPARα auto-induction was slightly higher in LoxP animals and similarly to GW7647, the expression of PPARα target genes were induced to a greater extent in LoxP animals compared to NRCA1-KO^{Alb} mice, reinforcing our observation that NRCA1 is required for the full activation of PPARα.

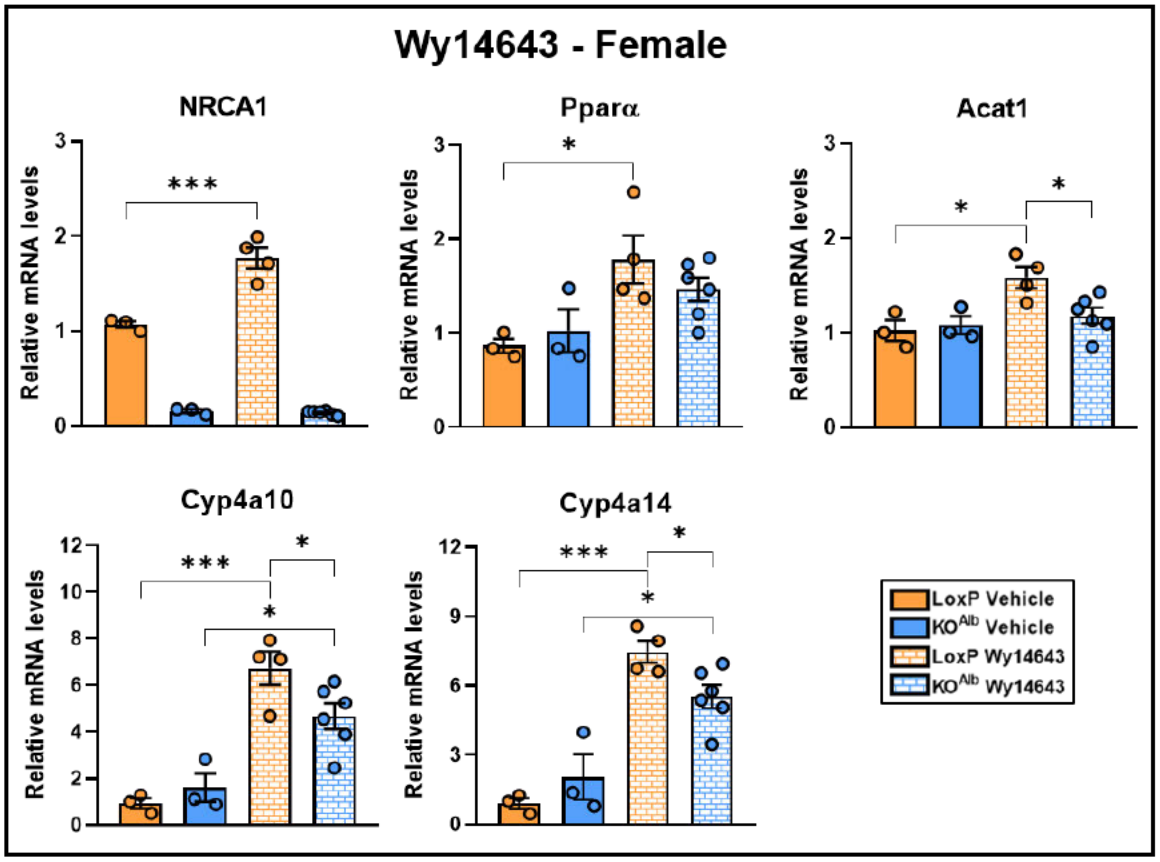

Figure 27: NRCA1 is required to fully activate PPARα by Wy14643. Female animals were subjected to a 4-hour treatment through oral gavage with vehicle or GW7647. LoxP vehicle (orange), NRCA1-KO^{Alb} mice vehicle (blue), LoxP GW7647 (orange, white tiled) and NRCA1-KO^{Alb} mice GW7647 (blue, white tiled). RT-qPCR was performed to analyze the expression of NRCA1 and PPARα target genes. Data represented as mean ± SEM. One-way Anova test coupled with multiple-comparisons was performed. * $P < 0.05$, ** $P < 0.01$, *** $P < 0.001$.

We also treated 16-week old male mice with a single dose of GW7647. However, male NRCA1-KO^{Alb} mice were able to induce PPARα target genes to a similar extent as LoxP mice upon GW7647 treatment (Figure 28). These results suggest that agonist treatment has different kinetics between female and male mice.

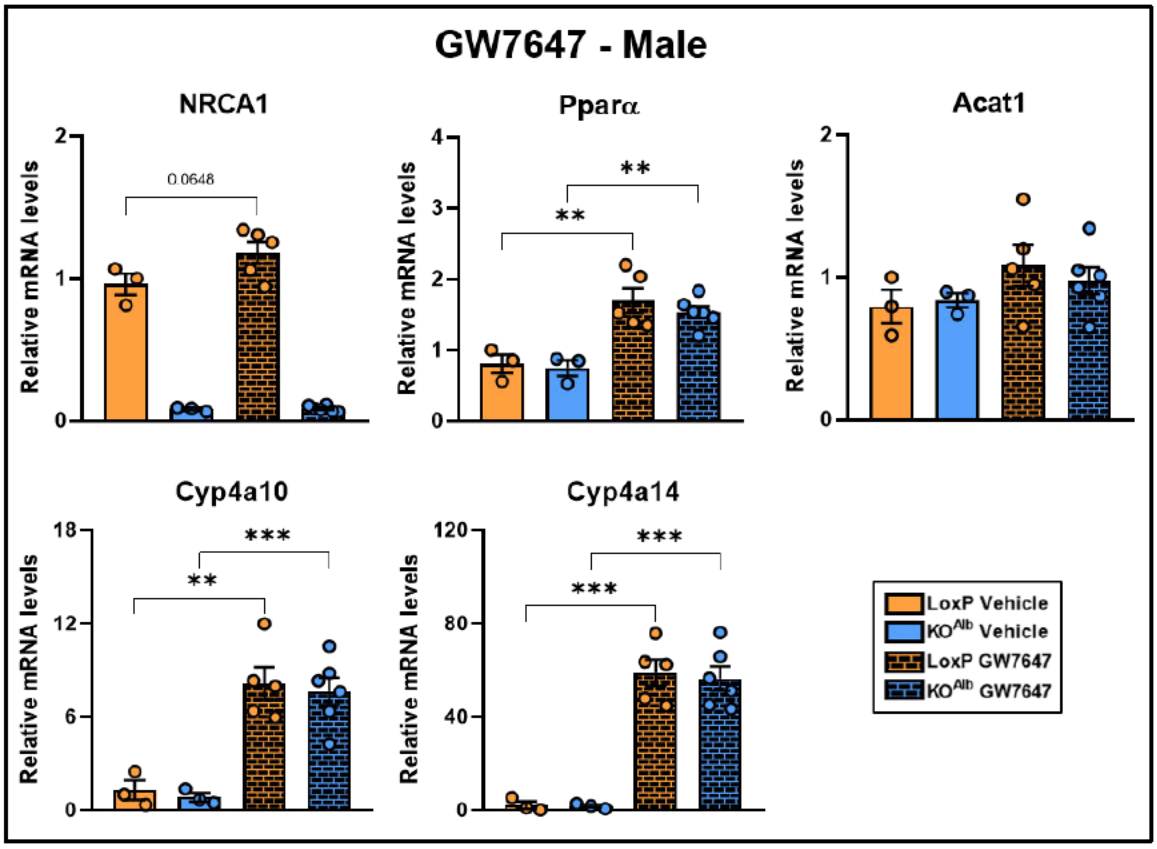

Figure 28: NRCA1 ablation does not affect PPARα activation by GW7647. Male animals were subjected to a 4-hour treatment through oral gavage with vehicle or GW7647. LoxP vehicle (orange), NRCA1-KO^{Alb} mice vehicle (blue), LoxP GW7647 (orange, black tiled) and NRCA1-KO^{Alb} mice GW7647 (blue, black tiled). RT-qPCR was performed to analyze the expression of NRCA1 and PPARα target genes. Data represented as mean ± SEM. One-way Anova test coupled with multiple-comparisons was performed.

4.1.6. NRCA1 ablation impairs PPARα activation by agonist upon methionine- and choline-deficient diet

PPARα has a strong protective role against the development of MASLD[39]. NRCA1 ablation leads to impaired PPARα activation and enhanced hepatic fat accumulation. Therefore, we wondered whether NRCA1-KO^{Alb} mice would be more susceptible to develop MASLD and MASH. The methionine- and choline-deficient diet (MCD) is a research diet used to model MASLD in mice, however it causes a dramatic weight loss that is not observed in humans[105]. A 0.1% supplementation of methionine in drinking water can circumvent this non-physiological weight loss[106]. The duration of the MCD diet regime is typically 3 weeks[106]. We subjected female LoxP and NRCA1-KO^{Alb} mice at around the age of 8 weeks to a one-week MCD diet to induce an acute liver stress. At the day of sacrifice, we treated mice with a single dose of vehicle or GW7647 for 4 hours and we checked the expression of PPARα target genes.

NRCA1 was not induced by GW7647 (Figure 29), as previously observed in female mice (Figure 26). GW7647 enhanced the expression of Cyp4a10 and Cyp4a14 in MCD diet-fed LoxP mice, but not so much in NRCA1-KO^{Alb} mice (Figure 29). This indicates that PPARα cannot be fully activated by agonist in female mice upon acute diet-induced liver stress. Surprisingly, MCD diet-fed NRCA1-KO^{Alb} mice had upregulated levels of Cyp4a10 and Cyp4a14 compared to MCD diet-fed LoxP animals, and GW7647 treatment did not cause an increase in the expression of Cyp4a10 and Cyp4a14, but rather a decrease (Figure 29).

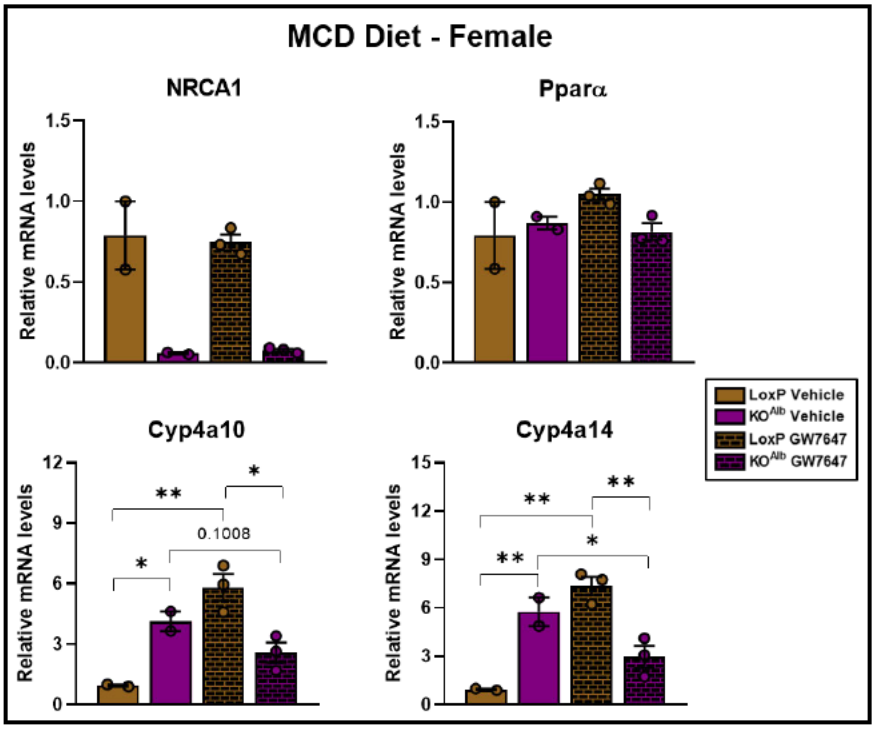

Figure 29: Effects of acute MCD diet and single dose GW7647 treatment on the expression of NRCA1, PPARα, Cyp4a10 and Cyp4a14 in female LoxP and NRCA1-KO^{Alb} mice. Female mice around the age of 8 weeks were subjected to a one-week MCD diet regime and treated with a single dose of GW7647 on the day of sacrifice.). RT-qPCR was performed to analyze the expression of NRCA1 and PPARα target genes. Data represented as mean ± SEM. One-way Anova test coupled with multiple-comparisons was performed. * $P < 0.05$, ** $P < 0.01$, *** $P < 0.001$.

We also subjected male LoxP and NRCA1-KO^{Alb} mice around the age of 8 weeks to a 3-week MCD diet regime supplemented with 0.1% methionine in drinking water to induce fatty liver and liver fibrosis. As NRCA1 ablation prevents full activation of PPARα by agonists, and PPARα agonists are known to ameliorate fatty liver and fibrosis in MCD-induced MASLD mouse models[107–109], we treated LoxP and NRCA1-KO^{Alb} mice with PPARα during the whole duration of the MCD diet regime.

Chronic treatment with GW7647 induced the expression of NRCA1 in male mice fed with MCD diet (Figure 30). Interestingly, PPARα expression was downregulated in NRCA1-KO^{Alb} mice in response to MCD diet, which was maintained upon GW7647 treatment (Figure 30). However, NRCA1-KO^{Alb} mice were able to induce the expression of Cyp4a10 and Cyp4a14 to a similar extent as LoxP mice upon chronic GW7647 treatment (Figure 30). However, there were only 3 NRCA1-KO^{Alb} mice able to induce Cyp4a10 and Cyp4a14 upon GW7647 to a similar levels as LoxP mice. By removing the values of the 3 "super responder" NRCA1-KO^{Alb} mice, we could observe that induction of Cyp4a10 and Cyp4a14 in these mice was impaired upon chronic GW7647 treatment (Figure 31).

In all, these results indicate that activation of PPARα in response to acute or chronic treatment with GW7647 is impaired in both female and male NRCA1-KO^{Alb} mice subjected to acute and chronic regime of MCD diet. However, in male mice, there is a minor subpopulation of NRCA1-KO^{Alb} mice that can fully activate PPARα in response to GW7647.

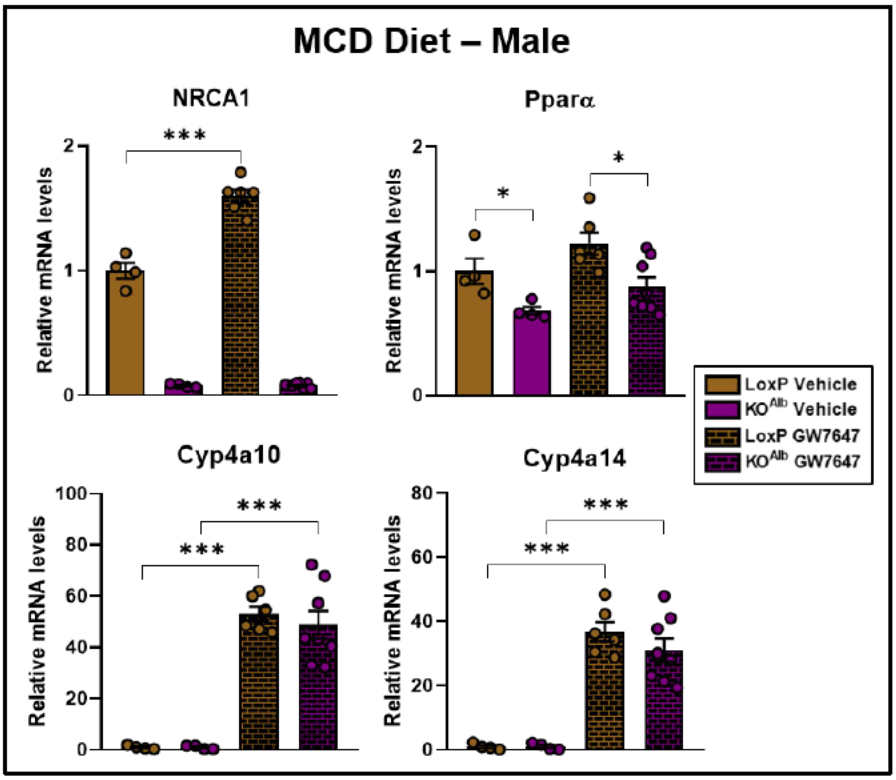

Figure 30: Effects of chronic MCD diet and GW7647 treatment on the expression of NRCA1, PPARα, Cyp4a10 and Cyp4a14 in male LoxP and NRCA1-KO^{Alb} mice. Male mice around the age of 8 weeks were subjected to a 3-week MCD diet regime and treated with GW7647 during the duration of the MCD diet. RT-qPCR was performed to analyze the expression of NRCA1 and PPARα target genes. Data represented as mean ± SEM. One-way Anova test coupled with multiple-comparisons was performed. * $P < 0.05$, ** $P < 0.01$, *** $P < 0.001$.

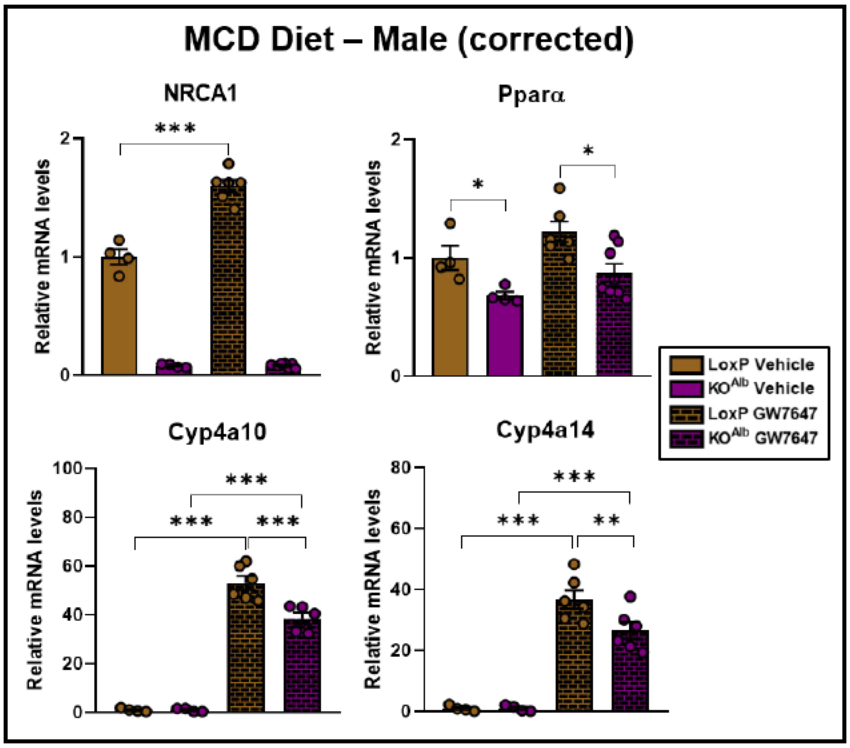

Figure 31: Effects of chronic MCD diet and GW7647 treatment on the expression of NRCA1, PPARα, Cyp4a10 and Cyp4a14 in male LoxP and NRCA1-KO^{Alb} mice. Male mice around the age of 8 weeks were subjected to a 3-week MCD diet regime and treated with GW7647 during the duration of the MCD diet. RT-qPCR was performed to analyze the expression of NRCA1 and PPARα target genes. The values of the 3 super responder NRCA1-KO^{Alb} mice were removed from Cyp4a10 and Cyp4a10. Data represented as mean ± SEM. One-way Anova test coupled with multiple-comparisons was performed. * $P < 0.05$, ** $P < 0.01$, *** $P < 0.001$.

4.2. Characterization of NRCA1-KO^{Alb} mice

4.2.1. Standard diet

4.2.1.1. Male mice

Male NRCA1-KO^{Alb} mice on a standard diet did not show major differences in body and tissue weight nor body composition at 16 weeks of age [redacted] When we analyzed body weight across ages, we observed an age-dependent increase in body weight, (Figure 32A), but NRCA1-deficient mice gained more weight during aging (Figure 32B). There were no differences across ages nor between genotypes in fasting-induced weight loss (Figure 32C), nor in fed (Figure 32D) and fasted (Figure 32E) liver weight.

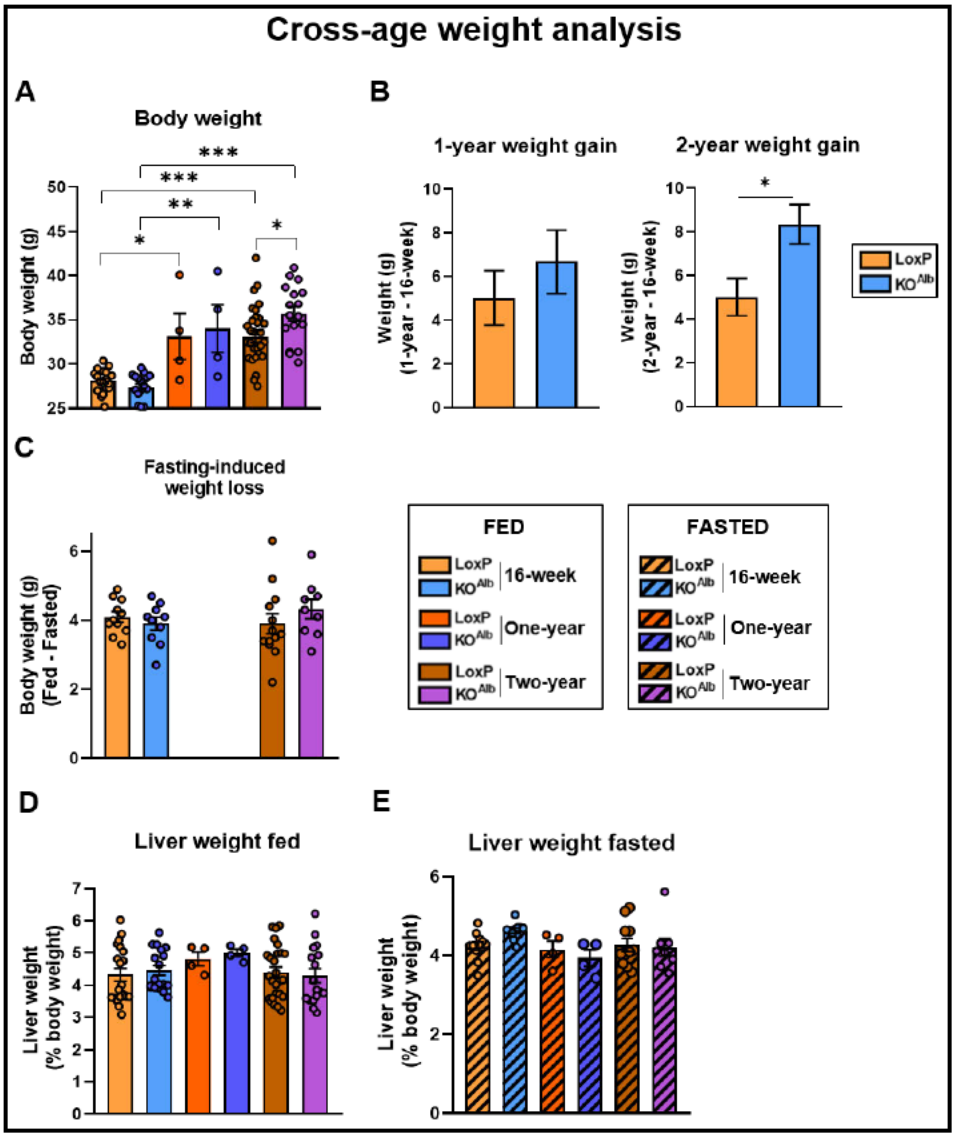

Figure 32: NRCA1 ablation leads to increased body weight gain during aging in male mice. **A**) Body weight. **B**) Age-dependent body weight gain. **C**) Fasting-induced weight loss. **D**) Liver weight under fed conditions. **E**) Liver weight under fasting conditions. Data represented as mean ± SEM. One-way Anova test coupled with multiple-comparisons was performed. * $P < 0.05$, ** $P < 0.01$, *** $P < 0.001$.

In addition, one-year old and two-year old NRCA1-KO^{Alb} mice showed enhanced accumulation of fat in the liver under fasting conditions (Figure 33 and Figure 34). These results are in agreement with the observation that PPARα activation is impaired in one-year old and two-year old NRCA1-KO^{Alb} animals upon fasting (Figure 16 and Figure 19).

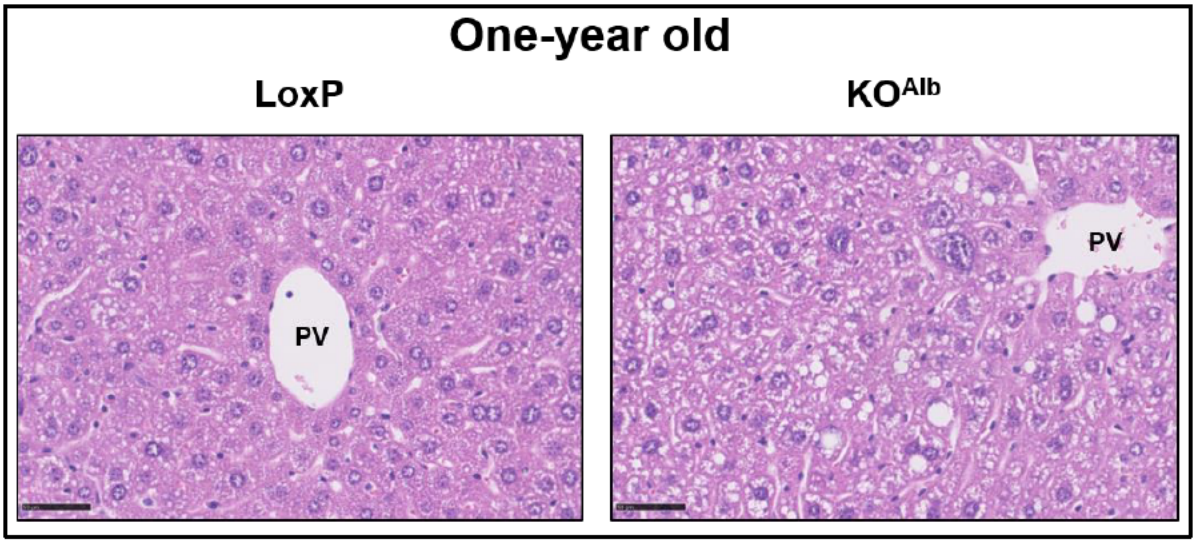

Figure 33: NRCA1 ablation leads to increased hepatic fat accumulation in one-year old male mice. One-year old LoxP and NRCA1-KO^{Alb} mice were subjected to overnight fasting (16 h). Livers were collected and subjected to hematoxylin and eosin staining. White rounded structures indicate lipid droplets. PV portal vein, scale bar 50 µm.

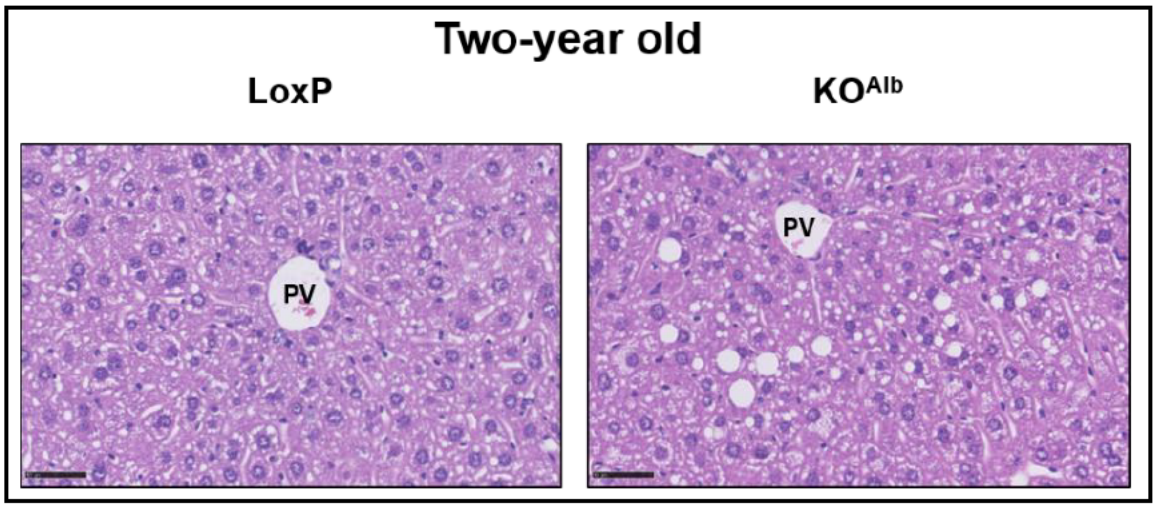

Figure 34: NRCA1 ablation leads to increased hepatic fat accumulation in one-year old male mice. Two-year old LoxP and NRCA1-KO^{Alb} mice were subjected to overnight fasting. Livers were collected and subjected to hematoxylin and eosin staining. White rounded structures indicate lipid droplets. PV portal vein, scale bar 50 µm.

4.2.1.2. Female mice

NRCA1 ablation did not cause any changes in body weight in 16-week old female mice (Figure 35A). However, NRCA1-KO^{Alb} female mice lost more body weight upon overnight fasting (16 h) (Figure 35B). There were no differences in liver weight between genotypes (Figure 35C/D). Histological analysis showed that NRCA1-KO^{Alb} female mice had enhanced hepatic fat accumulation upon fasting, similarly to male mice. This observation is consistent with impaired fasting-induced PPARα activation (Figure 14).

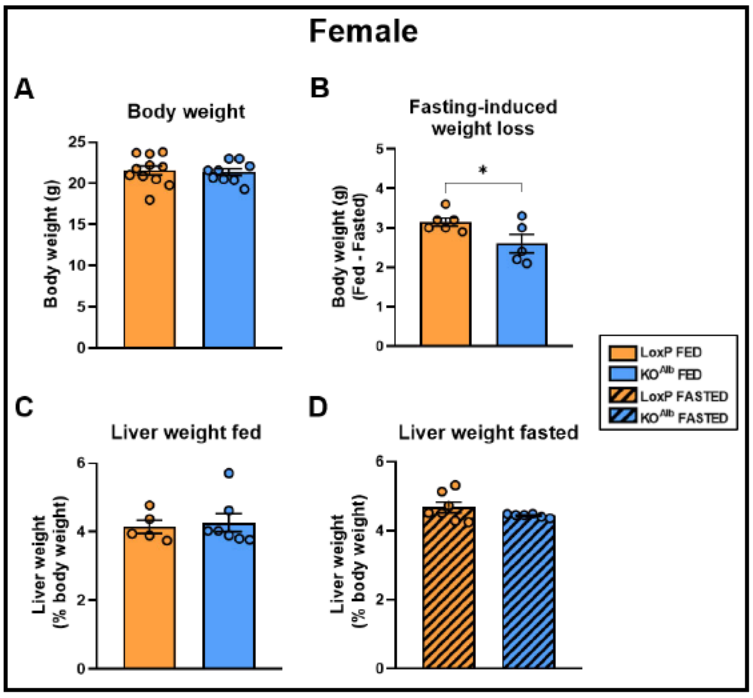

Figure 35: NRCA1 ablation reduces weight loss upon overnight fasting in female mice. A) Body weight. **B**) Fasting-induced weight loss. **C**) Liver weight in fed conditions. **D**) Liver weight in fasting conditions. Data represented as mean ± SEM. Unpaired Student's t-test was performed. * $P < 0.05$.

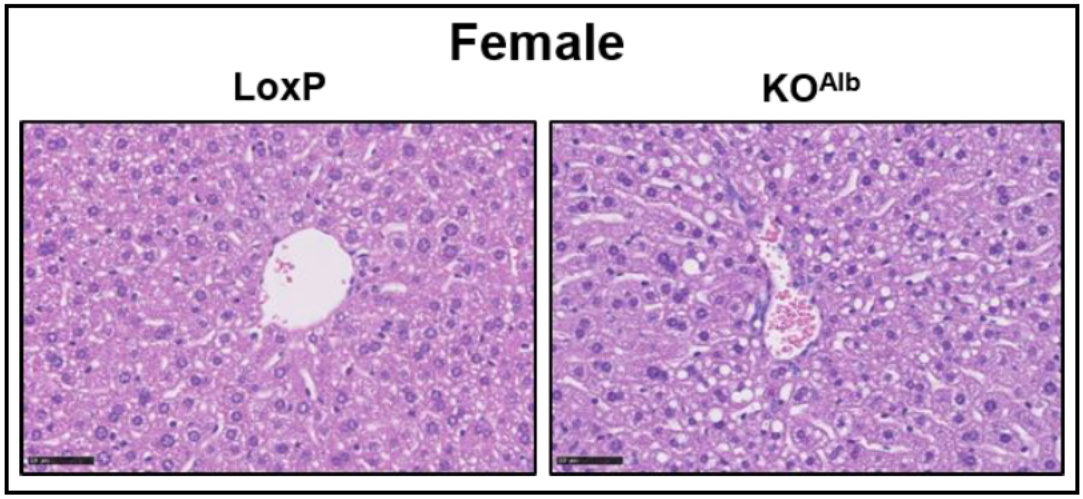

Figure 36: NRCA1 ablation leads to increased hepatic fat accumulation in 16-week old female mice. 16-week old LoxP and NRCA1-KO^{Alb} mice were subjected to overnight fasting. Livers were subjected to hematoxylin and eosin staining. White rounded structures indicate lipid droplets. PV portal vein, scale bar 50 µm.

4.2.2. Methionine- and choline-deficient diet

4.2.2.1. Male mice

We have described that NRCA1 ablation leads to impaired PPARα activation and enhanced hepatic fat accumulation. Therefore, we wondered whether NRCA1-KO^{Alb} mice would be more susceptible to develop MASLD and MASH and whether NRCA1 ablation has any effects on MASLD treatment with PPARα agonists. Therefore, we subjected LoxP and NRCA1-KO^{Alb} mice around the age of 8 weeks to a 3-week MCD diet regime supplemented with 0.1% methionine in drinking water to induce fatty liver and liver fibrosis. In addition, we treated LoxP and NRCA1-KO^{Alb} mice with vehicle or the PPARα agonist GW7647 during the whole duration of the MCD diet regime (Figure 37).

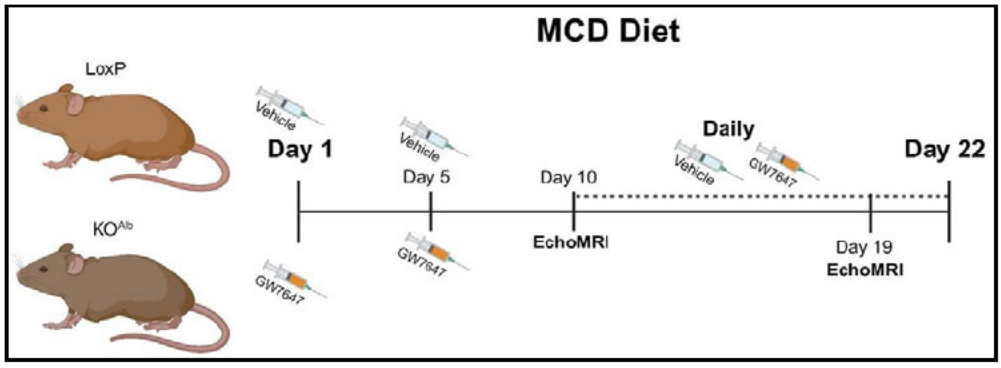

Figure 37: Overview of MCD diet regime. 8-week old LoxP and NRCA1-KO^{Alb} were fed an MCD diet supplemented with 0.1% methionine in drinking water for 21 days. Mice were treated through oral gavage with vehicle or GW7647 (5 mg/kg) on day 1 and day 5. On day 10, mice body composition was measured via EchoMRI. Starting from day 10, mice were treated with vehicle or GW7647 every day until they were sacrificed on day 21. Endpoint body composition was measured again on day 18. Created with BioRender.

The MCD diet supplemented with 0.1% methionine did not cause much changes in total body weight (Figure 38A). On one hand, body weight did not change in LoxP animals treated with vehicle (Figure 38B), but a small body weight decrease could be detected upon GW7647 treatment at day 10 and day 22 (Figure 38C). On the other hand, NRCA1-KO^{Alb} mice treated with vehicle had a tiny decrease in body weight at day 10, which was normalized at day 22 (Figure 38D). However, NRCA1-KO^{Alb} mice treated with GW7647 showed a significant decrease in body weight at day 10, which was further exacerbated at day 22 (Figure 38E). When calculating weight loss in LoxP mice, GW7647 did not have any major effect at day 10 (Figure 38F) nor at day 22 (Figure 38G). However, GW7647 induced significant weight loss in NRCA1-KO^{Alb} mice at day 10 (Figure 38F), which was even greater at day 22 (Figure 38G). Interestingly, only two doses of GW7647 were sufficient to enhance weight loss in NRCA1-KO^{Alb} mice (Figure 38F).

GW7647 treatment caused an increase in liver weight, which was more prominent in LoxP mice (Figure 38H), therefore GW7647-induced liver weight gain was slightly higher in LoxP animals (Figure 38I). Surprisingly, there were 3 out of 8 NRCA1-KO^{Alb} mice that had increased liver weight comparable to LoxP animals. Interestingly, these 3 NRCA1-KO^{Alb} mice did not show impaired PPARα activation upon agonist treatment (Figure 30).

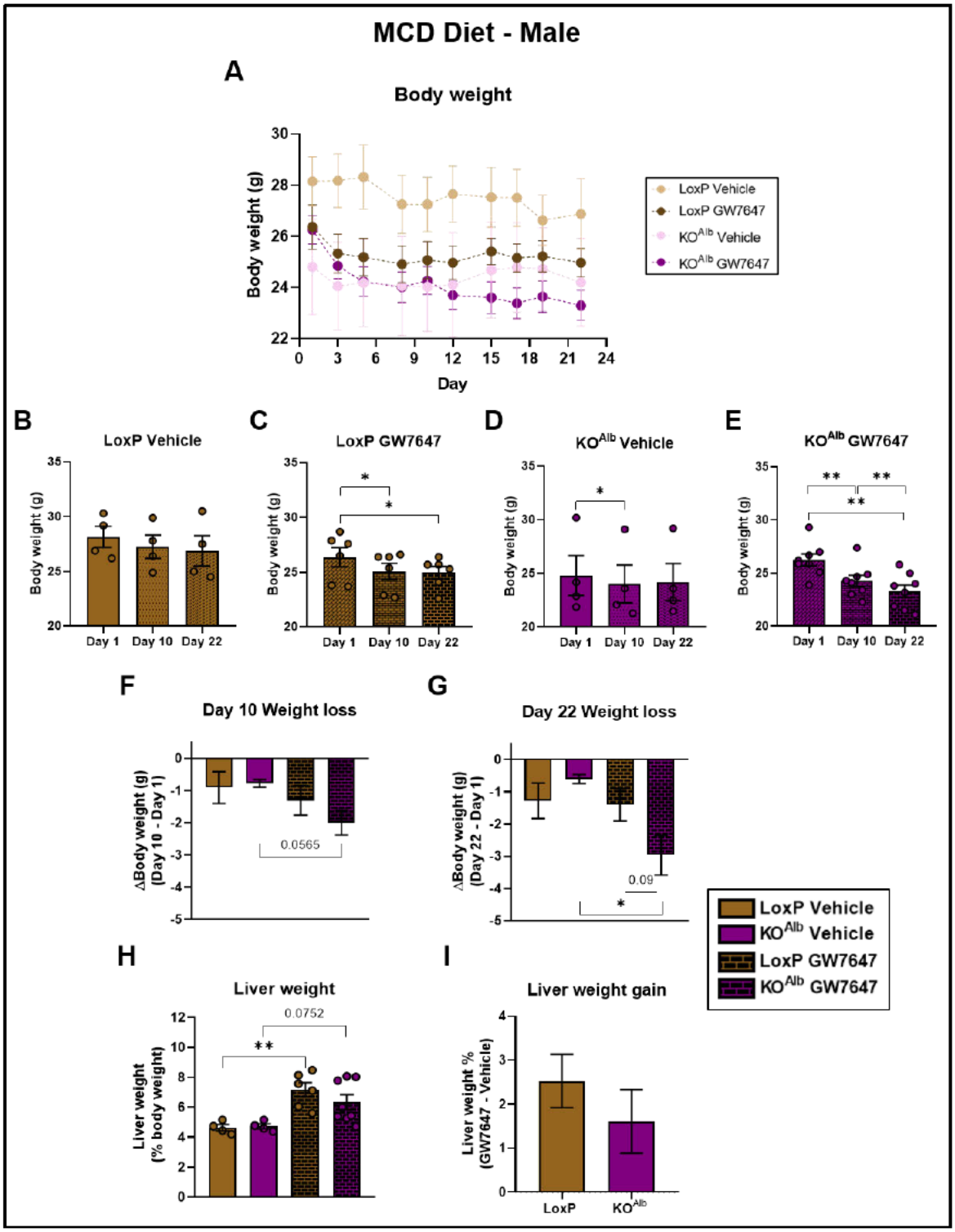

Figure 38: Effects of MCD diet and GW7647 treatment on body weight of male LoxP and NRCA1-KO^{Alb} mice. **A**) Body weight during MCD diet and GW7647 treatment. **B**) Body weight at day 10 and 22 of LoxP mice treated with vehicle. **C**) Body weight at day 10 and 22 of LoxP mice treated with GW7647. **D**) Body weight at day 10 and 19 of NRCA1-KO^{Alb} mice treated with vehicle. **E**) Body weight at day 10 and 22 of NRCA1-KO^{Alb} mice treated with vehicle. **F**) Weight loss at day 10. **G**) Weight loss at day 22. **H**) Liver weight. **I**) GW7647-induced liver weight gain. Data represented as mean ± SEM. Unpaired Student's t-test and One-way Anova test coupled with multiple-comparisons were performed. * $P < 0.05$, ** $P < 0.01$, *** $P < 0.001$.

We analyzed body composition of mice at day 10 of the MCD diet, after two doses of GW7647, and at day 19, after 9 daily doses plus the previous two doses (Figure 37). At day 10, NRCA1-KO^{Alb} mice had higher lean mass compared to LoxP mice (Figure 39A), however these differences were normalized at day 19 (Figure 39B). Treatment with GW7647 enhanced lean mass in mice of both genotypes at day 10 (Figure 39A) and at day 19 (Figure 39B). LoxP mice tended to gain more lean mass at day 10 than NRCA1-KO^{Alb} mice (Figure 39C), however this gain was normalized at day 19 (Figure 39D).

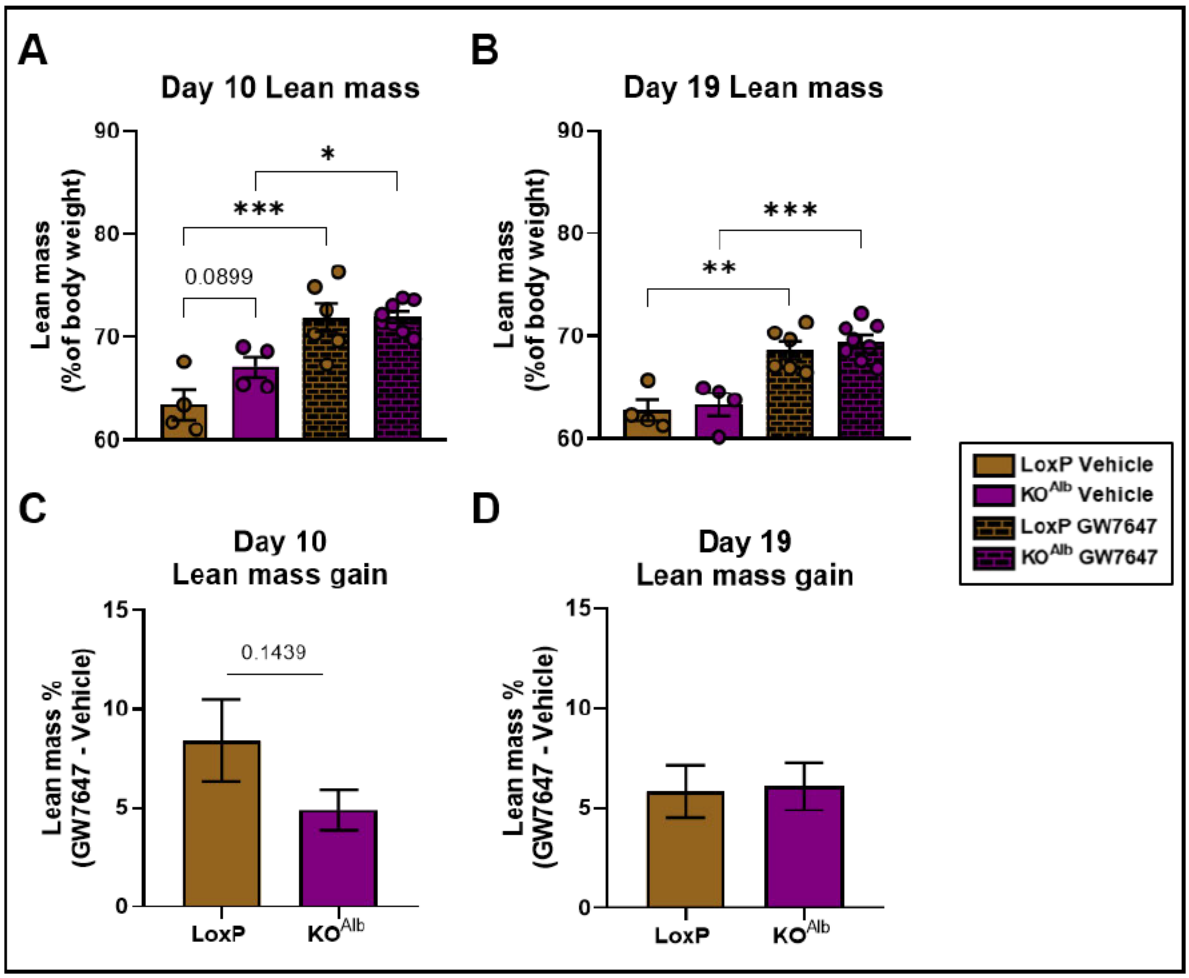

Figure 39: Effects of MCD diet and GW7647 treatment on lean mass of LoxP and NRCA1-KO^{Alb} mice. A) Lean mass at day 10. **B**) Lean mass at day 19. **C**) GW7647-induced lean mass gain at day 10 **D**) GW7647-induced lean mass gain at day 19. Data represented as mean ± SEM. One-way Anova test coupled with multiple-comparisons was performed. * $P < 0.05$, ** $P < 0.01$, *** $P < 0.001$.

In keeping with the data on lean mass, NRCA1-KO^{Alb} mice had lower fat mass at day 10 compared to LoxP mice (Figure 40A), but these differences were normalized at day 19 (Figure 40B), similarly to lean mass. Treatment with GW7647 decreased fat mass in mice of both genotypes at day 10 (Figure 40A) and at day 19 (Figure 40B). Concomitantly, epididymal WAT weight was slightly decreased by GW7647 treatment in both genotypes. LoxP mice tended to lose more fat mass at day 10 than NRCA1-KO^{Alb} mice (Figure 40C), however this loss was normalized at day 19 (Figure 40D).

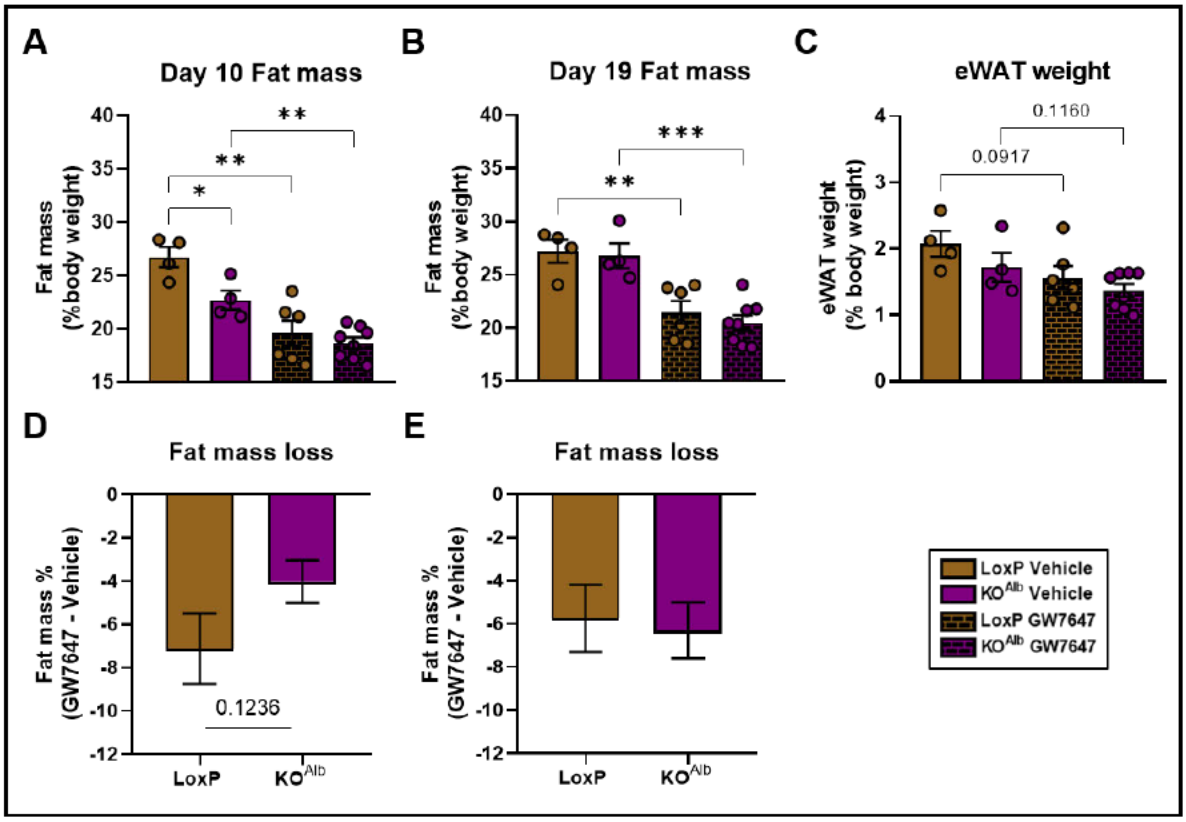

Figure 40: Effects of MCD diet and GW7647 treatment on fat mass of LoxP and NRCA1-KO^{Alb} mice. A) Fat mass at day 10. **B**) Fat mass at day 19. **C**) GW7647-induced fat mass loss at day 10 **D**) GW7647-induced fat mass loss at day 19. Data represented as mean ± SEM. Unpaired Student's t-test and One-way Anova test coupled with multiple-comparisons were performed. * $P < 0.05$, ** $P < 0.01$, *** $P < 0.001$.

All these results seem to indicate that at the beginning of the MCD diet there are differences in body composition between genotypes. However, these differences are abrogated upon extended feeding with MCD diet, probably through adaptation mechanisms. Moreover, two doses of GW7647 in a time window of 10 days were sufficient to trigger changes in body composition, namely an enhancement of lean mass and a loss of fat mass, which were more prominent in LoxP mice, without major changes in body weight.

4.2.2.2. Female mice

PPARα activation was impaired in female mice upon fasting and PPARα agonist treatment (4.1.5). Therefore, we have also evaluated the effects of one-week MCD diet in female LoxP and NRCA1-KO^{Alb} mice. In this regard, we subjected female mice around 8 weeks of age to a one-week MCD diet regime. Moreover, at day 7 we treated them with a single dose of GW7647 for 4 hours.

One week of MCD diet did not cause major changes in body weight nor in liver weight in female mice (Figure 41A/B). We observed a moderate decrease in body weight in LoxP mice after one week of MCD diet (Figure 41C), but not in NRCA1-KO^{Alb} animals (Figure 41D). In keeping with this, body weight loss tended to be enhanced in LoxP animals (Figure 41E). Interestingly, activation of PPARα upon a single dose of GW7647 was also impaired in female NRCA1-KO^{Alb} animals upon one week of MCD diet (Figure 29).

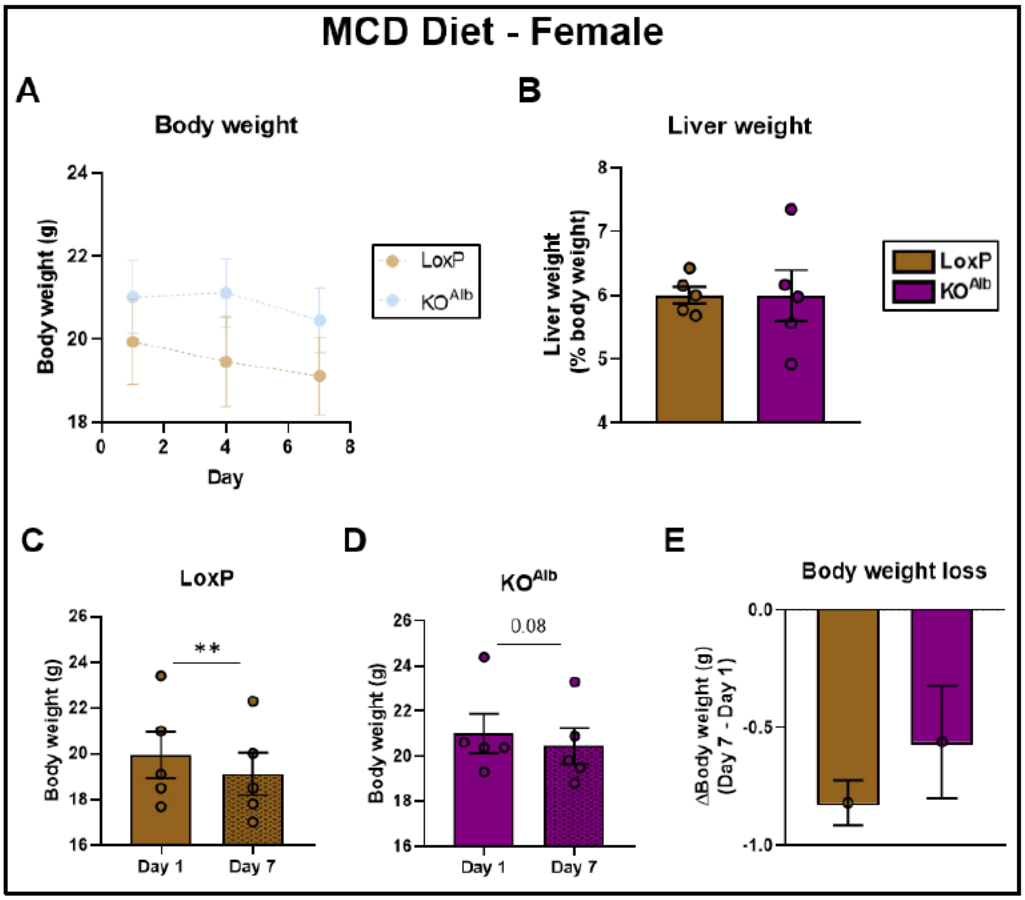

Figure 41: Effects of one-week MCD diet on body weight of female LoxP and NRCA1-KO^{Alb} mice. **A**) Body weight during one-week MCD diet. **B**) Liver weight. **C**) Body weight at day 1 and 7 of LoxP mice. **D**) Body weight at day 1 and 7 of NRCA1-KO^{Alb} mice. **E**) Body weight loss at day 7. Data represented as mean ± SEM. Unpaired and paired Student's t-test were performed. * $P < 0.05$.

4.3. Interactome studies reveal a role of NRCA1 in chromatin and epigenetic regulation

4.3.1. Generation and validation of NRCA1-TurboID construct

In order to dissect the molecular mechanism by which NRCA1 activates PPARα, we aimed to study the interactome of NRCA1. To do this, we used the BioID technology, a proximity labelling high-throughput screening method used to map protein-protein interactions in living cells and in whole organisms[110]. This method consists of fusing a biotin ligase with a protein of interest, and it has the ability to identify transient interactions. The biotin ligase biotinylates proteins near the protein of interest within a ~10 nm-radius[110]. Biotinylated proteins are selectively enriched with biotin-affinity pull-down and analyzed through mass spectrometry to identify binding partners. Typically, in BioID experiments, a control condition with the biotin ligase alone is used to rule out unspecific binding partners (Figure 42).

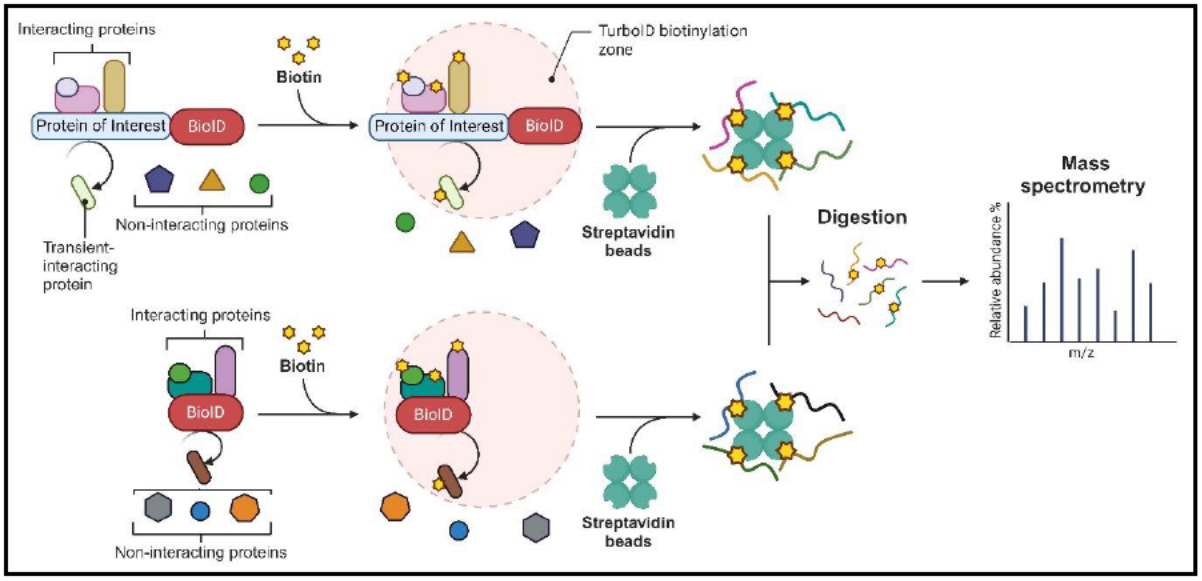

Figure 42: BioID experiment overview. A construct containing the protein of interest fused with a biotin ligase (BioID) is expressed in cells. Cells are incubated with exogenous biotin to induce biotinylation and then collected and lysed. Biotinylated proteins are enriched with biotin-affinity pulldown, i.e., with beads conjugated with streptavidin, which has a strong affinity for biotin. Proteins are subjected to digestion to obtain short peptides, which analyzed through mass spectrometry. Cells expressing BioID alone are used as control for unspecific interactions. Created with BioRender.

The BioID technology is based on the *E.Coli* promiscuous biotin ligase BirA. However, slow kinetics is a major limitation of BioID, as it requires long incubation times with biotin to induce biotinylation (i.e. 12 to 24 hours)[111]. To overcome this limitation, two faster versions of BioID were engineered using yeast display-based direct evolution on BirA, and were named TurboID (TID) and miniTurboID (mTID)[112]. TID and mTID can induce biotinylation with as little as 10 minute incubation with biotin[112], which make them ideal to study interactome dynamics. Therefore, we decided to fuse NRCA1 with TID or mTID.

To generate the fusion construct, we performed molecular cloning as described in 7.4.2.1. However, we only managed to fuse NRCA1 with TID and not mTID. TID is a biotin ligase that has a molecular weight of around 35 kDa. We fused TID at the C-terminus of NRCA1, as addition of a big tag at the N-terminus of NRCA1, such as GFP tag, disrupts its exit from the nucleus (unpublished data). The fusion construct will be referred as NRCA1-TID hereafter. NRCA1-TID contains an HA tag at the N-terminus and a V5 tag in between NRCA1 and TurboID (Figure 43).

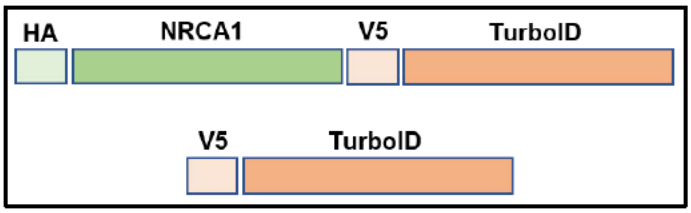

Figure 43: Scheme of NRCA1-TID fusion protein and TID alone. Created with BioRender.

Next, we proceeded to characterize the NRCA1-TID fusion protein. Biotin ligase activity can be detected quite easily through western blot analysis with streptavidin (SA)-conjugated horseradish peroxidase (HRP), as SA has a strong affinity for biotin (Figure 44). A particularity of biotin ligases is self-biotinylation, which is why a prominent 37 kDa band can be detected with SA-HRP in the presence of biotin (Figure 44). SA-HRP can also detect endogenous proteins that require biotin as cofactor, such as carboxylases[113], for this reason a 70 kDa and 140 kDa band can be observed in the absence of biotin (Figure 44).

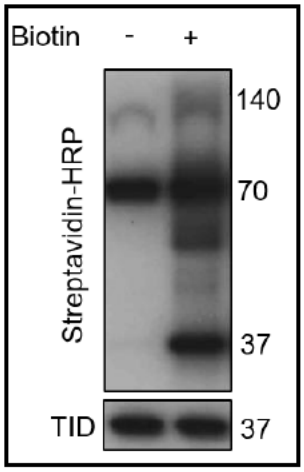

Figure 44: Detection of biotin ligase activity. HEK293T cells were transiently transfected with a plasmid encoding for TID for 24 hours. After transfection, cells were treated with (+) or without (-) 50 µM biotin during 1 hour. Cells were collected and lysed to obtain protein extracts. Western blot analysis was performed to detect biotinylation using streptavidin-HRP. Biotinylated proteins can be seen as a smear. TID was detected using an antibody against V5-tag.

First, we checked whether biotin ligase activity was preserved in NRCA1-TID. For this, we incubated cells expressing Flag-NRCA1, TID and NRCA1-TID with increasing concentrations of biotin. Biotin ligase activity was detected only in cells expressing TID or NRCA1-TID, as biotinylation is not expected to occur in cells expressing F-TP (Figure 45).

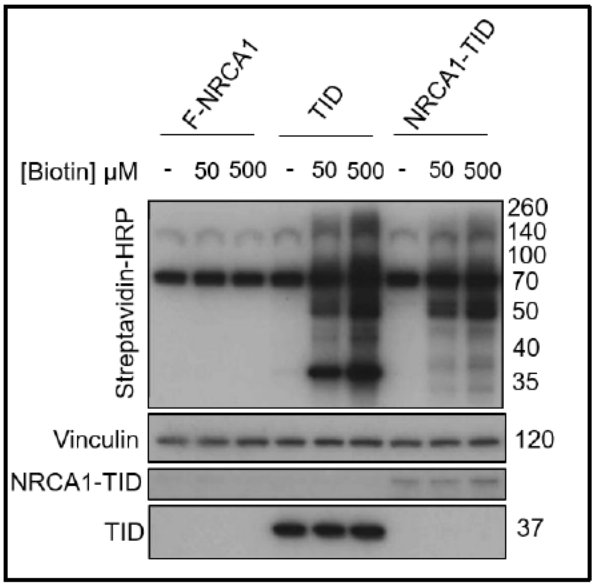

Figure 45: Biotin ligase activity is preserved in NRCA1-TID. HEK293T cells were transiently transfected with plasmids encoding for Flag-NRCA1 (F-TP), TurboID (TID) or NRCA1-TurboID (NRCA1-TID) for 24 hours. After transfection, cells were treated with 50 µM or 500 µM biotin during 1 hour. Cells were collected and lysed to obtain protein extracts. Western blot analysis was performed to detect biotinylation using streptavidin-HRP. NRCA1-TID was detected using an antibody against NRCA1. TID was detected using an antibody against V5-tag.

As NRCA1 is a protein that shuttles between the nucleus and cytoplasm[73], we performed subcellular fractionation to assess biotinylation in cytosolic and nuclear fractions. Nuclear fractions can be divided into soluble, also known as nucleoplasm, and insoluble, which contains chromatin. We also purified chromatin to assess biotinylation in chromatin (Figure 46).

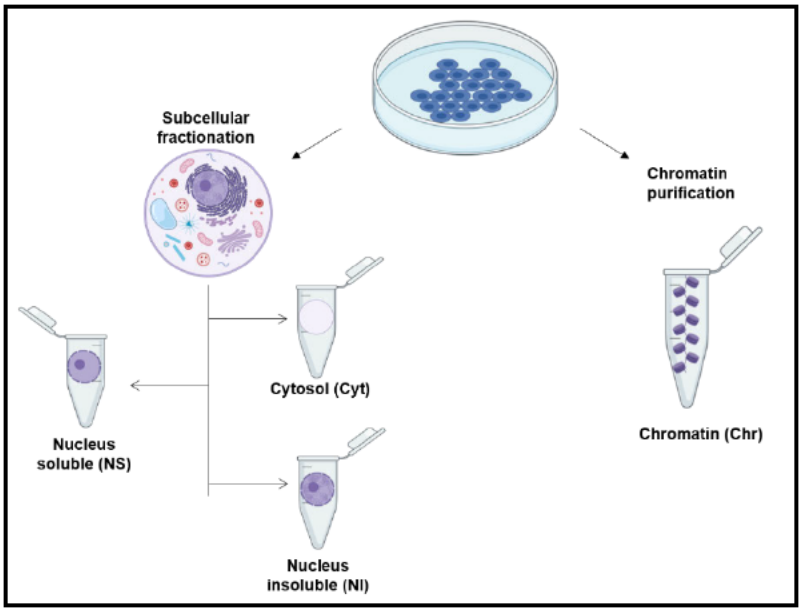

Figure 46: Subcellular fractionation assay and chromatin purification. Two plates of cells were used in this experimental setup. One of the plates was used for subcellular fractionation, which yielded cytosolic (Cyt), nuclear soluble (NS) and nuclear insoluble (NI) fractions. The other plate was used for chromatin purification, yielding chromatin (Chr). Created with BioRender.

Biotinylation occurred in all subcellular compartments, including chromatin, as shown by western blot analysis with SA-HRP (Figure 47A). To ensure there was no cross-contamination among the different fractions, we performed western blot analysis to detect markers of each fraction. GAPDH was only enriched in cytosolic fraction, RING1A was enriched in nuclear soluble fraction and slightly enriched in nuclear insoluble and in chromatin, histone H2A was only enriched in nuclear insoluble fraction and in chromatin (Figure 47B). TurboID and NRCA1-TID were found in all the compartments. Surprisingly, Flag-NRCA1 was mostly enriched in nuclear insoluble fraction and in chromatin (Figure 47B).

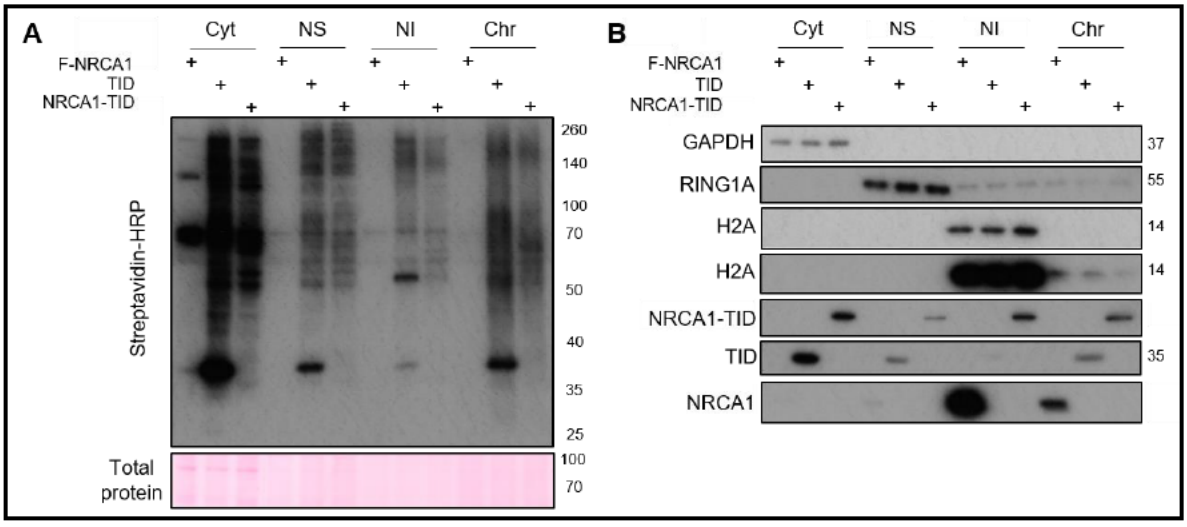

Figure 47: Biotinylation occurs in all subcellular fractions and chromatin. HEK293T cells were transiently transfected with plasmids encoding for Flag-NRCA1 (F-TP), TurboID (TID) or NRCA1-TurboID (NRCA1-TID) for 24 hours. After transfection, cells were treated with 50µM biotin during 1 hours. Cells were collected and subcellular fractionation was performed, yielding cytosolic (Cyt), nuclear soluble (NS) and nuclear insoluble (NI) fractions. In parallel, chromatin (Chr) was also obtained through chromatin purification. **A)** Western blot analysis was performed to detect biotinylation using streptavidin-HRP. Biotinylated proteins can be seen as a smear. **B)** Western blot analysis was performed to detect protein markers of different fractions to ensure proper fraction enrichment.

Next, we optimized the amount of SA-coated magnetic beads for the biotin-affinity pulldown assay. For this, we incubated protein extracts with different amounts of beads. The ideal ratio of beads (µL)/protein (mg) to enrich for biotinylated proteins was 20 µL of beads/mg of protein, as no biotinylated proteins remained in the flowthrough fractions (Figure 48B). NRCA1 is an activator of autophagy, for that reason we included a starvation condition (EBSS) in order to identify NRCA1 binding partners under basal and nutrient deprivation conditions.

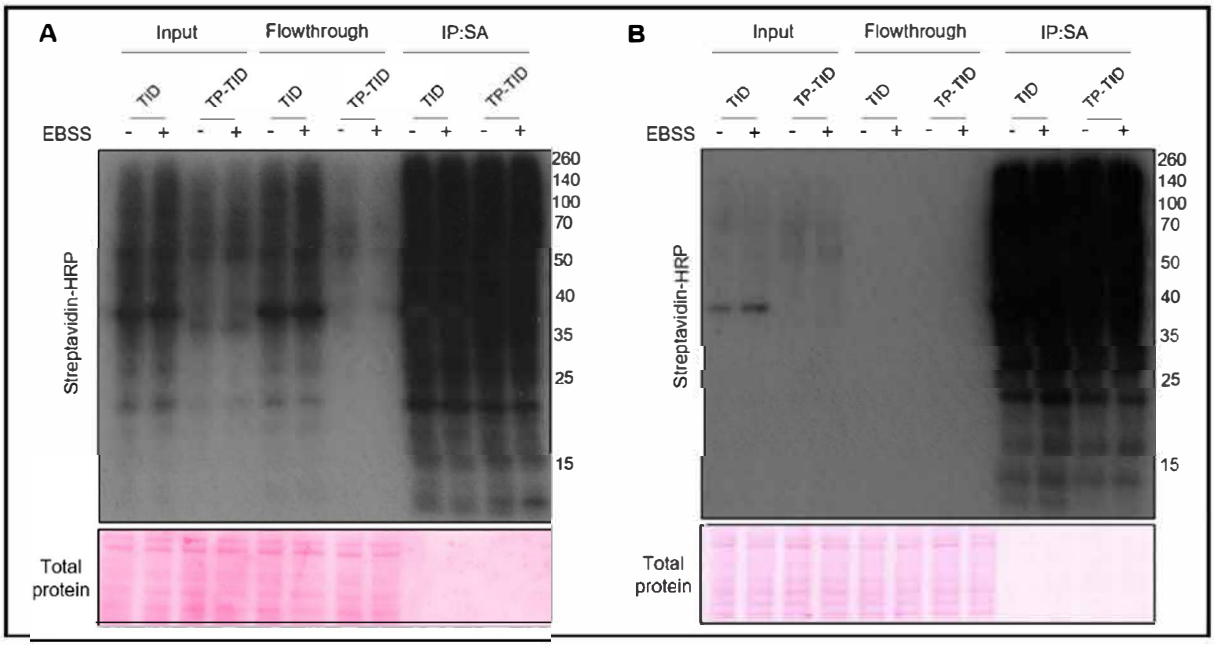

Figure 48: Optimization of biotin-affinity pulldown assay. HEK293T cells were transfected with plasmids encoding for TurboID (TID) or NRCA 1-TurboID (NRCA 1-TID or Target Protein (TP)-TiD) for 24 hours. After transfection, cells were incubated with (+) or without (-) starvation media EBSS and 50µM biotin for 1 hour. Cells were collected and lysed, and pulldown assay with streptavidin-coated magnetic beads was performed. Western blot analysis was performed to detect biotinylation using HRP-conjugated streptavidin. A considerable enrichment of biotinylated proteins can be seen in the pulldown fractions (IP:SA). **A)** Protein extracts were incubated with a ratio of 12 µL beads/mg of protein. **B)** Protein extracts were incubated with a ratio of 20 µL beads/ mg of protein.

NRCA1 interacts with key proteins that are located in autophagosomes, such as GABARAP and LC3[redacted]. To validate whether NRCA1-TID is a functional NRCA1 protein, we performed biotin-affinity pulldown assays with SA-coated magnetic beads to check whether NRCA1-TID was able to interact with proteins located in autophagosomes. Pulldown with SA-coated beads is very efficient as it yields a huge enrichment of biotinylated proteins (Figure 48B). NRCA1-TID is able to interact with several proteins involved in autophagy, including GABARAP, under basal and autophagy-activating conditions (starvation) (Figure 49).

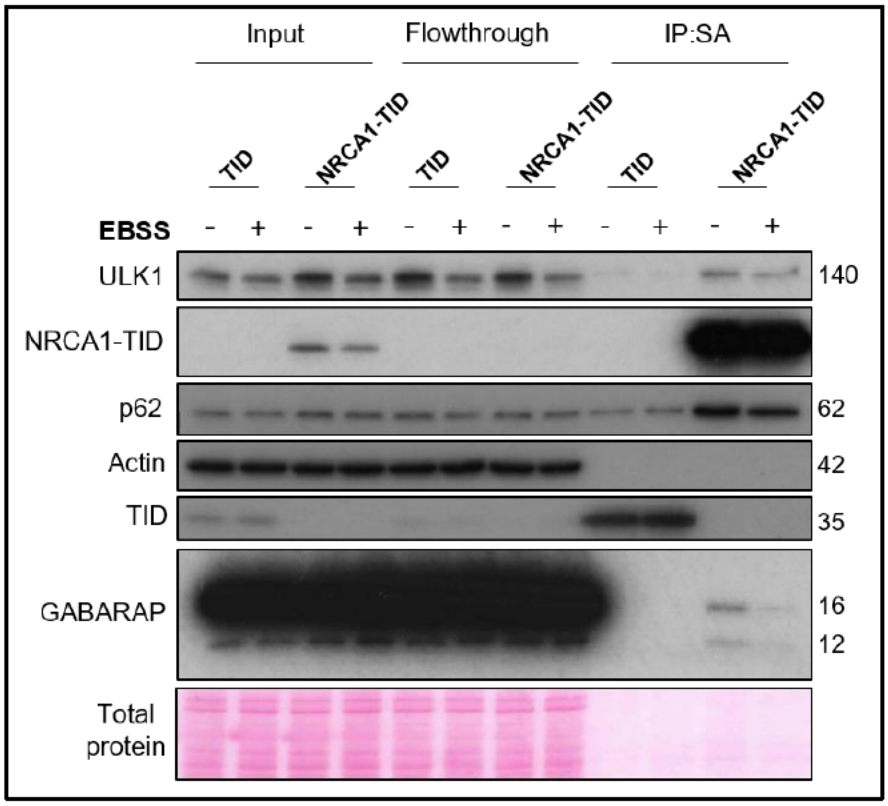

Figure 49: NRCA1-TID interacts with known NRCA1 interactors. HEK293T cells were transfected with plasmids encoding for TurboID (TID) or NRCA1-TurboID (NRCA1-TID) for 24 hours. After transfection, cells were incubated with (+) or without (-) starvation media EBSS and 50µM biotin for 1 hour. Cells were collected and lysed, and pulldown assay with streptavidin-coated magnetic beads was performed. **A)** Western blot analysis of different proteins involved in autophagy. Enrichment of ULK1, p62 and GABARAP in pulldown fractions (IP:SA) of NRCA1-TID-transfected cells indicates interaction. **B)** Quantification of ULK1, p62 and GABARAP enrichment in IP:SA fractions. One-way Anova test coupled with multiple-comparisons was performed. * $P < 0.05$, ** $P < 0.01$, *** $P < 0.001$.

4.3.2. Mass spectrometry pilot experiment

After validating NRCA1-TID, we performed a pilot experiment. TID alone was used as a control for unspecific interactions. To ensure that the TurboID worked, we checked whether we could detect known NRCA1 interactors in the proteomics analysis. To maximize discovery in the proteomics analysis, we run the samples through two different mass spectrometers (Orbitrap Lumos and Orbitrap Eclipse), performed protein identification and quantification using two different search engine platforms (MaxQuant and Proteome Discoverer) and used two different interactome analysis algorithms (SAINTe and SAINTq), as described in 7.5.2. By setting a fold-change (FC) ≥ 2.5 and a Bayesian false discovery rate (BFDR) ≤ 0.1, we identified 401 and 296 binding partners under basal and starvation conditions, respectively. 169 proteins were shared between the two conditions, 228 proteins were exclusive for basal conditions and 128 proteins were exclusive for starvation conditions (Figure 50) We could detect NCOR1, a nuclear corepressor protein, known to interact with NRCA1, under both conditions. We could also detect ATG2B under both conditions, a protein involved in autophagy regulation[114].

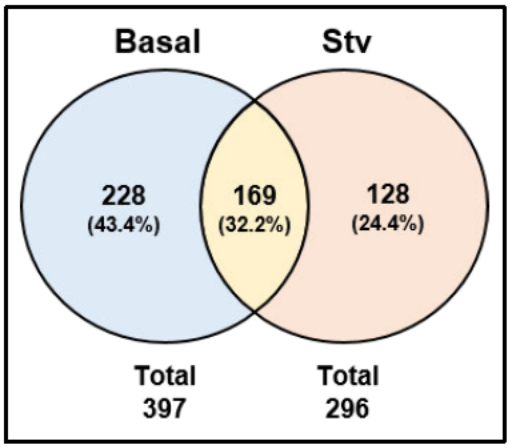

Figure 50: Venn diagram of proteomics analysis. Comparison between basal and starvation (Stv) conditions.

We performed gene set enrichment analysis (GSEA). Under basal conditions, top enriched gene sets indicate that NRCA1 interacts with many chromatin-binding proteins that are involved in the epigenetic regulation of gene expression (Figure 51). These data suggest that NRCA1 may be involved in the regulation of epigenetics, which would be in agreement with the role NRCA1 plays in transcription regulation (2.3.1).

Even though Venn diagram analysis showed 24.4% of exclusive interactors under starvation conditions (Figure 50), top enriched gene sets under starvation were very similar to that of basal conditions (Figure 52). These results suggest that while starvation induces some changes in NRCA1 interactors, these interactors are involved in the same biological processes, molecular functions and cellular components.

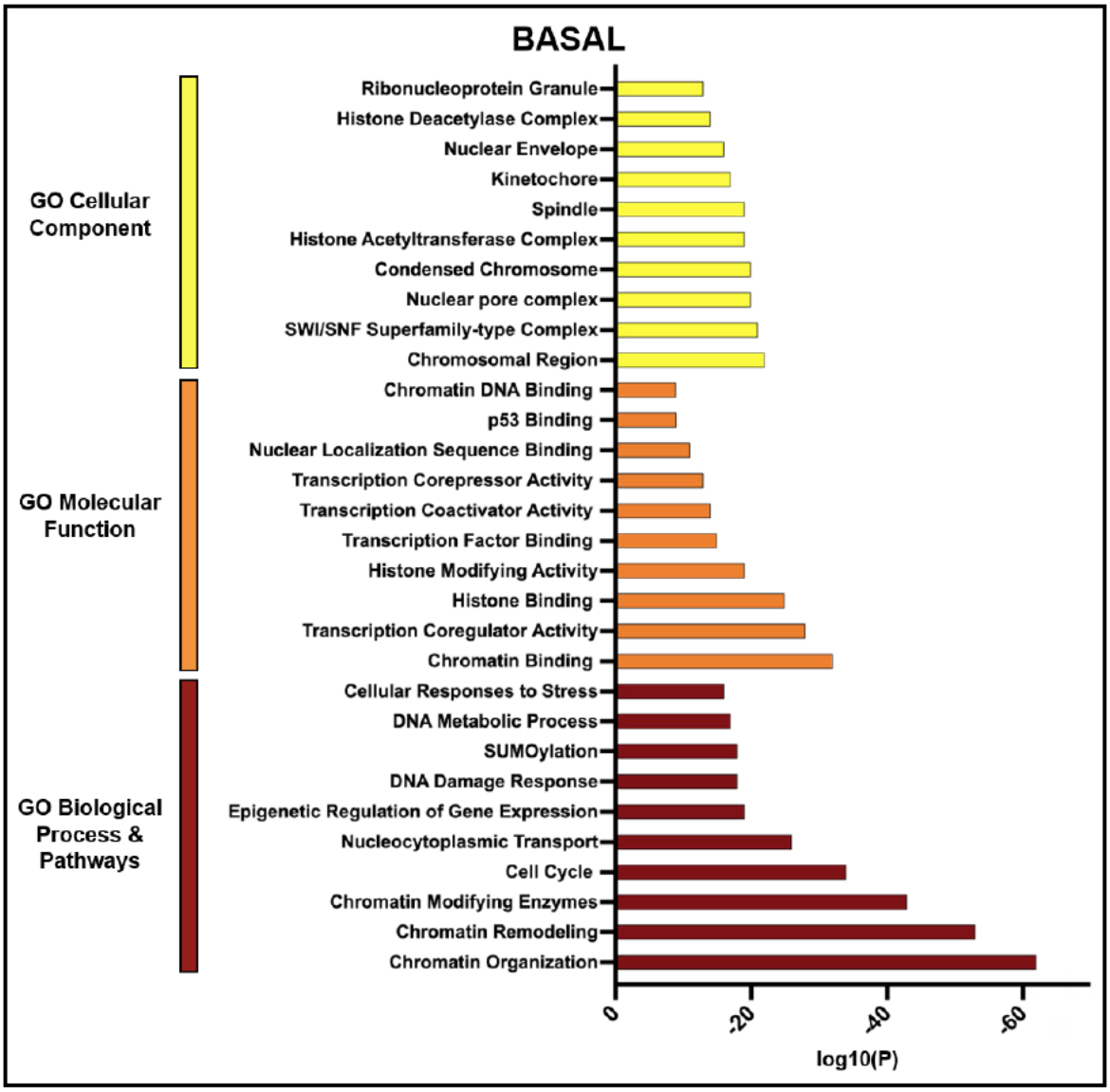

Figure 51: Gene set enrichment analysis of binding partners under basal conditions. Top 10 enriched gene ontology (GO) terms for biological process and pathways, molecular function, and cellular component are shown. Analysis was performed using Metascape software[115]. Statistical significance is shown as log10 of the p value.

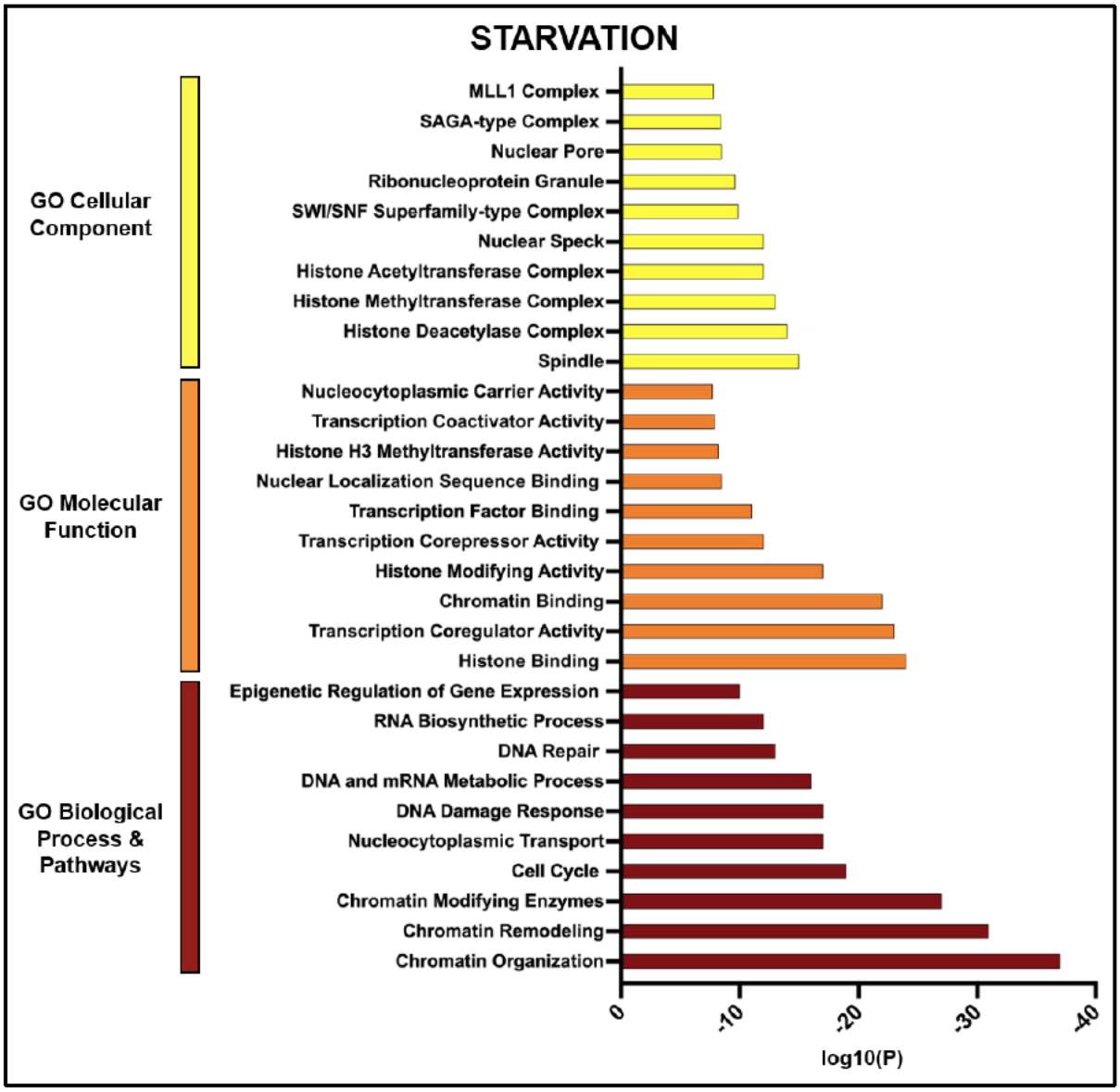

Figure 52: Gene set enrichment analysis of binding partners under starvation conditions. Top 10 enriched gene ontology (GO) terms for biological process and pathways, molecular function, and cellular component are shown. Analysis was performed using Metascape software[115]. Statistical significance is shown as log10 of the p value.

4.3.3. Mass spectrometry experiment

In the pilot experiment, gene sets enriched under starvation conditions were very similar to that of basal conditions, therefore, we decided not to perform the proteomic analysis under starvation conditions. Although the pilot experiment was performed with one biological replicate and three technical replicates, the detection of NCOR1, which is a known interactor of NRCA1, provided us confidence that the TurboID assay worked.

We performed the mass spectrometry experiment with 4 biological replicates. To maximize discovery in the analysis, we used the same strategy as in the pilot experiment. We run the samples through two different mass spectrometers (Orbitrap Lumos and Orbitrap Eclipse), performed protein identification and quantification using two different search engine platforms (MaxQuant and Proteome Discoverer) and used two different interactome analysis algorithms (SAINTe and SAINTq), as described in 7.5.2. We noticed that in this experiment, we needed to be less restrictive with the BFDR to identify interactors, therefore we set a BFDR ≤ 0.2, but we increased the fold-change (FC) ≥ 3. We identified a total of 233 interactors.

In the interactome studies, we were particularly interested in finding ubiquitin ligases as NRCA1 has a UIM (Figure 5), and also because ubiquitin ligases regulate stability of their target proteins through degradation[116], including NRs[117,118]. In the pilot experiment, we detected several ubiquitin ligases, including RING1, UBR5, and UBE2O, among others.

In this experiment, we could again detect NCOR1, and also GABARAPL2, another known interactor of NRCA1 involved in the regulation of autophagy. In addition, we could also detect the ubiquitin ligases identified in the pilot experiment (RING1, UBR5 and UBE2O). Next, we performed GSEA. Top enriched gene sets (Figure 53) were similar to those enriched in the pilot experiment (Figure 51). The most significant gene ontology (GO) terms for biological process, molecular function and cellular component were all related to chromatin, histone modifications and epigenetics (Figure 53). Interestingly, NRCA1 seems to interact with many proteins that bind to NRs and have coregulator activity (Figure 54), which could explain NRCA1 NR coactivator activity, including activation of PPARα observed in this thesis.

Since many of the interactors found in the pilot and in the actual experiment were the same, and GSEA yielded similar results, we decided to combine both datasets and performed GSEA (Figure 55). This resulted in a total number of 526 binding partners that were enriched in gene sets related to chromatin, epigenetic regulation, transcription coregulators, and nuclear receptors.

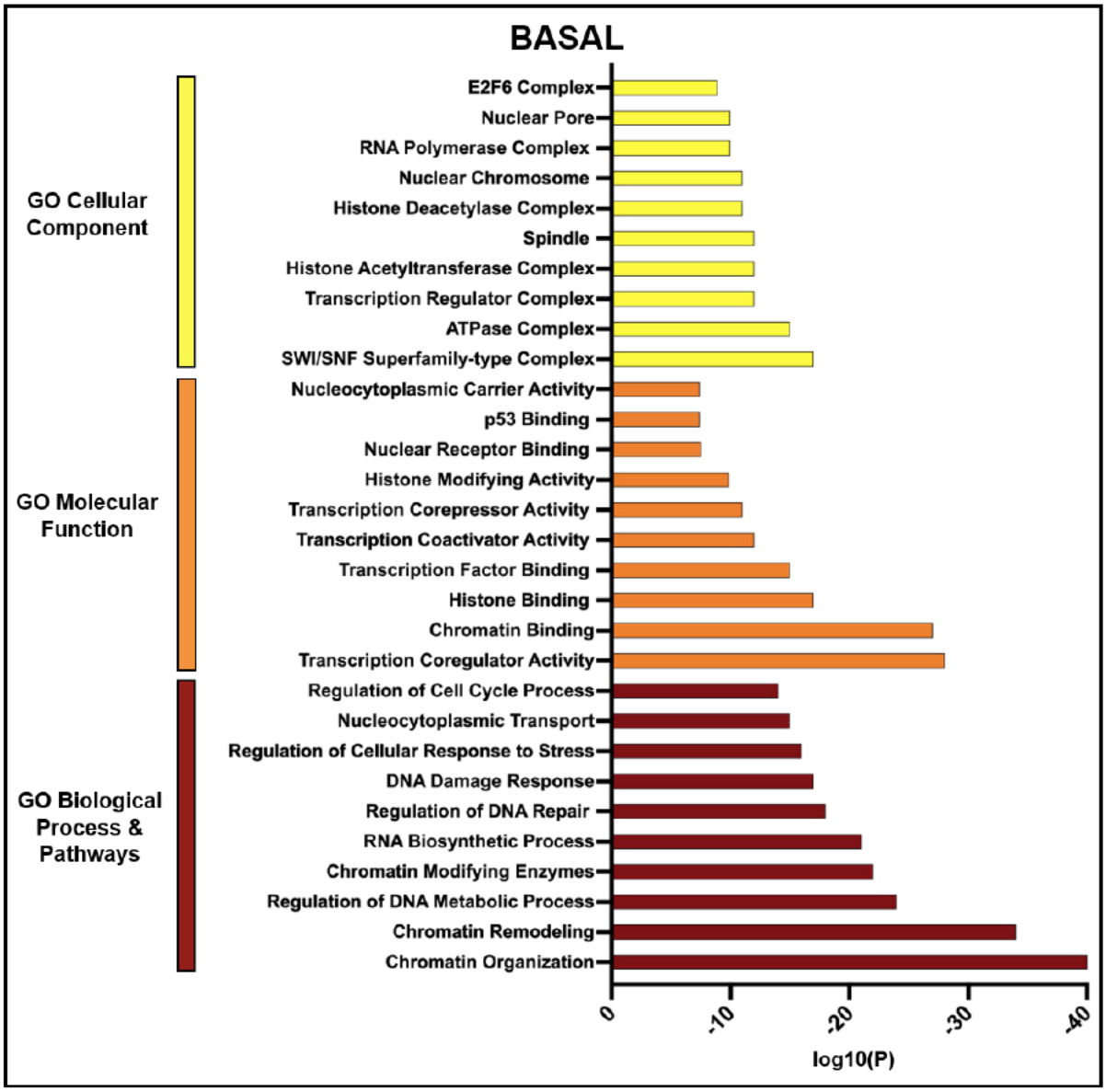

Figure 53: Gene set enrichment analysis of binding partners under basal conditions. Top 10 enriched gene ontology (GO) terms for biological process and pathways, molecular function, and cellular component are shown. Analysis was performed using Metascape software[115]. Statistical significance is shown as log10 of the p value.

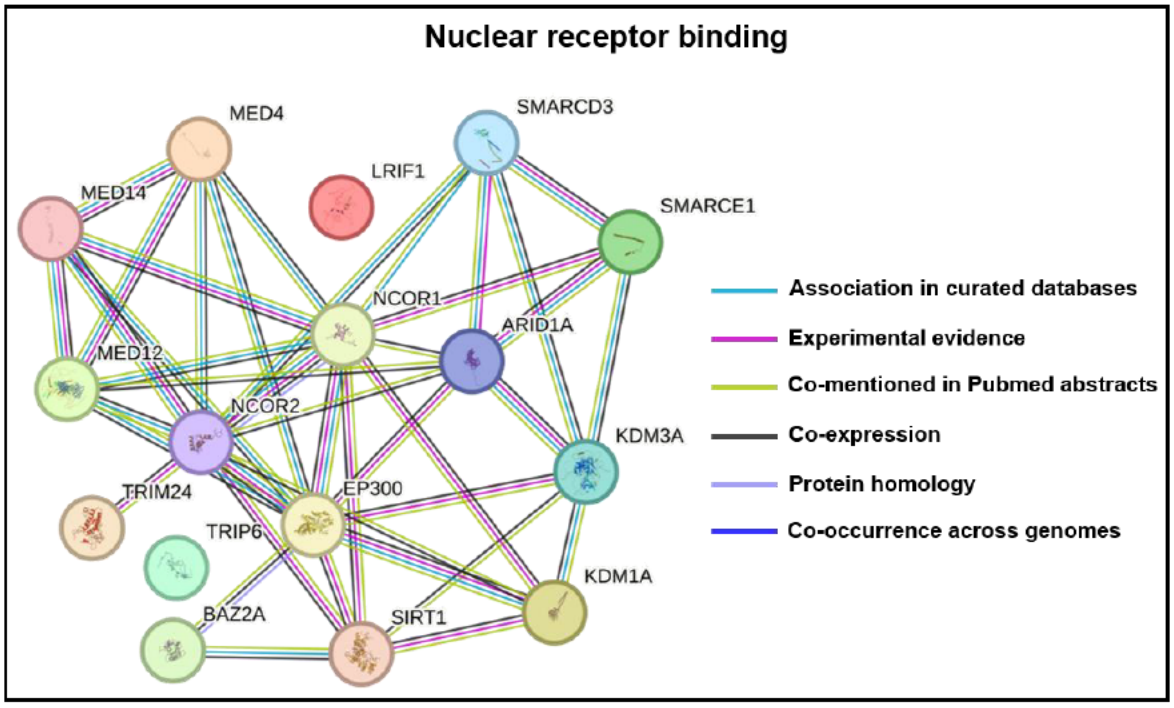

Figure 54: Interaction network of proteins with nuclear receptor binding function found in our proteomic analysis. Each node represents a protein. The content in the nodes shows that there is a known or predicted 3D structure for that particular protein. Different coloured edges represent protein-protein associations at different levels, i.e. proteins that jointly contribute to a shared function, although it does not necessarily mean they are physically binding to each other. Elaborated with StringDB.

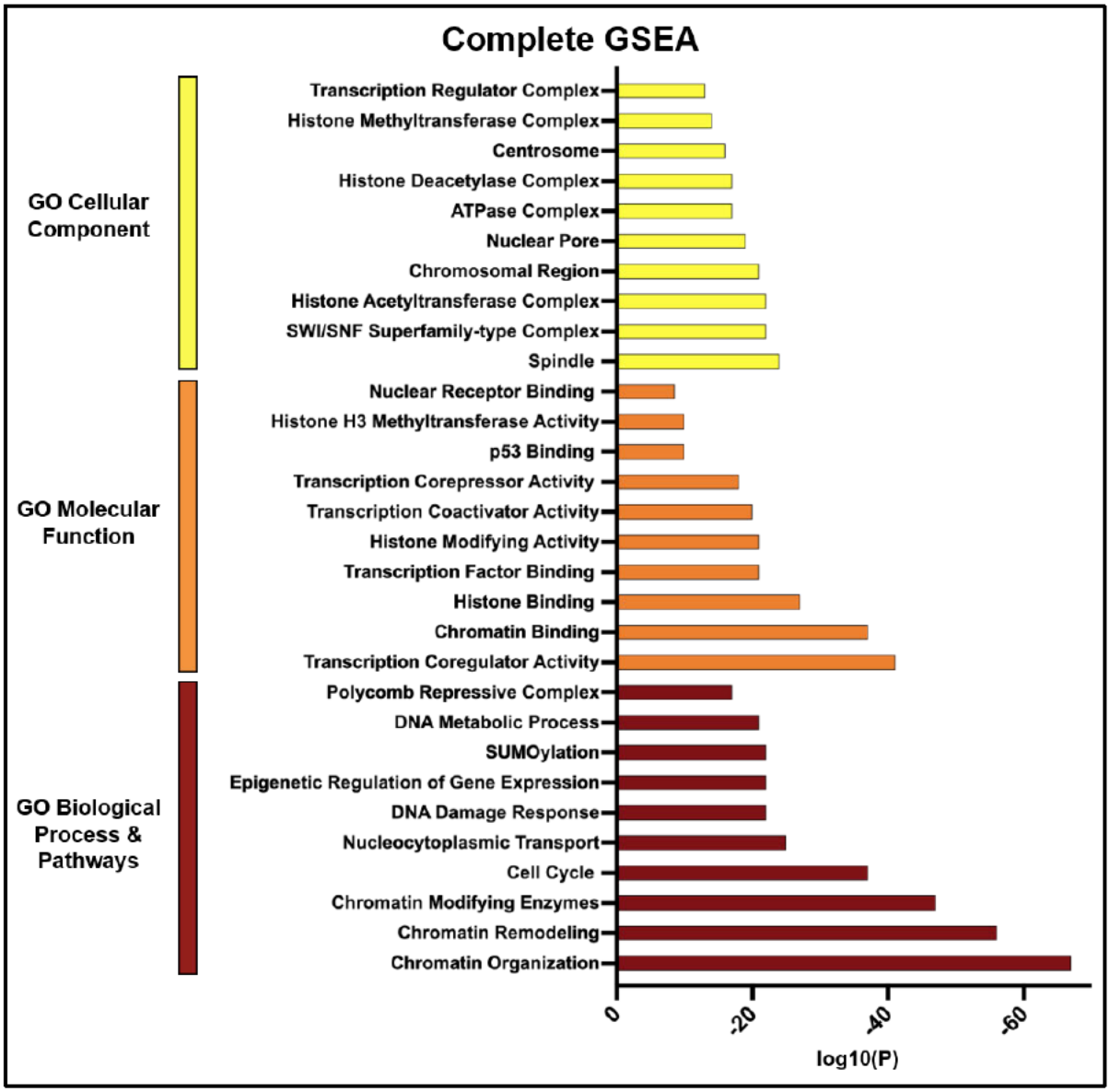

Figure 55: Gene set enrichment analysis of binding partners under basal conditions identified in the pilot experiment and in the final experiment. Top 10 enriched gene ontology (GO) terms for biological process and pathways, molecular function, and cellular component are shown. Analysis was performed using Metascape software[115]. Statistical significance is shown as log10 of the p value.

4.3.4. Validation of interactors

As we mentioned previously, we were particularly interested in finding ubiquitin ligases in the interactome studies. The ubiquitin ligases that we identified in the proteomic analysis were RING1, UBE2O and UBR5. Ubiquitin ligases are key players in the ubiquitination cascade. First, ubiquitin is activated in an ATP-dependent manner by ubiquitin-activating enzymes (E1s), followed by the transfer of the activated ubiquitin to ubiquitin-conjugating enzymes (E2s), thereby forming an E2~ubiquitin complex. Finally, ubiquitin can be transferred to the substrate directly by the E2[119] or via ubiquitin ligases (E3s). E3s act as a scaffold by binding to both the substrate and the E2s~ubiquitin complex to facilitate substrate ubiquitination[116]. When the E2~ubiquitin—E3—substrate complex is formed, depending on the type of E3, ubiquitin is transferred by the E2 (this is the case for RING E3s, the predominant type of E3s) or by the E3 itself (this is the case for HECT E3s and RING-between-RING E3s)[120] (Figure 56).

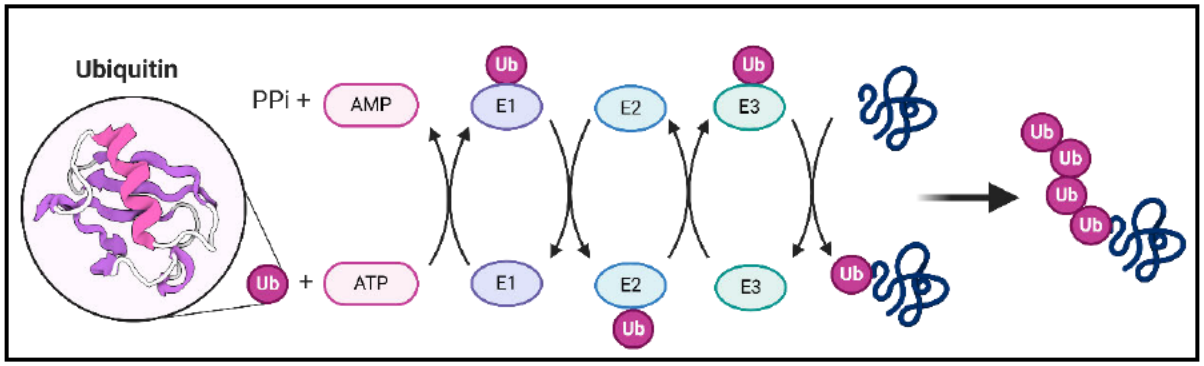

Figure 56: Overview of ubiquitination cascade. Created with BioRender.

RING1, also known as RING1A, is the catalytic core of the polycomb repressive complex 1 (PRC1)[121]. RING1A has a paralog protein, RING1B (also known as RNF2), which can also be the catalytic component of PRC1[121]. The PRC1 is a chromatin-binding complex that monoubiquitinates histone H2A at lysine 119 (H2AK119ub1) to mediate transcriptional repression on target genes. RING1A and RING1B have non-redundant functions in mouse development, as RING1B deficiency arrests embryo development during gastrulation[122], whereas RING1A null embryos reach birth, although with some alterations in the axial skeleton[123]. However, mouse embryonic stem cells expressing catalytically-inactive RING1B retained some H2AK119ub1, indicating that RING1A also contributes to H2AK119ub1[124]. In fact, it has been shown that RING1B is the main E3 responsible for H2AK119ub1 in pluripotent cells[125]. However, in breast cancer cells, it seems that RING1A is more important for H2AK119ub1 than RING1B[126]. Interestingly, PRC1 seems to target genes involved in the regulation of metabolism in mouse embryonic stem cells[127] and breast cancer cells[126]. The ubiquitination of histone H2A leads to recruitment of the polycomb repressive complex 2 (PRC2), which mediates trimethylation of H3 at lysine 27 (H3K27me3) to mediate transcriptional repression[128]. Interestingly, in our mass spectrometry experiment, we could also detect 19 other members of the PRC1 (Figure 57).

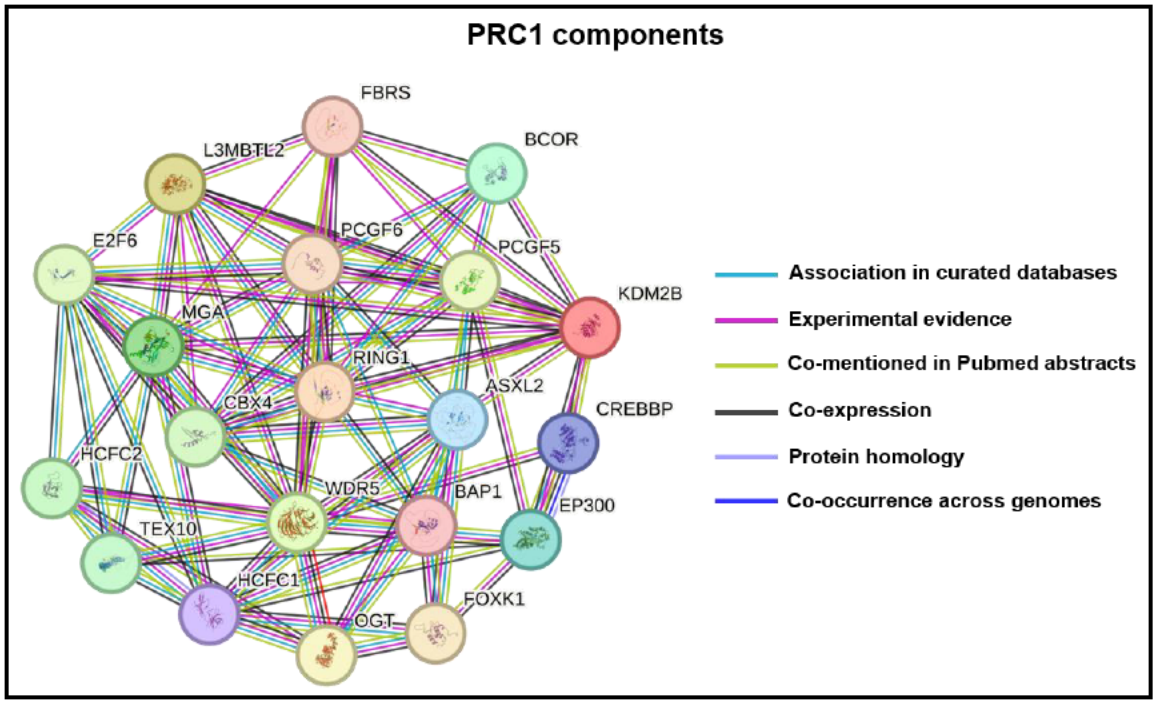

Figure 57: Interaction network of components of PRC1 detected in our proteomic analysis. Each node represents a protein. The content in the nodes shows that there is a known or predicted 3D structure for that particular protein. Different coloured edges represent protein-protein associations at different levels, i.e. proteins that jointly contribute to a shared function, although it does not necessarily mean they are physically binding to each other. Elaborated with StringDB.

UBE2O is a hybrid E2/E3 involved in many cellular functions[129]. Two independent studies showed that UBE2O is a quality control factor that marks orphan proteins for degradation[130,131], i.e. proteins that are subunits of multiprotein complexes that were not incorporated into the complexes, to maintain proteome homeostasis. For instance, UBE2O promotes the degradation of cytosolic orphan ribosomal proteins[130], which is necessary for terminal erythroid differentiation[131]. UBE2O also regulates several aspects of metabolism such as adipogenesis[132], skeletal muscle biology and insulin sensitivity[133] and liver lipid metabolism[134].

UBR5 is a HECT E3 involved in the regulation of nuclear processes. It is involved in the regulation of the DNA damage response at different levels[135–138]. UBR5 is a quality control factor of orphan transcriptional regulators[139]. Unpaired transcriptional subunits, which may arise from cellular stress, are degraded by UBR5, thus permitting the effective execution of gene expression programs[139]. Moreover, UBR5 was identified as a regulator of the stability of NRs by promoting the degradation of many NRs, including GR and ER, among others[117]. In this regard, UBR5 interacts with NRs in a ligand-dependent manner on chromatin, which may serve as a negative feedback mechanism to terminate ligand activation of NRs[117]. Interestingly, UBR5 was found to interact with WDR5[140] and BMI1[141], both components of PRC1. Along these lines, silencing of BMI1, RING1A or RING1B impaired UBR5 recruitment to damaged chromatin. The BMI1-containing PRC1 is involved in transcriptional repression on damaged chromatin in response to DNA damage[142] and UBR5 was identified as a downstream effector in this pathway[141].

Taking into consideration the literature regarding RING1A, UBE2O and UBR5, we proceeded to validate the interaction between NRCA1 and these E3s. First, we performed non-endogenous pulldown assays overexpressing Flag-tagged RING1A, UBE2O or UBR5 (as bait) and wild-type (WT) NRCA1 (as prey) in HEK293T cells. We could see interaction between NRCA1 and all the Flag-tagged E3s (Figure 58, Figure 59 and Figure 60).

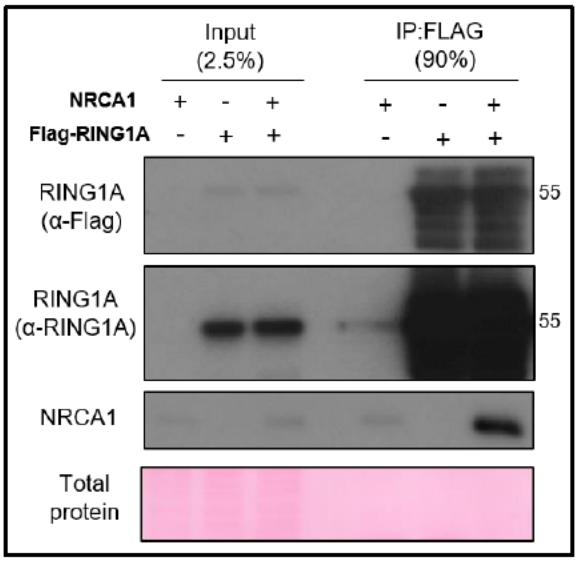

Figure 58: RING1A interacts with NRCA1. HEK293T cells were transiently co-transfected with a plasmid encoding for Flag-RING1A and a plasmid encoding for NRCA1. Cells were collected after 24 hours of transfection and lysed. Protein extracts were incubated with magnetic beads coated with anti-Flag monoclonal antibodies to pulldown Flag-tagged RING1A. Western blot analysis was performed to detect proteins of interest. A considerable enrichment of NRCA1 in IP:FLAG fractions can be observed, indicative of interaction.

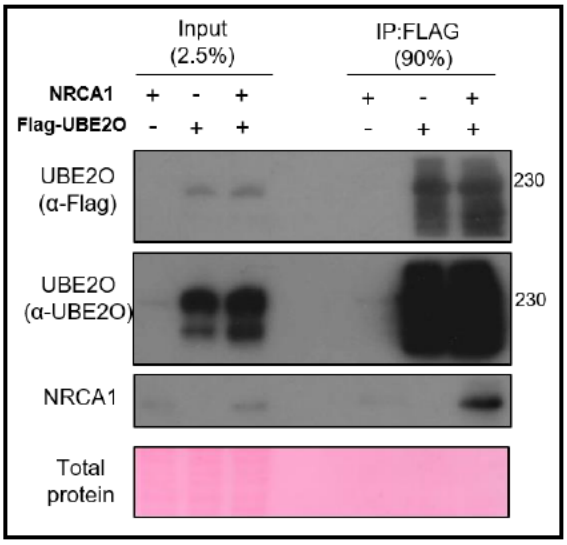

Figure 59: UBE2O interacts with NRCA1. HEK293T cells were transiently co-transfected with a plasmid encoding for Flag-UBE2O and a plasmid encoding for NRCA1. Cells were collected after 24 hours of transfection and lysed. Protein extracts were incubated with magnetic beads coated with anti-Flag monoclonal antibodies to pulldown Flag-tagged UBE2O. Western blot analysis was performed to detect proteins of interest. A considerable enrichment of NRCA1 in IP:FLAG fractions can be observed, indicative of interaction.

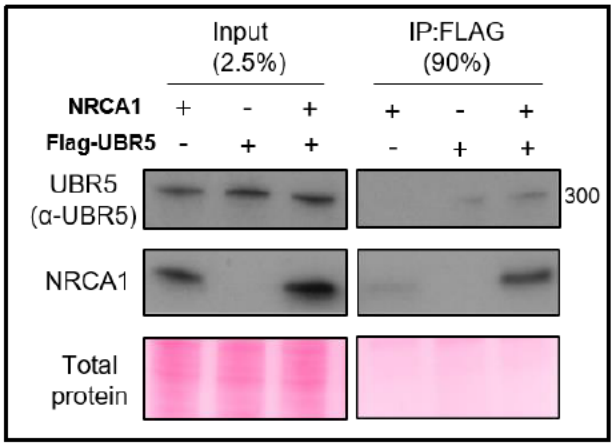

Figure 60: UBR5 interacts with NRCA1. HEK293T cells were transiently co-transfected with a plasmid encoding for Flag-UBR5 and a plasmid encoding for NRCA1. Cells were collected after 24 hours of transfection and lysed. Protein extracts were incubated with magnetic beads coated with anti-Flag monoclonal antibodies to pulldown Flag-tagged UBR5. Western blot analysis was performed to detect proteins of interest. A considerable enrichment of NRCA1 in IP:FLAG fractions can be observed, indicative of interaction.

To further validate these interactions, we conducted semi-endogenous pulldown assays in HeLa cells stably overexpressing GFP or NRCA1-GFP by using GFP as bait and detecting endogenous RING1A, UBE2O and UBR5. To validate the NRCA1-GFP cell line, we proved that NRCA1-GFP could interact with GABARAP and p62 (unpublished). Under these conditions, we could observe interaction between NRCA1 and the E3s (Figure 61).

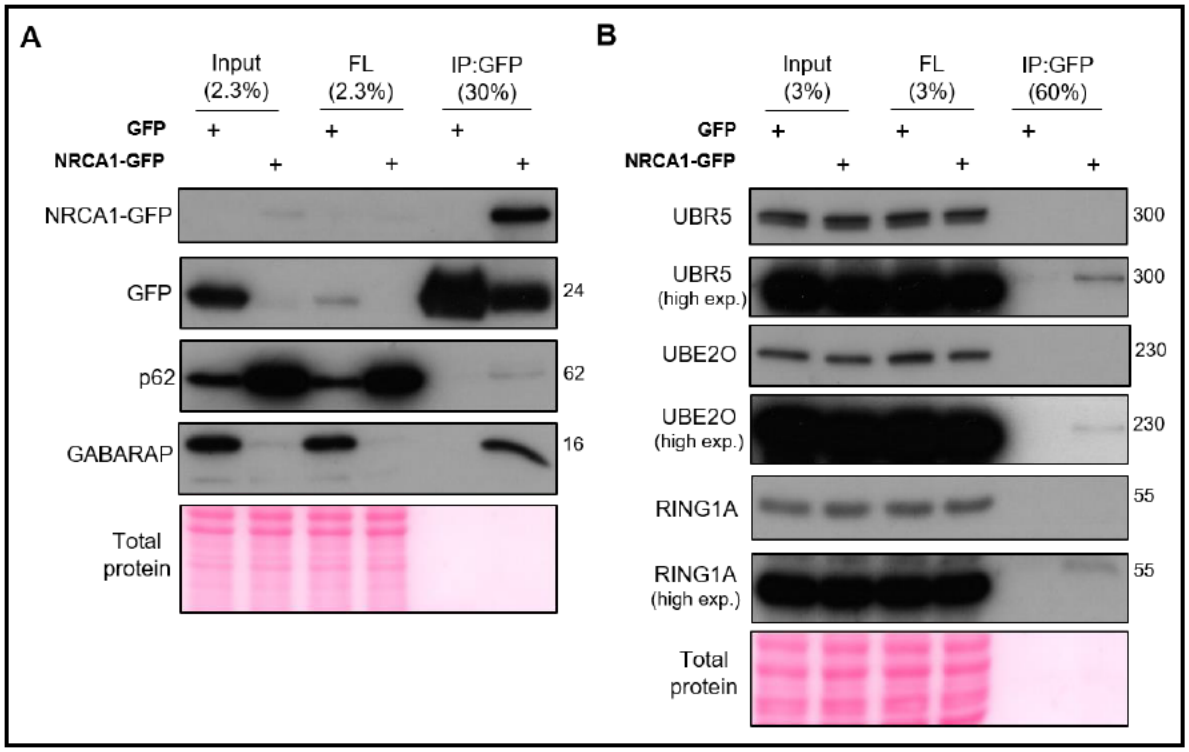

Figure 61: NRCA1 interacts with RING1A, UBE2O and UBR5. HeLa cells stably overexpressing GFP or NRCA1 (TP-GFP) were collected and lysed. Protein extracts were incubated with magnetic beads coated with GFP-trap. Western blot analysis was performed to detect proteins of interest. **A**) Shows interactions between NRCA1 and p62, and NRCA1 and GABARAP. **B**) Shows interaction between NRCA1 and E3s.

4.4. NRCA1 is a chromatin-binding protein

Considering the GSEA data from the interactome studies (Figure 55), and that NRCA1 interacts with RING1A and UBR5, we asked whether NRCA1 could be a chromatin-binding protein. To elucidate this, we performed subcellular fractionation assays and chromatin purification assays (Figure 46). We checked this in HEK293T transiently overexpressing Flag-NRCA1 and WT NRCA1. We observed that both proteins were highly enriched in nuclear insoluble fraction and purified chromatin (Figure 62). We could also see endogenous NRCA1 enriched in chromatin in different cell lines, including SH-SY5Y and Ishikawa (Figure 63), and HAP1 and C2C12 cells (Figure 64).

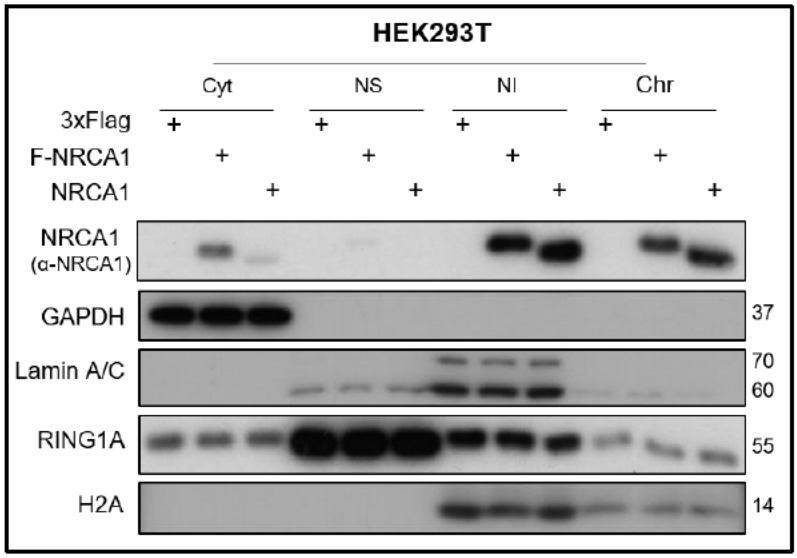

Figure 62: NRCA1 is a chromatin-binding protein. HEK293T cells were transiently transfected with plasmids encoding for 3xFlag, Flag-NRCA1 (F-TP) or WT NRCA1 in two different plates. After 24 hours of transfection, one of the plates was used for subcellular fractionation, which yielded cytosolic (Cyt), nuclear soluble (NS) and nuclear insoluble (NI) fractions. The other plate was used for chromatin purification, yielding chromatin (Chr). Western blot analysis was performed to detect proteins of interest in the different fractions.

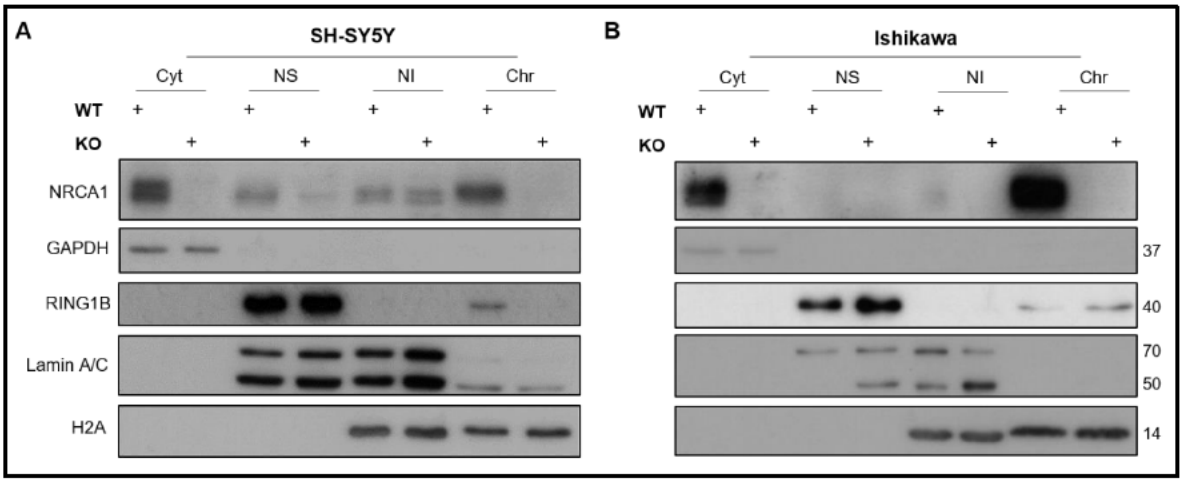

Figure 63: Endogenous NRCA1 is a chromatin-binding protein in SH-SY5Y and Ishikawa cells. Western blot analysis of different fractions in WT and KO SH-SY5Y (**A**) and Ishikawa (**B**) cells.

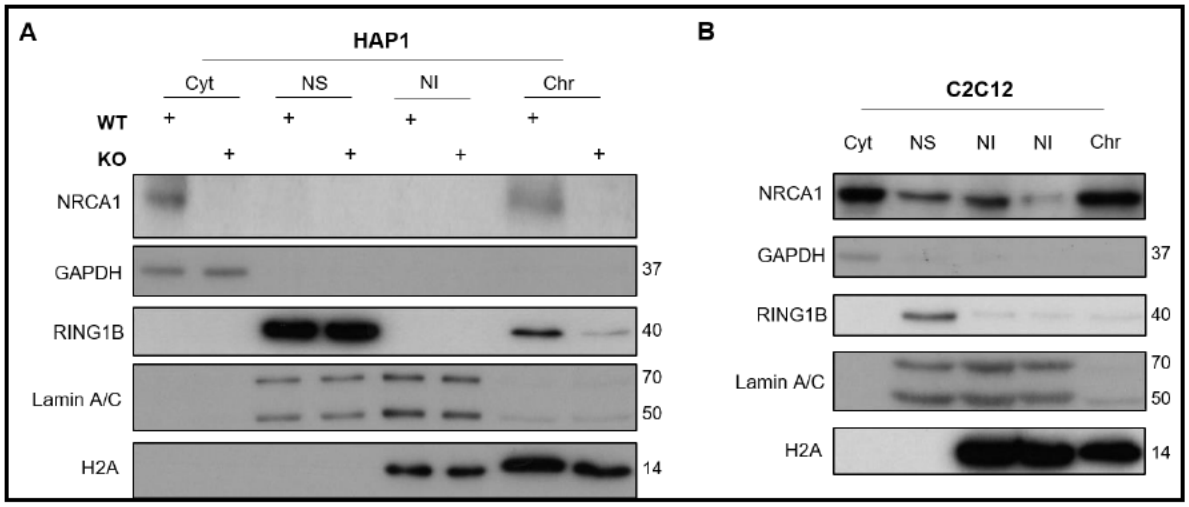

Figure 64: Endogenous NRCA1 is a chromatin-binding protein in HAP1 and C2C12 cells. Western blot analysis of different fractions in WT and KO HAP1 cells (**A**) and WT C2C12 cells (**D**).

We have shown that NRCA1 is a chromatin-binding protein that interacts with many proteins involved in the regulation of chromatin dynamics and epigenetics in *in vitro* cell models. Chromatin and epigenetic regulators are involved in the modulation of gene transcription by NRs through changes in chromatin dynamics and epigenetic marks (2.1.2). Therefore, it would be possible that NRCA1 regulates PPARα activity through interactions with chromatin and epigenetic regulators. Interestingly, we observed that NRCA1 is also found on chromatin in mouse livers (Figure 65).

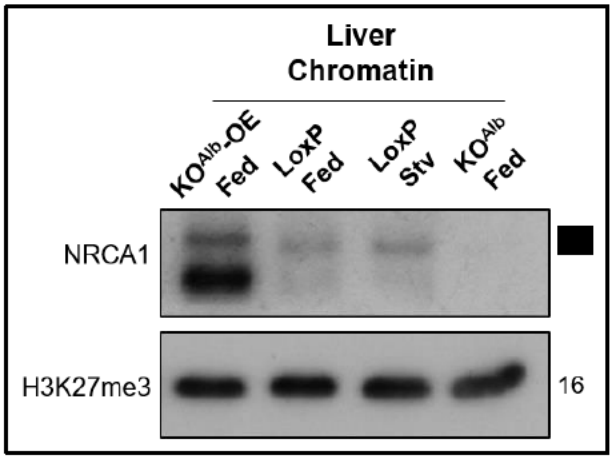

Figure 65: NRCA1 is a chromatin-binding protein in mouse liver. Livers were collected from liver specific NRCA1-KO overexpressing NRCA1 by adenoviral vector (KO^{Alb}-OE) fed mice, from LoxP fed and fasted (Stv) mice, and from liver-specific NRCA1 fed mice (KO^{Alb}). Chromatin was purified from these livers and western blot analysis was performed.

4.5. UBR5 regulates NRCA1 protein levels, apoptosis and autophagy

4.5.1. UBR5 ablation upregulates NRCA1 protein levels

In our proteomics analysis we identified UBR5 as a potential interactor of NRCA1 (4.3.3). We then validated the interaction between NRCA1 and UBR5 using two different pulldown approaches (Figure 58 and Figure 61). We became interested in UBR5 because it was shown to be involved in the degradation and stability of nuclear receptors[117]. As UBR5 is an E3, we hypothesized that interaction between UBR5 and NRCA1 would implicate ubiquitination of NRCA1, leading to its degradation through the proteasome.

To study whether UBR5 regulates NRCA1 protein stability, we generated UBR5-deficient cells using the Ishikawa cell line with the CRISPR-CAS9 technology (UBR5$^{-/-}$). We chose this cell line because we already had NRCA1-deficient Ishikawa cells[redacted]. UBR5 was fully depleted and NRCA1 and RING1A proteins levels were upregulated in UBR5-deficient cells (Figure 66), suggesting that UBR5 could be an E3 that targets NRCA1 and RING1A for ubiquitination and subsequent degradation through the proteasome.

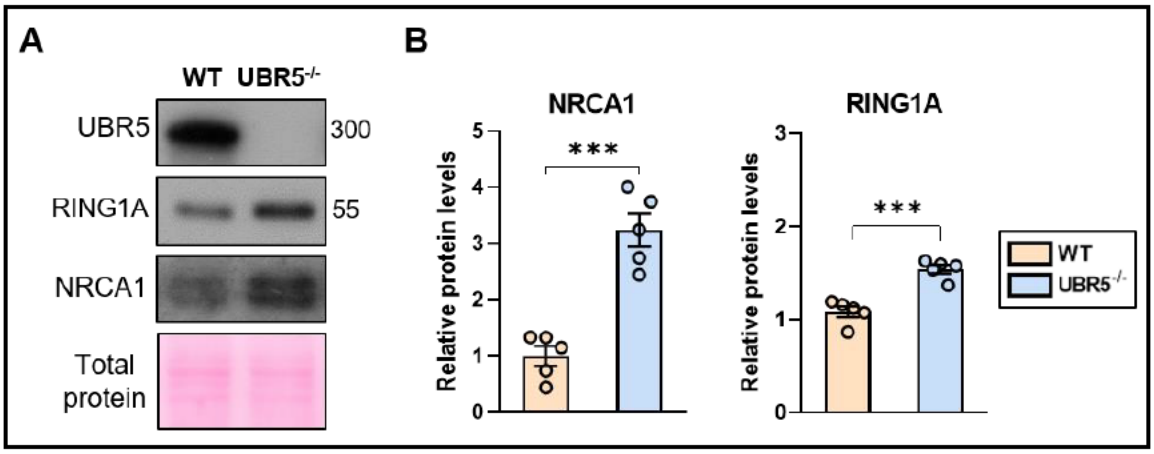

Figure 66: UBR5 ablation upregulates [redacted] and RING1A protein levels. A) Western blot analysis of WT and UBR5-KO (UBR5$^{-/-}$) Ishikawa cells. **B**) Quantification. Data represented as mean ± SEM. Student's t-test was performed. *** $P < 0.001$.

Interestingly, NRCA1 ablation in Ishikawa cells downregulated UBR5 protein levels (Figure 67), suggesting that there is a mutual regulation between NRCA1 and UBR5, with opposing effects. NRCA1 depletion also upregulated RING1A protein levels (Figure 67), similarly to UBR5$^{-/-}$ cells. It could be that NRCA1 acts as a scaffold that allows UBR5 to interact with RING1A so that it can ubiquitinate it and mark it for degradation. Therefore, in the absence of NRCA1, UBR5 can no longer interact with RING1A and ubiquitinate it, thus leading to an upregulation of RING1A protein levels.

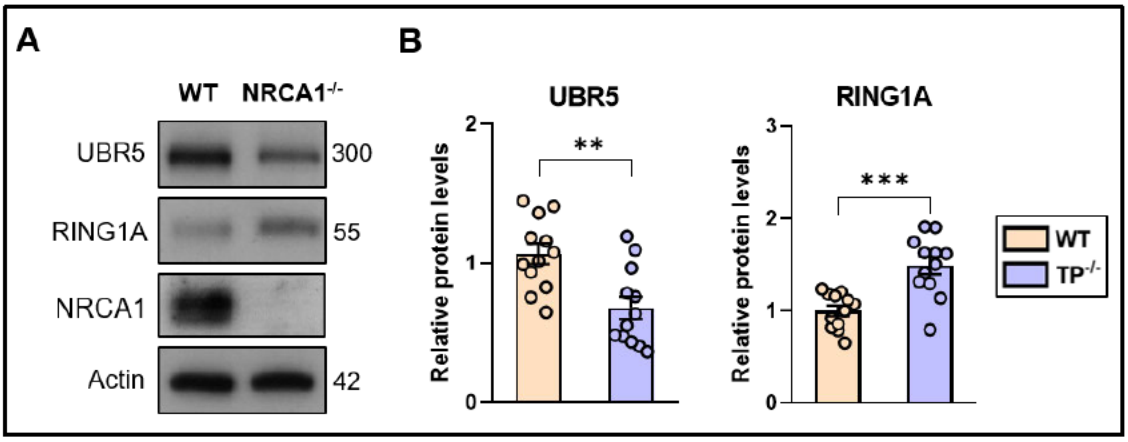

Figure 67: NRCA1 ablation downregulates UBR5 and upregulates RING1A protein levels. A) Western blot analysis of WT and NRCA1-KO ($TP^{-/-}$) Ishikawa cells. **B**) Quantification. Data represented as mean ± SEM. Student's t-test was performed. ** $P < 0.01$, *** $P < 0.001$.

4.5.2. UBR5 ablation enhances autophagy flux

As described in 2.3.2, NRCA1 is an activator of autophagy. Therefore, we wanted to assess whether UBR5 ablation, which leads to an upregulation of NRCA1, had any effects on autophagy. Because autophagy is a proteolytic pathway, an initial step to evaluate alterations in autophagy is to assess protein levels of autophagosome markers under basal and starvation conditions, such as p62 and LC3B, since they are bona fide autophagy substrates[143]. Along these lines, we subjected WT and UBR5$^{-/-}$ to a 10-hour starvation pulse. First, we observed that starvation causes a marked downregulation of p62 and LC3B protein levels, which is consistent with them being autophagy substrates (Figure 68). UBR5 ablation in basal conditions causes a remarkable decrease in p62 and LC3B protein levels, similar to those observed in WT cells under starvation conditions, suggesting that autophagy may be accelerated in UBR5$^{-/-}$ cells (Figure 68). Moreover, starvation in UBR5$^{-/-}$ cells further decreases protein levels of p62 and LC3B. Starvation does not alter protein levels of UBR5 nor NRCA1, though we observed a tendency towards increased levels (Figure 68). Interestingly, as we previously reported (Figure 66), NRCA1 is upregulated in UBR5$^{-/-}$ cells in basal conditions, and starvation seemed to downregulate its protein levels (Figure 68).

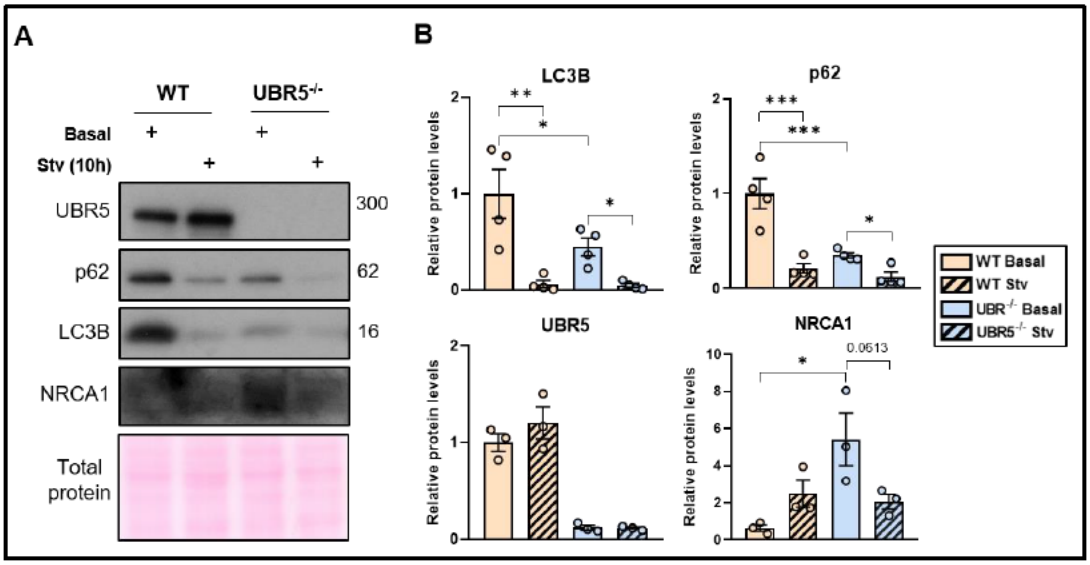

Figure 68: UBR5 ablation causes a downregulation in the autophagy proteins p62 and LC3B. WT and UBR5$^{-/-}$ Ishikawa cells were cultured with DMEM (Basal) or EBSS (Stv) for 10 hours and collected to obtain protein extracts. **A**) Western blot analysis. **B**) **Quantification**. Data represented as mean ± SEM. One-way Anova test coupled with multiple-comparisons was performed. * $P < 0.05$, ** $P < 0.01$, *** $P < 0.001$.

We have previously validated the interaction between NRCA1 and UBE2O and RING1A. Therefore, we also checked whether starvation and UBR5 ablation affected these other two E3s. Interestingly, we observed in WT cells that starvation causes UBE2O protein levels to increase, whereas RING1A protein levels are decreased due to starvation (Figure 69). UBR5 ablation did not cause alterations in UBE2O in basal conditions, but it did increase RING1A protein levels. Moreover, we observed a starvation-induced decrease in RING1A (Figure 69). These results suggest that starvation increases UBE2O stability, which is lost upon UBR5 deletion; and that starvation decreases RING1A stability and that perhaps UBR5 is an E3 that marks RING1A for degradation, as its levels are increased in UBR5$^{-/-}$ cells.

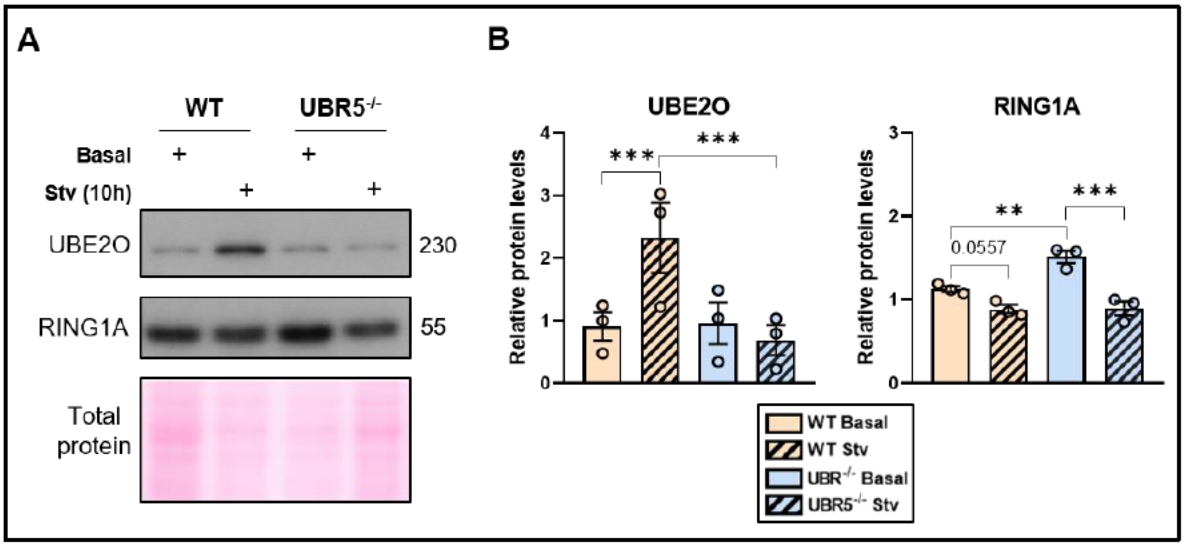

Figure 69: UBR5 ablation causes alterations in UBE2O and RING1A protein levels. WT and UBR5$^{-/-}$ Ishikawa cells were cultured with DMEM (Basal) or EBSS (Stv) for 10 hours and collected to obtain protein extracts. **A**) Western blot analysis. **B**) Quantification. Data represented as mean ± SEM. One-way Anova test coupled with multiple-comparisons was performed. * $P < 0.05$, ** $P < 0.01$, *** $P < 0.001$.

Decreased protein levels of p62 and LC3B in UBR5$^{-/-}$ cells, which was further exacerbated upon starvation, suggested there were alterations in autophagy upon UBR5 ablation. To evaluate whether autophagy activity was compromised, we measured autophagy flux[143] in basal and starvation conditions, as described in 7.4.3, through western blot analysis. A 5-hour starvation pulse was used to evaluate starvation-induced autophagy, alongside a 5-hour treatment with Bafilomycin A1.

Autophagy flux studies indicated that UBR5 ablation leads to a two-fold increase in basal and starvation-induced autophagy flux when assessing flux of p62 and LC3B-II (Figure 70). These results show that UBR5 ablation promotes basal and starvation-induced autophagy, thus indicating that UBR5 is an inhibitor of autophagy.

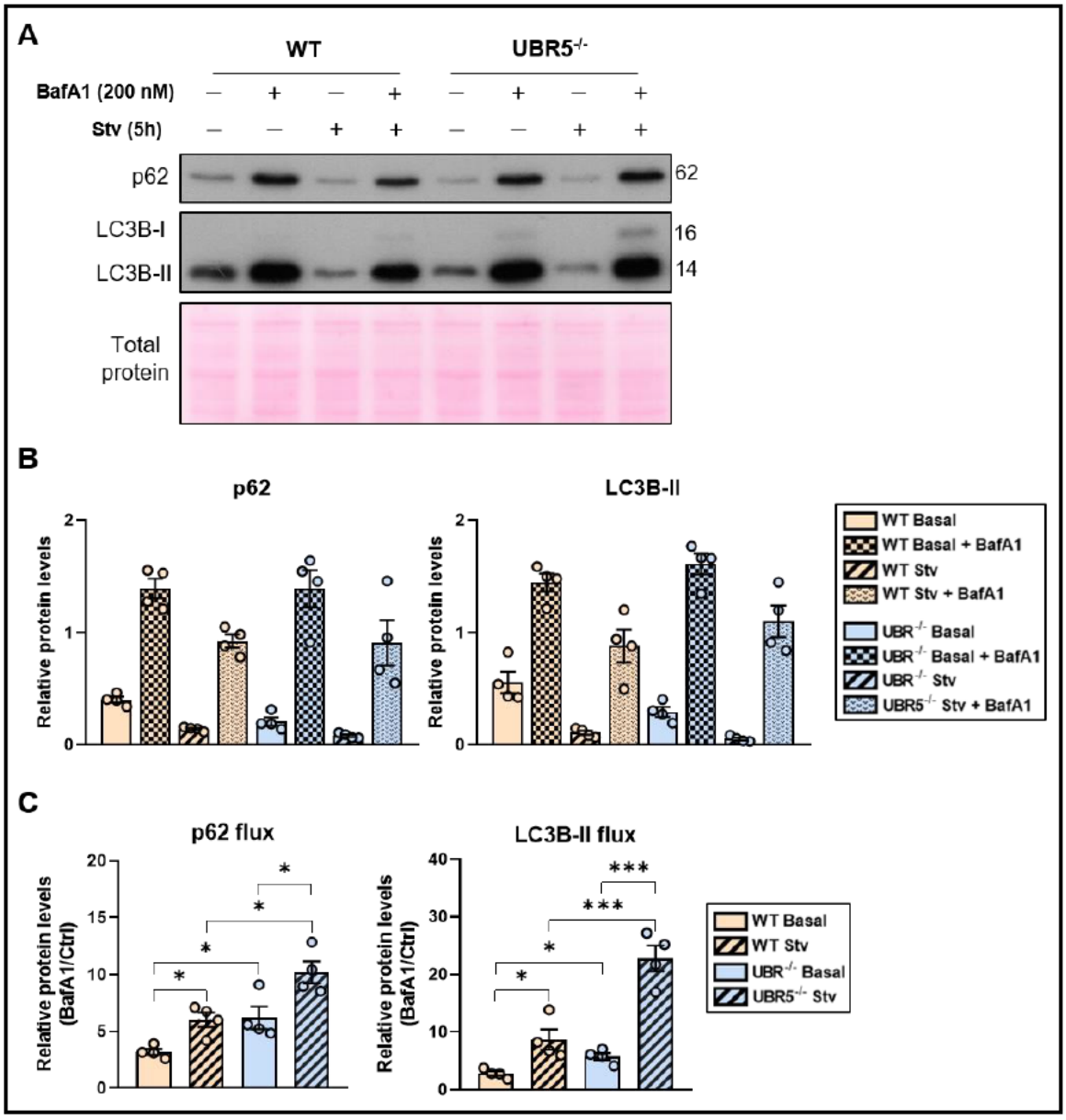

Figure 70: UBR5 ablation enhances autophagy flux. WT and UBR5$^{-/-}$ Ishikawa cells were cultured with DMEM (Basal) or EBSS (Stv) for 5 hours in the absence or presence of Bafilomycin A1 and collected to obtain protein extracts. **A**) Western blot analysis. **B**) Quantification of total protein levels. **C**) Quantification of flux. Data represented as mean ± SEM. One-way Anova test coupled with multiple-comparisons was performed. * $P < 0.05$, ** $P < 0.01$, *** $P < 0.001$.

We also measured the levels of UBR5, NRCA1, UBE2O, RING1A, and RING1B under the conditions used to study autophagy flux. We observed that UBR5 levels do not change upon starvation nor upon inhibition of autophagy (Figure 71A/B). In keeping with this, flux analysis show that UBR5 is not degraded through autophagy (Figure 72A).

In WT cells, UBE2O protein levels are upregulated upon a 5-hour starvation pulse, similarly to what we observed upon a 10-hour starvation pulse, and its levels are further increased when autophagy is inhibited (Figure 71A/C). Moreover, UBR5 ablation prevented these upregulations to occur (Figure 71A/C). Flux analysis indicate that UBE2O is not an autophagy substrate (Figure 72B).

NRCA1 levels are upregulated in UBR5$^{-/-}$ cells in basal conditions, as we observed earlier (Figure 71A/D). We also observed that NRCA1 levels are remarkably upregulated in starved cells upon autophagy inhibition, which are further upregulated upon UBR5 ablation (Figure 71A/D). This is consistent with flux analysis, as they indicate that NRCA1 can be degraded through autophagy upon starvation, and that UBR5 ablation enhances it (Figure 72C). This results indicate that NRCA1 is an autophagy substrate under starvation conditions.

RING1A is upregulated in UBR5$^{-/-}$ cells in basal conditions, as we observed earlier, and it is dramatically downregulated in starved UBR5$^{-/-}$ cells when autophagy is inhibited (Figure 71A/E). In addition, flux analysis show that starvation decreases degradation of RING1A through autophagy, which is further reduced upon UBR5 ablation (Figure 72D). However, UBR5 ablation alone does not reduce RING1A autophagic degradation (Figure 72D).

RING1B is also upregulated in UBR5$^{-/-}$ cells in basal conditions, and it is also dramatically downregulated in starved UBR5$^{-/-}$ cells when autophagy is inhibited (Figure 71A/F). Autophagy inhibition also downregulated RING1B levels in UBR5$^{-/-}$ cells in basal conditions. In keeping with this, flux analysis show, similarly to RING1A, that starvation decreases autophagic degradation of RING1B, which is also further reduced upon UBR5 ablation (Figure 72E). But, unlike RING1A, UBR5 ablation alone also reduced RING1B autophagic degradation (Figure 72D).

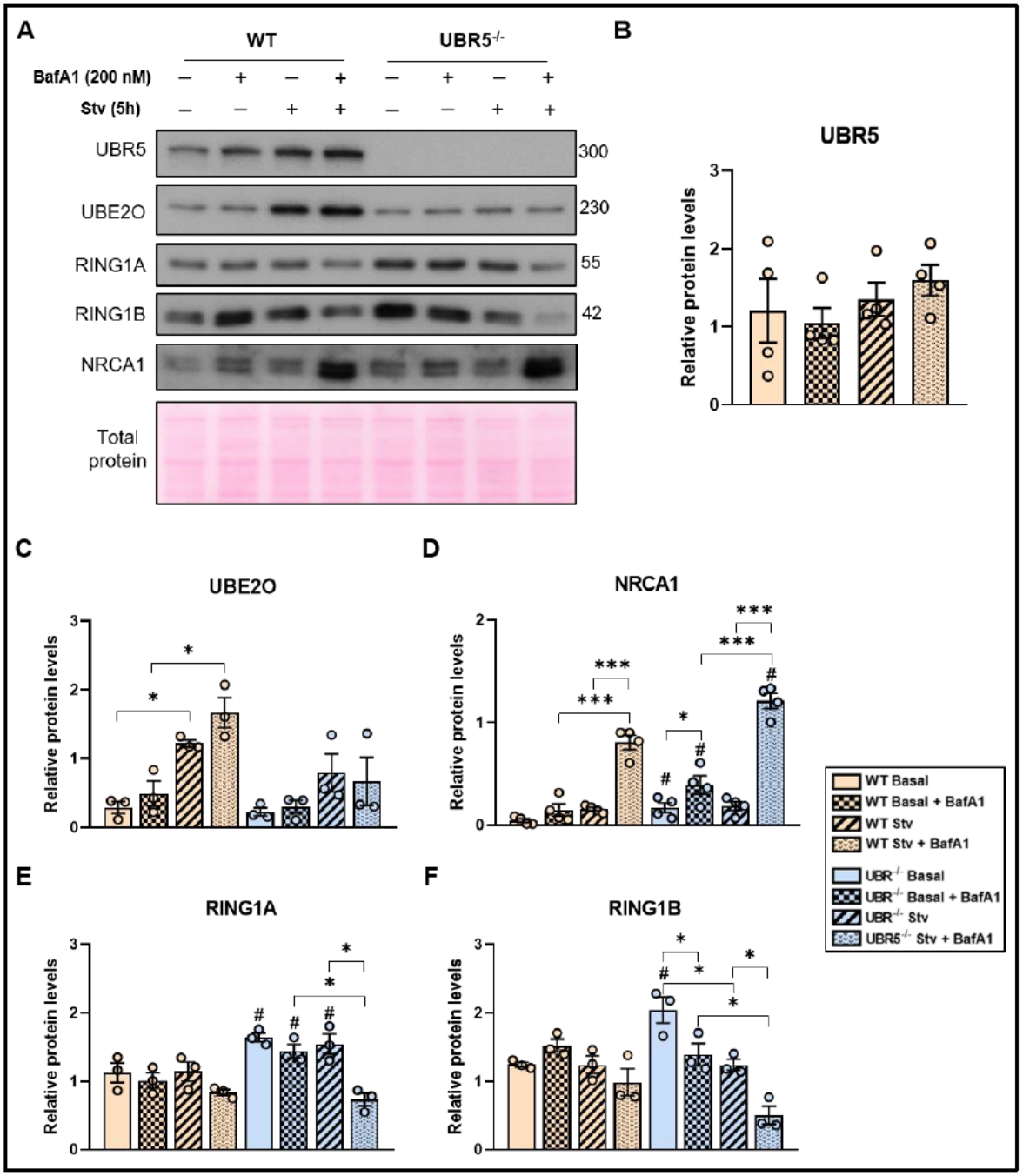

Figure 71: Effects of autophagy inhibition and starvation in on the protein levels of UBR5, UBE2O, NRCA1, RING1A and RING1B in WT and UBR5$^{-/-}$ cells. **A**) Western blot analysis. **B**) Quantification of UBR5. **C**) Quantification of UBE2O. **D**) Quantification of NRCA1. **E**) Quantification of RING1A. **F**) Quantification of RING1B. Data represented as mean ± SEM. One-way Anova test coupled with multiple-comparisons was performed. * P < 0.05, ** P < 0.01, *** P < 0.001. # denotes significance between cell lines.

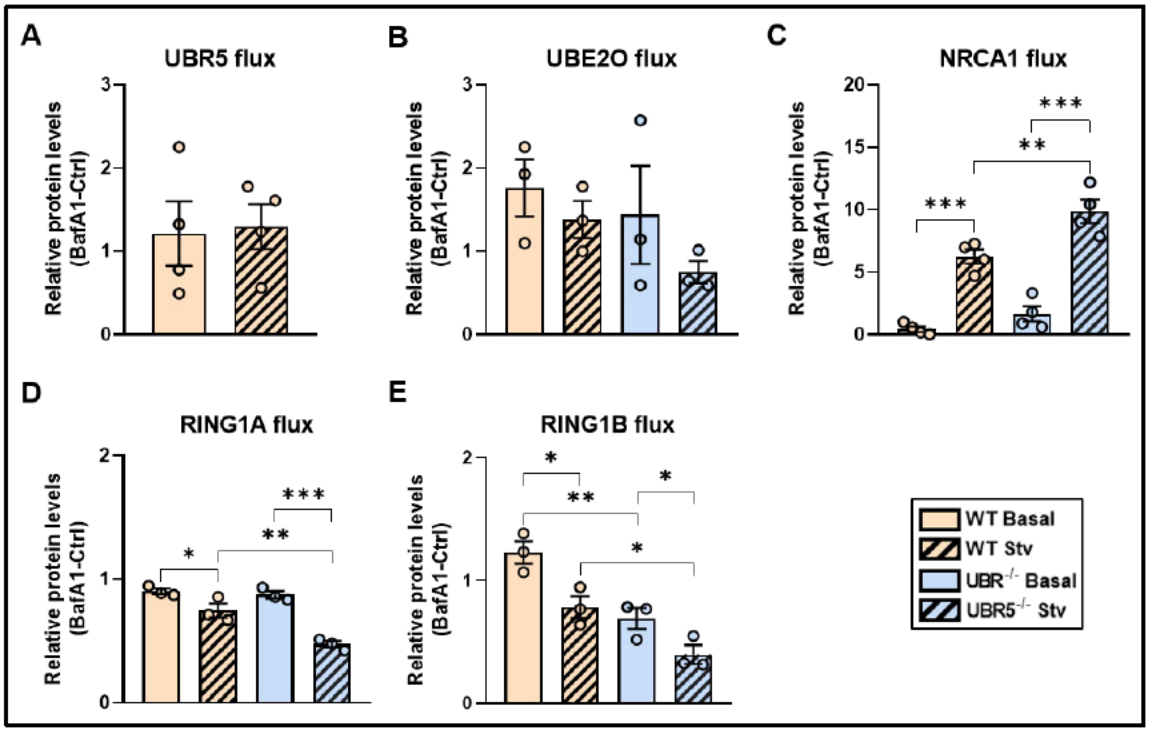

Figure 72: Autophagic degradation of UBR5, UBE2O, NRCA1, RING1A and RING1B. A) Flux quantification of UBR5. **B**) Flux quantification of UBE2O. **C**) Flux quantification of NRCA1. **D**) Flux quantification of RING1A. **E**) Flux quantification of RING1B.

4.5.3. UBR5 ablation promotes starvation-induced apoptosis

Because NRCA1 is also an activator of apoptosis, and excessive autophagy can trigger what is known as autophagic cell death or autophagy-dependent cell death[144,145]. Therefore, we evaluated the effects of a 10-hour starvation pulse on apoptosis markers, such as poly (ADP-ribose) polymerase-1 (PARP-1) and CASP3. Briefly, when apoptosis is triggered, caspases, including CASP3, are activated to promote proteolysis of key structural proteins and modulate the activity of a different array of enzymes[146]. Caspase activation often requires their own cleavage by other caspases[146]. PARP-1 is an enzyme that is cleaved by caspases during apoptosis[147]. Therefore, cleaved PARP-1 and CASP3 can be monitored to evaluate activation of apoptosis. We observed that a 10-hour starvation pulse induced apoptosis, as WT cells showed increased cleavage of PARP-1 and CASP3 (Figure 73). Interestingly, UBR5$^{-/-}$ cells showed a similar or even higher cleavage of PARP-1 and CASP3 than WT cells under starvation conditions. Moreover, starvation in UBR5$^{-/-}$ cells led to a dramatic increase in cleaved PARP-1 and CASP3 (Figure 73). These results suggest that UBR5 ablation promotes apoptosis, perhaps through the action of NRCA1, as it is upregulated in UBR5$^{-/-}$ cells (Figure 66).

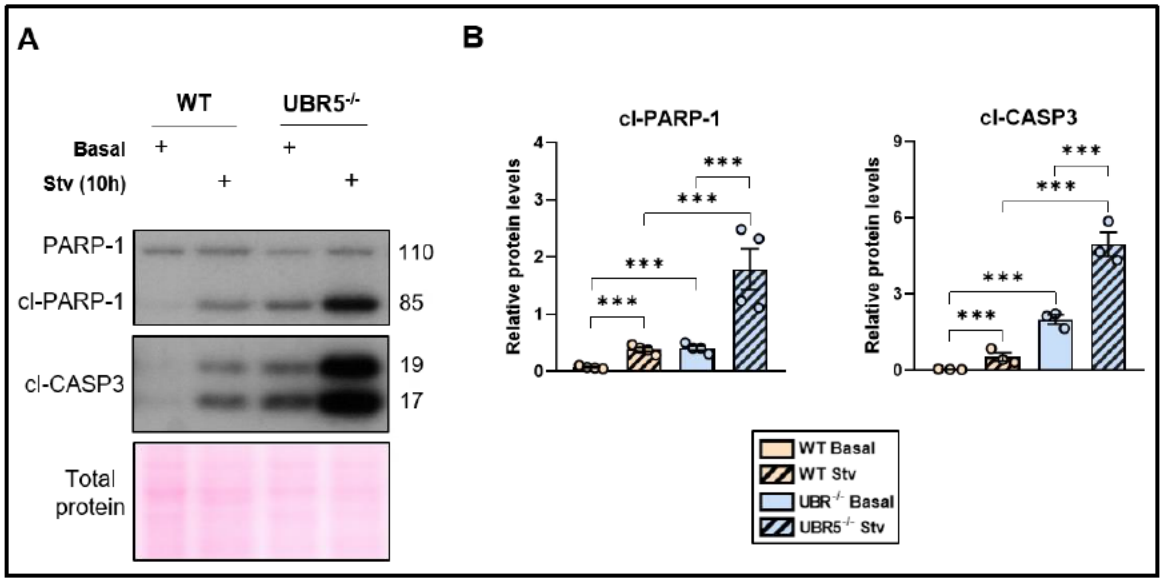

Figure 73: UBR5 ablation promotes starvation-induced apoptosis. WT and UBR5$^{-/-}$ Ishikawa cells were cultured with DMEM (Basal) or EBSS (Stv) for 10 hours and collected to obtain protein extracts. **A**) Western blot analysis. **B**) **Quantification**. Data represented as mean ± SEM. One-way Anova test coupled with multiple-comparisons was performed. * $P < 0.05$, ** $P < 0.01$, *** $P < 0.001$.

We also checked activation of apoptosis in the autophagy flux studies. We observed that UBR5$^{-/-}$ cells are more sensitive to starvation-induced apoptosis and apoptosis triggered by autophagy blockade, as evidenced by increased cleavage of PARP-1 and CASP3 (Figure 74). When autophagy inhibition is combined with starvation, massive apoptosis occurs in UBR5$^{-/-}$ cells, suggesting that UBR5 has an anti-apoptotic role in the context of autophagy-dependent cell death.

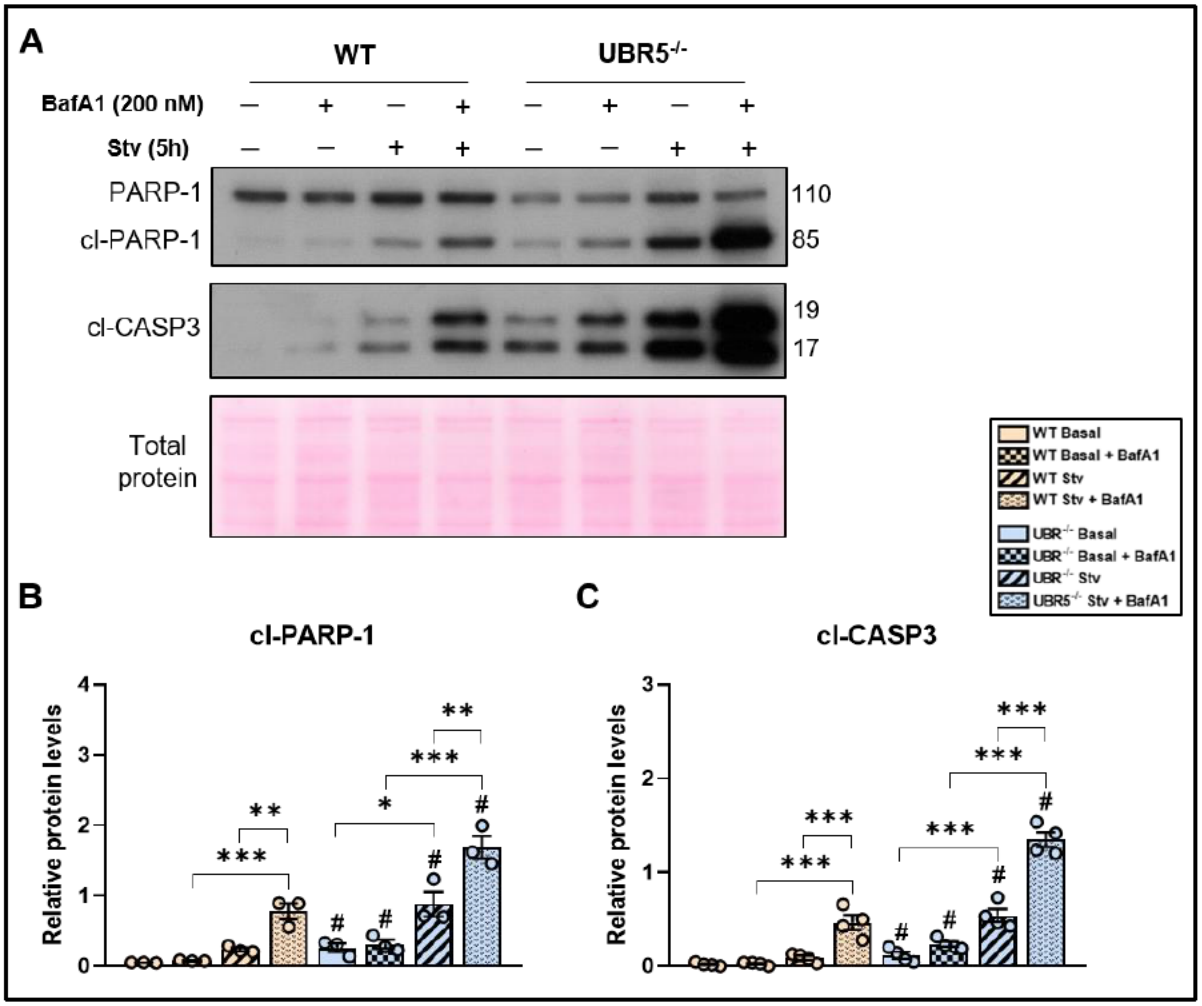

Figure 74: UBR5 ablation sensitizes cells to starvation and autophagy inhibition-induced cell death. A) Western blot analysis. **B**) Quantification of cl-PARP-1. **C**) Quantification of cl-CASP3. . Data represented as mean ± SEM. One-way Anova test coupled with multiple-comparisons was performed. * $P < 0.05$, ** $P < 0.01$, *** $P < 0.001$. # denotes significance between cell lines.

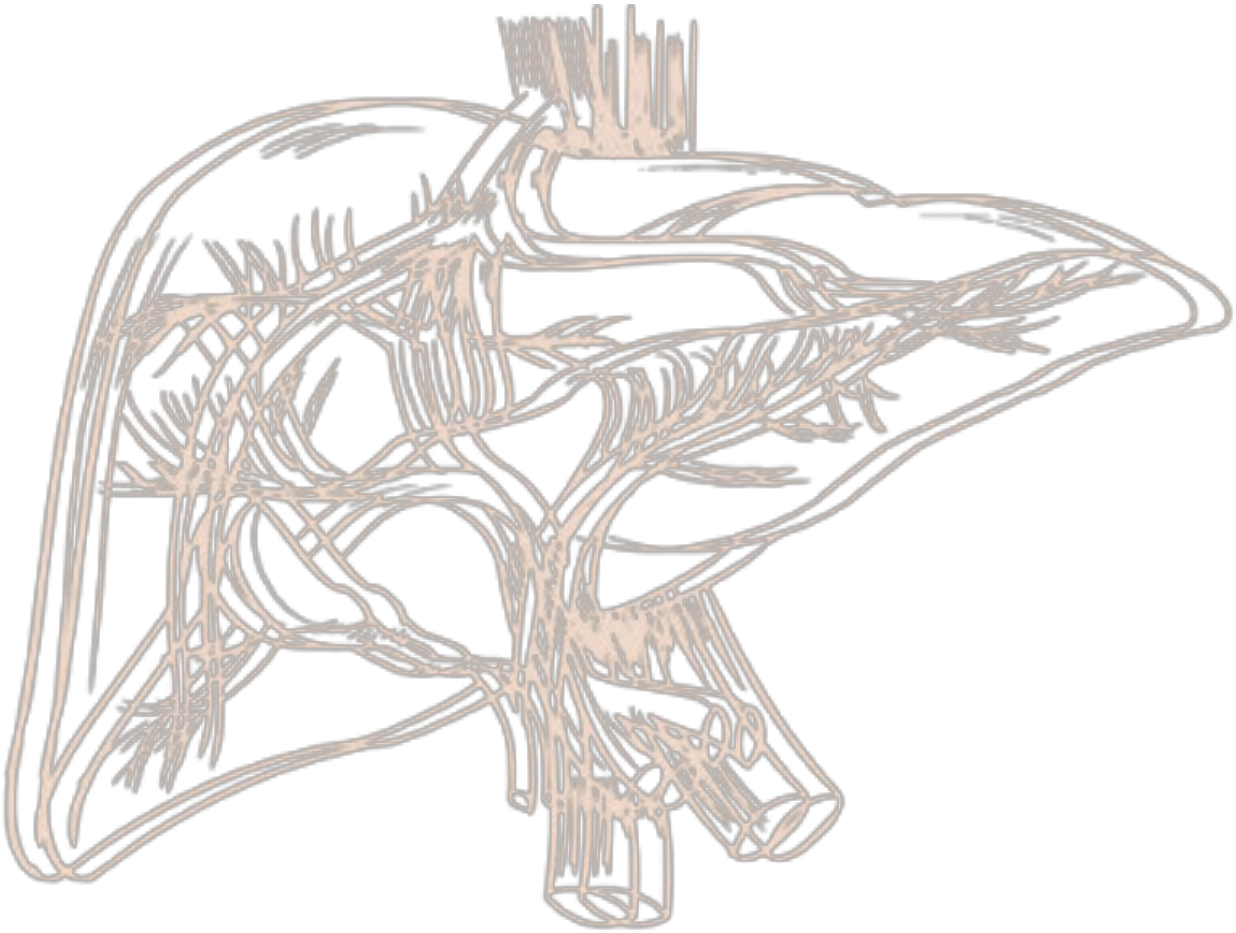

DISCUSSION

5. DISCUSSION

5.1. NRCA1 is a novel PPARα activator

5.1.1. NRCA1 ablation impairs PPARα activation

In this thesis, we have identified NRCA1 as a novel activator of PPARα in response to fasting *in vivo*. These findings are consistent with previous work in the lab that showed that NRCA1 can act as a coactivator of TRα, PPARγ, GRα, VDR and ERα in *in vitro* luciferase reporter assays[redacted]. We have observed in 16-week old male mice that ablation of NRCA1 impairs the activation of PPARα in response to overnight fasting (16 h), which leads to a decreased upregulation of PPARα target genes that are essential for FAO and KB synthesis in response to fasting (Figure 8).

It is known that fasting induces intrahepatic lipid accumulation in rodents and in humans[148–150], most likely due to the uptake of FFAs coming from adipose tissue lipolysis[151], which serve as a source for energy through FAO, and building blocks for processes such as gluconeogenesis and KB synthesis, among other processes[152]. Along these lines, as a consequence of impaired PPARα activation, fasted NRCA1-KO^{Alb} mice showed increased hepatic triglyceride levels compared to LoxP mice (Figure 9A) and decreased plasma β-hydroxybutyrate levels (Figure 9B). Because FAO predominantly occurs in mitochondria and peroxisomes, it would be interesting to measure mitochondrial and peroxisomal fatty acid oxidation rates in NRCA1-KO^{Alb} livers[153].

We have also evaluated the activation of PPARα upon fasting in a tamoxifen-inducible total KO model (NRCA1-KO^{Ubc}). In this model, unlike the NRCA1-KO^{Alb} model, NRCA1 ablation does not occur at the embryonic level but upon feeding a tamoxifen-containing diet. Mice around the age of 8 weeks are fed with a tamoxifen-containing diet for 4 weeks, so they are 12-week old on the sacrifice day. The NRCA1-KO^{Ubc} mouse model was previously characterized[redacted]. These mice have a slight increase in body weight and enhanced WAT weight compared to LoxP mice. Interestingly, this increase in WAT mass was not due to adipocyte hypertrophy, but due to adipocyte hyperplasia, which is considered a less pathogenic form of obesity[redacted]. We observed that 12-week old male NRCA1-KO^{Ubc} also had impaired activation of PPARα, as evidenced by blunted upregulation of PPARα target genes (Figure 11). These results indicate that NRCA1 ablation also impairs PPARα activation in a metabolic context characterized by hyperplasic obesity.

The effects of NRCA1 ablation on PPARα activation also occur in female mice (Figure 14). Moreover, we have uncovered sex-dependent differences in the activation of PPARα in response to fasting. In keeping with this, male mice show a much higher upregulation of Cyp4a10 (around tenfold) in response to fasting compared to female mice (Figure 15), which is a gene extremely sensitive to PPARα activation. This may suggest that female mice require a minor activation of PPARα to handle the lipid overload under fasting conditions, whereas male mice need a higher activation of PPARα.

The effects of NRCA1 ablation on PPARα activation are maintained during aging in male mice. We observed that PPARα activation is impaired in one-year old (Figure 16) and in two-year old (Figure 19) male NRCA1-KO^{Alb} mice. It has been suggested in the literature that PPARα activity declines with age[40]. Our data not only confirms this, but also indicate that NRCA1 ablation further exacerbates the age-dependent decline in PPARα activity (Figure 20). Concomitantly, one-year old and two-year old mice also show increased hepatic lipid content in fasting conditions (Figure 33 and Figure 34).

Fasting is the physiological condition that activates PPARα. Concomitantly, refeeding inhibits PPARα[36,154]. In this regard, it would also be interesting whether NRCA1 ablation has any effects on refeeding-induced PPARα inhibition.

Fasting elicits a complex metabolic response affecting several tissues[155]. We have shown that NRCA1 is necessary for a correct PPARα activation in response to fasting. To further confirm that NRCA1 is required for PPARα activation, we made use of PPARα agonists. With PPARα agonists, we make sure that we are specifically targeting PPARα, as fasting can trigger a plethora of pathways. We subjected 16-week old female mice to a single dose of GW7647 through oral gavage and collected livers 4 hours after the treatment. NRCA1-KO^{Alb} mice treated with GW7647 showed impaired activation of PPARα, as evidenced by blunted upregulation of PPARα itself, ACAT1, Cyp4a10 and Cyp4a14 (Figure 26) and similar results were obtained when mice were treated with the PPARα agonist Wy14643 (Figure 27). These results confirm that NRCA1 is indeed required for the full activation of PPARα in the presence of ligand.

Strikingly, GW7647 treatment in 16 week old male mice did not show differences in the activation of PPARα between genotypes. Male NRCA1-KO^{Alb} mice were able to induce the expression of PPARα target genes at the same levels as LoxP mice (Figure 28). Similarly to sex-dependent differences in the activation of PPARα in response to fasting, it could be that agonist treatment has different kinetics in male mice. It would be interesting to evaluate how aged male NRCA1-KO^{Alb} mice respond to PPARα agonist treatment.

Hepatic autophagy is a cellular process that is also important in the fasting response as livers with defective autophagy also show a dramatic accumulation of hepatic TGs[61] under fasting conditions. Apart from impaired upregulation of PPARα target genes upon fasting, we also observed impaired expression of autophagy genes during fasting in NRCA1-KO^{Alb} and NRCA1-KO^{Ubc} mice (Figure 13). This is in agreement with the impaired autophagy flux detected in primary hepatocytes isolated from NRCA1-KO^{Alb} mice [redacted]. Interestingly, it was established that PPARα controls the transcriptional activation of autophagy, acting as a transcription factor for autophagy genes[36]. Therefore, it NRCA1 may be regulating the expression of autophagy genes upon fasting via PPARα.

The molecular mechanism by which NRCA1 regulates the activation of PPARα in response to fasting or agonists remains to be elucidated. We have shown that NRCA1 ablation does not cause changes in the expression of PPARα coregulators in fed nor in fasting conditions (Figure 10). It has been reported that PPARα can regulate its own expression as a feed-forward mechanism[103]. In keeping with this, PPARα binds to PPREs that are present in the promoter region of PPARα to enhance its own expression[103]. In our studies we have detected that PPARα autoinduction is also impaired in NRCA1-KO^{Alb} mice in some of the cohorts (Figure 10, Figure 11 and Figure 16), but not in all of them. Therefore, impaired PPARα activation upon fasting is unlikely to be driven by impaired autoinduction of PPARα.

In our *in vitro* studies, we uncovered that NRCA1 binds to many proteins that are involved in the regulation of chromatin dynamics and epigenetics. Interestingly, some of these proteins have nuclear receptor binding function. Therefore, it could be that NRCA1 regulates PPARα activation through interactions with these epigenetic players, discussed in 5.3. Interestingly, we have shown that NRCA1 interacts with UBR5, and that there is a functional interaction between these two proteins. In this regard, UBR5 ablation leads to upregulation of NRCA1, and NRCA1 ablation leads to downregulation of UBR5 (4.5.1). Results from UBR5$^{-/-}$ cells suggest that UBR5 is an E3 that ubiquitinates NRCA1 for degradation.

Interestingly, UBR5 was identified as an E3 that promotes nuclear receptor degradation upon ligand binding[117], perhaps as a feedback loop mechanism to terminate nuclear receptor activation. However, in this study[117], the implications of UBR5 in the degradation and regulation of PPARα was not evaluated. Therefore, it would be interesting to study if there is a functional interaction between NRCA1 and UBR5 in liver cells. It might be that NRCA1 regulates UBR5 function, thus regulating the degradation of PPARα upon agonist treatment or fasting. UBR5 not only could be degrading PPARα, but also NRCA1 to shut down PPARα activation.

5.1.2. NRCA1 may be a PPARα target gene

An interesting observation is the upregulation of NRCA1 expression upon overnight (Figure 12). In this regard, NRCA1 expression is upregulated in response to fasting in 16-week, one-year old and two-year old mice, as well as in 16-week female mice. This prompted us to think that perhaps NRCA1 could be under the transcriptional control of PPARα. In keeping with this, when we treated female mice with the agonist GW7647, expression of NRCA1 was not induced (Figure 26). However, treatment with the agonist Wy14643 led to a remarkable upregulation of NRCA1 (Figure 27). Moreover, chronic treatment with GW7647 in male mice fed with MCD diet during 3 weeks induced the expression of NRCA1 (Figure 30). Discrepancies observed with different agonists may be due to the fact that GW7647 is almost a thousand-fold more potent than Wy14643. In this regard, the dose we used with Wy14643 was only ten times lower compared to the dose we used with GW7647.

If NRCA1 is a PPARα target gene, it should contain PPAR-responsive elements (PPREs). We explored the PPARgene database[156], which can provide predictions on whether queried genes may contain PPAR-responsive elements based on verified target genes, although it is not specific for PPARα, as it may also apply for PPARγ and PPARδ. Surprisingly, NRCA1 was predicted as a PPAR target gene with a medium confidence level and we obtained 4 putative PPREs, one of which may be conserved in mouse and rat.

To further investigate whether NRCA1 is a PPARα target gene, luciferase reporter assays with the putative PPREs from NRCA1 should be performed. It would also be essential to perform ChIP experiments to assess whether PPARα binds to the NRCA1 gene. Considering our data that NRCA1 is required to fully activate PPARα, if NRCA1 is a PPARα target it would constitute a feed-forward loop to ensure maximum activation of PPARα in response to fasting.

5.2. Characterization of NRCA1-KO^{Alb} mice

5.2.1. Standard diet

Male NRCA1-KO^{Alb} mice fed a standard diet did not have any changes in body and liver weight nor body composition at 16 weeks of age [redacted]. Body weight is known to increase due to aging[157]. Interestingly, NRCA1-KO^{Alb} mice gained more body weight during aging compared to LoxP littermates (Figure 32). It has been reported that liver-specific PPARα-KO (PPARα-KO^{Alb}) mice gain more weight during aging[39]. Since NRCA1 ablation impairs PPARα activation, it could be that increased age-associated body weight gain in NRCA1-KO^{Alb} mice is due to impaired PPARα activation.

PPARα-KO^{Alb} mice are also characterized by increased liver weight at the age of 18 weeks[158], but age-associated liver weight gain in PPARα-KO^{Alb} mice has not been documented. We observed that in NRCA1-KO^{Alb} mice, liver weight was not increased in young nor in old mice, probably because PPARα activation in these mice is only partially impaired in contrast to PPARα-KO^{Alb} mice. Increased hepatic fat accumulation upon fasting in NRCA1-KO^{Alb} mice is consistent with increased hepatic fat accumulation upon fasting observed in PPARα-KO^{Alb} mice[39]. Moreover, aged PPARα-KO^{Alb} mice develop fatty liver spontaneously[39].

As described previously, NRCA1 activates autophagy through interactions with key protein involved in autophagy regulation (2.3.2). Moreover, we have uncovered in this thesis that NRCA1 can also regulate hepatic autophagy at the transcriptional level, most likely through the action of PPARα[36]. Moreover, autophagy flux is impaired in primary hepatocytes isolated from NRCA1-KO^{Alb} mice livers [redacted]. It has been reported that hepatic autophagy, more specifically lipophagy, is very important to prevent fat accumulation in the liver in response to HFD[61]. In addition, it has been widely reported that autophagy is impaired in conditions that favor the development of MASLD in mice[56], including HFD. Furthermore, activation of lipophagy with a synthetic lipophagy adapter using adeno-associated virus ameliorated steatohepatitis in mouse MASLD models[64]. In keeping with this, it would be likely that NRCA1-KO^{Alb} mice, apart from impaired FAO and KB synthesis, it also has impaired lipophagy due to impaired PPARα activation. Therefore, it would be interesting to assess in NRCA1-KO^{Alb} livers whether there is increased accumulation of autophagosome-containing lipid droplets.

5.2.2. High-fat diet

Characterization of NRCA1-KO^{Alb} mice under HFD was described in [redacted].

Under 16 weeks of HFD, NRCA1-KO^{Alb} mice showed impaired glucose metabolism. In this regard, fasting blood glucose was higher in NRCA1-deficient animals, and plasma insulin levels tended to be higher. Concomitantly, homeostasis model index of insulin resistance (HOMA-IR) values were higher in NRCA1-KO^{Alb} animals, indicating increased insulin resistance. These mice were also glucose intolerant, as indicated by glucose tolerance test. However, in contrast, HFD-fed PPARα-KO^{Alb} mice did not show glucose intolerance, but were actually more glucose tolerant compared to HFD-fed LoxP animals, in spite of developing more severe MASLD[158]. This suggests that insulin resistance in HFD-fed NRCA1-KO^{Alb} animals may involve a PPARα-independent mechanism.

Analysis of livers showed that NRCA1-KO^{Alb} mice had enhanced liver weight upon HFD without differences in total body weight, food intake nor fecal excretion between genotypes. Histological analysis of livers showed increased number and size of lipid droplets in NRCA1-KO^{Alb} animals. In addition, Oil-Red-O staining and biochemical measurement of hepatic triglycerides showed enhanced lipid accumulation in livers of HFD-fed NRCA1-KO^{Alb} mice [redacted]. These results do not fit with our observations in that expression of PPARα target genes in response to 16 weeks of HFD is not impaired in NRCA1-KO^{Alb} animals (Figure 21). It could be due to a PPARα-independent mechanism, or also because the treatment with HFD was too long and the overload of lipids from the diet bypassed the effects of NRCA1 ablation. Lipidomic analysis of livers from mice fed a HFD for 16 weeks showed a significant remodeling of several types of lipids upon NRCA1 ablation (unpublished data). As fatty acids are the natural PPARα ligands, it could be that the extensive remodeling of lipids in NRCA1-KO^{Alb} livers impedes the effects of NRCA1 ablation on PPARα activation. Upon 8 weeks of HFD, NRCA1-KO^{Alb} mice also tended to accumulate more hepatic fat [redacted]. It would be interesting to check whether PPARα activation is impaired upon 8 weeks of HFD.

Upon 8 weeks of HFD, NRCA1-KO^{Alb} mice also accumulate more cholesterol in liver [redacted]. However, when HFD is extended to 16 weeks, hepatic cholesterol in NRCA1-KO^{Alb} mice is normalized. Studies with 16 weeks of WD showed that bile acid metabolism is impaired upon [redacted] ablation. In this regard, NRCA1-KO^{Alb} mice fed a WD for 16 weeks had decreased levels of bile acids in plasma and feces [redacted]. It has been reported that bile acids can induce the expression of PPARα[159]. Therefore, it would be interesting to analyze bile acid metabolism in NRCA1-KO^{Alb} mice fed upon 8 weeks and 16 weeks of HFD. It could be that 16 weeks of HFD leads to increased bile acids, which in turn activate PPARα, thus bypassing the effects of NRCA1 ablation. However, despite PPARα being activated to the levels of LoxP mice, NRCA1-KO^{Alb} mice still accumulate more hepatic lipid.

Staining of liver sections with Sirius Red and Masson's trichrome to detect extracellular collagen as a marker of tissue fibrosis showed slight increase in fibrosis due to HFD, but there were no differences between genotypes. However, when stained with an antibody against

F4/80, a specific marker for monocytes and macrophages used to assess liver inflammation, NRCA1-KO^{Alb} mice showed increased F4/80-positive area in response to HFD, whereas LoxP mice did not show this kind of increase when fed a HFD. This suggests that NRCA1 has a protective role against HFD-induced liver inflammation. Moreover, HFD-fed NRCA1-deficient mice had a tendency towards increased plasma levels of ALT and AST, which are used a biochemical parameters of liver damage.

In all, prolonged HFD caused enhanced hepatic fat accumulation in NRCA1-KO^{Alb} mice, even though PPARα activation was not impaired in these mice. Moreover, NRCA1-KO^{Alb} animals were more insulin resistant compared to LoxP littermates after 16 weeks of HFD, and had slightly increased infiltration of F4/80-positive immune cells and elevated levels of ALT and AST. These results indicate that NRCA1 has a protective role in response to prolonged HFD independent of PPARα.

5.2.3. Western diet

Characterization of NRCA1-KO^{Alb} mice under 16 weeks of WD was described in [redacted].

Unlike HFD, NRCA1-KO^{Alb} mice fed a WD for 16 weeks showed impaired PPARα activation (Figure 24). Surprisingly, this was not accompanied by enhanced hepatic fat accumulation. In addition, despite impaired PPARα activation, WD-fed NRCA1-KO^{Alb} mice did not show any signs of enhanced liver damage [redacted].

WD-fed NRCA1-KO^{Alb} mice showed altered bile acid metabolism, as in decreased plasma and fecal levels of bile acids. These mice also show a remodeling of certain lipid species compared to LoxP animals. Elevated bile acids are toxic for the liver[33]. Moreover, elevated blood bile acids has been reported in MASLD patients, and they can cause liver injury and drive MASLD development[160]. Perhaps the decrease in plasma and fecal levels of bile acids is so beneficial for the liver that bypasses the impaired PPARα activation. Maybe the remodeling of certain lipid species also contributes to these beneficial effects.

WDs are widely used to model MASLD because they have been reported to better phenocopy human MASLD, because they also induce obesity and insulin resistance[160]. In most studies, mice are fed with WD during at least 24-32 weeks to model MASLD[160]. It is likely that 16 weeks of WD are not sufficient to see changes in liver damage even though we observe impaired PPARα activation in WD-fed NRCA1-KO^{Alb} mice.

5.2.4. Methionine- and choline-deficient diet

The MCD diet is also used to model MASLD in mice, however it causes a dramatic weight loss that is not observed in humans[105] and it does not mimic the metabolic dysfunction associated with human MASLD[161]. Therefore, its use for preclinical MASLD models is under debate[160]. The MCD diet drives liver damage by impairing hepatic lipid export due to the lack of phosphatidylcholine, the main constituent of VLDLs[160]. It also induces lipolysis, which is why it induces weight loss, thus releasing massive amounts of FFAs that reach the liver. The main advantage of the MCD diet is that it can induce a MASLD-like phenotype in a short period of time (3 weeks)[106] in contrast to WDs (24-32 weeks)[160]. Moreover, a 0.1% supplementation of methionine in drinking water can circumvent the non-physiological weight loss[106].

PPARα has a strong protective role against the development of MASLD[39] and treatment with PPARα agonists ameliorates the disease in MASLD mouse models[107–109]. NRCA1 ablation leads to impaired PPARα activation and enhanced hepatic fat accumulation. Therefore, we wondered whether NRCA1-KO^{Alb} mice would be more susceptible to develop MASLD and whether they would respond worse to PPARα therapy in the context of MASLD. To test this, we subjected mice around the age of 8 weeks to 3 weeks of MCD diet and chronic treatment with GW7647 as described previously (Figure 37).

Feeding with MCD diet supplemented with 0.1% methionine in drinking water did not cause detrimental weight loss in vehicle-treated animals (Figure 38B/D), as reported in the literature[106]. However, two doses of GW7647 separated by a time window of 5 days induced weight loss in both LoxP and NRCA1-KO^{Alb} mice (Figure 38C/E). Weight loss tended to be higher in NRCA1-KO^{Alb} mice (Figure 38F). After 11 daily doses of GF7647, NRCA1-KO^{Alb} mice kept losing more weight, but body weight in LoxP was maintained (Figure 38C/E). The total weight loss induced by GW7647 was significantly higher in NRCA1-KO^{Alb} mice compared to LoxP animals (Figure 38G). It has been reported that chronic treatment with the PPARα agonist Wy14643 during MCD diet feeding caused weight loss in LoxP mice, but not in total PPARα-KO mice[162], however, the mechanisms are unknown.

Liver weight was similar between both genotypes upon MCD diet. However, LoxP mice treated with GW7647 showed a remarkable increase in liver weight (Figure 38H). Chronic treatment with Wy14643 in MCD diet-fed mice also induced an increase in liver weight[162]. Chronic treatment with the PPARα agonist GW9578 also led to increased liver weight in obese AKR/J mice[163]. These results are consistent with the known effects of PPARα activation on hepatocyte proliferation[164,165]. GW7647-induced liver weight gain was also observed in NRCA1-KO^{Alb} mice, but to a lower extent (Figure 38H). In fact, there were only 3 out of 8 mice that had a prominent increase in liver weight, suggesting that most NRCA1-KO^{Alb} mice respond worse to GW7647-treatment. Concomitantly, if we remove those 3 “super-responder” NRCA1-KO^{Alb} mice, PPARα activation by GW7647 is clearly impaired in NRCA1-KO^{Alb} animals. Interestingly, plasmas collected from the NRCA1-KO^{Alb} mice with impaired PPARα activation were yellowish compared to vehicle-treated animals and LoxP GW-7647 treated animals. Histological analysis will be seminal to determine the state of the livers and evaluate whether MCD diet has differential effects between genotypes, and whether GW7647 treatment has any effects between genotypes on top of MCD diet.

We also measured body composition at day 10 after two doses of GW7647 and at day 19, after 9 daily doses of GW7647 plus the previous two doses. To begin with, NRCA1-KO^{Alb} mice showed enhanced lean mass (Figure 39A) and reduced fat mass (Figure 40A) at day 10 of MCD diet. Strikingly, two doses of GW7647 induced a significant increase in lean mass in both genotypes (Figure 39A), however the total GW7647-induced lean mass gain tended to be higher in LoxP mice (Figure 39C). Two doses of GW7647 induced a significant loss in fat mass in both genotypes (Figure 40A), and total GW7647-induced fat mass loss tended to be higher in LoxP mice as well (Figure 40C).

Nevertheless, the differences in body composition observed at day 10 were abrogated at day 19 (Figure 39B, Figure 40B). In addition, the higher GW7647-induced lean mass gain and fat mass loss in LoxP animals were no longer observed at day 19 (Figure 39D, Figure 40D). We do not know whether this adaptation in body composition at day 19 in NRCA1-KO^{Alb} mice is due to prolonged MCD diet treatment, prolonged GW7647 treatment or a combined effect of both.

We also subjected female mice to MCD diet. However, in this case, we only fed the female mice with MCD diet during one week to evaluate the effects of NRCA1 ablation in response to an acute lipid overload stress in the liver. Liver weights were similar in both genotypes (Figure 41B) after one week of MCD diet, but it caused a modest decrease in body weight in female mice of both genotypes (Figure 41C/D). At the day 7 of MCD diet mice were treated with GW7647 for 4 hours. PPARα activation by GW7647 was clearly impaired in NRCA1-KO^{Alb} female mice (Figure 29). Strikingly, vehicle-treated NRCA1-KO^{Alb} mice showed enhanced expression of Cyp4a10 and Cyp4a14 compared to vehicle-treated LoxP mice (Figure 29). In fact, GW7647 treatment caused a downregulation in the expression of Cyp4a10 and Cyp4a14 in NRCA1-KO^{Alb} animals (Figure 29). It has been reported that MCD diet induces an increase in the expression of Cyp4a14[39,166]. This increased expression is associated to MASLD progression, as overexpression of Cyp4a14 induced fatty liver[166], whereas Cyp4a14 ablation ameliorated MCD diet-induced MASLD[166]. In this regard, Cyp4a14 overexpression upregulated the expression of CD36, a lipid transporter that mediates fatty acid uptake in hepatocytes[166]. Moreover, Cyp4a14-KO mice showed attenuated expression of Cyp4a14 upon MCD diet compared to LoxP animals[166], suggesting that increased CD36 expression by Cyp4a14 drives MASLD.

PPARα agonism has been shown to ameliorate MASLD in mouse models in numerous studies[107–109], and it induces the expression of Cyp4a14. However, studies in Cyp4a14-KO mice and mice with Cyp4a14 overexpression have shown that Cyp4a14 is a driver of MASLD pathogenesis[166].

We have evaluated the effects of NRCA1 ablation in the activation of PPARα by GW7647 in an MCD diet-induced MASL model in male and female mice. Our results indicate that PPARα activation in NRCA1-KO^{Alb} animals in response to GW7647 is impaired in male and female mice fed with MCD diet. Histological analysis will be key to evaluate whether NRCA1 ablation has detrimental effects in the pathogenesis of MASLD, and whether NRCA1 ablation prevents amelioration of MASLD by GW7647.

5.3. NRCA1 is a chromatin-binding protein that interacts with the epigenetic machinery

In this study, by using the BioID technology for interactome analysis, we have identified the binding partners of NRCA1. One of the advantages of the BioID technology is the detection of transient interactors, as well as the detection of indirect interactors, for instance proteins that interact with a NRCA1 interactor but not directly with NRCA1 but are detected because of their vicinity with NRCA1. Therefore, the concept of "proximome" has arisen from BioID studies[167], to indicate the proximity nature of the BioID assay. For our proteomics analysis, we have used an exhaustive strategy by harnessing two different mass spectrometers, two different database searching software and two different interactome analysis algorithms. Therefore, we could be less restrictive with the BFDR and FC values in identifying interactors. Most binding partners we identified, under basal and starvation conditions, are proteins that are in some way regulating chromatin dynamics and epigenetics. Although starvation does induce some changes in the specific interacting partners, these changes are not reflected when performing GSEA, suggesting that the functions and processes that are regulated by the starvation-induced interactors are the same as those regulated by interactors in basal conditions.

As described in 2.3.2, NRCA1 is an activator of autophagy and is constantly shuttling between the nucleus and the cytoplasm. However, upon autophagy-activating conditions, such as starvation, there is a considerable increase in the pool of cytoplasmic NRCA1 in puncta-like structures. Therefore, we would have expected an increase in the number of cytoplasmic interactors in the BioID experiment under starvation conditions. It could be that starvation-induced cytoplasmic translocation of NRCA1-TID is somehow impaired by the attachment of TurboID at the C-terminus of NRCA1. However, attachment of GFP at the C-terminus of NRCA1 does not alter cytoplasmic translocation of NRCA1 under autophagy-activating conditions (unpublished data). It could also be that a one-hour starvation pulse was not sufficient to remodel the proximome of NRCA1.

Given the role of NRCA1 in autophagy, we also expected to identify new interactors involved in the regulation of autophagy. In this regard, we identified ATG2B in our mass spectrometry analysis, however, when we attempted to validate the interaction through pulldown assays in HeLa cells stably overexpressing NRCA1-GFP, we could not detect interactions between NRCA1 and ATG2B. Interestingly, in our validation studies of the NRCA1-TID construct (4.3.1), when we performed biotin-affinity pulldown assays we could observe interaction between NRCA1 and p62 (Figure 49), which we further validated with the NRCA1-GFP system. However, we were not able to detect p62 as an interactor in the proteomics analysis. These results indicate the presence of false negatives in the proteomics analysis.

Previous work in our laboratory showed that NRCA1 is a coactivator of several nuclear receptors in the presence of their ligands, including TRα, PPARγ, GRα, VDR and ERα. These experiments were performed using luciferase reporter assays containing responsive elements for said nuclear receptors. However, the molecular mechanism by which NRCA1 mediated

the activation of these nuclear receptors in the presence of their ligands remains to be elucidated. Now that we have uncovered the interacting partners of NRCA1, it would not be far-fetched to hypothesize that NRCA1 acts as a coactivator of nuclear receptors by interacting with epigenetic players in the presence of ligand. More specifically, as NRCA1 enhances the activation of nuclear receptors upon ligand binding, these interactions between NRCA1 and epigenetic regulators may act to favor the incorporation of epigenetic marks that open the chromatin to allow gene transcription (ON marks), or to suppress the incorporation of epigenetic marks that close the chromatin to prevent gene transcription (OFF marks), or a combination of both. Interestingly, we have also demonstrated in mouse liver that NRCA1 indeed acts as a coactivator of PPARα, as lack of NRCA1 impairs PPARα activation by fasting and by agonist.

Validation of the interaction between NRCA1 and RING1A and NRCA1 and UBR5, and the identification of several other members of the PRC1 in our mass spectrometry analysis prompted us to think that NRCA1 could also be a chromatin-binding protein. We performed subcellular and chromatin purification assays using several cell lines and we were able to detect NRCA1 in purified chromatin of all the cell lines tested. We could also detect it in the chromatin purified from mouse livers. It would be interesting to check whether NRCA1 binds directly to DNA or through another partner that does interact with DNA, which can be assessed with electrophoretic mobility shift assay (EMSA). Interestingly, the amino acid sequence of NRCA1 contains two regions that are rich in basic amino acid residues, from 138-152 and 169-203 (Figure 5) that could be for interaction with DNA. NRCA1 as a chromatin-binding protein raises the question whether it is bound to specific DNA sequences and to what genes it is bound. ChIP-seq analysis could be performed to answer these questions. Given the tissue-specific roles of NRCA1, it would not be surprising if NRCA1 were bound to different sequences and genes depending on the tissue. Antibodies to perform ChIP are usually the limiting factor in ChIP-seq studies, therefore good-quality antibodies are needed for this type of experiments. To date, we have not been able to identify any commercial antibody that works well to detect NRCA1 in western blot analysis, let alone to immunoprecipitate endogenous NRCA1. We have an in-house made antibody that can recognize and detect endogenous NRCA1 in western blot analysis, but it has limited capacity to immunoprecipitate overexpressed NRCA1. The lack of a good NRCA1 antibody constitutes a seminal limitation in studying its cellular and molecular functions.

NRCA1 interacts with RING1A, and it is in close proximity to other members of the PRC1. The PRC1 ubiquitinates histone H2A to mediate gene repression[121]. We hypothesize that a possible mechanism by which NRCA1 regulates PPARα activation is through its interaction with RING1A and the PRC1. There is no reported role of the PRC1 in liver metabolism. Interestingly, RING1B silencing in breast cancer cells, the paralog of RING1A, upregulates genes involved in fatty acid metabolism[126]. As PRC1 is a repressive complex, and NRCA1 is an activator of PPARα, it would be reasonable that NRCA1 prevents the action of PRC1 on PPARα target genes upon activation of PPARα by fasting or agonists. However, when NRCA1 is ablated, PRC1 can repress PPARα target genes, even in the presence of agonists or upon fasting. Therefore, it would be interesting to assess whether NRCA1 ablation promotes PRC1 occupancy on PPARα target genes through ChIP-Seq analysis.

5.4. UBR5 regulates NRCA1 protein levels

In this thesis, we have uncovered that NRCA1 interacts with UBR5. To study whether there was any functional interaction between these two proteins, we generated Ishikawa cells lacking UBR5. What we first noticed in UBR$^{-/-}$ cells was an upregulation of NRCA1 protein levels (Figure 66), suggesting that UBR5 could be an E3 involved in the ubiquitination and proteasomal degradation of NRCA1. Interestingly, NRCA1 deletion in Ishikawa cells downregulated UBR5 protein levels (Figure 67), indicating a mutual functional interaction.

Not only did UBR5 ablation upregulated NRCA1 protein levels, but it also enhanced NRCA1-related processes. On one hand, UBR5 deletion sensitized cells to apoptosis under basal conditions, to starvation-induced apoptosis and to autophagy-inhibition-induced apoptosis (Figure 73, Figure 74). On the other hand, UBR$^{-/-}$ cells showed enhanced basal autophagy flux and starvation-induced autophagy flux (Figure 70). Interestingly, autophagy flux studies indicated that UBR5 ablation enhanced NRCA1 degradation through autophagy (Figure 72). It has been widely reported that when proteasome substrates can no longer be degraded by the proteasome (e.g. when proteins aggregate), they become substrates for autophagic degradation[116].

Considering the data concerning UBR5 and NRCA1, it will be essential to demonstrate that UBR5 indeed ubiquitinates and targets NRCA1 for proteasomal degradation. UBR5 is an E3 that belongs to the N-end rule pathway[168]. This proteolytic pathway mainly targets short-lived proteins[168], and NRCA1 is a short-lived protein with a half-life of around 5 hours [redacted]. The N-end rule pathway requires the generation of a degron at the N-terminus of target proteins through various mechanisms[168]. Degrons are amino acid sequences used by E3s to recognize their substrates for subsequent ubiquitination. Interestingly, NRCA1 only contains 3 lysine residues that could be ubiquitinated. Triple mutation of these residues increased dramatically increased the half-life of NRCA1. It would be very interesting to assess the half-life of NRCA1 in UBR5-depleted cells, and in UBR$^{-/-}$ cells with re-expression of WT UBR5 or catalytically-dead UBR5 mutant.

The identification of UBR5 as the potential E3 that targets NRCA1 opens up the possibility to modulate NRCA1-related processes, such as autophagy and apoptosis via UBR5. NRCA1 has been reported to sensitize cancer cells to death receptor-dependent apoptosis[redacted]. In keeping with this, UBR5 inhibitors could be produced to enhance the pro-apoptotic effects of NRCA1 in the context of cancer treatment.

Another interesting observation is that UBR5-depleted cells and NRCA1-depleted cells show upregulated RING1A levels, suggesting there is functional interaction between these 3 proteins. It could be that UBR5 also targets RING1A for degradation. This could require NRCA1, maybe to act as a scaffold to promote UBR5-RING1A interaction, which is why NRCA1 ablation also leads to upregulation of RING1A protein levels.

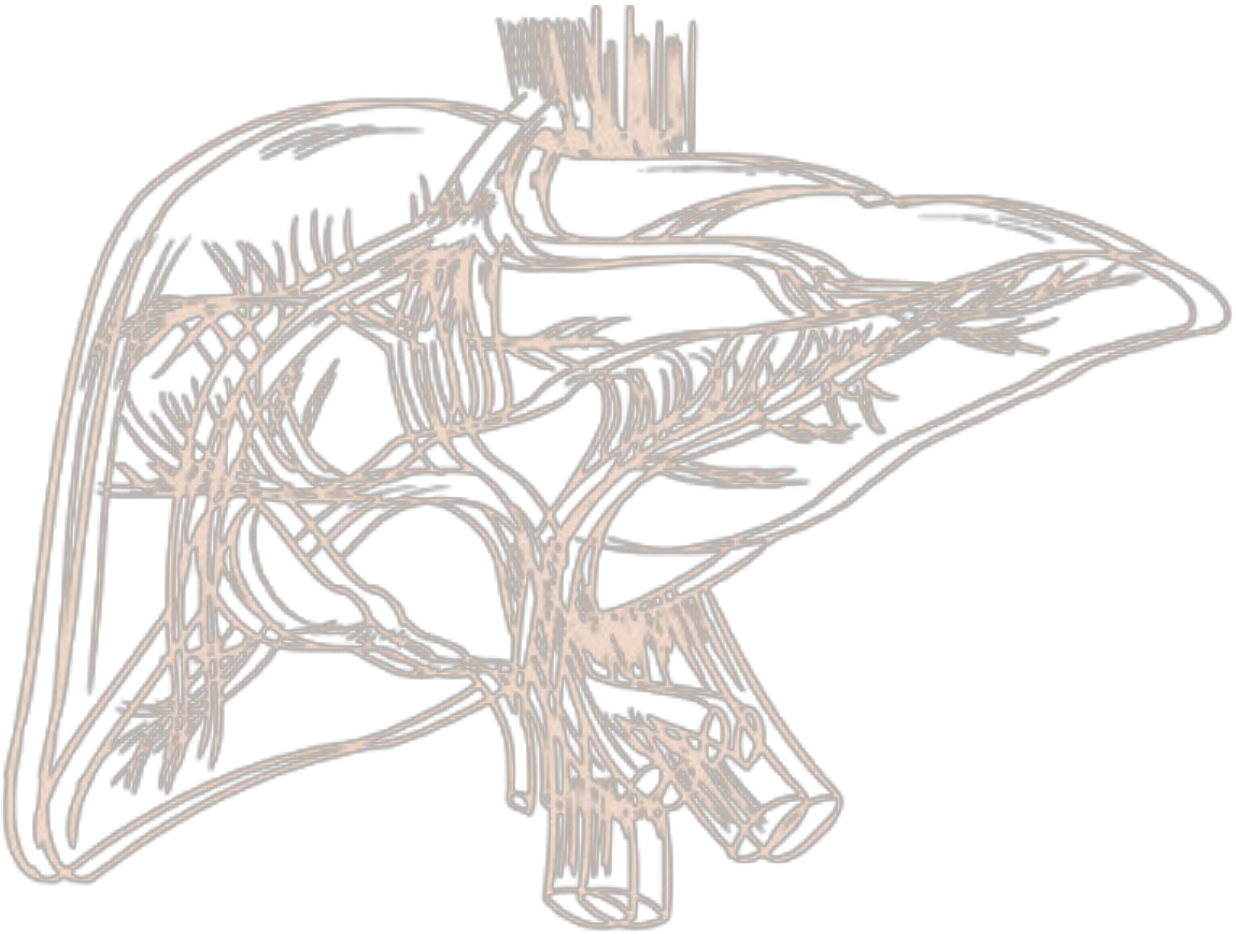

CONCLUSIONS

6. CONCLUSIONS

The data obtained from *in vivo* studies allow us to propose the following conclusions:

1. Liver-specific and total NRCA1 ablation impairs hepatic PPARα activation by overnight fasting in 12-week, 16-week, one-year and two-year old male mice and in 16-week old female mice. This is accompanied by enhanced hepatic fat accumulation upon overnight fasting.
2. NRCA1 expression is upregulated in response to overnight fasting in female and male mice of all ages.
3. Aging impairs fasting-induced induction of NRCA1, and PPARα activation by overnight fasting, which is further exacerbated by NRCA1 ablation.
4. PPARα activation by agonist is impaired by NRCA1 ablation in standard diet-fed female mice, but not in male mice.
5. PPARα activation by agonist is impaired by NRCA1 ablation in MCD-diet fed female mice and male mice.

The data obtained from *in vitro* studies allow us to propose the following conclusions:

1. NRCA1 is a chromatin-binding protein in different cell lines and in mouse liver.
2. NRCA1 predominantly interacts with proteins involved in the regulation of chromatin dynamics and epigenetics. Many of these proteins have nuclear receptor binding function and are members of the PRC1.
3. NRCA1 interacts with RING1A, UBE2O and UBR5 through co-immunoprecipitation assays.
4. There is functional interaction between NRCA1, UBR5 and RING1A. On one hand, NRCA1 ablation leads to UBR5 downregulation. On the other hand, UBR5 ablation causes upregulation of NRCA1. Ablation of either NRCA1 or UBR5 leads to an upregulation of RING1A.
5. UBR5 ablation enhances basal and starvation-induced autophagy flux, and promotes apoptosis under basal and starvation conditions.

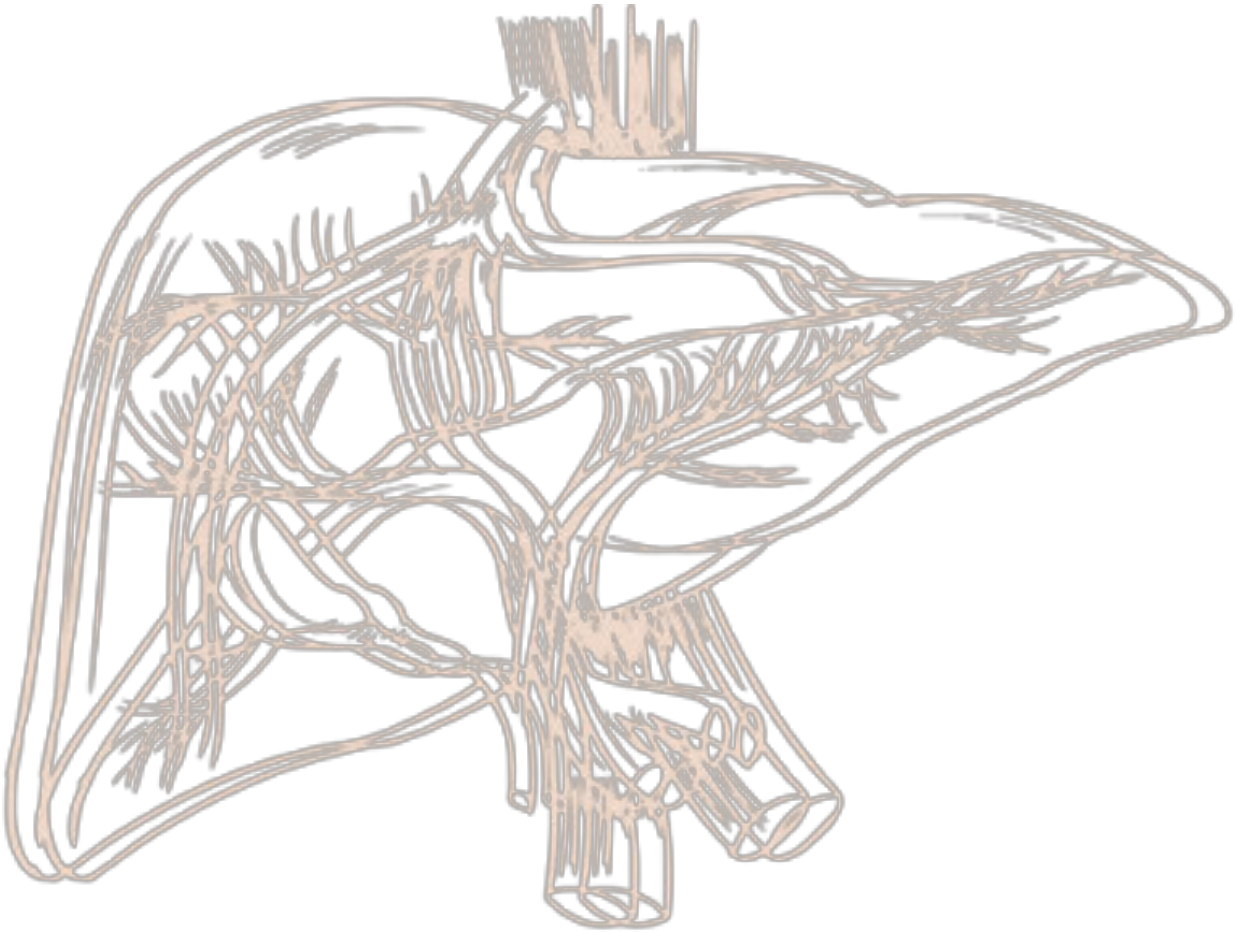

MATERIALS & METHODS

7. MATERIALS AND METHODS

7.1. Materials

7.1.1. Primers, primary and secondary antibodies

Table 1: Sequences of primers used in this thesis.

Target gene	Forward	Reverse
Arp	AAGCGCGTCCTGGCATTGTCT	CCGCAGGGGCAGCAGTGGT
Acat1	CTACATGGGCAATGTCATCCA	TGCGCCCAGTGTTGCT
Acox1	TTACGTCACGTTTACCCCGG	ACCAGCTTCCCCGACTGAA
Atg5	CCCCTGAAGATGGAGAGAAGAG	TCCTGACTCAAGGTGGTTCC
Atg12	CTGGTGGCCTCGGAACAGT	CATGCCTGGGATTTGCAGT
Atg16l	CTGGGATATCCGGTCAGAGAG	TCTCCACTTTCCCTGTCAGC
Cd36	ATGGGCTGTGATCGGAACTG	GTCTTCCCAATAAGCATGTCTCC
Cpt1a	CTCCGCCTGAGCCATGAAG	CACCAGTGATGATGCCATTCT
Cyp2c55	ACACACACAAGCACTTTGTCA	GCTTCTGCTGGTAATCTGCG
Cyp4a10	AGAACTTCCCAAGTGCCTTTC	GCAAACCATACCCATTAGCCTTT
Cyp4a14	GGCAGTCCAATTCTACTTACGA	CTCCTTGTCCTTCAGATGGT
Gabarap	AAGAGGAGCATCCGTTCGAGA	GCTTTGGGGGCTTTTTCCAC
Gabarapl1	GGACCACCCCTTCGAGTATC	CCTCTTATCCAGATCAGGGACC
Gabarapl2	TCGGGCTCTCAGATTGTTGAC	ATGGCCTTCTCGGAGGGAA
Lc3a	TTGGTCAAGATCATCCGGT	GCTCACCATGCTGTGCTGG
Lc3b	CCCACCAAGATCCCAGTGAT	CCAGGAACTTGGTCTTGTCCA
Ncor1	TGCGTCAGCTTTCTGTGATTCCACC	TGATTTCTGCCTCTGCGTTTTCCAT
Pgc-1α	AGCCGTGACCACTGACAACGAG	GCTGCATGGTTCTGAGTGCTAAG
Pparα	TGCAAACTTGGACTTGAACG	AGGAGGACAGCATCGTGAAG
Rxr	ACTTCTCTACCCAGGTGAAC	GATATCCTCAGTGCTGCTC
Sirt1	TCCCTCAAAGTAAGACCAGTAGC	TGCCACCCACACCTCTTCAT

Table 2: List of primary antibodies used in this thesis.

Target	Host	Dilution	Source
β-Actin	Mouse	1:10000	Sigma Aldrich, A1978
CASP3	Rabbit	1:1000	CST, 9662S
Cyp4a	Mouse	1:1000	Santa Cruz, sc-271983
Flag	Rabbit	1:1000	CST, 1672368S
GABARAP	Rabbit	1:1000	CST, 13733S
GAPDH	Rabbit	1:1000	CST, 2118S
GFP	Goat	1:1000	CST, ab5450
H2A	Rabbit	1:1000	CST, 12349S
H3K27me3	Rabbit	1:1000	CST, 1679733S
Lamin A/C	Mouse	1:500	Santa Cruz, sc-376248
LC3B	Rabbit	1:1000	1672775S, CST
PARP-1	Rabbit	1:1000	9542S, CST
p62	Guinea pig	1:1000	PROGEN, GP62-C
RING1A	Rabbit	1:1000	CST, 13069S
RING1B	Rabbit	1:1000	CST, 5694T
SA-HRP	-	1:50000	Jackson Immuno, 016-030-084
NRCA1	Mouse	1:500	In house
UBE2O	Rabbit	1:1000	Bethyl Labs, A301-873A-T
UBR5	Rabbit	1:1000	CST, 65344S
ULK1	Rabbit	1:1000	CST, 1678054S
Vinculin	Mouse	1:5000	Santa Cruz, sc-73614

Table 3: List of secondary antibodies used in this thesis.

Target	Host	Dilution	Source
Anti-goat-HRP	Mouse	1:10000	Santa Cruz, sc-2354
Anti-guinea pig-HRP	Goat	1:10000	Jackson Immuno, 106-035-003
Anti-mouse-HRP	Donkey	1:10000	Jackson Immuno, 715-035-150
Anti-rabbit-HRP	Donkey	1:10000	Jackson Immuno, 711-035-152
Anti-mouse IRDeye 800CW	Donkey	1:5000	Licor, 926-32212
Anti-rabbit DyLight 800	Goat	1:5000	Thermo Fisher, SA5-35571

Table 4: List of plasmids used in this thesis.

Plasmid	Source
V5-TurboID-NES_pCDNA3	Addgene, #107169
pSG5 EDD (Flag-UBR5)	Addgene, #37191
pcDNA3.1-3xFLAG-TEV-UBE2O	Addgene, #105718
Flag-RING1A	Kindly gifted by Dr. Zhaoyuan Hou

7.1.2. General buffers and solutions

Table 5: RIPA lysis buffer.

Component	Final concentration	Source
EDTA	1 mM	Merck Millipore, 324503
EGTA	1 mM	Sigma-Aldrich, E4378
NaCl	150 mM	Sigma-Aldrich, 71376
Triton X-100	1% (v/v)	Sigma-Aldrich, I3021
SDS	0.1% (w/v)	Sigma-Aldrich, 11667289001
Sodium deoxycholate	0.5% (w/v)	Sigma-Aldrich, D6750
TRIS-HCl 7.5	50 mM	Sigma-Aldrich, 10812846001

Table 6: Flag-IP buffer

Component	Final concentration	Source
EDTA	1 mM	Merck Millipore, 324503
NaCl	150 mM	Sigma-Aldrich, 71376
Triton X-100	1% (v/v)	Sigma-Aldrich, T8787
TRIS-HCl pH 7.5	50 mM	Sigma-Aldrich, 10812846001

Table 7: Protein loading dye (4x)

Component	Final concentration	Source
Bromophenol blue	0.04% (w/v)	Sigma-Aldrich, 114391
DL-Dithiothreitol	1 mM	Sigma-Aldrich, D0632
NN,-dimethyl formamide	4% (w/v)	Sigma-Aldrich, D4551
Glycerol	40% (w/v)	Sigma-Aldrich, G5516
SDS	8% (w/v)	Sigma-Aldrich, 11667289001
Tris-HCl	240 mM	Sigma-Aldrich, 10812846001

Table 8: Phosphate-buffered saline

Component	Final concentration	Source
$Na_2HPO_4 \cdot 2H_2O$	9 mM	Sigma-Aldrich, 71643
NaCl	136.9 mM	Sigma-Aldrich, 71376
KCl	2.7 mM	Sigma-Aldrich, 60130
KH_2PO_4	1.5 mM	Sigma-Aldrich, 5655

Table 9: Separation gel for SDS-PAGE

Component	Final concentration	Source
Acrylamide (30%)	20-44.7% (v/v)	Sigma-Aldrich, A3699
APS	0.07% (v/v)	Bio-Rad, 1610700
dH_2O	28.5-53.2% (v/v)	Milli-Q® Direct
SDS	0.1% (w/v)	Sigma-Aldrich, 11667289001
Separation buffer: TrisHCl 1.5 M	25% (v/v)	Sigma-Aldrich, 10812846001
TEMED	0.07% (v/v)	Bio-Rad, 1610800

Table 10: Stacking buffer for SDS-PAGE

Component	Final concentration	Source
Acrylamide (30%)	5% (v/v)	Sigma-Aldrich, A3699
APS	0.07% (v/v)	Bio-Rad, 1610700
dH_2O	60% (v/v)	Milli-Q® Direct
SDS	0.1% (w/v)	Sigma-Aldrich, 11667289001
Stacking buffer: TrisHCl 0.5 M	25% (v/v)	Sigma-Aldrich, 10812846001
TEMED	0.07% (v/v)	Bio-Rad, 1610800

7.2. *In vivo* methods

7.2.1. Generation of liver-specific NRCA1 knockout model

The NRCA1 liver-specific knockout model (NRCA1-LKO) was initially generated [redacted]. This was performed using the Cre/Lox recombination technology to delete a specific region within the NRCA1 gene. NRCA1 $^{LoxP/LoxP}$ mice were previously used in our group by [redacted]. Those mice were transgenically modified to contain two LoxP recombination sites within the NRCA1 gene, which were placed before exon 3 and after exon 4 of the sequence (Figure 75). The activity of the Cre recombinase causes the excision of Exon 3 (containing the start codon ATG) and Exon 4, resulting in NRCA1 protein ablation, specifically in hepatocytes.

The NRCA1 liver-specific knockout model was generated by crossing homozygous NRCA1$^{LoxP/LoxP}$ mice with a strain expressing the Cre recombinase under the hepatocyte-specific albumin promoter. Both mouse strains had a pure C57BL/6J genetic background. This crossing resulted in a first generation of heterozygous mice (Alb-Cre$^{-/+}$, NRCA1$^{LoxP-/LoxP+}$). These mice were further crossed to obtain littermates of the two desired genotypes:

- Alb-Cre$^{-/-}$, NRCA1$^{LoxP+/LoxP+}$: Mice with normal NRCA1 expression due to the absence of Cre recombinase. These mice are further referred to as LoxP or control mice.
- Alb-Cre$^{-/+}$, NRCA1$^{LoxP+/LoxP+}$: Mice with hepatocyte-specific ablation of NRCA1. These mice are further referred to as NRCA1-KO^{Alb} or KO^{Alb} mice.

All mice assigned to experiments have been shown to be homozygous for carrying the LoxP sequence by genotyping. Furthermore, mice were genotyped for Cre recombinase. Mice containing the sequence coding for Cre recombinase were considered NRCA1-LKO mice, and littermates lacking this sequence were used as controls. The genotypes were confirmed at the end of experiments on mRNA and protein level after necropsy.

Figure 75: Generation of the NRCA1 liver-specific knockout mouse model. Created with BioRender.

7.2.2. Genotyping of mice

Genotyping of NRCA1-KO^{Alb} was performed by extraction of genomic DNA from tail tips obtained at weaning. Extracted DNA was subsequently amplified by PCR. Finally, PCR-products were separated based on size through electrophoresis in agarose and visualized using SYBR™ Safe DNA Gel Stain.

7.2.2.1. Genomic DNA extraction

Extraction of genomic DNA from mouse tail tips was performed as follows:

1. Tail tips are digested in 500 µL tail tip lysis buffer containing Proteinase K (Material and Methods, Table 1) overnight at 55℃ and shaking at 450 rpm.
2. Proteinase K is deactivated at 80℃ for 2 min.
3. Samples are cooled down on ice and centrifuged at 18,000g for 15 min at RT.
4. Supernatant is transferred to new vials containing 500 µL isopropanol and is mixed by inverting.
5. Vials are centrifuged at 14,000g for 10 min at RT and supernatant is discarded.

6. The pellet is washed with 500 µL 70% ethanol.
7. Samples are centrifuged at 14,000g for 5 min at RT and supernatant is discarded.
8. Pellets are dried for 1h.
9. Isolated DNA is resuspended in 500 µL of water and heated for 2 min at 65°C.

7.2.2.2. Genotyping by polymerase chain reaction

To determine the genotype of mice, sequences of DNA were amplified by polymerase chain reaction (PCR) using two different primer sets for Cre and LoxP (Material and Methods, Table 25). Using this technique, selected sequences can be amplified exponentially to a concentration that allows visual detection in an agarose gel upon DNA staining with SYBR™ Safe DNA Gel Stain.

Cre-primer pair targets a sequence of about [redacted] bp within the Cre recombinase gene and will only be amplified and detected in Cre-positive animals, as seen in Figure 66. Animals expressing Cre recombinase under the hepatocyte-specific albumin promoter, as well as NRCA1-KO^{Alb}, show bands of [redacted] bp. Cre-negative animals can be identified by the absence of the 640 bp band in the agarose gel.

The second primer pair is directed against the NRCA1 sequence, resulting in an about [redacted] bp band in wild-type animals and an about [redacted] bp band in animals, where LoxP sequences are inserted in the genomic DNA (Figure 76). Genotyping of Albumin-Cre mice and C57BL/6J wildtype mice results in a band detected at around [redacted] bp, while all experimental animals were transgenic for LoxP sites inserted within the NRCA1 gene sequence.

Figure 76: Genotyping of experimental animals by PCR. PCR-products visualized in an agarose gel after electrophoresis. [redacted].

7.2.3. Oral gavage

Oral gavage was performed adhering to the following protocol and by Vanessa Hernàndez, our animal technician:

1. Weigh the mouse to determine the appropriate dosing volume. The volume should not exceed 100 µL/10 grams of body weight, with a maximum of 300 µL to be administered.
2. Restrain the mouse by gently gripping the dorsal neck.
3. Draw up the calculated volume, attach the feeding needle to the syringe and slightly lubricate it with water.
4. Grasp the skin over the shoulders and hold the mouse upright so that it cannot push the gavage tube away with the front feet. Gently pull the head backward.
5. Slide the needle into the mouth behind and to the left of the incisor teeth and over the tongue and slowly advance the needle into the oral cavity. Avoid rotating the needle.
6. When insertion is properly achieved, slowly administer the solution.
7. Once the solution is administered, remove the gavage tube smoothly and return the mouse to its cage.
8. Keep the mouse under observation for at least 15 minutes for signs of pain or distress, such as breathing difficulties or bleeding.
9. Monitor animals at least once between 12-24 hours after dosing and check for the above-mentioned signs of distress.
10. Dosing may be repeated up to 3 times within a 24 hour period.

Oral gavage solutions were prepared in aqueous solution containing 10% DMSO, 40% PEG300, 5% Tween-80 and 45% PBS. For GW7647, mice were administered a 5 mg/kg dose. For Wy14643, mice were administered a 50 mg/kg dose.

7.2.4. Body composition measurement

To measure body composition, the EchoMRI™ equipment was used, which measures fat, lean, total water and free water mass. The system utilizes quantitative nuclear magnetic resonance for analysis. Animals are placed inside a plastic holder and inserted into the system without the need for sedation or anesthesia. The determined fat mass is the total of all fat molecules within the animal expressed as equivalent weight of canola oil. The lean mass includes all body parts that contain water excluding fat, bone minerals, hair and claws. Free water consists mostly of urine within the bladder, while total water includes free water as well as water contained in lean mass.

7.2.5. Research diets

Table 11: List of diets used in this thesis

Diet name	Source
Chow diet	Special diets services, RMI, 801151
HFD diet: 60% kcal fat	Research Diets, D12492i
WD: 40% kcal fat, 0.2% cholesterol (w/w), 35% sucrose (w/w	Research Diets, D12079Bi
MCD diet	Research Diets, A06071305

7.3. *Ex vivo* methods

7.3.1. Histological analysis of liver samples

The morphology of mouse livers was analyzed microscopically using various standard staining techniques. Mice were sacrificed by cervical dislocation and liver tissue was collected immediately after. The liver was washed in PBS to remove residual blood and the right median lobe was cut in half using a scalpel. One part was immersed in 4 % paraformaldehyde and incubated overnight, while the other part was embedded in OCT solution and frozen in liquid nitrogen-cooled isopentane. Paraformaldehyde fixed livers were washed in PBS and stored at 4 ℃ before being transferred to the Histopathology Facility of the IRB. OCT embedded samples were stored at -80 ℃.

Samples were processed by the Histopathology Facility of the IRB. They performed tissue embedding in paraffin, cutting of sections, mounting onto slides and staining. Livers were stained using hematoxylin and eosin (H/E), Periodic acid–Schiff stain (PAS), Masson's trichrome stain and Sirius red stain. Furthermore, immunohistochemistry was performed for the macrophage marker F4/80. OCT embedded samples were cut, mounted and stained using Oil-Red-O (ORO). Slides were scanned using the NanoZoomer 2.0-HT (Hamamatsu). Quantification of F4/80- and ORO-stained livers was performed by analyzing three different regions per sample. The stained area per image was determined using the ImageJ software.

7.4. *In vitro* methods

7.4.1. Cell culture

During this PhD thesis, several cell lines were used to perform *in vitro* experiments, including AML12, C2C12 myoblasts, HAP1, HeLa, HEK293T, Ishikawa, mouse embryonic fibroblasts (MEFs) and SHSY-5Y cells. Cells were cultured at 37℃ in incubators with a humidified atmosphere of 5 % CO2 and 95% air. Before reaching confluency, cells were passaged using trypsin every 2 - 3 days. To seed cells for experiments, cells were counted as described in Material and Methods, 7.4.3. Culture media for each cell line is detailed in the following tables:

To freeze cells, freezing media containing fetal bovine serum (FBS) with 10 % dimethylsulfoxide (DMSO) as a cryoprotective agent and vials of frozen cells were stored at -80℃. Frozen cells were thawed in a water bath set to 37℃ and quickly mixed with pre-warmed culture media. The solution was centrifuged for 3 min at 300g to resuspend the cell pellet in DMSO-free.

To seed cells for experiments, cells are detached with trypsin and resuspended with culture media. 10 µl of cellular suspension is mixed with 10 µl of trypan blue and pipetted into a Neubauer chamber for cell counting. Finally, the desired amount of cells are seeded onto the cell culture vessel of choice.

For transient transfection experiments, the desired amount of cells are seeded onto the cell culture vessel of choice. Transfection solution is prepared by mixing 150 mM NaCl, polyethylenimine and the plasmid of interest and incubated for 20 minutes. Next, cells are incubated with transfection solution for 4 hours and media is removed for fresh media.

Table 12: Composition of culture media for C2C12, HeLa, HEK293T and SHSY-5Y cells.

Component	Final concentration	Source
DMEM	500 mL	Gibco, 41966
FBS	10% (v/v)	Sigma-Aldrich, F7525
Penicillin-Streptavidin	1% (v/v)	Gibco™, 15140122
HEPES	25 mM	Sigma-Adlrich, H4034

Table 13: Composition of culture media for Ishikawa cells.

Component	Final concentration	Source
MEM	500 mL	Gibco, 31095
FBS	5% (v/v)	Sigma-Aldrich, F7525
Penicillin-Streptavidin	1% (v/v)	Gibco™, 15140122
HEPES	25 mM	Sigma-Adlrich, H4034

Table 14: Composition of culture media for HAP1 cells.

Component	Final concentration	Source
IMDM	500 mL	Gibco, 12440
FBS	5% (v/v)	Sigma-Aldrich, F7525
Penicillin-Streptavidin	1% (v/v)	Gibco™, 15140122
HEPES	25 mM	Sigma-Adlrich, H4034

Table 15: Composition of culture media for AML12 cells.

Component	Final concentration	Source
DMEM-F12 GlutaMax	500 mL	Gibco, 31331028
FBS	10% (v/v)	Sigma-Aldrich, F7525
ITS (Insulin, Transferrin, Selenium)	1x	Sigma-Aldrich, 41400045
Dexamethasone	40 ng/ul	Sigma-Aldrich, D1756
Penicillin-Streptavidin	1% (v/v)	Gibco™, 15140122
HEPES	25 mM	Sigma-Adlrich, H4034

Table 16: Other reagents used in cell culture.

Reagent	Source
DMSO	Fisher Chemical, 10080110
Trypan Blue	Sigma-Aldrich, F7525
Trypsin-EDTA	Sigma-Aldrich, 41400045
Polyethylenimine	Polysciences, PEI 25000, 23966-2
Wy-14643	MedChemExpress, HY-16995
GW7647	Abcam, ab141124

7.4.2. TurboID

7.4.2.1. Molecular cloning

To clone the NRCA1-TurboID fusion vector, we used the Gibson Assembly cloning method. Briefly, this method allows for the joining of multiple DNA fragments in a single, isothermal reaction (Figure 77).

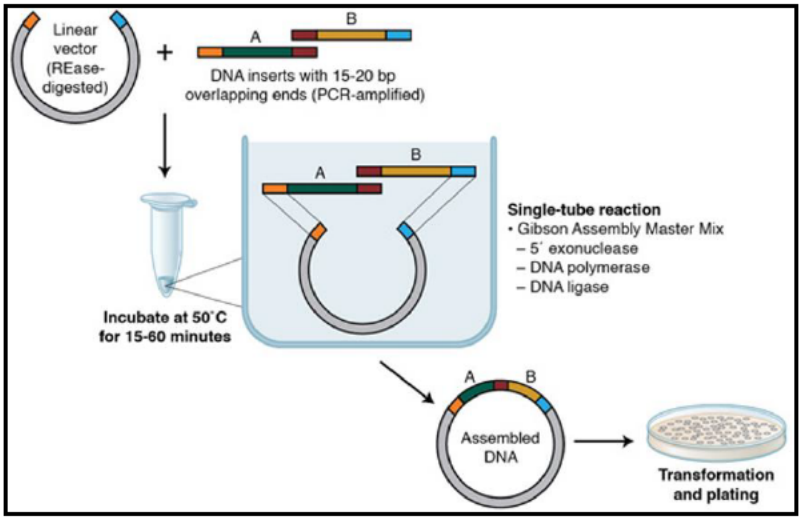

Figure 77: Overview of Gibson Assembly cloning method. Gibson Assembly employs three enzymatic activities in a single-tube reaction: 5´ exonuclease, the 3´ extension activity of a DNA polymerase and DNA ligase activity. The 5´ exonuclease activity chews back the 5´ end sequences and exposes the complementary sequence for annealing. The polymerase activity then fills in the gaps on the annealed regions. A DNA ligase then seals the nick and covalently links the DNA fragments together. The NEB Gibson Assembly Master Mix enables rapid assembly at 50˚C. Adapted from https://www.neb.com/en/applications/cloning-and-synthetic-biology/dna-assembly-and-cloning/gibson-assembly.

To perform the Gibson Assembly cloning method, we used the following protocol:

1. Generation of DNA inserts with overlapping ends through PCR amplification: primers used to amplify DNA inserts of interest can be found on (Table 6).
2. Digestion of backbone vector: we used as backbone vector a vector containing the TurboID insert (Figure 78). For digestion, we used HindIII and NheI restriction enzymes.
3. Amplified DNA inserts and digested vector were run in 1.5% agarose gels and purified using the Macherey-Nagel Nucleospin gel and PCR clean-up kit. Purified samples were quantified using NanoDrop 2000 UV-Vis Spectrophotometer.
4. We used a 5:1 insert to vector ratio for the Gibson reaction. For this, we mixed 50 ng of vector, 250 ng of insert and 5 µL of Gibson master mix reagent in a total volume of 10 µL in a PCR tube (on ice). Next, we incubated the samples at 50ºC in a thermocycler for 1 hour. After the reaction, assembly products were frozen at -20ºC.

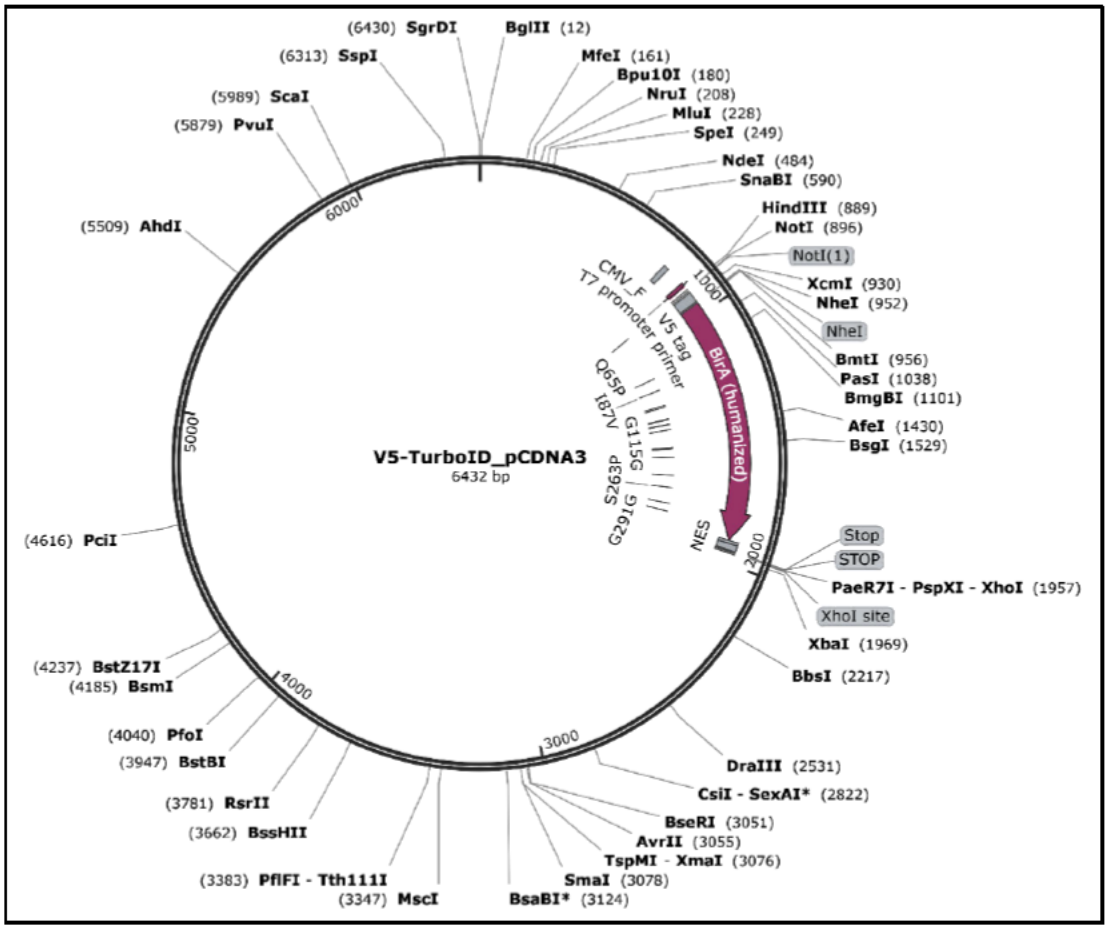

Figure 78: Map of the vector containing the TurboID insert. Created with SnapGene.

7.4.2.2. Bacteria transformation

NEB 10-β competent *E.Coli* cells were transformed with Gibson assembly products as follows:

1. Thaw NEB 10-β competent *E.Coli* cells on ice for 10 minutes.
2. Add 2 µL of Gibson assembly product to the bacteria. Carefully flick the tube 4-5 times to mix cells and DNA without vortexing and place on ice for 30 minutes.
3. Heat shock the mixture of bacteria and DNA at 42ºC for 30 seconds and place on ice for 5 minutes.
4. Add 950 µL of room temperature lysogeny broth (LB) and place at 37ºC for 1 hour with vigorously shaking (250 rpm).
5. Warm ampicillin selection plates at 37ºC.
6. Centrifuge samples at 2000 rpm for 3 minutes and remove 800 µL of LB.
7. Resuspend the pellet with remaining volume, add suspension to a selection plate and incubate overnight.

7.4.2.3. Plasmid verification and amplification

If cloning was successful, colonies will form on the selection plate. To verify the plasmid, we grew single colony bacteria in a 5 mL bacterial culture tube overnight with LB supplemented with 100 µg/mL ampicillin. The next day, we purified plasmid using the NucleoSpin Plasmid, Mini kit for plasmid DNA and sent the plasmid for sequencing.

Once the plasmid was verified, we amplified the plasmid. To do so, we transformed Top 10 *E.Coli* as described in [redacted]. with the purified plasmid f rom the previous step. Single colony was grown in a 5 mL bacterial culture tube overnight with LB supplemented with 100 µg/mL ampicillin. The next day, 1 mL of the bacterial culture was further grown overnight in a Erlenmeyer flask containing 200 mL of LB supplemented with 100 µg/mL ampicillin. The next day, plasmid was purified using Macherey-Nagel NucleoBond Xtra Maxi and sent for sequencing.

7.4.2.4. Turbo-ID protocol

Day 1: Seeding HEK293T cells

Seed $10*10^6$ HEK293T cells onto 15 cm dishes (2 dishes should give you enough protein).

Day 2: Transfection

Transfect cells with PEI.

Day 3: Addition of exogenous biotin and collect cells

Add biotin to a final concentration of 50 µM and incubate for 2 hours. Collect cells and proceed with affinity purification (freeze cell pellet at -80ºC if you are not performing the pull-down the same day).

Day 4: Affinity purification with streptavidin-coated magnetic beads (Pierce Thermo Fisher). "Detailed protocol"

1. Resuspend the cell pellet with 1.5 ml of RIPA lysis buffer (see recipe on the next page).
2. Incubate 1h on an end-over-end rotator at 4ºC.
3. Centrifuge at 16,000g for 30 minutes. (In the meantime, pre-equilibrate the magnetic beads with 1ml of lysis buffer twice in a LoBind microtube).
4. Take 10% of the lysate for western blot input analysis.
5. Incubate lysate with streptavidin-coated magnetic beads in a LoBind microtube (Eppendorf). **Note**: in our hands, what works the best is 20 µl of beads / 1 mg of protein. Adjust the amount of beads accordingly.
6. Incubate the lysates with the beads on an end-over-end rotator at 4ºC for 3 hours.
7. Take 10% of the supernatant for western blot flowthrough analysis.
8. Transfer the beads to a new LoBind microtube and wash them once with 1ml of lysis buffer and twice with 1 ml of 50 mM ammonium bicarbonate (pH 8).
9. Transfer the beads to a new LoBind microtube and wash two more times with 1 ml of 50 mM ammonium bicarbonate (pH 8).

10. Resuspend the beads in 50 mM ammonium bicarbonate (pH 8). **Example:** if you used 180 µl of beads, resuspend the beads in 180 µl of ammonium bicarbonate.
11. Take a small amount of the beads to analyze the IP fraction through western blot for quality control purposes. **Note**: 180 µl of beads / 60 µl of 1x sample buffer. Boil the beads with sample buffer at 95ºC for 10 minutes at 600 rpm.
12. Snap-freeze the rest of the beads and keep them at -80ºC until performing on-bead digestion.

7.4.3. Determination of autophagy flux

Autophagic flux describes the complete process of degradation of cellular components into its breakdown products by autophagy, including phagophore and autophagosome formation, fusion with the lysosome and subsequent degradation and release of recycled material back into the cytosol[143]

The macrolide Bafilomycin A1 (BafA1) disrupts autophagic flux via two distinct ways. First, BafA1 blocks lysosomal acidification and enzyme activation by inhibiting the proton pump V-ATPase. Furthermore, it also prevents autophagosome-lysosome fusion by inhibiting the endoplasmic reticulum calcium pump Ca-P60A/SERCA [redacted].

Assessment of autophagic flux was performed as follows:

1. 10^6 cells are seeded into 6 cm dishes.
2. The following day, media is removed, and cells are washed with PBS.

3a. To assess basal autophagy flux, culture media containing 200 nM Bafilomycin A1 or an equal volume of a DMSO vehicle was added to cells.

3b. To assess starvation-induced autophagy flux, EBSS media containing 200 nM Bafilomycin A1 or an equal volume of a DMSO vehicle was added to cells.

4. After four hours of incubation, cells were harvested for protein extraction (as described in 7.5.4.2).
5. A detailed explanation on how to calculate autophagy flux is provided (Figure 79).

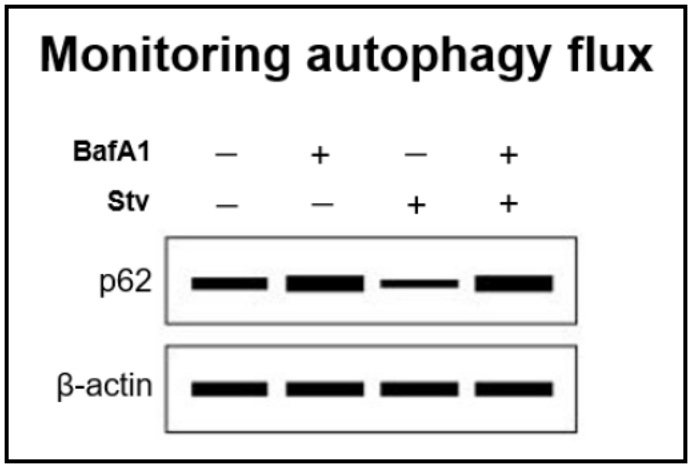

Figure 79: How to calculate autophagy flux *in vitro*. 4 conditions are needed to calculate autophagy flux: cells in basal conditions without inhibitor of autophagy ($BafA1^-$, Stv^-), cells in basal conditions treated with inhibitor of autophagy ($BafA1^+$, Stv^-), cells in starvation conditions without inhibitor of autophagy ($BafA1^-$, Stv^+), and cells in starvation treated with inhibitor of autophagy ($BafA1^+$, Stv^+). Treatment with inhibitor of autophagy, such as Bafilomycin A1, leads to a build-up of p62. This build-up corresponds to the amount of p62 that should have been degraded through autophagy. In keeping with this, we can estimate the flux of p62 and by doing the following calculation[143]: $flux = \frac{p62\ levels\ in\ the\ presence\ of\ BafA1}{p62\ levels\ in\ the\ absence\ of\ BafA1}$. The same procedure can be applied to LC3B-II. These calculation provides an estimation of basal and starvation-induced autophagy flux. Image adapted from[169].

7.5. Molecular biology methods

7.5.1. Analysis of gene expression by real time quantitative PCR

7.5.1.1. RNA extraction

RNA was extracted using TRIzol™ and purified using Purelink™ RNA Mini High Yield columns by following the manufacturer's instructions. RNA extraction from cells was performed by removing media, adding 500 µL of lysis buffer (provided within the kit) to 6-well plates and scraping of cells. In case of tissues, pieces of about 30 mg were put into pre-chilled tubes containing three zirconium oxide beads and 500 µL cold TRIzol™. Tissue was homogenized using the Mini-Beadbeater disrupter (Bio Spec Products) for 30 s at 3,400 oscillations per minute. The extracted RNA of cells and tissues was purified as follows:

1. 100 µL of chloroform is added to every 500 µL of TRIzol™, mixed thoroughly and incubated at RT for 2 min.
2. Samples are centrifuged for 15 min at 12,000g and 4℃ to achieve phase separation.
3. The upper aqueous phase is carefully removed and added to 300 µL of pre-chilled 70% ethanol.
4. The sample is transferred to a spin cartridge and centrifuged for 30 s at RT. The flow-through is discarded.
5. 700 µL Wash Buffer I is added to the spin cartridge followed by another centrifugation step. Flow-through is again discarded.
6. 80 µLPureLink™ DNase mixture is added directly to the surface of the spin cartridge membrane and incubated for 15 min at RT.
7. 500 µL Wash Buffer II is added to the spin cartridge followed by another centrifugation. Flow-through is again discarded.
8. Step 8 is repeated.
9. The empty spin cartridge is centrifuged for 1 min at 12,000g and RT to dry the membrane with bound RNA.
10. 30µL of pre-warmed RNase-free water (70℃) is added and incubated for 1 min.
11. The spin cartridge is inserted into a recovery tube and centrifuged for 1 min at 12,000g and RT.
12. Eluted RNA is stored at -80 ℃.

7.5.1.2. RNA quantification

The quantity and purity of RNA was determined by spectrophotometry using the NanoDrop 2000 UV-Vis Spectrophotometer. The concentration of RNA is given in ng/µL. The purity of the RNA is specified by two different absorbance ratios. Nucleotides, RNA and DNA absorb light at 260 nm, whereas proteins, phenol and other contaminants have a strong absorbance at 280 nm. A 260 / 280 ratio that is considerably lower than 2.0 indicates a contamination of a given sample. Contaminants such as carbohydrates, EDTA and phenol have absorbance near 230 nm. Thus, a 260 / 230 ratio that lies within the expected range of 2.0 - 2.2 is used as a secondary measure of nucleic acid purity.

7.5.1.3. Complementary single-stranded DNA preparation

Complementary single-stranded DNA (cDNA) is synthetized from an RNA template in a process called reverse transcription using the enzyme Reverse transcriptase (RT). In course of this thesis, cDNA was synthesized using qScript® cDNA SuperMix following the manufacturer's instructions:

1. An amount of 1 µg RNA is brought to a final volume of 16 µL using UltraPure™ Distilled Water and 4 µL qScript® cDNA SuperMix is added to each reaction.
2. After thoroughly mixing the reactions, cDNA is synthesized using the GeneAmp® thermocycler by incubating the samples with the following conditions:
    - 5 min at 25 ℃
    - 30 min at 42 ℃
    - 5 min at 85 ℃
    - 4 ℃ on hold
3. Once the samples cooled down to 4 ℃, they are diluted 1:50 using UltraPure™ Distilled Water. Subsequently, 6 µL of this cDNA dilution is used for every reaction during quantitative polymerase chain reaction.

7.5.1.4. Real time quantitative PCR

Real time quantitative polymerase chain reaction (RT-qPCR) was performed in 384-well plates using the thermocycler QuantStudio™ 6 Flex Real-Time PCR System. Each sample was measured in triplicates and all measurements were normalized to β-actin. Reactions contained 6 ng of cDNA, 625 nM of forward and reverse primers, 6 µL of SYBR Green PCR Master Mix in a final volume of 16 µL.

The RT-qPCR is performed in three distinct steps. First, there is an initial denaturation step at 95 ℃ for 10 min. This is followed by 40 cycles of 15 s of 95 ℃ and 1 min at 60 ℃. During the last step a melting curve is recorded, which serves as a positive control that only one specific PCR-product was amplified. The melting curve is generated by constantly detecting fluorescence while the temperature is increasing 0.05 ℃ / s. Rising temperatures cause dissociation of double-stranded DNA molecules, resulting in a decrease of SYBR®Green fluorescence. Melting temperatures are specific for each DNA molecule. Thus, RT-qPCRs that amplified a specific target will show a melting curve with one single peak, while RT-qPCRs that were unspecific will generate curves with multiple peaks.

7.5.2. Proteomics

All the procedures in this section were performed by the Mass Spectrometry and Proteomics core facility of IRB Barcelona.

7.5.2.1. Sample preparation

Tryptic digestion was performed directly on beads by incubating them with 1 µg of trypsin in a solution of 50% of beads in 50 mM NH_4HCO_3 (ABC buffer) at 37ºC overnight. The following morning, an additional 1 µg trypsin was added and incubated for 2 h more at 37°C.

Beads were pelleted by centrifugation at 2,000 g for 5 min, and the supernatant was transferred to a fresh Eppendorf tube. Beads were washed once with 100 µL of 50 mM ABC buffer, and these washes were pooled with the first supernatant. FA was added to the eluates to a 1% final concentration (in the case of magnetic beads, complete separation of the beads is performed with a magnetic separation rack). Samples were cleaned up through C18 tips (polyLC C18 tips) and peptides were eluted with 80% acetonitrile, 1% TFA in water. Next, samples were diluted to a final concentration of 20% acetonitrile and 0.25% TFA and loaded into SCX columns (polyLC),; peptides were eluted in 5% NH_4OH, 30% methanol. Finally, samples were evaporated to dry in the Speed Vac, reconstituted in 50 µL and diluted 1:8 with 3% acetonitrile, 1% FA aqueous solution for MS analysis.

7.5.2.2. LC-MSMS analysis

Two types of nano-LC-MS/MS set up were used in this work.

Evosep-Eclipse

Diluted peptides were loaded to a Evotip C18 µ-precolumn (Evosep) following the commercial instruction. Peptides were separated using a C18 analytical column EV1106 column (150 µm × 150 mm, 1.9 µm) (Evosep) using a Evosep One (EV-1000, Evosep) chromatographic system with a 88 min run. The column outlet was directly connected to an Orbitrap Eclipse™ Tribrid (Thermo Scientific). The mass spectrometer was operated in a DDA mode. Survey MS scans were acquired in the Orbitrap with the resolution (defined at 200 m/z) set to 120,000. The lock mass was user-defined at 445.12 m/z in each Orbitrap scan. The top speed (most intense) ions per scan were fragmented by CID with a NCE of 30 % and detected in the linear ion trap. The ion count target value was 400,000 and 10,000 for the survey scan and for the MS/MS scan respectively. Target ions already selected for MS/MS were dynamically excluded for 15 s. RF Lens were tuned to 30 %. Minimal signal required to trigger MS to MS/MS switch was set to 5,000. The spectrometer was working in positive polarity mode and singly charge state precursors were rejected for fragmentation.

Dionex-Lumos

Peptides were analyzed using an Orbitrap Fusion Lumos Tribrid mass spectrometer (Thermo Scientific, Waltham, MA, USA) equipped with a Thermo Scientific Dionex Ultimate 3000 ultrahigh-pressure chromatographic system (Thermo Scientific, Waltham, MA, USA) and an Advion Triversa Nanomate (Advion Inc Biosciences Ithaca, NY, USA) as the nanospray interface. C18 trap (300 µm × 5 mm, C18 PepMap100, 5 µm, 100 Å; Thermo Scientific,

Waltham, MA, USA) and C18 analytical columns (NanoEase MZ HSS T3 column (75 µm×250 mm, 1.8 µm, 100 Å); Waters, Milford, MA, USA) were used for the chromatographic separation at a 250 nL/min flow rate and 60 min gradient from 1 to 35 % B (A = 0.1% FA in water, B = 0.1 % FA in acetonitrile). The mass spectrometer was operated in a DDA mode using Orbitrap resolution in the MS1 (120 k) and Ion Trap in MS2; ions were fragmented by CID with a 35 % NCE. The ion count target value was 400,000 and 10,000 for the survey scan and for the MS/MS scan respectively. Target ions already selected for MS/MS were dynamically excluded for 30 s. RF Lens were tuned to 30%. Minimal signal required to trigger MS to MS/MS switch was set to 5,000. The spectrometer was working in positive polarity mode and singly charge state precursors were rejected for fragmentation.

Orbitrap Eclipse & Lumos Tune Application 3.5.3890 and 4.0.4091 and Xcalibur versions 4.5.445.18 and 4.6.67.17 were used to operate the instruments and to acquire data, respectively

7.5.2.3. Database search

We also used a twin strategy using the searching softwares MQ and PD. We tried to keep the big majority of MQ and PD parameters as analogous as possible taking into account that they are completely different database search tools.

MaxQuant

We used MQ (v1.6) with its Andromeda search engine[170–175]. We used the Human proteome from SwissProt (released in 2021), the SwissProt [redacted] Mouse protein sequence, and the list of common contaminants as a protein database (released in 2017). The search was run against the target and the decoy databases in order to determine the FDR. Only peptides and proteins with an FDR below 1 % were considered as positive identifications. Some of the most relevant search parameters were trypsin (allowing for two missed cleavage sites) as digesting enzyme; oxidation in methionine and acetylation in protein N-terminus, as dynamic modifications; 10 ppm as precursor mass tolerance; and 0.6 Da as MS/MS mass tolerance.

Proteome Discoverer

We used PD (v2.5) with Sequest HT as a search engine. We used the Human proteome from SwissProt (released in 2021), the SwissProt [redacted] Mouse protein sequence, and the list of common contaminants as a protein database (released in 2017). Both searches were run against the target and the decoy databases in order to determine the FDR with the Percolator algorithm[176,177]. Only PSMs with an FDR below 1 % were considered as positive identifications. Some of the most relevant search parameters were trypsin (allowing for two missed cleavage sites) as digesting enzyme; oxidation in methionine, acetylation in protein N-terminus, and methyl group loss with and without acetylation in protein N-terminus, as dynamic modifications; 10 ppm as precursor mass tolerance; and 0.6 Da as MS/MS mass tolerance[176].

7.5.2.4. Interactome analysis

Similarly as we did for the database search, we followed a twin strategy for the interactome analysis based on two different scoring algorithms called SAINTq[178] and SAINTexpress[179] and analyzed PD and MQ outputs in parallel.

SAINTq

The SAINTq-based interactome analysis uses protein abundances to score potential interactors. We drop contaminant and decoy identifications and only abundances from unique peptides for protein groups were sent to SAINTq scoring algorithm. The resulting list with potential interactors was initially filtered by requiring FC ≥ 3 and BFDR ≤ 0.02.

SAINTexpress

The SAINTexpress-based interactome analysis uses PSMs counts to score potential interactors. Additionally as we did with SAINTq, with SAINTexpress we also analyzed the combination of PD and MQ outputs (PD+MQ). This combined dataset is constructed by taking the maximum PSM count between PD and MQ, for a given prey and a given sample. As usual, contaminant and decoy identifications were removed and only unique peptides for protein groups were sent to the SAINTexpress scoring algorithm. The resulting list with potential interactors was initially filtered by requiring FC ≥ 3 and BFDR ≤ 0.02.

7.5.3. Transcriptomics

7.5.3.1. Interactome analysis

RNA was extracted as in 7.5.1.1.

7.5.3.2. Library preparation and sequencing

Library preparation was performed by the Functional Genomics Core Facility of IRB Barcelona. Briefly, total RNA extractions were quantified with the Nanodrop One (Thermo Fisher), and RNA integrity was assessed with RNA ScreenTape assay of the Tapestation 4200 platform (Agilent). Libraries for RNA-seq were prepared at IRB Barcelona Functional Genomics Core Facility. Briefly, rRNA depletion and library preparation was performed from 1 µg of total RNA and used to generate dual-indexed cDNA libraries with the Illumina Stranded Total RNA Prep, Ligation with Ribo-Zero Plus kit (Illumina) and UD Indexes Set A (Illumina). Ten cycles of PCR amplification were applied to all libraries.

Sequencing-ready libraries were quantified using the Qubit dsDNA HS assay (Invitrogen) and quality controlled with the Tapestation HS D5000 assay (Agilent). An equimolar pool was prepared with the sixteen libraries and submitted for sequencing at the Centre for Genomic Regulation. A final qPCR quality control was performed before sequencing in an Illumina NextSeq2000. Sequencing output was 703 Million 50-bp single-end reads and at least 39 million of reads were obtained for each library.

7.5.3.3. Analysis

Genome and annotation versions

The dataset consists of single end reads. The genome version used for alignment was mouse mm10 with annotations from GENCODE version M25[180].

RNASeq data preprocessing and alignment

Single-end reads were aligned to the corresponding genome using STAR (v2.7.10a)[181] with default parameters. STAR indexes were built using the GENCODE annotation with versions referenced above. SAM files were converted to BAM and sorted using sambamba (v0.6.70)[182]. Gene counts were obtained with the featureCounts function from the Rsubread package[183] with the GTF file corresponding to the annotation used for indexing the genome.

RNASeq differential expression and functional enrichment

All analyses were performed in the R programming language version 4.1.3[184] unless otherwise stated. Differential analyses were performed using the DESeq2 package[185]. Functional enrichment was performed using the roastgsa package[186]. Gene set analysis was performed employing the regularized rlog transformed matrix. The Broad Hallmarks gene set collection[187] was downloaded from[188] and gene ontology and KEGG pathways from[189,190] (v3).

7.5.4. Western Blot

Western blotting is a commonly used technique to detect proteins of interest within a protein extract. First, protein homogenates are prepared from cells or tissues. The concentration of protein is quantified, and samples are prepared for gel electrophoresis, a procedure that separates proteins based on their size. An electrical current is used to transfer the proteins from the gel onto a membrane. The membrane is then incubated in solutions containing specific antibodies to detect selected proteins. The primary antibody is designed to bind the protein of interest, while the secondary antibody is directed against the primary antibody. Secondary antibodies are often conjugated to a fluorophore or enzymes like horseradish peroxidase (HRP). These conjugates allow detection of desired proteins by imaging systems (such as the Odyssey® Fc Imaging System) or by incubating the membrane with a substrate solution (ECL). HRP, which is conjugated to the secondary antibody, catalyzes the conversion of chemiluminescent substrates, which emits low intensity light that can be detected using X-ray films. Finally, detected signals can be quantified by densitometric analysis.

7.5.4.1. Protein extraction from tissues

1. Pieces of about 20 - 30 mg tissue are added to tubes containing 600 µL RIPA buffer and three zirconium oxide beads.
2. Tubes are inserted into the Mini-Beadbeater disruptor (Bio Spec Products) and homogenized for 30 s at 3,400 oscillations per minute.
3. Samples are rotated for 30 min at 4 ℃.
4. Homogenates are centrifuged at 18,200 g for 10 min at 4 ℃.

5. Supernatant is collected and quantified (Material and Methods, 7.5.4.3) and adjusted to 5 µg / µL.

7.5.4.2. Protein extraction from cells

1. Culture dishes (6 or 10 cm dishes) are placed on ice and cells were harvested in culture media using a cell scraper.
2. Cell suspension is transferred to pre-chilled 2 mL microcentrifuge tubes and centrifuged at 300g at 4℃ for 5 min (5427 R, Eppendorf™).
3. The supernatant is removed, and the pellet is washed once with ice-cold PBS.
4. Centrifugation at 1,600 rpm at 4 ℃ for 5 min.
5. Supernatant is removed and the cell pellet is frozen at -80 ℃.
6. The cell pellet is resolved in RIPA buffer and incubated on ice for 15 min.
7. Samples are centrifuged at 18,200 g for 10 min at 4 ℃.
8. Supernatant is collected and protein content is quantified (Material and Methods, 7.5.4.3) and adjusted to 5 µg/µL.

7.5.4.3. Protein extract quantification

Protein homogenates were quantified using Pierce™ BCA Protein Assay Kit following the manufacturer's instructions. This procedure is based on the generation of a violet compound in amounts proportional to the protein concentration of the sample. In an alkaline environment, proteins within the sample reduce Cu2+ to Cu1+, which is also known as the Biuret reaction. Bicinchoninic acid (BCA) is highly sensitive to Cu1+ cations and is converted into purple reaction products that can be quantified by measuring the absorbance at 562 nm using a spectrophotometer. Samples are measured in duplicates. The kit contains an albumin standard solution with a concentration of 2 mg/mL that was used to prepare a standard curve (Water was used as a blank):

1. An albumin standard curve ranging from 1 to 20 mg is pipetted into wells of a microtiter plate.
2. Samples (2 µL) are added to microtiter wells.
3. BCA reagent B is diluted 1:50 with BCA reagent A and 200 µL of the solution are added to each well.
4. The plate is incubated at 37 ℃ for 30 min.
5. Finally, the absorbance at 562 nm is detected using a microplate reader (BioTek®, Sunrise®).

Protein concentration of samples is calculated by interpolating the unknown value from the standard curve.

7.5.4.4. Sample preparation

Protein homogenates are brought to a desired concentration with ultrapure water. Three volumes of sample are mixed with one volume of 4X loading dye and samples are boiled at 95 ℃ for 5 min to denature proteins. Protein homogenates destined for detection of high molecular weight proteins by western blot were not boiled.

7.5.4.5. Sodium dodecyl sulfate-polyacrylamide gel electrophoresis

Sodium dodecyl sulfate–polyacrylamide gel electrophoresis (SDS-PAGE) was performed using the Mini-Protean system (Bio-Rad). Gels of 1.5 mm depth were poured between two clean glass plates (sandwich of spacer and short glass). Depending on the molecular weight of the proteins of interest, a 6-13 % acrylamide separation gel is prepared (Material and Methods, Table 10), poured between the glasses and topped with isopropanol to straighten the gels surface. The gel is allowed to polymerize. The stacking gel is prepared (Material and Methods, (Table 11) and added on top of the polymerized separation gel after elimination of the isopropanol layer. Depending on the volume of samples, 1.5 mm thick 10- or 15-well combs were inserted into the stacking gel to create wells of 66 µL or 40 µL, respectively. The gel was allowed to polymerize before the comb was removed. Gels were used immediately or stored up to 4 days at 4 °C.

Glass sandwiches containing polymerized gels were placed into the electrophoresis system. The buffer tank was filled with electrophoresis buffer (Material and Methods, Table 12). The gel was allowed to equilibrate for 15 min before the protein standard (Material and Methods, Table 15) and samples were loaded into the wells. The electrophoresis chamber was closed using a lid that is connected to the power supply. The gel was run using a constant electrical potential difference of 90 V until the migration front reached the bottom of the gel.

7.5.4.6. Transfer of proteins to PVDF membranes

After SDS-PAGE, proteins need to be transferred from the gel to a membrane in order to be detected. In course of this thesis PVDF membranes (Material and Methods, Table 16) that require activation in 100 % methanol prior to transfer, were used. In order to transfer the proteins, a sandwich out of filter papers (Whatman®), sponges, gel and membrane was prepared in color-coded cassettes in a box filled with transfer buffer (Material and Methods, Table 13). Care was taken to avoid bubbles between the layers, which prevent the transfer of proteins. The sandwich was assembled in the following order:

1. A sponge soaked in transfer buffer is placed on the black part of the cassette.
2. A transfer buffer-soaked filter paper is placed on top of the sponge.
3. The gel containing separated proteins is equilibrated in transfer buffer and placed onto the filter paper.
4. A piece of PVDF membrane, activated for 1 min in methanol, is placed onto the gel.
5. Another filter paper, soaked in transfer buffer, is placed on top of the membrane.
6. A transfer buffer-soaked sponge is placed on top of the filter paper.
7. The transparent part of the cassette is pressed onto the layers and is then closed.

The cassette was inserted into the transfer tank. The color-coded cassettes and electrodes of the tank ensure the correct orientation of the gel and membrane during transfer. A cooling unit was inserted into the transfer tank before it was filled with transfer buffer. The transfer chamber was closed using a lid that is connected to the power supply. The power was turned on, and the gel was run for 999 min using an electrical current of 90 mA. After the transfer, the membrane is removed from the cassette and is used for immunodetection of proteins (7.5.4.8).

7.5.4.7. Total protein staining

To proof the homogeneous transfer of proteins onto PVDF membranes, as well as determining the relative protein amount of a sample, used to normalize the signal of a target of interest, reversible staining of total protein was performed. This step is done immediately after the transfer of proteins onto membranes and before the blocking step.

- For immunodetection of proteins of interest with fluorescence-based secondary antibodies, the membrane is rinsed with dH2O and stained with the Revert™ 700 Total Protein Stain solution for 5 min at RT with agitation. The membrane is washed twice with a washing solution (6.7% v/v acetic acid, 30% v/v methanol) for 2 min each. The membrane is rinsed with dH2O and is scanned using the Odyssey® Fc Imaging System. Images are acquired using the Image Studio™ Software, according to the manufacturer's instruction. After detection, the membrane is destained with a reversal solution (0.1% w/v NaOH,30% v/v methanol) for 5-10 min until the color of stained proteins disappears. Afterwards, the membrane is washed three times with dH2O and once with PBS containing 0.1 % (v / v) Tween-20 (PBST), for 5 min each. The membrane is now ready for the immunodetection of proteins of interest (7.5.4.8).
- For immunodetection of proteins of interest with HRP-based secondary antibodies, the membrane is rinsed with dH2O and stained with Ponceau S solution (0.1% w/v in 5% acetic acid). The membrane is washed 3 times with dH20 and is scanned with a conventional scanner. The membrane is destained with TBS containing 0.1% (v/v) Tween-20 (TBS-T). The membrane is now ready for the immunodetection of proteins of interest (7.5.4.8).

7.5.4.8. Immunodetection of proteins of interest

Proteins transferred onto a membrane can be immunodetected using primary antibodies that specifically bind to proteins of interest, and secondary antibodies directed against primary antibodies. Immunodetection consists of four main steps including blocking, incubation with primary and secondary antibody and finally detection.

First, the membrane is placed into a blocking solution of TBS-Tsupplemented with 5% (w/v) skimmed milk powder. The membrane is incubated for one hour on a shaker with agitation (100 rpm). This step reduces background signals by blocking non-specific binding sites for antibodies using a solution rich in proteins.

The blocked membrane is then immersed in the primary antibody solution. Specific conditions depend on the antibody that is used and are described in detail in Material and Methods, Table 27. Membranes are incubated overnight inside 50 mL tubes placed on a TubeRoller™ at 4 ℃. After incubation, the membranes are washed three times using TBS-T for 10 min each. The washing steps are performed with agitation on a shaker at RT.

The membrane that is now free of unbound primary antibody is immersed in a secondary antibody solution that is prepared in PBST containing 5% (w/v) skimmed milk powder. Specific conditions are detailed in Material and Methods, Table 28. Secondary antibodies target primary antibodies and are conjugated to fluorophores or enzymes that allow their detection. Membranes are incubated for 1h at RT and with agitation. After incubation,

the membranes are washed three times using TBST for 5 min each. In case of fluorescently labelled secondary antibodies, membranes were washed one more time using TBS without Tween-20.

Lastly, the protein of interest is detected. This was done in two different ways, depending on the secondary antibodies that were used. Membranes incubated with HRP-conjugated secondary antibodies were incubated with a substrate solution (ECL™, GE Healthcare) according to the manufacturer's instructions. Briefly, solution A (luminol solution) and solution B (peroxidase solution) are mixed (1:1) and the surface of the membrane is covered. After 1 min of incubation, excess solution is removed, and the membranes were placed between plastic sheets into an X-ray film cassette. Depending on the intensity of the signal, standard or high-sensitive films were exposed to the membranes for different times inside a dark room. The exposed films were subsequently developed using the Hyper Processor Model AM4 (Amersham Pharmacia Biotech).

In the case of membranes incubated with fluorescently labelled secondary antibodies, the membranes were scanned using the Odyssey® Fc Imaging System and the Images were acquired using the Image Studio™ Software, according to the manufacturer's instruction.

7.5.4.9. Densitometry analysis of protein relative levels

In order to determine the relative amount of the proteins of interest and housekeeping proteins, developed X-ray films were scanned using the HP Officejet Pro X576dw printer. The software Image J (Fiji) was used to quantify the density (intensity) of bands on the X-ray scans.

7.5.4.10. Membrane stripping

Restore™ Western Blot Stripping Buffer was used to remove primary and secondary antibodies from PVDF membranes in order to incubate the same membrane using different antibodies. Membranes were incubated in Stripping Buffer for 15 min, followed by blocking and incubation with another set of primary and secondary antibodies.

7.5.5. Chromatin purification (cell lines)

1. Start experiment with $10 \cdot 10^6$ cells. Crosslink nuclear proteins adding formaldehyde for 10 min directly to the medium to a final concentration of 1% at RT in a rocking platform.
2. Stop the crosslinking by adding Glycine (in PBS) to a final concentration of 125 mM and incubate for 5 min at RT in a rocking platform.
3. Wash the cells with ice-cold PBS. Wash again the cells adding ice-cold PBS supplemented with a protease inhibitor cocktail and collect the cells by scraping.
4. Centrifuge at 1,500g for 5 min at 4ºC. Discard SN and resuspend in 10mL of ChIP Wash A buffer.
5. Incubate 10 min at 4ºC on a rotatory wheel and centrifuge at 1500xg, 5 min at 4ºC.
6. Discard SN and resuspend in 10mL of ChIP Wash B buffer.
7. Incubate 10 min at 4ºC on a rotatory wheel and centrifuge at 1500xg, 5 min at 4ºC.
8. Discard SN and resuspend in 4,5mL of Lysis Buffer.
9. Add 0.5 mL 10% SDS, and invert the tube 5 times. Centrifuge 5' at 1500xg at 4ºC
10. Discard SN (without disturbing fluffy pellet), add 50 µL of Lysis Buffer, and invert the tube 5 times → centrifuge 5' at 1500xg at 4ºC
11. Discard SN (without disturbing fluffy pellet), add 50 µL of Lysis Buffer, and invert the tube 5 times → centrifuge 5' at 1500xg at 4ºC
12. Discard SN and resuspend in Lysis Buffer up to 2mL (take into consideration the pellet volume) and add 20 µL PMSF (stock 100mM -> 1mM) + 20 µL 10% SDS.
13. Aliquot in microtubes (500 µL) and sonicate (30s-30s) (7-10-12-14 cycles) to optimize sonication and obtain 300-500 bp fragments
14. Mix the lysates and add 2mL (1960 µL Lysis Buffer + 20 µL PMSF + 20 µL 10% SDS)
15. Add 0.42 mL 10% Triton X100, 42 µL 10% sodium deoxycholate and 150 µL 4M NaCl.
16. Incubate 10 min in a rotatory wheel at 4ºC. Aliquot and centrifuge 5' max speed at 4ºC.
17. Pool all SN and discard the pellets
18. Separate 100 µL to decrosslink and check DNA size and aliquot the rest in 0.5 mL and store at -80ºC.

Table 17: ChIP Wash A buffer

Component	Final concentration	Source
HEPES pH 7.9	10 mM	Sigma-Adlrich, H4034
EDTA	10 mM	Meck Millipore, 324503
EGTA	0.5 mM	Sigma-Aldrich, E4378
Triton X100	0.25%	Sigma-Aldrich, T8787

Table 18: ChIP Wash B buffer

Component	Final concentration	Source
HEPES pH 7.9	10 mM	Sigma-Adlrich, H4034
EDTA	10 mM	Meck Millipore, 324503
EGTA	0.5 mM	Sigma-Aldrich, E4378
Triton X100	0.25%	Sigma-Aldrich, T8787
NaCl	100 mM	Sigma-Aldrich, 71376

Table 19: Lysis buffer

Component	Final concentration	Source
TrisHCl pH 7.9	10 mM (pH 7.9)	Sigma-Aldrich, 10812846001
EDTA	10 mM	Meck Millipore, 324503

7.5.6. Chromatin purification (tissue)

Chromatin purification from tissue was performed using the ChIP-IT High Sensitivity® kit from Active Motif (53040).

7.5.7. Subcellular fractionation

Subcellular fractionation was performed using the NE-PER™ Nuclear and Cytoplasmic kit from Thermo Scientific™ (78833).

7.6. Statistical analysis

In this PhD thesis, data are presented as mean ± SEM. Different statistical tests have been used depending on the number of groups that were analyzed. These include, unpaired Student's t-test, paired Student's t-test and One-way ANOVA test coupled with multiple comparisons Significance was established at $p < 0.05$. Statistical analysis was applied mostly to data from $n \geq 3$ independent experiments.

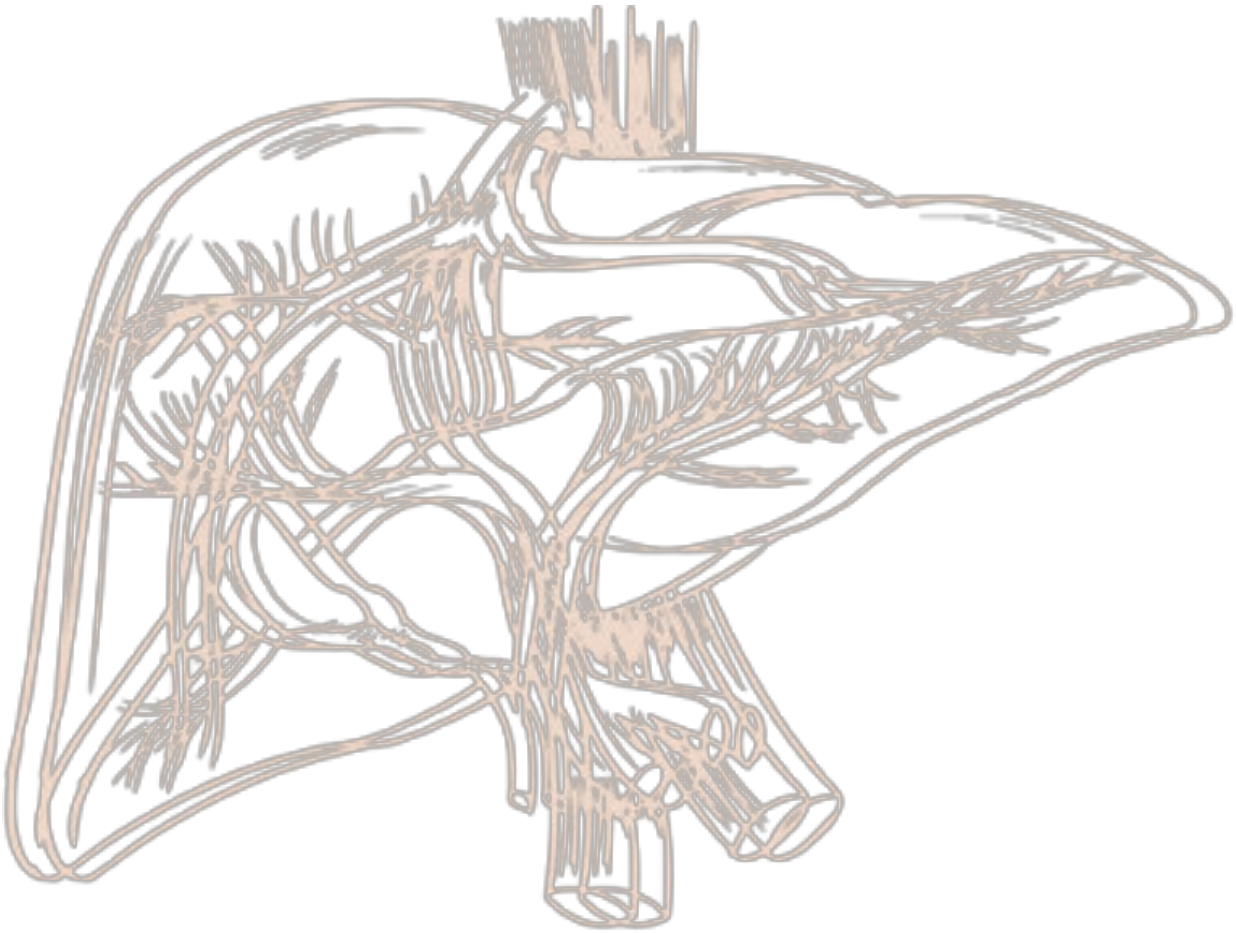

REFERENCES

8. REFERENCES

1. Petersen, M. C., Vatner, D. F. & Shulman, G. I. Regulation of hepatic glucose metabolism in health and disease. *Nat. Rev. Endocrinol.* **13**, 572–587 (2017).
2. Alves-Bezerra, M. & Cohen, D. E. Triglyceride Metabolism in the Liver. in *Comprehensive Physiology* 1–22 (John Wiley & Sons, Ltd, 2017). doi:https://doi.org/10.1002/cphy.c170012.
3. Hodges, R. E. & Minich, D. M. Modulation of Metabolic Detoxification Pathways Using Foods and Food-Derived Components: A Scientific Review with Clinical Application. *J. Nutr. Metab.* **2015**, (2015).
4. Kuscuoglu, D. *et al.* Liver – master and servant of serum proteome. *J. Hepatol.* **69**, 512–524 (2018).
5. Stefan, N. & Häring, H. The role of hepatokines in metabolism. *Nat. Rev. Endocrinol.* **9**, 144–152 (2013).
6. Rinella, M. E. *et al.* A multisociety Delphi consensus statement on new fatty liver disease nomenclature. *Hepatology* **78**, 1966–1986 (2023).
7. Loomba, R., Friedman, S. L. & Shulman, G. I. Mechanisms and disease consequences of nonalcoholic fatty liver disease. *Cell* **184**, 2537–2564 (2021).
8. Chalasani, N. *et al.* The diagnosis and management of nonalcoholic fatty liver disease: Practice guidance from the American Association for the Study of Liver Diseases. *Hepatology* **67**, 328–357 (2018).
9. Singh, S. *et al.* Fibrosis Progression in Nonalcoholic Fatty Liver vs Nonalcoholic Steatohepatitis: A Systematic Review and Meta-analysis of Paired-Biopsy Studies. *Clin. Gastroenterol. Hepatol.* **13**, 643-654.e9 (2015).
10. Loomba, R., Lim, J. K., Patton, H. & El-Serag, H. B. AGA Clinical Practice Update on Screening and Surveillance for Hepatocellular Carcinoma in Patients With Nonalcoholic Fatty Liver Disease: Expert Review. *Gastroenterology* **158**, 1822–1830 (2020).
11. Lazarus, J. V. *et al.* NAFLD — sounding the alarm on a silent epidemic. *Nat. Rev. Gastroenterol. Hepatol.* **17**, 377–379 (2020).
12. Irimia, J. M. *et al.* Lack of liver glycogen causes hepatic insulin resistance and steatosis in mice. *J. Biol. Chem.* **292**, 10455–10464 (2017).
13. Eslam, M., Valenti, L. & Romeo, S. Genetics and epigenetics of NAFLD and NASH : Clinical impact. *J. Hepatol.* **68**, 268–279 (2018).
14. Makkonen, J., Pietiläinen, K. H., Rissanen, A., Kaprio, J. & Yki-Järvinen, H. Genetic factors contribute to variation in serum alanine aminotransferase activity independent of obesity and alcohol: a study in monozygotic and dizygotic twins. *J. Hepatol.* **50**, 1035–1042 (2009).
15. BasuRay, S., Smagris, E., Cohen, J. C. & Hobbs, H. H. The PNPLA3 variant associated with fatty liver disease (I148M) accumulates on lipid droplets by evading ubiquitylation. *Hepatology* **66**, (2017).
16. Bruce, K. D. *et al.* Maternal High-Fat Feeding Primes Steatohepatitis in Adult Mice Offspring, Involving Mitochondrial Dysfunction and Altered Lipogenesis Gene Expression. *Hepatology* **50**, 1796–1808 (2009).

17. Schwimmer, J. B. *et al.* Heritability of nonalcoholic fatty liver disease. *Gastroenterology* **136**, 1585–1592 (2009).

18. Shao, Y., Chen, S., Han, L. & Liu, J. Pharmacotherapies of NAFLD: updated opportunities based on metabolic intervention. *Nutr. Metab.* **20**, 1–18 (2023).

19. Vilar-Gomez, E. *et al.* Weight loss through lifestyle modification significantly reduces features of nonalcoholic steatohepatitis. *Gastroenterology* **149**, 367-378.e5 (2015).

20. Orci, L. A. *et al.* Exercise-based Interventions for Nonalcoholic Fatty Liver Disease: A Meta-analysis and Meta-regression. *Clin. Gastroenterol. Hepatol.* **14**, 1398–1411 (2016).

21. Oh, S. *et al.* High-intensity aerobic exercise improves both hepatic fat content and stiffness in sedentary obese men with nonalcoholic fatty liver disease. *Sci. Rep.* **7**, 1–12 (2017).

22. Sung, K. C. *et al.* Effect of exercise on the development of new fatty liver and the resolution of existing fatty liver. *J. Hepatol.* **65**, 791–797 (2016).

23. Oh, S. *et al.* Moderate to vigorous physical activity volume is an important factor for managing nonalcoholic fatty liver disease: A retrospective study. *Hepatology* **61**, 1205–1215 (2015).

24. Pipitone, R. M. *et al.* MAFLD: a multisystem disease. *Ther. Adv. Endocrinol. Metab.* **14**, 20420188221145548 (2023).

25. Scholtes, C. & Giguère, V. Transcriptional control of energy metabolism by nuclear receptors. *Nat. Rev. Mol. Cell Biol.* **23**, 750–770 (2022).

26. Kim, J. K., Samaranayake, M. & Pradhan, S. Epigenetic mechanisms in mammals. *Cell. Mol. Life Sci.* **66**, 596–612 (2009).

27. Rudraiah, S., Zhang, X. & Wang, L. Nuclear Receptors as Therapeutic Targets in Liver Disease: Are We There Yet? *Annu. Rev. Pharmacol. Toxicol.* **56**, 605–626 (2016).

28. Panzitt, K. & Wagner, M. FXR in liver physiology: Multiple faces to regulate liver metabolism. *Biochim. Biophys. Acta - Mol. Basis Dis.* **1867**, 166133 (2021).

29. Liss, K. H. H. & Finck, B. N. PPARs and nonalcoholic fatty liver disease. *Biochimie* **136**, 65–74 (2017).

30. Braissant, O., Foufelle, F., Scotto, C., Dauça, M. & Wahli, W. Differential expression of peroxisome proliferator-activated receptors (PPARs): tissue distribution of PPAR-alpha, -beta, and -gamma in the adult rat. *Endocrinology* **137**, 354–366 (1996).

31. Russo-Savage, L. & Schulman, I. G. Liver X receptors and liver physiology. *Biochim. Biophys. Acta - Mol. Basis Dis.* **1867**, 166121 (2021).

32. Sun, Y., Demagny, H. & Schoonjans, K. Emerging functions of the nuclear receptor LRH-1 in liver physiology and pathology. *Biochim. Biophys. Acta - Mol. Basis Dis.* **1867**, 166145 (2021).

33. Shin, D.-J. & Wang, L. Bile Acid-Activated Receptors: A Review on FXR and Other Nuclear Receptors. *Handb. Exp. Pharmacol.* **256**, 51–72 (2019).

34. Clifford, B. L. *et al.* FXR activation protects against NAFLD via bile-acid-dependent reductions in lipid absorption. *Cell Metab.* **33**, 1671-1684.e4 (2021).

35. Seok, S. *et al.* Transcriptional regulation of autophagy by an FXR-CREB axis. *Nature*

516, 108–111 (2014).

36. Lee, J. M. *et al.* Nutrient-sensing nuclear receptors coordinate autophagy. *Nature* **516**, 112–115 (2014).

37. Kersten, S. *et al.* Peroxisome proliferator-activated receptor α mediates the adaptive response to fasting. *J. Clin. Invest.* **103**, 1489–1498 (1999).

38. Pawlak, M., Lefebvre, P. & Staels, B. Molecular mechanism of PPARα action and its impact on lipid metabolism, inflammation and fibrosis in non-alcoholic fatty liver disease. *J. Hepatol.* **62**, 720–733 (2015).

39. Montagner, A. *et al.* Liver PPARα is crucial for whole-body fatty acid homeostasis and is protective against NAFLD. *Gut* **65**, 1202–1214 (2016).

40. Wan, J. *et al.* Aging-induced aberrant RAGE / PPAR α axis promotes hepatic steatosis via dysfunctional mitochondrial β oxidation. *Aging Cell* **19**, 1–14 (2020).

41. Gong, Z., Tas, E., Yakar, S. & Muzumdar, R. Hepatic lipid metabolism and non-alcoholic fatty liver disease in aging. *Mol. Cell. Endocrinol.* **455**, 115–130 (2017).

42. Bento, C. F. *et al.* Mammalian Autophagy: How Does It Work? *Annu. Rev. Biochem.* **85**, 685–713 (2016).

43. Schuck, S. Microautophagy - distinct molecular mechanisms handle cargoes of many sizes. *J. Cell Sci.* **133**, (2020).

44. Kaushik, S. & Cuervo, A. M. The coming of age of chaperone-mediated autophagy. *Nat. Rev. Mol. Cell Biol.* **19**, 365–381 (2018).

45. Nakatogawa, H. Mechanisms governing autophagosome biogenesis. *Nat. Rev. Mol. Cell Biol.* **21**, 439–458 (2020).

46. Gatica, D., Lahiri, V. & Klionsky, D. J. Cargo recognition and degradation by selective autophagy. *Nat. Cell Biol.* **20**, 233–242 (2018).

47. Alers, S., Loffler, A. S., Wesselborg, S. & Stork, B. Role of AMPK-mTOR-Ulk1/2 in the Regulation of Autophagy: Cross Talk, Shortcuts, and Feedbacks. *Mol. Cell. Biol.* **32**, 2–11 (2012).

48. Russell, R. C. *et al.* ULK1 induces autophagy by phosphorylating Beclin-1 and activating VPS34 lipid kinase. *Nat. Cell Biol.* **15**, 741–750 (2013).

49. Seglen, P. O. & Gordon, P. B. 3-Methyladenine: Specific inhibitor of autophagic/lysosomal protein degradation in isolated rat hepatocytes. *Proc. Natl. Acad. Sci.* **79**, 1889–1892 (1982).

50. Geng, J. & Klionsky, D. J. The Atg8 and Atg12 ubiquitin-like conjugation systems in macroautophagy. 'Protein Modifications: Beyond the Usual Suspects' Review Series. *EMBO Rep.* **9**, 859–864 (2008).

51. Tanida, I. *et al.* HsAtg4B/HsApg4B/autophagin-1 cleaves the carboxyl termini of three human Atg8 homologues and delipidates microtubule-associated protein light chain 3- and GABAA receptor-associated protein-phospholipid conjugates. *J. Biol. Chem.* **279**, 36268–36276 (2004).

52. Nakatogawa, H. Two ubiquitin-like conjugation systems that mediate membrane formation during autophagy. *Essays Biochem.* **55**, 39–50 (2013).

53. Martens, S. & Fracchiolla, D. Activation and targeting of ATG8 protein lipidation. *Cell*

Discov. **6**, 1–11 (2020).

54. Johansen, T. & Lamark, T. Selective Autophagy: ATG8 Family Proteins, LIR Motifs and Cargo Receptors. *J. Mol. Biol.* **432**, 80–103 (2020).

55. Klionsky, D. J. *et al.* Guidelines for the use and interpretation of assays for monitoring autophagy (3rd edition). *Autophagy* **12**, 1–222 (2016).

56. Sun-Wang, J. L., Yarritu-Gallego, A., Ivanova, S. & Zorzano, A. The ubiquitin-proteasome system and autophagy: self-digestion for metabolic health. *Trends Endocrinol. Metab.* **32**, 594–608 (2021).

57. Ueno, T. & Komatsu, M. Autophagy in the liver: Functions in health and disease. *Nat. Rev. Gastroenterol. Hepatol.* **14**, 170–184 (2017).

58. Napolitano, G. & Ballabio, A. TFEB at a glance. *J. Cell Sci.* **129**, 2475–2481 (2016).

59. Naito, T., Kuma, A. & Mizushima, N. Differential contribution of insulin and amino acids to the mtorc1-autophagy pathway in the liver and muscle. *J. Biol. Chem.* **288**, 21074–21081 (2013).

60. Liu, G. Y. & Sabatini, D. M. mTOR at the nexus of nutrition, growth, ageing and disease. *Nat. Rev. Mol. Cell Biol.* **21**, (2020).

61. Singh, R. *et al.* Autophagy regulates lipid metabolism. *Nature* **458**, 1131–1135 (2009).

62. Yang, L., Li, P., Fu, S., Calay, E. S. & Hotamisligil, G. S. Defective hepatic autophagy in obesity promotes ER stress and causes insulin resistance. *Cell Metab.* **11**, 467–478 (2010).

63. Toledo, M. *et al.* Autophagy Regulates the Liver Clock and Glucose Metabolism by Degrading CRY1. *Cell Metab.* **28**, 268-281.e4 (2018).

64. Minami, Y. *et al.* Liver lipophagy ameliorates nonalcoholic steatohepatitis through extracellular lipid secretion. *Nat. Commun.* **14**, (2023).

65. Sun-Wang, J. L., Ivanova, S. & Zorzano, A. The dialogue between the ubiquitin-proteasome system and autophagy: implications in ageing. *Aging Res. Rev.* **64**, 1–18 (2020).

66. González-Rodríguez, A. *et al.* Impaired autophagic flux is associated with increased endoplasmic reticulum stress during the development of NAFLD. *Cell Death Dis.* **5**, (2014).

67. [redacted] (2005).

68. [redacted] (2007).

69. [redacted] (2012).

70. [redacted] (2009).

71. [redacted] (2013).

72. [redacted] (2010).

73. [redacted] (2012).

74. [redacted] (2019).

75. [redacted] (2023).

76. [redacted] (2019).

77. [redacted] 2014).

78. [redacted] (2004).

79. [redacted] (2010).

80. [redacted] (2016).

81. [redacted] (2009).

82. [redacted] (2009).

83. [redacted] (2020).

84. [redacted] (2015).

85. [redacted] (2019).

86. [redacted] (2017).

87. [redacted] (2022) [redacted]

88. [redacted] (2018).

89. [redacted] (2014).

90. [redacted] (2019).

91. [redacted] (2006).

92. [redacted] (2019).

93. [redacted] (2019).

94. [redacted] (2009).

95. [redacted] (2014).

96. [redacted] (2015).

97. [redacted] (2015).

98. [redacted] (2017).

99. [redacted] (2017).

100. [redacted] (2011).

101. [redacted] (2019).

102. Kersten, S., Rakhshandehroo, M., Knoch, B. & Müller, M. Peroxisome proliferator-activated receptor alpha target genes. *PPAR Res.* **2010**, (2010).

103. Aibara, D. *et al.* Gene repression through epigenetic modulation by PPARA enhances hepatocellular proliferation. *iScience* **25**, 104196 (2022).

104. Patsouris, D., Reddy, J. K., Müller, M. & Kersten, S. Peroxisome proliferator-activated receptor α mediates the effects of high-fat diet on hepatic gene expression. *Endocrinology* **147**, 1508–1516 (2006).

105. Machado, M. V. *et al.* Mouse models of diet-induced nonalcoholic steatohepatitis reproduce the heterogeneity of the human disease. *PLoS One* **10**, 1–16 (2015).

106. Matsumoto, M. *et al.* An improved mouse model that rapidly develops fibrosis in non-alcoholic steatohepatitis. *Int. J. Exp. Pathol.* **94**, 93–103 (2013).

107. Honda, Y. *et al.* Pemafibrate, a novel selective peroxisome proliferator-activated receptor alpha modulator, improves the pathogenesis in a rodent model of nonalcoholic steatohepatitis. *Sci. Rep.* **7**, 1–11 (2017).

108. Okishio, S. *et al.* PPARα agonist and metformin co-treatment ameliorates NASH in mice induced by a choline-deficient, amino acid-defined diet with 45% fat. *Sci. Rep.* **10**, 1–11 (2020).

109. Ip, E., Farrell, G., Hall, P., Robertson, G. & Leclercq, I. Administration of the potent PPARalpha agonist, Wy-14,643, reverses nutritional fibrosis and steatohepatitis in mice. *Hepatology* **39**, 1286–1296 (2004).

110. Roux, K. J., Kim, D. I., Burke, B. & May, D. G. BioID: A Screen for Protein-Protein Interactions. *Curr. Protoc. Protein Sci.* **91**, 19.23.1-19.23.15 (2018).

111. May, D. G., Scott, K. L., Campos, A. R. & Roux, K. J. Comparative Application of BioID and TurboID for Protein-Proximity Biotinylation. *Cells* **9**, (2020).

112. Branon, T. C. *et al.* Efficient proximity labeling in living cells and organisms with TurboID. *Nat. Biotechnol.* **36**, 880–898 (2018).

113. Chandler, C. S. & Ballard, F. J. Multiple biotin-containing proteins in 3T3-L1 cells. *Biochem. J.* **237**, 123–130 (1986).

114. Valverde, D. P. *et al.* ATG2 transports lipids to promote autophagosome biogenesis. *J. Cell Biol.* **218**, 1787–1798 (2019).

115. Zhou, Y. *et al.* Metascape provides a biologist-oriented resource for the analysis of systems-level datasets. *Nat. Commun.* **10**, (2019).

116. Pohl, C. & Dikic, I. Cellular quality control by the ubiquitin-proteasome system and autophagy. *Science (80-.).* **366**, 818–822 (2019).

117. Tsai, J. M. *et al.* UBR5 forms ligand-dependent complexes on chromatin to regulate nuclear hormone receptor stability UBR5 forms ligand-dependent complexes on chromatin to regulate nuclear hormone receptor stability. *Mol. Cell* **83**, 2753–2767 (2023).

118. Hehl, L. A. & Schulman, B. A. To be (in a transcriptional complex) or not to be (promoting UBR5 ubiquitylation): That is an answer to how degradation controls gene expression. *Mol. Cell* **83**, 2616–2618 (2023).

119. Hoeller, D. *et al.* E3-Independent Monoubiquitination of Ubiquitin-Binding Proteins. *Mol. Cell* **26**, 891–898 (2007).

120. Morreale, F. E., Walden, H., Es, R. & Ring, A. SnapShot : Types of Ubiquitin Ligases. *Cell* **165**, 248-248.e1 (2016).

121. Piunti, A. & Shilatifard, A. The roles of Polycomb repressive complexes in mammalian development and cancer. *Nat. Rev. Mol. Cell Biol.* **22**, 326–345 (2021).

122. Voncken, J. W. *et al.* Rnf2 (Ring1b) deficiency causes gastrulation arrest and cell cycle inhibition. *Proc. Natl. Acad. Sci. U. S. A.* **100**, 2468–2473 (2003).

123. del Mar Lorente, M. *et al.* Loss- and gain-of-function mutations show a polycomb group function for Ring1A in mice. *Development* **127**, (2000).

124. Blackledge, N. P. *et al.* PRC1 Catalytic Activity Is Central to Polycomb System Function. *Mol. Cell* **77**, 857-874.e9 (2020).

125. de Napoles, M. *et al.* Polycomb group proteins ring1A/B link ubiquitylation of histone H2A to heritable gene silencing and X inactivation. *Dev. Cell* **7**, 663–676 (2004).

126. Chan, H. L. *et al.* Polycomb complexes associate with enhancers and promote oncogenic transcriptional programs in cancer through multiple mechanisms. *Nat. Commun.* **9**, (2018).

127. Brookes, E. *et al.* Polycomb associates genome-wide with a specific RNA polymerase

II variant, and regulates metabolic genes in ESCs. *Cell Stem Cell* **10**, 157–170 (2012).

128. Blackledge, N. P. & Klose, R. J. The molecular principles of gene regulation by Polycomb repressive complexes. *Nat. Rev. Mol. Cell Biol.* **22**, 815–833 (2021).
129. Ullah, K., Zubia, E., Narayan, M., Yang, J. & Xu, G. Diverse roles of the E2/E3 hybrid enzyme UBE2O in the regulation of protein ubiquitination, cellular functions, and disease onset. *FEBS J.* **286**, 2018–2034 (2019).
130. Yanagitani, K., Juszkiewicz, S. & Hegde, R. S. UBE2O is a quality control factor for orphans of multiprotein complexes. *Science (80-.).* **357**, 472–475 (2017).
131. Nguyen, A. T. *et al.* UBE2O remodels the proteome during terminal erythroid differentiation. *Science (80-.).* **357**, (2017).
132. Zhang, X. *et al.* Fine-tuning BMP7 signalling in adipogenesis by UBE2O/E2-230K-mediated monoubiquitination of SMAD6. *EMBO J.* **32**, 996–1007 (2013).
133. Vila, I. K. *et al.* A muscle-specific UBE2O/AMPKα2 axis promotes insulin resistance and metabolic syndrome in obesity. *JCI Insight* **4**, (2019).
134. Ma, M. *et al.* UBE2O promotes lipid metabolic reprogramming and liver cancer progression by mediating HADHA ubiquitination. *Oncogene* **41**, 5199–5213 (2022).
135. Gudjonsson, T. *et al.* TRIP12 and UBR5 suppress spreading of chromatin ubiquitylation at damaged chromosomes. *Cell* **150**, 697–709 (2012).
136. Zhang, T., Cronshaw, J., Kanu, N., Snijders, A. P. & Behrens, A. UBR5-mediated ubiquitination of ATMIN is required for ionizing radiation-induced ATM signaling and function. *Proc. Natl. Acad. Sci. U. S. A.* **111**, 12091–12096 (2014).
137. Cipolla, L. *et al.* UBR5 interacts with the replication fork and protects DNA replication from DNA polymerase η toxicity. *Nucleic Acids Res.* **47**, 11268–11283 (2019).
138. Li, C. G. *et al.* PPARγ Interaction with UBR5/ATMIN Promotes DNA Repair to Maintain Endothelial Homeostasis. *Cell Rep.* **26**, 1333-1343.e7 (2019).
139. Mark, K. G. *et al.* Orphan quality control shapes network dynamics and gene expression. *Cell* **186**, 3460-3475.e23 (2023).
140. Guarnaccia, A. D. *et al.* Impact of WIN site inhibitor on the WDR5 interactome. *Cell Rep.* **34**, 108636 (2021).
141. Sanchez, A. *et al.* BMI1-UBR5 axis regulates transcriptional repression at damaged chromatin. *Proc. Natl. Acad. Sci. U. S. A.* **113**, 11243–11248 (2016).
142. Chagraoui, J., Hébert, J., Girard, S. & Sauvageau, G. An anticlastogenic function for the Polycomb Group gene Bmi1. *Proc. Natl. Acad. Sci. U. S. A.* **108**, 5284–5289 (2011).
143. Klionsky, D. J. *et al.* Guidelines for the use and interpretation of assays for monitoring autophagy (4th edition). *Autophagy* 1–382 (2021) doi:10.1080/15548627.2020.1797280.
144. Galluzzi, L. *et al.* Molecular mechanisms of cell death: Recommendations of the Nomenclature Committee on Cell Death 2018. *Cell Death Differ.* **25**, 486–541 (2018).
145. Denton, D. & Kumar, S. Autophagy-dependent cell death. *Cell Death Differ.* **26**, 605–616 (2019).
146. Kiraz, Y., Adan, A., Kartal Yandim, M. & Baran, Y. Major apoptotic mechanisms and genes involved in apoptosis. *Tumor Biol.* **37**, 8471–8486 (2016).

147. Chaitanya, G. V., Alexander, J. S. & Babu, P. P. PARP-1 cleavage fragments: Signatures of cell-death proteases in neurodegeneration. *Cell Commun. Signal.* **8**, 1–11 (2010).

148. Hashimoto, T. *et al.* Defect in Peroxisome Proliferator-activated Receptor ␣ -inducible Fatty Acid Oxidation Determines the Severity of Hepatic Steatosis in Response to Fasting *. *J. Biol. Chem.* **275**, 28918–28928 (2000).

149. Heijboer, A. C. *et al.* Sixteen hours of fasting differentially affects hepatic and muscle insulin sensitivity in mice. *J. Lipid Res.* **46**, 582–588 (2005).

150. Moller, L., Stodkilde-Jorgensen, H., Jensen, F. T. & Jorgensen, J. O. L. Fasting in healthy subjects is associated with intrahepatic accumulation of lipids as assessed by 1H-magnetic resonance spectroscopy. *Clin. Sci. (Lond).* **114**, 547–552 (2008).

151. Saponaro, C., Gaggini, M., Carli, F. & Gastaldelli, A. The Subtle Balance between Lipolysis and Lipogenesis: A Critical Point in Metabolic Homeostasis. *Nutrients* **7**, 9453–9474 (2015).

152. Rui, L. Energy metabolism in the liver. *Compr. Physiol.* **4**, 177–197 (2014).

153. Huynh, F. K., Green, M. F., Koves, T. R. & Hirschey, M. D. Measurement of fatty acid oxidation rates in animal tissues and cell lines. *Methods Enzymol.* **542**, 391–405 (2014).

154. Inagaki, T. *et al.* Endocrine Regulation of the Fasting Response by PPARα-Mediated Induction of Fibroblast Growth Factor 21. *Cell Metab.* **5**, 415–425 (2007).

155. Tang, D. *et al.* Fasting: From Physiology to Pathology. *Adv. Sci.* **10**, 2204487 (2023).

156. Fang, L. *et al.* PPARgene: A Database of Experimentally Verified and Computationally Predicted PPAR Target Genes. *PPAR Res.* **2016**, 6042162 (2016).

157. Sasaki, T. Age-Associated Weight Gain, Leptin, and SIRT1: A Possible Role for Hypothalamic SIRT1 in the Prevention of Weight Gain and Aging through Modulation of Leptin Sensitivity. *Front. Endocrinol. (Lausanne).* **6**, (2015).

158. Régnier, M. *et al.* Hepatocyte-specific deletion of Pparα promotes NAFLD in the context of obesity. *Sci. Rep.* **10**, 1–15 (2020).

159. Torra, I. P. *et al.* Bile acids induce the expression of the human peroxisome proliferator-activated receptor α gene via activation of the farnesoid X receptor. *Mol. Endocrinol.* **17**, 259–272 (2003).

160. Gallage, S. *et al.* A researcher's guide to preclinical mouse NASH models. *Nat. Metab.* **4**, 1632–1649 (2022).

161. Machado, M. V. *et al.* Mouse models of diet-induced nonalcoholic steatohepatitis reproduce the heterogeneity of the human disease. *PLoS One* **10**, e0127991 (2015).

162. Ip, E. *et al.* Central role of PPARalpha-dependent hepatic lipid turnover in dietary steatohepatitis in mice. *Hepatology* **38**, 123–132 (2003).

163. Harrington, W. W. *et al.* The Effect of PPARalpha, PPARdelta, PPARgamma, and PPARpan Agonists on Body Weight, Body Mass, and Serum Lipid Profiles in Diet-Induced Obese AKR/J Mice. *PPAR Res.* **2007**, 97125 (2007).

164. Brocker, C. N. *et al.* Hepatocyte-specific PPARA expression exclusively promotes agonist-induced cell proliferation without influence from nonparenchymal cells. *Am. J.*

Physiol. Gastrointest. Liver Physiol. **312**, G283–G299 (2017).

165. Xie, G. *et al.* Hepatocyte Peroxisome Proliferator–Activated Receptor α Enhances Liver Regeneration after Partial Hepatectomy in Mice. *Am. J. Pathol.* **189**, 272–282 (2019).
166. Zhang, X. *et al.* Ablation of cytochrome P450 omega-hydroxylase 4A14 gene attenuates hepatic steatosis and fibrosis. *Proc. Natl. Acad. Sci. U. S. A.* **114**, 3181–3185 (2017).
167. Tauber, M. *et al.* An mTORC1-GRASP55 signaling axis controls unconventional secretion to reshape the extracellular proteome upon stress. *Mol. Cell* **81**, 3275–3293 (2021).
168. Tasaki, T., Sriram, S. M., Park, K. S. & Kwon, Y. T. The N-End rule pathway. *Annu. Rev. Biochem.* **81**, 261–289 (2012).
169. Yoshii, S. R. & Mizushima, N. Monitoring and measuring autophagy. *Int. J. Mol. Sci.* **18**, 1–13 (2017).
170. Cox, J. & Mann, M. {MaxQuant} enables high peptide identification rates, individualized p.p.b.-range mass accuracies and proteome-wide protein quantification. *Nature Biotechnology* vol. 26 1367–1372 (2008).
171. Cox, J., Michalski, A. & Mann, M. Software lock mass by two-dimensional minimization of peptide mass errors. *J. Am. Soc. Mass Spectrom.* **22**, 1373–1380 (2011).
172. Cox, J. *et al.* Accurate proteome-wide label-free quantification by delayed normalization and maximal peptide ratio extraction, termed {MaxLFQ}. *Mol. Cell. Proteomics* **13**, 2513–2526 (2014).
173. Schaab, C., Geiger, T., Stoehr, G., Cox, J. & Mann, M. Analysis of high accuracy, quantitative proteomics data in the {MaxQB} database. *Mol. Cell. Proteomics* **11**, M111.014068 (2012).
174. Tyanova, S. *et al.* Visualization of {LC-MS/MS} proteomics data in {MaxQuant}. *Proteomics* **15**, 1453–1456 (2015).
175. Tyanova, S., Temu, T. & Cox, J. The {MaxQuant} computational platform for mass spectrometry-based shotgun proteomics. *Nat. Protoc.* **11**, 2301–2319 (2016).
176. Käll, L., Canterbury, J. D., Weston, J., Noble, W. S. & MacCoss, M. J. Semi-supervised learning for peptide identification from shotgun proteomics datasets. *Nat. Methods* **4**, 923–925 (2007).
177. Käll, L., Storey, J. D., MacCoss, M. J. & Noble, W. S. Posterior error probabilities and false discovery rates: two sides of the same coin. *J. Proteome Res.* **7**, 40–44 (2008).
178. Teo, G. *et al.* {SAINTq}: Scoring protein-protein interactions in affinity purification - mass spectrometry experiments with fragment or peptide intensity data. *Proteomics* **16**, 2238–2245 (2016).
179. Teo, G. *et al.* {SAINTexpress}: improvements and additional features in Significance Analysis of {INTeractome} software. *J. Proteomics* **100**, 37–43 (2014).
180. Frankish, A. *et al.* GENCODE reference annotation for the human and mouse genomes. *Nucleic Acids Res.* **47**, D766–D773 (2019).
181. Dobin, A. *et al.* STAR: Ultrafast universal RNA-seq aligner. *Bioinformatics* **29**, 15–21 (2013).

182. Tarasov, A., Vilella, A. J., Cuppen, E., Nijman, I. J. & Prins, P. Sambamba: Fast processing of NGS alignment formats. *Bioinformatics* **31**, 2032–2034 (2015).

183. Liao, Y., Smyth, G. K. & Shi, W. The R package Rsubread is easier, faster, cheaper and better for alignment and quantification of RNA sequencing reads. *Nucleic Acids Res.* **47**, e47 (2019).

184. Team, R. C. R: A language and environment for statistical computing. *R Foundation for Statistical Computing* https://www.r-project.org/ (2021).

185. Love, M. I., Huber, W. & Anders, S. Moderated estimation of fold change and dispersion for RNA-seq data with DESeq2. *Genome Biol.* **15**, 550 (2014).

186. Caballé-Mestres, A., Berenguer-Llergo, A. & Stephan-Otto Attolini, C. Roastgsa: a comparison of rotation-based scores for gene set enrichment analysis. *BMC Bioinformatics* **24**, 408 (2023).

187. Liberzon, A. *et al.* The Molecular Signatures Database (MSigDB) hallmark gene set collection. *Cell Syst.* **1**, 417–425 (2015).

188. No Title. https://www.gsea-msigdb.org/gsea/msigdb.

189. Subramanian, A. *et al.* Gene set enrichment analysis: a knowledge-based approach for interpreting genome-wide expression profiles. *Proc. Natl. Acad. Sci. U. S. A.* **102**, 15545–15550 (2005).

190. Liberzon, A. *et al.* Molecular signatures database (MSigDB) 3.0. *Bioinformatics* **27**, 1739–1740 (2011).

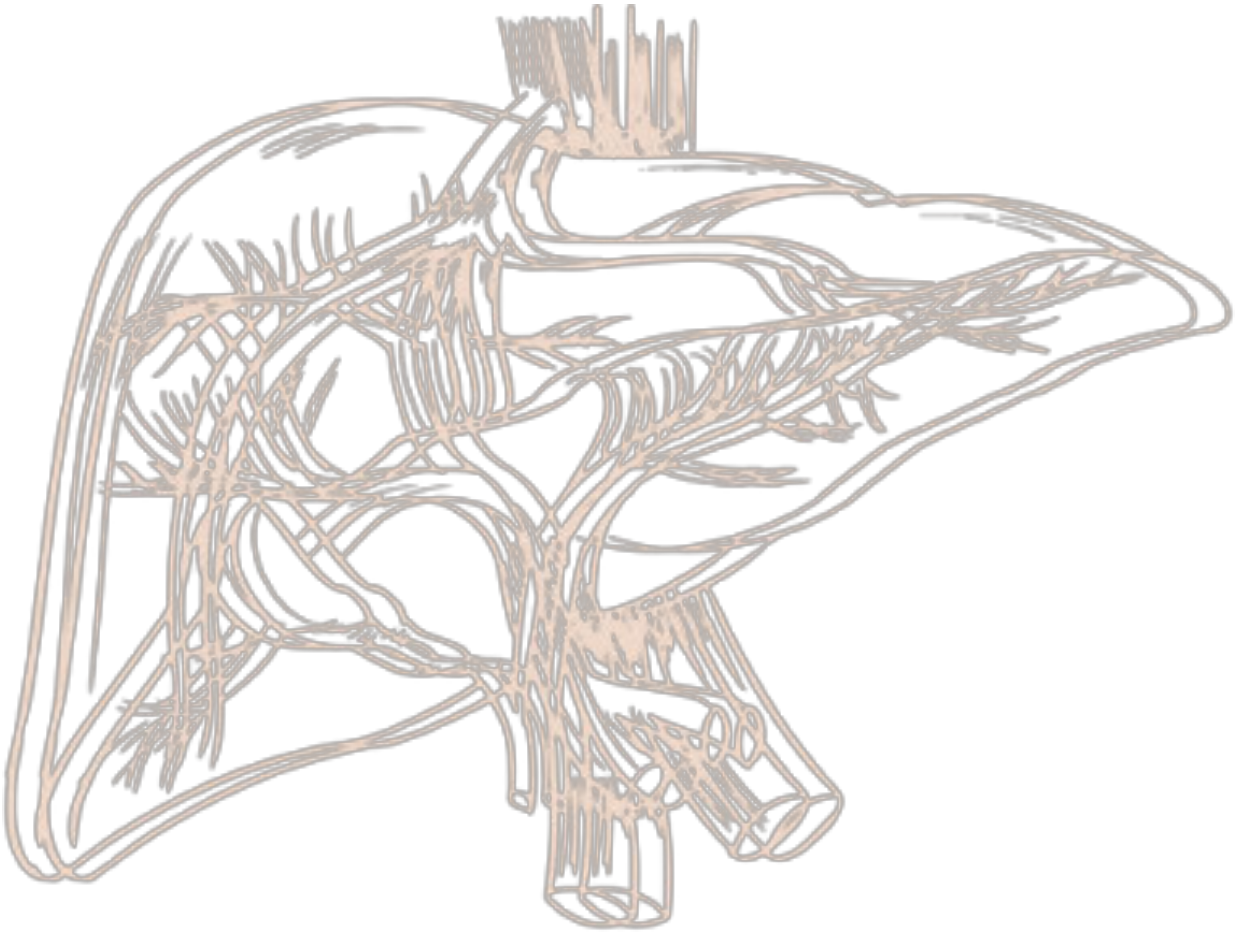

APPENDIX 1

CellPress

Trends in
Endocrinology & Metabolism

Review

The ubiquitin-proteasome system and autophagy: self-digestion for metabolic health

Jia Liang Sun-Wang,[1,2,3,*] Alex Yarritu-Gallego,[4,5] Saška Ivanova,[1,2,3] and Antonio Zorzano[1,2,3,*]

Type 2 diabetes mellitus (T2DM) is a global health challenge. Therefore, understanding the molecular mechanisms underlying the pathophysiology of T2DM is key to improving current therapies. Loss of protein homeostasis leads to the accumulation of damaged proteins in cells, which results in tissue dysfunction. The elimination of damaged proteins occurs through the ubiquitin-proteasome system (UPS) and autophagy. In this review, we describe the mutual regulation between the UPS and autophagy and the involvement of these two proteolytic systems in metabolic dysregulation, insulin resistance, and T2DM. We propose that alterations in the UPS or autophagy contribute to triggering insulin resistance and the development of T2DM. In addition, these two pathways emerge as promising therapeutic targets for improving insulin resistance.

Diabetes mellitus (DM): a major global health issue

DM is the most common metabolic disease and one of the top ten causes of death worldwide [1]. The prevalence of DM has increased dramatically in recent decades. In 2017, around 425 million people between 20 and 79 years of age lived with DM and this number is estimated to rise to 629 million by 2045 [2]. DM is characterized by impaired glucose homeostasis, which results in hyperglycemia. DM is classified into different disease categories and the most prevalent is type 2 DM (T2DM). T2DM is characterized by a gradual loss of insulin production by pancreatic β-cells and the progressive development of insulin resistance in metabolically relevant tissues, such as skeletal muscle, adipose tissue, liver, and brain, most likely due to alterations in the insulin signaling pathway [3].

One of the major risk factors in the development of T2DM is obesity, a detrimental metabolic condition [4]. The prevalence of obesity has also risen tremendously over recent decades due to industrialization, sedentary lifestyles, and diets based on processed foods [4,5]. Another relevant risk factor in T2DM is aging [3]. The metabolic derangements in T2DM patients can lead to numerous health complications, including cardiovascular, renal, and neurodegenerative disease, thus impairing their healthspan and lifespan [6]. Therefore, T2DM poses a serious threat to global health that needs to be tackled following the United Nations Sustainable Development Goal 3 (SDG3) to 'ensure healthy lives and promote well-being for all at all ages' [7]. A better understanding of the molecular mechanisms leading to insulin resistance and to β-cell failure will permit the prevention of T2DM, as well as allowing for more efficient and personalized treatments. Therefore, based on recent data, we propose that the ubiquitin-proteasome system (UPS) and autophagy participate in the pathophysiology of T2DM.

Cellular protein degradation machinery

The UPS

The UPS targets most cellular proteins for degradation to the 26S proteasome (proteasome hereafter), a multiprotein complex formed by the 20S core particle (CP) and the 19S regulatory particle (RP) [8]. Proteins that are targeted to the proteasome are previously subjected to ubiquitination (Box 1). Ubiquitinated substrates are recognized and bound directly to ubiquitin

Highlights

Alterations in the ubiquitin-proteasome system (UPS) and autophagy are associated with metabolic disorders, including obesity and type 2 diabetes.

The proteasome activity is downregulated in liver, pancreas, and adipose tissue under insulin resistant conditions and the proteasome is required for the metabolic activity of brown adipocytes and for β-cell function.

A deficient autophagy triggers insulin resistance in liver and it leads to varying alterations in conferring susceptibility to obesity and on adipogenesis.

The UPS and autophagy regulate each other. The 26S proteasome is regulated by autophagy activity through a process named proteaphagy. Autophagy activity is controlled through the action of E3 ubiquitin ligases and deubiquitinases that participate in the different phases of autophagosome formation and fusion with lysosomes.

Therapeutic interventions targeting the UPS and autophagy improve metabolic health.

[1]Institute for Research in Biomedicine (IRB Barcelona), Barcelona Institute of Science and Technology (BIST), Barcelona, Spain
[2]Departament de Bioquímica i Biomedicina Molecular, Facultat de Biologia, Universitat de Barcelona, Barcelona, Spain
[3]CIBER de Diabetes y Enfermedades Metabólicas Asociadas, Barcelona, Spain
[4]Department of Nephrology and Medical Intensive Care, Charité-Universitätsmedizin Berlin, Berlin, Germany
[5]Experimental and Clinical Research Center, a Cooperation of Charité-Universitätsmedizin Berlin and Max Delbruck Center for Molecular Medicine, Berlin, Germany

 https://doi.org/10.1016/j.tem.2021.04.015

*Correspondence:
jialiang.sunwang@irbbarcelona.org (J.L. Sun-Wang) and
antonio.zorzano@irbbarcelona.org (A. Zorzano).

Box 1. Ubiquitination as a 'degrade-me' signal

Ubiquitination, also referred to as ubiquitylation, is a post-translational modification that involves the covalent attachment of one (monoubiquitination) or multiple (polyubiquitination) ubiquitin monomers to the ε-amino group of a lysine residue. Ubiquitin is a small regulatory protein of 8.6 kDa, ubiquitously expressed in eukaryotic organisms. Ubiquitination occurs through a sequence of enzymatic reactions catalyzed by ubiquitin-activating enzymes (E1s), ubiquitin-conjugating enzymes (E2s), and ubiquitin ligases (E3s). E3s provide substrate specificity for ubiquitination, a feature that explains why humans and other eukaryotic organisms have hundreds of genes that encode for E3s [109]. Polyubiquitin chains can be generated through the consecutive addition of ubiquitin molecules to any lysine residue of the previous ubiquitin: M1, K6, K11, K27, K29, K33, K48, and K63, thus offering a wide variety of linkage types to regulate many cellular functions [110]. In this regard, K48-, K29-, and K11-polyubiquitin chains are signals for proteasome degradation, whereas K63 chains are involved in autophagy degradation and in the regulation of protein activity.

Therefore, ubiquitin is a common molecular player shared by the UPS and autophagy. But how the different types of polyubiquitin chains target a substrate protein to the proteasome or to autophagy remains to be elucidated. Furthermore, p62 constitutes a key player, as it is not only an autophagic adaptor, but also a proteasome shuttling factor [111]. Thus, p62 can be considered a dual proteasomal and autophagic receptor, suggesting that other autophagic adaptors with similar biochemical properties may also act as dual receptors. Recent findings showed that the choice between proteasomal and autophagic degradation depends on the ability of p62 to oligomerize [112,113]. When p62 is in an oligomeric state, it binds with higher preference to K63-linked polyubiquitin chains [112]. By contrast, K48-linked polyubiquitin chains can disrupt p62 oligomers, suggesting that a nonoligomeric state favors proteasomal degradation, whereas an oligomeric state favors autophagic degradation [112]. Moreover, the generation of artificial receptors has revealed that oligomeric receptors are inefficient in the degradation of soluble substrates compared with monomeric receptors [113]. By contrast, only oligomeric receptors are capable of promoting autophagic degradation of aggregation-prone substrates [113]. In conclusion, the choice which of the two degradation systems (i.e., proteasomal or autophagic) will be used depends on several factors: (i) polyubiquitin linkage type, (ii) receptor oligomerization state, and (iii) substrate aggregation state.

receptors located at the 19S RP of the proteasome or indirectly through **proteasome-shuttling factors** (see Glossary) [9]. Substrates are then committed to degradation through an ATP-dependent and irreversible binding step to the 19S RP. Prior to degradation, ubiquitin conjugates are removed by **deubiquitinating enzymes (DUBs)**, thereby allowing the reutilization of ubiquitin. The timely degradation of substrates and the clearance of damaged proteins by the proteasome contributes to protein homeostasis (proteostasis).

Autophagy

Autophagy targets cytosolic components, including proteins and organelles, to the lysosome for degradation. Three types of autophagy occur in mammals: macroautophagy [10], **microautophagy** [11], and **chaperone-mediated autophagy (CMA)** [12]. Macroautophagy (autophagy hereafter) is the most characterized type of autophagy and it requires the formation of autophagosomes, namely double-membrane vesicles that deliver the **cargo** to lysosomes (Figure 1). Once autophagosomes are formed, they fuse with lysosomes into autolysosomes, where the cargo and autophagosomes are degraded into building blocks that are recycled by the cell. Autophagy is a tightly regulated process that requires a complex signaling cascade and **ATG proteins**. **mTORC1** and **AMPK**, two key metabolic sensors, control the initial events in autophagosome biogenesis [13] (Figure 1).

Autophagy can take place in a nonselective manner (nonselective autophagy), which involves the random uptake of cytosolic material for degradation (e.g., upon nutrient deprivation). However, during selective autophagy, autophagosomes recruit specific cellular components [14]. Selective degradation through autophagy receives a distinct nomenclature, depending on the cargo recruited: aggrephagy (protein aggregates), mitophagy (mitochondria), etc. The degradation of cellular material by autophagy serves as a quality control mechanism to maintain homeostasis. More specifically, aggrephagy contributes to the maintenance of proteostasis.

Mechanisms of interaction between the UPS and autophagy

UPS and autophagy share molecular players (e.g., ubiquitin and **p62**) (Box 1) and there is increasing evidence that they regulate each other. In this section, we describe mechanisms of interaction between the UPS and autophagy and discuss their implications in proteostasis.

Proteaphagy: the clearance of proteasomes by autophagy

Degradation of proteasomes through autophagy, also referred to as proteaphagy, was first hinted at through early observations in rat liver, in 1995 [15]. However, it was not until recently that the degradation of proteasomes through autophagy was described in mammalian cells [16], yeast [17], and plants [18]. In mammals, proteaphagy is activated upon amino acid and serum (AAS) deprivation (Figure 2). The 20S CP and 19S RP subunits are highly enriched in autophagosome–lysosome fractions and are dramatically reduced in whole-cell lysates after 24–30 hours of AAS starvation [16]. Upon AAS starvation, 19S RP subunits are ubiquitinated, a process that is necessary for proteasome uptake by autophagosomes [16]. However, the E3s responsible for the ubiquitination of the 19S RP under AAS deprivation remain to be described. p62 was identified as the autophagic adaptor necessary for proteasome recruitment into autophagosomes via the UBA domain [16].

Proteasome inhibitors (PIs) also activate proteaphagy [19–21] (Figure 2) and induce ubiquitination of the 19S RP, a process mediated by the E3 STUB1 [19]. Ubiquitination of the 19S RP promotes the reversible sequestration of proteasomes in **aggresomes** by p62, which could lead to two distinct outcomes. On one hand, removal of PIs from the cellular medium rescues proteasomes, resulting in the recovery of proteasomal activity. On the other hand, continued exposure to PIs induces the clearance of aggresome-associated proteasomes through autophagy [19], thus pointing to crosstalk between aggrephagy and proteaphagy.

Interestingly, genetically and chemically induced proteasome impairment upregulates autophagy, with p62 playing a central role, and also activates the **proteasome recovery pathway (PRP)** through the transcription factor **Nrf1** [22]**.** Activation of autophagy under deficient proteasomal degradation relies on multiple mechanisms, including the activation of the unfolded protein response (UPR) associated with endoplasmic reticulum (ER) stress [23,24] and the stabilization of the master transcription factor of lysosomal and autophagy genes TFEB [25], among others [22]. Therefore, upregulation of autophagy, activation of the PRP, and induction of proteaphagy may be a coordinated response for the disposal of defective proteasomes, the clearance of substrates that should have been degraded by the proteasome, and the synthesis of new proteasomes to maintain proteostasis.

The mechanisms underlying proteaphagy are coming to light, but the physiological role of this process remains elusive. In the context of starvation and in contrast to *in vitro* studies [16], there are no changes in proteasome abundance in mouse skeletal muscle and liver after 24 and 48 hours of fasting [26]. However, proteasomes are present in the hepatic lysosomes of fasted rats [15]. Furthermore, starvation increases proteasome activity in muscle and liver [26] and in cultured cells [27], observations that thus question the physiological relevance of starvation-induced proteaphagy.

In the context of oxidative stress, proteaphagy may be a relevant cytoprotective mechanism. In this connection, oxidative stress causes protein damage and misfolding, resulting in an initial upregulation of the UPS to deal with misfolded proteins. However, if oxidative stress persists, it may enhance the formation of aggregates that can overwhelm the proteasome and induce proteotoxic stress [28]. In these conditions and in an attempt to restore proteostasis,

Glossary

Aggresomes: cytoplasmic inclusions that isolate misfolded proteins and prevent them from harming the cell. Aggresomes form when the protein degradation machinery is overwhelmed (e.g., upon proteasome inhibition).
AMPK: AMP-activated protein kinase. AMPK is an energy sensor that is activated when cellular energy levels run low, thus promoting catabolism.
ATG proteins: Atg stands for 'autophagy-related'. Atg proteins form the core macroautophagic machinery.
ATG8: a ubiquitin-like protein that is conjugated to autophagosome membranes and is involved in cargo recruitment and autophagosome biogenesis in yeast. Mammals have six ATG8 homologs that perform similar functions (LC3A, LC3B, LC3C, GABARAP, GABARAP-L1, and GATE-16). The most studied ATG8 homolog in mammals is LC3B, a *bona fide* autophagosome marker [130].
Cargo: cellular material to be degraded in the lysosome.
Chaperone-mediated autophagy (CMA): a form of autophagy that targets only proteins that bear a KFERQ sequence (or KFERQ-like sequence) for degradation by the lysosome. Proteins with the KFERQ sequence are delivered to the lysosomal membrane by chaperones, where they interact with lysosomal-associated membrane protein 2 isoform A (LAMP2A). LAMP2A then forms a pore that allows translocation of the proteins to the lysosomal lumen for degradation.
Deubiquitinating enzyme (DUB): DUBs catalyze the removal of ubiquitin from ubiquitinated proteins. Humans have more than 100 genes that encode for DUBs [109].
Microautophagy: a form of autophagy that does not require the formation of autophagosomes for cargo delivery to the lysosome. Instead, the lysosomal membrane invaginates to take up the cargo.
mTORC1: mammalian target of rapamycin complex 1. mTORC1 is a protein kinase complex that acts as a metabolic sensor. It is activated by nutrients, such as growth factors and amino acids, and it promotes anabolism while it inhibits catabolism through the phosphorylation of downstream target proteins. When nutrients are scarce, mTORC1 is inactive. mTORC1 can also be chemically inhibited by rapamacyin.

proteaphagy could be jointly activated with aggrephagy to degrade blocked proteasomes and aggregated proteins.

Regulation of the autophagic machinery by ubiquitination

E3 ubiquitin ligases are essential players in the UPS. In addition, recent studies have shown that ubiquitination of ATG proteins is a fundamental process in the regulation of autophagy. Many components of the autophagic machinery are subjected to different types of ubiquitination by a wide variety of E3s (Table 1). Based on the data, K48-linked ubiquitination of ATG proteins promotes their proteasomal degradation and may serve as a regulatory signal to restrict autophagy when it is not necessary (i.e., under nutrient-rich conditions) or as a signal to terminate autophagy to prevent overactivation. On the contrary, other linkage types of ubiquitin chains may regulate the activity of ATG proteins to promote autophagy under autophagy-activating conditions.

Ubiquitination is a reversible process that can be antagonized by DUBs. Interestingly, DUBs also play a role in the regulation of autophagy by removing ubiquitin chains. For instance, K48-linked ubiquitin chains in ULK1 can be removed by USP20 to prevent its proteasomal degradation, thus stabilizing ULK1 and promoting autophagy [29]; whereas K63-linked ubiquitin chains in ULK1 can be removed by USP1, thus suppressing autophagy [30].

The importance of the regulation of autophagy by E3s and DUBs has been demonstrated by a recent study [31]. In this connection, K29/K48 ubiquitination of the class III PI3-kinase subunit VPS34 by UBE3C promotes its proteasomal degradation, thus suppressing autophagy. Ubiquitin chains on VPS34 can be removed by TRABID [31]. Under ER stress and proteotoxic stress induced by PIs, UBE3C interaction with VPS34 is diminished, resulting in decreased VPS34 ubiquitination and VPS34 stabilization [31]. Interestingly, mice fed with a high-fat diet (HFD) exhibit reduced levels of TRABID and VPS34, decreased autophagy, and develop hepatic steatosis. Under these conditions, overexpression of TRABID in HFD-fed mice restored VPS34 protein levels and autophagy and alleviated steatosis [31]. Therefore, the timely action of E3s and DUBs modulates autophagy to preserve proteostasis and tissue homeostasis.

The UPS and autophagy in metabolic disease

Understanding the molecular mechanisms underlying the development of insulin resistance and T2DM is key to designing novel therapeutic approaches. In this section, we discuss the implications of the UPS and autophagy in obesity, insulin resistance, and T2DM. We propose that these pathways are promising therapeutic targets for the treatment of metabolic diseases.

The UPS and metabolic homeostasis

Proteasome activity is reduced in livers from *ob/ob* and *db/db* mice [32] and also in adipocytes from obese insulin-resistant human subjects [33]. Proteolysis by the proteasome is also impaired in the brains of streptozotocin-induced diabetic rats [34] and the spontaneous obese rat WNIN/Ob [35]. Gene expression of proteasome subunits is reduced in the livers of *db/db* mice [36] and in mouse heart upon HFD [37]. HFD also impairs proteasome activity in mouse white adipose tissue (WAT), brown adipose tissue (BAT), and liver [32,33,38]. These findings indicate that UPS function is altered under conditions characterized by obesity or insulin resistance.

Recent data have provided strong evidence that the UPS is required in nonshivering thermogenesis and that inhibition of the proteasome represses the expression of metabolic genes such as UCP1 or PGC1α and induces ER stress in BAT [38]. Furthermore, proteasome activity mediated by the transcription factor Nrf1 is essential for BAT thermogenic adaptation and metabolic health in mice [38]. BAT-specific deletion of Nrf1 reduces proteasome activity, which is exacerbated by a

Nrf1: nuclear factor erythroid 2-related factor 1. A transcription factor that modulates the expression of proteasome subunits.
p62: also referred to as SQSTM1 (sequestosome 1). p62 is a multifunctional protein involved in cell signaling, autophagy, and proteasomal degradation. It contains a UBA domain, which recognizes ubiquitinated proteins, a LIR, which recognizes Atg8 homologs at the autophagosome membrane, and a PB1 domain, which serves for oligomerization and for interaction with proteasomes. The presence of these domains allows p62 to act as an autophagic adaptor and as a proteasome-shuttling factor [131].
Proteasome inhibitors (PIs): small molecules that inhibit proteasomal degradation, thus inducing proteotoxic stress. These inhibitors are extensively used for research and therapeutic purposes. For instance, the proteasome inhibitor bortezomib has been in clinical use for multiple myeloma for more than 10 years [132].
Proteasome recovery pathway (PRP): a mechanism mediated by the transcription factor Nrf1 that upregulates the synthesis of proteasome subunits upon proteasome inhibition [133].
Proteasome-shuttling factors: ubiquitin receptors that shuttle ubiquitinated proteins to the proteasome for degradation. These proteins contain a UBL (ubiquitin-like) domain that is recognized by proteasome intrinsic ubiquitin receptors and a UBA (ubiquitin-associated) domain that recognizes ubiquitinated proteins [134].

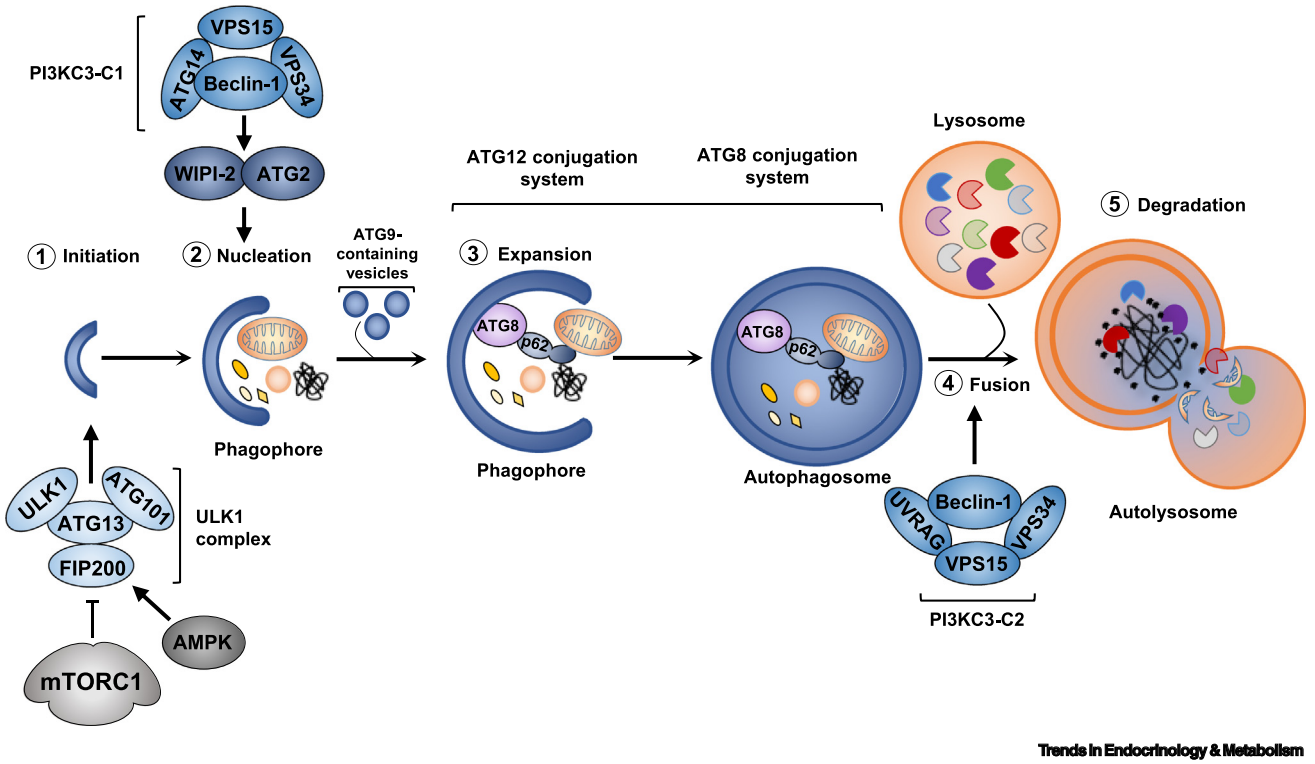

Figure 1. Autophagy. Autophagy is initiated by the ULK1 complex, which can be activated via mTORC1 inhibition or AMPK activation (1). The nucleation step results in the formation of the phagophore and requires the class III phosphatidylinositol 3-kinase complex I (PI3KC3-C1) and the WIPI2-ATG2 complex (2). Phagophore expansion and maturation into autophagosome requires delivery of membranes by ATG9-containing vesicles and the conjugation of **ATG8** homolog proteins to the phagophore membrane (3). Autophagic adaptors such as p62 mediate cargo recruitment. ATG8 proteins are also required for cargo recruitment and are conjugated to autophagosome membranes through the action of the ATG12 and ATG8 conjugation systems. Autophagic cargo can be ubiquitinated, which may be essential for recognition by adaptor proteins [14], which recognize both the cargo and the autophagosome membrane. For instance, p62 binds ubiquitinated protein aggregates and ubiquitinated mitochondria through a UBA (ubiquitin-associated) domain and interacts with LC3B (an ATG8 protein) anchored at the autophagosome membrane through an LC3-interacting region (LIR). The fusion between autophagosomes and lysosomes is mediated by the class III phosphatidylinositol 3-kinase complex II (PI3KC3-C2) (4). The fusion event results in the formation of autolysosomes, where cargo and autophagic adaptors are degraded (5).

HFD and results in the secretion of proinflammatory cytokines in plasma and systemic insulin resistance (Table 2) [38]. Interestingly, intra-BAT injection of adenoviruses encoding for either Nrf1 or the proteasome activator PA28α in diet-induced obese mice and *ob/ob* mice enhances proteolysis by the proteasome, which in turn ameliorates insulin resistance [38]. In addition, ablation of the proteasome activator PA28 results in ER stress in the liver, leading to hepatic insulin resistance and exacerbated glucose intolerance upon HFD [32]. Moreover, proteasome inhibition induces ER stress and impairs insulin signaling in adipocytes [33]. Taken together, these data indicate that the UPS is involved in metabolic homeostasis and it emerges as a possible target for the treatment of insulin resistance and T2DM.

By contrast, proteasome activity is increased in myotubes derived from obese insulin-resistant individuals [39]. This differential profile of changes in proteasome activity in skeletal muscle suggests that the UPS plays distinct roles in different tissues to handle insulin resistance. The observation that the PI bortezomib attenuates palmitic acid-induced ER stress, inflammation, and insulin resistance in myotubes [40] further supports the notion that the UPS in muscle is differentially regulated in comparison with other tissues. This upregulation in UPS activity in myotubes derived from obese insulin-resistant subjects might be due to increased transcriptional activity of Forkhead Box (Fox) O transcription factors, which coordinate the transcription of genes

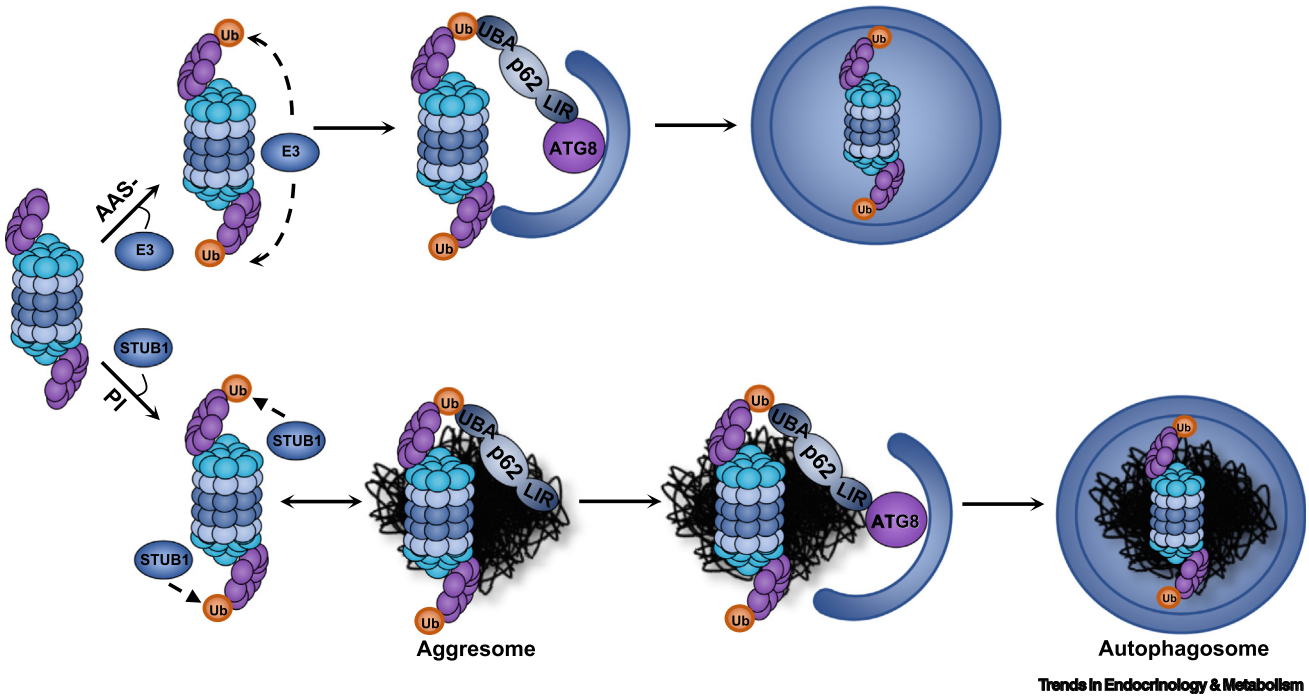

Figure 2. Mechanisms of proteaphagy. Proteaphagy can be triggered by amino acid and serum (AAS) starvation and by proteasome inhibition (PI). AAS starvation-induced proteaphagy promotes the ubiquitination of the 19S regulatory particle (RP) by an unknown E3. Ubiquitinated proteasomes are recognized by the UBA domain of p62, which recruits proteasomes into autophagosomes for lysosomal degradation. PI-induced proteaphagy triggers the ubiquitination of the 19S RP by the E3 STUB1. Ubiquitinated proteasomes are sequestered into aggresomes in a reversible manner by p62. If PI persists, proteasomes and aggresomes are engulfed by autophagosomes and then targeted to the lysosome for degradation. Abbreviations: LIR, LC3-interacting region; Ub, ubiquitin.

related to the UPS, including E3s and proteasome subunits [41]. Insulin inhibits FoxO activity [42], thereby downregulating UPS-related genes and proteasomal degradation. However, the inhibitory action of insulin on FoxO is lost upon insulin resistance, with a concomitant increase in UPS activity [41,42]. FoxO1, 3, and 4 control the muscle-specific expression of the E3s Atrogin-1 and MuRF-1, the main E3s that are responsible for muscle atrophy, which may be a reason for FoxO-dependent increase in UPS activity that only occurs in muscle [41,43]. It is unclear whether FoxO1, 3, and 4 regulate expression of E3s in liver or in adipose tissues. Additional experimental data on proteasome activity in muscle and other metabolically relevant tissues is required to fully understand UPS regulation in insulin-resistant conditions in humans and in animal models.

Autophagy in metabolic fitness

Alterations in autophagy have also been documented in the context of obesity. The protein levels of ATG5, ATG7, ATG12, and Beclin-1 are reduced in the livers of HFD-fed mice [44,45] and in *ob/ob* mice, together with autophagy flux [46]. ATG7 protein levels are also decreased in mouse heart upon HFD [47]. Muscles of patients with T2DM also showed attenuated expression of ATG proteins, including ATG5 and p62 [48], repressed autophagic signaling through the ULK1 complex [48], and decreased levels of the autophagy activator TP53INP2, suggesting impaired autophagy flux [49].

By contrast, HFD increases the levels of ATG5 and ATG12 [45] and enhances autophagy flux in mouse WAT [50]. It has also been reported that autophagy is necessary for adipogenesis [51]. Increased autophagic flux in WAT upon HFD may be an adaptive response to increase the

Table 1. List of E3s that regulate autophagy through the ubiquitination of ATG proteins

	ATG	E3	Ub[a]	Condition[b]	Result[c]	Refs
Initiation	ULK1	TRAF6	K63	Short starvation	+	[114]
		NEDD4L	K48	Prolonged starvation	–	[115]
		KLHL20	K48	Prolonged starvation	–	[116]
	ATG13	LUBAC	M1	Short starvation	+	[117]
Nucleation	Beclin-1	TRAF6	K63	TLR4 activation	+	[118]
		TRIM50	K63	Short starvation	+	[119]
		KLHL20	K48	Prolonged starvation	–	[116]
		RNF216	K48	Prolonged starvation	–	[120]
	WIPI2	HUWE1	K48	Nutrient rich	–	[121]
		CUL4	K48	Mitosis activation	–	[122]
	VPS34	UBE3C	K29 K48	Basal	–	[31]
	VPS34	KLHL20	K48	Prolonged starvation	–	[116]
	ATG9	Met30	K48	Nutrient rich	–	[123]
Expansion	ATG16L	CUL3-gigaxonin	K48	Basal	+	[124]
	ATG4	RNF5	K48	Basal	–	[125]
	GABARAP	MIB1	K48	Basal	–	[126]
	p62	UBE2D2/3[d]	K63?	PIs treatment	+	[127]
		NEDD4	K63	Basal	+	[128]
Fusion	UVRAG	SMURF1	K29 K33	Basal	+	[129]

[a]The linkage type of the ubiquitination is detailed in the 'Ub' column.
[b]The cellular conditions under which these ubiquitination events were identified are detailed in the 'Condition' column.
[c]The outcome of the ubiquitination events is listed in the 'Result' column as favoring (+) or suppressing (–) autophagy.
[d]UBE2D2 and UBE2D3 are E2s.

number of adipocytes in order to store excess fat or it could also be a consequence of increased lipid droplet (LD) biosynthesis, as LDs contribute to autophagosome biogenesis [52].

Suppression of autophagy in WAT and liver impairs metabolic homeostasis in mouse models (Table 2) [46,53,54]. Simultaneous deletion of ATG3 or ATG16L in mouse WAT and BAT leads to the accumulation of dysfunctional mitochondria and toxic lipid peroxides, which in turn induce WAT inflammation and systemic insulin resistance [53]. Interestingly, autophagy plays a seminal role in lipid metabolism [55] and WAT biology [51]. In this regard, ablation of the autophagy activator TP53INP2 promotes adipose hyperplasia, thus leading to hyperplasic obesity [56], a less pathogenic form of obesity [57]. Currently available data reveal a multiplicity of potential mechanisms behind what we refer to autophagy and the need for more in-depth studies.

In mouse liver, ATG5 deletion impairs fasting-induced hepatic steatosis (Table 2) [58]. Lack of ATG7 in mouse liver increases ER stress, impairs hepatic insulin signaling, and induces systemic insulin resistance, which are restored upon ATG7 re-expression [46]. Moreover, ATG7 ablation in mouse liver impairs glucose homeostasis as a result of alterations in gluconeogenesis [54]. By contrast, mice lacking ATG7 in muscle are protected from diet-induced obesity and insulin resistance due to metabolic adaptations induced by FGF21 [59], a hormone secreted in response to nutrient challenges to restore metabolic homeostasis [60]. Suppression of autophagy in muscle leads to mitochondrial dysfunction, oxidative stress, ER stress, and the subsequent

Table 2. *In vivo* metabolic effects of altered UPS or autophagy

Genotype[a]	Organ	UPS/ autophagy	Model	Metabolic phenotype	Refs
Nrf1$^{-/-}$	BAT	↓UPS	Regular or HFD, mice	Mitochondrial dysfunction, ER stress, inflammation, and insulin resistance	[38]
Nrf1 adOE	BAT	↑UPS	HFD, *ob/ob* mice	Improved insulin sensitivity	[38]
PA28α adOE	BAT	↑UPS	HFD, *ob/ob* mice	Improved insulin sensitivity	[38]
PA28$^{-/-}$	Whole body	↓UPS	Regular or HFD, mice	ER stress and insulin resistance	[32]
ATG3$^{-/-}$	WAT BAT	↓Autophagy	Regular diet, mice	Mitochondrial dysfunction, inflammation, and insulin resistance	[53]
ATG16L$^{-/-}$	WAT BAT	↓Autophagy	Regular diet, mice	Inflammation and insulin resistance	[53]
TP53INP2$^{-/-}$	Whole body	= Autophagy	HFD, mice	Increased adiposity w/o altering glucose homeostasis	[56]
ATG5$^{-/-}$	Liver	↓Autophagy	Fasting, mice	Impaired fasting-induced hepatic steatosis	[58]
ATG7 adKD	Liver	↓Autophagy	Regular diet, mice	ER stress and insulin resistance	[46]
ATG7 adOE	Liver	↑ Autophagy	*ob/ob*, mice	↓ER stress, improved insulin sensitivity	[46]
ATG7$^{-/-}$	Liver	↓Autophagy	Regular diet, mice	Impaired gluconeogenesis	[54]
ATG7$^{-/-}$	Muscle	↓Autophagy	HFD, mice	Mitochondrial dysfunction, ER stress, FGF21 secretion, and improved insulin sensitivity	[59]
FUNDC1$^{-/-}$	Muscle	↓Autophagy	HFD, mice	Mitochondrial dysfunction, FGF21 secretion, and improved insulin sensitivity	[61]
ATG7$^{-/-}$	β-cells	↓Autophagy	Regular or HFD diet, mice	Mitochondrial dysfunction, ↓β-cell mass, ↓insulin production, and hyperglycemia	[73] [74]

[a]Abbreviations: adOE, adenoviral overexpression; adKD, adenoviral knockdown.

secretion of FGF21 (Table 2) [59]. This FGF21-dependent metabolic adaptation is also observed in mice upon muscle-specific deletion of FUNDC1, a mitophagy adaptor [61].

In all, available data indicate that autophagy plays a role in the regulation of metabolic homeostasis and that it undergoes adaptations in metabolic disorders. Additionally, recent data reveal that small molecules that induce autophagy exert beneficial effects in obese insulin-resistant mice [62]. Thus, chronic treatment with a chemical compound named MSL-7, which activates autophagy, improves glucose homeostasis and insulin sensitivity in *ob/ob* mice and HFD-induced obese mice and these effects occur in the absence of changes in body weight [62]. Additionally, administration of the plant metabolite Rg2, a steroid glycoside that induces autophagy, ameliorates insulin resistance and reduces body weight gain in HFD-fed mice [63]. Improvement of insulin sensitivity by Rg2 is autophagy-dependent, as this effect is lost in autophagy-deficient mice [63]. Moreover, autophagy enhancers attenuate diabetic cardiomyopathy in rat and mouse models by mitigating oxidative stress [64–66]. Based on these observations, autophagy emerges as a potential target to ameliorate insulin resistance and diabetic complications in obese and T2DM patients.

Altered UPS and autophagy in the progression of metabolic disease

Alterations in the UPS and autophagy may pave the way for the progression of metabolic disease. β-Cell dysfunction is the definitive alteration that triggers T2DM [67]. β-Cells secrete insulin together with amylin, also referred to as islet amyloid polypeptide (IAPP). Accumulating evidence suggests that IAPP aggregation is involved in β-cell dysfunction in the context of T2DM (Figure 3) [68]. Interestingly, the UPS and autophagy have been reported to regulate IAPP turnover in β-cells (Figure 3) [69]. In addition, proteasomal degradation and autophagy are impaired in the pancreatic islets of T2DM patients [69,70], thus leading to a marked accumulation of ubiquitinated proteins [69]. Autophagy is also suppressed in β-cells of HFD-fed and diabetic

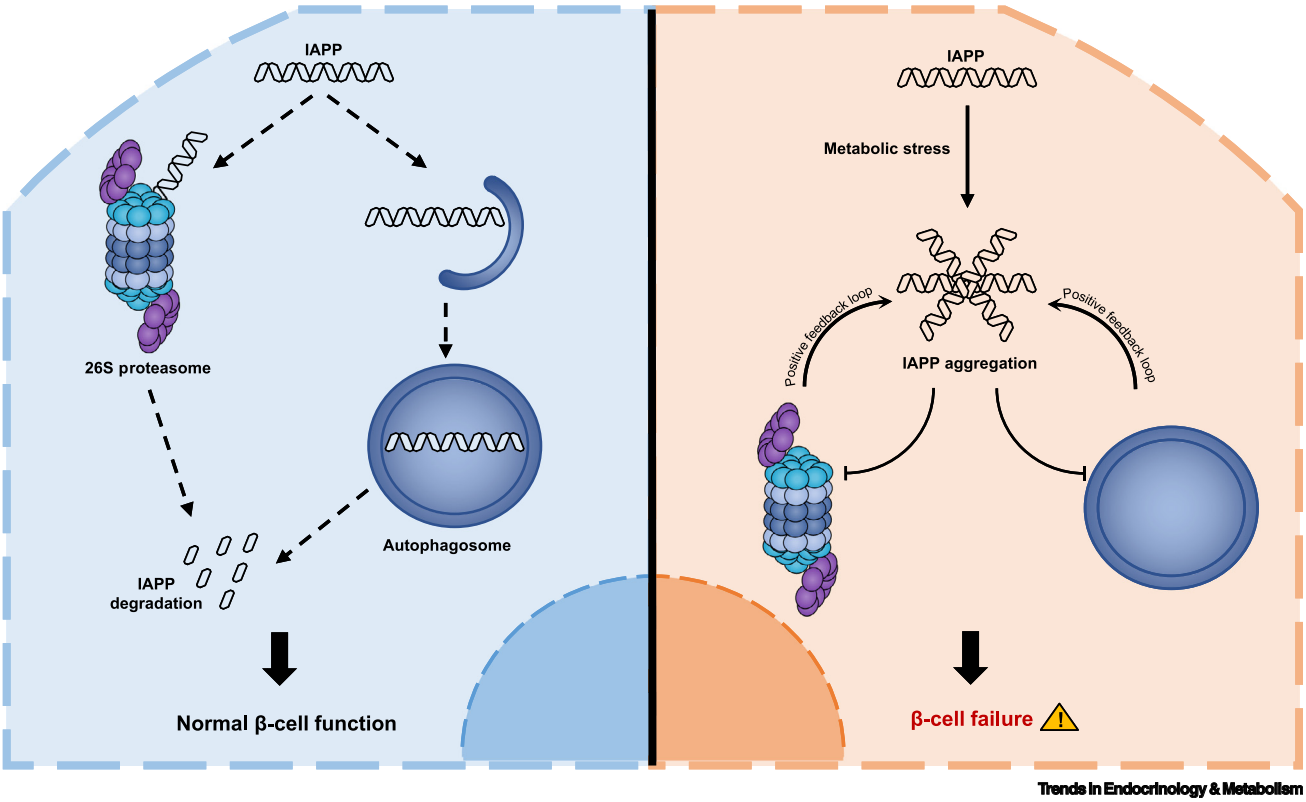

Figure 3. The ubiquitin-proteasome system (UPS) and autophagy preserve β-cell function by degrading islet amyloid polypeptide (IAPP). The UPS and autophagy contribute to preservation of β-cell function by degrading IAPP (broken arrows, left panel). However, UPS and autophagy function in β-cells decline under metabolic stress [e.g., high glucose, oxidative stress, endoplasmic reticulum (ER) stress, mitochondrial dysfunction, etc.], thus allowing IAPP to form toxic aggregates. IAPP aggregates further inhibit the UPS and autophagy, generating a vicious cycle that exacerbates IAPP aggregation, which eventually leads to β-cell failure.

mice [71], and deletion of autophagy in mouse β-cells enhances IAPP-induced apoptosis [72], thus reducing β-cell mass [73–75]. By contrast, the autophagy enhancer MSL-7 improves IAPP clearance and β-cell function and ameliorates diabetes in an IAPP-induced diabetes mouse model [76]. In keeping with this, the autophagy activator rapamycin decreases β-cell apoptosis and improves insulin secretion in human pancreatic islets from T2D donors [77]. Chronic exposure to high glucose in INS-1E β-cells and human pancreatic islets reduces proteasome activity, increases the accumulation of ubiquitinated proteins, and triggers ER stress and apoptosis [78]. Furthermore, the PI MG-132 promotes apoptosis in INS-1E β-cells and human pancreatic islets [78]. Moreover, hyperglycemia also impairs autophagy in INS-1E β-cells [70]. Interestingly, IAPP aggregates have been proposed to inhibit the UPS and autophagy [79]. These observations suggest the interesting notion that metabolic stress in prediabetic individuals is responsible for UPS and autophagy dysfunction in β-cells, ultimately resulting in β-cell failure. In short, UPS and autophagy collaborate to maintain metabolic health by degrading IAPP and ameliorating oxidative stress in β-cells, thus improving β-cell survival and function (Figure 3). However, therapeutic strategies aiming at enhancing autophagy in β-cells should be carefully considered, as excessive activation of autophagy promotes the degradation of insulin secretory granules, thereby reducing insulin secretion and impairing glucose tolerance [80]. Additionally, short-term inhibition of autophagy in β-cells improves β-cell function upon HFD through changes in the lipidome [81,82], suggesting that suppressing autophagy for a short time may also be beneficial.

Metabolic alterations, including enhanced reactive oxygen species (ROS) production, mitochondrial dysfunction, and increased ER stress, are characteristic of insulin resistance and T2DM and they may precede the development of these conditions [83–85]. Interestingly, mitochondrial dysfunction has been reported to impair autophagy and also UPS function [86,87] (Figure 4). Thus, ablation of the mitochondrial fusion protein Mitofusin 2 (Mfn2) promotes mitochondrial dysfunction, causes insulin resistance, and reduces autophagy flux in cells and in skeletal muscle [86,88,89]. However, despite decreased autophagy flux, lack of Mfn2 in skeletal muscle activates an adaptive mitophagy pathway via HIF1α and BNIP3 to minimize mitochondrial damage [87], suggesting that mitochondrial stress can induce mitophagy even when autophagy activity is reduced. Moreover, mutations in respiratory complex I reduce the assembly and activity of the proteasome [87]. Deficiencies in the UPS and autophagy have also been associated with mitochondrial dysfunction in cells [90], muscle [59,61,91], BAT [38], WAT [53], β-cells [92], and heart [93]. Alterations in the UPS and autophagy also cause ER stress in liver [32,46], muscle [59], and adipocytes [33]. Altogether, these data suggest that mitochondrial dysfunction contributes to the alterations in UPS and autophagy function under prediabetic conditions. Furthermore, altered UPS and autophagy may in turn establish a feed-forward loop that exacerbates

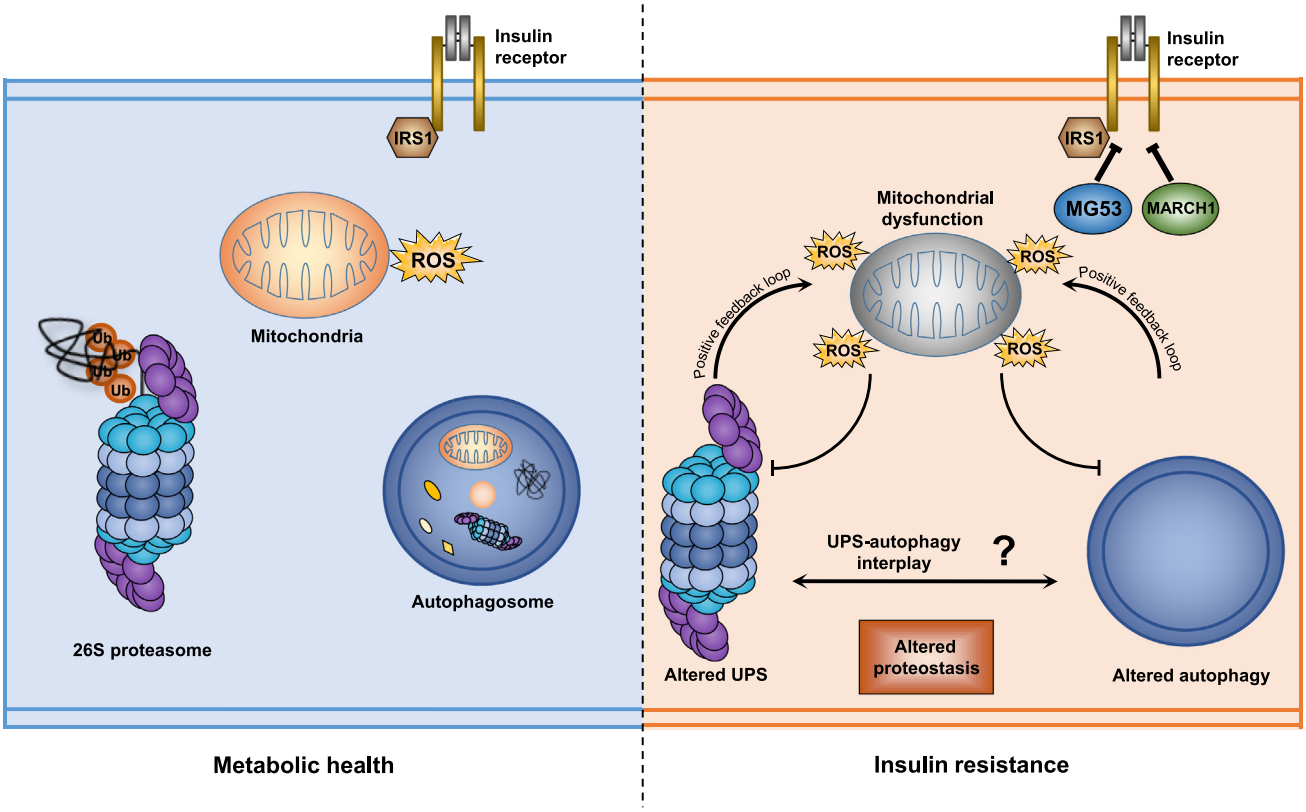

Figure 4. Alterations in the ubiquitin-proteasome system (UPS) and autophagy under insulin resistance. Cells from healthy individuals are characterized by normal mitochondrial function and mild levels of oxidative stress. Functional UPS and autophagy contribute to the maintenance of proteostasis, thus preserving insulin signaling and metabolic health (left). However, under metabolic stress, for example, in the context of obesity, cells are characterized by upregulation of the E3s MG53 and MARCH1, mitochondrial dysfunction, chronic oxidative stress, and endoplasmic reticulum (ER) stress (not shown). Increased expression of MG53 and MARCH1 promotes proteasomal degradation of the insulin receptor and insulin receptor substrate 1 (IRS1), thus impairing insulin signaling. Mitochondrial dysfunction may contribute to alterations in the UPS and autophagy. In turn, alterations in both proteolytic systems may exacerbate mitochondrial dysfunction and ER stress (not shown), thus aggravating insulin resistance and leading to β-cell failure and the development of type 2 diabetes mellitus (right). Abbreviation: ROS, reactive oxygen species.

mitochondrial dysfunction and ER stress, thus aggravating insulin resistance in peripheral tissues and leading to β-cell failure and the development of T2DM (Figure 4).

Physical exercise and calorie restriction have been widely considered to have beneficial effects in T2DM patients [94,95]. UPS activity is enhanced in human skeletal muscle after high-intensity exercise [26], in mouse muscle and liver upon fasting [26], and in the brain of WNIN/Ob rats upon calorie restriction [35]. Autophagy is also enhanced upon exercise in mouse [96] and human muscle [97] and this exercise-induced adaptation in autophagy is required for glucose homeostasis in mice [96]. Intermittent fasting preserves β-cell function in an autophagy-dependent manner in obese mice [71]. Moreover, long-term calorie restriction in humans increases the expression of ATG genes, including ULK1 and Beclin-1 [98]. Interestingly, intermeal fasting in mice activates autophagy in liver, adipose tissue, muscle, and brain, thus conferring systemic metabolic benefits [99]. The modulation of the UPS and autophagy may contribute to the beneficial metabolic effects associated with exercise and calorie restriction.

Ubiquitination in metabolic homeostasis

The insulin signaling pathway is also regulated by ubiquitination [100]. Several E3s have been identified to play a role in metabolic homeostasis. Expression of the E3s MG53 and MARCH1 is upregulated in muscle and WAT from obese human subjects and HFD-treated mice [101,102]. In this context, MG53 and MARCH1 promote proteasomal degradation of the insulin receptor (IR) and the IR substrate 1 (IRS1), leading to insulin resistance [101,102] (Figure 4). By contrast, ablation of these E3s prevents insulin resistance upon HFD [101,102]. Additionally, MG53 has been identified as a myokine with insulin-desensitizing effects secreted by muscle [103]. Circulating MG53 acts as an allosteric inhibitor of the IR by binding to its extracellular domain, and neutralization of MG53 with an antibody enhances insulin sensitivity in *db/db* mice [103]. Furthermore, global deletion of MKRN1 protects mice from diet-induced obesity and diabetes through AMPK stabilization and activation in liver, WAT, and BAT [104].

DUBs also contribute to metabolic fitness. Along these lines, chronic ER stress in mice upregulates USP14, which stabilizes 3′,5′-cyclic monophosphate-responsive element binding (CREB) protein (CBP), thus enhancing glucagon action, gluconeogenesis, and hyperglycemia [105]. Liver-specific deletion of USP14 reduced hepatic glucose output and improved hyperglycemia and glucose intolerance in HFD-treated mice [105]. USP14 has also been reported to increase the stability of fatty acid synthase (FASN) and USP14 levels are upregulated in HFD-fed mice and in *db/db* mice [106]. Overexpression of USP14 increases hepatic triglyceride content and promotes steatosis [106]. By contrast, knockdown of USP14 reduces liver triglyceride content, alleviates steatosis, and improves glucose metabolism in *db/db* mice [106]. Another study in mice has shown that UPS20 is a positive regulator of cholesterol biosynthesis under fed conditions by stabilizing HMG-CoA reductase, the rate-limiting enzyme in cholesterol synthesis [107]. Interestingly, genetic ablation or pharmacological inhibition of USP20 in mice improves insulin sensitivity, reduces diet-induced body weight gain, and increases energy expenditure [107]. Liver-specific overexpression of USP18 improves lipid metabolism and insulin sensitivity in mice fed with a HFD by suppressing TAK1 activity and the nuclear factor kappa B signaling pathways, whereas hepatic ablation of USP18 exacerbates steatosis and glucose intolerance upon HFD [108]. In all, these data suggest that ubiquitination dynamics governed by E3s and DUBs can also be a potential therapeutic target to promote metabolic fitness.

Concluding remarks

Alterations in both the UPS and autophagy have been documented in the context of obesity, insulin resistance, and T2DM in mouse models and human subjects. However, further research

Outstanding questions

Are the alterations that occur in the UPS or autophagy in specific tissues responsible for the development of insulin resistance and β-cell dysfunction?

What are the molecular bases for the alterations in the UPS and autophagy in the context of obesity, insulin resistance, and T2DM? What are the mechanisms by which these alterations impair metabolic health?

Does proteaphagy play a relevant role in the maintenance of energy homeostasis and in metabolic disorders? To answer these questions, we need a thorough understanding of the processes that regulate proteaphagy and the design and implementation of molecular tools to study this process *in vivo*.

Are specific E3 ubiquitin ligases or deubiquitinases involved in the dysregulation of autophagy upon metabolic diseases? If so, it would be pertinent to identify the intracellular signals that activate or inhibit them.

is required in animal models and humans to fully elucidate tissue-specific alterations in these two processes (see Outstanding questions). There is accumulating evidence that the modulation of these degradation pathways have beneficial effects on metabolism. Therefore, it is reasonable to put forward the UPS and autophagy as promising targets to improve the metabolic profile of obese and T2DM patients.

The UPS and autophagy share molecular players and regulate each other in a timely manner. On one hand, autophagy can regulate the UPS through proteaphagy, which can be activated under certain stress conditions, including starvation and proteasome inhibition. On the other hand, the UPS can regulate autophagy dynamics through the action of E3s and DUBs. The molecular aspects of the interplay between the UPS and autophagy are still far from being fully understood. Moreover, the physiological relevance of this inter-regulation has yet to be investigated (see Outstanding questions) and it will be key to analyze whether the interplay between the UPS and autophagy is essential to maintain metabolic homeostasis.

Recent data suggest that mitochondrial dysfunction contributes to the alterations in the UPS and autophagy in tissues under insulin resistance. We propose that impaired proteostasis due to alterations in the UPS and autophagy exacerbates mitochondrial dysfunction and ER stress, ultimately resulting in β-cell failure and promoting the transition from insulin resistance to T2DM. In this regard, it would be relevant to study whether alterations in the UPS and autophagy occur in the natural course of T2DM development.

Acknowledgments

Due to space constraints, we have not included all relevant references in this growing field, so we kindly ask readers for their understanding and apologize to authors. This study was supported by research grants from MINECO and MICINN (SAF2016-75246R and PID2019-106209RB-I00, respectively), the Generalitat de Catalunya (Grant 2017SGR1015), CIBERDEM ('Instituto de Salud Carlos III'), the Fundación Ramon Areces (CIVP18A3942), the Fundación BBVA, the Fundació Marató de TV3 (20132330), and EFSD. J.L.S-W. is a recipient of an FPU PhD fellowship (FPU18/00340) from the 'Ministerio de Universidades', Spain. A.Y-G is a recipient of a fellowship within the Marie Sklodowska-Curie Innovative Training Network 'TrainCDKis' under the Marie Sklodowska-Curie grant agreement No 860977. A.Z. is a recipient of an ICREA 'Academia' Award (Generalitat de Catalunya). We gratefully acknowledge institutional funding from MINECO through the Centres of Excellence Severo Ochoa Award and from the CERCA Programme of the Generalitat de Catalunya.

Declaration of interests

No interests are declared.

References

1. World Health Organization (2020) *The Top 10 Causes of Death*, WHO
2. Cho, N.H. *et al.* (2018) IDF diabetes atlas: global estimates of diabetes prevalence for 2017 and projections for 2045. *Diabetes Res. Clin. Pract.* 138, 271–281
3. DeFronzo, R.A. *et al.* (2015) Type 2 diabetes mellitus. *Nat. Rev. Dis. Prim.* 1, 1–23
4. Hruby, A. and Hu, F.B. (2015) The epidemiology of obesity: a big picture. *Pharmacoeconomics* 33, 673–689
5. The GBD (2015) Obesity Collaborators (2017) Health effects of overweight and obesity in 195 countries over 25 years. *N. Engl. J. Med.* 377, 13–27
6. Harding, J.L. *et al.* (2019) Global trends in diabetes complications: a review of current evidence. *Diabetologia* 62, 3–16
7. The United Nations General Assembly (2015) *Transforming Our World: The 2030 Agenda for Sustainable Development, United Nations*.
8. Collins, G.A. and Goldberg, A.L. (2017) The logic of the 26S proteasome. *Cell* 169, 792–806
9. Bard, J.A.M. *et al.* (2018) Structure and function of the 26S proteasome. *Annu. Rev. Biochem.* 87, 697–724
10. Bento, C.F. *et al.* (2016) Mammalian autophagy: how does it work? *Annu. Rev. Biochem.* 85, 685–713
11. Schuck, S. (2020) Microautophagy - distinct molecular mechanisms handle cargoes of many sizes. *J. Cell Sci.* 133
12. Kaushik, S. and Cuervo, A.M. (2018) The coming of age of chaperone-mediated autophagy. *Nat. Rev. Mol. Cell Biol.* 19, 365–381
13. Nakatogawa, H. (2020) Mechanisms governing autophagosome biogenesis. *Nat. Rev. Mol. Cell Biol.* 21, 439–458
14. Gatica, D. *et al.* (2018) Cargo recognition and degradation by selective autophagy. *Nat. Cell Biol.* 20, 233–242
15. Cuervo, A.M. *et al.* (1995) Degradation of proteasomes by lysosomes in rat liver. *Eur. J. Biochem.* 227, 792–800
16. Cohen-Kaplan, V. *et al.* (2016) p62- and ubiquitin-dependent stress-induced autophagy of the mammalian 26S proteasome. *Proc. Natl. Acad. Sci. U. S. A.* 113, E7490–E7499
17. Marshall, R.S. *et al.* (2016) Autophagic turnover of inactive 26S proteasomes in yeast is directed by the ubiquitin receptor Cue5 and the Hsp42 chaperone. *Cell Rep.* 16, 1717–1732

18. Marshall, R.S. *et al.* (2015) Autophagic degradation of the 26S proteasome is mediated by the dual ATG8/ubiquitin receptor RPN10 in *Arabidopsis*. *Mol. Cell* 58, 1053–1066
19. Choi, W.H. *et al.* (2020) Aggresomal sequestration and STUB1-mediated ubiquitylation during mammalian proteaphagy of inhibited proteasomes. *Proc. Natl. Acad. Sci. U. S. A.* 117, 19190–19200
20. Hashimoto, E. *et al.* (2020) Enhanced O-GlcNAcylation mediates cytoprotection under proteasome impairment by promoting proteasome turnover in cancer cells. *iScience* 23, 101299
21. Goebel, T. *et al.* (2020) Proteaphagy in mammalian cells can function independent of ATG5/ATG7. *Mol. Cell. Proteomics* 19, 1120–1131
22. Sun-Wang, J.L. *et al.* (2020) The dialogue between the ubiquitin-proteasome system and autophagy: implications in ageing. *Aging Res. Rev.* 64, 1–18
23. Yorimitsu, T. *et al.* (2006) Endoplasmic reticulum stress triggers autophagy. *J. Biol. Chem.* 281, 30299–30304
24. Ding, W.X. *et al.* (2007) Linking of autophagy to ubiquitin-proteasome system is important for the regulation of endoplasmic reticulum stress and cell viability. *Am. J. Pathol.* 171, 513–524
25. Li, C. *et al.* (2019) Proteasome inhibition activates autophagy-lysosome pathway associated with TFEB dephosphorylation and nuclear translocation. *Front. Cell Dev. Biol.* 7, 1–8
26. VerPlank, J.J.S. *et al.* (2019) 26S proteasomes are rapidly activated by diverse hormones and physiological states that raise cAMP and cause Rpn6 phosphorylation. *Proc. Natl. Acad. Sci. U. S. A.* 116, 4228–4237
27. Zhao, J. *et al.* (2015) MTOR inhibition activates overall protein degradation by the ubiquitin proteasome system as well as by autophagy. *Proc. Natl. Acad. Sci. U. S. A.* 112, 15790–15797
28. Myeku, N. *et al.* (2016) Tau-driven 26S proteasome impairment and cognitive dysfunction can be prevented early in disease by activating cAMP-PKA signaling. *Nat. Med.* 22, 46–53
29. Kim, J.H. *et al.* (2018) The deubiquitinating enzyme USP20 stabilizes ULK1 and promotes autophagy initiation. *EMBO Rep.* 19, 1–17
30. Raimondi, M. *et al.* (2019) USP1 (ubiquitin specific peptidase 1) targets ULK1 and regulates its cellular compartmentalization and autophagy. *Autophagy* 15, 613–630
31. Chen, Y.-H. *et al.* (2021) VPS34 K29/K48 branched ubiquitination governed by UBE3C and TRABID regulates autophagy, proteostasis and liver metabolism. *Nat. Commun.* 12, 1322
32. Otoda, T. *et al.* (2013) Proteasome dysfunction mediates obesity-induced endoplasmic reticulum stress and insulin resistance in the liver. *Diabetes* 62, 811–824
33. Díaz-Ruiz, A. *et al.* (2015) Proteasome dysfunction associated to oxidative stress and proteotoxicity in adipocytes compromises insulin sensitivity in human obesity. *Antioxid. Redox Signal.* 23, 597–612
34. Shruthi, K. *et al.* (2019) Ubiquitin-proteasome system and ER stress in the brain of diabetic rats. *J. Cell. Biochem.* 120, 5962–5973
35. Shruthi, K. *et al.* (2016) Amelioration of neuronal cell death in a spontaneous obese rat model by dietary restriction through modulation of ubiquitin proteasome system. *J. Nutr. Biochem.* 33, 73–81
36. Guzmán-Flores, M. *et al.* (2016) Comparative Proteomics of Liver of the Diabetic Obese db/db and Non-Obese or Diabetic Mice. *Curr. Proteomics* 13, 231–236
37. Vileigas, D.F. *et al.* (2019) Landscape of heart proteome changes in a diet-induced obesity model. *Sci. Rep.* 9, 1–16
38. Bartelt, A. *et al.* (2018) Brown adipose tissue thermogenic adaptation requires Nrf1-mediated proteasomal activity. *Nat. Med.* 24, 292–303
39. Bollinger, L.M. *et al.* (2015) Skeletal muscle myotubes in severe obesity exhibit altered ubiquitin-proteasome and autophagic/lysosomal proteolytic flux. *Obesity* 23, 1185–1193
40. Kwak, H.J. *et al.* (2016) Bortezomib attenuates palmitic acid-induced ER stress, inflammation and insulin resistance in myotubes via AMPK dependent mechanism. *Cell. Signal.* 28, 788–797
41. Milan, G. *et al.* (2015) Regulation of autophagy and the ubiquitin-proteasome system by the FoxO transcriptional network during muscle atrophy. *Nat. Commun.* 6, 1–14
42. O'Neill, B.T. *et al.* (2016) Insulin and IGF-1 receptors regulate FoxO-mediated signaling in muscle proteostasis. *J. Clin. Invest.* 126, 3433–3446
43. Bodine, S.C. *et al.* (2001) Identification of ubiquitin ligases required for skeletal muscle atrophy. *Science* 294, 1704–1708
44. Guo, R. *et al.* (2017) Adiponectin deficiency rescues high-fat diet-induced hepatic injury, apoptosis and autophagy loss despite persistent steatosis. *Int. J. Obes.* 41, 1403–1412
45. López-Vicario, C. *et al.* (2015) Inhibition of soluble epoxide hydrolase modulates inflammation and autophagy in obese adipose tissue and liver: role for omega-3 epoxides. *Proc. Natl. Acad. Sci. U. S. A.* 112, 536–541
46. Yang, L. *et al.* (2010) Defective hepatic autophagy in obesity promotes ER stress and causes insulin resistance. *Cell Metab.* 11, 467–478
47. Wang, S. *et al.* (2018) ALDH2 protects against high fat diet-induced obesity cardiomyopathy and defective autophagy: role of CaM kinase II, histone H3K9 methyltransferase SUV39H, Sirt1, and PGC-1α deacetylation. *Int. J. Obes.* 42, 1073–1087
48. Møller, A.B. *et al.* (2017) Altered gene expression and repressed markers of autophagy in skeletal muscle of insulin resistant patients with type 2 diabetes. *Sci. Rep.* 7, 1–11
49. Sala, D. *et al.* (2014) Autophagy-regulating TP53INP2 mediates muscle wasting and is repressed in diabetes. *J. Clin. Invest.* 124, 1914–1927
50. Mizunoe, Y. *et al.* (2017) Involvement of lysosomal dysfunction in autophagosome accumulation and early pathologies in adipose tissue of obese mice. *Autophagy* 13, 642–653
51. Ferhat, M. *et al.* (2019) Autophagy in adipose tissue physiology and pathophysiology. *Antioxid. Redox Signal.* 31, 487–501
52. Shpilka, T. *et al.* (2015) Lipid droplets and their component triglycerides and steryl esters regulate autophagosome biogenesis. *EMBO J.* 34, 2117–2131
53. Cai, J. *et al.* (2018) Autophagy ablation in adipocytes induces insulin resistance and reveals roles for lipid peroxide and Nrf2 signaling in adipose-liver crosstalk. *Cell Rep.* 25, 1708–1717
54. Toledo, M. *et al.* (2018) Autophagy regulates the liver clock and glucose metabolism by degrading CRY1. *Cell Metab.* 28, 268–281
55. Singh, R. *et al.* (2009) Autophagy regulates lipid metabolism. *Nature* 458, 1131–1135
56. Romero, M. *et al.* (2018) TP53INP2 regulates adiposity by activating β-catenin through autophagy-dependent sequestration of GSK3β. *Nat. Cell Biol.* 20, 443–454
57. Longo, M. *et al.* (2019) Adipose tissue dysfunction as determinant of obesity-associated metabolic complications. *Int. J. Mol. Sci.* 20, 2358
58. Li, Y. *et al.* (2018) Impaired fasting-induced adaptive lipid droplet biogenesis in liver-specific Atg5-deficient mouse liver is mediated by persistent nuclear factor-like 2 activation. *Am. J. Pathol.* 188, 1833–1846
59. Kim, K.H. *et al.* (2013) Autophagy deficiency leads to protection from obesity and insulin resistance by inducing Fgf21 as a mitokine. *Nat. Med.* 19, 83–92
60. Martínez-Garza, Ú. *et al.* (2019) Fibroblast growth factor 21 and the adaptive response to nutritional challenges. *Int. J. Mol. Sci.* 20, 1–21
61. Fu, T. *et al.* (2018) Mitophagy directs muscle-adipose crosstalk to alleviate dietary obesity. *Cell Rep.* 23, 1357–1372
62. Lim, H. *et al.* (2018) A novel autophagy enhancer as a therapeutic agent against metabolic syndrome and diabetes. *Nat. Commun.* 9, 1438
63. Fan, Y. *et al.* (2017) Identification of natural products with neuronal and metabolic benefits through autophagy induction. *Autophagy* 13, 41–56
64. Xie, Z. *et al.* (2011) Improvement of cardiac functions by chronic metformin treatment is associated with enhanced cardiac autophagy in diabetic OVE26 mice. *Diabetes* 60, 1770–1778
65. Wang, B. *et al.* (2014) Resveratrol-enhanced autophagic flux ameliorates myocardial oxidative stress injury in diabetic mice. *J. Cell. Mol. Med.* 18, 1599–1611

66. Zhang, L. *et al.* (2016) Early administration of trimetazidine attenuates diabetic cardiomyopathy in rats by alleviating fibrosis, reducing apoptosis and enhancing autophagy. *J. Transl. Med.* 14, 1–13
67. Chen, C. *et al.* (2017) Human beta cell mass and function in diabetes: recent advances in knowledge and technologies to understand disease pathogenesis. *Mol. Metab.* 6, 943–957
68. Mukherjee, A. *et al.* (2015) Type 2 diabetes as a protein misfolding disease. *Trends Mol. Med.* 21, 439–449
69. Bhowmick, D.C. and Jeremic, A. (2018) Functional proteasome complex is required for turnover of islet amyloid polypeptide in pancreatic β-cells. *J. Biol. Chem.* 293, 14210–14223
70. Ji, J. *et al.* (2019) Type 2 diabetes is associated with suppression of autophagy and lipid accumulation in β-cells. *J. Cell. Mol. Med.* 23, 2890–2900
71. Liu, H. *et al.* (2017) Intermittent fasting preserves beta-cell mass in obesity-induced diabetes via the autophagy-lysosome pathway. *Autophagy* 13, 1952–1968
72. Shigihara, N. *et al.* (2014) Human IAPP-induced pancreatic β cell toxicity and its regulation by autophagy. *J. Clin. Invest.* 124, 3634–3644
73. Jung, H.S. *et al.* (2008) Loss of autophagy diminishes pancreatic β cell mass and function with resultant hyperglycemia. *Cell Metab.* 8, 318–324
74. Ebato, C. *et al.* (2008) Autophagy is important in islet homeostasis and compensatory increase of beta cell mass in response to high-fat diet. *Cell Metab.* 8, 325–332
75. Sheng, Q. *et al.* (2017) Autophagy protects pancreatic beta cell mass and function in the setting of a high-fat and high-glucose diet. *Sci. Rep.* 7, 1–10
76. Kim, J. *et al.* (2021) An autophagy enhancer ameliorates diabetes of human IAPP-transgenic mice through clearance of amyloidogenic oligomer. *Nat. Commun.* 12, 183
77. Bugliani, M. *et al.* (2019) Modulation of autophagy influences the function and survival of human pancreatic beta cells under endoplasmic reticulum stress conditions and in type 2 diabetes. *Front. Endocrinol. (Lausanne)* 10, 1–10
78. Broca, C. *et al.* (2014) Proteasome dysfunction mediates high glucose-induced apoptosis in rodent beta cells and human islets. *PLoS One* 9, 1–11
79. Press, M. *et al.* (2019) Protein aggregates and proteostasis in aging: amylin and β-cell function. *Mech. Ageing Dev.* 177, 46–54
80. Yamamoto, S. *et al.* (2018) Autophagy differentially regulates insulin production and insulin sensitivity. *Cell Rep.* 23, 3286–3299
81. Huang, C. *et al.* (2019) Kisspeptin-activated autophagy independently suppresses non-glucose-stimulated insulin secretion from pancreatic β-cells. *Sci. Rep.* 9, 1–12
82. Chu, K.Y. *et al.* (2020) Short-term inhibition of autophagy benefits pancreatic β-cells by augmenting ether lipids and peroxisomal function, and by countering depletion of n-3 polyunsaturated fatty acids after fat-feeding. *Mol. Metab.* 40, 101023
83. Tangvarasittichai, S. (2015) Oxidative stress, insulin resistance, dyslipidemia and type 2 diabetes mellitus. *World J. Diabetes* 6, 456
84. Rocha, M. *et al.* (2020) Mitochondria and T2D: role of autophagy, ER stress, and inflammasome. *Trends Endocrinol. Metab.* 31, 725–741
85. Oakes, S.A. and Papa, F.R. (2015) The role of endoplasmic reticulum stress in human pathology. *Annu. Rev. Pathol. Mech. Dis.* 10, 173–194
86. Sebastián, D. *et al.* (2016) Mfn2 deficiency links age-related sarcopenia and impaired autophagy to activation of an adaptive mitophagy pathway. *EMBO J.* 35, 1677–1693
87. Meul, T. *et al.* (2020) Mitochondrial regulation of the 26S proteasome. *Cell Rep.* 32, 108059
88. Muñoz, J.P. *et al.* (2013) Mfn2 modulates the UPR and mitochondrial function via repression of PERK. *EMBO J.* 32, 2348–2361
89. Sebastián, D. *et al.* (2012) Mitofusin 2 (Mfn2) links mitochondrial and endoplasmic reticulum function with insulin signaling and is essential for normal glucose homeostasis. *Proc. Natl. Acad. Sci. U. S. A.* 109, 5523–5528
90. Sulkshane, P. *et al.* (2020) Inhibition of proteasome reveals basal mitochondrial ubiquitination. *J. Proteome* 229, 103949
91. Carnio, S. *et al.* (2014) Autophagy impairment in muscle induces neuromuscular junction degeneration and precocious aging. *Cell Rep.* 8, 1509–1521
92. Aoyagi, K. *et al.* (2016) VAMP7 regulates autophagy to maintain mitochondrial homeostasis and to control insulin secretion in pancreatic β-cells. *Diabetes* 65, 1648–1659
93. Shirakabe, A. *et al.* (2016) Drp1-dependent mitochondrial autophagy plays a protective role against pressure overload-induced mitochondrial dysfunction and heart failure. *Circulation* 133, 1249–1263
94. Hamasaki, H. (2016) Daily physical activity and type 2 diabetes: a review. *World J. Diabetes* 7, 243
95. Barnosky, A.R. *et al.* (2014) Intermittent fasting vs daily calorie restriction for type 2 diabetes prevention: a review of human findings. *Transl. Res.* 164, 302–311
96. He, C. *et al.* (2012) Exercise-induced BCL2-regulated autophagy is required for muscle glucose homeostasis. *Nature* 481, 511–515
97. Schwalm, C. *et al.* (2015) Activation of autophagy in human skeletal muscle is dependent on exercise intensity and AMPK activation. *FASEB J.* 29, 3515–3526
98. Yang, L. *et al.* (2016) Long-term calorie restriction enhances cellular quality-control processes in human skeletal muscle. *Cell Rep.* 14, 422–428
99. Martinez-Lopez, N. *et al.* (2017) System-wide benefits of intermeal fasting by autophagy. *Cell Metab.* 26, 856–871
100. Balaji, V. *et al.* (2018) Ubiquitylation pathways in insulin signaling and organismal homeostasis. *BioEssays* 40, 1–10
101. Song, R. *et al.* (2013) Central role of E3 ubiquitin ligase MG53 in insulin resistance and metabolic disorders. *Nature* 494, 375–379
102. Nagarajan, A. *et al.* (2016) MARCH1 regulates insulin sensitivity by controlling cell surface insulin receptor levels. *Nat. Commun.* 7, 12639
103. Wu, H.K. *et al.* (2019) Glucose-sensitive myokine/cardiokine MG53 regulates systemic insulin response and metabolic homeostasis. *Circulation* 139, 901–914
104. Lee, M.S. *et al.* (2018) Loss of the E3 ubiquitin ligase MKRN1 represses diet-induced metabolic syndrome through AMPK activation. *Nat. Commun.* 9, 3404
105. Liu, B. *et al.* (2019) Sustained ER stress promotes hyperglycemia by increasing glucagon action through the deubiquitinating enzyme USP14. *Proc. Natl. Acad. Sci. U. S. A.* 116, 21732–21738
106. Liu, B. *et al.* (2018) Proteome-wide analysis of USP14 substrates revealed its role in hepatosteatosis via stabilization of FASN. *Nat. Commun.* 9, 1–12
107. Lu, X.Y. *et al.* (2020) Feeding induces cholesterol biosynthesis via the mTORC1–USP20–HMGCR axis. *Nature* 588, 479–484
108. An, S. *et al.* (2017) USP18 protects against hepatic steatosis and insulin resistance through its deubiquitinating activity. *Hepatology* 66, 1866–1884
109. Liu, L. *et al.* (2019) UbiHub: a data hub for the explorers of ubiquitination pathways. *Bioinformatics* 35, 2882–2884
110. Akutsu, M. *et al.* (2016) Ubiquitin chain diversity at a glance. *J. Cell Sci.* 129, 875–880
111. Seibenhener, M.L. *et al.* (2004) Sequestosome 1/p62 is a polyubiquitin chain binding protein involved in ubiquitin proteasome degradation. *Mol. Cell. Biol.* 24, 8055–8068
112. Wurzer, B. *et al.* (2015) Oligomerization of p62 allows for selection of ubiquitinated cargo and isolation membrane during selective autophagy. *eLife* 4, 1–28
113. Lu, K. *et al.* (2017) Receptor oligomerization guides pathway choice between proteasomal and autophagic degradation. *Nat. Cell Biol.* 19, 732–739
114. Nazio, F. *et al.* (2013) MTOR inhibits autophagy by controlling ULK1 ubiquitylation, self-association and function through AMBRA1 and TRAF6. *Nat. Cell Biol.* 15, 406–416
115. Nazio, F. *et al.* (2016) Fine-tuning of ULK1 mRNA and protein levels is required for autophagy oscillation. *J. Cell Biol.* 215, 841–856
116. Liu, C.C. *et al.* (2016) Cul3-KLHL20 ubiquitin ligase governs the turnover of ULK1 and VPS34 complexes to control autophagy termination. *Mol. Cell* 61, 84–97

117. Chu, Y. *et al.* (2020) LUBAC and OTULIN regulate autophagy initiation and maturation by mediating the linear ubiquitination and the stabilization of ATG13. *Autophagy* Published online June 26, 2020. https://doi.org/10.1080/15548627.2020.1781393
118. Shi, C.S. and Kehrl, J.H. (2010) TRAF6 and A20 regulate lysine 63-linked ubiquitination of Beclin-1 to control TLR4-induced autophagy. *Sci. Signal.* 3, 1–10
119. Fusco, C. *et al.* (2018) TRIM50 regulates Beclin 1 proautophagic activity. *Biochim. Biophys. Acta Mol. Cell Res.* 1865, 908–919
120. Xu, C. *et al.* (2014) Regulation of autophagy by E3 ubiquitin ligase RNF216 through BECN1 ubiquitination. *Autophagy* 10, 2239–2250
121. Wan, W. *et al.* (2018) mTORC1-regulated and HUWE1-mediated WIPI2 degradation controls autophagy flux. *Mol. Cell* 72, 303–315
122. Lu, G. *et al.* (2019) Suppression of autophagy during mitosis via CUL4-RING ubiquitin ligases-mediated WIPI2 polyubiquitination and proteasomal degradation. *Autophagy* 15, 1917–1934
123. Feng, Y. *et al.* (2020) Downregulation of autophagy by Met30-mediated Atg9 ubiquitination. *Proc. Natl. Acad. Sci. U. S. A.* 118, e2005539118
124. Scrivo, A. *et al.* (2019) Gigaxonin E3 ligase governs ATG16L1 turnover to control autophagosome production. *Nat. Commun.* 10, 1–14
125. Kuang, E. *et al.* (2012) Regulation of ATG4B stability by RNF5 limits basal levels of autophagy and influences susceptibility to bacterial infection. *PLoS Genet.* 8, e1003007
126. Joachim, J. *et al.* (2017) Centriolar satellites control GABARAP ubiquitination and GABARAP-mediated autophagy. *Curr. Biol.* 27, 2123–2136
127. Peng, H. *et al.* (2017) Ubiquitylation of p62/sequestosome1 activates its autophagy receptor function and controls selective autophagy upon ubiquitin stress. *Cell Res.* 27, 657–674
128. Lin, Q. *et al.* (2017) The HECT E3 ubiquitin ligase NEDD4 interacts with and ubiquitylates SQSTM1 for inclusion body autophagy. *J. Cell Sci.* 130, 3839–3850
129. Feng, X. *et al.* (2019) Ubiquitination of UVRAG by SMURF1 promotes autophagosome maturation and inhibits hepatocellular carcinoma growth. *Autophagy* 15, 1130–1149
130. Johansen, T. and Lamark, T. (2020) Selective autophagy: ATG8 family proteins, LIR motifs and cargo receptors. *J. Mol. Biol.* 432, 80–103
131. Danieli, A. and Martens, S. (2018) P62-mediated phase separation at the intersection of the ubiquitin-proteasome system and autophagy. *J. Cell Sci.* 131, jcs214304
132. Manasanch, E.E. and Orlowski, R.Z. (2017) Proteasome inhibitors in cancer therapy. *Nat. Rev. Clin. Oncol.* 14, 417–433
133. Radhakrishnan, S.K. *et al.* (2010) Transcription factor Nrf1 mediates the proteasome recovery pathway after proteasome inhibition in mammalian cells. *Mol. Cell* 38, 17–28
134. Zientara-Rytter, K. and Subramani, S. (2019) The roles of ubiquitin-binding protein shuttles in the degradative fate of ubiquitinated proteins in the ubiquitin-proteasome system and autophagy. *Cells* 8, 40

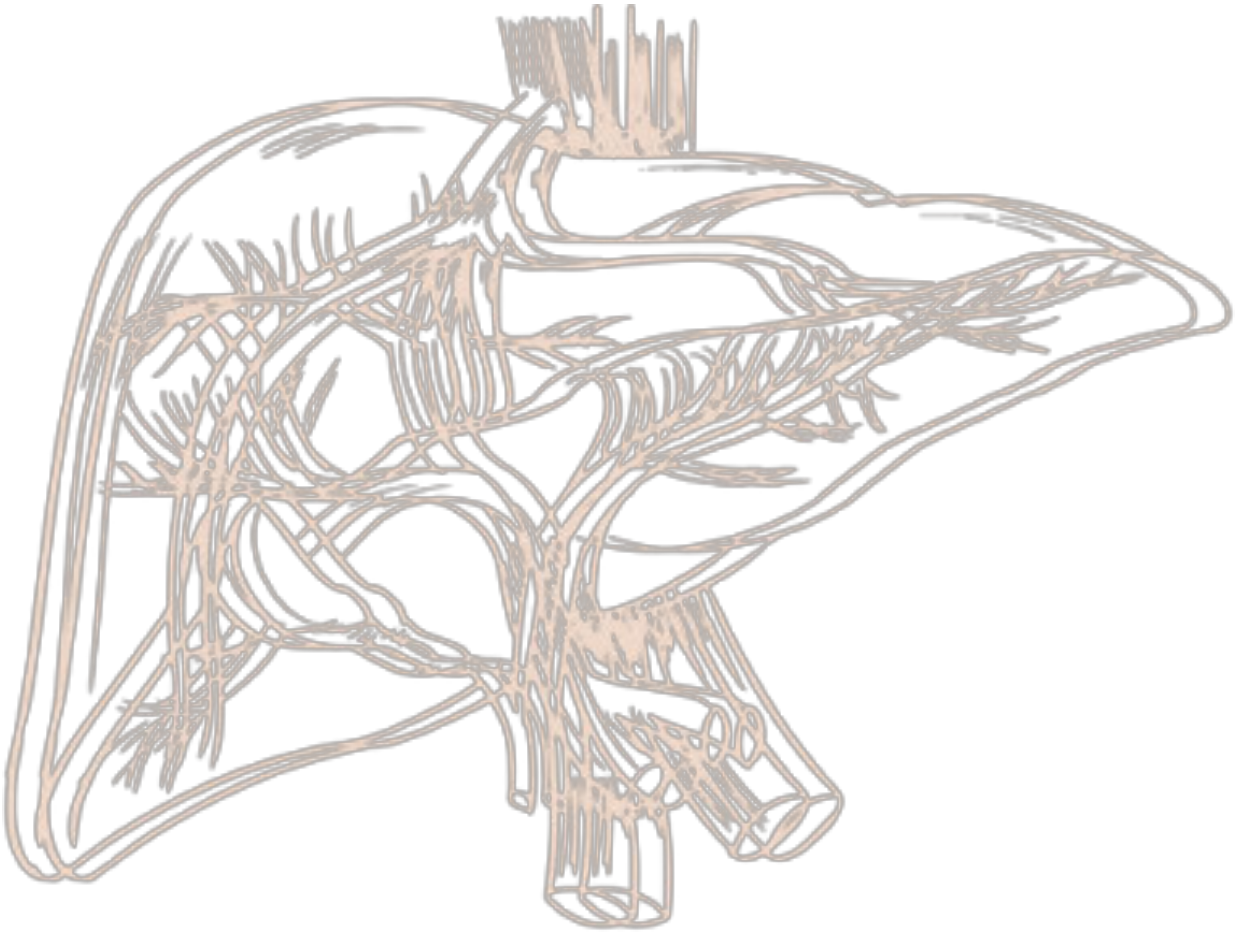

APPENDIX 2

Ageing Research Reviews 64 (2020) 101203

Contents lists available at ScienceDirect

Ageing Research Reviews

journal homepage: www.elsevier.com/locate/arr

Review

The dialogue between the ubiquitin-proteasome system and autophagy: Implications in ageing

Jia Liang Sun-Wang [a,b,c], Saška Ivanova [a,b,c], Antonio Zorzano [a,b,c,*]

[a] Institute for Research in Biomedicine (IRB Barcelona), Barcelona Institute of Science and Technology (BIST), Barcelona, Spain
[b] Departament de Bioquímica i Biomedicina Molecular, Facultat de Biologia, Universitat de Barcelona, Barcelona, Spain
[c] CIBER de Diabetes y Enfermedades Metabólicas Asociadas, Barcelona, Spain

ARTICLE INFO

Keywords:
Proteostasis
Autophagy
Ubiquitin-proteasome system
Ageing
UPS-autophagy crosstalk

ABSTRACT

Dysregulated proteostasis is one of the hallmarks of ageing. Damaged proteins may impair cellular function and their accumulation may lead to tissue dysfunction and disease. This is why protective mechanisms to safeguard the cell proteome have evolved. These mechanisms consist of cellular machineries involved in protein quality control, including regulators of protein translation, folding, trafficking and degradation. In eukaryotic cells, protein degradation occurs via two main pathways: the ubiquitin-proteasome system (UPS) and the autophagy-lysosome pathway. Although distinct pathways, they are not isolated systems and have a complementary nature, as evidenced by recent studies. These findings raise the question of how autophagy and the proteasome crosstalk. In this review we address how the two degradation pathways impact each other, thereby adding a new layer of regulation to protein degradation. We also analyze the implications of the UPS and autophagy in ageing.

1. Introduction

1.1. The ubiquitin-proteasome system

The ubiquitin-proteasome system (UPS) targets the vast majority of cellular proteins (70–80 %) to the proteasome for degradation (Collins and Goldberg, 2017). Proteins that undergo proteasomal degradation are previously ubiquitinated, which consists of the conjugation of one or more ubiquitin molecules to one or multiple lysine residues of the substrate (Akutsu et al., 2016). Ubiquitin conjugation is orchestrated by an enzymatic cascade that contributes to the modulation of the half-lives of substrate proteins, ranging from seconds to days. First, ubiquitin is activated in an ATP-dependent manner by ubiquitin-activating enzymes (E1s), followed by the transfer of the activated ubiquitin to ubiquitin-conjugating enzymes (E2s), thereby forming an E2~ubiquitin complex. Finally, ubiquitin can be transferred to the substrate directly by the E2 (Hoeller et al., 2007) or via ubiquitin ligases (E3s). E3s act as a scaffold by binding to both the substrate and the E2s~ubiquitin complex to facilitate substrate ubiquitination (Pohl and Dikic, 2019). When the E2~ubiquitin—E3—substrate complex is formed, depending on the type of E3, ubiquitin is transferred by the E2 (this is the case for RING E3s, the predominant type of E3s) or by the E3 itself (this is the case for HECT E3s and RING-between-RING E3s) (Morreale et al., 2016). The human genome encodes for at least 2 E1s, 41 E2s and 634 E3s (Liu et al., 2019). E3s provide substrate specificity and this feature explains why cells express hundreds of these enzymes and why they have emerged as novel therapeutic targets for modulating the half-life of disease-causing proteins (Zheng and Shabek, 2017). Ubiquitin can be removed by deubiquitinating enzymes (DUBs), which further regulate the fate and function of substrates by reverting the effects of ubiquitination. In the context of proteasomal degradation, DUBs allow the continuous recycling of ubiquitin (Collins and Goldberg, 2017) (Fig. 1). There are at least 113 DUBs encoded in the human genome (Liu et al., 2019).

The 26S proteasome is a 2.5 MDa multiprotein complex composed of two different subcomplexes, namely the 20S core particle (CP) and the 19S regulatory particle (RP), and it is found in the cytoplasm and nucleus of all eukaryotic cells. The 20S CP, also known as the 20S proteasome, has a barrel-shape structure formed by 7 α-subunits (α_{1-7}) and 7 β-subunits (β_{1-7}) that are arranged in 4 stacked heteroheptameric rings, which in turn form 2 outer α-rings and 2 inner β-rings (Tanaka, 2009; Budenholzer et al., 2017; Rousseau and Bertolotti, 2018) (Fig. 1). The CP is responsible for proteolytic activity, which is attributed to the β-rings, specifically to subunits β_1, β_2 and β_5, each of which exerts distinct proteolytic activity, also known as caspase-like, trypsin-like and

* Corresponding author at: Institute for Research in Biomedicine (IRB Barcelona), Barcelona Institute of Science and Technology (BIST), Barcelona, Spain.
E-mail address: antonio.zorzano@irbbarcelona.org (A. Zorzano).

https://doi.org/10.1016/j.arr.2020.101203
Received 20 July 2020; Received in revised form 9 October 2020; Accepted 25 October 2020
Available online 29 October 2020

chymotrypsin-like activity, respectively (Tanaka, 2009; Budenholzer et al., 2017; Rousseau and Bertolotti, 2018). The 2 outer α-rings serve as a gate to regulate polypeptide access to the proteolytic chamber and as an anchoring platform for the 19S RP (Marshall and Vierstra, 2019). This particle, also known as PA700 (proteasome activator of 700 kDa), is bound to the 20S CP in an ATP-dependent manner (Chu-Ping et al., 1994). It has two components, namely the base and the lid, which control substrate recognition, unfolding and translocation into the catalytic site of the 20S CP through the α-rings (Collins and Goldberg, 2017; Finley, 2009; Bhattacharyya et al., 2014). The base contains a total of 10 subunits, 6 AAA^+-ATPase proteins forming a ring that is in contact with the α-ring of the CP, and 4 non-ATPase proteins, of which 3 are intrinsic ubiquitin receptors. Ubiquitin recognition at the proteasome can also be mediated by external proteins that are not integral subunits of the proteasome, also known as extrinsic ubiquitin receptors or proteasome shuttling factors (Bard et al., 2018). The lid contains 9 non-ATPase subunits, one of which is a deubiquitinase. The 19S RP has the following functions: (i) initial binding of ubiquitinated substrates by the ubiquitin receptors located in the base; and (ii) commitment of the substrate to degradation, which requires ATP hydrolysis, protein unfolding and 20S CP gate opening by the ATPase subunits in the base and substrate deubiquitination (Collins and Goldberg, 2017) by the lid (Fig. 1).

Proteasome composition can be heterogeneous depending on the cellular context and cell type. This diversity stems from the existence of other catalytic subunits and RPs. The catalytic subunits β_1, β_2 and β_5 form the standard 20S proteasome, but can be replaced by subunits β_{1i}, β_{2i} and β_{5i} (Fig. 2) in response to inflammation (IFN-γ), giving rise to the 20S immunoproteasome (Johnston-Carey et al., 2015). The 20S immunoproteasome was initially described in immune cells, where it plays a key role in antigen processing, antigen presentation and T cell biology (Murata et al., 2018). The 19S RP can also be replaced by other regulatory complexes that control substrate entry into the 20S CP to assemble distinct forms of proteasomes (Fig. 2). These regulatory complexes are ATP-independent, in contrast to the 19S, and include the 11S RP (also known as PA28 or REG) and PA200 (also known as PSME4), but their functions have not been as widely characterized as those of the 19S RP (Collins and Goldberg, 2017). PA28 consists of subunits PA28α, PA28β and PA28γ (Cascio, 2014). PA28α and PA28β are inducible by IFN-γ (Cascio, 2014), they form a heteroheptameric ring with an $\alpha_4\beta_3$ stoichiometry (Huber and Groll, 2017), they are implicated in immunity (Murata et al., 2018) and locate mainly to the cytosol (Brooks et al., 2000). In contrast, PA28γ forms a homoheptameric ring and it is not involved in immunity, but it participates in cell cycle regulation (Mao et al., 2008), DNA repair (Levy-barda et al., 2011), male fertility (Huang et al., 2016) and it resides mainly in the nucleus (Brooks et al., 2000). PA200 is also nuclear and has been implicated in DNA repair (Ustrell et al., 2002) and male fertility (Huang et al., 2016). However, the mechanism of action of these alternative RPs are poorly understood. The heterogeneity of proteasome composition is further enriched by the ability of these RPs to form hybrid proteasomes with the 19S RP at one end of the 20S proteasome and with PA28 at the other end (Cascio et al., 2002) (Fig. 2). Of note, there is increasing evidence that the 20S proteasome alone is able to degrade unfolded proteins (Ben-Nissan and Sharon, 2014).

1.2. The autophagy-lysosome pathway

Autophagy is a cytoprotective pathway that delivers cytosolic components (e.g. proteins, organelles) to the lysosomes for degradation

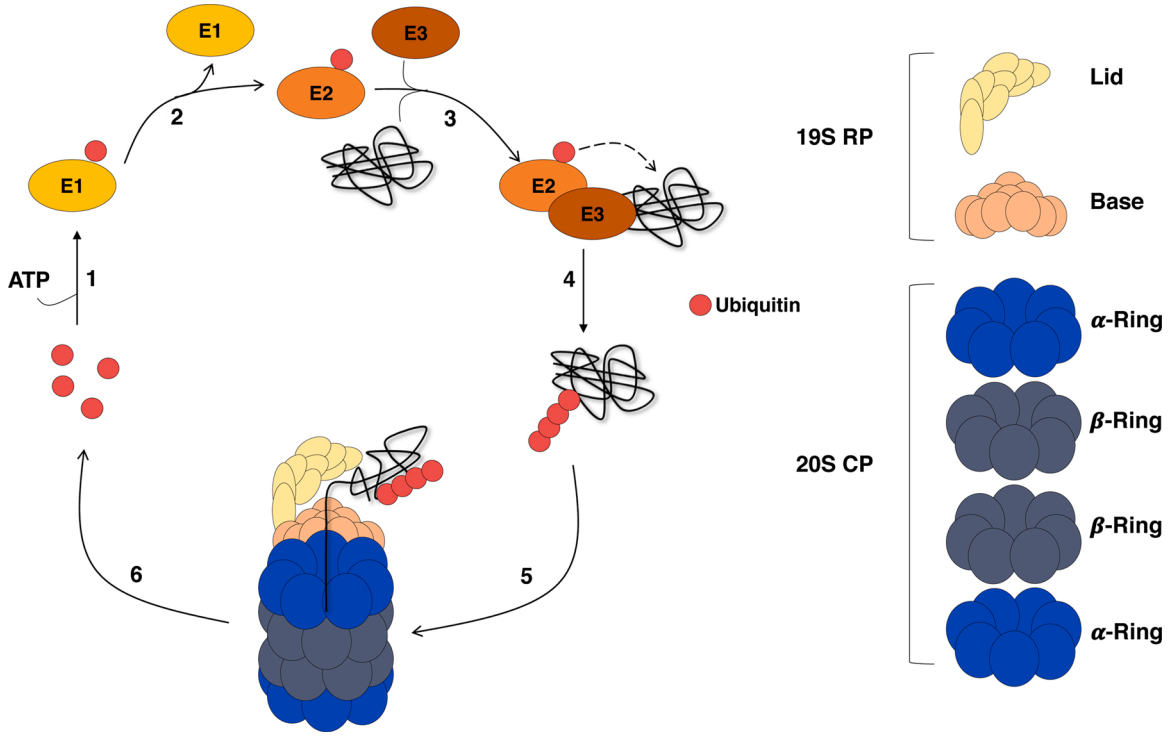

Fig. 1. The ubiquitin-proteasome system.
Degradation through the UPS (left) is initiated by the ATP-dependent activation of ubiquitin (Ub) through an E1 (1). The activated Ub is transferred to an E2 (2). An E3 serves as a docking platform for the substrate protein and the E2-Ub complex to mediate Ub ligation to the substrate (3). The substrate protein acquires multiple ubiquitin moieties attached through ubiquitin conjugation (4). The substrate protein can be recognized by the proteasome itself or can be delivered to it by a shuttle factor such as p62, which recognizes the ubiquitin chains in the substrate via its UBA domain and the proteasome through its PB1 domain (5). The proteolytic activity of the proteasome results in small peptides and the prior deubiquitination by DUBs allows the recycling of Ub (6). Structure of the 26S proteasome (right). The 19S RP is formed by the lid (substrate deubiquitination) and the base (substrate binding and unfolding, and 20S CP gate opening). The 20S CP is formed by α-rings (substrate gating) and β-rings (substrate proteolysis).

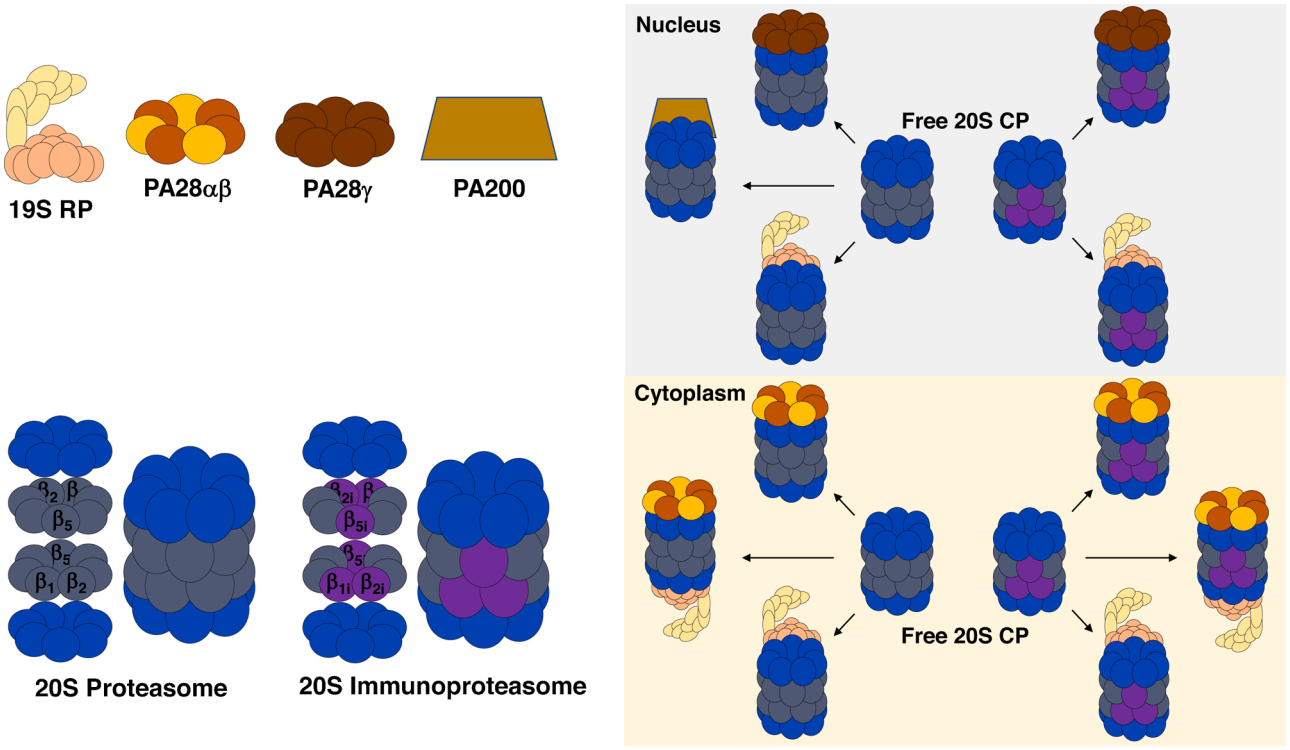

Fig. 2. Heterogeneity of proteasome composition.
Proteasome composition can vary depending on the cellular context and the cell type. This heterogeneity stems from the existence of several RPs, including 19S RP, PA28αβ, PA28γ and PA200 (top-left), and different catalytic subunits that can replace the standard catalytic subunits, resulting in immunoproteasomes (bottom-left). 20S CPs can be present in a free form without RPs or be assembled with RPs in distinct combinations, giving rise a heterogeneous population of proteasomes. For instance, in the nucleus, free 20S CPs can be assembled with PA28γ and PA200, which are involved in DNA repair (top-right). In the cytosol, free 20S CPs can be assembled with the 19S RP to target ubiquitinated proteins, with PA28αβ to target oxidized proteins or with both to form hybrid proteasomes.

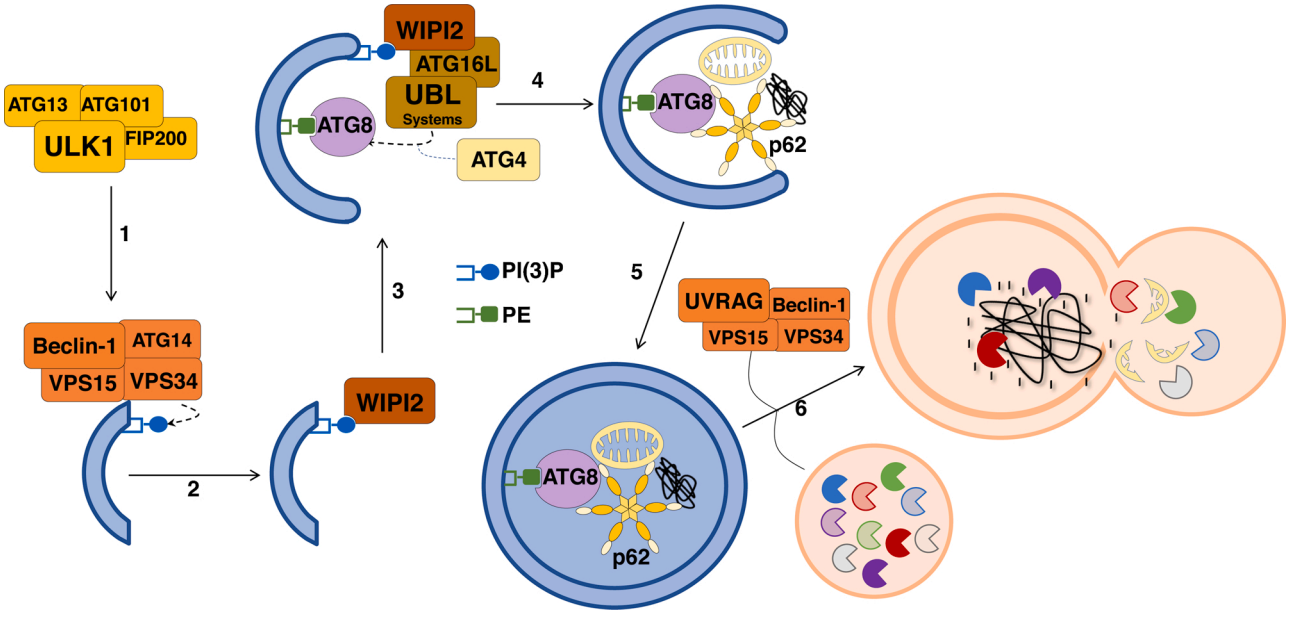

Fig. 3. The autophagy-lysosome pathway.
Degradation through the autophagy-lysosome pathway is initiated by the ULK1 complex, which activates the VPS34 complex (1). The VPS34 complex I catalyses the formation of phosphatidyl-inositol 3-phosphates (PI(3)P) on the membrane of the nascent phagophore, which allows nucleation of the phagophore and recruitment of WIPI2 (2), a PI(3)P effector. WIPI2 recruits the ubl-conjugation systems that promote the conjugation of ATG8 proteins to the membrane of the phagophore (3). The assembly of the autophagic machinery allows elongation of the phagophore (4). p62 in its oligomeric state recognizes protein aggregates and other cellular structures, such as mitochondria, through the UBA domain and recruits them to maturating phagophores via LC3-interaction through the LIR sequence. The phagophore matures into an autophagosome (5), which eventually fuses with the lysosome with the aid of the VPS34 complex II (6), which contains hydrolytic enzymes, resulting in autolysosomes where the engulfed cargo is degraded.

(Galluzzi et al., 2017). Three types of autophagy have been described in mammals: macroautophagy (Bento et al., 2016a), microautophagy (Li et al., 2012) and chaperone-mediated autophagy (Kaushik and Cuervo, 2018). The most widely characterized type of autophagy is macroautophagy (autophagy from here on). Autophagy is initiated by a complex signaling cascade that enables the formation of double-membrane organelles called autophagosomes around the cellular material to be degraded, also known as 'cargo' (Bento et al., 2016b). Cargo is often also ubiquitinated. The initial structure that precedes the autophagosome is called phagophore. The upstream signaling complex in autophagosome biogenesis is the ULK1 complex, formed by the heterotetramer ULK1, ATG13, ATG101 and FIP200 (Fig. 3). This complex plays a central role in autophagy signaling as it is regulated by the mammalian target of rapamycin complex 1 (mTORC1) and the AMP-activated protein kinase (AMPK), both key metabolic sensors (Alers et al., 2012). The ULK1 complex anchors at autophagosome assembly sites, where it recruits, phosphorylates and activates the class III phosphoinositide 3-kinase (PI3K) complex I (also known as VPS34 complex) (Russell et al., 2013)— composed of Vps34 (also known as the catalytic subunit), Vps15 (also known as the regulatory subunit), Beclin-1 and ATG14. This complex generates phosphatidylinositol 3-phosphates (PI3Ps) at phagophores (Seglen and Gordon, 1982) for the anchoring of the ATG2-WIPI complex, a PI3P effector that allows the recruitment of downstream machinery (Bento et al., 2016a) (Fig. 3).

Downstream of ATG2-WIPI are the ubiquitin-like (UBL) conjugation systems. As their name indicates, these systems resemble ubiquitin conjugation systems and they consist of a UBL protein, an E1-like enzyme, an E2-like enzyme and an E3-like enzyme (Geng and Klionsky, 2008). The autophagic machinery contains two UBL-conjugation systems with shared factors: ATG12 and ATG8 are UBL proteins, ATG7 acts as an E1-like enzyme, ATG10 and ATG3 as E2-like enzymes and the conjugated ATG12-ATG5-ATG16 L complex as an E3-like enzyme. In the first conjugation system, ATG12 is conjugated to ATG5 through ATG7 and ATG10 and subsequently binds to ATG16 L to form an E3-like enzyme complex. In the second conjugation system, ATG8 is processed by the cysteine protease ATG4 (Tanida et al., 2004) and conjugated to phosphatidylethanolamine (PE) moieties present in nascent autophagosomes through ATG7, ATG3 and the ATG12-ATG5-ATG16 L complex (Geng and Klionsky, 2008; Nakatogawa, 2013) (Fig. 3). Conjugated ATG8 to PE is referred to as ATG8-II and serves many functions: (i) further recruitment of upstream factors, generating a positive feedback loop, (ii) elongation and closure of nascent autophagosomes, (iii) cargo recruitment and (iv) fusion of autophagosomes with lysosomes (Martens and Fracchiolla, 2020). Mammalian cells express 6 distinct ATG8 homolog proteins, of which the most widely studied is LC3B (Johansen and Lamark, 2020). In this regard, LC3B-II serves as a bonafide autophagosome marker (Klionsky et al., 2016).

Autophagosomes recruit cargo through a variety of adaptor proteins, also known as autophagic adaptors or receptors, such as p62 (Gatica et al., 2018). These adaptors recognize both the cargo, through ubiquitin-associated (UBA) domains and ATG8 proteins in the autophagosome membrane via LC3-interacting regions (LIR) (Johansen and Lamark, 2020) (Fig. 3). Once the cargo has been engulfed, autophagosomes fuse with lysosomes, forming autolysosomes, where the cargo and autophagosomes themselves are degraded into recyclable building blocks (Fig. 3). Autophagosome-lysosome fusion requires several factors, including membrane tethering factors (Nakamura and Yoshimori, 2017) and the class III PI3K complex II, formed by Vps34, Vps15, Beclin-1 and UVRAG (UV radiation resistance-associated gene). In this regard, UVRAG promotes fusion events by activating Vps34 (Liang et al., 2008), but this function is antagonized by the interaction between UVRAG and RUBCN (Sun et al., 2011) (rubicon). Additionally, mTORC1 phosphorylates UVRAG to enhance the interaction with RUBCN under nutrient-rich conditions (Kim et al., 2015) — an interesting observation that links mTORC1 to autophagy initiation and maturation. Autophagosomes can engulf random cellular material in a process termed bulk autophagy, or they can be highly selective depending on the cellular context. In the context of proteostasis, autophagy is upregulated upon proteotoxic stress to target protein aggregates (Lim et al., 2015), which are also conjugated with ubiquitin moieties, similarly to the UPS. The degradation of protein aggregates through autophagy is also known as aggrephagy (Stolz et al., 2014).

1.3. Ubiquitin and p62 function in UPS and autophagy

Despite being different degradation mechanisms, the UPS and autophagy share some molecular players, ubiquitin being one of the most common. Ubiquitin is a small regulatory protein (8.6 kDa) that is *ubiquitously* expressed in eukaryotic organisms and is essential for protein ubiquitination. The incorporation of ubiquitin to target proteins can occur at one or multiple lysine (K) residues, where either a single ubiquitin molecule (mono- and multi-monoubiquitination, respectively) or ubiquitin polymers (polyubiquitination) are added. Ubiquitin chains or polymers can be generated through the consecutive attachment of ubiquitin molecules to the N-terminus (Met1), to a lysine residue of the substrate, or to a lysine residue of the previous ubiquitin (Lys6, Lys11, Lys27, Lys29, Lys33, Lys48, Lys63), thus offering many possibilities to assemble homotypic (ubiquitin chains that contain a single linkage type) or heterotypic conjugates (ubiquitin chains that contain mixed linkages) and therefore providing a wide range of regulatory signals. The cellular outcomes of ubiquitination depend not only on chain topology but also on other factors, such as the timing and reversibility of the reaction, or enzyme and substrate localization, thus adding a layer of complexity to the ubiquitin code (Akutsu et al., 2016).

Cellular functions of the ubiquitin code can be classified into proteolytic and non-proteolytic. The former refers to the ability of ubiquitin to modulate the degradation rate of proteins through the UPS or the autophagy-lysosome pathway, while processes such as the regulation of protein interactions, activity or localization fall into the category of non-proteolytic functions, which have been extensively reviewed elsewhere (Chen and Sun, 2009; Komander and Rape, 2012). The main ubiquitin polymers that contribute to the regulation of proteasomal degradation are Lys48-linked chains, as their levels increase rapidly upon proteasome blockade (Peng et al., 2003; Xu et al., 2009; Kaiser et al., 2011; Kim et al., 2011). In addition, the presence of Lys11 linkages in heterotypic ubiquitin conjugates constitutes a strong proteasomal degradation signal (Meyer and Rape, 2014; Grice et al., 2015). In contrast, Lys63-linked chains are involved in the lysosomal degradation of membrane proteins (Huang et al., 2006; Mukhopadhyay and Riezman, 2007) and degradation of protein aggregates through autophagy, as autophagic receptors bind to Lys63-linked chains with higher preference (Kirkin et al., 2009).

Another molecular player shared by the two degradation systems is the p62/SQSTM1 protein. p62 is a multifunctional stress-inducible scaffold protein involved in many cellular processes, for example, it serves as a receptor for autophagy and as a signaling hub for mTORC1 activation (Sánchez-Martın and Komatsu, 2018; Sánchez-Martín et al., 2019). In the context of protein degradation, p62 is a well-characterized ubiquitin receptor, and it contains an UBA domain (Kirkin et al., 2009). It is also able to interact with the proteasome via its Phox and Bem1p (PB1) domain (Seibenhener et al., 2004) and with ATG8 autophagy proteins via its LIR domain (Pankiv et al., 2007). Proteomic studies have not found evidence for the binding of p62 to proteasomes under basal conditions, although p62 association with the proteasome was robustly detected under proteasome inhibition conditions (Choi et al., 2020).

The ability of p62 to interact with key elements from both systems, together with its ability to oligomerize (Wurzer et al., 2015), allows it to escort ubiquitinated proteins to the proteasome as a shuttle factor (Seibenhener et al., 2004) or to autophagosomes as an autophagy receptor. The question as to how p62 "decides" which pathway to deliver ubiquitinated substrates to remains to be fully elucidated. However, recent findings indicate that pathway selection may depend on the

oligomeric state of the receptor (Lu et al., 2017). When p62 adopts an oligomeric or filamentous state, K48-linked ubiquitin chains are less efficiently bound to the complex than K63-linked chains. However, K48-linked chains disrupt p62 oligomers more effectively (Wurzer et al., 2015), thereby suggesting that an oligomeric state favors autophagy while a non-oligomeric state is involved in proteasomal degradation. Oligomerization of p62 can be induced by proteotoxic stress, i.e. accumulation of protein aggregates, as observed upon proteasome inhibition (Peng et al., 2017). The involvement of p62 in the crosstalk between the UPS and autophagy raises the question as to whether other autophagic receptors also participate. Such participation would highly depend on the molecular and biochemical characteristics of the receptors, that is to say, whether they can interact with the proteasome.

Ubiquitin and p62 serve as the bridge between the UPS and autophagy (Fig. 4) and, together with other factors, they coordinate a functional crosstalk between the two systems, which is important for cell adaptation to environmental cues. Alterations in the ubiquitin-proteasome system or in autophagy contribute to the pathogenesis of several human diseases, such as cancer and neurodegenerative disorders (e.g. Parkinson disease and Alzheimer's disease) (Rousseau and Bertolotti, 2018; Yang and Klionsky, 2020).

2. Regulation of autophagy by the UPS

2.1. Autophagy upregulation by a deficient UPS

Accumulating evidence indicates that autophagy is upregulated under conditions of deficient degradation of ubiquitinated proteins by the UPS, such as upon proteasome inhibition by bortezomib, epoxomicin and MG-132, among others. These compounds have been widely used for research purposes and some of them as anti-cancer agents (Manasanch and Orlowski, 2017). For instance, inhibition of the proteasome by MG-132 induced autophagy in colon cancer cells (Wu et al., 2008) and rat alveolar macrophages (Fan et al., 2018). In addition, the proteasome inhibitor bortezomib increased autophagy in HeLa cells (Laussmann et al., 2011), melanoma cell lines (Selimovic et al., 2013), human prostate cancer cells (Zhu et al., 2010), immortalized mouse embryonic cells (Zhu et al., 2010) (MEFs) and human breast cancer cell lines (Milani et al., 2009). Proteasome impairment induced by genetic manipulation, e.g. genetic ablation of proteasomal subunits, also activated autophagy (Zhu et al., 2010; Pandey et al., 2007). Moreover, in an in vivo fly model of the neurodegenerative disease spinobulbar muscular atrophy, characterized by UPS impairment and the accumulation of ubiquitin-positive protein aggregates, autophagy is upregulated to compensate deficient UPS degradation (Pandey et al., 2007). All these studies reported enhanced autophagy by monitoring increased expression of autophagy genes, increased LC3B-II protein levels under basal conditions and increased formation of LC3-positive puncta also under basal conditions. However, none of these studies performed autophagy flux assessment, the gold standard assay to measure autophagic activity (Klionsky et al., 2016).

The molecular mechanisms underlying this cellular compensation are not fully understood. It has been proposed that the unfolded protein response (UPR), a protein quality control mechanism that is activated in the ER upon a variety of stressors (Hetz et al., 2015), provides a link between UPS impairment and autophagy upregulation. In multiple myeloma cells, proteasome inhibition causes the accumulation of misfolded proteins in the ER lumen, thus activating the UPR (Obeng et al., 2006) and its three signaling branches: PERK, IRE1α and ATF6, which have been reviewed elsewhere (Hetz et al., 2015). However, another study using multiple myeloma cells reported that proteasome inhibition promoted the disruption of the UPR rather than its activation (Lee et al., 2003). Along these lines, bortezomib enhanced the formation of autophagosomes as seen through electron microscopy, as well as the transcription of autophagy-related genes (ATG) through the activation of the PERK-eIF2α-ATF4 axis in human prostate cancer cells (Zhu et al., 2010) and the activation of the IRE1α-ASK1-JNK1 axis in melanoma cells (Selimovic et al., 2013). In melanoma cells, the upregulation of autophagy was associated with apoptosis, but whether increased cell death was dependent on autophagy was not assessed (Selimovic et al., 2013). In contrast, in other cancer cell lines, bortezomib was found to enhance cell death by blocking autophagy (Kao et al., 2014).

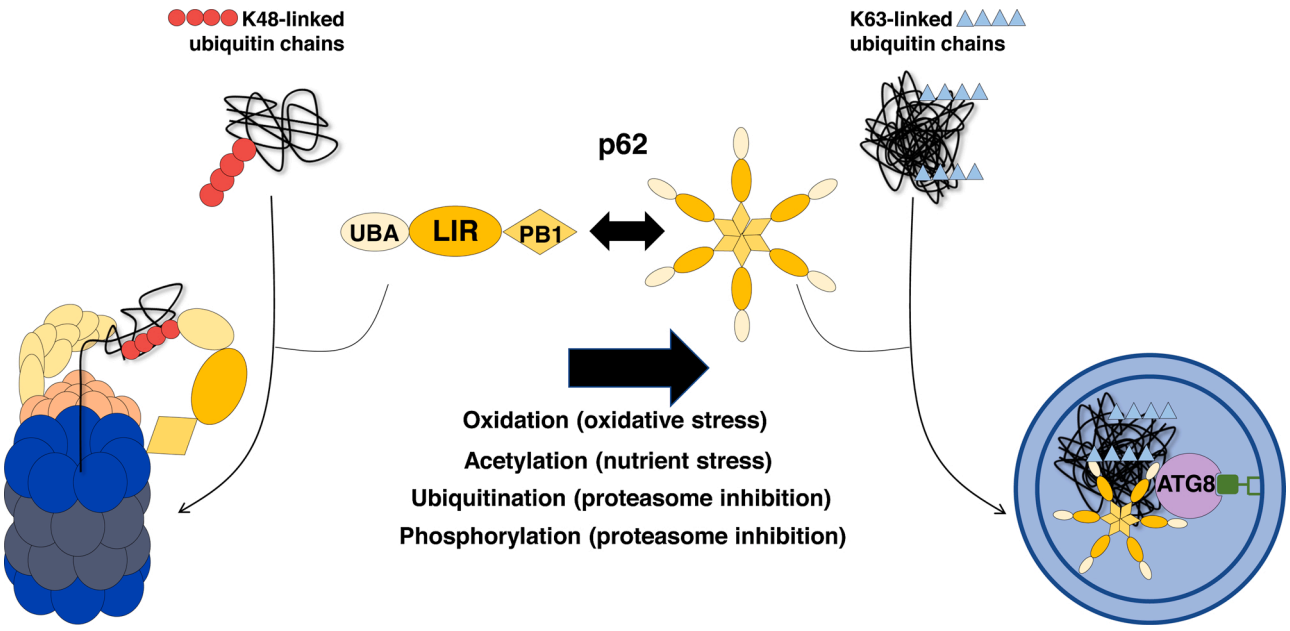

Fig. 4. Overview of UPS and autophagy crosstalk.
Ubiquitin and p62 are central players in the communication between the two protein quality control systems. On one hand, the proteasome degrades single proteins in a one-by-one fashion. On the other hand, autophagy can target clusters of proteins that may even be aggregated. For proteasomal degradation, substrates are usually tagged with K48-linked ubiquitin chains, whereas for autophagy-lysosome degradation, K63-linked ubiquitin chains are usually utilized. In its monomeric form, p62, a triple ubiquitin- proteasome-autophagy receptor, can act as a shuttle, bringing protein substrates to the proteasome to facilitate their degradation. Additionally, upon oligomerization, which can occur under certain cellular contexts, p62 can serve as an autophagy receptor to recruit cargo into autophagosomes.

The transcription factor EB (TFEB), a master regulator of lysosome biogenesis and autophagy (Napolitano and Ballabio, 2016), also participates in the upregulation of autophagy upon proteasome inhibition. TFEB coordinates the transcription of genes involved in the autophagy-lysosome pathway in response to environmental cues and it is degraded by the UPS (Sha et al., 2017). Under nutrient-rich conditions, TFEB activity is limited due to mTORC1-mediated phosphorylation (Napolitano and Ballabio, 2016). Upon starvation, phosphorylated TFEB is ubiquitinated by STUB1 (Sha et al., 2017) and degraded by the proteasome to increase the pool of non-phosphorylated TFEB, which can homodimerize to become transcriptionally active and activate autophagy, as STUB1 deletion in MEFs reduced the expression of ATG genes as well as the formation of LC3 positive puncta (Sha et al., 2017). A recent report showed that MG-132-induced proteasome inhibition enhanced the levels of TFEB and facilitated its nuclear translocation, thereby increasing the expression of genes related to the autophagy-lysosome pathway, such as LC3 and LAMP1 in neuroblastoma and HEK 293 cells (Li et al., 2019). An interesting study links TFEB to ER stress (Martina et al., 2016). Along this line, ER stressors cause TFEB translocation to the nucleus in a PERK-dependent and mTORC1-independent manner in MEF and ARPE-19 (human retinal pigment epithelium) cells, thus upregulating the transcription of other UPR genes like ATF6 (Martina et al., 2016). This observation may integrate TFEB and the UPR into the proteasome inhibition response to enhance autophagy (Fig. 5).

The transcription factors Nrf1 (also named NFE2L1, nuclear factor erythroid-2-like 1) and Nrf2 (NFE2L2, nuclear factor erythroid-2-like 2), members of the cap'n'collar basic leucine zipper (CnC-bZip) family of transcription factors and master regulators of the anti-oxidative stress response, are important in the compensation mechanism (Fig. 5). Whereas immature Nrf1 is a glycoprotein embedded in the ER, Nrf2 resides in the cytoplasm. It has been documented that Nrf1 mediates the rapid induction of GABARAPL1 and p62 expression upon proteasome inhibition in several human cell lines (Sha et al., 2018), a key event to isolate non-degraded proteins into insoluble aggregates and to deliver them to autophagosomes for lysosomal clearance. ER-bound Nrf1 is cleaved by the protease DDI2 (Koizumi et al., 2016) (DNA-damage inducible 1 homolog 2) upon proteasome dysfunction. Interestingly, Nrf1 activation not only upregulates p62 levels but also the expression of proteasome subunits, to mediate the proteasome recovery pathway, also known as the proteasome "bounce-back" mechanism (Radhakrishnan et al., 2010). Similarly, Nrf2 is also a dual activator of the expression of autophagy genes (Pajares et al., 2016), including p62, and proteasome genes (Kwak et al., 2003). Upon proteasome dysfunction, Nrf2 has been reported to activate autophagy in mouse liver as seen by increased formation of p62 positive puncta, increased p62 phosphorylation and increased p62 degradation (Kageyama et al., 2014), and the proteasome bounce-back mechanism in fruit flies (Tsakiri et al., 2013a). Interestingly, Nrf2 is a proteasome substrate. Under normal conditions, Nrf2 is bound to Keap1, which serves as a substrate adaptor for the E3 ubiquitin ligase Cul3, which in turn ubiquitinates Nrf2 to promote its proteasomal degradation, thus limiting its activity (McMahon et al., 2003). Therefore, Nrf2 protein levels may increase upon proteasome deficiency and enhance its transcriptional activity. Furthermore, Nrf2 has been reported to be phosphorylated by PERK in MEF cells upon glucose deprivation (Cullinan and Diehl, 2004), one of the branches of the UPR, and it may be activated by ER stress. Nonetheless, it remains uncertain whether Nrf2 activation upon proteasome inhibition is dependent on the UPR.

As mentioned before p62 is a key player in the crosstalk between the UPS and autophagy, as it is a receptor shared by both systems. Under conditions in which the proteasome is inhibited, the main ubiquitin chains that accumulate are the K48-linked chains (Komander and Rape, 2012). These bind less efficiently to oligomeric p62 and disrupt its oligomerization more effectively (Wurzer et al., 2015). This observation suggests that proteins that are accumulated/aggregated upon proteasome blockade need further modification by E3s, such as the addition of K63-linked chains, which preferentially bind to oligomeric p62.

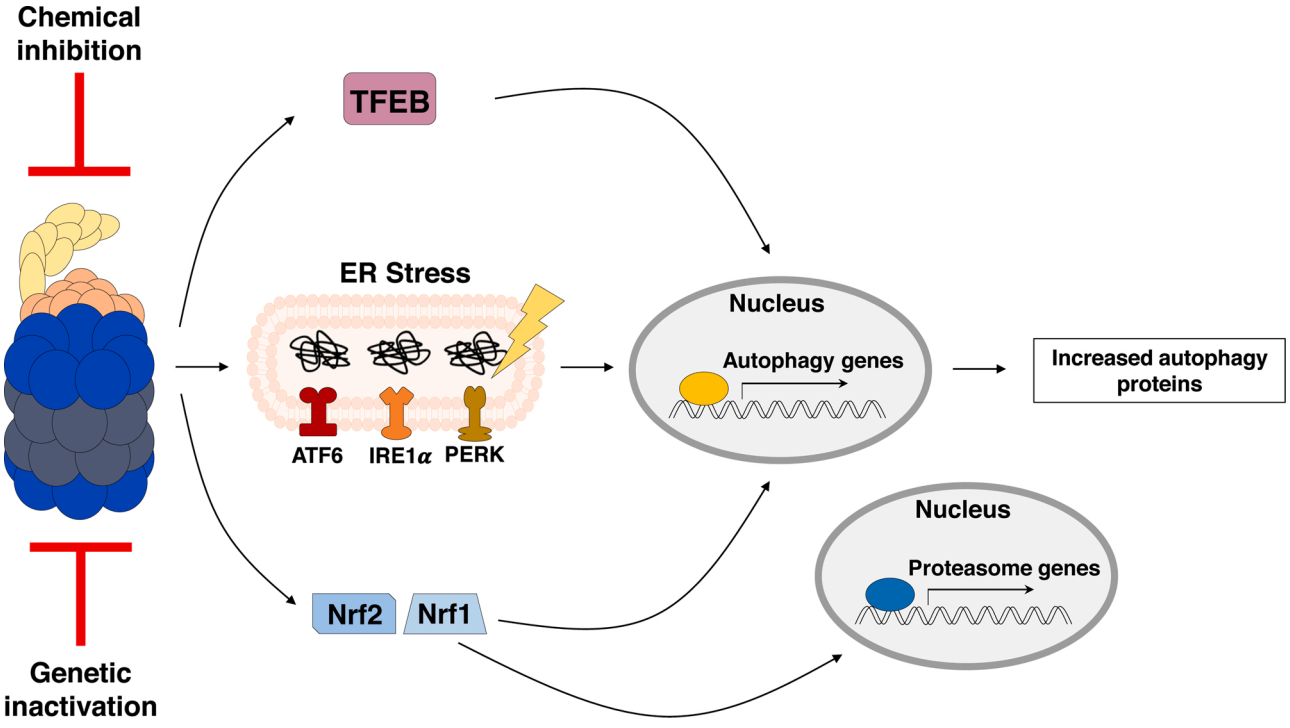

Fig. 5. UPS deficiency leads to autophagy upregulation through the integration of several signals.
ER stress can be triggered upon proteasome deficiency, leading to the activation of the UPR and the consequent transcription of ATG genes. Nrf1/2 and TFEB may accumulate due to proteasome inhibition, contributing to the expression of ATG genes and to the overall upregulation of autophagy. Nrf1/2 accumulation may also activate the proteasome recovery pathway.

Interestingly, p62 oligomerizes through its PB1 domain, which also recognizes the proteasome. Therefore, p62 oligomerization may also favor autophagy by abolishing the interaction with proteasomes, though further affinity and binding studies are required. In addition, blocking proteasomal degradation induced p62 phosphorylation by several protein kinases Thus promoting upregulation of aggrephagy (Lim et al., 2015; Matsumoto et al., 2011).

2.2. Autophagy regulation by E3 ubiquitin ligases

Ubiquitination of the core autophagic machinery is an important regulatory mechanism. It affects all the steps involved in autophagosome formation and maturation, from the initial upstream signaling by the ULK1 complex to autophagosome-lysosome fusion, thus ensuring a tight control under different cellular contexts (Grumati and Dikic, 2018; Chen et al., 2019). E3s are key players in the UPS as they are essential for substrate ubiquitination and, more importantly, they provide substrate specificity. Therefore, we consider important to describe the regulation of autophagy by E3 ubiquitin ligases, although it does not necessarily constitute a mechanism of crosstalk between the two degradation pathways.

2.2.1. Autophagy initiation

ULK1 and VPS34 are the major components that drive autophagy initiation and autophagosome formation. Both complexes are regulated via phosphorylation and ubiquitination. ULK1 is ubiquitinated by a variety of E3s (Zachari and Ganley, 2017), such as the TNF receptor-associated factor 6 (TRAF6). TRAF6 adds K63-linked ubiquitin chains to ULK1 to enhance its stability, thus increasing its activity (Fig. 6). However, the recruitment of TRAF6 to ULK1 requires the cofactor AMBRA1, a binding partner of the VPS34 complex (Nazio et al., 2013), in a mechanism that is dependent on mTOR inhibition. Additionally, activated ULK1 phosphorylates AMBRA1, initiating a positive feedback loop and promoting AMBRA1 autophagy functions, i.e. activation of the VPS34 complex. ULK1 is also ubiquitinated by the NEDD4-like E3 ubiquitin ligase (NEDD4L), which, in contrast to TRAF6, induced ULK1 proteasomal degradation upon autophagy progression (Nazio et al., 2016) (Fig. 6). The cullin-3 E3 ligase complex Cul3-KLHL20 also induced ULK1 ubiquitination and subsequent proteasomal degradation (Liu et al., 2016) during prolonged starvation. Taken together, NEDD4L- and Cul3-induced ubiquitination of ULK1 ensures timely regulation of autophagy, thus preventing its overactivation. The mitochondrial E3 MUL1 has also been reported to ubiquitinate ULK1 upon selenite-induced mitophagy (Li et al., 2015) to promote its proteasomal degradation, which could serve to halt mitophagy.

2.2.2. Phagophore nucleation

VPS34 activity is regulated by the ubiquitination of Beclin-1 (Hill et al., 2019). Beclin-1 is a substrate of TRAF6-mediated K63-linked ubiquitination, which activated the VPS34 complex and TLR4-induced autophagy in macrophages (Shi and Kehrl, 2010). The interaction between TRAF6 and Beclin-1 seems to be direct (Shi and Kehrl, 2010). A parallel study showed that K63-linked ubiquitination of Beclin-1 is also driven by AMBRA1 (Xia et al., 2013), although the specific E3 was not elucidated. Based on the data, it may be that the E3 is either TRAF6 or the Cul4-ligase complex, as AMBRA1 is part of the Cul4-ligase complex. TRIM50, another E3, also ubiquitinated Beclin-1 in a K63-dependent manner to enhance its interaction with ULK1 and promote autophagy (Fusco et al., 2018) (Fig. 6). Beclin-1 is negatively regulated through K48-linked chains by the E3 ligase complexes Cul3-KLHL20 (Liu et al., 2016) and RNF216 (Xu et al., 2014), leading to its degradation by the proteasome. The E3 NEDD4 induced Beclin-1 ubiquitination with K11- and K63-linked chains (Platta et al., 2012). Whereas K11-ubiquitination targeted Beclin-1 for proteasomal degradation, K63-linked ubiquitination by NEDD4 was not further examined for its possible role in the regulation of autophagy. The two different ubiquitination patterns could presumably occur in a general context under different cellular conditions; for instance, K63-linked ubiquitination could be more predominant under autophagy-activating conditions, whereas K11-induced proteasomal degradation could be more pronounced under conditions where autophagy is not required or could serve as a termination signal after a long induction of autophagy.

Moreover, PI3P effectors, such as WIPI2, which are downstream of the VPS34 complex, also undergo ubiquitination. The E3 HUWE1 mediates WIPI2 ubiquitination in an mTORC1-dependent fashion (Wan

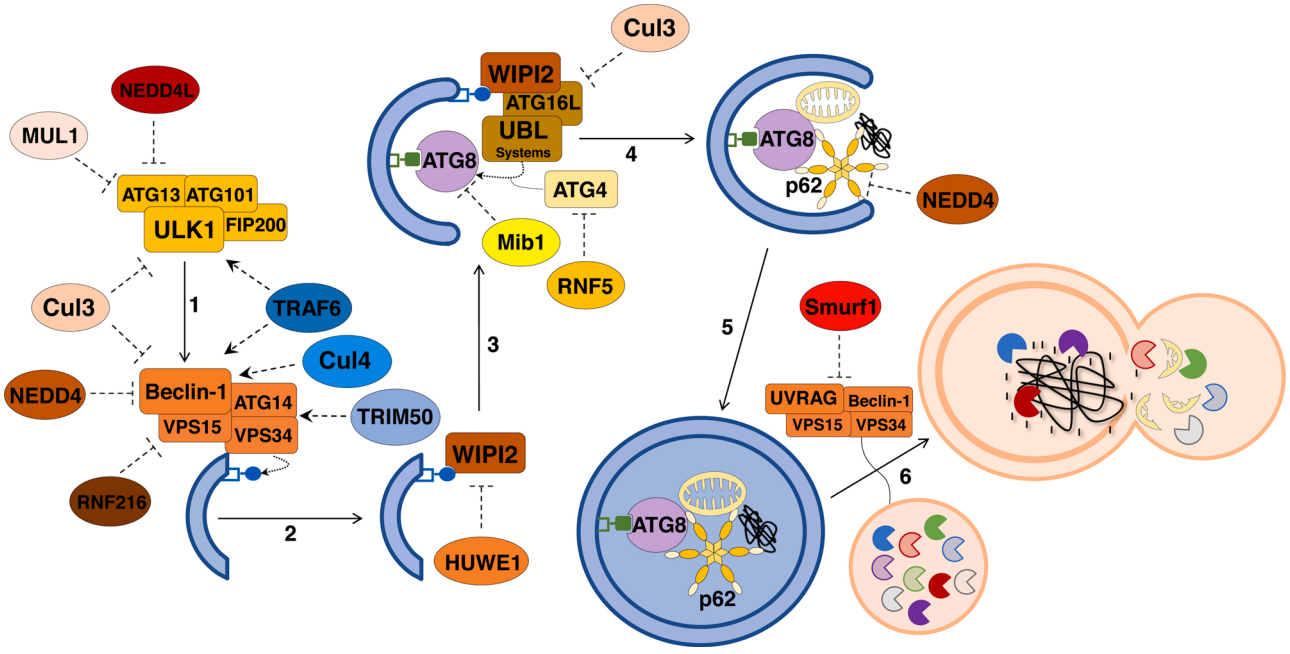

Fig. 6. Overview of autophagy-regulating E3s.
Every step of autophagosome formation and maturation is subjected to ubiquitin regulation. Some E3s negatively regulate autophagy (blunt dashed arrows), whereas others activate autophagy (pointy dashed arrows).

et al., 2018) (Fig. 6). When nutrients are available, mTORC1 is activated and it phosphorylates WIPI2. This step is necessary for the recruitment of HUWE1 to WIPI2 and its subsequent ubiquitination, which promotes WIPI2 degradation via the proteasome, thus keeping autophagy switched off. Also, Cul4-RING E3s marked WIPI2 for proteasomal degradation during mitosis to ensure that autophagy is shut down during cellular division (Lu et al., 2019).

2.2.3. Phagophore elongation and autophagosome maturation

Ubiquitination also modulates the UBL conjugation systems. ATG16 L K48-linked ubiquitination is driven by gigaxonin (Scrivo et al., 2019), a substrate adaptor for Cul3 E3 complexes (Fig. 6), which promoted the degradation of ATG16 L by both the proteasome and autophagy, although K63-linked ubiquitination was not reported. A recent study showed that correct turnover of ATG16 L is necessary for the proper elongation of autophagosomes and the maintenance of basal autophagic flux, as deletion of gigaxonin caused aberrant accumulation of ATG16 L and impaired autophagosome production and autophagy flux (Scrivo et al., 2019). It would be interesting to study whether ATG16 L turnover is also necessary for autophagosome elongation under autophagy-activating conditions.

The cysteine protease ATG4, which cleaves ATG8 to facilitate its lipidation, is a substrate of the E3 RNF5 (Kuang et al., 2012) (Fig. 6). Under basal conditions, RNF5 ubiquitination of ATG4 promoted its proteasomal degradation, thereby limiting autophagy. On the other hand, upon starvation, ATG4-RNF5 interaction was attenuated, preventing ATG4 from being degraded by the proteasome and thus favoring autophagy. The centrosome-residing E3 Mib1 promoted GABARAP (ATG8 family member) proteasomal degradation by adding K48-linked ubiquitin chains. However, during starvation, the centriolar satellite protein PCM1 interacted with GABARAP and prevented Mib1-mediated ubiquitination, thus allowing the recruitment of GABARAP to autophagosomes (Joachim et al., 2017) (Fig. 6). Modulation of GABARAP levels by the proteasome raises the question as to whether other ATG8 proteins, such as LC3B, also undergo E3-mediated proteasomal degradation. In this regard, NEDD4 interacts with LC3B but does not ubiquitinate LC3B. This interaction was required for NEDD4-induced ubiquitination of p62 (Sun et al., 2017) (Fig. 6). It has also been shown that NEDD4 directly interacts with p62 and mediates its ubiquitination to promote aggrephagy (Lin et al., 2017). Several studies further confirmed that ubiquitination of p62 is required for its function as an autophagic receptor (Peng et al., 2017; Lee et al., 2017), but the mechanism remains elusive. To unravel how p62 ubiquitination regulates its function in autophagy, it would be pertinent to study whether modifications by ubiquitin are involved in p62 oligomerization, a process that facilitates cargo recruitment for autophagy degradation (Wurzer et al., 2015). Recently, our laboratory showed that TP53INP2, an autophagic protein that binds to all mammalian ATG8 proteins (Sancho et al., 2012), also interacts with TRAF6 to facilitate caspase-8 K63-linked ubiquitination during death receptor-induced apoptosis (Ivanova et al., 2019). Whether TP53INP2 modulates TRAF6 activity during autophagy and promotes K63-linked ubiquitination of the core autophagic machinery remains to be documented. Furthermore, UVRAG, a component of the class III PI3K complex II, is ubiquitinated by the E3 Smurf1, which incorporates non-canonical K29/K33-linked ubiquitin chains that reduce its binding to RUBCN, thus enhancing autophagy (Feng et al., 2019).

Given all these observations, it appears that K63-linked ubiquitination promotes autophagy, whereas K11- and K48-linked chains target components of the autophagic machinery to proteasomal degradation, thus blocking autophagy (Fig. 6). K63-linked ubiquitination of the autophagic machinery occurs upon autophagy-activating stimuli, such as starvation. It would, therefore, be interesting to study whether ubiquitination also serves as a termination signal by promoting the clearance of the autophagic machinery, thus returning autophagic flux to basal levels. In this regard, K11- and K48-linked ubiquitination may contribute to signaling the termination of autophagy. Interestingly, recent studies show that DUBs deubiquitinate proteins from the core autophagic machinery to promote or inhibit autophagy, depending on the type of ubiquitin linkage chains that they remove. For instance, ULK1 K63-linked ubiquitination by TRAF6 can be reverted by the DUB USP1 to prevent autophagy (Raimondi et al., 2019); and its proteasomal degradation signal can be antagonized by USP20 (Kim et al., 2018). In short, the coordinated action of E3s and DUBs contributes to the regulation of autophagy dynamics.

The molecular signals that stimulate E3s to activate or inhibit autophagy under certain conditions remain largely unknown. Some E3s are subjected to tight regulation by post-translational modifications in order to avoid unwanted protein ubiquitination, such as phosphorylation (Zheng and Shabek, 2017; Song and Luo, 2019). Therefore, it is not unreasonable to speculate that E3s that enhance autophagy may be activated by phosphorylation events or lack thereof upon autophagy-activating stimuli, e.g. lack of mTORC1 phosphorylation or phosphorylation by AMPK, and the contrary for autophagy-inhibiting E3s. To shed light on this, a comprehensive study of post-translational modifications of E3s involved in autophagy regulation should be conducted under autophagy-activating and -inhibiting conditions.

3. Regulation of the UPS by autophagy

Degradation of the proteasome by autophagy was first indicated in in vivo studies showing the accumulation of proteasomes in rat liver lysosomes (Cuervo et al., 1995). It was not until two decades later that proteasome subunits were found to accumulate in plant cells with mutations in ATG genes (Marshall et al., 2015). The same study revealed that, upon nitrogen starvation, 26S proteasomes co-localized with ATG8-marked autophagosomes, thereby indicating that 26S proteasomes can indeed be degraded through the autophagy-lysosome pathway, in a process termed proteaphagy (Marshall et al., 2015). Further analysis showed that chemical inhibition or genetic disruption of the proteasome stimulates ubiquitination of the 19S RP to promote proteasome autophagic clearance mediated by Rpn10 (also known as Psmd4). Rpn10 is a ubiquitin-proteasome receptor that, under this condition, becomes an autophagy receptor, delivering inactive proteasomes to autophagosomes (Marshall et al., 2015) (Fig. 7). Rpn10 association with the proteasome 19S RP increases upon its ubiquitination and interacts with ATG8 through a ubiquitin-interacting motif (UIM) rather than a LIR domain (Marshall et al., 2015). The role of Rpn10 as an autophagy receptor for the selective recruitment of inactive proteasomes was further confirmed by the observation that inhibitor-induced proteaphagy is blocked in RPN10 mutant plant cells (Marshall et al., 2015). However, Rpn10 and ubiquitination of the 19S RP are not involved in nitrogen starvation-induced proteaphagy. This observation suggests the existence of other autophagy receptors that target proteasomes to autophagosomes under different stress conditions and therefore diverse proteaphagic pathways, similarly to mitochondria, which also undergo distinct mitophagic routes (Youle and Narendra, 2011).

Proteaphagy has also been described in yeast (Waite et al., 2016; Nemec et al., 2017; Marshall et al., 2016; Marshall and Vierstra, 2018) and in mammalian cells (Cohen-Kaplan et al., 2016). In these cells, RPN10 does not interact with ATG8 (Marshall et al., 2016). In yeasts, Cue5 ubiquitin receptor acts as an autophagic receptor for inactive proteasomes (Marshall et al., 2016), however, a receptor for nitrogen starvation-induced proteaphagy remains to be identified (Fig. 7). Yeast proteaphagy required prior aggregation of impaired proteasomes in insoluble protein deposit (IPOD) structures mediated by Hsp42 (Marshall et al., 2016). Proteasome inhibition also induced proteasome ubiquitination in yeast (Marshall et al., 2016), but whether this process occurred before or after proteasome aggregation into IPOD structures remains elusive. Other yeast studies reported that nitrogen starvation induced rapid degradation of proteasomes, a process that required their encapsulation in cytoplasmic puncta (probably endosomes) mediated by

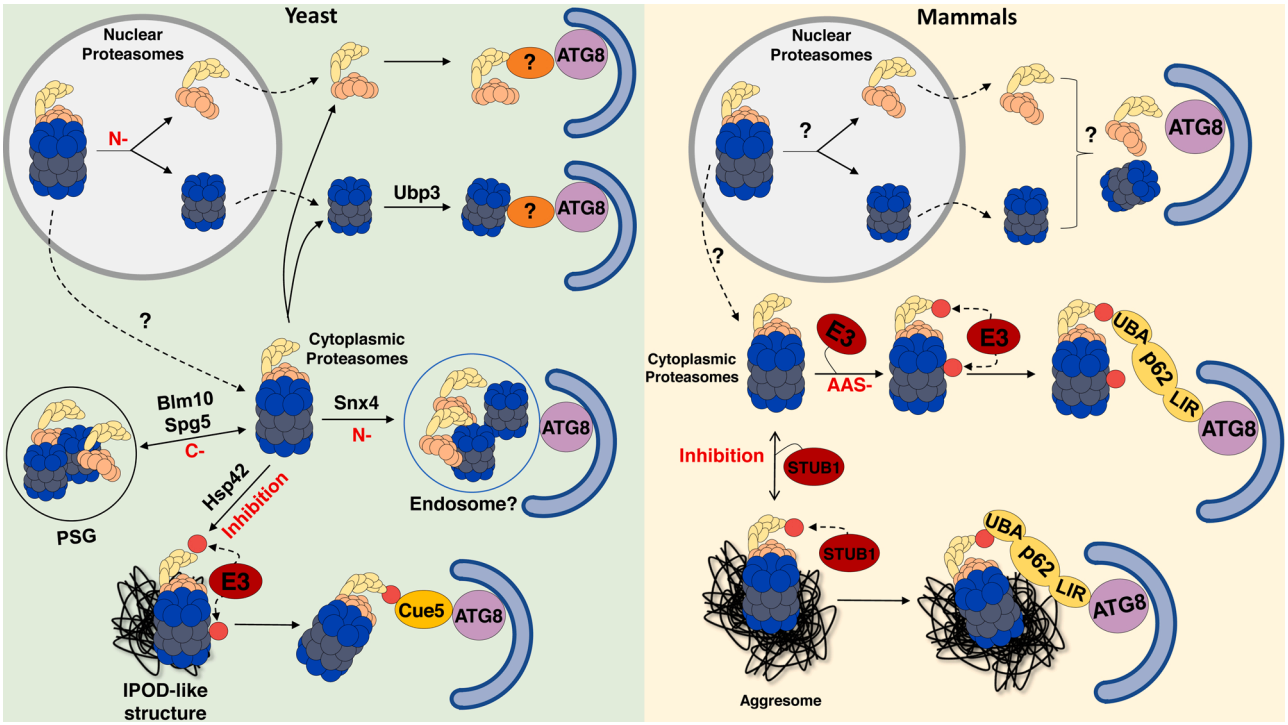

Fig. 7. Overview of proteaphagy in yeast and mammals.
In yeast cells (left), proteaphagy is activated in response to different stressors. Under nitrogen starvation (N-), nuclear proteasomes can dissociate into the 19S RP and 20S CP and exit the nucleus, but it is not known whether they exit the nucleus as a whole complex. Once in the cytoplasm, whole proteasomes and subcomplexes can be encapsulated in a Snx4-dependent manner (perhaps into endosomes) before engulfment by autophagosomes. Subcomplexes can also be targeted separately upon nitrogen starvation: 20S CP degradation is Ubp3-dependent, whereas 19S RP degradation is not. Upon chemical inhibition (MG-132), proteasomes are aggregated into IPOD-like structures and ubiquitinated (although the order of events remains elusive), after which they are recognized by Cue5 and recruited to autophagosomes. However, carbon starvation (C-) stimulates the reversible mobilization of proteasomes into PSG. In mammalian cells (right), proteaphagy can be stimulated by amino acid and serum starvation and proteasome inhibition. Whether proteasomes also dissociate in the nucleus and whether this is prior to nuclear exit remains elusive. Contrary to yeast, proteasomes are ubiquitinated upon amino acid and serum starvation (AAS-), which is necessary for the association of p62. During mammalian proteaphagy of inhibited proteasomes, proteasomes are ubiquitinated by STUB1 and sequestered into p62-positive aggresomes in a reversible manner. p62 binds ubiquitinated proteasomes through the UBA domain and recruits them to autophagosomes via the LIR motif.

Snx4 (Nemec et al., 2017) before engulfment by autophagosomes (Fig. 7). Conversely, nitrogen starvation did not induce proteasome ubiquitination (Marshall et al., 2016). Additional observations indicated that carbon starvation does not rapidly induce proteaphagy (Waite et al., 2016; Marshall and Vierstra, 2018). Instead, it triggers the formation of proteasome storage granules (PSGs), where proteasomes are protected from degradation (Marshall and Vierstra, 2018) as a mechanism that favors cell survival (Fig. 7). When nutrients are available, proteasomes stored in PSGs can be remobilized to promote renewed growth (Marshall and Vierstra, 2018). However, if carbon starvation is prolonged, proteasomes may slowly undergo proteaphagy (Marshall and Vierstra, 2018).

In mammalian cells, p62 mediates proteaphagy (Cohen-Kaplan et al., 2016) under conditions of amino acid and serum deprivation for 24−30 h (Fig. 7), which results in a more than 50 % reduction in proteasome subunit protein levels. Contrary to yeast and plants, amino acid and serum starvation in HeLa cells induced heavy ubiquitination of several proteasome subunits, including Rpn1, Rpn2, Rpn10 and Rpn13. Ubiquitinated proteasomes are recognized by p62 through its UBA domain and delivered to autophagosomes through the interaction with LC3B (Cohen-Kaplan et al., 2016). Under these conditions, the PB1 domain of p62 does not appear to be essential for proteasome recognition (Cohen-Kaplan et al., 2016). This observation raises the question as to whether other proteaphagic routes are present in mammalian cells, triggered by environmental cues other than starvation, such as proteasome inhibition (Choi et al., 2020), and whether autophagy receptors other than p62 are involved in these forms of selective proteaphagy. In this regard, in mammalian cells, proteasome subunits are also ubiquitinated upon proteasome inhibition (Choi et al., 2020; Besche et al., 2014), which signals proteasome inactivation (Besche et al., 2014) and degradation through proteaphagy (Choi et al., 2020). During proteaphagy of inhibited proteasomes in mammalian cells, ubiquitinated proteasomes are sequestered into p62-positive aggresomes in a reversible fashion, allowing the rescue of proteasomes (Marshall and Vierstra, 2018). This observation suggests, alongside the reported rapid induction of p62 upon proteasome blockade (Sha et al., 2018), that p62 also serves as the autophagic receptor for inactive proteasomes in mammals. Moreover, autophagy is upregulated when proteasomes are inactive (see section 2.1), suggesting that this compensation mechanism also governs the dynamics of proteaphagy. A question that remains open is the identity of the E3s involved in the ubiquitination of the proteasome before its lysosomal degradation and the type of ubiquitin chains that are incorporated. In this regard, several E3s associate with the proteasome in yeast and humans (Saeki, 2017). Interestingly, the E3s Ube3c and RNF181 ubiquitinate the Rpn13 and Rpt1 subunits, respectively, in response to the chemical inhibition of the proteasome in HEK293 cells (Besche et al., 2014). Rpn13 is a proteasomal ubiquitin receptor, and its ubiquitination reduced the capacity of the proteasome to bind and degrade ubiquitinated proteins (Besche et al., 2014). It would be worth investigating whether Rpn13 ubiquitination is necessary for mammalian proteaphagy. Furthermore, amino acid starvation also induced the ubiquitination of proteasome-associated E3s (Cohen-Kaplan et al., 2016), such as HUWE1 and KCMF1, thereby pointing to a coordinated regulation of proteaphagy under stress conditions. A recent report has identified STUB1 as the E3 responsible for the ubiquitination of mammalian proteasomes during proteaphagy of inhibited proteasomes

(Choi et al., 2020).

The subcellular localization of proteasomes is highly variable and dynamic among different cell types (Enenkel, 2014). Numerous studies support the hypothesis that proteasome localization is predominantly nuclear in highly proliferating cells, whereas it is mostly cytoplasmic in non-dividing cells (Enenkel, 2014). In the proteaphagy studies in yeast cells, proteasomes seemed to accumulate in the nucleus in basal conditions but then shifted to the vacuole (the lysosome equivalent in yeast (Li and Kane, 2009) upon nitrogen starvation and proteasome inhibition (Marshall et al., 2016). Similar results were found in mammalian cells under amino acid and serum starvation (Cohen-Kaplan et al., 2016). These findings raise the question as to how the proteasome overcomes the nuclear barrier in order to be targeted to the vacuole. One possible explanation could be that nuclear proteasomes are degraded by autophagy alongside the nucleus, in a process termed nucleophagy (Papandreou and Tavernarakis, 2019; Mijaljica and Devenish, 2013). Studies in yeast revealed that nitrogen starvation-induced proteaphagy of nuclear proteasomes do not require nucleophagy but do depend on the nuclear export machinery (Nemec et al., 2017). Follow-up studies suggested that nuclear proteasomes can undergo dissociation before nuclear export for their autophagic degradation (Nemec et al., 2017). Interestingly, other reports in yeast showed that proteaphagy can target proteasome subcomplexes separately upon nitrogen starvation (Waite et al., 2016), and even upon proteasome inhibition (Marshall et al., 2016). In this regard, nitrogen starvation induced the dissociation of the subcomplexes. Additionally, the autophagic clearance of the 20S CP depended on the DUB Ubp3, the yeast homolog of human Usp10, whereas degradation of the 19S RP was Ubp3-independent (Waite et al., 2016; Marshall and Vierstra, 2018), suggesting distinct pathways for each subcomplex. Moreover, proteasome subcomplexes can be mobilized separately to PSGs upon carbon starvation (Marshall and Vierstra, 2018), thereby further supporting the notion that proteasome subcomplexes can be targeted separately. However, several questions remain open: (i) can cytoplasmic proteasomes also be targeted as separated subcomplexes? (ii) is proteasome dissociation a pre-requisite for proteaphagy? (iii) what are the factors that regulate this dissociation prior to proteaphagy? (iv) are different autophagic receptors involved in the recognition of proteasome subcomplexes? (v) are all these molecular mechanisms also present in mammalian proteaphagy? and (vi) what is the physiological role of proteaphagy? Regarding this last question, a recent study showed that proteasome subunit levels are not altered in muscle or liver of mice fasted for 24 or 48 h (VerPlank et al., 2019), contrasting the in vitro findings (Cohen-Kaplan et al., 2016). This might be due to the fact that cells used in the in vitro studies were LC3B-overexpressing HeLa cells. Therefore, the importance of proteaphagy in vivo needs to be thoroughly investigated.

Given the role of autophagy in the degradation of proteasomes, a compelling question is how deficiencies in autophagy or proteaphagy affect proteasome function. In this regard, it would be of interest to design chemical or genetic approaches to inhibit proteaphagy. Accumulation of proteasomes would be expected upon autophagy inhibition, as reported previously (Marshall et al., 2015), but whether this accumulation enhances or impairs proteasome function remains elusive. In this respect, an increase in proteasome activity and subunit levels (at both mRNA and protein levels) has been described upon pharmacological inhibition and RNA interference of autophagy in colon cancer cell lines (Wang et al., 2013). These observations could be attributed to a decreased proteaphagy. Autophagy-deficient cells have been reported to activate Nrf2 through the accumulation of p62, as p62 sequesters Keap1 in inclusion bodies, thus blocking Nrf2 proteasomal degradation (Komatsu et al., 2010). The activation of Nrf2 upon autophagy deficiency may also contribute to the increase in proteasome function by upregulating the expression of proteasome subunits (Kwak et al., 2003). Another study using HeLa cells showed decrease in degradation of proteasome substrates following autophagy inhibition by compromised delivery of substrates to the proteasome (Korolchuk et al., 2009), and independent of changes in proteasome activity. This impairment in the delivery of substrates was due to p62 accumulation in autophagy-deficient cells, which sequestered proteasome substrates in aggregates (Korolchuk et al., 2009). Along these lines, genetic ablation of autophagy genes in *C. elegans* decreased proteasome degradation, although independently of p62 accumulation (Jha and Holmberg, 2020). In light of the above, it is possible that autophagy-compromised cells upregulate the expression of proteasome subunits to enhance proteasome function as a compensatory mechanism, similar to how autophagy is upregulated following proteasome inhibition. However, this compensation may be hindered by the accumulation of p62.

4. Coordinated regulation of the UPS and autophagy

We have analyzed the regulation of autophagy by UPS, and also the degradation of proteasomes through autophagy. These examples document the crosstalk between UPS and autophagy, and may also permit to explain cell adaptation under specific stress conditions.

There is also broad evidence indicating that under some other conditions, autophagy and UPS are regulated in parallel. In this regard, mTOR inhibition or amino acid starvation activates protein degradation by up-regulation of both UPS and autophagy in cultured cells (Zhao et al., 2015). The rapid activation of the UPS was characterized by increased K48 ubiquitin conjugation and ubiquitin-dependent degradation of growth-related proteins such as HMGCS1, SUPT6H, α-taxilin and Myst2. This process permits to slow down anabolic processes while providing building blocks for energy production to sustain the most vital biological pathways under mTOR inhibition. These results are in agreement with studies that showed coordinated activation of the UPS and autophagy through FoxO transcription factors in muscle cells upon denervation or fasting that lead to muscle atrophy (Zhao et al., 2007; Mammucari et al., 2007). Similar observations were also reported in vivo, where deletion of FoxO transcription factors in mice attenuated muscle atrophy upon denervation by reducing the expression of atrogenes, namely genes involved in the UPS and autophagy (Milan et al., 2015). FoxO transcription factors are negatively regulated by the insulin/IGF-1 (IIS) pathway (Brown and Webb, 2018), which is activated under nutrient repletion conditions. In fed conditions, mTOR is also activated (Bar-Peled and Sabatini, 2014), which together with the activation of the IIS pathway is set to repress both the UPS and autophagy.

Oxidative stress also upregulates the UPS and autophagy through the action of the transcriptional factor Nrf2 (Pajares et al., 2016; Pickering et al., 2012; Jain et al., 2010) and post-translational mechanisms discussed in the next section. This may constitute a cytoprotective mechanism to prevent the accumulation of oxidized and damaged proteins harmful for cells.

UPS and autophagy activity are also subjected to regulation by exercise (VerPlank et al., 2019; Grumati et al., 2011; He et al., 2012; Schwalm et al., 2015). Studies performed in human and rat skeletal muscles show increased Rpn6 phosphorylation and proteasome activity after exercise, through a mechanism dependent on cAMP and the activation of PKA (VerPlank et al., 2019). Exercise also induced autophagy in mouse skeletal muscle, which required the phosphorylation of BCL2 (He et al., 2012), probably by AMPK (Schwalm et al., 2015). The physiological implications of exercise-mediated upregulation of the UPS and autophagy may be to enhance the capacity to degrade misfolded proteins as a result of mechanic damage due to muscle contraction or as a result of oxidative damage by free radicals due to increased mitochondrial metabolism. This increase in overall proteolysis may also contribute to the degradation of proteins that are not needed for muscle recovery after exercise.

Interestingly, it has been reported that the UPS can be upregulated upon certain stimuli independently of autophagy. In this regard, increasing intracellular levels of cGMP enhanced 26S proteasomal degradation of proteins without affecting autophagy in neuroblastoma

and HEK293 cells (VerPlank et al., 2020). The same authors reported increased 26S proteasome activity upon stimuli that rise cAMP levels in several cell lines and mouse tissues (VerPlank et al., 2019; Lokireddy et al., 2015). However, these stimuli had no effect on basal autophagy in mouse primary hepatocytes, but did inhibit Torin1-induced autophagy in mouse C2C12 myotubes and HEK293 cells (VerPlank et al., 2019).

5. UPS and autophagy crosstalk during oxidative stress

The UPS and the autophagy-lysosome pathway form a complex protein quality control network that contributes to the overall surveillance of protein degradation in order to ensure a healthy proteome and prevent the deleterious effects of the accumulation of misfolded and damaged proteins (e.g. oxidized proteins) into aggregates. The presence of protein aggregates and the accumulation of aberrant proteins in different cell types are characteristic of a wide range of human diseases, including neurodegenerative disorders (Chiti and Dobson, 2017) (e.g. Huntington's disease and Parkinson's disease), metabolic disorders (e.g. type 2 diabetes (Mukherjee et al., 2015) and cancer (Deshaies, 2014). Both degradation systems work hand in hand to prevent these events. However, several lines of evidence indicate that disease-causing aberrant proteins impair the activity of the proteasome and autophagy, thus leading to a positive feedback loop that favors the accumulation of toxic proteins.

When proteins are translated, they fold into their native conformation in order to undertake their functions, but this folding process may also yield misfolded or unfolded proteins. Proteins with aberrant folding are recognized by molecular chaperones, such as Hsp70 and Hsp90, which prevent their aggregation and attempt to re-fold these proteins (Bukau et al., 2006) before they are directed to degradation. These chaperones also interact with E3s (Kevei et al., 2017) to couple protein re-folding with proteasomal degradation. In this regard, when the chaperone machinery fails to re-fold client proteins, chaperone-bound E3s, such as the C-terminus of Hsc70-interacting protein (Murata et al., 2001) (CHIP), ubiquitinate unfolded and misfolded proteins to mark them for degradation through the proteasome (Kevei et al., 2017), thus ensuring protein quality control under normal conditions. However, under stress conditions, such as oxidative stress, the number of misfolded and damaged proteins increases, thus requiring cells to push their protein quality control systems to handle this kind of insult (Korovila et al., 2017).

In the presence of acute oxidative stress, 26S proteasomes are inhibited and dissociate into 20S CPs and 19S RPs in a reversible manner. This dissociation allows the generation of 20S proteasomes, which increases cellular capacity to remove oxidized proteins independently of ATP and ubiquitin, although it leads to the accumulation of ubiquitinated proteins (Wang et al., 2010; Livnat-Levanon et al., 2014; Wang et al., 2017). This dissociation is conserved from yeast to humans, and it depends on the Ecm29 protein, as Ecm29 deletion prevents proteasome dissociation (Wang et al., 2010, 2017). However, the molecular mechanism by which Ecm29 dissociates the 19S RP from the 20S CP remains elusive. Mitochondrial dysfunction-induced oxidative stress also triggered proteasome dissociation through the generation of ROS (Livnat-Levanon et al., 2014). This dissociation may also allow the 20S proteasome to be associated with other RPs. In this regard, the association between PA28αβ and the 20S proteasome increased rapidly upon H_2O_2 treatment in MEF cells (Pickering and Davies, 2012) and enhanced the degradation of oxidized proteins (Pickering and Davies, 2012; Pickering et al., 2010).

Proteasomes are tightly regulated by a wide variety of post-translational modifications (Kors et al., 2019). Interestingly, a number of post-translational modifications on the proteasome, such as S-glutathionylation, occur when cells are under oxidative stress (Demasi et al., 2003; Silva et al., 2012; Leme et al., 2019; Zmijewski et al., 2009). H_2O_2 induced S- glutathionylation on residues Cys76 and Cys221 of the α_5 subunit (Demasi et al., 2003; Silva et al., 2012) increased α-ring gate opening and conferred resistance to oxidative stress in yeast (Silva et al., 2012; Leme et al., 2019). Whether this also occurs in mammalian cells remains elusive. It would be interesting to study whether oxidative stress-induced post-translational modifications are also involved in proteasome dissociation. In addition to post-translational modifications on the proteasome, oxidative stress has been reported to enhance the expression of 20S proteasomes, PA28 RPs and PA200 (Pickering et al., 2010), mostly through the activation of Nrf2 (Pickering et al., 2012), thus contributing to overall cellular anti-oxidant defense. Oxidative stress triggers conformational changes in Keap1 through the oxidation of critical cysteine residues, a process that abolishes its binding to Nrf2, resulting in Nrf2 stabilization and activation (Espinosa-Diez et al., 2015). In short, under acute oxidative stress, the proteasome undergoes a series of reversible modifications and remodeling, thus providing an adaptive response that allows rapid degradation of damaged and oxidized proteins in an ATP- and ubiquitin-independent fashion while undermining the clearance of ubiquitinated proteins. Interestingly, a study performed in cultured rat hippocampal neurons revealed that only a 20 % of the proteasomes are being actively used under unstressed conditions, leaving an 80 % of proteasomes unengaged (Filomeni et al., 2015). It may be possible that oxidative stress mobilizes this excess of non-active proteasomes (Fig. 8).

Oxidative stress has also been reported to activate autophagy through various mechanisms (Filomeni et al., 2015; Zhang et al., 2019). Oxidative stress can induce ER stress, which in turn triggers the UPR (Zhang et al., 2019) (Fig. 5). A key transcription factor involved in the upregulation of autophagy in response to oxidative stress is Nrf2 (Pajares et al., 2016). p62 has been described to interact with Keap1 and promote its degradation via autophagy, thus freeing and activating Nrf2 (Komatsu et al., 2010). Interestingly, as Nrf2 upregulates gene expression of autophagy genes (Pajares et al., 2016), including p62 (Jain et al., 2010), a positive feedback loop is generated that further enhances Nrf2 activation (Jain et al., 2010). Therefore, Nrf2 serves as a nexus that upregulates both the UPS and autophagy during oxidative stress. Whether oxidative stress induces post-translational modifications on the autophagic machinery to stimulate autophagy remains an open debate (Filomeni et al., 2015). In this regard, oxidative stress induced the oxidation of 2 conserved cysteine residues of p62, namely Cys105 and Cys113, which are located in the PB1 domain (Carroll et al., 2018). This enhanced p62 oligomerization resulted in increased autophagy flux and stress resistance (Carroll et al., 2018). Oxidative stress also inhibited the ATG8-delipidating activity of ATG4, which is necessary for correct autophagosome formation (Scherz-Shouval et al., 2007).

When the UPS is saturated, misfolded and damaged proteins may form large insoluble protein aggregates (Hyun et al., 2003) that can no longer be removed by the proteasome. Additionally, protein aggregates further inhibit the proteasome (Bence et al., 2001; Lindersson et al., 2004; Díaz-Hernández et al., 2006; Myeku et al., 2016). Under these circumstances, autophagy can be activated. The communication between the overwhelmed UPS and autophagy involves a complex integration of signals that results in an overall upregulation of autophagy (Fig. 5), with p62 as the key player in the crosstalk. In this regard, p62 oligomerizes, and then captures and isolates protein aggregates into structures called aggresomes to minimize their toxicity (Komatsu et al., 2007) and delivers them to autophagosomes for lysosomal clearance (Pankiv et al., 2007). p62 may also target saturated proteasomes to autophagy under these conditions (Marshall et al., 2015, 2016; Cohen-Kaplan et al., 2016). It would be interesting to examine whether autophagy-activating E3s are also involved in the crosstalk between the UPS and autophagy upon oxidative insults. Taken together, proper communication between the UPS and autophagy is essential for a coordinated response against environmental cues, such as oxidative stress (Fig. 8).

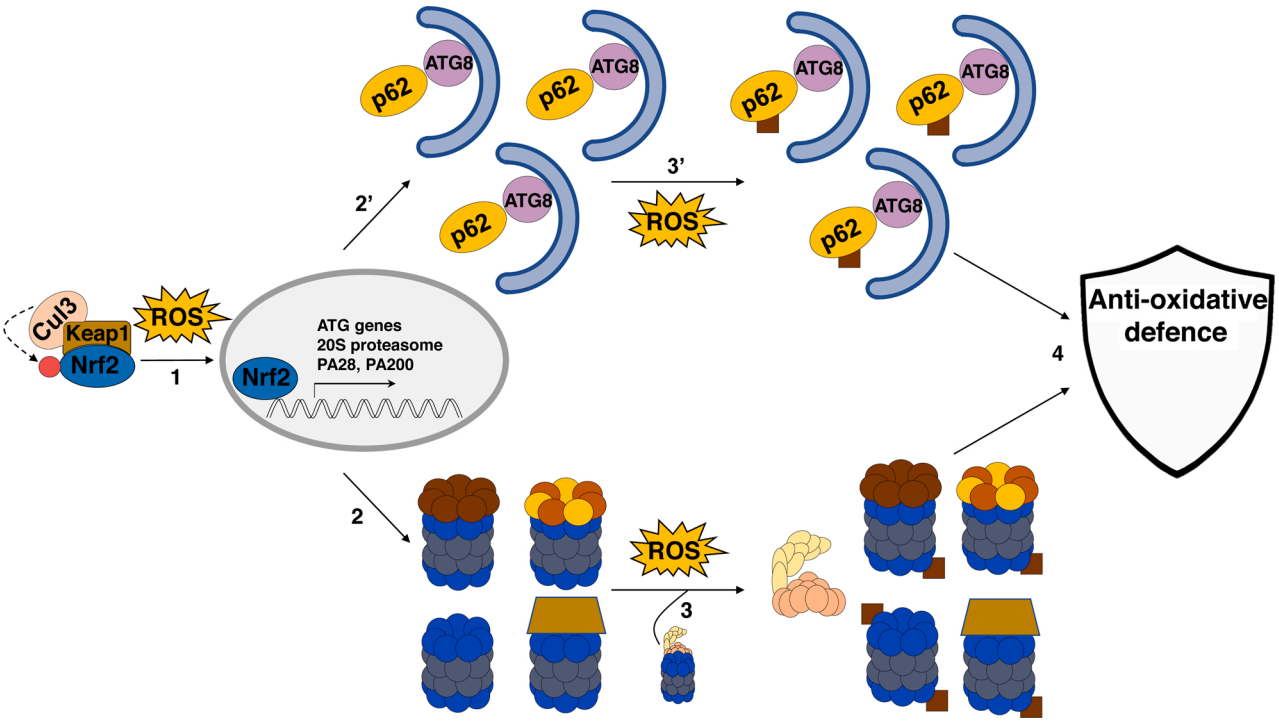

Fig. 8. UPS and autophagy at the crossroads of oxidative stress.
Proteins are oxidized and damaged upon oxidative stress and their accumulation can be toxic for cells. Under normal conditions, Nrf2 is bound to Keap1, which acts a substrate adaptor for Cul3, thus promoting Nrf2 ubiquitination (red circle) and proteasomal degradation. However, oxidative stress, e.g. reactive oxygen species (ROS), can induce the oxidation of cysteine residues in Keap1, thereby stimulating the release of Nrf2 into the nucleus and its activation(1). Once in the nucleus, Nrf2 stimulates the transcription of antioxidant response genes, including 20S proteasome subunit genes, PA28, PA200 and ATG genes, among others. This increases the number of proteasomes (2) and enhances the formation of autophagosomes (2′). ROS can also induce 26S proteasome dissociation into free 19S RP and 20S CP, post-translational modifications (brown squares) on the proteasome and may also mobilize non-active proteasomes to increase the cellular capacity to degrade oxidized proteins (3). ROS can also oxidize p62 (brown squares), which enhances autophagy flux (3′). This adaptive response increases the capacity of cells to degrade oxidized and damaged proteins, thus granting cells protection against oxidative stress (4).

6. UPS and autophagy in ageing

During ageing, many cellular pathways and functions deteriorate, leading to detrimental cellular processes such as mitochondrial dysfunction (Sebastián et al., 2017) and cellular senescence (Childs et al., 2015), which in turn contribute to the pathophysiology of age-related diseases, including cardiovascular, metabolic and neurodegenerative disorders and cancer. Protein quality control is also dampened in ageing organisms, resulting in the accumulation of toxic protein aggregates, a hallmark of ageing (López-Otín et al., 2013). Therefore, special attention has been made to study the effects of ageing on the UPS and the autophagy-lysosome pathway.

6.1. UPS

UPS dysfunction can occur at different levels, i.e. due to decreased expression of proteasome subunits, changes in the subunit composition, decreased peptidase activity and alterations in the expression and activity of ubiquitin conjugation enzymes. Early gene expression studies in the brain and skeletal muscle of mice, and isolated human fibroblasts revealed reduced expression of proteasome subunits and ubiquitin-related enzymes in old mice compared to young counterparts (Lee et al., 1999, 2000; Ly et al., 2000), but whether this decrease in the expression of proteasome subunits led to declined proteolysis was not reported. This reduced expression of proteasome subunits was reversed by a calorie-restricted diet (Lee et al., 1999, 2000). Proteasome content was also markedly downregulated in epidermal cells in elderly humans, correlating with decreased peptidase activity (Petropoulos et al., 2000), and also in rat heart (Bulteau et al., 2002). Moreover, the proteolytic activity of the 26S proteasome was decreased in fruit flies upon ageing due to alterations in the assembly of the 19S RP with the 20S CP (Vernace et al., 2007; Tonoki et al., 2009). An increase in the content of 20S immunoproteasomes was observed in aged rat muscle, but proteasome activity was decreased (Ferrington et al., 2005). These observations suggest that muscles respond to ageing by upregulating immunoproteasomes, albeit futilely, most likely due to the multi-layered effects of ageing, like chronic oxidative stress, which may influence its activity in a different manner than acute oxidative stress. It would be of interest to study the post-translational landscape of proteasomes from aged organisms.

In aged mice, overall proteasome activity has also been observed to be reduced in primary hepatocytes (Tomaru et al., 2012) and liver (Rodriguez et al., 2010), both 20S and 26S activities were reduced in white adipose tissue (Dasuri et al., 2011) (WAT) and in skeletal muscle (Strucksberg et al., 2010; Hwee et al., 2014; Fernando et al., 2019) from aged mice, along with a decreased content of 20S subunits and increased accumulation of oxidized proteins (Dasuri et al., 2011). However, another study reported increased proteasome content and activity in the hindlimb muscles of aged rats, an observation that was associated with muscle wasting and sarcopenia (Altun et al., 2010). Ageing effects on the proteasome might occur differently depending on the tissue or cell type, as proteasome activity varies across tissues (Fredriksson et al., 2012; Vilchez et al., 2012a; Tsakiri et al., 2013b), and even across different types of muscle and myofiber (Fernando et al., 2019; Raz et al., 2017). In this regard, aged somatic tissues in fruit flies exhibited lower proteasome content and activity than aged reproductive tissues (Tsakiri et al., 2013b). in vivo measurements in *C. elegans* showed that body-wall muscle cells display a less severe decline in proteasome activity compared to dorso-rectal neurons (Hamer et al., 2010) during ageing. The role of the UPS in ageing is also evidenced by studies that show

increased resistance to oxidative stress and increased life span upon enhancement of proteasome function through genetic approaches in *C. elegans* (Ghazi et al., 2007; Vilchez et al., 2012b; Chondrogianni et al., 2015), fruit flies (Tonoki et al., 2009) and yeast (Kruegel et al., 2011). Moreover, a genetically engineered mouse model with reduced chymotrypsin-like activity shows a shorter life span compared to normal mice (Tomaru et al., 2012), whereas a fly model with increased chymotrypsin-like activity exhibited a prolonged life span (Nguyen et al., 2019). Interestingly, skin fibroblasts derived from healthy centenarians show higher expression of proteasome subunits and higher proteasome activity compared to those of old adults under 100 years of age (Chondrogianni et al., 2000). Similar observations have been performed in livers of long-lived naked mole-rats (Rodriguez et al., 2012). These observations suggest that active proteasome activity is beneficial for healthy ageing.

6.2. Autophagy

A compelling question is whether autophagy ameliorates reduced proteasome function in ageing through the compensation mechanisms discussed in previous sections (Fig. 5). However, the general view is that autophagy function also declines during ageing, and improvement of autophagy function promotes longevity in several animal models (Alvers et al., 2009; Harrison et al., 2009; Bjedov et al., 2010; Robida-Stubbs et al., 2012; Zhang et al., 2014; Simonsen et al., 2008; Pyo et al., 2013; Lapierre et al., 2013; Ulgherait et al., 2014), similarly to the UPS. Conversely, a study in *C. elegans* showed that autophagy flux increases with age in several tissues, including the intestine, muscle and neurons (Chapin et al., 2015). Another report suggested a shift from proteasomal degradation to autophagy-lysosome degradation during ageing in primary human fibroblasts and rat brains, where autophagy is upregulated (Gamerdinger et al., 2009). An explanation of these rather controversial data could be that the effects of ageing on the autophagy-lysosome pathway are context- and time-dependent and that the specimens analyzed were not old enough to show reduced autophagy. In this regard, the upregulation of autophagy may occur early during ageing as a mechanism to compensate decreased proteasomal function and may then decline in later stages of ageing. To shed light on this hypothesis, an extensive analysis of the two proteolytic systems should be performed in different tissues and at different stages of ageing. An interesting study showed that healthy human centenarians have increased protein levels of Beclin-1 compared to young adults (Emanuele et al., 2014), suggesting that enhanced autophagy promotes healthy ageing, thus prolonging life span. This hypothesis is further supported by studies in model animals whose life span is increased upon pharmacological (e.g. rapamycin (Alvers et al., 2009; Harrison et al., 2009; Bjedov et al., 2010; Robida-Stubbs et al., 2012; Zhang et al., 2014)) or genetic induction of autophagy (Simonsen et al., 2008; Harrison et al., 2009; Bjedov et al., 2010; Robida-Stubbs et al., 2012; Zhang et al., 2014; Simonsen et al., 2008; Pyo et al., 2013; Lapierre et al., 2013; Ulgherait et al., 2014), although rapamycin may affect many other processes apart from autophagy (Li et al., 2014).

Taken together, all these data indicate that the UPS and the autophagy-lysosome pathway are protein quality control systems involved in the ageing process and that they are essential to maintain a healthy life span. The current view is that the activity of the two degradation systems declines during ageing. This decline may partially be attributed to the detrimental effects of chronic oxidative stress and other mechanisms. Along these lines, age-associated loss of Nrf2 activity has been reported in mouse liver and auditory cortex (Li et al., 2018; Zhang et al., 2012), rat liver (Suh et al., 2004; Shih and Yen, 2007), human bronchial epithelial cells (Zhou et al., 2018) and skeletal muscle of sedentary human individuals (Safdar et al., 2010). Moreover, the long-lived naked mole rat exhibited higher Nrf2 expression and activity compared to conventional laboratory mice, and Nrf2 expression and activity were positively correlated to maximum life span potential across rodent species (Lewis et al., 2015). These observations suggest that age-related loss of Nrf2 function is involved in the age-associated decline of the UPS and autophagy. Interestingly, recent work from our lab demonstrated a decrease in the expression of mitofusin-2 (MFN2) in aged mice, a key protein in mitochondrial dynamics (Liesa et al., 2009), which led to decreased autophagy and the accumulation of damaged mitochondria. These observations point to the involvement of MFN2 in the age-related decline of autophagy, and probably also the UPS, as mitochondrial dysfunction was reported to modulate proteasome composition (Livnat-Levanon et al., 2014).

However, it is not clear whether, despite this decline in activity, the two systems are still able to communicate with each other.

The impairment of both degradation systems upon ageing leads to the accumulation of protein aggregates that can react with other cellular components resulting in highly crosslinked un-degradable oxidized material such as lipofuscin (Reeg and Grune, 2015; Moreno-García et al., 2018). Lipofuscin, also known as the “age pigment”, accumulates in the cytosol and in the lysosomal lumen and has detrimental effects for cells (Höhn and Grune, 2013). In this regard, it has been reported that lipofuscin inhibits proteasomal degradation by competitive binding to the 20S proteasome (Höhn et al., 2011). The proposed mechanism involves the recognition of hydrophobic amino acid patches on the surface of lipofuscin by the 20S proteasome. Due to the un-degradable nature of lipofuscin, these aggregates remain attached to the 20S proteasome, thus preventing the degradation of oxidized proteins and aggravating the accumulation of protein aggregates (Höhn et al., 2011). Lysosomal lipofuscin accumulation is present in mouse models that recapitulate neurodegenerative disorders characterized by impaired autophagic flux (Shacka et al., 2007; Dehay et al., 2012; Brandenstein et al., 2015; Wavre-Shapton et al., 2015). Additionally, lipofuscin accumulation appears to impair lysosomal degradation (Terman et al., 1999), probably by interfering with lysosomal function, which may hinder aggrephagy. Therefore, lipofuscin establishes a positive feedback loop that causes further alterations in the UPS and autophagy and further accumulation of toxic protein aggregates.

6.3. UPS and autophagy crosstalk

The expression of p62, as well as that of other autophagy-related genes, decreases with age in mouse liver (Kwon et al., 2012). Also, generic deletion of p62 reduced life span and accelerated ageing in mice (Kwon et al., 2012). This mouse model exhibited early-onset mitochondrial dysfunction in brain, liver and heart, and this dysfunction was correlated with a downregulation of the Nrf2-dependent antioxidant pathway, thus contributing to the accelerated ageing phenotype. However, autophagy was not examined in this mouse model. Induction of p62 expression in middle-aged flies extended life span by improving mitochondrial fitness (Aparicio et al., 2019), which is coherent with the observation that p62 is involved in mitophagy (Ashrafi and Schwarz, 2013). In *C. elegans*, p62 overexpression induced autophagy, improved proteostasis, and subsequently extended life span (Kumsta et al., 2019). The decline in p62 during ageing (Kwon et al., 2012) may have various implications in the crosstalk between the UPS and autophagy that have not been explored to date. An important implication might be the impairment of proteaphagy. Acute oxidative stress has been shown to induce various post-translational modifications in the proteasome thereby modulating its activity as an adaptive response. However, little is known whether this stress can alter proteaphagy. In this regard, oxidative stress promoted p62 oligomerization and enhanced autophagy flux (Carroll et al., 2018). Therefore, the promotion of proteaphagy when oxidative stress overwhelms the UPS would appear to be logical. Oxidative stress is a hallmark of ageing (López-Otín et al., 2013; Finkel and Holbrook, 2000) and may be a mechanism by which proteasome activity declines with age. Furthermore, autophagy is also downregulated in aged organisms, suggesting that not only proteasome activity but also proper disposal of deficient proteasomes is impaired in

these organisms. In this context, it would, therefore, be relevant to examine the effects of chronic oxidative stress on proteaphagy and whether proteaphagy flux is attenuated in aged organisms.

A recent study performed in rat hippocampus showed that UPS-autophagy crosstalk is attenuated in aged organisms (Gavilán et al., 2015). In this study, authors show that upon proteasome inhibition, young rats are capable of upregulating autophagy as a compensation mechanism, whereas aged rats are not. This compensation seems to rely on the activation of the insulin/IGF-1 (IIS) pathway in young mice, which is lost in aged mice (Gavilán et al., 2015). In another study, livers from young mice were able to enhance proteasomal degradation to compensate for impaired chaperone-mediated autophagy (Schneider et al., 2015). However, this compensation mechanism was not observed in aged mice. The mechanisms underlying the loss of functional crosstalk compensation among proteolytic systems upon ageing requires further elucidation.

The involvement of E3s in ageing and age-related diseases is starting to be understood. The ageing process is governed by signaling pathways, including mTOR, AMPK and insulin/IGF-1 (IIS) (Kenyon, 2010). Whereas reduced mTOR signaling contributes to lifespan extension (Liu and Sabatini, 2020), increased AMPK signaling supports longevity (Salminen and Kaarniranta, 2012), most likely through the effects of autophagy (Liu and Sabatini, 2020). The IIS pathway is closely linked to the activation of the mTOR signaling pathway and it contributes to longevity through the effect of various transcription factors, including the FoxO family and Nrf2 (van Heemst, 2010; Kevei and Hoppe, 2014). Attenuation of the IIS pathway activates these transcription factors and promotes the expression of genes, among others, involved in the UPS and autophagy (Milan et al., 2015), which may contribute to their pro-longevity effects (Webb and Brunet, 2014). The IIS, mTOR and AMPK signaling pathways have been reported to be regulated by a complex integration of ubiquitin signals mediated by E3s (Ronnebaum et al., 2014; Jiang et al., 2019). Along these lines, the E3 CHIP regulates multiple IIS/mTOR signaling components, including Akt (Su et al., 2011), the p85 subunit of PI3K (Ko et al., 2014) and SGK1 (Belova et al., 2006), all of them through K48-linked ubiquitination-induced proteasomal degradation, along with many other E3s (Balaji et al., 2018). A recent study showed that CHIP also regulates insulin receptor (INSR) turnover through mono-ubiquitination, which triggers the endocytic-lysosomal degradation of the receptor in *C. elegans*, the fruit fly, and HEK293 cells (Tawo et al., 2017). In this regard, CHIP mediates INSR degradation under normal conditions, thus limiting insulin signaling and prolonging life span in *C. elegans*, whereas under proteotoxic conditions, CHIP is recruited to accumulated damaged proteins and cannot mono-ubiquitinate the INSR, thereby reducing the pro-longevity effects of CHIP (Tawo et al., 2017). Therefore, with age, CHIP might function exclusively in the degradation of accumulated proteins. In addition, CHIP-deficient mice have shorter lifespans and exhibit an altered protein quality control, as reflected by a decline in proteasome activity and accumulation of damaged proteins (Min et al., 2008). In *C. elegans*, the CUL-1 E3 ligase complex regulates longevity by increasing the transcriptional activity of FoxO (Ghazi et al., 2007). Additionally, FoxO transcription factors are also subjected to ubiquitin-dependent proteasomal degradation, which is mediated by the E3s SKP2 and Mdm2 (Huang and Tindall, 2011). The lifespan-prolonging effects of reduced IIS is well-established in invertebrate models, but is rather controversial in mammals as decreased IIS may lead to insulin resistance, a detrimental condition often associated with ageing and that eventually results in type 2 diabetes (T2D) and a shorter lifespan (Vitale et al., 2019). This controversy is most likely due to the complexity of the IIS pathway in mammals gained through evolution (van Heemst, 2010), e.g. tissue-specific expression of components of the signaling pathway. In light of the above, the pro-longevity effects of reduced IIS are not so clear in mammals and may largely depend on those components of the pathway that are regulated in tissue-specific contexts and the extent to which the pathway is repressed.

7. Concluding remarks

The UPS and the autophagy-lysosome pathway are not isolated protein degradation systems. Through crosstalk mechanisms, they work hand in hand as guardians of the proteome, protecting it from environmental stress. Ubiquitin, p62 and E3s are central elements of the communication between the two systems. The UPS regulates the activity of the autophagy-lysosome pathway through the modulation of transcription factors, which may depend on the cellular context. On the other hand, autophagy regulates the activity of the UPS through the clearance of proteasomes. Understanding the dialogue between the UPS and autophagy is of paramount importance in the search for drugs to block one pathway or the other. For instance, in the context of cancer, proteasome inhibitors are currently under clinical use for cancer therapy, such as bortezomib, but some types of cancer show resistance (Manasanch and Orlowski, 2017), which could partially be due to the crosstalk between the UPS and autophagy-lysosome pathway, resulting in the upregulation of the latter. However, autophagy upregulation by deficient proteasome should be revised by performing autophagy flux studies. Although several crosstalk mechanisms have been described, the communication between these two systems is just starting to be elucidated. In this regard, further research is needed to address how the upregulation of one system affects the other. Furthermore, the physiological role of proteaphagy is unknown. The activity of the two degradation pathways are also coordinately regulated in order to respond to environmental cues, such as oxidative stress, and this coordination may be achieved through the mechanisms discussed in this review.

Studies performed in model organisms suggest that UPS and autophagy function decline during ageing and may contribute to the pathogenesis of age-related diseases, including neurodegenerative and metabolic disorders. However, human studies are scarce. Understanding how ageing and oxidative stress negatively affect the function of the UPS and autophagy and also their crosstalk is key for the future development of clinical approaches to abrogate the deleterious effects of ageing and to promote healthy ageing. In this regard, enhancing these proteolytic systems has emerged as an attractive therapeutic strategy. However, this is a challenging task, as overactivation of these protein quality control systems in aged individuals may also be detrimental. Also, the UPS and autophagy play distinct roles in different tissues in the development of age-related metabolic disorders. This topic has been extensively investigated in the context of autophagy through the genetic manipulation of autophagy genes. However, physiological studies in the context of the UPS are scarce and should therefore be reinforced. Moreover, E3 ubiquitin ligases are becoming attractive therapeutic targets in ageing, and in the pathophysiology of age-related diseases such as metabolic syndrome and type 2 diabetes, and future studies should focus on understanding their role in the crosstalk between the UPS and autophagy, their molecular characteristics such as substrate-specificity, tissue-specific expression and their abundance or redundancy.

Acknowledgements

Due to space constraints, we have not included all relevant references in this growing field, so we kindly ask readers for their understanding. We would like to thank Alex Yarritu-Gallego, MSc, for insightful discussions about ageing. We would also like to thank Dr. Bernat Crosas (Institut de Biologia Molecular de Barcelona, CSIC) for critical reading of the manuscript. This study was supported by research grants from MINECO (SAF2016-75246R), MICINN (PID2019-106209RB-I00), the Generalitat de Catalunya (Grant 2017SGR1015), CIBERDEM ("Instituto de Salud Carlos III"), the Fundación Ramon Areces (CIVP18A3942), the Fundación BBVA, the Fundació Marató de TV3 (20132330), and EFSD. J.L.S.-W. is a recipient of an FPU PhD fellowship (FPU18/00340) from MICINN, Spain. A.Z. is a recipient of an ICREA "Academia" Award (Generalitat de Catalunya). We gratefully acknowledge institutional funding from MINECO and MICINN through

the Centres of Excellence Severo Ochoa Award, and from the CERCA Programme of the Generalitat de Catalunya.

References

Akutsu, M., Dikic, I., Bremm, A., 2016. Ubiquitin chain diversity at a glance. J. Cell. Sci. 129, 875–880.

Alers, S., Loffler, A.S., Wesselborg, S., Stork, B., 2012. Role of AMPK-mTOR-Ulk1/2 in the regulation of autophagy: cross talk, shortcuts, and feedbacks. Mol. Cell. Biol. 32, 2–11.

Altun, M., et al., 2010. Muscle wasting in aged, sarcopenic rats is associated with enhanced activity of the ubiquitin proteasome pathway. J. Biol. Chem. 285, 39597–39608.

Alvers, A.L., et al., 2009. Autophagy is required for extension of yeast chronological life span by rapamycin. Autophagy 5, 847–849.

Aparicio, R., Rana, A., Walker, D.W., 2019. Upregulation of the autophagy adaptor p62/SQSTM1 prolongs health and lifespan in middle-aged Drosophila. Cell Rep. 28, 1029–1040 e5.

Ashrafi, G., Schwarz, T.L., 2013. The pathways of mitophagy for quality control and clearance of mitochondria. Cell Death Differ. 20, 31–42.

Balaji, V., Pokrzywa, W., Hoppe, T., 2018. Ubiquitylation pathways in insulin signaling and organismal homeostasis. BioEssays 40, 1–10.

Bard, J.A.M., et al., 2018. Structure and function of the 26S proteasome. Annu. Rev. Biochem. 87, 697–724.

Bar-Peled, L., Sabatini, D.M., 2014. Regulation of mTORC1 by amino acids. Trends Cell Biol. 24, 400–406.

Belova, L., et al., 2006. Ubiquitin-proteasome degradation of serum- and glucocorticoid-regulated kinase-1 (SGK-1) is mediated by the chaperone-dependent E3 ligase CHIP. Biochem. J. 400, 235–244.

Bence, N.F., Sampat, R.M., Kopito, R.R., 2001. Impairment of the ubiquitin-proteasome system by protein aggregation. Science (80-.) 292, 1552–1555.

Ben-Nissan, G., Sharon, M., 2014. Regulating the 20S proteasome ubiquitin-independent degradation pathway. Biomolecules 4, 862–884.

Bento, C.F., et al., 2016a. Mammalian autophagy: how does it work? Annu. Rev. Biochem. 85, 685–713.

Bento, C.F., et al., 2016b. Mammalian autophagy: how does it work? Annu. Rev. Biochem. 85, 685–713.

Besche, H.C., et al., 2014. Autoubiquitination of the 26S proteasome on Rpn13 regulates breakdown of ubiquitin conjugates. EMBO J. 33, 1159–1176.

Bhattacharyya, S., Yu, H., Mim, C., Matouschek, A., 2014. Regulated protein turnover: snapshots of the proteasome in action. Nat. Rev. Mol. Cell Biol. 15, 122–133.

Bjedov, I., et al., 2010. Mechanisms of life span extension by rapamycin in the fruit fly Drosophila melanogaster. Cell Metab. 11, 35–46.

Brandenstein, L., Schweizer, M., Sedlacik, J., Fiehler, J., Storch, S., 2015. Lysosomal dysfunction and impaired autophagy in a novel mouse model deficient for the lysosomal membrane protein Cln7. Hum. Mol. Genet. 25, 777–791.

Brooks, P., et al., 2000. Subcellular localization of proteasomes and their regulatory complexes in mammalian cells. Biochem. J. 346, 155–161.

Brown, A.K., Webb, A.E., 2018. Chapter seven - regulation of FOXO factors in mammalian cells. In: Ghaffari, S. (Ed.), Forkhead FOXO Transcription Factors in Development and Disease, 127. Academic Press, pp. 165–192.

Budenholzer, L., Cheng, C.L., Li, Y., Hochstrasser, M., 2017. Proteasome structure and assembly. J. Mol. Biol. 429, 3500–3524.

Bukau, B., Weissman, J., Horwich, A., 2006. Molecular Chaperones and Protein Quality Control. Cell 125, 443–451.

Bulteau, A.L., Szweda, L.I., Friguet, B., 2002. Age-dependent declines in proteasome activity in the heart. Arch. Biochem. Biophys. 397, 298–304.

Carroll, B., et al., 2018. Oxidation of SQSTM1/p62 mediates the link between redox state and protein homeostasis. Nat. Commun. 9, 1–11.

Cascio, P., 2014. PA28αβ: The enigmatic magic ring of the proteasome? Biomolecules 4, 566–584.

Cascio, P., Call, M., Petre, B.M., Walz, T., Goldberg, A.L., 2002. Properties of the hybrid form of the 26S proteasome containing both 19S and PA28 complexes. EMBO J. 21, 2636–2645.

Chapin, H.C., Okada, M., Merz, A.J., Miller, D.L., 2015. Tissue-specific autophagy responses to aging and stress in C. elegans. Aging (Albany. NY) 7, 419–434.

Chen, Z.J., Sun, L.J., 2009. Nonproteolytic functions of ubiquitin in cell signaling. Mol. Cell 33, 275–286.

Chen, R.H., Chen, Y.H., Huang, T.Y., 2019. Ubiquitin-mediated regulation of autophagy. J. Biomed. Sci. 26, 1–12.

Childs, B.G., Durik, M., Baker, D.J., Van Deursen, J.M., 2015. Cellular senescence in aging and age-related disease: from mechanisms to therapy. Nat. Med. 21, 1424–1435.

Chiti, F., Dobson, C.M., 2017. Protein Misfolding, Amyloid Formation, and Human Disease: A Summary of Progress Over the Last Decade. Annu. Rev. Biochem. 86, 27–68.

Choi, W.H., et al., 2020. Aggresomal sequestration and STUB1-mediated ubiquitylation during mammalian proteaphagy of inhibited proteasomes. Proc. Natl. Acad. Sci. 117, 19190–19200.

Chondrogianni, N., Petropoulos, I., Franceschi, C., Friguet, B., Gonos, E.S., 2000. Fibroblast cultures from healthy centenarians have an active proteasome. Exp. Gerontol. 35, 721–728.

Chondrogianni, N., Georgila, K., Kourtis, N., Tavernarakis, N., Gonos, E.S., 2015. 20S proteasome activation promotes life span extension and resistance to proteotoxicity in Caenorhabditis elegans. FASEB J. 29, 611–622.

Chu-Ping, M., Vu, J.H., Proske, R.J., Slaughter, C.A., DeMartino, G.N., 1994. Identification, purification, and characterization of a high molecular weight, ATP-dependent activator (PA700) of the 20 S proteasome. J. Biol. Chem. 269, 3539–3547.

Cohen-Kaplan, V., et al., 2016. p62- and ubiquitin-dependent stress-induced autophagy of the mammalian 26S proteasome. Proc. Natl. Acad. Sci. U. S. A. 113, E7490–E7499.

Collins, G.A., Goldberg, A.L., 2017. The logic of the 26S proteasome. Cell 169, 792–806.

Cuervo, A.M., Palmer, A., Rivett, A.J., Knecht, E., 1995. Degradation of proteasomes by lysosomes in rat liver. Eur. J. Biochem. 227, 792–800.

Cullinan, S.B., Diehl, J.A., 2004. PERK-dependent activation of Nrf2 contributes to redox homeostasis and cell survival following endoplasmic reticulum stress. J. Biol. Chem. 279, 20108–20117.

Dasuri, K., et al., 2011. Proteasome alterations during adipose differentiation and aging: links to impaired adipocyte differentiation and development of oxidative stress. Free Radic. Biol. Med. 51, 1727–1735.

Dehay, B., et al., 2012. Loss of P-type ATPase ATP13A2/PARK9 function induces general lysosomal deficiency and leads to Parkinson disease neurodegeneration. Proc. Natl. Acad. Sci. 109, 9611–9616.

Demasi, M., Silva, G.M., Netto, L.E.S., 2003. 20 S proteasome from Saccharomyces cerevisiae is responsive to redox modifications and is S-glutathionylated. J. Biol. Chem. 278, 679–685.

Deshaies, R.J., 2014. Proteotoxic crisis, the ubiquitin-proteasome system, and cancer therapy. BMC Med. 12, 1–14.

Díaz-Hernández, M., et al., 2006. Inhibition of 26S proteasome activity by huntingtin filaments but not inclusion bodies isolated from mouse and human brain. J. Neurochem. 98, 1585–1596.

Emanuele, E., et al., 2014. Can enhanced autophagy be associated with human longevity? Serum levels of the autophagy biomarker beclin-1 are increased in healthy centenarians. Rejuvenation Res. 17, 518–524.

Enenkel, C., 2014. Proteasome dynamics. Biochim. Biophys. Acta - Mol. Cell Res. 1843, 39–46.

Espinosa-Diez, C., et al., 2015. Antioxidant responses and cellular adjustments to oxidative stress. Redox Biol. 6, 183–197.

Fan, T., et al., 2018. Proteasome inhibition promotes autophagy and protects from endoplasmic reticulum stress in rat alveolar macrophages exposed to hypoxia-reoxygenation injury. J. Cell. Physiol. 233, 6748–6758.

Feng, X., et al., 2019. Ubiquitination of UVRAG by SMURF1 promotes autophagosome maturation and inhibits hepatocellular carcinoma growth. Autophagy 15, 1130–1149.

Fernando, R., et al., 2019. Low proteasomal activity in fast skeletal muscle fibers is not associated with increased age-related oxidative damage. Exp. Gerontol. 117, 45–52.

Ferrington, D.A., Husom, A.D., Thompson, L.V., 2005. Altered proteasome structure, function, and oxidation in aged muscle. FASEB J. 19, 1–24.

Filomeni, G., De Zio, D., Cecconi, F., 2015. Oxidative stress and autophagy: the clash between damage and metabolic needs. Cell Death Differ. 22, 377–388.

Finkel, T., Holbrook, N.J., 2000. Oxidants, oxidative stress and the biology of ageing. Nature 408, 239–247.

Finley, D., 2009. Recognition and processing of ubiquitin-protein conjugates by the proteasome. Annu. Rev. Biochem. 78, 477–513.

Fredriksson, Å., et al., 2012. Effects of aging and reproduction on protein quality control in soma and gametes of Drosophila melanogaster. Aging Cell 11, 634–643.

Fusco, C., et al., 2018. TRIM50 regulates Beclin 1 proautophagic activity. Biochim. Biophys. Acta - Mol. Cell Res. 1865, 908–919.

Galluzzi, L., et al., 2017. Molecular definitions of autophagy and related processes. EMBO J. 36, 1811–1836.

Gamerdinger, M., et al., 2009. Protein quality control during aging involves recruitment of the macroautophagy pathway by BAG3. EMBO J. 28, 889–901.

Gatica, D., Lahiri, V., Klionsky, D.J., 2018. Cargo recognition and degradation by selective autophagy. Nat. Cell Biol. 20, 233–242.

Gavilán, E., et al., 2015. Age-related dysfunctions of the autophagy lysosomal pathway in hippocampal pyramidal neurons under proteasome stress. Neurobiol. Aging 36, 1953–1963.

Geng, J., Klionsky, D.J., 2008. The Atg8 and Atg12 ubiquitin-like conjugation systems in macroautophagy. 'protein modifications: beyond the usual suspects' review series. EMBO Rep. 9, 859–864.

Ghazi, A., Henis-Korenblit, S., Kenyon, C., 2007. Regulation of Caenorhabditis elegans lifespan by a proteasomal E3 ligase complex. Proc. Natl. Acad. Sci. U. S. A. 104, 5947–5952.

Grice, G.L., et al., 2015. The proteasome distinguishes between Heterotypic and homotypic Lysine-11-Linked polyubiquitin chains. Cell Rep. 12, 545–553.

Grumati, P., Dikic, I., 2018. Ubiquitin signaling and autophagy. J. Biol. Chem. 293, 5404–5413.

Grumati, P., et al., 2011. Physical exercise stimulates autophagy in normal skeletal muscles but is detrimental for collagen VI-deficient muscles. Autophagy 7, 1415–1423.

Hamer, G., Matilainen, O., Holmberg, C.I., 2010. A photoconvertible reporter of the ubiquitin-proteasome system in vivo. Nat. Methods 7, 473–478.

Harrison, D.E., et al., 2009. Rapamycin fed late in life extends lifespan in genetically heterogeneous mice. Nature 460, 392–395.

He, C., et al., 2012. Exercise-induced BCL2-regulated autophagy is required for muscle glucose homeostasis. Nature 481, 511–515.

Hetz, C., Chevet, E., Oakes, S.A., 2015. Proteostasis control by the unfolded protein response. Nat. Cell Biol. 17, 829–838.

Hill, S.M., Wrobel, L., Rubinsztein, D.C., 2019. Post-translational modifications of Beclin 1 provide multiple strategies for autophagy regulation. Cell Death Differ. 26, 617–629.
Hoeller, D., et al., 2007. E3-independent monoubiquitination of ubiquitin-binding proteins. Mol. Cell 26, 891–898.
Höhn, A., Grune, T., 2013. Lipofuscin: formation, effects and role of macroautophagy. Redox Biol. 1, 140–144.
Höhn, A., et al., 2011. Lipofuscin inhibits the proteasome by binding to surface motifs. Free Radic. Biol. Med. 50, 585–591.
Huang, H., Tindall, D.J., 2011. Regulation of FOXO protein stability via ubiquitination and proteasome degradation. Biochim. Biophys. Acta - Mol. Cell Res. 1813, 1961–1964.
Huang, F., Kirkpatrick, D., Jiang, X., Gygi, S., Sorkin, A., 2006. Differential regulation of EGF receptor internalization and degradation by multiubiquitination within the kinase domain. Mol. Cell 21, 737–748.
Huang, L., Haratake, K., Miyahara, H., Chiba, T., 2016. Proteasome activators, PA28γ and PA200, play indispensable roles in male fertility. Sci. Rep. 6, 2–10.
Huber, E.M., Groll, M., 2017. The mammalian proteasome activator PA28 forms an asymmetric α4β3 complex. Structure 25, 1473–1480 e3.
Hwee, D.T., Baehr, L.M., Philp, A., Baar, K., Bodine, S.C., 2014. Maintenance of muscle mass and load-induced growth in Muscle RING Finger 1 null mice with age. Aging Cell 13, 92–101.
Hyun, D.H., Lee, M.H., Halliwell, B., Jenner, P., 2003. Proteasomal inhibition causes the formation of protein aggregates containing a wide range of proteins, including nitrated proteins. J. Neurochem. 86, 363–373.
Ivanova, S., et al., 2019. Regulation of death receptor signaling by the autophagy protein TP53INP2. EMBO J. 38, e99300.
Jain, A., et al., 2010. p62/SQSTM1 is a target gene for transcription factor NRF2 and creates a positive feedback loop by inducing antioxidant response element-driven gene transcription. J. Biol. Chem. 285, 22576–22591.
Jha, S., Holmberg, C.I., 2020. Tissue-specific impact of autophagy genes on the ubiquitin-proteasome system in C. elegans. Cells 9.
Jiang, Y., Su, S., Zhang, Y., Qian, J., Liu, P., 2019. Control of mTOR signaling by ubiquitin. Oncogene 38, 3989–4001.
Joachim, J., et al., 2017. Centriolar satellites control GABARAP ubiquitination and GABARAP-Mediated autophagy. Curr. Biol. 27, 2123–2136 e7.
Johansen, T., Lamark, T., 2020. Selective autophagy: ATG8 family proteins, LIR motifs and cargo receptors. J. Mol. Biol. 432, 80–103.
Johnston-Carey, H.K., Pomatto, L.C.D., Davies, K.J.A., 2015. The Immunoproteasome in oxidative stress, aging, and disease. Crit. Rev. Biochem. Mol. Biol. 51, 268–281.
Kageyama, S., et al., 2014. Proteasome dysfunction activates autophagy and the Keap1-Nrf2 pathway. J. Biol. Chem. 289, 24944–24955.
Kaiser, S.E., et al., 2011. Protein standard absolute quantification (PSAQ) method for the measurement of cellular ubiquitin pools. Nat. Methods 8, 691–696.
Kao, C., et al., 2014. Bortezomib enhances cancer cell death by blocking the autophagic flux through stimulating ERK phosphorylation. Cell Death Dis. 5, e1510–12.
Kaushik, S., Cuervo, A.M., 2018. The coming of age of chaperone-mediated autophagy. Nat. Rev. Mol. Cell Biol. 19, 365–381.
Kenyon, C.J., 2010. The genetics of ageing. Nature 464, 504–512.
Kevei, É., Hoppe, T., 2014. Ubiquitin sets the timer: impacts on aging and longevity. Nat. Struct. Mol. Biol. 21, 290–292.
Kevei, É., Pokrzywa, W., Hoppe, T., 2017. Repair or destruction—an intimate liaison between ubiquitin ligases and molecular chaperones in proteostasis. FEBS Lett. 591, 2616–2635.
Kim, W., et al., 2011. Systematic and quantitative assessment of the ubiquitin-modified proteome. Mol. Cell 44, 325–340.
Kim, Y.M., et al., 2015. MTORC1 phosphorylates UVRAG to negatively regulate autophagosome and endosome maturation. Mol. Cell 57, 207–218.
Kim, J.H., et al., 2018. The deubiquitinating enzyme USP20 stabilizes ULK1 and promotes autophagy initiation. EMBO Rep. 19, 1–17.
Kirkin, V., McEwan, D.G., Novak, I., Dikic, I., 2009. A role for ubiquitin in selective autophagy. Mol. Cell 34, 259–269.
Klionsky, D.J., et al., 2016. Guidelines for the use and interpretation of assays for monitoring autophagy (3rd edition). Autophagy 12, 1–222.
Ko, H.R., et al., 2014. P42 Ebp1 regulates the proteasomal degradation of the p85 regulatory subunit of PI3K by recruiting a chaperone-E3 ligase complex HSP70/CHIP. Cell Death Dis. 5, 1–12.
Koizumi, S., et al., 2016. The aspartyl protease DDI2 activates Nrf1 to compensate for proteasome dysfunction. Elife 5, 1–10.
Komander, D., Rape, M., 2012. The ubiquitin code. Annu. Rev. Biochem. 81, 203–229.
Komatsu, M., et al., 2007. Homeostatic levels of p62 control cytoplasmic inclusion body formation in autophagy-deficient mice. Cell 131, 1149–1163.
Komatsu, M., et al., 2010. The selective autophagy substrate p62 activates the stress responsive transcription factor Nrf2 through inactivation of Keap1. Nat. Cell Biol. 12, 213–223.
Korolchuk, V.I., Mansilla, A., Menzies, F.M., Rubinsztein, D.C., 2009. Autophagy inhibition compromises degradation of ubiquitin-proteasome pathway substrates. Mol. Cell 33, 517–527.
Korovila, I., et al., 2017. Proteostasis, oxidative stress and aging. Redox Biol. 13, 550–567.
Kors, S., Geijtenbeek, K., Reits, E., Schipper-Krom, S., 2019. Regulation of proteasome activity by (Post-)transcriptional mechanisms. Front. Mol. Biosci. 6.
Kruegel, U., et al., 2011. Elevated proteasome capacity extends replicative lifespan in saccharomyces cerevisiae. PLoS Genet. 7.
Kuang, E., et al., 2012. Regulation of ATG4B stability by RNF5 limits basal levels of autophagy and influences susceptibility to bacterial infection. PLoS Genet. 8.
Kumsta, C., et al., 2019. The autophagy receptor p62/SQST-1 promotes proteostasis and longevity in C. Elegans by inducing autophagy. Nat. Commun. 10, 1–12.
Kwak, M.-K., Wakabayashi, N., Greenlaw, J.L., Yamamoto, M., Kensler, T.W., 2003. Antioxidants enhance mammalian proteasome expression through the Keap1-Nrf2 signaling pathway. Mol. Cell. Biol. 23, 8786–8794.
Kwon, J., et al., 2012. Assurance of mitochondrial integrity and mammalian longevity by the p62-Keap1-Nrf2-Nqo1 cascade. EMBO Rep. 13, 150–156.
Lapierre, L.R., et al., 2013. The TFEB orthologue HLH-30 regulates autophagy and modulates longevity in Caenorhabditis elegans. Nat. Commun. 4.
Laussmann, M.A., et al., 2011. Proteasome inhibition can induce an autophagy-dependent apical activation of caspase-8. Cell Death Differ. 18, 1584–1597.
Lee, C.K., Klopp, R.G., Weindruch, R., Prolla, T.A., 1999. Gene expression profile of aging and its retardation by caloric restriction. Science (80-.) 285, 1390–1393.
Lee, C.K., Weindruch, R., Prolla, T.A., 2000. Gene-expression profile of the ageing brain in mice. Nat. Genet. 25, 294–297.
Lee, A.H., Iwakoshi, N.N., Anderson, K.C., Glimcher, L.H., 2003. Proteasome inhibitors disrupt the unfolded protein response in myeloma cells. Proc. Natl. Acad. Sci. U. S. A. 100, 9946–9951.
Lee, Y.J., et al., 2017. Keap1/Cullin3 modulates p62/SQSTM1 activity via UBA domain ubiquitination. Cell Rep. 19, 188–202.
Leme, J.M.M., et al., 2019. Mutations of Cys and Ser residues in the α5-subunit of the 20S proteasome from Saccharomyces cerevisiae affects gating and chronological lifespan. Arch. Biochem. Biophys. 666, 63–72.
Levy-barda, A., et al., 2011. Involvement of the nuclear proteasome activator PA28 γ in the cellular response to DNA double-strand breaks a n d e s i o s c i e n c e o n o t d i s t r i b u t e. Cell Cycle 10, 4300–4310.
Lewis, K.N., et al., 2015. Regulation of Nrf2 signaling and longevity in naturally long-lived rodents. Proc. Natl. Acad. Sci. U. S. A. 112, 3722–3727.
Li, S.C., Kane, P.M., 2009. The yeast lysosome-like vacuole: endpoint and crossroads. Biochim. Biophys. Acta 1793, 650–663.
Li, W.W., Li, J., Bao, J.K., 2012. Microautophagy: lesser-known self-eating. Cell. Mol. Life Sci. 69, 1125–1136.
Li, J., Kim, S.G., Blenis, J., 2014. Rapamycin: one drug, many effects. Cell Metab. 19, 373–379.
Li, J., et al., 2015. Mitochondrial outer-membrane E3 ligase MUL1 ubiquitinates ULK1 and regulates selenite-induced mitophagy. Autophagy 11, 1216–1229.
Li, Y., et al., 2018. Age-associated decline in Nrf2 signaling and associated mtDNA damage may be involved in the degeneration of the auditory cortex: implications for central presbycusis. Int. J. Mol. Med. 42, 3371–3385.
Li, C., et al., 2019. Proteasome inhibition activates autophagy-lysosome pathway associated with TFEB dephosphorylation and nuclear translocation. Front. Cell Dev. Biol. 7, 1–8.
Liang, C., et al., 2008. Beclin1-binding UVRAG targets the class C Vps complex to coordinate autophagosome maturation and endocytic trafficking. Nat. Cell Biol. 10, 776–787.
Liesa, M., Palacín, M., Zorzano, A., 2009. Mitochondrial dynamics in mammalian health and disease. Physiol. Rev. 89, 799–845.
Lim, J., et al., 2015. Proteotoxic stress induces phosphorylation of p62/SQSTM1 by ULK1 to regulate selective autophagic clearance of protein aggregates. PLoS Genet. 11, 1–28.
Lin, Q., et al., 2017. The HECT E3 ubiquitin ligase NEDD4 interacts with and ubiquitylates SQSTM1 for inclusion body autophagy. J. Cell. Sci. 130, 3839–3850.
Lindersson, E., et al., 2004. Proteasomal inhibition by α-Synuclein filaments and oligomers. J. Biol. Chem. 279, 12924–12934.
Liu, G.Y., Sabatini, D.M., 2020. mTOR at the nexus of nutrition, growth, ageing and disease. Nat. Rev. Mol. Cell Biol. 21.
Liu, C.C., et al., 2016. Cul3-KLHL20 ubiquitin ligase governs the turnover of ULK1 and VPS34 complexes to control autophagy termination. Mol. Cell 61, 84–97.
Liu, L., et al., 2019. UbiHub: a data hub for the explorers of ubiquitination pathways. Bioinformatics 35, 2882–2884.
Livnat-Levanon, N., et al., 2014. Reversible 26S proteasome disassembly upon mitochondrial stress. Cell Rep. 7, 1371–1380.
Lokireddy, S., Kukushkin, N.V., Goldberg, A.L., 2015. cAMP-induced phosphorylation of 26S proteasomes on Rpn6/PSMD11 enhances their activity and the degradation of misfolded proteins. Proc. Natl. Acad. Sci. 112, E7176–E7185.
López-Otín, C., Blasco, M.A., Partridge, L., Serrano, M., Kroemer, G., 2013. The hallmarks of aging. Cell 153, 1194.
Lu, K., Den Brave, F., Jentsch, S., 2017. Receptor oligomerization guides pathway choice between proteasomal and autophagic degradation. Nat. Cell Biol. 19, 732–739.
Lu, G., et al., 2019. Suppression of autophagy during mitosis via CUL4-RING ubiquitin ligases-mediated WIPI2 polyubiquitination and proteasomal degradation. Autophagy 15, 1917–1934.
Ly, D.H., Lockhart, D.J., Lerner, R.A., Schultz, P.G., 2000. Mitotic misregulation and human aging. Science (80-) 287, 2486–2492.
Mammucari, C., et al., 2007. FoxO3 controls autophagy in skeletal muscle in vivo. Cell Metab. 6, 458–471.
Manasanch, E.E., Orlowski, R.Z., 2017. Proteasome inhibitors in cancer therapy. Nat. Rev. Clin. Oncol. 14, 417–433.
Mao, I., Liu, J., Li, X., Luo, H., 2008. REGγ, a proteasome activator and beyond? Cell. Mol. Life Sci. 65, 3971–3980.
Marshall, R.S., Vierstra, R.D., 2018. Proteasome storage granules protect proteasomes from autophagic degradation upon carbon starvation. Elife 7, 1–38.
Marshall, R.S., Vierstra, R.D., 2019. Dynamic regulation of the 26S proteasome: from synthesis to degradation. Front. Mol. Biosci. 6.

Marshall, R.S., Li, F., Gemperline, D.C., Book, A.J., Vierstra, R.D., 2015. Autophagic degradation of the 26S proteasome is mediated by the dual ATG8/Ubiquitin receptor RPN10 in Arabidopsis. Mol. Cell 58, 1053–1066.
Marshall, R.S., McLoughlin, F., Vierstra, R.D., 2016. Autophagic turnover of inactive 26S proteasomes in yeast is directed by the ubiquitin receptor Cue5 and the Hsp42 chaperone. Cell Rep. 16, 1717–1732.
Martens, S., Fracchiolla, D., 2020. Activation and targeting of ATG8 protein lipidation. Cell Discov. 6, 1–11.
Martina, J.A., Diab, H.I., Brady, O.A., Puertollano, R., 2016. TFEB and TFE3 are novel components of the integrated stress response. EMBO J. 35, 479–495.
Matsumoto, G., Wada, K., Okuno, M., Kurosawa, M., Nukina, N., 2011. Serine 403 phosphorylation of p62/SQSTM1 regulates selective autophagic clearance of ubiquitinated proteins. Mol. Cell 44, 279–289.
McMahon, M., Itoh, K., Yamamoto, M., Hayes, J.D., 2003. Keap1-dependent proteasomal degradation of transcription factor Nrf2 contributes to the negative regulation of antioxidant response element-driven gene expression. J. Biol. Chem. 278, 21592–21600.
Meyer, H., Rape, M., 2014. Enhanced protein degradation by branched ubiquitin chains. Cell 157, 910–921.
Mijaljica, D., Devenish, R.J., 2013. Nucleophagy at a glance. J. Cell. Sci. 126, 4325–4330.
Milan, G., et al., 2015. Regulation of autophagy and the ubiquitin-proteasome system by the FoxO transcriptional network during muscle atrophy. Nat. Commun. 6.
Milani, M., et al., 2009. The role of ATF4 stabilization and autophagy in resistance of breast cancer cells treated with Bortezomib. Cancer Res. 69, 4415–4423.
Min, J.-N., et al., 2008. CHIP deficiency decreases longevity, with accelerated aging phenotypes accompanied by altered protein quality control. Mol. Cell. Biol. 28, 4018–4025.
Moreno-García, A., Kun, A., Calero, O., Medina, M., Calero, M., 2018. An overview of the role of Lipofuscin in age-related neurodegeneration. Front. Neurosci. 12, 464.
Morreale, F.E., Walden, H., Es, R., Ring, A., 2016. SnapShot: types of ubiquitin ligases. Cell 165, 248-248.e1.
Mukherjee, A., Morales-Scheihing, D., Butler, P.C., Soto, C., 2015. Type 2 diabetes as a protein misfolding disease. Trends Mol. Med. 21, 439–449.
Mukhopadhyay, D., Riezman, H., 2007. Proteasome-independent functions of ubiquitin in endocytosis and signaling. Science (80-.) 315, 201–205.
Murata, S., Minami, Y., Minami, M., Chiba, T., Tanaka, K., 2001. CHIP is a chaperone-dependent E3 ligase that ubiquitylates unfolded protein. EMBO Rep. 2, 1133–1138.
Murata, S., Takahama, Y., Kasahara, M., Tanaka, K., 2018. The immunoproteasome and thymoproteasome: functions, evolution and human disease. Nat. Immunol. 19, 923–931.
Myeku, N., et al., 2016. Tau-driven 26S proteasome impairment and cognitive dysfunction can be prevented early in disease by activating cAMP-PKA signaling. Nat. Med. 22, 46–53.
Nakamura, S., Yoshimori, T., 2017. New insights into autophagosome-lysosome fusion. J. Cell. Sci. 130, 1209–1216.
Nakatogawa, H., 2013. Two ubiquitin-like conjugation systems that mediate membrane formation during autophagy. Essays Biochem. 55, 39–50.
Napolitano, G., Ballabio, A., 2016. TFEB at a glance. J. Cell. Sci. 129, 2475–2481.
Nazio, F., et al., 2013. MTOR inhibits autophagy by controlling ULK1 ubiquitylation, self-association and function through AMBRA1 and TRAF6. Nat. Cell Biol. 15, 406–416.
Nazio, F., et al., 2016. Fine-tuning of ULK1 mRNA and protein levels is required for autophagy oscillation. J. Cell Biol. 215, 841–856.
Nemec, A.A., Howell, L.A., Peterson, A.K., Murray, M.A., Tomko, R.J., 2017. Autophagic clearance of proteasomes in yeast requires the conserved sorting nexin Snx4. J. Biol. Chem. 292, 21466–21480.
Nguyen, N.N., et al., 2019. Proteasome β5 subunit overexpression improves proteostasis during aging and extends lifespan in Drosophila melanogaster. Sci. Rep. 9, 1–12.
Obeng, E.A., et al., 2006. Proteasome inhibitors induce a terminal unfolded protein response in multiple myeloma cells. Blood 107, 4907–4916.
Pajares, M., et al., 2016. Transcription factor NFE2L2/NRF2 is a regulator of macroautophagy genes. Autophagy 12, 1902–1916.
Pandey, U.B., et al., 2007. HDAC6 rescues neurodegeneration and provides an essential link between autophagy and the UPS. Nature 447, 859–863.
Pankiv, S., et al., 2007. p62/SQSTM1 binds directly to Atg8/LC3 to facilitate degradation of ubiquitinated protein aggregates by autophagy. J. Biol. Chem. 282, 24131–24145.
Papandreou, M.E., Tavernarakis, N., 2019. Nucleophagy: from homeostasis to disease. Cell Death Differ. 26, 630–639.
Peng, J., et al., 2003. A proteomics approach to understanding protein ubiquitination. Nat. Biotechnol. 21, 921–926.
Peng, H., et al., 2017. Ubiquitylation of p62/sequestosome1 activates its autophagy receptor function and controls selective autophagy upon ubiquitin stress. Cell Res. 27, 657–674.
Petropoulos, I., et al., 2000. Increase of oxidatively modified protein is associated with a decrease of proteasome activity and content in aging epidermal cells. Journals Gerontol. - Ser. A Biol. Sci. Med. Sci. 55, 220–227.
Pickering, A.M., Davies, K.J.A., 2012. Differential roles of proteasome and immunoproteasome regulators Pa28αβ, Pa28γ and Pa200 in the degradation of oxidized proteins. Arch. Biochem. Biophys. 523, 181–190.
Pickering, A.M., et al., 2010. The immunoproteasome, the 20S proteasome and the PA28αβ proteasome regulator are oxidative-stress-adaptive proteolytic complexes. Biochem. J. 432, 585–594.
Pickering, A.M., Linder, R.A., Zhang, H., Forman, H.J., Davies, K.J.A., 2012. Nrf2-dependent induction of proteasome and Pa28αβ regulator are required for adaptation to oxidative stress. J. Biol. Chem. 287, 10021–10031.
Platta, H.W., Abrahamsen, H., Thoresen, S.B., Stenmark, H., 2012. Nedd4-dependent lysine-11-linked polyubiquitination of the tumour suppressor Beclin 1. Biochem. J. 441, 399–406.
Pohl, C., Dikic, I., 2019. Cellular quality control by the ubiquitin-proteasome system and autophagy. Science (80-.) 366, 818–822.
Pyo, J.O., et al., 2013. Overexpression of Atg5 in mice activates autophagy and extends lifespan. Nat. Commun. 4, 1–9.
Radhakrishnan, S.K., et al., 2010. Transcription factor Nrf1 mediates the proteasome recovery pathway after proteasome inhibition in mammalian cells. Mol. Cell 38, 17–28.
Raimondi, M., et al., 2019. USP1 (ubiquitin specific peptidase 1) targets ULK1 and regulates its cellular compartmentalization and autophagy. Autophagy 15, 613–630.
Raz, V., et al., 2017. Proteasomal activity-based probes mark protein homeostasis in muscles. J. Cachexia Sarcopenia Muscle 8, 798–807.
Reeg, S., Grune, T., 2015. Protein oxidation in aging: does it play a role in aging progression? Antioxid. Redox Signal. 23, 239–255.
Robida-Stubbs, S., et al., 2012. TOR signaling and rapamycin influence longevity by regulating SKN-1/Nrf and DAF-16/FoxO. Cell Metab. 15, 713–724.
Rodriguez, K.A., Gaczynska, M., Osmulski, P.A., 2010. Molecular mechanisms of proteasome plasticity in aging. Mech. Ageing Dev. 131, 144–155.
Rodriguez, K.A., Edrey, Y.H., Osmulski, P., Gaczynska, M., Buffenstein, R., 2012. Altered composition of liver proteasome assemblies contributes to enhanced proteasome activity in the exceptionally long-lived naked mole-rat. PLoS One 7.
Ronnebaum, S.M., Patterson, C., Schisler, J.C., 2014. Minireview: hey U(PS): metabolic and proteolytic homeostasis linked via AMPK and the ubiquitin proteasome system. Mol. Endocrinol. 28, 1602–1615.
Rousseau, A., Bertolotti, A., 2018. Regulation of proteasome assembly and activity in health and disease. Nat. Rev. Mol. Cell Biol. 19, 697–712.
Russell, R.C., et al., 2013. ULK1 induces autophagy by phosphorylating Beclin-1 and activating VPS34 lipid kinase. Nat. Cell Biol. 15, 741–750.
Saeki, Y., 2017. Ubiquitin recognition by the proteasome. J. Biochem. 161, 113–124.
Safdar, A., deBeer, J., Tarnopolsky, M.A., 2010. Dysfunctional Nrf2-Keap1 redox signaling in skeletal muscle of the sedentary old. Free Radic. Biol. Med. 49, 1487–1493.
Salminen, A., Kaarniranta, K., 2012. AMP-activated protein kinase (AMPK) controls the aging process via an integrated signaling network. Ageing Res. Rev. 11, 230–241.
Sánchez-Martín, P., Saito, T., Komatsu, M., 2019. p62/SQSTM1: 'Jack of all trades' in health and cancer. FEBS J. 286, 8–23.
Sánchez-Martın, P., Komatsu, M., 2018. p62/SQSTM1 – steering the cell through health and disease. J. Cell. Sci. 131.
Sancho, A., et al., 2012. Dor/tp53inp2 and tp53inp1 constitute a metazoan gene family encoding dual regulators of autophagy and transcription. PLoS One 7.
Scherz-Shouval, R., et al., 2007. Reactive oxygen species are essential for autophagy and specifically regulate the activity of Atg4. EMBO J. 26, 1749–1760.
Schneider, J.L., et al., 2015. Loss of hepatic chaperone-mediated autophagy accelerates proteostasis failure in aging. Aging Cell 14, 249–264.
Schwalm, C., et al., 2015. Activation of autophagy in human skeletal muscle is dependent on exercise intensity and AMPK activation. FASEB J. 29, 3515–3526.
Scrivo, A., Codogno, P., Bomont, P., 2019. Gigaxonin E3 ligase governs ATG16L1 turnover to control autophagosome production. Nat. Commun. 10, 1–14.
Sebastián, D., Palacín, M., Zorzano, A., 2017. Mitochondrial Dynamics: Coupling Mitochondrial Fitness with Healthy Aging. Trends Mol. Med. 23, 201–215.
Seglen, P.O., Gordon, P.B., 1982. 3-Methyladenine: specific inhibitor of autophagic/lysosomal protein degradation in isolated rat hepatocytes. Proc. Natl. Acad. Sci. 79, 1889–1892.
Seibenhener, M.L., et al., 2004. Sequestosome 1/p62 is a polyubiquitin chain binding protein involved in ubiquitin proteasome degradation. Mol. Cell. Biol. 24, 8055–8068.
Selimovic, D., et al., 2013. Bortezomib/proteasome inhibitor triggers both apoptosis and autophagy-dependent pathways in melanoma cells. Cell. Signal. 25, 308–318.
Sha, Y., Rao, L., Settembre, C., Ballabio, A., Eissa, N.T., 2017. STUB1 regulates TFEB -induced autophagy–lysosome pathway. EMBO J. 36, 2544–2552.
Sha, Z., Schnell, H.M., Ruoff, K., Goldberg, A., 2018. Rapid induction of p62 and GABARAPL1 upon proteasome inhibition promotes survival before autophagy activation. J. Cell Biol. 217, 1757–1776.
Shacka, J.J., et al., 2007. Cathepsin D deficiency induces persistent neurodegeneration in the absence of bax-dependent apoptosis. J. Neurosci. 27, 2081–2090.
Shi, C.S., Kehrl, J.H., 2010. TRAF6 and A20 regulate lysine 63-linked ubiquitination of Beclin-1 to control TLR4-induced Autophagy. Sci. Signal. 3, 1–10.
Shih, P.-H., Yen, G.-C., 2007. Differential expressions of antioxidant status in aging rats: the role of transcriptional factor Nrf2 and MAPK signaling pathway. Biogerontology 8, 71–80.
Silva, G.M., et al., 2012. Redox control of 20S proteasome gating. Antioxidants Redox Signal. 16, 1183–1194.
Simonsen, A., et al., 2008. Promoting basal levels of autophagy in the nervous system enhances longevity and oxidant resistance in adult Drosophila. Autophagy 4, 176–184.
Song, L., Luo, Z.Q., 2019. Post-translational regulation of ubiquitin signaling. J. Cell Biol. 218, 1776–1786.
Stolz, A., Ernst, A., Dikic, I., 2014. Cargo recognition and trafficking in selective autophagy. Nat. Cell Biol. 16, 495–501.
Strucksberg, K.H., Tangavelou, K., Schröder, R., Clemen, C.S., 2010. Proteasomal activity in skeletal muscle: a matter of assay design, muscle type, and age. Anal. Biochem. 399, 225–229.
Su, C.H., et al., 2011. Akt phosphorylation at Thr308 and Ser473 is required for CHIP-mediated ubiquitination of the kinase. Cell. Signal. 23, 1824–1830.

Suh, J.H., et al., 2004. Decline in transcriptional activity of Nrf2 causes age-related loss of glutathione synthesis, which is reversible with lipoic acid. Proc. Natl. Acad. Sci. U. S. A. 101, 3381–3386.
Sun, Q., et al., 2011. The RUN domain of Rubicon is important for hVps34 binding, lipid kinase inhibition, and autophagy suppression. J. Biol. Chem. 286, 185–191.
Sun, A., et al., 2017. The E3 ubiquitin ligase NEDD4 is an LC3-interactive protein and regulates autophagy. Autophagy 13, 522–537.
Tanaka, K., 2009. The proteasome: overview of structure and functions. Proc. Jpn. Acad. Ser. B Phys. Biol. Sci. 85, 12–36.
Tanida, I., et al., 2004. HsAtg4B/HsApg4B/autophagin-1 cleaves the carboxyl termini of three human Atg8 homologues and delipidates microtubule-associated protein light chain 3- and GABAA receptor-associated protein-phospholipid conjugates. J. Biol. Chem. 279, 36268–36276.
Tawo, R., et al., 2017. The ubiquitin ligase CHIP integrates proteostasis and aging by regulation of insulin receptor turnover. Cell 169, 470–482 e13.
Terman, A., Dalen, H., Brunk, U.T., 1999. Ceroid/lipofuscin-loaded human fibroblasts show decreased survival time and diminished autophagocytosis during amino acid starvation. Exp. Gerontol. 34, 943–957.
Tomaru, U., et al., 2012. Decreased proteasomal activity causes age-related phenotypes and promotes the development of metabolic abnormalities. Am. J. Pathol. 180, 963–972.
Tonoki, A., et al., 2009. Genetic evidence linking age-dependent attenuation of the 26S proteasome with the aging process. Mol. Cell. Biol. 29, 1095–1106.
Tsakiri, E.N., et al., 2013a. Proteasome dysfunction in Drosophila signals to an Nrf2-dependent regulatory circuit aiming to restore proteostasis and prevent premature aging. Aging Cell 12, 802–813.
Tsakiri, E.N., et al., 2013b. Differential regulation of proteasome functionality in reproductive vs. Somatic tissues of Drosophila during aging or oxidative stress. FASEB J. 27, 2407–2420.
Ulgherait, M., Rana, A., Rera, M., Graniel, J., Walker, D.W., 2014. AMPK modulates tissue and organismal aging in a non-cell-autonomous manner. Cell Rep. 8, 1767–1780.
Ustrell, V., Hoffman, L., Pratt, G., Rechsteiner, M., 2002. Pa200, a nuclear proteasome activator involved in DNA repair. EMBO J. 21, 3516–3525.
van Heemst, D., 2010. Insulin, IGF-1 and longevity. Aging Dis. 1, 147–157.
Vernace, V.A., Arnaud, L., Schmidt-Glenewinkel, T., Figueiredo-Pereira, M.E., 2007. Aging perturbs 26S proteasome assembly in Drosophila melanogaster. FASEB J. 21, 2672–2682.
VerPlank, J.J.S., Lokireddy, S., Zhao, J., Goldberg, A.L., 2019. 26S Proteasomes are rapidly activated by diverse hormones and physiological states that raise cAMP and cause Rpn6 phosphorylation. Proc. Natl. Acad. Sci. U. S. A. 116, 4228–4237.
VerPlank, J.J.S., et al., 2020. CGMP via PKG activates 26S proteasomes and enhances degradation of proteins, including ones that cause neurodegenerative diseases. Proc. Natl. Acad. Sci. U. S. A. 117, 14220–14230.
Vilchez, D., et al., 2012a. Increased proteasome activity in human embryonic stem cells is regulated by PSMD11. Nature 489, 304–308.
Vilchez, D., et al., 2012b. RPN-6 determines C. elegans longevity under proteotoxic stress conditions. Nature 489, 263–268.
Vitale, G., Pellegrino, G., Vollery, M., Hofland, L.J., 2019. ROLE of IGF-1 system in the modulation of longevity: controversies and new insights from a centenarians' perspective. Front. Endocrinol. (Lausanne) 10, 1–11.
Waite, K.A., De-La Mota-Peynado, A., Vontz, G., Roelofs, J., 2016. Starvation induces proteasome autophagy with different pathways for core and regulatory particles. J. Biol. Chem. 291, 3239–3253.
Wan, W., et al., 2018. mTORC1-regulated and HUWE1-Mediated WIPI2 degradation controls autophagy flux. Mol. Cell 72, 303–315 e6.
Wang, X., Yen, J., Kaiser, P., Huang, L., 2010. Regulation of the 26S proteasome complex during oxidative stress. Sci. Signal. 3 ra88–ra88.
Wang, X.J., et al., 2013. A novel crosstalk between two major protein degradation systems. Autophagy 9, 1500–1508.
Wang, X., et al., 2017. The proteasome-interacting Ecm29 protein disassembles the 26S proteasome in response to oxidative stress. J. Biol. Chem. 292, 16310–16320.
Wavre-Shapton, S.T., et al., 2015. Photoreceptor phagosome processing defects and disturbed autophagy in retinal pigment epithelium of Cln3Δex1-6 mice modelling juvenile neuronal ceroid lipofuscinosis (Batten disease). Hum. Mol. Genet. 24, 7060–7074.
Webb, A.E., Brunet, A., 2014. FOXO transcription factors: key regulators of cellular quality control. Trends Biochem. Sci. 39, 159–169.
Wu, W.K.K., et al., 2008. Induction of autophagy by proteasome inhibitor is associated with proliferative arrest in colon cancer cells. Biochem. Biophys. Res. Commun. 374, 258–263.
Wurzer, B., et al., 2015. Oligomerization of p62 allows for selection of ubiquitinated cargo and isolation membrane during selective autophagy. Elife 4, 1–28.
Xia, P., et al., 2013. WASH inhibits autophagy through suppression of Beclin 1 ubiquitination. EMBO J. 32, 2685–2696.
Xu, P., et al., 2009. Quantitative proteomics reveals the function of unconventional ubiquitin chains in proteasomal degradation. Cell 137, 133–145.
Xu, C., et al., 2014. Regulation of autophagy by E3 ubiquitin ligase RNF216 through BECN1 ubiquitination. Autophagy 10, 2239–2250.
Yang, Y., Klionsky, D.J., 2020. Autophagy and disease: unanswered questions. Cell Death Differ. 858–871. https://doi.org/10.1038/s41418-019-0480-9.
Youle, R.J., Narendra, D.P., 2011. Mechanisms of mitophagy. Nat. Rev. Mol. Cell Biol. 12, 9–14.
Zachari, M., Ganley, I.G., 2017. The mammalian ULK1 complex and autophagy initiation. Essays Biochem. 61, 585–596.
Zhang, H., et al., 2012. Nrf2-regulated phase II enzymes are induced by chronic ambient nanoparticle exposure in young mice with age-related impairments. Free Radic. Biol. Med. 52, 2038–2046.
Zhang, Y., et al., 2014. Rapamycin extends life and health in C57BL/6 mice. Journals Gerontol. - Ser. A Biol. Sci. Med. Sci. 69 A, 119–130.
Zhang, Z., et al., 2019. Redox signaling and unfolded protein response coordinate cell fate decisions under ER stress. Redox Biol. 25, 101047.
Zhao, J., et al., 2007. FoxO3 coordinately activates protein degradation by the autophagic/lysosomal and proteasomal pathways in atrophying muscle cells. Cell Metab. 6, 472–483.
Zhao, J., Zhai, B., Gygi, S.P., Goldberg, A.L., 2015. MTOR inhibition activates overall protein degradation by the ubiquitin proteasome system as well as by autophagy. Proc. Natl. Acad. Sci. U. S. A. 112, 15790–15797.
Zheng, N., Shabek, N., 2017. Ubiquitin ligases: structure, function, and regulation. Annu. Rev. Biochem. 86, 129–157.
Zhou, L., Zhang, H., Davies, K.J.A., Forman, H.J., 2018. Aging-related decline in the induction of Nrf2-regulated antioxidant genes in human bronchial epithelial cells. Redox Biol. 14, 35–40.
Zhu, K., Dunner, K., McConkey, D.J., 2010. Proteasome inhibitors activate autophagy as a cytoprotective response in human prostate cancer cells. Oncogene 29, 451–462.
Zmijewski, J.W., Banerjee, S., Abraham, E., 2009. S-glutathionylation of the Rpn2 regulatory subunit inhibits 26 S proteasomal function. J. Biol. Chem. 284, 22213–22221.

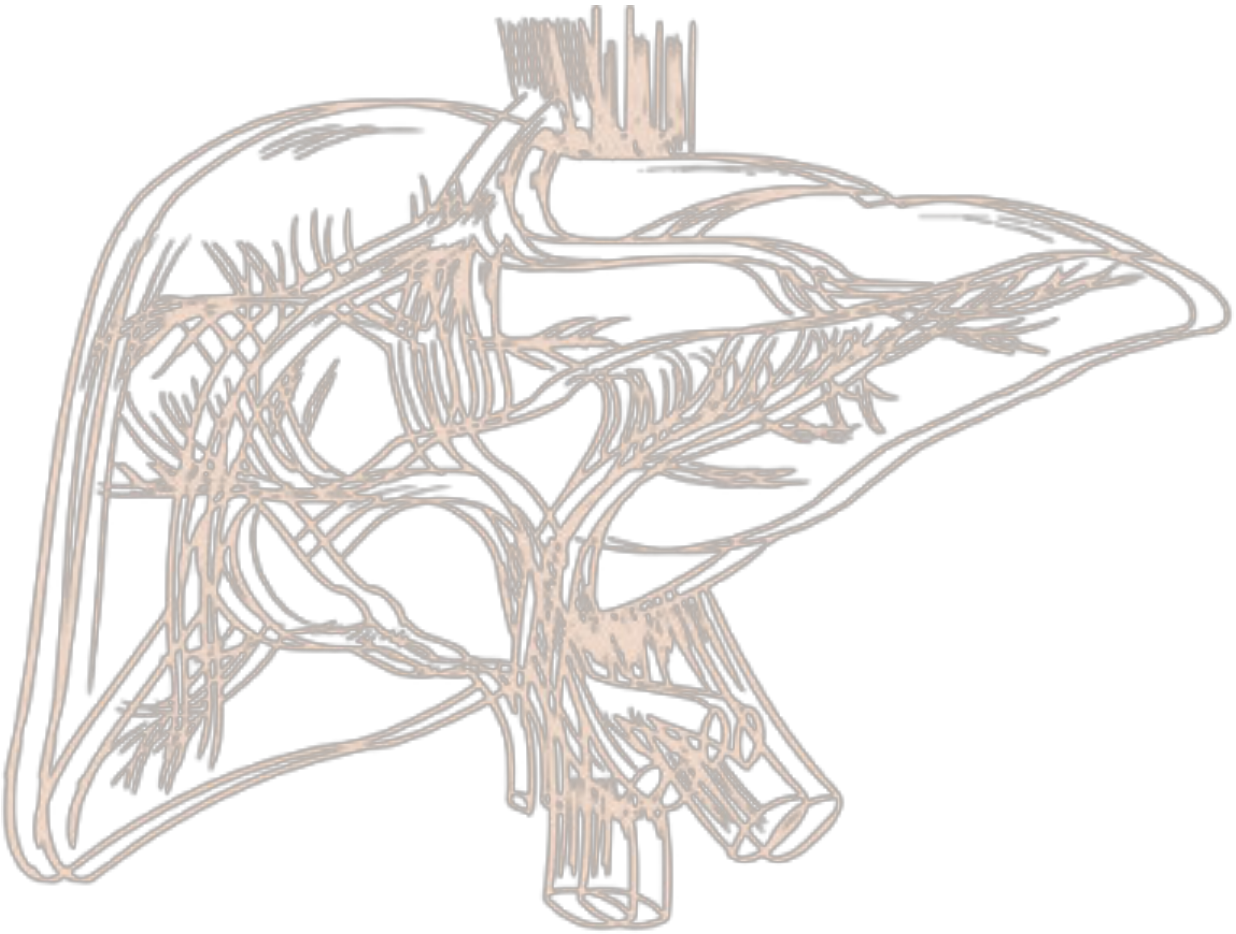

APPENDIX 3

Chem

CellPress

Article

Facilitated Diffusion of Proline across Membranes of Liposomes and Living Cells by a Calix[4]pyrrole Cavitand

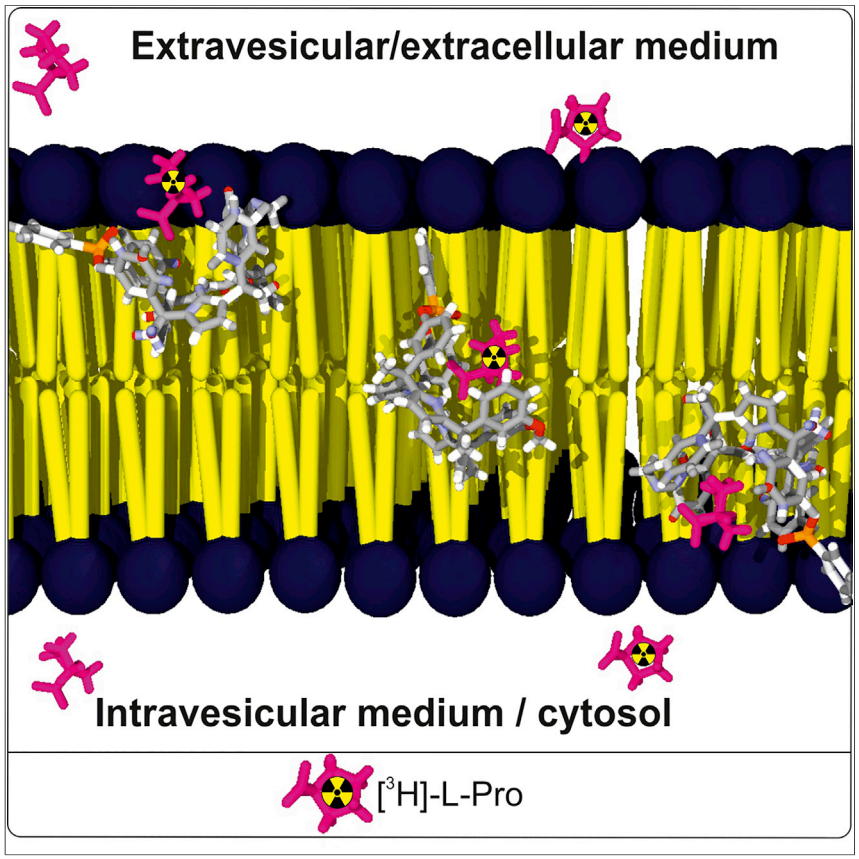

Few studies assess the amino acid transport properties of synthetic carriers using liposomal and cell membranes. Herein, we apply an optimized radiometric assay to demonstrate the selective transport of L-Pro across liposomal membranes by the means of a synthetic calix[4]pyrrole cavitand. Moreover, we show that the carrier also contributes to the overall uptake of L-Pro in HeLa cells. These unprecedented results augur well for the potential application of calix[4]pyrroles as therapeutic tools for L-Pro-dependent diseases, including some cancers and hyperprolinemia.

Luis Martínez-Crespo, Jia Liang Sun-Wang, Andres Felipe Sierra, ..., Paola Bartoccioni, Manuel Palacín, P. Ballester

manuel.palacin@irbbarcelona.org (M.P.)
pballester@iciq.es (P.B.)

HIGHLIGHTS

A calix[4]pyrrole transports amino acids across liposomal and cell membranes

Radiometric assays show L-Pro transport selectivity over other natural amino acids

The synthetic carrier contributes to the overall uptake of L-Pro in cultured cells

The synthetic carrier is not cytotoxic under transport conditions

Martínez-Crespo et al., Chem 6, 3054–3070
November 5, 2020
https://doi.org/10.1016/j.chempr.2020.08.018

CellPress

Chem

Article

Facilitated Diffusion of Proline across Membranes of Liposomes and Living Cells by a Calix[4]pyrrole Cavitand

Luis Martínez-Crespo,[1] Jia Liang Sun-Wang,[1,2,4] Andres Felipe Sierra,[1] Gemma Aragay,[1] Ekaitz Errasti-Murugarren,[2] Paola Bartoccioni,[2,3] Manuel Palacín,[2,3,4,*] and P. Ballester[1,5,6,*]

SUMMARY

The transport of anions and cations through liposomal membranes facilitated by synthetic carriers has been widely described. In contrast, analogous studies describing the facilitated transport of amino acids (aa) are scarce. We describe the use of calix[4]pyrrole receptors as synthetic carriers for the facilitated diffusion of aa across membranes of liposomes and living cells. We demonstrate that a calix[4]pyrrole cavitand is highly effective and selective for the facilitated diffusion of L-proline (L-Pro). We propose a mobile carrier diffusion mechanism to explain the observed aa facilitated diffusion process. The transport process involves the formation of a 1:1 complex between the carrier and the aa (e.g., L-Pro⊂1). We also describe the unprecedented application of a synthetic carrier to contribute to the uptake of L-Pro in human cells in addition to that mediated by the natural transporters. The reported results augur well for the potential use of aa synthetic carriers in therapeutic applications.

INTRODUCTION

Cell membranes are selectively permeable to the passage of biologically relevant polar molecules, either neutral or charged, as well as simple monoatomic ions. The reduced solubility of these compounds in the hydrophobic core of the membrane is responsible for its impermeability. The low solubility also translates to reduced rates for their passive diffusion through phospholipid bilayers in living cells and liposomes.[1] As the transport of neutral and charged molecules, as well as small ions, across cell membranes, plays a crucial role in the metabolism energetics and cell signaling of living organisms, it demands the existence of specific carrier and channel proteins to regulate this process. Missing or defective endogenous carriers and channels underlie a number of human diseases, such as cystic fibrosis (Cl^- transport deficiency)[2] or primary inherited aminoacidurias (defects in the renal absorption of amino acids)[3,4] among many others. On the one hand, the development of synthetic molecules, aka carriers, that are able to facilitate the transport of biologically relevant molecules and ions across liposomal membranes is an important goal in supramolecular chemistry. On the other hand, it also constitutes a sensible approach with therapeutic potential in the treatment of the diseases mentioned above.

Many examples of synthetic carriers able to transport monoatomic anions and cations through synthetic lipid membranes and living cell membranes can be found in literature.[5–9] In contrast, the number of reports describing the facilitated transport of amino acids (aa) across lipid bilayers using synthetic carriers is scarce.[10,11] Most of

The Bigger Picture

Important diseases in the modern society, including cancer, aminoacidurias, and neurodegenerative disorders, might be provoked by missing or defective amino acid transporters at the cell membrane. Synthetic receptors capable of transporting amino acids across cell membranes could serve as therapeutic tools to tackle these diseases. To date, few studies concerning synthetic transporters of amino acids were performed using liposomal membranes. Moreover, as far as we are aware, there are no literature precedents reporting the amino acid transport properties of synthetic receptors through membranes of living cells. This work describes the use of a calix[4]pyrrole-based synthetic carrier for the facilitated transport of amino acids across the membranes of liposomes. It also represents the first account reporting the ability of a synthetic carrier to contribute to the L-Pro influx of living cells.

the reported examples describing synthetic carriers able to mediate the transport of aa across lipophilic membranes are based on the results of U-tube transport experiments. In these types of experiments, a non-polar organic solvent i.e., $CHCl_3$ is used to mimic a lipophilic bilayer.[12,13] Nevertheless, the potential biological/therapeutic application of any developed synthetic aa carrier demands the assessment of its transport activity in synthetic liposomes and living cells.

An early example of the facilitated diffusion of aa across lipophilic bilayers was reported by Stillwell.[14] This work demonstrated that the uptake of aa into lipid vesicles could be stimulated by the formation of an imine between the primary amine of the aa and several water-soluble aldehydes. A few years later, Sunamoto et al., reported the first example of a photo-responsive spiropyran-based synthetic carrier that mediated the efflux of phenylalanine from the interior of a liposome to the extravesicular media.[15] The authors attributed the facilitated transport to the formation of a 1:1 complex between the zwitterionic forms of both the merocyanine-isomer of the carrier and the phenylalanine, which increased the solubility of the latter in the lipophilic membrane. The amount of extravesicular aa was quantified using a fluorescent assay involving the reaction of fluorescamine with the primary amine of the effluxed aa.

More recently, the groups of Hou and Gale published two elegant contributions describing the facilitated diffusion of aa through lipid bilayers. Remarkably, the two reported approaches are substantially different.[10,11] On the one hand, Hou and co-workers demonstrated that peptide-appended pillar[n]arenes (n=5,6) function as artificial channels facilitating aa transport across liposomal membranes.[10] Their assessment of the transport activity of the synthetic channels relied on the quantification of the concentration of extravesicular aa (i.e., efflux experiments) also using the fluorescamine method. The reported transport activities were derived from the ratio of transport rate constants measured in the presence and absence of the synthetic channel. Liposomes embedding the more active tubular channel showed a 3-fold increase in transport activity for the polar glycine (Gly) compared with the liposomes lacking the artificial channel.

On the other hand, Gale and co-workers described a dynamic covalent approach for the facilitated transmembrane transport of aa.[11] They showed that the combination of squaramide **6** (Figure 1) with the lipophilic and electrophilic aldehyde **7** (Figure 1) produced a synergistic effect on the transport of Gly across liposomal membranes. The facilitated transport of Gly was proposed to derive from the assembly of a three-component hydrogen-bonded complex involving the two NHs of the squaramide and the carboxylate group (COO^-) of the Gly imine or hemiaminal. In turn, the imine or hemiaminal of Gly resulted from the reaction of its primary NH_2 groups with the carbonyl of the aldehyde (Figure 1). The authors also developed a new fluorescent assay based on liposomes entrapping a calcein-Cu^{2+} complex to measure the Gly influx.

It is rather complex to compare the transport effectiveness of the two approaches described above for Gly. Not only are the experimental conditions of the transport experiments different (influx versus efflux) but also the quantification methods.

The examples of facilitated transport of aa described above used fluorescence spectroscopy to assess the intravesicular or extravesicular aa concentrations after efflux or influx processes. Notwithstanding that fluorescence assays are highly valuable and easy to implement in the laboratory for quantitative kinetic studies, they are

[1]Institute of Chemical Research of Catalonia (ICIQ), Barcelona Institute of Science and Technology (BIST), Avgda. Països Catalans 16, 43007 Tarragona, Spain

[2]Institute for Research in Biomedicine, Barcelona Institute of Science and Technology (BIST), Barcelona, Spain

[3]Centro de Investigación Biomédica en Red de Enfermedades Raras (CIBERER), 08028 Barcelona, Spain

[4]Department of Biochemistry and Molecular Biomedicine, Faculty of Biology, University of Barcelona, 08028 Barcelona, Spain

[5]ICREA, Pg. Lluís Companys, 23, 08018-Barcelona, Spain

[6]Lead Contact

*Correspondence: manuel.palacin@irbbarcelona.org (M.P.), pballester@iciq.es (P.B.)

https://doi.org/10.1016/j.chempr.2020.08.018

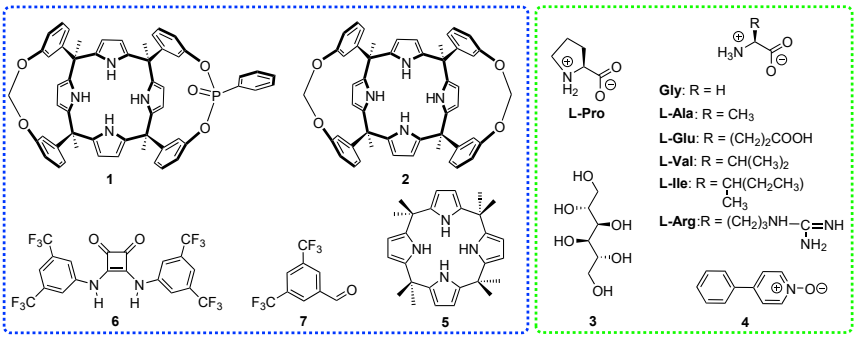

Figure 1. Molecular Structures of Synthetic Carriers and Substrates

Molecular structures of the synthetic carriers (blue box) and the substrates (green box) used in this work.

prone to significant errors caused by unspecific transport of other species. Radiotracer assays have been shown to be very useful in determining the kinetics of influx and efflux processes of biologically relevant molecules across liposomal membranes and living cell membranes.[16–18] Their implementation requires the use of dedicated laboratories, the safe handling, and disposal of used hazardous radioisotopes, and time-consuming autoradiographic treatments. However, all these shortcomings and limitations are compensated by the unequivocal molecular identification of the species responsible for the radiation level.

We reported that "two walls" and "four walls" calix[4]pyrroles are effective carriers of mono- and polyatomic anions through phospholipid membranes.[19,20] It is worth noting that the different substitutions at the meso-aromatic panels of the calix[4]pyrrole resulted in a dramatic change of the anion transport activity. Moreover, we and others have shown that α,α,α,α-isomers of aryl-extended calix[4]pyrroles and their cavitand derivatives are able to bind small polar molecules in aqueous and organic solutions with high efficiency and significant selectivity.[21–23] In this regard, we reported that the mono-phosphonate bridged calix[4]pyrrole cavitand **1** was an effective receptor for creatinine binding in CD_2Cl_2 solution (Figure 1).[24] Remarkably, simple molecular modeling studies revealed that L-Pro was also a good fit in terms of shape, size, and functional groups complementary with the binding site provided by cavitand **1**. For this reason and given our previous experience in the pre-insertion of calix[4]pyrroles carriers in liposomal membranes, we decided to undertake the evaluation of the mono-phosphonate calix[4]pyrrole cavitand **1** as an aa transporter.

Facilitating L-Pro transport with synthetic carriers is relevant in the context that recent reports identified the important role of intracellular concentration of L-Pro in the tumorigenic potential[25] and metastasis formation[26] of some cancer cells. The development of synthetic carriers selective to L-Pro transport might be exploited as therapeutic tools in some cancers as well as in other inherited deficiencies related to L-Pro metabolism in cells, such as hyperprolinemia type I and type II.[25]

Herein, we describe our results to facilitate the liposomal membrane transport of aa using pre-inserted cavitand **1**. We used optimized radiometric assays for the assessment of the aa concentration in influx and efflux experiments. The used assay is derived from those employed in transport studies of aa with natural transport proteins.[27,28] The developed radiometric assay reduces the risk of false-positive responses and low reproducibility that we encountered when using the fluorescent labeling methods reported in literature. We found that cavitand **1** selectively

facilitated the transport of L-Pro. In addition, we propose a carrier-facilitated transport mechanism involving the formation of a 1:1 Pro⊂**1** inclusion complex for the process. We also discovered that calix[4]pyrrole cavitand **1** is more efficient in facilitating the diffusion of L-Pro than the analog cavitand **2**, lacking the phosphonate group, or the octamethyl calix[4]pyrrole **5**, deprived from an aromatic cavity (Figure 1). The transport activity of **1** for L-Pro seems to be on par with that determined for a supramolecular system described by Gale.[11] However, none of the previously described amino acid synthetic carriers showed selectivity for L-Pro transport.

Finally, we also studied the facilitated transport of L-Pro in human HeLa cells by embedding the calix[4]pyrrole cavitand **1** in liposomes. The obtained results suggest that cavitand **1** increases the L-Pro uptake of the cells at high extracellular substrate concentrations (i.e., 20 mM).

RESULTS AND DISCUSSION

First, we evaluated the affinity of cavitand **1** toward a reduced set of natural aa in CD_2Cl_2 solution. Owing to the low solubility of natural aa in CD_2Cl_2 solution, we performed a series of solid-liquid extraction experiments. Thus, we added an excess of the solid amino acid (L-Pro, L-Ala, Gly, L-Glu, L-Arg, L-Val, and L-Ile) to separate CD_2Cl_2 solutions of cavitand **1** at mM concentration. After shaking the resulting suspension for 5 min, the solid was filtered off and the resulting solution was analyzed by ^{1}H NMR spectroscopy. Remarkably, only the extraction experiment of L-Pro produced significant changes in the ^{1}H NMR spectrum of **1** (Figures S1 and S2). We observed a single set of proton signals for the receptor that was assigned to the bound cavitand **1**. The pyrrole NH's moved downfield compared with those in free **1** ($\Delta\delta \sim 2.5$ ppm). This observation indicated their involvement in hydrogen-bonding interactions. We also detected five new broad signals resonating at δ = 0.15, 0.97, 1.40, 1.72, 2.71 ppm that were assigned to the protons of L-Pro bound in the aromatic cavity of **1** (Figure S1h). The integrals of the proton signals of bound **1** and included L-Pro assigned a 1:1 stoichiometry to the complex. Taken together, these results indicated that cavitand **1** extracted 1 equiv of L-Pro to CD_2Cl_2 solution forming a deep inclusion complex for which we estimated a K_a (L-Pro⊂**1**) > 10^6 M^{-1}.[29]

Gratifyingly, single crystals of the L-Pro⊂**1** complex suitable for X-ray diffraction grew from vapor diffusion of pentane into a dichloromethane solution of the complex. The X-ray structure of the L-Pro⊂**1** complex (Figure 2) revealed that L-Pro is deeply included in the aromatic cavity of **1**. In the L-Pro⊂**1** complex, four hydrogen-bonding interactions are established between the pyrrole NHs of **1** and the oxygen atoms of the carboxylate group of L-Pro. In addition, the oxygen atom of the P=O group at the upper rim of the cavitand **1** has one additional ionic hydrogen bond with the protonated amino group of L-Pro.

^{13}C(1)-Proline Transport Experiments Monitored by ^{13}C NMR Assays

Evidence of L-Pro transport facilitated by cavitand **1** was initially derived from a ^{13}C NMR assay.[30] We prepared large unilamellar and multilamellar liposomes (mean diameter ~ 800 nm) of egg-yolk phosphatidylcholine (EYPC) loaded with a buffered solution of L-Pro (e.g., 200 mM L-Pro, 10 mM HEPES, pH 7.4). We suspended the prepared liposomes in an isosmotic medium containing ^{13}C-labeled L-Pro (^{13}C(1)-L-Pro, 200 mM) and stirred the mixture for 60 min. The ^{13}C NMR spectrum of the suspension showed a single sharp signal resonating at δ = 175.8 ppm. We assigned this sharp signal to the ^{13}C in the carbonyl carbon atom (^{13}C(1)) of both extravesicular and intravesicular, if any, enriched L-Pro. Next, we added an aqueous solution of

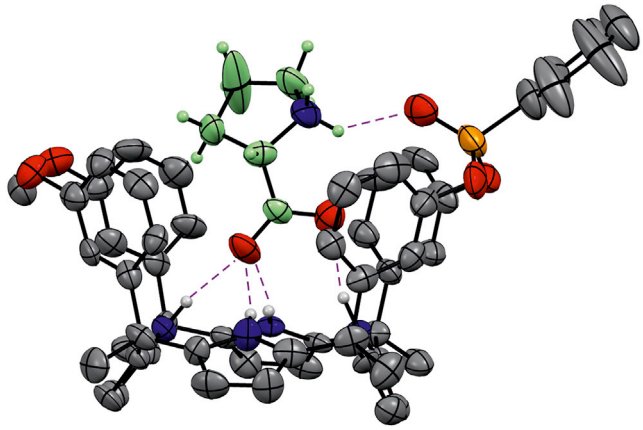

Figure 2. X-Ray Crystal Structure of the L-Pro⊂1 Complex
Thermal ellipsoids set at 50% probability; the H atoms of the Pro guest are shown as spheres of 0.3 Å. L-Pro and its C and H atoms shown in light green. Purple dashed lines indicate H-bond interactions. The non-polar hydrogen atoms of cavitand **1** are omitted for clarity.

paramagnetic Mn^{2+} (1 mM $MnSO_4$) in order to induce a selective broadening of the ^{13}C signal of extravesicular enriched L-Pro and acquired a new ^{13}C NMR spectrum of the resulting suspension.[30] The obtained results show that for liposomes not embedding the transporter, there is a slow diffusion of L-Pro reflected by a small signal of $^{13}C(1)$ corresponding to the intravesicular, unaffected $^{13}C(1)$-L-Pro resonating at δ = 175.8 ppm (Figure 3C-left panel). Not surprisingly, the liposomal membrane is impermeable to the paramagnetic Mn^{2+}. We performed analogous experiments using liposomes containing **1** embedded in their membranes (0.1 % carrier/EYPC molar ratio [mr]). In this case, we observed an enhancement of the $^{13}C(1)$ signal of intact, intravesicular $^{13}C(1)$-L-Pro after the Mn^{2+} addition (Figure 3D-left panel). We ascribe this result to the facilitated diffusion of L-Pro mediated by carrier **1**. The subsequent lysis of the liposomes, induced by the addition of a detergent, produced the broadening of the residual sharp signal resonating at δ = 175.8 ppm because the Mn^{2+} can now interact with all $^{13}C(1)$-L-Pro molecules (Figure 3F-left panel).

The increase in the concentration of **1** embedded in the phospholipid membrane (i.e., 0.1% to 1% mr **1**:EYPC) did not provoke significant changes in the ^{13}C NMR spectra of the liposomes registered after Mn^{2+} addition (Figures 3D and 3E -left panel). Most likely, at 0.1% mr of **1**, the equilibrium between intra- and extravesicular concentrations of $^{13}C(1)$-L-Pro is reached after the 60 min delay used for monitoring the transport experiments.

We performed analogous transport experiments using L-alanine enriched with ^{13}C in the carbonyl carbon atom ($^{13}C(1)$-L-Ala) (Figure 3-right panel). We selected L-Ala as an example of non-cyclic α-amino acid, which was not quantitatively extracted by cavitand **1** in the solid-liquid extraction experiments (Figure S1B). Interestingly, we observed that the transport of L-Ala was facilitated only when **1** was embedded in the liposomes at 1% mr (**1**:EYPC) (Figure 3E-right panel). The ^{13}C NMR spectra of the suspensions of the liposomes registered after the addition of Mn^{2+} without embedded carrier or with carrier 1 embedded at 0.1% mr are identical (Figures 3C and 3D -right panel). The similar intensities of the sharp ^{13}C NMR signals for the intravesicular $^{13}C(1)$ of the aa in L-Ala and L-Pro transport experiments of liposomes lacking the embedded carrier indicate that the two aa feature similar passive diffusion rates across the membrane. The larger efficiency of **1** in facilitating the transport

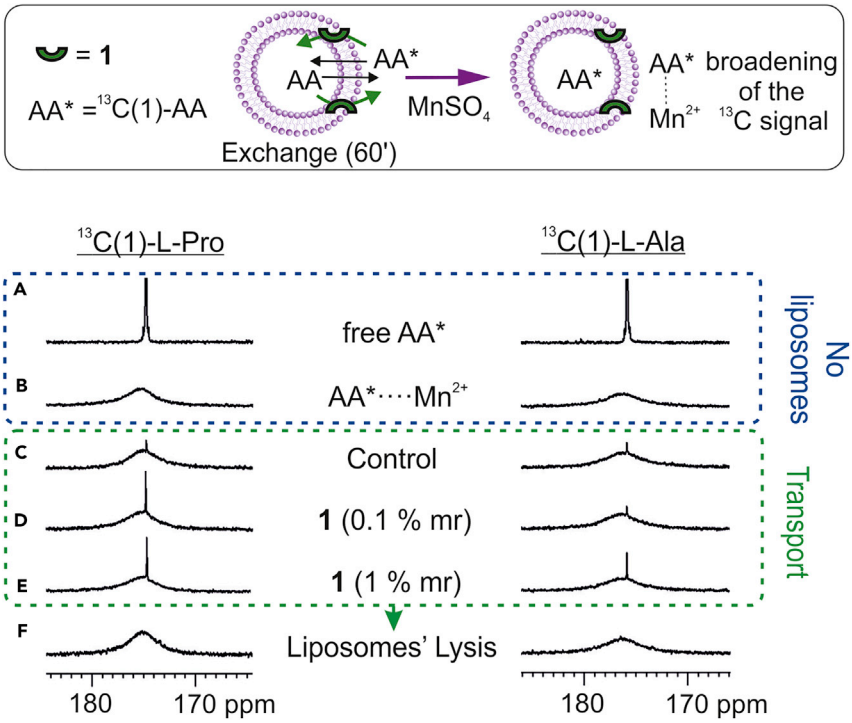

Figure 3. Monitoring the aa Transport by ^{13}C NMR

(A and B) (Top) Schematic representation of the ^{13}C NMR assay used to monitor aa transport. (Bottom) Blue box: ^{13}C NMR spectra of $^{13}C(1)$-L-Pro (left) and $^{13}C(1)$-L-Ala (right) in 9:1 H_2O:D_2O before (A) and after (B) the addition of $MnSO_4$.

(C–E) Green box: ^{13}C NMR spectra of EYPC liposomes in 9:1 H_2O:D_2O with different carrier mr (0 C, 0.1% D, and 1% E): the spectra were acquired after 60 min of aa transport time and following the addition of $MnSO_4$.

(F) ^{13}C NMR spectra registered after the lysis of the liposomes used for the transport experiment of L-Pro (left) and L-Ala (right) by the addition of detergent. Initial conditions: intravesicular (L-Pro (left panel) or L-Ala (right panel) 200 mM, HEPES 10 mM, pH 7.4); extravesicular ($^{13}C(1)$-L-Pro (left) or $^{13}C(1)$-L-Ala (right) 200 mM and HEPES 10 mM, pH 7.4).

of L-Pro correlates well with the extraction properties derived from the solid-liquid experiments.

Quantification of the Amino Acid Transport Efficiency and Kinetics across Liposomal Membranes Embedding Calix[4]Pyrrole Cavitand 1

The above NMR studies are not suitable for quantitative kinetic studies of the transport process owing to their long acquisition times. Thus, we assessed the transport kinetics using [^3H] radiolabeled aa. In a typical influx experiment (see Experimental Procedures section and Supplemental Information), liposomes were incubated with unlabeled aa (i.e., L-Pro unless indicated otherwise) with a trace of the radiolabeled aa. At the desired times, transport was stopped by adhering liposomes to nitrocellulose filters and washed in ice-cooled buffer and the trapped radioactivity counted.

The control time course curve of an L-Pro influx experiment using liposomes lacking the embedded synthetic carrier is shown in Figure 4A as a dashed gray line. The curve shows a reduced slope indicative of a slow rate for the passive diffusion of the amino acid across the liposomal membrane (~20 pmol in 60 min) (Figure 4A). When carrier **1** is embedded into the liposomal membrane (0.1% mr) the rate of the L-Pro influx increases significantly (up to ~100 pmol in 60 min) (Figure 4A

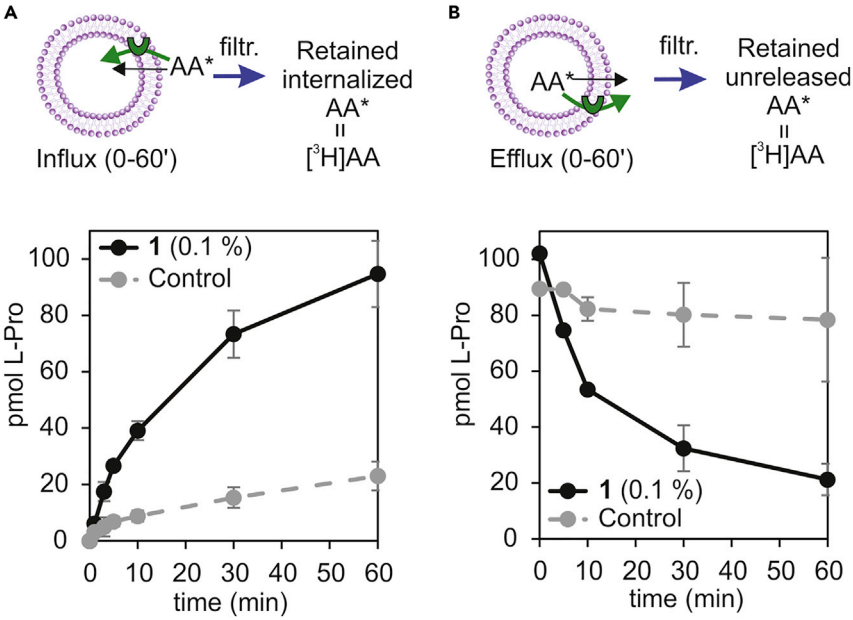

Figure 4. Influx and Efflux Radiometric Assay

(A and B) Upper panel: schematic representations of the influx (A) and efflux (B) kinetic experiments of L-Pro transport across liposomal membranes quantified using radiometric assays. The black arrows indicate L-Pro transport due to passive diffusion and green arrows facilitated transport of L-Pro through carrier **1**. Lower panel: time course curves (solid black lines) corresponding to the influx (A) and efflux (B) experiments of L-Pro using liposomes incorporating **1** (0.1% mr) within the membrane. In both cases, the L-Pro values (pmol) are calculated as the average of three different experiments and the error bars correspond to the standard deviation. The slashed time course curves in gray correspond to L-Pro transport due to passive diffusion. The black time course curves represent L-Pro total transport (diffusion + facilitated transport).

continuous black line), supporting that the transport of L-Pro across the lipid bilayer is facilitated by carrier **1**. After 60 min of transport, the ratio of the amount (pmols) of L-Pro present in the liposomes having embedded the carrier at 0.1% mr with that of the liposomes lacking the carrier was used to quantify the transport efficiency of **1**. This ratio assigns a 5-fold increase of the facilitated transport compared with the simple passive diffusion of the aa through the membrane. This result is consistent with the data obtained using the ^{13}C NMR spectroscopy assay (Figure 3).

To analyze the integrity and permeability of the liposomal bilayer upon inserting carrier **1**, we performed transport experiments using [^{14}C]-D-mannitol **3** (Figure 1) as a model system of a polar compound that should be membrane impermeable (Figure S3). We did not observe noticeable differences in the influx transport experiments of D-mannitol using liposomes embedding carrier **1** at 1% mr and control liposomes lacking the carrier. In all transport experiments, at 60 min the amount of D-mannitol present in the liposomes was ~10 pmol. The results support that the liposomal membrane integrity is not significantly altered by the insertion of carrier **1** and that the carrier does not facilitate the transport of D-mannitol **3**. Likewise, the reduced amount of D-mannitol present in the liposomes at the end of the transport experiments is indicative of a slower passive diffusion of the saccharide compared with the aa.

Next, we monitored efflux transport experiments of radiolabeled [^{3}H]-L-Pro by slightly modifying the radiotracer assay used in the influx counterparts. The efflux experiments aimed at supporting that activity of carrier **1** worked in the two senses of

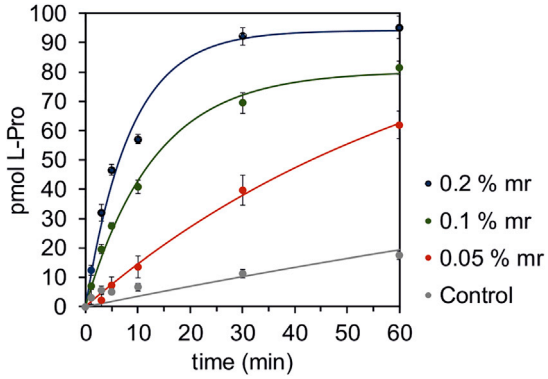

Figure 5. L-Pro Influx Transport Experiments at Different Carrier:Lipid Molar Ratio

Non-linear fits (curves) of the experimental data of L-Pro influx transport experiments (points) obtained at different carrier:lipid % mr (0%, 0.05% red, 0.1% green and 0.2% blue mr) to the theoretical kinetic model of a reversible first-order reaction. In all cases, the L-Pro values were calculated as the average of three different transport experiments replicates and the error bars correspond to the standard deviation.

the transport process (Figure 4B). For these experiments, liposomes (with and without embedded carrier **1**) were loaded with a buffered solution of the radiotracer (100 mM of NaCl, 10 mM HEPES, pH 7.4, 100 μM of L-Pro, and 20.8 μCi/mL [^{3}H]-L-Pro) (see Experimental Procedures section). An aliquot of the liposomes containing the tracer aa (24 μL) was diluted in an identical buffer solution (180 μL) (100 mM of NaCl and 10 mM HEPES, pH 7.4) not containing the aa. The aa efflux was monitored by quantifying the residual ^{3}H activity level present in the liposomes at the indicated times. The obtained results indicated that liposomes with carrier **1** embedded in their membranes experienced a faster efflux of the aa (~80 pmol L-Pro in 60 min) compared with the control counterparts (~10 pmol L-Pro in 60 min) (Figure 4B).[31]

Having demonstrated the facilitated transport of L-Pro in liposomes with carrier **1** embedded, we assessed the transport kinetics at different concentrations of the carrier (Figure 5). It is worth to note that, after 60 min of transport, a similar amount of L-Pro (~80–100 pmol) was present in the liposomes with 0.2% and 0.1% mr of **1**. This value (~80–100 pmol of L-Pro) also coincided with the initial value of L-Pro in the radiometric efflux experiments (Figure 4B). Most likely, this is the equilibrium amount of L-Pro present in the prepared volume of liposomes under the described experimental conditions.

We performed a non-linear fitting of the experimental time course curves obtained in the L-Pro influx experiments with liposomes embedding different concentrations of the carrier to a kinetic model for a reversible first-order reaction. This approach to analyzing influx kinetic data was previously described in the literature.[32,33] The fits of the experimental data to the theoretical model were consistent, allowing us to derive apparent rate constant values (k) for the L-Pro influx experiments (Figure 5, see Supplemental Information for details). Not surprisingly, we found that the rate constant values increased linearly with the carrier concentration ($k = 2.4 \times 10^{-4}$ s^{-1}, 1.3×10^{-3} s^{-1}, and 2.0×10^{-3} s^{-1} for 0.05, 0.1%, and 0.2% mr, respectively). The transport rate constant using liposomes lacking the carrier was determined as $k_0 = 6.7 \times 10^{-5}$ s^{-1}. Hou and co-workers defined the transport activity (A) of their channels at a certain concentration, as the ratio between the transport rate constant (in the presence of transporter) and that of the passive diffusion (in the absence of

transporter) ($A = k/k_0$). Remarkably, the synthetic artificial channels reported by Hou and co-workers also showed a linear dependence of A with the mr of the transporter at low transporter concentrations (i.e., channel:lipid mr < 0.2%).[10] They calculated a maximum of a 3-fold increase in activity, A, for the facilitated passive transport of Gly for a 0.05 % channel:lipid mr. Remarkably, using calix[4]pyrrole cavitand **1** we obtained a 4-fold increase in transport activity using a 0.05 % carrier **1**:EYPC mr and we reached a 30-fold increase in A using a 0.2% **1**:EYPC mr.

The effect of the extravesicular concentration of L-Pro (10–10^4 μM) in the transport efficiency of **1** was studied at a fixed transport time (i.e., 180 s; i.e., linear conditions of transport in this time period). We observed a linear relationship between the amount of L-Pro present in the liposomes at t = 180 s and the used extravesicular concentration of L-Pro up to 10,000 μM concentration (Figure S4).

In short, the analysis of the kinetic data for the influx transport experiments performed at different concentrations of carrier **1** and L-Pro hinted to the existence of linear relationships between both concentrations of the embedded carrier (**1**) and extravesicular aa (L-Pro) and the influx rates of the aa in the liposomes. This result demonstrates that carrier **1** did not reach saturation kinetics in the range of the studied concentration.

Considering the reduced size of the molecular structure of carrier **1** (14 × 10 Å, Figure S5)[34] compared with the thickness of the liposomal membrane (>30 Å) we favor a mobile carrier mechanism for the facilitated diffusion process of L-Pro by **1** than cavitand **1** behaving as an artificial channel. In nature, carrier diffusion proteins typically display a maximum value of rate transport owing to saturation of the binding sites of the carrier (saturation kinetics). Most likely, the non-saturation kinetics observed for **1** are related to the low binding constant L-Pro⊂**1** complex when formed in the liposomal membranes.[26]

Transport Studies of L-Pro in the Presence of a Competitive Binding Guest for Carrier 1

To further demonstrate the role of **1** as a carrier for the facilitated transport of L-Pro, we performed transport experiments in the presence of a competitive binding guest.

Pyridine *N*-oxides are known to form thermodynamically and kinetically highly stable complexes with aryl-extended calix[4]pyrroles ($K > 10^4\ M^{-1}$) in polar and non-polar organic solvents and water.[21,35] We performed influx transport experiments of L-Pro in the presence of increasing concentrations of 4-phenylpyridine *N*-oxide **4** (0–100 μM) in the extravesicular transport buffer (Figure 1). We used freshly prepared liposomes with 0.1% mr of embedded carrier 1. In all transport experiments, the extravesicular concentration of L-Pro (100 μM) was maintained constant (Figure S6). For each transport experiment at different *N*-oxide concentrations, we performed control experiments with liposomes lacking carrier **1**. The value of the amount of L-Pro obtained in the control experiments was subtracted from that obtained in the experiments with liposomes having **1** embedded. The subtracted value of L-Pro (pmol) was used to assess the magnitudes of the effective competitive transport (ECT). We defined ECT to be the ratio between the amounts of L-Pro present in the liposomes at the end of two different transport experiments. In one of them, we used extravesicular buffer containing a defined concentration of the *N*-oxide. In the other, the extravesicular buffer did not contain the *N*-oxide. Consequently, an ECT value of 1 indicates that the competing guest has no effect on the transport experiment. The obtained data are graphically represented in Figure 6. Interestingly, an increase in

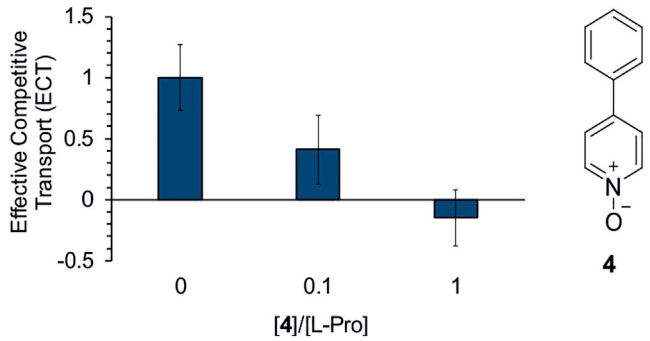

Figure 6. Effective Competitive Transport

ECT of **1** (0.1% mr) in the presence of 4-phenylpyridine-*N*-oxide **4** as a competitive guest. Transport was measured at a fixed transport time (180 s) with an extravesicular concentration of L-Pro 100 μM with and without the carrier at different concentrations of *N*-oxide (0, 10, and 100 μM). The ECT (see main text for details) in the absence of **4** was set to be equal to 1. The ECT values were calculated as the average of three transport experiments replicates. The error bars correspond to the propagated errors from the standard deviation values.

the concentrations of the *N*-oxide **4** produced a sensitive reduction in ECT value. Most likely, the *N*-oxide **4** preferentially diffuses into the liposomal membrane. There, it competes with L-Pro for the binding site of the embedded carrier **1** (**4**⊂**1** versus L-Pro⊂**1** complex). This binding competition effectively reduces the amount of carrier **1** available to facilitate the transport of L-Pro, resulting in the observed decrease of L-Pro present in the liposomes at the end of the transport experiment.

Studies of the aa Transport Selectivity of Carrier 1

We also undertook influx transport experiments of L-Ala with liposomes embedding carrier **1** at two different concentrations (0.1% and 1% mr; Figure S7). We measured almost identical quantities of L-Ala present in control liposomes (no carrier) and liposomes with 0.1% mr of embedded carrier **1**. Increasing the **1**/EYPC molar ratio to 1% provoked a significant increase in the quantity of L-Ala present in the liposomes (influx). This observation is in line with the transport results obtained using the ^{13}C NMR assay (Figure 3, bottom). Most likely, the observed selectivity is due to the better fit in terms of shape, size, and functional groups of the L-Pro within the cavity of the calix[4]pyrrole receptor.

In addition to L-Pro and L-Ala, the ability of carrier **1** to transport other natural aa (L-Glu, L-Arg, Gly, L-Val, and L-Ile) was also studied using the radiometric influx assay and liposomes having a 0.1% mr concentration of embedded carrier **1**. We defined the transport selectivity of the carrier for each aa as the ratio between the amount (pmols) of aa transported in the liposomes embedding carrier **1** after 5[36] and 30 min of transport to that obtained in an analogous L-Pro transport (Figure 7). All the aa quantities were corrected by subtracting the corresponding amount produced by their passive diffusion (Figure S8). The obtained results demonstrated that carrier **1** features a remarkable selectivity for the facilitated transport of L-Pro over the other studied aa. The transport of L-Glu, Gly, and L-Ala were not facilitated significantly by embedding carrier **1** in the liposomes' membrane. Moreover, more lipophilic aa, such as L-Val and L-Ile, did not show significant differences between the passive diffusion and facilitated transport with liposomes embedding 0.1% mr of **1** (See Figure S8). In contrast, the transport of L-Arg seems to be slightly facilitated in liposomes embedding **1**. These findings are in good agreement with the

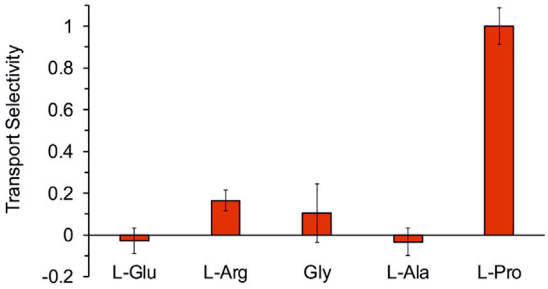

Figure 7. Transport Selectivity

Determined transport selectivity values for **1** (0.1% mr) with different natural radioactive-labeled aa. To facilitate comparison, we defined the transport selectivity value as the ratio of the amount of aa present in the liposomes at the end of a transport experiment with that measured for L-Pro in an identical run. The amount of L-Pro produced the larger determining value, thus the transport selectivity of the carrier for L-Pro is set to be equal to 1. The transported amount of aa was measured at a fixed time (300 s) for an extravesicular concentration of 100 μM. In all cases, the transport selectivity values were calculated as the average of three transport experiment replicates. The error bars correspond to the propagated errors from the standard deviation values. The results of L-Val and L-Ile are not included in the figure owing to their large rate of passive diffusion. See Figure S8 for details.

extraction properties of carrier **1** derived from solid-liquid experiments performed with the aa series. L-Pro was extracted into the dichloromethane solution by **1** to a larger extent than any other aa.

Studies of L-Pro Transport Using Other Synthetic Carriers

We became interested in studying the aa transport properties of other synthetic carriers based on a calix[4]pyrrole scaffold, i.e., **2** and **5** (Figure 1). Cavitand **2** is a bis-methylene bridged analog of cavitand **1**. Octamethyl calix[4]pyrrole **5** contains the binding site of the calix[4]pyrrole core but lacks the aromatic cavity. Solid-liquid extraction experiments of L-Pro with receptors **2** and **5** in dichloromethane solution did not induce noticeable changes in the ^{1}H NMR spectrum of the free host (Figures S9 and S10). These results indicate that in dichloromethane solution L-Pro has a reduced affinity for **2** and **5** compared with **1**.[37] It is worth reminding that receptor **1** was able to extract 1 equiv of L-Pro in analogous solid-liquid extraction experiments (Figure S1). We performed influx experiments of L-Pro using liposomes with carriers **2** and **5** embedded in their membranes at 0.1% mr (100 μM of aa). The change with time of the amount of L-Pro present in the liposomes embedding octamethyl calix[4]pyrrole **5** (Figure S11) was almost identical to the one measured in control experiments using liposomes lacking the carrier (i.e., passive diffusion). On the other hand, liposomes embedding cavitand **2** displayed noticeable changes in the amount of L-Pro at longer transport times (i.e., 30–60 min) compared with the control. In any case, the facilitated transport of L-Pro with carrier **2** embedded in the membrane was less significant (i.e., ~40 pmol L-Pro in 60 min; Figure S11) than that provided by cavitand **1** (~90 pmol in 60 min; Figure S11). Together, these results demonstrate that cavitand **1** is a privileged carrier for the facilitated transport of L-Pro across liposomal membranes.

In order to compare the transport abilities of cavitand **1** for L-Pro with those of other synthetic carriers described in literature, we performed L-Pro influx transport experiments using a multimolecular carrier system closely related to the one described by Gale and co-workers mainly for Gly transport.[11] However, the changes in L-Pro concentration were monitored using the radiometric assay optimized in this work instead of the fluorescent method described by the authors. In our L-Pro influx transport experiments, the squaramide **6** (Figure 1) was pre-inserted (embedded) in the

liposomes at a 0.1% mr. We start monitoring the kinetics of the transport of L-Pro after the addition of aldehyde **7** as a DMSO solution (10% mr and 1% vol DMSO). Interestingly, we observed that the modified[38] Gale's carrier system was also efficient in facilitating the transport of L-Pro (Figure S12) albeit at a lower transport rate than **1** (Figure 4A). This result supports the suitability of our optimized radiometric assay also in the study of the transport abilities of multimolecular self-assembled carrier systems.

We conclude that the calix[4]pyrrole cavitand **1** displayed a moderate improvement in transport abilities of L-Pro compared with the modified multimolecular carrier system developed by Gale et al., (**6** and **7**) (Figures 4A, S11, and S12). It is worth noting that Gale's three components assembly carrier system was designed to facilitate the transport of aa like L-Ala and Gly (i.e., L-Pro was not studied in their work).

Study of the Facilitated L-Pro Transport in HeLa Cells

Bearing in mind the potential use of calix[4]pyrrole derivatives as therapeutic tools, we wanted to assess whether cavitand **1** was able to transport L-Pro across the membrane of human cells. To do so, HeLa cells were pre-incubated with POPC (1-palmitoyl-2-oleyl-*sn*-glycero-3-phosphocholine) derived liposomes (~100 nm mean diameter) with cavitand **1** embedded in the membrane at 10% mr (POPC-**1**). Control experiments without carrier **1** were also performed (control, POPC).

Transport experiments were performed in choline chloride (ChoCl) medium (sodium-free medium), to minimize endogenous L-Pro transport (i.e., functional ablation of sodium-dependent transporters). The overall concentration of L-Pro in HeLa cells was increased upon POPC-**1** treatment (1–10 μM) compared with control conditions when a high concentration of extracellular L-Pro (i.e., 20 mM) was assayed (Figure 8A). This increase in L-Pro uptake was not detectable when 1 mM concentration of substrate was used (Figures 8A and S13). Transport experiments at additional substrate concentrations (1, 2, 5, 10, and 20 mM) were also performed (Figure S14). These additional results suggest that the increase in L-Pro uptake upon POPC-**1** treatment is only noticeable at high substrate concentrations. Indeed, at 20 mM of L-Pro concentration, the L-Pro transport into cells attributed to cavitand **1** was $1.2 \times 10^4 \pm 1.4 \times 10^3$ pmols/min·mg protein (Figure 8), which corresponds to a ~35% increase in L-Pro uptake with respect to control conditions (Figures S13 and S14). These results are in agreement with the linear dependency of the L-Pro concentration in the mM range mediated by compound **1** (Figure 5).

In all, our results suggest that cavitand **1** contributes to L-Pro uptake on top of the transport mediated by natural transporters (Figure 8B). To the best of our knowledge, this is the first report showing aa transport mediated by a synthetic carrier in cultured cells. This is reminiscent of transport of inorganic anions in epithelial cells mediated by synthetic carriers.[39] Carrier proteins are integral membrane proteins featuring the binding pocket accessible on both sides of biological membranes. In brief, transport occurs by binding the corresponding substrate at one side of the membrane (e.g., extracellular solution, *cis* side). Through conformational changes, they access the trans-side to release the substrate. Finally, re-opening the *cis* side closes the transport cycle for a new transport event. This is known as the alternative access model (Figure 8B).[40] In contrast, cavitand **1**, with an approximate size of 14 Å by 10 Å, is not able to access simultaneously both sides of biological membranes (~30 Å). This remark suggests that cavitand **1** might diffuse within the membrane (e.g., liposomes or the plasma membrane of HeLa cells), and eventually, upon reaching the membrane surface, binds the substrate (e.g., L-Pro). Afterward, diffusion of

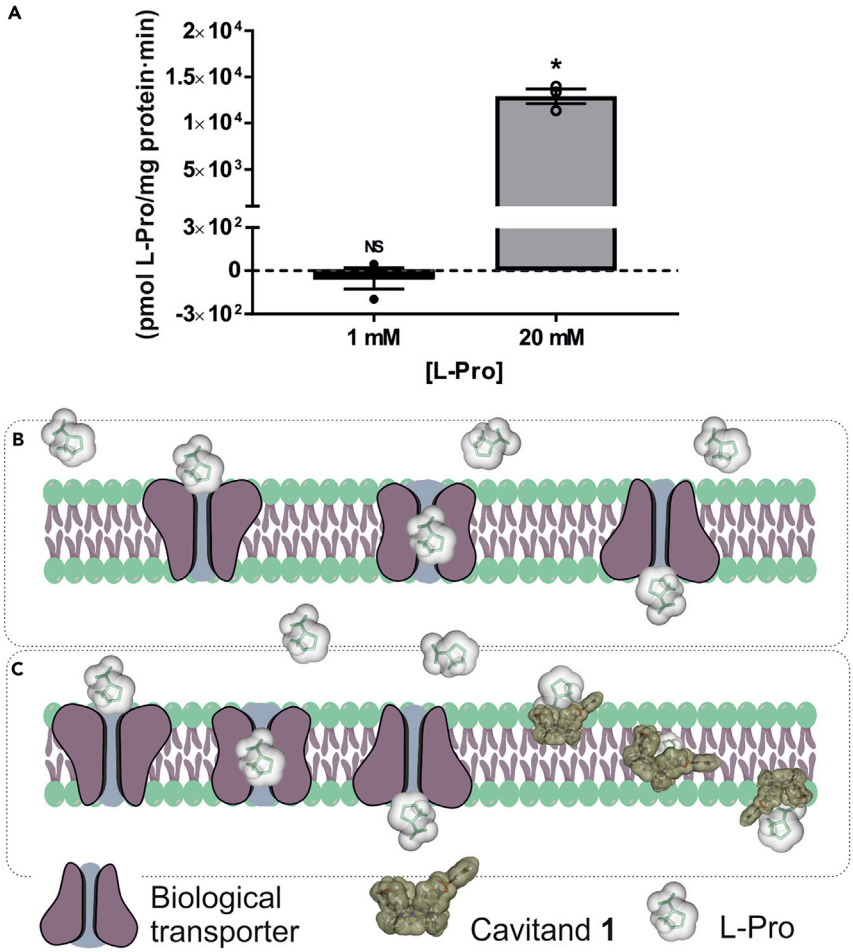

Figure 8. L-Pro Transport Experiments in HeLa Cells

(A) Plot of the results obtained for the L-Pro transport experiments using HeLa cells. HeLa cells were incubated with POPC or POPC-**1** and L-Pro transport activity was measured at different substrate concentrations using L-[^{3}H]-Pro. The y-axis represents the pmol of L-[^{3}H]-Pro internalized by cells treated with POPC-**1** after subtraction of pmol of L-[^{3}H]-Pro internalized by cells treated with POPC (control experiment). Data is presented as mean ± SEM of 3 independent experiments and was analyzed using a two-tail unpaired Student's t test ($\alpha = 0.05$). Error bars correspond to the standard error of the mean (SEM). NS, no significant differences. *$p < 0.05$. Cartoons of the proposed transport mechanism are shown in (B and C).

(B) Normal cells express specific transporters that are in charge of L-Pro transport across the membrane;

(C) Cells that are treated with POPC-**1** incorporate the cavitand **1** in the membrane, which contributes to L-Pro transport together with endogenous transporters, thereby enhancing overall L-Pro uptake. The cartoon (C) highlights that the size of the synthetic carrier (even not drawn to scale) does not allow it to reach both sides of the membrane simultaneously as is the case for the biological transporter.

the L-Pro⊂**1** complex within the membrane would access the *trans* side (i.e., inner volume) to finally release the substrate (Figure 8C). This transport mechanism, as in the case of transporter proteins,[41] should result in saturation of the transport at high substrate concentrations, when all the transporter binding sites are occupied. Remarkably, the experimental results show a linear increase of the L-Pro concentration in the liposomes with the increase of external L-Pro substrate concentration either in liposomes (up to 10 mM L-Pro) or in HeLa cells. Most likely, this is caused by the low affinity of cavitand **1** for L-Pro in the membrane.

Conclusions

We have shown that calix[4]pyrrole cavitand **1** facilitates aa transport across artificial (liposomes) and biological (cultured cells) membranes. Based on the experimental results we propose that cavitand **1** transports L-Pro through a mobile carrier mechanism involving the formation of a 1:1 complex (L-Pro⊂**1**). Remarkably, we calculated a 30-fold increase in L-Pro transport activity using liposomes embedding cavitand **1** (0.2 % carrier 1:EYPC mr and 100 μM substrate concentration) compared with liposomes lacking the embedded carrier. Moreover, we demonstrated that carrier **1** displays a remarkable selectivity for the facilitated transport of L-Pro over L-Glu, L-Arg, Gly, and L-Ala. In contrast, in HeLa cultured cells cavitand **1** mediates L-Pro transport only at high concentrations of substrate (~20 mM) with a moderate increase in L-Pro uptake over background (endogenous transporters at the cell membrane). These preliminary results in cells are promising and augur well for the potential application of calix[4]pyrroles as therapeutic tools for the modulation of aa transport and in the delivery of aa-derived drugs to tackle diseases that are of interest to the current society, such as cancer, aminoacidurias, and neurodegenerative disorders.[42] However, further modifications to the molecular structure of **1** are needed to increase the intrinsic transport activity of this synthetic carrier in order to approach the transport capacity of cell-endogenous transporters.

EXPERIMENTAL PROCEDURES

Resource Availability

Lead Contact

Further information and requests for resources and reagents should be directed and will be fulfilled by the Lead Contact, Professor Pablo Ballester (pballester@iciq.es).

Materials Availability

This study did not generate new unique reagents.

Data and Code availability

The published article includes all datasets generated during this study. Crystallographic data for L-Pro⊂**1** complex reported in this paper has been deposited in the Cambridge Structural Database CSD, CCDC: 1984688.

Manuscript available at SSRN: https://ssrn.com/abstract=3554084 or https://doi.org/10.2139/ssrn.3554084.

General

All chemicals were purchased from commercial sources and used without further purification unless otherwise stated.^{13}C-labeled aa were purchased from Sigma Aldrich. Radiolabeled compounds and scintillation reagents were acquired from Perkin Elmer. Compounds **1**, **2**, and **5** were prepared following the reported procedures.[24,43] EYPC, POPC, the mini-extruder set, and Nucleophore® 1 μm pore diameter polycarbonate membranes were acquired from Avanti® Polar Lipids, Inc. Lipid solutions were prepared using HPLC grade chloroform supplied by Riedel-de Haën Honeywell. All aqueous solutions were prepared using deionized water from a Millipore filtration system.

^{1}H NMR, ^{13}C NMR, and ^{31}P NMR spectra were acquired in a Bruker Avance 400 Ultrashield spectrometer. The radioactivity was counted with a β-scintillation counter LSC-7200 Hitachi Aloka Medical.

NMR Transport Experiments

In a typical experiment, 250 μL of aa⊂EYPC liposomes stock solution (see Supplemental Information for details) were mixed with 250 μL of transport buffer (200 mM ^{13}C(1)-L-Pro or ^{13}C(1)-L-Ala, 10 mM HEPES, pH 7.4) in an NMR tube. The mixture was stirred for 60 min at room temperature. Afterward, 55 μL of D_2O and 25 μL of aqueous $MnSO_4$ (20 mM) were added and the ^{13}C NMR spectrum was registered.

Liposomes' Radiometric Assays

Influx Experiments

In a typical experiment, 24 μL of EYPC liposomes stock solution (see Supplemental Information for details) were added to 180 μL of transport buffer (100 μM of L-aa, [^{3}H]-L-aa 0.5 μCi, 100 mM NaCl, 10 mM HEPES, pH 7.4) in an Eppendorf tube.[44] The mixture was homogenized and incubated at room temperature for a concrete time of transport (t = 1–60 min). Afterward, ~1 mL of cold stopping buffer (5 mM of L-aa, 100 mM NaCl, 10 mM HEPES, pH 7.4, 0°C–4°C) was added. The mixture was immediately homogenized and filtered through a nitrocellulose filter (0.45 μm pore diameter). The filters were washed with cold stopping buffer (3 × 2 mL) and dried in the air for at least 30 min. Finally, the filters were plugged in 3 mL of scintillation liquid, and radioactivity was counted with a β-counter. Transport points were performed by triplicate for each condition (i.e., transport time, concentration of transporter).

Efflux Experiments

In a typical experiment, 24 μL of [^{3}H]-L-Pro⊂EYPC liposomes stock solution (see Supplemental Information for details) were added to 936 μL of buffer (100 mM NaCl, 10 mM HEPES, pH 7.4) in an Eppendorf tube. The mixture was homogenized and incubated at room temperature for a concrete time of transport (t = 5–60 min). Afterward, ~1 mL of cold stopping buffer (5 mM of L-Pro, 100 mM NaCl, 10 mM HEPES, pH 7.4, 0°C–4°C) was added. The mixture was immediately homogenized and filtered through a nitrocellulose filter (0.45 μm pore diameter). The filters were washed with cold stopping buffer (3 × 2 mL) and dried in the air for at least 30 min. Finally, the filters were plugged in 3 mL of scintillation liquid, and radioactivity was counted with a β-counter. Transport points were performed by triplicate for each condition (i.e., transport time, concentration of transporter).

HeLa Cells Radiometric Assays

HeLa cells were maintained at 37°C in a humidified 5% CO_2 environment in DMEM supplemented with 10% fetal bovine serum, 50 units mL^{-1} penicillin, 50 μg mL^{-1} streptomycin, and 2 mM L-glutamine. Cells were incubated with 1 mL of POPC suspension (10 μM in PBS) or POPC-**1** suspension (10 μM POPC and 1 μM **1** in PBS) for 10 min at 37°C. After incubation, aa uptake was measured by exposing replicate cultures at 37°C to [^{3}H]-L-Pro (1 μCi/mL; Perkin Elmer) in sodium-free transport buffer (137 mM choline chloride, 5 mM KCl, 2 mM $CaCl_2$, 1 mM $MgSO_4$, and 10 mM HEPES, pH 7.4). Transport rates were determined using an incubation period of 1 min and increasing concentrations of cold aa. Assays were terminated by washing with an excess volume of chilled transport buffer. Cells were lysed using 0.1% SDS and 100 mM NaOH. Then radioactivity was counted in a Packard Tri-Carb Liquid Scintillation Counter, and 10 μL was used to determine protein content using the Pierce BCA kit (Pierce).

MTT (3-(4,5-dimethylthiazol-2-yl)-2,5-diphenyltetrazolium bromide) cell viability assays showed that cavitand **1** is not cytotoxic under the experimental conditions used

for the facilitated L-Pro transport radiometric experiments in HeLa cells (see Figure S16 for details).

SUPPLEMENTAL INFORMATION

Supplemental Information can be found online at https://doi.org/10.1016/j.chempr.2020.08.018.

ACKNOWLEDGMENTS

This work was supported by the Spanish Ministry of Science, Innovation and Universities (SAF2015-64869-R-FEDER, RTI2018-094211-B-100), MINECO (CTQ2017-84319-P), FEDER funds (SAF2015-64869-R-FEDER, RTI2018-094211-B-I00, CTQ2017-84319-P), the CERCA Programme/Generalitat de Catalunya, AGAUR, (2017 SGR 1123 and 2017 SGR 961) and Barcelona Institutute of Science and Technology (BIST), Spain. (2016 IGNITE Project – CALIX4TRANS). J.L.S.-W. is a recipient of an FPU PhD fellowship from the Spanish Ministry of Science, Innovation and Universities with reference number FPU18/00340. P.Bartoccioni was supported by a CIBERER contract. We gratefully acknowledge institutional funding to IRB-Barcelona from the MINECO through the Centres of Excellence Severo Ochoa Award and from the CERCA Programme of the Generalitat de Catalunya. We thank Dr. D. Hernandez and Dr. S. Sopeña for providing compounds 1 and 6, respectively. Prof. Jun-Li Hou and Prof. J. Montenegro are also acknowledged for their support at the initial stage of the project.

AUTHOR CONTRIBUTIONS

P.Ballester, L.M.-C., G.A., M.P., P.Bartoccioni, E.E.M., and J.L.S.-W. designed research; L.M.-C., J.L.S.-W., A.F.S., P. Bartoccioni, and G.A. performed research; A.F.S. contributed with the synthetic receptors 1, 2 and 5 and binding studies; P.Ballester, L.M.-C., G.A., M.P., P.Bartoccioni, E.E.M., and J.L.S.-W. analyzed data; and G.A., L.M.-C., M.P., and P.Ballester wrote the manuscript.

DECLARATION OF INTERESTS

The authors declare no competing interests.

Received: February 28, 2020
Revised: April 10, 2020
Accepted: August 25, 2020
Published: September 25, 2020

REFERENCES

1. Yang, N.J., and Hinner, M.J. (2015). Getting across the cell membrane: an overview for small molecules, peptides, and proteins. In Site-Specific Protein Labeling: Methods and Protocols, A. Gautier and M.J. Hinner, eds. (Springer), pp. 29–53.

2. Anderson, M.P., Gregory, R.J., Thompson, S., Souza, D.W., Paul, S., Mulligan, R.C., Smith, A.E., and Welsh, M.J. (1991). Demonstration that CFTR is a chloride channel by alteration of its anion selectivity. Science *253*, 202–205.

3. Torrents, D., Mykkänen, J., Pineda, M., Feliubadaló, L., Estévez, R., de Cid, R.d., Sanjurjo, P., Zorzano, A., Nunes, V., Huoponen, K., et al. (1999). Identification of SLC7A7, encoding y+LAT-1, as the lysinuric protein intolerance gene. Nat. Genet. *21*, 293–296.

4. Feliubadaló, L., Font, M., Purroy, J., Rousaud, F., Estivill, X., Nunes, V., Golomb, E., Centola, M., Aksentijevich, I., Kreiss, Y., et al. (1999). Non-type I cystinuria caused by mutations in SLC7A9, encoding a subunit (bo,+AT) of rBAT. Nat. Genet. *23*, 52–57.

5. Matile, S., Vargas Jentzsch, A., Montenegro, J., and Fin, A. (2011). Recent synthetic transport systems. Chem. Soc. Rev. *40*, 2453–2474.

6. Spooner, M.J., and Gale, P.A. (2015). Anion transport across varying lipid membranes - the effect of lipophilicity. Chem. Commun. (Camb.) *51*, 4883–4886.

7. Howe, E.N.W., Busschaert, N., Wu, X., Berry, S.N., Ho, J., Light, M.E., Czech, D.D., Klein, H.A., Kitchen, J.A., and Gale, P.A. (2016). pH-regulated nonelectrogenic anion transport by Phenylthiosemicarbazones. J. Am. Chem. Soc. *138*, 8301–8308.

8. Gale, P.A. (2011). From anion receptors to transporters. Acc. Chem. Res. *44*, 216–226.

9. Gale, P.A., Pérez-Tomás, R., and Quesada, R. (2013). Anion transporters and biological systems. Acc. Chem. Res. *46*, 2801–2813.

10. Chen, L., Si, W., Zhang, L., Tang, G.F., Li, Z.T., and Hou, J.L. (2013). Chiral selective transmembrane transport of amino acids through artificial channels. J. Am. Chem. Soc. *135*, 2152–2155.

11. Wu, X., Busschaert, N., Wells, N.J., Jiang, Y.B., and Gale, P.A. (2015). Dynamic covalent

transport of amino acids across lipid bilayers. J. Am. Chem. Soc. *137*, 1476–1484.

12. Bozkurt, S., Yilmaz, M., and Sirit, A. (2012). Chiral calix[4]arenes bearing amino alcohol functionality as membrane carriers for transport of chiral amino acid methylesters and mandelic acid. Chirality *24*, 129–136.

13. Sessler, J.L., and Andrievsky, A. (1998). Efficient transport of aromatic amino acids by Sapphyrin–Lasalocid conjugates. Chem. Eur. J. *4*, 159–167.

14. Stillwell, W. (1976). Facilitated diffusion of amino acids across bimolecular lipid membranes as a model for selective accumulation of amino acids in a primordial protocell. Biosystems *8*, 111–117.

15. Sunamoto, J., Iwamoto, K., Mohri, Y., and Kominato, T. (1982). Liposomal membranes. 13. Transport of an amino acid across liposomal bilayers as mediated by a photoresponsive carrier. J. Am. Chem. Soc. *104*, 5502–5504.

16. Klein, R.A., Moore, M.J., and Smith, M.W. (1971). Selective diffusion of neutral amino acids across lipid bilayers. Biochim. Biophys. Acta *233*, 420–433.

17. Westmark, P.R., and Smith, B.D. (1996). Boronic acids facilitate the transport of ribonucleosides through lipid bilayers. J. Pharm. Sci. *85*, 266–269.

18. Westmark, P.R., Gardiner, S.J., and Smith, B.D. (1996). Selective monosaccharide transport through lipid bilayers using boronic acid carriers. J. Am. Chem. Soc. *118*, 11093–11100.

19. Adriaenssens, L., Estarellas, C., Vargas Jentzsch, A., Martinez Belmonte, M., Matile, S., and Ballester, P. (2013). Quantification of nitrate-pi interactions and selective transport of nitrate using calix[4]pyrroles with two aromatic walls. J. Am. Chem. Soc. *135*, 8324–8330.

20. Martínez-Crespo, L., Sun-Wang, J.L., Ferreira, P., Mirabella, C.F.M., Aragay, G., and Ballester, P. (2019). Influence of the insertion method of aryl-extended calix[4]pyrroles into liposomal membranes on their properties as anion carriers. Chem. Eur. J. *25*, 4775–4781.

21. Escobar, L., Aragay, G., and Ballester, P. (2016). Super aryl-extended calix[4]pyrroles: synthesis, binding studies, and attempts to gain water solubility. Chem. Eur. J. *22*, 13682–13689.

22. Peñuelas-Haro, G., and Ballester, P. (2019). Efficient hydrogen bonding recognition in water using aryl-extended calix[4]pyrrole receptors. Chem. Sci. *10*, 2413–2423.

23. Galán, A., Valderrey, V., and Ballester, P. (2015). Ordered co-encapsulation of chloride with polar neutral guests in a tetraurea calix[4]pyrrole dimeric capsule. Chem. Sci. *6*, 6325–6333.

24. Guinovart, T., Hernández-Alonso, D., Adriaenssens, L., Blondeau, P., Martínez-Belmonte, M., Rius, F.X., Andrade, F.J., and Ballester, P. (2016). Recognition and sensing of creatinine. Angew. Chem. Int. Ed. *55*, 2435–2440.

25. Sahu, N., Dela Cruz, D., Gao, M., Sandoval, W., Haverty, P.M., Liu, J., Stephan, J.P., Haley, B., Classon, M., Hatzivassiliou, G., and Settleman, J. (2016). Proline starvation induces unresolved ER stress and hinders mTORC1-dependent tumorigenesis. Cell Metab. *24*, 753–761.

26. Elia, I., Broekaert, D., Christen, S., Boon, R., Radaelli, E., Orth, M.F., Verfaillie, C., Grünewald, T.G.P., and Fendt, S.M. (2017). Proline metabolism supports metastasis formation and could be inhibited to selectively target metastasizing cancer cells. Nat. Commun. *8*, 15267.

27. Reig, N., Chillarón, J., Bartoccioni, P., Fernández, E., Bendahan, A., Zorzano, A., Kanner, B., Palacín, M., and Bertran, J. (2002). The light subunit of system b(o,+) is fully functional in the absence of the heavy subunit. EMBO J. *21*, 4906–4914.

28. Reig, N., del Rio, C., Casagrande, F., Ratera, M., Gelpí, J.L., Torrents, D., Henderson, P.J.F., Xie, H., Baldwin, S.A., Zorzano, A., et al. (2007). Functional and structural characterization of the first prokaryotic member of the L-amino acid transporter (LAT) family: a model for APC transporters. J. Biol. Chem. *282*, 13270–13281.

29. Assuming that the solubility of L-Pro in CD_2Cl_2 is lower than 1×10^{-4} M and after solid-liquid extraction only the 1:1 inclusion complex is observed in the ^{1}H NMR spectrum (L-Pro⊂1/free 1 ratio > 100), we estimated the lower limit of the stability constant K(L-Pro⊂1) to be 1×10^6 M^{-1}.

30. Davis, J.T., Gale, P.A., Okunola, O.A., Prados, P., Iglesias-Sánchez, J.C., Torroba, T., and Quesada, R. (2009). Using small molecules to facilitate exchange of bicarbonate and chloride anions across liposomal membranes. Nat. Chem. *1*, 138–144.

31. Note that the total amount of L-Pro loaded in the liposomes is the same that the maximum amount of L-Pro transported during the uptake experiments.

32. Chakrabarti, A.C., Clark-Lewis, I., Harrigan, P.R., and Cullis, P.R. (1992). Uptake of basic amino acids and peptides into liposomes in response to transmembrane pH gradients. Biophys. J. *61*, 228–234.

33. Redelmeier, T.E., Hope, M.J., and Cullis, P.R. (1990). On the mechanism of transbilayer transport of phosphatidylglycerol in response to transmembrane pH gradients. Biochemistry *29*, 3046–3053.

34. Estimated radius resulting from the sphere with the center located in the centroid calculated for the X-ray crystal structure of the L-Pro⊂**1** complex using the Discovery Studio Visualizer software.

35. Escobar, L., and Ballester, P. (2019). Quantification of the hydrophobic effect using water-soluble super aryl-extended calix[4]pyrroles. Org. Chem. Front. *6*, 1738–1748.

36. This time is within the range of initial rate conditions.

37. [L-Pro] extracted by **2** and **5** < 0.1 mM.

38. In our transport experiments, we pre-inserted squaramide 6 during the liposomes' preparation. In contrast, Gale and co-workers used the post-insertion method for both squaramide **6** and aldehyde **7** which were added as DMSO solutions just before the beginning of the transport.

39. Li, H., Valkenier, H., Judd, L.W., Brotherhood, P.R., Hussain, S., Cooper, J.A., Jurček, O., Sparkes, H.A., Sheppard, D.N., and Davis, A.P. (2016). Efficient, non-toxic anion transport by synthetic carriers in cells and epithelia. Nat. Chem. *8*, 24–32.

40. Krishnamurthy, H., Piscitelli, C.L., and Gouaux, E. (2009). Unlocking the molecular secrets of sodium-coupled transporters. Nature *459*, 347–355.

41. Bartoccioni, P., Fort, J., Zorzano, A., Errasti-Murugarren, E., and Palacín, M. (2019). Functional characterization of the alanine–serine–cysteine exchanger of *Carnobacterium* sp *AT7*. J. Gen. Physiol. *151*, 505–517.

42. Bröer, S., and Palacín, M. (2011). The role of amino acid transporters in inherited and acquired diseases. Biochem. J. *436*, 193–211.

43. Rothemund, P., and Gage, C.L. (1955). Concerning the structure of "Acetonepyrrole". J. Am. Chem. Soc. *77*, 3340–3342.

44. Analogous L-Pro transport studies were performed using 100 mM KCl and 100 mM Na_2SO_4 transport buffers instead of 100 mM NaCl. The results of the L-Pro facilitated transport experiments using KCl and Na_2SO_4 HEPES buffer did not show significant differences with respect to those performed using NaCl (Figure S15).

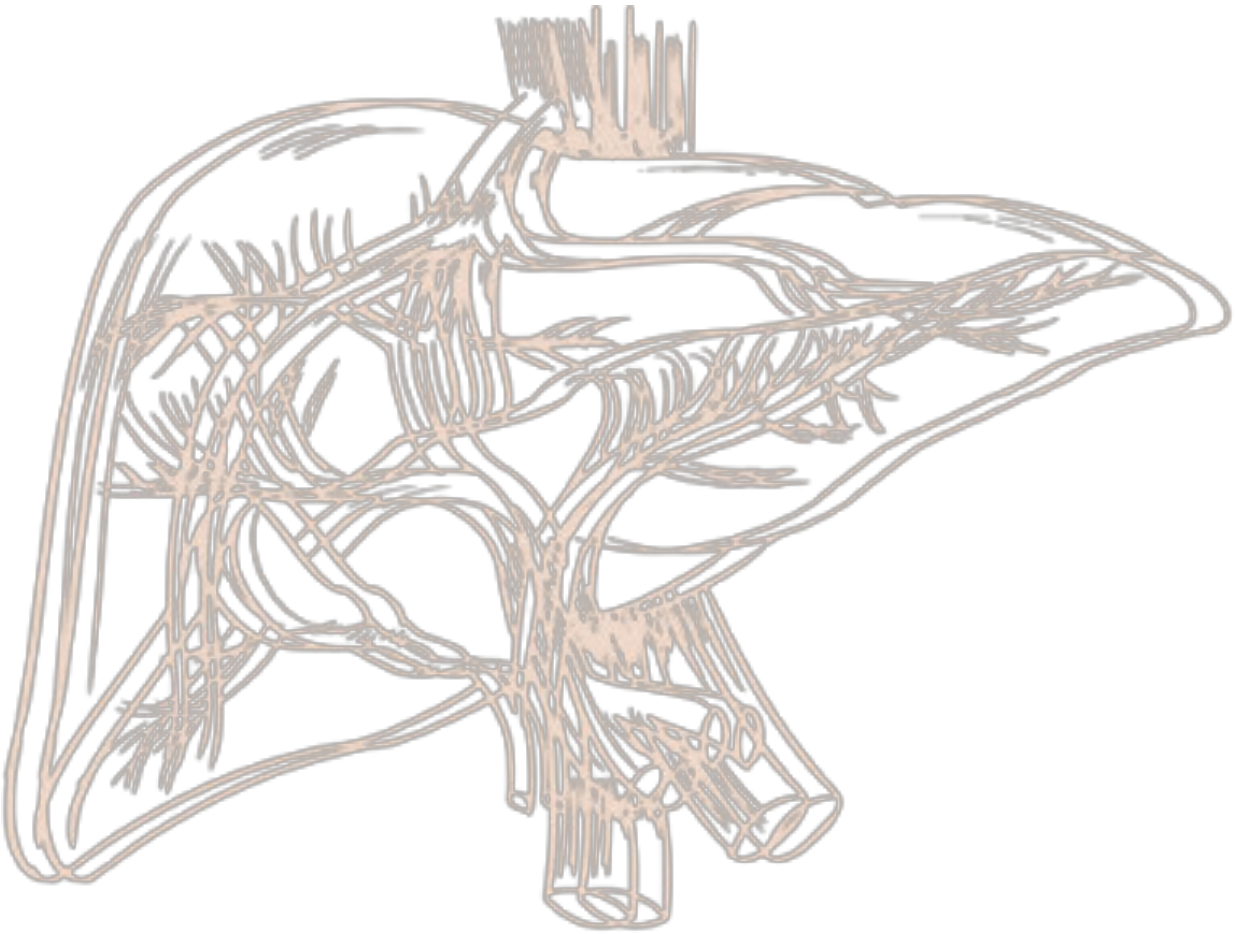

APPENDIX 4

Humanities & Social Sciences Communications

ARTICLE

https://doi.org/10.1057/s41599-020-00602-y OPEN

Barcelona's science diplomacy: towards an ecosystem-driven internationalization strategy

Alexis Roig [1,2], Jia Liang Sun-Wang [3] & Juan-Luis Manfredi-Sánchez [4]✉

Urban innovation ecosystems are set to play a prominent role in the internationalization and governance of big cities. By harboring solid scientific and technological assets and attracting both human and financial capital, they are best suited to become the pivotal actors of effective multi-stakeholder partnerships between the scientific community, public institutions, the private sector and civil society. In 2018, Barcelona's knowledge and innovation ecosystem came together to launch a comprehensive diplomatic strategy to put the city's science and technology at the forefront of global challenges. This paper presents the case study of Barcelona and discuss the opportunities for city-led science diplomacy as a formal, institutionalized practice aimed to reinforcing the insertion of local interests in the international scene while favouring the open interaction between the internal stakeholders involved.

[1] Barcelona Centre for International Affairs (CIDOB), Barcelona, Spain. [2] Barcelona Institute of International Studies (IBEI), Barcelona, Spain. [3] University of Barcelona, Barcelona, Spain. [4] University of Castilla-La Mancha, Toledo, Spain. ✉email: Juan.manfredi@uclm.es

Introduction

Global cities have gained prominence in academic literature on global governance. Their impact is visible in areas such as climate action (Bulkeley and Castán-Broto, 2013; Barber, 2017), migration (Bauder, 2016), human rights (Grigolo, 2019), industrial policy (Dijkstra et al., 2019) or global health. The city has become the unit of measure for innovation in public policy, thereby reshaping rules, and governance practices, including diplomacy.

An increasing number of cities are defining their strategies for internationalization and defining mechanisms that ensure an integral approach to foreign action (Curtis and Acuto, 2018), effective coordination among the different levels of government operating in international affairs (Kuznetsov, 2015), and adequate organization of its various stakeholders (Cerda-Bertomeu and Sarabia-Sanchez, 2016), as global perspectives and policies from different regions have become increasingly available to local arenas (Tavares, 2016; Nijman, 2016).

This context overcomes state-based approaches, extending the scope of foreign policy and diplomatic action. Global urban areas become active participants by operationalizing technological and innovation policies, expanding the activity of what global means for local governments. An innovation ecosystem does not emerge as an isolated central-government decision: entrepreneurs and researchers move to cities where universities, venture capital and human capital are found.

Global cities are contributing to realize "plural diplomacies" (Cornago, 2013). Old diplomatic structures and agendas may be not functional in the digital order, characterized by global economic flows, information and communication technologies, globalized labor markets, the start-up scene, or even environmental effects. Global cities pay attention to such transformations and respond in a new form of multilateralism -as city networks- and diplomatic practice. What *global* means for local governments makes sense in a sovereignty free debate, as global cities focus on implementing public policies instead of contesting state-nation configuration or other security issues traditionally related to realism.

Science and technology have become the cornerstones of growth within urban ecosystems, with direct consequences on economic and diplomatic activity. Likewise, science impacts the global projection of cities through values of internationalization, economic openness, innovation and demographic attraction of the so-called creative class (Florida, 2003). In this context, the following research question arises: what features make up the science diplomacy of the city of Barcelona? The hypothesis is as follows: the symbolic capital of the city allows differentiation through science and technology as sources of soft power.

This article sheds light on The Barcelona Science and Technology Diplomacy Hub (SciTech DiploHub), a unique experience on innovation and city diplomacy. The case of Barcelona serves as an example on how a global city can enhance its scientific and technological capacity to face local and global challenges, making use of its innovation ecosystem. The institution and its discourse exemplify new goals and methods in diplomatic action, particularly on the urban level.

The article employs the case study research method, defined as a qualitative small research, based on authors' fieldnotes, focused on a single phenomenon, and tracing a process linking causes with observed outcomes. Fieldnotes were taken during the design and execution of the project by two of its promoters and executive positions. Since two of the authors were involved in the launching of the project, the fieldnotes were taken during the meetings and gatherings with representatives of the public and private sector. The third author has collected experiences of promoters within various academic and professional activities such as events and conferences at Fundación Carolina 2018, Diplocat 2019, Fundación Banc Sabadell 2019, ESADE Business School 2020. In these quotes, the third author records explanations, questions from the public, or interventions by the co-authors. They are quotes and data published on the website of the institution under study. The case study research method is commonly used in social sciences to deepen one particular event, and "the goal of a good case study is to both produce knowledge about the case, but also provide some cumulative knowledge about the broader universe of cases" (Lamont, 2015). Regarding the limitations of the research method, authors provide auto-ethnographic account of -their experience. This auto-ethnographic exercise intends not to fall into complacency and, therefore, invites a third external author to counter overconfidence on the organization's own work. To provide evidence, where data are necessary, authors refer to public information openly distributed and available. The public–private status, promoters and members of the Ecosystem Board of Barcelona SciTech DiploHub are accessible on its website. As a non-profit organization, the information is more easily accessible and protected information is not violated.

Science and technology in city diplomacy

The rise of global cities takes place in parallel to that of the knowledge-based society and the digital economy. They have gained prominence in academic literature as the main driver behind productivity growth within a given territory. Before that, innovation policy was primarily intended to increase national technological competitiveness and spatial implications were considered only implicitly in the distribution of public funding (Boschma, 2005). Cities join the globalization process with the aim of benefiting from the advantages of an open and de-industrialized international economy. Educational services, the financial industry and research-intensive companies do not require factories, but access to knowledge and venture capital to develop market ideas and solutions. It is in this context that cities tap into innovation policies, thereby competing for the attraction of talent and creative classes, access to capital markets and technological expansion.

Science and innovation have both been drivers and followers of the globalization of cities and urban areas. Digital transformation reinforced the urban concentration, as complex economic system needs scale economies in investments, R&D, multimodal transports, access to banking and financial services, and other inputs. Global cities are those which concentrate production, population, capital markets, technologies and knowledge. Spatial concentration means hubs and clusters connected to the territory, thereby giving rise to the development of cluster economic theory (Porter, 1998; Ketels, 2013, G7, 2017). Network effects enhance the capacity for innovation by enabling people to mobilize resources, find relevant and reliable information quickly, and access appropriate knowledge sources and market outlets. This has led to the development of innovation-oriented regional policies (Ewers and Wettmann, 1980). Barcelona represents a reference case, built upon the symbolic capital of the city, which has harnessed its business and financial strength to articulate a narrative of a "global city", comparable to the one of Paris, London or Rome among other cities. The organization of the Olympic Games in 1992 itself consolidated the orientation of a service economy aligned with economic globalization.

Hubs are not only based on digital communities of activity, but on policies and institutions: "Complex knowledge, therefore does not travel well through digital communications channels and requires the richness of cities to be properly accumulated" (Balland et al., 2020). The global city is the preferred driver to

capitalize technological capabilities. Universities, colleges, and business schools provide graduates with intensive knowledge and expertize in management. Urban scaling and development economics require innovation, also in policy-making and governance (Roig, 2018).

In this context, cities compete with each other in the global arena for the raising of financial capital, the establishment of companies, the development of infrastructures or the execution of cultural and sports mega-events. The underlying economic logic holds that cities also compete in science and technology. In a hyperconnected system characterized by multimodal transport and digital technologies, the most competitive cities will attract more talent, better services and better cultural and educational resources, thereby increasing productivity. Competition does not consist on attracting industrial investments, but in providing cities with better services to join the geography of technological capitalism and corporate globalization (Taylor, 2012). Barcelona's non-capital status has driven the development of an economic model, which is highly dependent on the incorporation of its competitive assets and attractive into the globalization process. Science, higher education and the provision of cultural services allow to differentiate Barcelona from its competitors and create a particular economic offer.

The economic geography of urban cities has become an important vector of international political action. Opening up national economies to global markets has given cities a competitive role both within the same country and globally (Crescenzi et al., 2020; Leffel and Acuto, 2018). Cities host the headquarters of global corporations, commodity, currency and securities exchanges, producer services organizations, international governmental organizations, global conference centers and international transportation systems. As they grow in economic power, cities outstrip their national networks and demand responsibility in global governance (Acuto and Parnell, 2016; Bäckstrand et al., 2017). This is manifested in the demand for access to sources of power and mechanisms of influence in decision-making (Coll, 2015; Katz and Nowak, 2018; Schragger, 2016).

In order to understand how global cities are actorized, Ljungkvist explores "how the Global City's role in the globalized world is constructed and narrated locally" (2015, p. 2). Global cities are claiming political authority in foreign and security affairs (and not just a role in the globalized economy) on the basis of an emergent urban collective identity. According to Ljungkvist, reflexivity is crucial here: cities start referring to themselves as global cities and interacting with the world through policies and practices developed on behalf of their local societies.

As an example, the explicit withdrawal of some nation states from international cooperation, exemplified by the British decision to leave the European Union (EU) and the "America First" policies of the Trump administration, have propelled cities to take direct action in the international arena. While in the United Kingdom, the London City Hall launched the "London is Open" campaign as a first strategy to maintain close relations with EU neighbors, in the United States more than sixty mayors signed the "Chicago Climate Charter", committing to implement the goals of the Paris Agreement at the municipal level. These actions point to the advent of a multi-scalar global governance system in which cities are taking on some of the roles previously reserved for nation states, ranging from the creation of international policy-making frameworks and advocacy coalitions to formulating and implementing global agendas (Acuto, 2013).

Furthermore, the urban level promotes a flexible multi-stakeholder governance, open to cooperation among business, politics, civic society and higher education institutions. From an urban perspective, local governments around the world are increasingly interested in sharing best practices on local governance, particularly to encourage new linkages between their jurisdictions and the global environment (Burki et al., 1999; Cabrero Mendoza, 1995; Campbell, 2000). The multilevel governance includes regional and subnational level of government integration of such regional innovation systems in globally operating systems (Cooke, 2002; Koschatzky, 1997; Koschatzky and Sternberg, 2000; Marin and Mayntz, 1991). The literature offers examples in migration policies (Scholten and Pennix, 2016) and climate change (Hale, 2018; van der Heijden, 2019). This new governance models inspire the Ecosystem Board of Barcelona Science and Technology Diplomacy Hub (SciTech DiploHub), which integrates both public and private actors.

The urban voice makes sense in multilateral diplomacy, excluding the sovereignty debate (Rosenau, 1990). The New Urban Agenda—Habitat III elaborated a list of priorities in the international urban demands. The agenda identified five main pillars: (1) Strengthening the role of local governments (2) Commitment to creative solutions and innovative practices (3) Building inclusive alliances and citizen participation (4) Adopting an integrated and sustainable territorial development model, and (5) Monitoring, promoting public information and evaluating the impact of public policies. Cities are core actors for the achievement of the Sustainable Development Goals. Local effectiveness is also a consequence of coordinating activities, investments and decisions in networks of influence. Financing green or blue bonds, transferring technology, and supporting capacity building are opportunities for city collaboration. In the field of Sustainable Development Goals, "The Bellagio cities recognized that collective or coordinated purchasing policies, even among a small network of cities, could shape the market in powerful ways, given the aggregate scale of purchasing" (Pipa, 2019, p. 5). In all these cases, science and technology emerge as the cornerstones of public policies to provide specific, global, and shared solutions with other cities and urban territories.

City networks have also gained traction, with examples such as C40 cities (Davidson et al., 2019), the Global Covenant of Mayors for Climate and Energy or the Interreg program in the EU. The logic of the networks, distributed by themes, affinities and concerns impact. Acuto and Rayner consider that city networks are "formalized organizations with cities as their main members and characterized by reciprocal and established patterns of communication, policy-making and exchange" (2016, p. 1150). It seems there's no need for more networks but levering these and other partnerships to focus-oriented goals.

Literature recognizes city diplomacy as the "formal strategy in dealing with other governmental and non-governmental actors on an international stage" (Curtis and Acuto, 2018, p. 1). Cities will be part of the future world politics organization (Schragger, 2016). The broad definition fixes a second theoretical aspect: city diplomacy is flexible in formats and processes, opening avenues for participation. Business sectors, communities, universities, R&D labs, and other non-state actors contribute to the outcomes of city diplomacy, but not to international agreements. Such approach considers city diplomacy outcomes as the aggregate of product/services offered to increase the value for global issues effectively involved in city governance, i.e., according to their appropriate capacity. In the case of the city of Barcelona, its prestigious higher education institutions and cultural services, as well as its long-lasting business tradition, allowed the city to leverage capacity in science and technology. These were assets of the city's international action plan that favored Barcelona's diplomatic profile.

As stated above, in city diplomacy, the outcome is more relevant than international agreements. To understand city diplomacy, this paper establishes three conventional layers.

1. Promotion of the local industry and the internationalization of its economy. We find initiatives dedicated to attracting investments and companies, place branding, the protection of gastronomy, tourism of experiences or traditions. The *start-up nation* discourse today is not based on countries, but on geographical hubs. City networks compete against Silicon Valley to offer better conditions to increase the number and quality of high-tech companies. The expected conclusion is that economy represents a fast-track to understand globalization through urban lenses, and economic statecraft instruments are part of city diplomacy toolbox.
2. Political influence and representation in international organizations. There are different topics and approaches for matters related to climate change, the culture of peace, destination branding, health promotion or the right to decent housing. It is not a question of sovereignty, but of significant opportunity to face real problems by individual actions (cities alone) or in a collective (C40, UCLG) or cooperative manner (public and private initiatives). In traditional diplomacy, the Paris Agreement is an example of this new power architecture, mixing quality data (air pollution) and coordination (accountability) to counteract the effects of climate change.
3. Cultural and identity issues. There are many examples: the commemoration of historical events, linguistic immersion, architecture and landscape or cultural festivals. It is worth highlighting the growing use of memory policies to unite cultures and peoples, not necessarily identified with a State. However, at this point it is necessary to warn about rankings and other tools obsessed with marketing approaches to cultural dimensions of diplomacy. Place branding may be under public policy officers, not under PR strategists. The expected findings are the use of culture to profile the city, levering the power to attract people (tourists, investors) and companies.

As a result, the world is facing the rise of a diverse multilayered scenario in which cities and other non-state actors such as higher education institutions, corporations, research centers, and non-governmental organization (NGOs) are leveraging new intangible currencies, such as innovation, knowledge, and reputation on the adventure of going global while remaining anchored to the domestic matters (Weiss et al., 2013). Cities have the capacity to act globally because of the networked properties of the actors they host (Sassen, 1991; Castells, 1989; Taylor, 2012). This requires a "governance perspective, which acknowledges that multiple actors (public, civil society, and market actors) at multiple levels (from the local to the global) are now involved in governing, often through hybrid constellations that exist next to each other without hierarchical order" (Bouteligier, 2013, p. 13). These stakeholders are often based in innovation ecosystems within urban areas, which allows cities to gain global influence. Cities establish networks, engage in dialog and negotiations, facilitate public diplomacy, share best practices, encourage collaboration between international private and public entities, and ultimately influence world politics.

Within this context, the role of science in global governance is becoming crucial to ensure the effective uptake of high-quality scientific advice by policymakers. The global and scientific nature of these challenges calls out for international cooperation and places science at the forefront (The Royal Society & AAAS, 2010). With a view to the emerging global challenges, an increasing tendency can be observed in regional and urban policy to reject the classical economic promotion approach and move towards the development of soft intangible factors (Landabaso et al., 2001), including city diplomacy (Acuto, 2013; Glaeser et al., 2010) and science diplomacy (Van Langenhove and Boers, 2018). Cities are joining new collaborative platforms of influence (Tukianen et al., 2015), linking their domestic agendas with universal challenges of sustainability, economic growth and security and opening the door for the development of the aforementioned Urban Agenda. In addition, global challenges from climate change to global health, migrations and food and water security, together with rapid developments in areas such as artificial intelligence, robotics and gene editing require strong cross-border interactions between science, technology and civil society (6th World Science Forum, 2013). As Bulkeley and Betsill (2003, p. 9) explain "urban authorities have a significant but varied role in relation to urban planning, building codes, the provision of transportation and the supply of energy, water, and waste services […]. Given these powers and their democratic mandate as the local level of government, municipalities can, therefore, be seen as in a position to address the challenges of mitigating and adapting to climate change".

However, recent literature does not support the idea that cities will become the main actor in the fight against climate change due to its own inability to impose the legislative agenda on the national scale. City networks are powerful diplomatic actors, but they are still in the process of maturation to occupy the space reserved for states (Johnson, 2018; Smeds and Acuto, 2018). Both contributions on city diplomacy and cities in climate action appear to lack a clear contextualization of urban agency in relation to the role of globalizing national states—relations that can be considered to take place on a theoretical continuum between full antagonism and full cooperation.

In summary, both city diplomacy and science diplomacy, as manifestations of soft power, chart a different course from traditional national diplomacy. They have less structure, less direct influence, and fewer formal tools at their disposal (Nye, 2003; Skolnikoff, 1993; Wagner, 2002). As a result, they operate inside a framework that lends itself more easily to collaborative approaches and cooperation. In this regard, theoretical approaches on ecosystem theory, open innovation and the Triple Helix perspective on university-industry-government relationships have underscored the important role of public policy in facilitating these cooperative linkages between the institutional spheres of academic institutions, industry and government (Carayannis et al., 2018; Engel, 2015; Pique et al., 2018). According to the European Commission (2017), Barcelona stands out as an example of the Triple Helix model, built upon two main pillars: science and international recognition.

Within this theoretical framework, the case study of the Barcelona Science and Technology Diplomacy Hub (SciTech DiploHub) sets an example of how city diplomacy is configured as a formal practice at the crossroads of science, technology and international relations.

SciTech DiploHub, a public–private partnership in charge of deploying Barcelona's science diplomacy

Public and private in science city diplomacy. Barcelona's knowledge and innovation ecosystem came together to launch a comprehensive diplomatic strategy to put the city's science and technology at the forefront of sustainable development and global challenges in 2018. As a result, the Barcelona Science and Technology Diplomacy Hub (SciTech DiploHub) was created as non-profit public–private partnership backed by the city's research centers, universities, advocacy groups, start-ups, global corporations and public institutions with the aim to position Barcelona as a global lab in science diplomacy for cities around the world. SciTech

DiploHub has the mandate to elevate the role of science, technology and cities in foreign policy and make Barcelona a more influential player on the global stage by representing its knowledge and innovation ecosystem worldwide (Roig, 2018). The mandate is aligned with the academic literature of globalization and the aspirational desire to become a "superstar city" (Florida, 2003) through scientific and technological specialization. Influence in the technological arena does not depend on past inputs or assets, but can be built through an open ecosystem of executive education, investment and universities that endows scientific projects with an innovative orientation.

The first step towards the creation of Barcelona's science diplomacy was to identify the key actors in the city's innovation ecosystem. These included research institutions, higher education institutions, technological parks, scientific infrastructures, tech companies and start-ups, private foundations and public institutions. Higher education institutions are globally recognized, including the Times Higher Education—2019 World University Rankings (5th city of the world with the highest concentration of top 200 universities), the Innovation Cities Index (4th most innovative city in Europe and 21st most innovative city in the world), 5th European hub with most startup capital invested (Atomico dealroom—2018), and the Nature Top Science Cities Ranking 2019 (8th European city and scientific production). In executive education, Barcelona is considered the southern Europe hotspot with 2 business schools in the top 15 in the world, one of which has been ranked #1, according to The Financial Times—2020.

The main challenge encountered during the inception of the project was the lack of alignment of interests, priorities, and actions between the wide range of stakeholders in the ecosystem. It was identified that the internationalization strategies of the main players in the city were fundamentally reactive to competitive pressures such as declining domestic markets or scarce funding, rather than planned, sustainable long-term action plans. Moreover, uncoordinated or overlapping policies at different levels of government were identified as another relevant challenge to overcome. A foundational mission of SciTech DiploHub was thus to reduce thematic dispersion, align interests and priorities, achieve greater coherence with other government levels and dependencies, and build an international cooperation agenda in accordance with the city's development strategy.

It is critical that from the very outset, the action plan of the city's diplomatic strategy is arranged in an inclusive manner, taking into consideration the different stakeholders involved, who will necessarily be beneficiaries and active partners of the projects to be developed. The sustainability of a city-led science diplomacy strategy is thus dependant on the degree of legitimacy and acceptance among the local actors involved. These stakeholders seek to develop, within their legal-institutional framework, a series of actions that allow the city to insert itself internationally, thereby becoming international actors. In this regard, the local government is assumed as an interested party at the internal level, while civil society, academic institutions and private companies are external stakeholders and aim to obtain certain benefits of a political, functional, financial and non-financial nature. This strong relationship between the local government (the internally interested party) and the other stakeholders (external stakeholders) ensure that the city's diplomacy strategy is reflected in the action plans of each of the stakeholders involved, while, in turn, enabling that public policies are in alignment with the stakeholder's priorities, interests and needs.

In order to be able to specify the instruments required for the insertion of these stakeholders within the city's diplomatic action, as well as the potential interactions between them, it is important to conduct a strategic analysis of (i) "how" does the ecosystem want to be internationally perceived and (ii) "where" can the city be recognized as a relevant international partner, while (iii) assessing the competitive landscape and the international positioning of other global cities. The need for a global shared strategy is also driven by the necessity of a better governance. Good governance is characterized primarily by participation, transparency, inclusion and equity (UNESCAP, 2006). Gathering all stakeholders under the umbrella of science and technology can promote an equal participation of the ecosystem in the elaboration of transparent and efficient policies that will further benefit Barcelona's knowledge and innovation ecosystem and meet the needs of society while making the best use of common resources.

The launching of SciTech DiploHub, the Barcelona Science and Technology Diplomacy Hub, was supported by the Barcelona Manifesto, which compiled more than two hundred signatories by university deans, research institutions, all former city mayors, government ministers, business leaders and the city's most prominent scientists and technology experts, both in Barcelona and abroad. All the stakeholders from the ecosystem came together for the first time in a collective effort to launch the project (SciTech DiploHub, 2018). The foundation of the project through public–private collaboration stands out as a substantive novelty in science diplomacy, which is usually imposed through the top-down logic of central governments.

SciTech DiploHub is a non-profit public–private partnership backed by leading research centers, universities, non-profits, start-ups, corporations and public institutions that positions Barcelona as a global lab in science diplomacy for cities around the world. It has the mandate to elevate the role of science, technology and cities in foreign policy and make Barcelona a more influential player on the global stage through its contribution to global challenges. The main specific goals of the organization are (SciTech DiploHub, 2018):

- To consolidate Barcelona as an innovation capital, ready to meet the United Nations Sustainable Development Goals through science and technology (United Nations General Assembly, 2015).
- To position the city as an influential geopolitical actor through science diplomacy. Becoming a reliable partner thus paving the way for other global cities committed to developing their own science and technology diplomacy strategies.
- To promote a sound and inclusive multi-stakeholder dialog to design and deploy Barcelona's science diplomacy action plan, through partnerships among the scientific community, start-ups, policymakers, NGOs, the diplomatic corps, the private sector and civil society.
- To empower a global network of top scientists and technology experts educated in Barcelona to foster international cooperation, showcase our scientific strengths abroad and help us better understand and interpret key global issues.
- To become a world-class think tank where scientific expertize and innovation can be harnessed in support of an evidence-based local and foreign policy.

SciTech DiploHub implements a comprehensive action plan to deploy Barcelona's science and technology diplomacy strategy. It brings together consulates, international organizations and the city's innovation ecosystem to enhance collaborative projects; empowers the global diaspora of scientists and technology experts educated in Barcelona, the Barcelona Alumni network, and organizes international events to connect the city's ecosystem

with other global hotspots in science and technology. In addition, it offers capacity building and training in science diplomacy for city officers and diplomats; delivers policy advice for local city councils and partners with other international organizations, working as a think tank where scientific expertize can be harnessed in support of evidence-based policy (SciTech DiploHub, 2018). The following section will discuss two of the main initiatives of Barcelona's science diplomacy action plan: the Barcelona Alumni Network and The Barcelona Science and Technology Diplomatic Circle. These complementary tools are innovative in terms of soft power, since they articulate communities of interest, empower citizens outside of public institutions and allow dialog between different levels of government (central, regional and local government).

Networking Barcelona influencers. More attention has been paid in recent years to the role of higher education and talent mobility in public diplomacy and the contest for global influence. Some scholars have highlighted the "influence of high-quality human capital, local and global human network, and high-valued intellectual capacity" as elements of soft power in forming "an intangible regional network and leadership position, which will extend its long-term political, cultural, and social impacts in the region and beyond" (Cheng et al., 2011; Mok, 2012; Shields and Edwards, 2010).

Alumni play an important role as key allies and advocates of Barcelona's economic, social and cultural value beyond geographical areas. However, existent Alumni networks from the city's higher education institutions have dedicated minor efforts in establishing an international network of influence and these have been limited mainly to the regional arena. A direct consequence is a low representation and visibility of the city's higher education ecosystem in the international scene.

In this vein, the ecosystem's Alumni were identified as an underexploited crucial element of Barcelona's science diplomacy strategy as intercultural communicators, ambassadors of the city's knowledge ecosystem and education, business and trade promoters, thereby increasing the international recognition and visibility of the city's ecosystem. To untap this potential, the Barcelona Alumni network was launched as the global community of scientists, technology experts, researchers and innovation leaders trained in Barcelona and currently based abroad. The network currently gathers over one thousand members of more than thirty countries (Roig and Jiménez, 2019). Scientific specialization allows the emergence of a dynamic community, focused on thematic activities. Scientific dynamism serves as an accelerator of the diplomatic function: shared interests, as an essential characteristic of soft power, promote the development of an agenda of internationalization and influence. Thus, the institution acts as an umbrella organization, but not as a dominant actor in the relations between scientists linked to Barcelona. This structure represents a diplomatic innovation of interest for literature and, more specifically, for the practice of urban diplomacy.

By connecting and dynamizing this network, Barcelona Alumni creates opportunities for academic, scientific, and business partnerships, thus adding value to the ecosystem's research institutions and innovation industries while enhancing the ecosystem's competitiveness and influence. Simultaneously, it helps the Alumni to inform and encourage others to consider Barcelona as a reliable partner in science and technology, as well as promote the city as a reference destination for training and high education. It also enables the development of key talent pools for industry, investment and entrepreneurship that eventually support the economic development of the ecosystem. Finally, the Alumni network seeks to better understand international trends and strategic markets, allowing Barcelona's ecosystem to anticipate priorities, research programs and public policies.

The Barcelona Science and Technology Diplomatic Circle is a platform developed by SciTech DiploHub and the Barcelona City Council that engages in periodic visits and encounters between the more than one hundred diplomatic missions and international organizations serving Barcelona and leaders representing academia, the government and the private sector, which shape the innovation ecosystem of Barcelona. Heads of missions, counselors, attachés and officers dealing with science, technology and innovation from consulates, embassies and international organizations have the chance to find out new bonds with Barcelona's science and technology landscape, exchange best practices and connect back to their countries.

This initiative creates opportunities for networking and exchange of information, starting scientific collaborations that might be of global interest and enhancing diplomatic ties through science and technology. It also promotes Barcelona as a reference destination for doing research, investing and studying, thus contributing to the city branding and internationalization strategy. The diplomatic circle is partially inspired by analogous initiatives in other global cities, such as the Science and Technology Diplomatic Circle (STDC) in Boston, Singapore, Shanghai and Tokyo, and the Science Diplomats Club (SDC) in Washington. Barcelona leverages a pre-existent model to endow it with its own characteristics and adapt them to the specific context of the city. As with the first four cities, it includes the following elements: a high number of international students, a competitive educational network, investment capital, R&D centers, and a unique symbolic capital. Like Washington, Barcelona hosts a high number of resident scientists linked to the diplomatic and consular network located in the city.

Governance. SciTech DiploHub is a non-profit organization that establishes itself as the bridge linking together the wide array of stakeholders comprising Barcelona's innovation ecosystem, with the purpose of representing its assets and interests abroad and contributing to its internationalization. The participation of the ecosystem's stakeholders is channeled through the so-called "Ecosystem Board". Members of the Ecosystem Board consist of public and private entities that are mostly non-profit and devoted to the fields of science, technology, innovation and international relations. Currently, SciTech DiploHub has the support of the following entities (Table 1):

The institutions comprising the Ecosystem Board contribute to the realization of SciTech DiploHub's activities through the provision of financial resources. However, not only does the organization receive financial support from its partner institutions, but it is also granted the position of "ambassador of Barcelona's science and innovation ecosystem" in the international arena. This non-executive position gains relevance in the practice of soft power. The attribution of a status or power of representation, and the diplomatic connotations it encompasses, provides notoriety and uniqueness to the initiative. The ambassador role is novel in the urban domain, especially when referring to the representation of innovation ecosystems, and not to personalities depending on their career or assigned position.

Establishing an inclusive dialog with the urban stakeholders to be involved in the city's internationalization strategy throughout the entire process is a key ingredient for a fruitful public–private collaboration. This entails an effort to raise awareness among the multiple actors about the wide range of assets at their disposal, and therefore allowing them to build on complementarity by utilizing the diverse infrastructures, skills and funding sources.

Table 1 Institutions comprising the Ecosystem Board of SciTech DiploHub—Barcelona Science and Technology Diplomacy Hub.

Entity	Governance	Economy
Barcelona City Council	Public	Non-profit
Barcelona Supercomputing Center (BSC-CNS)	Public	Non-profit
Vall d'Hebron Research Institute (VHIR)	Public	Non-profit
Josep Carreras Leukemia Research Institute (IJC)	Public	Non-profit
Pompeu Fabra University	Public	Non-profit
Open University of Catalonia	Public	Non-profit
La Salle—Ramon Llull University	Private	Non-profit
Biocat—Bioregion of Catalonia	Public	Non-profit
Barcelona Tech City	Private	Non-profit
ACCIÓ-Agency for Business Competitiveness	Public	Non-profit
Fundació Catalunya-La Pedrera	Private	Non-profit
Fundació Banc Sabadell	Private	Non-profit
Fundació La Caixa	Private	Non-profit
Itnig	Private	For-profit
Catalan Foundation for Research and Innovation (FCRI)	Private	Non-profit
Advisory Council for Sustainable Development of Catalonia (CADS)	Public	Non-profit

Communication on a regular basis facilitates the exchange of ideas, information, and perspectives, as well as the mutual understanding of roles and responsibilities to ensure a more efficient decision-making process. A transparent process may contribute to a broader support for the projects under development and set the ground for building mutual trust among the involved partners. Trust is a fundamental element to the commitment of stakeholders, eventually enhancing the cooperative nature of the partnership.

As stated above, one of the main challenges was to align interests between stakeholders. Therefore, a great effort was put on establishing communication channels among all actors with the objective of allowing them to get acquainted with each other. Once the stakeholders have a certain knowledge about their respective interests and conflicts of interests, synergies can be more easily enhanced, and a shared global vision can be designed. In light of the above, SciTech DiploHub emerges as an institutionalized public–private partnership that serves as the pillar structure where public and private stakeholders in Barcelona's innovation ecosystem share and align their interests and missions, thereby converging into the implementation of its science diplomacy strategy and contributing to the city's international projection.

Discussion and conclusions

Urban innovation ecosystems are set to play a prominent role in the internationalization and governance of big cities. By harboring solid scientific and technological assets and attracting both human and financial capital, they are best suited to become the pivotal actors of effective multi-stakeholder partnerships between the scientific community, public institutions, the private sector and civil society. In response to the research question, the Barcelona Science and Technology Diplomacy is characterized by public–private collaboration. The case of Barcelona paves the way for other global innovation ecosystems to explore the opportunities for city-led science diplomacy as a formal, institutionalized practice aimed to reinforce the insertion of local interests in the international scene while favouring the open interaction between the city's internal stakeholders.

The second characteristic is the integration of actors with a strong international orientation. These include not only educational or scientific institutions, but also financial or business organizations. Barcelona's city-led science diplomacy strategy has not only reinforced the international influence of the urban innovation ecosystem but also favored the internal interaction between its main actors by: (i) delimiting the international action of the stakeholders involved, (ii) replacing the tendency towards "reactive internationalization" for a planned, sustainable internationalization strategy; (iii) improving the criteria to prioritize actions and initiatives; (iv) reducing thematic dispersion and aligning interests and priorities; (v) achieving greater coherence with other government levels and dependencies, and (vi) building an international cooperation agenda in accordance with the city's development strategy.

Barcelona's 'niche diplomatic action', focused on science and technology, comprises initiatives such as the Barcelona Alumni Network and The Barcelona Science and Technology Diplomatic Circle, which are true differentiating contributions in the execution of a soft power strategy adapted to cities. Overall, the city of Barcelona has made a substantial effort to adapt its international action to scientific and technological transformations. Knowledge, diplomacy and cities are meant to advance in an intertwined manner, reshaping urban policy planning. In short, Barcelona's case study contributes to understand an initial historical phase, when science and technology met city diplomacy. The designed model confirms the hypothesis of the symbolic capital of Barcelona. The desire for city membership, an esthetic heritage and the recent developments in science and technology, promote a unique style of urban diplomacy.

The very concept of city science diplomacy deserves further discussion. The dawn of this new urban chapter, which links both scientific knowledge and economic activity, will undoubtedly have an impact on global governance, as well as on international institutions and policies related to science and technology. The capacity to lead this new phenomenon will require a coordinated private and public response in accordance with the new multilayered diplomatic scenario. New capitalism, largely dependent on technological change and continuous innovation, will force cities to compete for R&D facilities, digital infrastructures, and innovation capabilities. Likewise, cities with greater capacity, either individually or within urban networks, will drive territorial inequality. The concentration of capital and talent can sharpen differences among territories and impact economic development, income inequality, or migration. It is not a minor matter. Therefore, city science diplomacy emerges as a relevant field to expand research on global governance.

Data availability

All data generated or analyzed during this study are included in this published article.

Received: 24 June 2020; Accepted: 10 September 2020;
Published online: 02 October 2020

References

Acuto M (2013) Global cities, governance and diplomacy: the urban link. Routledge New Diplomacy Studies, London

Acuto M, Parnell S (2016) Leave no city behind. Science 352(6288):873. https://doi.org/10.1126/science.aag1385

Acuto M, Rayner S (2016) City networks: breaking gridlocks or forging (new) lockins? International Affairs 92(5):1147–1166

Bäckstrand K, Kuyper JW, Linnér B et al. (2017) Non-state actors in global climate governance: From Copenhagen to Paris and beyond. Environ Polit 26(4). https://doi.org/10.1080/09644016.2017.1327485

Balland PA, Jara-Figueroa CI, Petralia S et al. (2020) Complex economic activities concentrate in large cities. Nat Human Behav 4:248–254. https://doi.org/10.2139/ssrn.3219155
Barber B (2017) Cool cities: urban sovereignty and the fix for global warming. University Press, New Haven
Bauder H (2016) Sanctuary cities: policies and practices in international perspective. Int Migr 55(2):174–187. https://doi.org/10.1111/imig.12308
Boschma R (2005) Rethinking regional innovation policy. In: Fuchs G, Shapira P (eds) Rethinking regional innovation and change. Economics of Science, Technology and Innovation. Springer, New York
Bouteligier S (ed) (2013) Cities, networks, and global environmental governance: spaces of innovation, places of leadership. Routledge, New York
Bulkeley H, Betsill MM (2003) Cities and climate change: urban sustainability and global environmental governance. Routledge, London
Bulkeley H, Castán-Broto V (2013) Government by experiment? global cities and the governing of climate change. Trans Inst Br Geogr 38(3):361–375. https://doi.org/10.1111/j.1475-5661.2012.00535.x
Burki S, Perry G, Dillinger W et al. (1999) Beyond the center: decentralizing the State. World Bank Latin American and Caribbean studies. World Bank, Washington DC
Cabrero Mendoza E (1995) La nueva gestión municipal en México. Análisis de experiencias innovadoras en gobiernos locales. Center for Economic Research and Training, Mexico DF
Campbell T (2000) The quiet revolution. The University of Pittsburgh Elgar, Pittsburgh
Carayannis EG, Grigoroudis E, Campbell D et al. (2018) The ecosystem as helix: an exploratory theorybuilding study of regional co-opetitive entrepreneurial ecosystems as quadruple/quintuple Helix innovation models. R&D Manage 48(1):148–162. https://doi.org/10.1111/radm.12300
Castells M (1989) The informational city. information technology, economic restructuring, and the urban-regional process. Basil Blackwell, Oxford
Cerda-Bertomeu MJ, Sarabia-Sanchez FJ (2016) Stakeholders' perceptions of place branding and the role of the public sector: an exploratory analysis. Place Branding and Public Diplomacy 12(4):299–313. https://doi.org/10.1057/s41254-016-0016-8
Cheng YC, Cheung AC, Yeun TW (2011). Development of a regional education hub: The case of Hong Kong. International Journal of Educational Management
Coll JM (2015). Cities emerging soft power: 5 key advantages for improved global governance. Barcelona: CIDOB
Cooke P (2002) Regional innovation systems: general findings and some new evidence from biotechnology clusters. Journal Technol Transf 27:133–145. https://doi.org/10.1023/A:1013160923450
Cornago N (2013) Plural diplomacies. Normative predicaments and functional imperatives. The Brill, Leiden
Crescenzi R, Iammarino S, Ioramashvili C et al. (2020) The geography of innovation and development: global spread and local hotspots. Geography and environment discussion paper series (4). London School of Economics and Political Science, London
Curtis S, Acuto M (2018) The foreign policy of cities. RUSI Journal 163(6):8–17. https://doi.org/10.1080/03071847.2018.1562014
Davidson K, Coenen L, Gleeson B (2019) A decade of C40: research insights and agendas for city networks. Glob Policy 10(4):697–708. https://doi.org/10.1111/1758-5899.12740
Dijkstra L, Poelman H, Rodríguez-Pose A (2019) The geography of EU discontent Reg Stud 54(6):737–753. https://doi.org/10.1080/00343404.2019.1654603
Engel JS (2015) Global clusters of innovation: lessons from silicon valley. Calif Manage Rev 57(2):36–65. https://doi.org/10.1525/cmr.2015.57.2.36
European Commission (2017) Rejuvenating Barcelona with digital technologies. Digital Transformation Monitor
Ewers HJ, Wettmann RW (1980) Innovation-oriented regional policy. Regional Studies 14:161–179
Florida R (2003) Cities and the creative class. City Community 2(1):1–19
G7 Academies' Joint Statement (2017) New economic growth: the role of science, technology, innovation and infrastructure. https://royalsociety.org/~/media/about-us/international/g-science-statements/2017-may-3-new-economic-growth.pdf?la=en-GB. Accessed 10 Jun 2020
Glaeser EL, Kerr W, Ponzetto G (2010) Clusters of entrepreneurships. Journal Urban Economics 67(1):150–168. https://doi.org/10.1016/j.jue.2009.09.008
Grigolo M (2019) The human rights city. Routledge, New York, San Francisco, Barcelona. London and New York
Hale T (2018) The role of sub-state and non-state actors in international climate process. Chatham House, London
Johnson C (2018) The power of cities in global climate politics: Saviours, supplicants or agents of change? Palgrave Macmillan, London
Katz B, Nowak J (2018) The new localism. how cities can thrive in the age of populism. Brookings Institution Press, New York
Ketels C (2013) Recent research on competitiveness and clusters: what are the implications for regional policy? Cambridge J Reg Econ Soc Adv 6 (2):269–284. https://doi.org/10.1093/cjres/rst008
Koschatzky K (ed) (1997) Technology-based firms in the innovation process: management, financing and regional networks. Physica-Verlag, Heidelberg
Koschatzky K, Sternberg R (2000) R&D cooperation in innovation systems–some lessons from the European Regional Innovation Survey (ERIS). Eur Plan Stud 8:487–501. https://doi.org/10.1080/713666415
Kuznetsov AS (2015). Theory and Practice of Paradiplomacy. Subnational governments in international affairs. New York: Routledge
Landabaso M, Oughton C, Morgan. K (2001). Innovation networks and regional policy in Europe. In Innovation Networks (pp. 243–273). Physica, Heidelberg
Lamont C (2015) Research methods in international relations. Sage, London
Leffel B, Acuto M (2018) Economic power foundations of cities in global governance. Glob Soc 32(3):281–301. https://doi.org/10.1080/13600826.2018.1433130
Ljungkvist K (ed) (2015) The global city 2.0: an international political actor. beyond economism? Uppsala University
Marin B, Mayntz R (1991) Policy networks: Empirical evidence and theoretical considerations. Westview Press, Boulde
Mok KHJ (2012) The rise of transnational higher education in Asia: student mobility and studying experiences in Singapore and Malaysia. High Educ Policy 25(2):225–241. https://doi.org/10.1057/hep.2012.6
Nye J (2003) The paradox of American power: why the world's only superpower can't go it alone. Oxford University Press, Oxford
Nijman JE (2016) Renaissance of the city as a global actor: The role of foreign policy and international law practices in the construction of cities as global actors" (Research Paper Series). Asser Institute, Center for International & European Law, The Hague. https://papers.ssrn.com/sol3/papers.cfm?abstract_id=2737805. Accessed 12 Jun 2020
Pipa AF (2019) Shaping the global agenda to maximize city leadership on the SDGs: the experiences of vanguard cities. Global Economy and Development at Brookings Institution, Nueva York
Pique J, Berbegal-Mirabent J, Etzkowitz (2018) Triple Helix and the evolution of ecosystems of innovation: the case of Silicon Valley. Triple Helix 5:11. https://doi.org/10.1186/s40604-018-0060-x
Porter ME (1998) Clusters and the new economics of competition. Harv Bus Rev 76:77–90
Roig A (2018) Towards a city-led Science Diplomacy: The rise of cities in a multilateral world and their role in a science-driven global governance. United Nations Institute for Training and Research
Roig A, Jiménez-Mausbach M (2019). SciTech DiploHub Barcelona Science and Technology Diplomacy Hub. In: Higher Education in the World 7. Humanities and Higher Education: Synergies between Science, Technology and Humanities, pp. 248–249. Global University Network for Innovation
Rosenau JN (1990) Turbulence in world politics: a theory of change and continuity. Princeton University Press, Princeton
Royal Society & American Association for the Advancement of Science (2010) New frontiers in science diplomacy. Royal Society, London
Sassen S (1991) The global city: New York, London, Tokyo. Princeton University Press, Princeton
Scholten P, Penninx R (2016) The multilevel governance of migration and integration. In: Garcés-Mascarenas B, Penninx R (eds) Integration processes and policies in Europe. Springer, pp. 91–108. https://doi.org/10.1007/978-3-319-21674-4_6
Schragger RC (2016) City power: urban governance in a global age. Oxford University Press, New York
SciTech DiploHub (2018) The Barcelona Manifesto. http://www.scitechdiplohub.org/manifesto/. Accessed 5 Jun 2020
Shields R, Edwards R (2010) Student mobility and emerging hubs in global higher education. In: Rust VD, Portnoi LM, Bagley SS (eds) Higher education, policy, and the global competition phenomenon. Palgrave Macmillan, New York
Skolnikoff EB (1993) The elusive transformation: science, technology, and the evolution of international politics. Princeton University Press, Princeton
Smeds E, Acuto M (2018) Networking cities after Paris: Weighing the ambition of urban climate change experimentation. Glob Policy 9(4):549–559. https://doi.org/10.1111/1758-5899.12587
Tavares R (2016) Paradiplomacy: cities and states as global players. Oxford University Press, Oxford
Taylor PJ (2012) The challenge facing word city network analysis. GaWC Research Bulletin 409. https://www.lboro.ac.uk/gawc/rb/rb409.html. Accessed 14 Oct 2019
Tukianen T, Leminen S, Westerlund M (2015) Cities as collaborative innovation platforms. Technology innovation. Manag Rev 5(10):16–23. https://doi.org/10.22215/timreview/933
UNESCAP (2006). What is Good Governance? United Nations Economic and Social Commissions for Asia and the Pacific

United Nations General Assembly (2015). Transforming our world: the 2030 Agenda for Sustainable Development, A/RES/70/1
Van der Heijden J (2019) Studying urban climate governance: Where to begin, what to look for, and how to make a meaningful contribution to scholarship and practice. Earth Syst Govern 1(1):Article 100005. https://doi.org/10.1016/j.esg.2019.100005
Van Langenhove L, Boers E (2018) Science diplomacy in search of a purpose in the populist era. United Nations University Institute on Comparative Regional Integration Studies (UNU-CRIS), 14
Wagner CS (2002) The elusive partnership: science and foreign policy. Sci Public Policy 29(6):409–417. https://doi.org/10.3152/147154302781780741
Weiss TG, Seyle DC, Coolidge K (2013). The rise of non-state actors in global governance: opportunities and limitations. One Earth Future foundation
World Science Forum (2013) Declaration. UNESCO, Rio de Janeiro

Acknowledgements

The paper is granted by Ministry of Science, Innovation and Universities of Spain (DiploCity-Grant reference RTI2018-096733-B-I00).

Competing interests

Two authors work at Barcelona Science and Technology Diplomacy Hub, while the third is an international scholar.

Additional information

Correspondence and requests for materials should be addressed to J.-L.M.-S.

Reprints and permission information is available at http://www.nature.com/reprints

Publisher's note Springer Nature remains neutral with regard to jurisdictional claims in published maps and institutional affiliations.

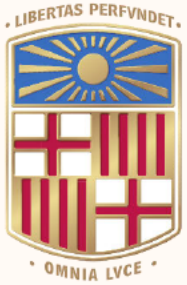

UNIVERSITAT DE BARCELONA